A Synthesis of Antarctic Neogene radiolarians: taxonomy, macroevolution and biostratigraphy

Dissertation
zur Erlangung des akademischen Grades
doctor rerum naturalium
(Dr. rer. nat.)
im Fach Biologie

eingereicht an der

Mathematisch-Naturwissenschaftlichen Fakultät I
der Humboldt-Universität zu Berlin

von

M.Sc. Johan Renaudie

Präsident der Humboldt-Universität zu Berlin
Prof. Dr. Jan-Hendrik Olbertz

Dekan der Mathematisch-Naturwissenschaftlichen Fakultät I
Prof. Dr. Stefan Hecht

Gutachter/innen: Dr. Prof. Taniel Danelian, Université de Lille (Frankreich)
PD Dr. Barbara Mohr, Museum für Naturkunde
Prof. Dr. Wolfgang Kiessling, Museum für Naturkunde

Tag der mündlichen Prüfung: 18/12/2012

Table of Contents

(1) The new species described in this chapter were published in *Journal of Micropalaeontology* (Renaudie & Lazarus 2012, in press).
(2) This chapter was modified and submitted to *Paleobiology* in May 2012.

Abstract

The Southern Ocean is the key to understand the Neogene climate evolution. Unfortunately the lack of a robust geochronological framework has hindered precise studies. Equally of interest is understanding how planktonic communities changed in relation with the evolution of these environments. Radiolarians are abundant in Antarctic Neogene sediments, diversified and consistently well-preserved. They should constitute not only an ideal testing ground for paleobiological studies but also a major resource for improved biostratigraphy. However, studies to date have focussed only on a small subset of this fauna.

In this study, a quantitative, taxonomically-complete dataset have been collected in various sites of the Southern Ocean, using 98 samples and ca. 7000 specimens per sample. Ca. 500 species were uncovered in this fauna, including 120 new to science.

The study of the macroevolutionary history of this fauna reveals that a significant, extinctionless ecological turnover, linked to a decrease in the evenness of the species' abundances and the rise of genus *Antarctissa* to dominance, occured at ca. 8 Ma, followed 3 My later by a significant diversity loss. Although the ecological event can be tentatively associated with a regional change in the composition of primary producers, the triggering event of the diversity loss is yet to be found.

The whole-fauna diversity history was compared to paleodiversity reconstructions computed using subsampling methodologies from the occurrences gathered in the Neptune database. The comparison shows that the main trends are retrieved by the subsampling procedures but also that substantial distortions make them poorly suited for detailed studies: the accuracy of these methods does not allow comparison with the paleoenvironmental history.

Finally a biostratigraphical analysis using the Constrained Optimization (CONOP) procedure was conducted on this whole-fauna dataset for the late Miocene - Pliocene sequence, after careful treatment of outliers. Although this analysis is still very much preliminary, it shows a coherent readjustement of the current age model for some sites by more than 1 My. This study also shows that 94 events seem reliable enough to be used to correlate Southern Ocean sites together. If confirmed, these events, along with the ca. 80 diatom events recently uncovered, would be a solid basis for a revised high-resolution chronological framework for the Southern Ocean.

Zusammenfassung

Der Südozean ist die Schlüsselregion zur Kenntnis der neogenen Klimaentwicklung. In diesem Zusammenhang ist die Untersuchung von planktonischen Gemeinschaften in Hinblick auf die Umweltentwicklung von großer Bedeutung. In antarktischen neogenen Sedimenten sind Radiolarien reichlich, in großer Diversität und einheitlich gut erhalten. Sie sind nicht nur perfekte Testobjekte für paläobiologischen Studien, sondern auch eine wichtige Quelle für eine verbesserte Biostratigraphie – bisher behinderte nämlich das Fehlen einer verlässlichen Geochronologie detaillierte Studien. Hier fokussieren sich die Untersuchungen nur auf einen kleinen Teildatensatz der Fauna.

Es wurde ein Datensatz aller Taxa von mehreren Standorten des Südozeans gesammelt: für alle der 98 Proben je ca. 7000 Radiolarien. Die Fauna enthält ca. 500 Arten (inclusive 120 neuer Taxa).

Die Untersuchung der Makroevolutionsgeschichte dieser Fauna zeigt, dass eine wesentliche ökologische Umwälzung, ohne wichtiges Aussterbeereignis, bezogen auf den Verlauf der Artengleichheit (evenness) und den Anstieg der Gattung *Antarctissa*, bei ca. 8 Ma erfolgte. Dann, 3 Mill. Jahre später, folgte ein wesentlicher Diversitätsverlust. Obwohl das ökologische Ereignis eventuell mit einer regionaler Änderung der Primärproduzenten assoziiert sein kann, ist der auslösende Faktor des Diversitätsabfalls unbekannt.

Außerdem zeigt der Vergleich zwischen der Diversitätsgeschichte dieser Fauna und einer Paläodiversitätsrekonstruktion südozeanischer Faunen, beruhend auf der Neptune Datenbank, daß der generelle Verläufe mit den Probenteilungsmethodologien (subsamplings methods) nachgezeichnet wird, jedoch diese Methodologien aufgrund grober Verzerrungen nicht geeignet für Detailstudien sind: die Genauigkeit dieser Methoden erlaubt keinen Vergleich mit der Paläoumweltsgeschichte.

Schließlich wurde eine biostratigraphische Analyse mittels der 'Constrained Optimization' (CONOP) Methode für die komplette Fauna vom Obermiozän bis zum Unterpliozän durchgeführt. Obwohl diese Analyse noch vorlaüfig ist, zeigt sich eine Angleichung des aktuellen Altersmodells um mehr als 1 Mill. Jahre. Diese Studie zeigt auch 94 neue, sichere Ereignisse, die für die stratigraphische Einordnung der Antarktischen Tiefseesedimente genutzt werden können. Im Falle einer Bestätigung, können diese Ereignisse zusammen mit den 80 neulich gefunden Diatomeenereignisse eine deste Basis für einen neuen hochauflösende geochronologischen Rahmen für den Bereich des Südozeans liefern.

Introduction

Rationale of the study

Understanding how life diversity is affected by environmental changes, and more generally what are the driving events of macroevolutionary patterns, is at the heart of ecological and paleobiological research. Resolving this issue both implies being able to accurately represent changes in the studied community and being able to correlate this community history with environmental changes.

The imperfection of most fossil records is the cause of a large array of biases preventing direct reconstruction of paleodiversity (e. g. Bush et al. 2004). Numerous methodologies have been developed to compensate some of those biases (e. g. Alroy 1996, 2000) but their accuracy could not be tested since the actual diversity of these fossil records is obviously unknown. Marine micropaleontology however does not have the limitations of most fossil records (Lazarus 2011) and therefore should constitute a unique resource for paleobiology and a reference standard for macroevolutionary research. Neogene radiolarians in particular have a rich (thanks to the DSDP/ODP deep sea drilling campaigns) and complete record.

Antarctic Neogene sediments are a key archive to understand major climatic and paleoceanographic events such as ice sheet growth during the middle Miocene, low-latitude upwelling system development during the late Miocene, Messinian events, early Pliocene warming and late Pleistocene glaciations. However the study of these events are hindered by the lack of a robust geochronologic framework, which is caused by the absence of carbonate microfossils in these sediments, widespread hiatuses and rapid changes in sedimentation rate: age model uncertainties are commonly higher than 1 My and thus prevent correlation at the needed resolution. In addition to the more widely employed diatoms, Antarctic Neogene sediments contain abundant well preserved radiolarians. These faunas are diverse, evolve rapidly and offer in principle a major resource for improved biostratigraphy and thus improved geochronology. However, studies to date have employed only a small fraction of the fauna and the available biostratigraphic resolution is only moderate.

Antarctic Neogene Radiolaria constitutes therefore an interesting testing ground for paleobiological research since this fauna offers the possibility to go beyond the two major current limitations of this discipline, given an improved recording effort. In this study, a quantitative, taxonomically-exhaustive dataset on this fauna was collected with the objective of giving an accurate representation of the community while improving local geochronology.

Radiolaria

1. A short history of radiolarian studies

Despite the early discovery of protists by van Leeuwenhoek (1674), the first radiolarian (*Sphaerozoum fuscum*) was only described briefly from the plankton in the early 19th century by the german botanist F. J. F. Meyen (1834). Soon after this discovery, Ehrenberg (1839) described the first fossil radiolarians (Polycystina) from the Neogene of Barbados. During the following years, Ehrenberg, Müller and Haeckel carried substantial work on both living and cenozoic radiolarians. Haeckel himself described over 3000 radiolarian taxa (Tanimura et al. 2009; Lazarus, subm.), mostly in his report from the H. M. S. Challenger Expedition. The higher level taxonomical framework established by Haeckel in this report, though widely recognized as being mostly artificial, is still partly the basis of today's radiolarian taxonomy, particularly for

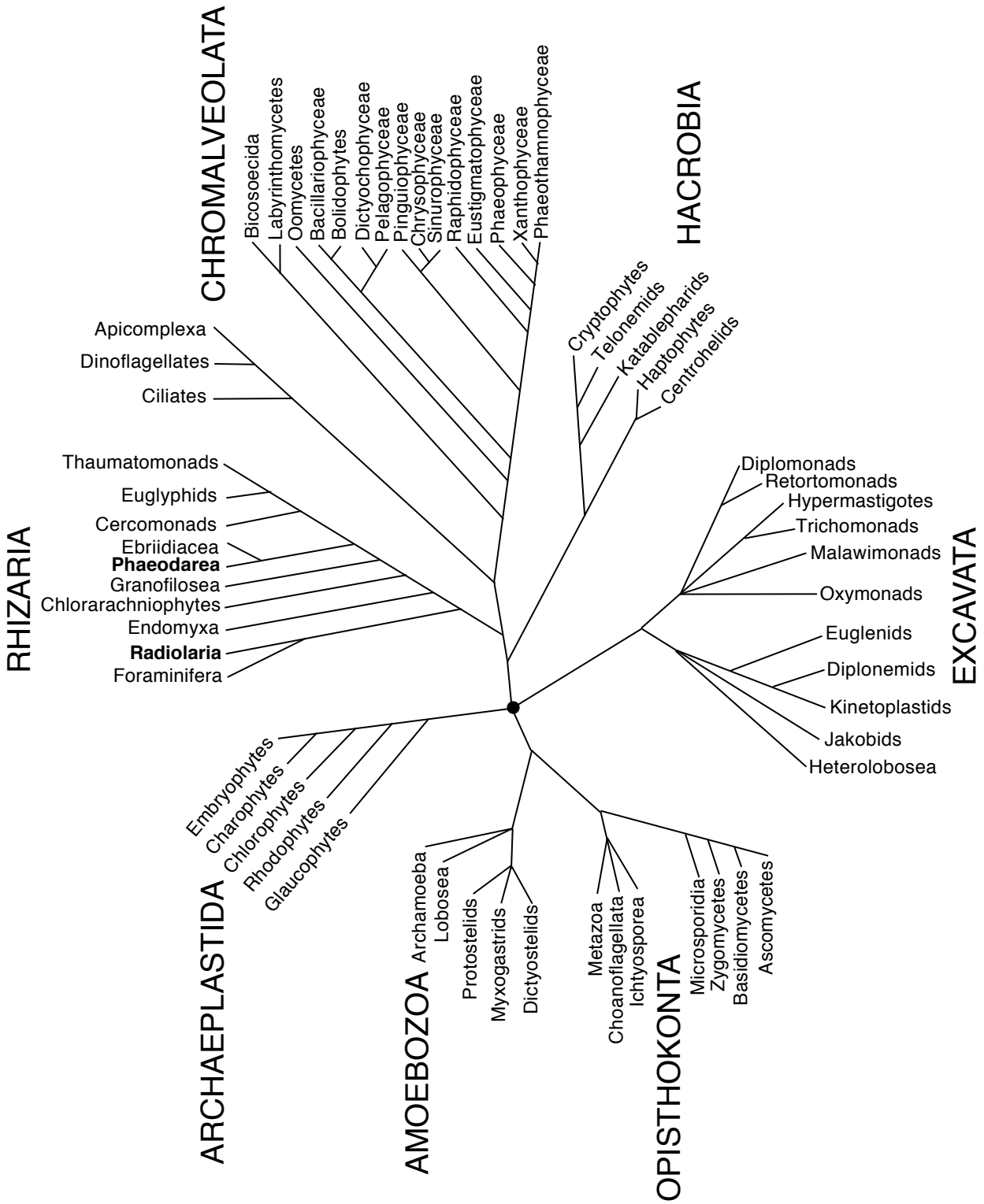

Figure 1.– The place of radiolarians amongst eukaryots.
(modified and redrawn after Bass et al. 2005, Keeling et al. 2005, Okamoto et al. 2009, Riisberg et al 2009)

Cenozoic genera.

The end of the 19th century and the beginning of the 20th century saw several major advances in the study of radiolarians: the first discovery of Mesozoic (Zittel 1876) and Paleozoic (Rüst 1892) radiolarians and the development of radiolarian systematic toward modern standards - e. g. Bütschli (1882) and Jørgensen (1905)'s description of the nasselarian skeleton. However, despite the fact that many early workers - such as Haeckel - studied both living and fossil radiolarians, it is only during the second part of the 20th century that proper ultrastructural studies (e. g. Hollande & Enjumet 1954; Cachon & Cachon 1971; Swanberg et al. 1985) detailed the cytology of the radiolarians and that the radiolarian taxonomy ceased to be purely based on skeleton morphology.

Meanwhile, thanks to a serie of long-term oceanographic and deep-sea drilling expeditions (most importantly the DSDP/ODP/IODP international expeditions from 1968 onwards), our knowledge of radiolarian diversity through time, of their geographic and stratigraphic distribution and of their evolution grew rapidly.

Modern studies on living radiolarians focus on understanding their ecology and their phylogenetic relationships using molecular data, while studies on fossil radiolarians try to sort out the impact of past environmental changes on radiolarian communities (for Cenozoic studies) or to understand their early evolution (for pre-Cenozoic studies). Fossil radiolarians are also used to study geologic questions, including determining the age of rocks and sediments, and to reconstruct past environmental conditions as part of paleoceanographic research.

2. Phylogeny

In Haeckel's classification of protists (Haeckel 1866), Radiolaria was part of the Rhizopoda Dujardin 1835, one of the eight main branches of Protista, and included at the time all single-celled organisms with pseudopodia. Radiolaria itself was composed of Acantharea Haeckel 1881, Polycystinea Ehrenberg 1838 and Phaeodarea Haeckel 1879. While Acantharea biomineralizes in strontium sulfate, both Polycystinea and Phaeodarea have skeleton of amorphous silicon. The latter also possess a characteristic pigmented granular cytoplasm: the 'phaeodium'.

Twentieth-century classifications, however, placed these three radiolarian groups (Radiolaria sensu Haeckel) in the protist group Sarcodina Schmarda 1871 (a group belonging to Sarcomastigophora Honigsberg & Balamuth 1963 and containing, basically, all amoeboid single-celled organisms; Levine et al. 1980). Acantharea, Polycystinea and Phaeodarea were united with Heliozoea Haeckel 1866 to form the Actinopoda Calkins 1901, on the basis of the presence of axopodia (i. e. differenciated pseudopodia sustained by microtubules).

This classification however was shown to be inconsistent with ultrastructural and molecular studies (Pawlowski 2008). Indeed Heliozoea were shown to be a cluster of protists belonging to widely different groups (Nikolaev et al. 2004). Only one group of Heliozoea, Taxopodida Fol 1883 (consisting of only one species, *Sticholonche zanclea* Hertwig 1877), appears to be related to Radiolaria.

According to the modern consensus (Adl et al. 2005; Keeling et al. 2005; Fig. 1), the three groups that form Radiolaria sensu Haeckel (Polycystinea, Acantharea and Phaeodarea) belong to the clade Rhizaria Cavalier-Smith 2002. However, while Polycystinea and Acantharea are, together with the Foraminifera d'Orbigny 1826, basal to the Rhizaria, Phaeodarea belongs to the crown-group, i. e. Cercozoa Cavalier-Smith 1998. The relationship between Polycystinea and Acantharea is still debated: either Polycystinea is polyphyletic and contains both Acantharea and *Sticholonche zanclea* (Takahashi et al. 2004; Yuasa et al. 2005; Fig. 2a) or Polycystinea is

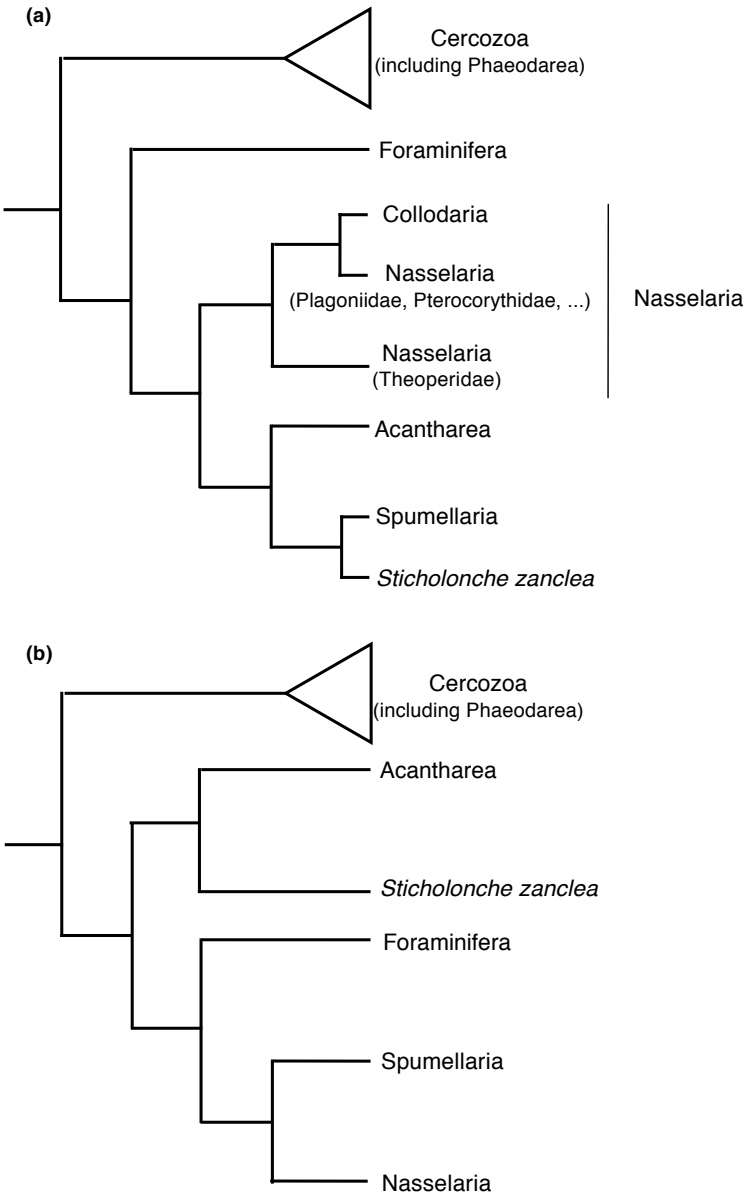

Figure 2.– Relationships between the different classical classes and orders of Haeckel's Radiolaria according to molecular phylogenies.

a) Polycystinea polyphyletic (based on 18S rDNA; Takahashi et al. 2004, Yuasa et al. 2005)
b) Polycystinea monophyletic (based on 18S and 28S rDNA; Krabberød et al. 2011)

The three families Thalassicollidae, Collosphaeridae and Sphaerozoidae (i. e. order Collodaria sensu De Wever et al. 2001) are nested in order Nassellaria.
Class Phaeodarea is, in all modern, molecular phylogenies, excluded from Radiolaria (Pollet et al. 2003; Nikolaev et al. 2004).

monophyletic (Krabberød et al. 2011; Fig. 2b) and so is the clade composed of Acantharea and *Sticholonche zanclea* (i. e. Spasmaria Cavalier-Smith 1993). The relationship of these two groups with Foraminifera is yet to be resolved; it seems however reasonable to think that Radiolaria (sensu stricto, i. e. excluding Phaeodarea) and Foraminifera are closely related, forming together Retaria Cavalier-Smith 1999 (Moreira et al. 2007).

Polycystinea is itself subdivided into different groups based, at first, on skeleton morphology. Classically those subdivisions were, in living polycystines radiolarians: Nassellaria Ehrenberg 1875 (with a skeleton having an axial symmetry, with an inner, spicular element; see Chapter 2, Fig. 2), Spumellaria Ehrenberg 1875 (with a skeleton having a radial symmetry) and Collodaria Haeckel 1887 (colonial forms with either no skeleton [family Thalassicollidae Haeckel 1862], a skeleton consisting of one single, smooth sphere [family Collosphaeridae Müller 1858] or composed of scattered spicules [family Sphaerozoidae Haeckel 1862]). Strong ultrustructural arguments for such a subdivision agree with the skeleton-based classification (see next paragraph). While the subdivision Nassellaria-Spumellaria fits relatively well to molecular phylogenies as well, Collodaria was found to be nested among Nassellaria in several molecular studies (Fig. 2a; Takahashi et al. 2004; Yuasa et al. 2005).

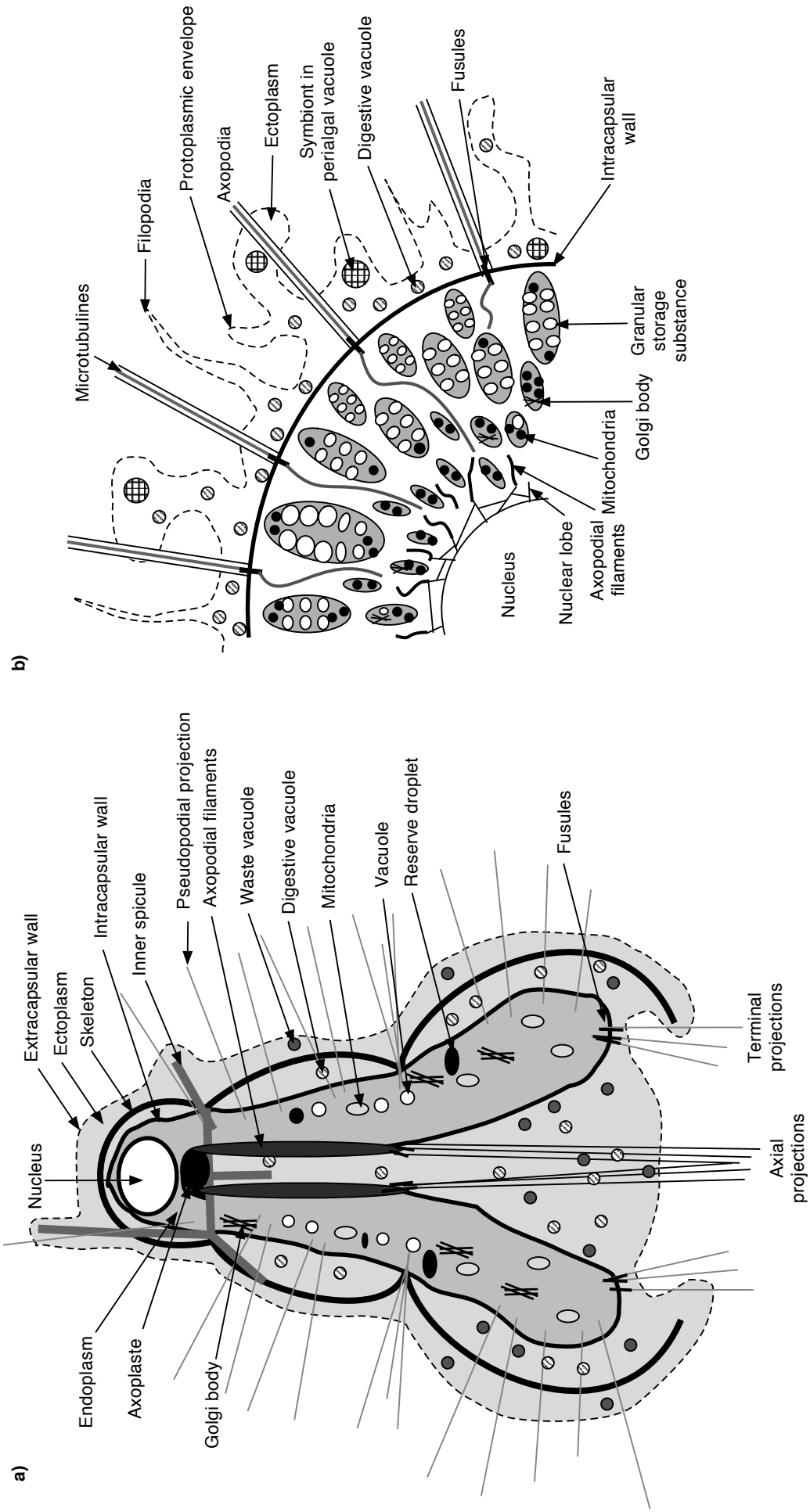

Figure 3.– Schematic illustration of Polycystine radiolarians cytology (redrawn and simplified after Suzuki & Aita 2011)
a) Nassellarian cytology; b) Spumellarian cytology.
In b, the skeleton is not represented because the relationship between the skeleton and the cytoplasm in spumellarians is not well understood to this date.

3. Cytology

Radiolarians have the particularity of having their cell divided into a nucleus, an endoplasm and an ectoplasm (see Fig. 3a and b). The nucleus is separated from the two others by a nucleic wall while the endoplasm and the ectoplasm are separated by a chitineous or pseudochitineous capsular wall (e. g. Anderson 1976; Suzuki & Aita 2011). The communication through the capsular wall occurs through organelles called fusules (Hollande & Enjumet 1953) or through fissures. The endoplasm contains various organelles such as the mithochondria, the ribosomes, the axoplast, golgi bodies, vacuoles and 'storage' organelles. The ectoplasm usually contains digestive vacuoles, waste vacuoles and perialgal vacuoles containing symbionts.

While the siliceous skeleton of nassellarians is contained entirely inside the extracapsular wall (Suzuki & Aita 2011), in spumellarians, the ectoplasm can contract inside the innermost cortical shell (Hollande & Enjumet 1960; Sugiyama & Anderson 1998; see also Chapter 2 Fig. 2). The skeleton is surrounded by an extension of the endoplasm and the ectoplasm (Swanberg et al. 1985), the cytokalymma, in which sites of silica secretion have been observed in polycystines radiolarians (Ogane et al. 2009b, 2010).

Axopodia are one of the main characteristics of Radiolaria: they are pseudopodia strengthened by bundles of microtubules. These microtubules are thought to be generated in the axoplast (which is an organelle specific to Radiolaria, present in the endoplasm; Cachon & Cachon, 1971) from which they extend, first, inside the endoplasm as axopodial filaments, and then to axopodia, in the ectoplasm, through fusules (Anderson 1977). Along with axopodia, polycystines radiolarians also possess regular pseudopodia as well as filopodia (Hollande & Enjumet 1954; Cachon & Cachon 1972a, b; Matsuoka 2007; Sugiyama et al. 2008).

In most Nassellarians, the endoplasm form lobes (Fig. 3a) joined in an apex that is situated in the cephalis (see Chapter 2 for skeleton terminology). The nucleus can be, in multisegmented forms, situated at the apex of those lobes but also, in other forms, anywhere else in those lobes. The axoplast however is, in all Nassellarians at the exception of family Trissocyclidae and forner 'Collodaria', situated in the cephalis, above the element of the inner spicule known as the median bar **MB** (Cachon & Cachon, 1971; Sugiyama & Anderson 1998).

In Spumellarians, the nucleus is usually central (Cachon & Cachon 1971; Suzuki et al. 2009b) and the endoplasm is divided in lobes that are elongated radially (see Fig. 3b).

Members of the nassellarian family Sphaerozoidae and Collosphaeridae are generally multinucleated (Anderson 1976; Suzuki et al. 2009b) with nuclei scattered in the intracapsulum (i. e. inside the intracapsular wall).

4. Ecology

Radiolarians are omnivorous (e. g. Anderson et al. 1984; Swanberg & Caron 1991), grazing on bacteria (e. g. Gowing 1986; Matsuoka 2007) and phytoplankton (Anderson 1978) as well as hunting zooplankton (Swanberg & Caron 1991; Matsuoka 2007). They can feed on prey of various size, ranging from bacterioplankton to small pelagic metazoans such as nauplius larvae and copepods (e. g. Swanberg 1979; Swanberg & Anderson 1985). Their feeding mechanism varies from one group to the other but usually relies on an active use of axopods or pseudopods (Matsuoka 2007; Sugiyama et al. 2008). Detritivory is also a feeding behavior that has been observed, specifically in phaeodarians (Gowing 1986). On the other side of the food chain, the main (known) predators of radiolarians are copepods (e. g. Harding 1974), amphipods (Swanberg 1979) or other small metazoans such as pelagic crabs (Lipps & Valentine 1970).

The relatively loose gelatinous ectoplasm of the radiolarian cell provides a viable

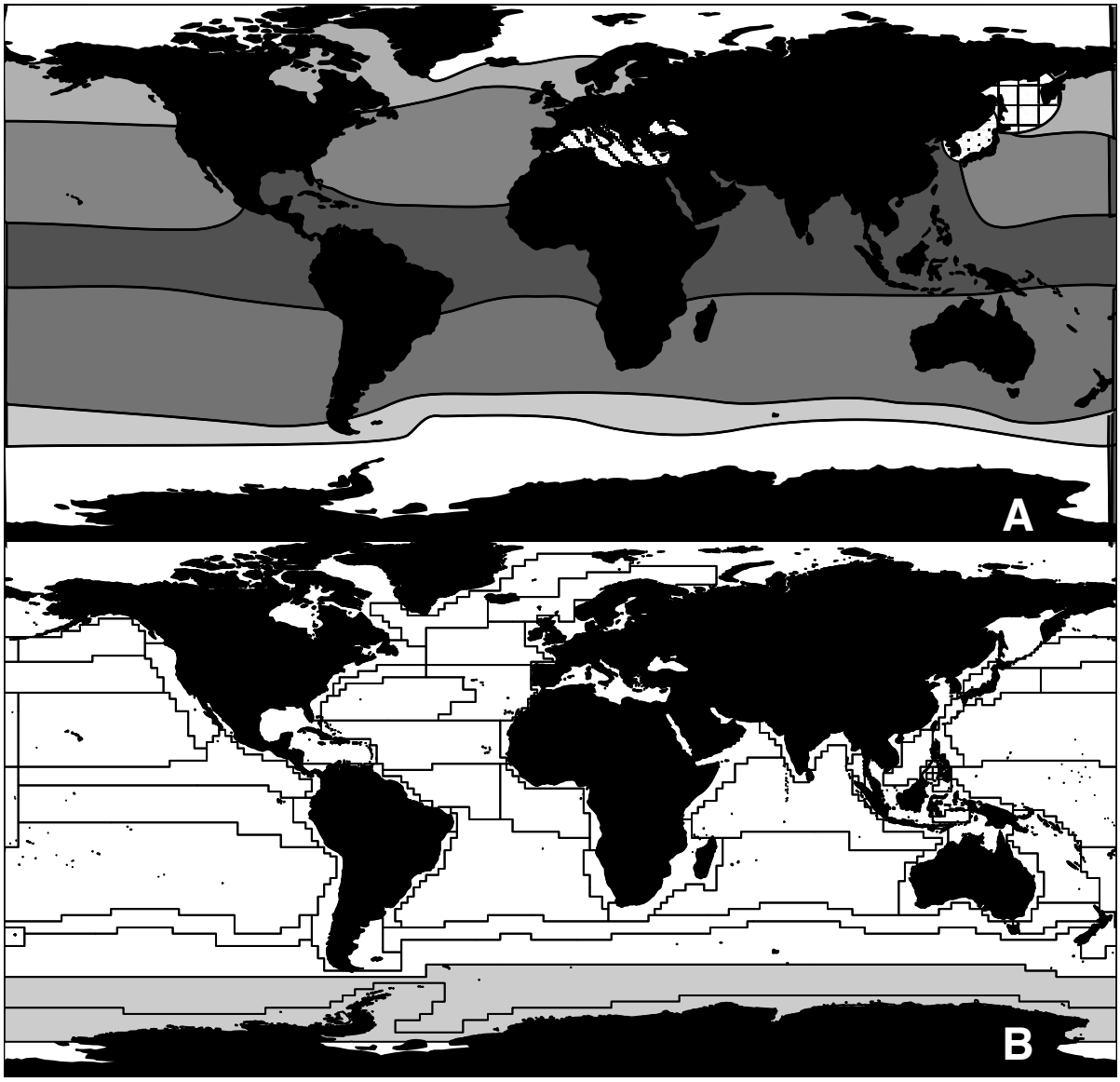

Figure 4.– Planktonic biogeographical provinces.
A. Main biomes.
In white, polar regions; in light grey, subpolar regions; in medium grey, 'transitional' (subtropical) regions; in dark grey, equatorial regions. Mediterranean Sea, Sea of Japan and Sea of Okhotsk are figured in motifs (respectively: dashed, dotted and checkered).
B. The detailed 56 pelagic biogeographic provinces as defined by Longhurst (1995).
In light grey the two provinces (open ocean and coastal) contained in the Southern Ocean.
Maps redrawn and simplified after Longhurst 1995, 1998 and Goll 1976, using data numerized by VLIZ 2009.

ecosystem to a large number of symbionts or parasites. Phototrophic symbionts are common in a large number of radiolarian species: these are mainly dinoflagellates (Anderson 1983), although some prasinophytes (a family of chlorophytes) have been observed in some cases (Anderson 1976; Gast & Caron 2001). Generally, the algal symbionts are situated in the ectoplasm, in perialgal vacuoles, but symbionts in the endoplasm have also been observed (Anderson & Matsuoka 1992). Ectoplasmic symbionts are usually situated at the periphery of the protoplasm during the day and migrate towards the central capsule during the night or during a stress period (Hollande & Carré 1974).

Hyperiid amphipods have been observed parasitizing colonies of collodarians (Swanberg 1979; Swanberg & Harbison 1980) while parasitic dinoflagellates (mainly genus *Duboscquella* Chatton 1920; Harada et al. 2007) have been found infecting solitary spumellarians (Suzuki et al. 2009c) and nassellarians (Dolven et al. 2007; Harada et al. 2007).

Coloniality is widespread in the families Collosphaeridae and Sphaerozoidae. They are generally a few centimeters long but can reach 2 meters in the case of *Collozoum caudatum* Swanberg & Anderson 1981. The shape of the colonies vary greatly from one species to another and even in one single species (Swanberg 1979). They are generally very rich in photosymbionts but still prey on other planktonic organisms (Swanberg 1979).

5. Biogeography

Longhurst 1995, 1998 proposed a classification of the world pelagic flora and fauna in four biomes and 56 provinces (Fig. 4B) based on physical and chemical constraints. The four biomes were the polar domain, the westerlies domain (subpolar), the trade-winds domain (subtropical and equatorial) and the coastal domain. Those four domains are based on the forcing physical parameter that conditions the depth of the mixed-layer: in the polar biome, the brackish surface layer resulting from the partial melting of the sea ice in spring is this parameter; in the subpolar biome it is the westerlies winds; in the subtropical to equatorial biome the geostrophic currents linked to trade winds and in the coastal biome, the occurrence of upwellings and other local processes affecting the nutrient inputs (Longhurst 1998). The first three biomes are physically delimited by oceanic fronts (the polar and the subtropical fronts; see **§3.1**; Sournia 1994; Longhurst 1998). As for the 56 ecological provinces shown on Figure 4B, these are linked primarily to the distribution, quantity and type of chlorophyll as observed by colorimetry in remote sensing studies (Longhurst 1995).

In radiolarians, the four biomes mentioned above are clearly distinct, with the addition of the equatorial zone as a fifth domain (Goll & Bjørklund 1974; Boltovskoy 1998a; Fig. 4A). Indeed, apart from a few cosmopolitan species, radiolarian species tend to be "endemic" to one or a few of these biomes (Goll & Bjørklund 1974; Boltovskoy et al. 2010). The 56 provinces however are hardly recognizable in term of species presence or absence, even if changes in absolute abundances of some species are sometimes noticeable from one province to the other (e. g. Boltovskoy et al. 2010). Only three provinces however do present somewhat distinctive faunas: the Mediterannean Sea, the Sea of Okhotsk and the Sea of Japan (Lazarus 2011). All three are marginal basins with limited connection to the open ocean. Polar faunas usually have a certain degree of endemicity and some cases of bipolarity (i. e. species endemic to both poles) have been reported (Stepanjants et al. 2006).

Radiolarians are known from all depths of the water column (e. g. Not et al. 2007; Boltovskoy et al. 2010). However precise studies on living depth of given species are hindered by the difficulty of gathering uncontaminated data from lower layers of the water column due to the sinking shells of upper layers unhabitants. Molecular-based ecological studies have the same issue since DNA can survive long enough the death of the individual to sink and contaminate lower layers as well. However, RNA does not and can provide uncontaminated information (Not et al. 2009) but RNA-based studies are, to date, few. From the information gathered to date it seems that the global distirbution of radiolarians in the water column follows that of most heterotrophic planktonic groups, i. e. a higher density between the base of the photic zone and the top of the thermocline (e. g. Kling 1979; Tanaka & Takahashi 2008; Boltovskoy et al. 2010).

6. The fossil record of radiolarians

Because the silicon content in phaeodarian and in polycystine skeletons is different, polycystines have a rich fossil record, while phaeodarians are rarely preserved. Because of the high solubility of strontium sulfate, acantharians are, to date, unkown from the fossil record:

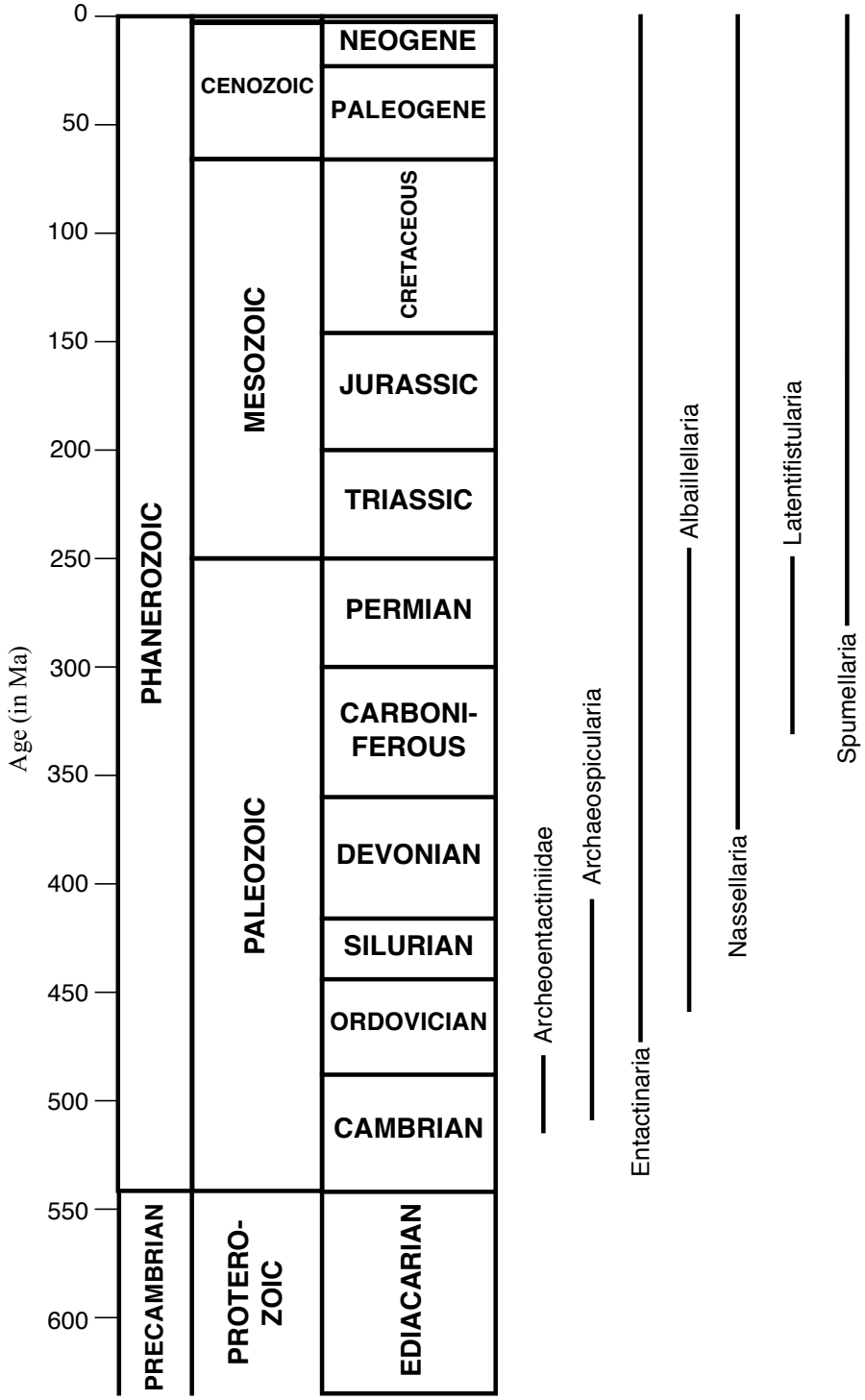

Figure 5.– Fossil record of the main groups of polycystines radiolarians.
Based on data from De Wever et al. 2003, Maletz 2011, Pouille et al. 2011.

however it has been hypothesized (e. g. Bernstein et al. 1998) that the formation of the deep-sea mineral known as barite (a barium oxide) is linked to acantharian biological activity (acantharians being the only known organisms to biomineralize strontium and barium), therefore the presence of barite might be an indirect fossil evidence of acantharian presence.

Considering these two facts, the fossil record of Radiolaria (sensu Haeckel) is therefore principally the fossil record of Polycystinea.

Apart from the two modern groups discussed above (Spumellaria and Nassellaria, including the former 'Collodaria'), other putative Polycystines groups are known only as fossils. They include: Entactinaria Kozur & Mostler 1992 (spherical forms with an inner spicular

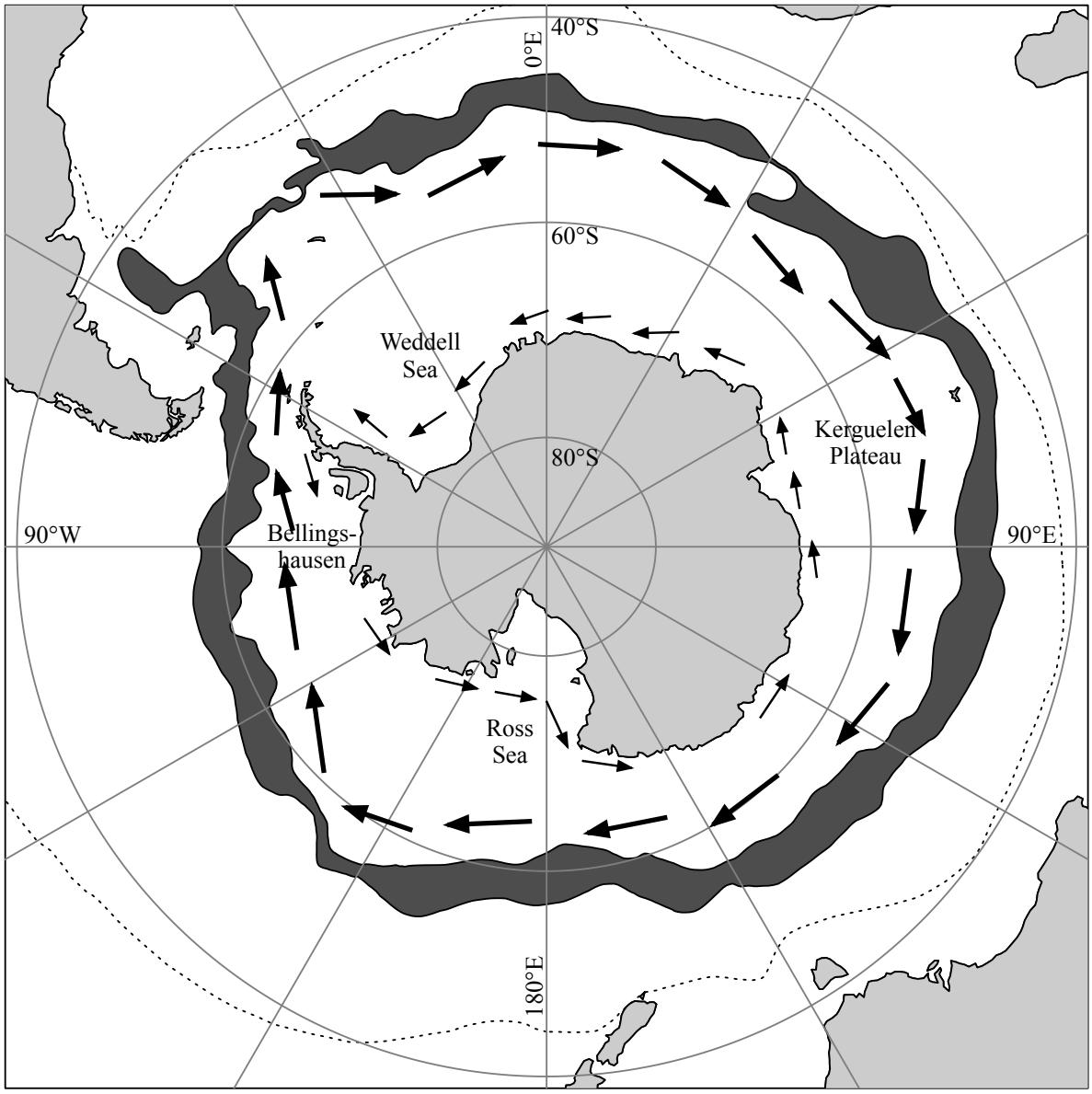

Figure 6.– Map of the Southern Ocean with Polar Front and main surface currents.
The Polar Frontal Zone is figured in dark grey and the Subtropical Front as a dotted line (both after Orsi et al. 1995); the Antarctic Circumpolar Current is indicated by large arrows and the Coastal Countercurrent by small arrows (both after Tchernia 1980).
Map created using R (R Development Core Team 2011) along with package GEOmap (Lees 2010).

element that evokes the element found in nassellarians), Latentifistularia Caridroit et al. 1999 (skeleton organized around an heteropolar, hollow, inner sphere), Albaillellaria Deflandre 1953 (skeleton with bilateral symmetry and a triactine spicular element), Archaeospicularia Dumitrica et al. 2000 (consisting of interlocking spicules) and the enigmatic family Archeoentactiniidae Won in Won & Below 1999. To this family belong the earliest known radiolarians (Maletz 2011; Pouille et al. 2011). Early Paleozoic faunas are constituted essentially of archaeospicularians, entactinarians and albaillellarians, while late Paleozoic faunas includes also latentifistularians and nassellarians. After the early Triassic, only nassellarians, spumellarians and entactinarians are known. Entactinarians, while highly diversified in the Paleozoic and the Mesozoic, become relict in the Cenozoic. The only cenozoic family unanimously recognized as belonging to Entactinaria is the Orosphaeridae Haeckel 1887 (Friend & Riedel 1967; Kozur & Mostler 1992); but several other families currently classified as belonging to Spumellaria are considered by

some authors as belonging to Entactinaria (e. g. De Wever et al. 2001). These families contain several living representatives, however no molecular studies have been done to date to confirm or infirm their affinity to one group or the other.

Paleoenvironmental context to this study

1. The Southern Ocean

Frontal system.– The Southern Ocean has the unique characteristic of not being limited by any continents; instead, it is separated from the Atlantic, the Indian and the Pacific Oceans by a serie of oceanographic, drifting limits called fronts. These fronts are all marked in the uppermost layer of the water column by a tightening of the spacing of isotherms, i. e. a clear shift in the temperature gradient.

The northernmost limit is the Subtropical Front (or Subtropical Divergence; Deacon 1933). It roughly follows the 40°S parallel and encompasses both the tip of South America and that of Southern New Zealand. South of the Subtropical Front lies the Subantarctic Front. Between the two extends the Subantarctic Zone. Close to the Subantarctic Front is the Polar Front: both delimit the so-called Polar Frontal Zone (or Antarctic Convergence; Deacon 1933), which lies at more or less 50°S in the Atlantic and Indian sectors, and 60°S in the Pacific sector (Orsi et al. 1995). This zone is a significant biogeographical barrier (e. g. Longhurst 1995): indeed, directly south of the Polar Front flows the Antarctic Circumpolar Current (ACC). This strong current effectively maintains pelagic populations south from the Polar Front. It flows clockwise around the globe and is associated to the strong Westerlies winds that flow around 55°S. The Antarctic Zone of the Southern Ocean is the zone delimited to the south by Antarctica and to the north by the Polar Front.

Coastal Countercurrent & the Ross Sea and Weddell Sea gyres.– Some minor (in comparison with the ACC) currents are noticeable in the Antarctic Zone of the Southern Ocean: the Coastal Countercurrent in particular is a weaker current, flowing anticlockwise around Antarctica from the Bellingshausen Sea to the Weddell Sea. This current is driven by the Easterlies winds which flow at ca. 70°S and tightly follows the continent. As a result of the joint action of this countercurrent and the ACC, two (main) cyclonic gyres are formed, one in the Weddell Sea, the other offshore the Ross Sea. The contact between westward and eastward currents is sometimes referred to as the Antarctic Divergence (Tchernia 1980).

The Antarctic Bottom Water.– Because of the formation of the sea ice and the discharge from the continental ice shelf of cold continental water, the surface water in both the Weddell and the Ross Sea is both colder and has an higher concentration of salt than the deeper water brought to those seas by the ACC (e. g. Gill 1973; Orsi et al. 1999). Therefore this surface water, being denser, sinks along the continental margin to a depth of ca. 4000m where it is injected in the global, thermohaline 'Ocean Conveyor Belt' (Broecker 1987).

2. Cenozoic Evolution of the Southern Ocean

Evolution of the Antarctic Circumpolar Current.– At the beginning of the Cenozoic, Antarctica was still bound to South America and Australia. During the Eocene those three continents drifted apart, however continental crust barriers in the paths between Antarctica and Australia (i. e. the Tasmanian Gateway) and between Antarctica and South America (i. e. the Drake Passage) were

partially too shallow to allow currents to flow through them (see Fig. 7). It is estimated that the Tasmanian Gateway opened to shallow waters in the latest Eocene (ca. 35.5 Ma; Stickley et al. 2004) and to deeper waters in the earliest Oligocene (ca. 30.2 Ma; Stickley et al. 2004). The Drake Passage Opening timing is still debated, with ages ranging from 41 Ma (Scher & Martin 2006) to 28 Ma (Lawver & Gahagan 2003). Whatever age is correct, it is safe to think that, at the end of Oligocene, both passages had opened and the Antarctic Circumpolar Current (ACC) was therefore fully formed.

Some authors have shown reconstructions with a West Antarctica Seaway (or Transantarctic Seaway) during the Paleogene (e. g. Cande et al. 2000; Cooke et al. 2002). Indeed without its continental ice-sheet and with an high sea-level, West Antarctica would be nothing more than an archipelago; thus allowing currents to flow from the Ross Sea to the Weddell Sea and creating a proto-ACC. The closing of this putative seaway may have occurred either in the Late Oligocene (Cooke et al. 2002) or in the Early Miocene (Nelson & Cooke 2001; Lawver & Gahagan 2003), depending on authors.

Evolution of the East & West Antarctic Ice Sheet.– The eastern, continental part of Antarctica (east of the Transantarctic Mountains) is considered to be the home of the earliest Cenozoic ice cover. Indeed, the first stable East Antarctic Ice Sheet is thought to have settled in the latest Eocene-earliest Oligocene (Ehrmann & Mackensen 1992; De Conto & Pollard 2003). The age of the formation of the West Antarctic Ice Sheet however is still under scrutiny: there are evidences for a formation as soon as the late Oligocene (e. g. Anderson & Schipp 2001; Sorlien et al. 2007) but it may have been an unstable, episodic ice sheet. The consensus tends to be that the formation of a permanent West Antarctic Ice Sheet happened somewhen during the late Miocene (e. g. Kennett & van der Broch 1986). There are nonetheless signs that it retreated several times during the Pliocene and Pleistocene (e. g. Scherer et al. 1998; Naish et al. 2009).

Evolution of the Polar Front.– Although an oceanographic front has been noticed in the late Eocene at ca. 50°S (Barron & Paterson 1991; Lazarus & Caulet 1994), it is only during the Oligocene that a true Polar Front is present and well defined in the Southern Ocean (Nelson & Cooke 2001), following the establishment of the ACC and East Antarctic Ice Sheet. This front expanded progressively from the Oligocene onwards (e. g. Cervato & Burckle 2003).

Evolution of the Bottom Water.– As noted above, the formation of the Antarctic Bottom Water, and therefore to some extent the current global thermohaline circulation, is directly linked to the presence of ice sheets on the Antarctic continent, of the sea ice extent and of the Antarctic Circumpolar Current. None of the three elements where present during the Eocene. Hence, the Eocene ocean lacked true Antarctic Bottom Water which, together with North Atlantic Deep Water (also absent in the Eocene; e. g. Wei & Peleo-Alampay 1997; Billups 2002), makes the modern cold deep ocean and the 'Conveyor Belt' function as it does today. However it has been inferred that, during the Paleocene and the Eocene, cool water from polar regions, together with warm saline bottom water formed in middle to low latitude (e. g. Kennett & Stott 1990) combined to form a global thermohaline circulation, albeit with deep waters (at ca. 10°C) much warmer than those of today (Barron & Peterson 1991).

Figure 7.– Paleogeographic reconstructions of the Southern Ocean during the Cenozoic.
Bold line represents the reconstructed Polar Front and arrows the main surface currents. Light grey area represents reconstructed shallow (possibly emerged) shelfs..
Redrawn and simplified after Lazarus & Caulet 1994, Cooke et al. 2002 and Lawver & Gahagan 2003. The base maps where produced using GPlates (Boyden et al. 2011) and R (R Development Core Team 2011) along with packages maptools (Lewin-Koh & Bivand 2012) and rgdal (Keith et al. 2012).

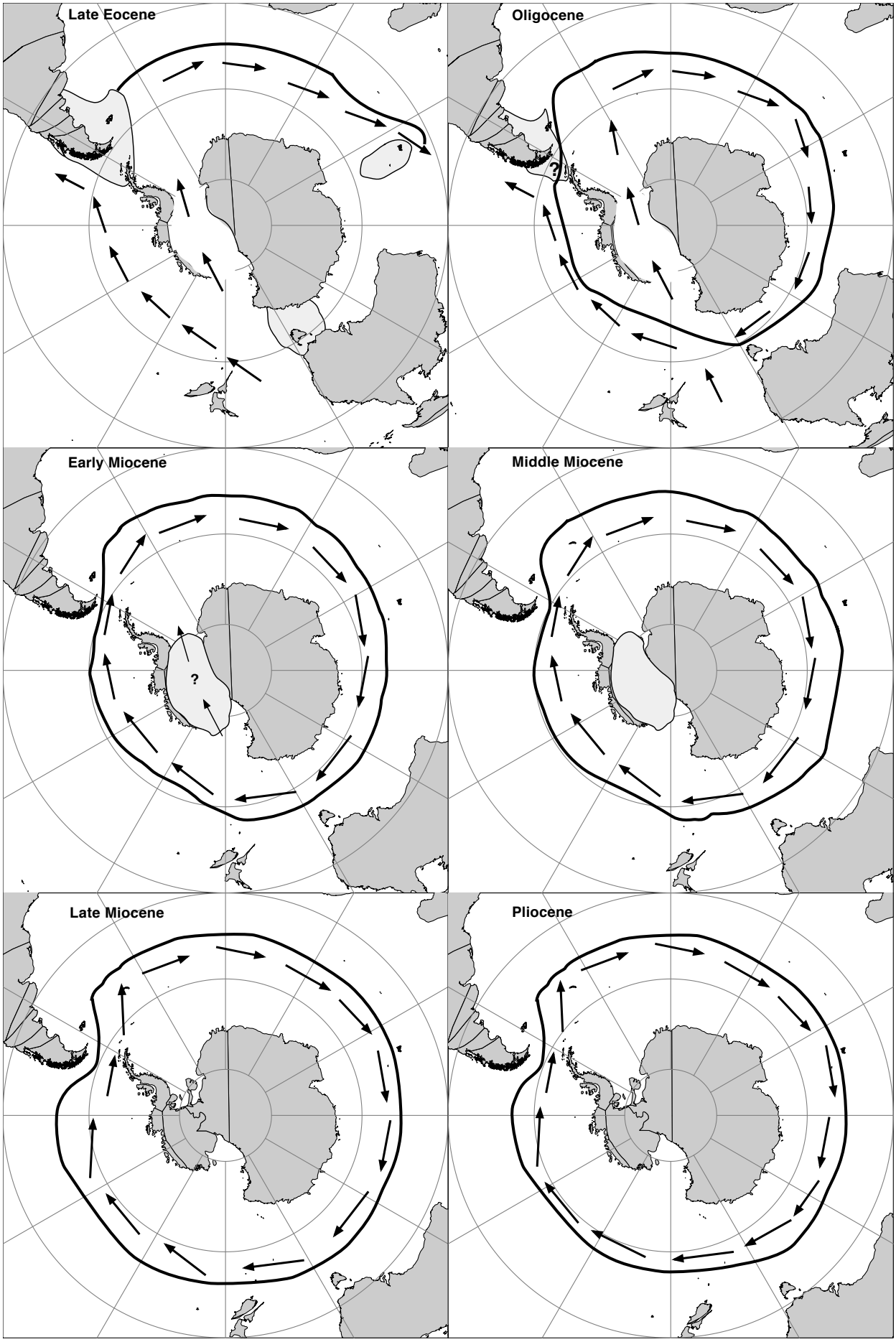
Late Eocene
Oligocene
?
Early Miocene
?
Middle Miocene
Late Miocene
Pliocene

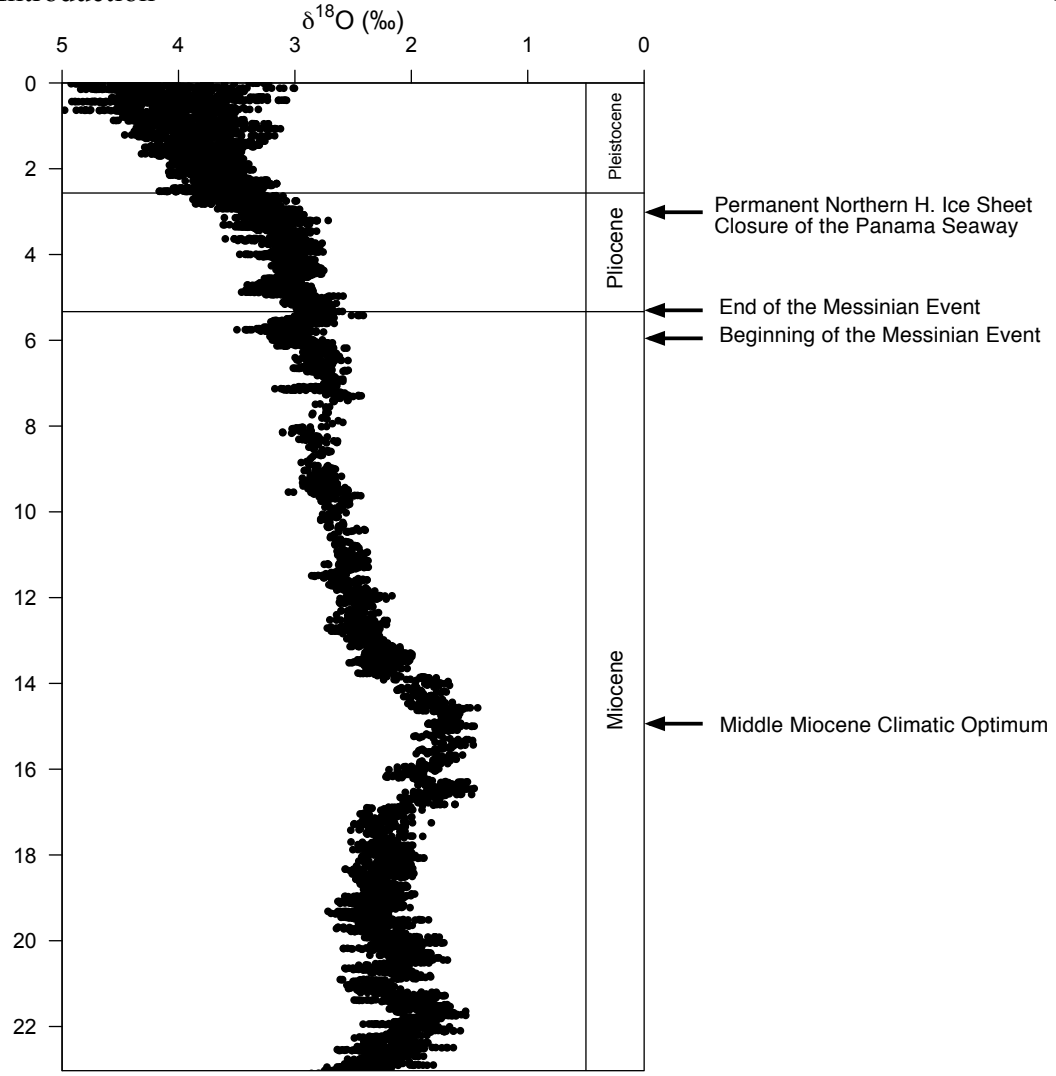

Figure 8.– Summary of global Neogene events. $\partial^{18}O$ curve from Zachos et al. 2001.

The formation of Antarctic Bottom Water is thought to have started (at least in the Atlantic sector) during the Oligocene (Diester-Haass et al. 1996; Lawver & Galahan 2003), along with the opening of both the Tasman Gateway and the Drake Passage and the subsequent formation of the ACC. Althought there is evidence that its exact location, its strength (i. e. the volume of water concerned) and its direction shifted several times from the Oligocene to the Pliocene (Schlüter & Ünzelmann-Neben 2008), it is thought to have existed continuously since that time.

3. Global Neogene paleoclimatology and paleoceanography

Middle Miocene climatic transition..– The global climatic evolution of the Neogene, as inferred from benthic foraminifera $\partial^{18}O$ (Fig. 8; Zachos et al. 2001), shows a period of high temperature (the last climatic optima of the Cenozoic), the so-called Middle Miocene Climatic Optimum, from ca. 17 Ma to ca. 15 Ma (e. g. Wright et al. 1992; Zachos et al. 2001). At ca. 15 Ma and until ca 12 Ma, an abrupt shift in $\partial^{18}O$ implies a rapid cooling and possibly also an increase in ice sheet volume: among other possible causes, this cooling is likely to be linked to the increasing importance of the Southern Ocean component of the Bottom Water over the northern, warmer component (Wright et al. 1992; Flower & Kennett 1994).

Messinian isolation of the Mediterranean Sea.– During the latest Miocene, the Mediterranean

Sea became isolated from the Atlantic Ocean (Hsü et al. 1973) from 5.6 Ma to 5.3 Ma (Krijgsman et al. 1999). This event, known as the Messinian Salinity Crisis, impacted indirectly global oceanography: indeed the lack of relatively dense, saline overflow water from the Mediterranean Sea into the Atlantic Ocean hindered to some extent the formation of Bottom Water in the Arctic (Blanc & Duplessy 1982; Müller et al. 1991), since this Mediterranean Overflow Water is, today, one of the main source of salinity for the North Atlantic Deep Water formation (Reid 1979).

Closure of the Panama and the Indonesian Seaway.– South and North America drifted toward one another during most of the Cenozoic until eventually the Central America Seaway closed up. This closure seems to have occured between ca. 13 Ma and 2.6 Ma (timing of its definitive closure; Lunt et al. 2008) with a closure of the deep circulation in the Seaway at about 4.6 Ma (Haug & Tiedemann 1998). This event have been widely considered as the possible trigger for the establishment of the Northern Hemisphere Ice Sheet and, hence, of the modern Atlantic thermohaline circulation (e. g. Schmidt 2007). More or less simultaneously, between the Indian and the Pacific Ocean, the Indonesian Gateway is also narrowed (ca. 3-4 Ma; Cane & Molnar 2001). As for the Panama Seaway, this event probably helped triggering the formation of the modern Pacific circulation.

Northern Hemisphere Ice Sheet.– Although simulations from models by De Conto et al. 2008 showed that the Northern Hemisphere Glaciation could have started as early as 23 Ma, all evidence show that it probably occurred around 3.6 Ma (e. g. Mudelsee & Raymo 2005; Meyers & Hinnov 2007). The causes of this glaciation remains uncertain, however the Panama Seaway closure and the subsequent intensification of the Gulf Stream (Flower 1999) may have helped. As a consequence to the Northern Hemisphere Glaciation, global temperature dropped at the onset of the Pleistocene.

4. Antarctic Neogene sedimentological record

Antarctic Neogene sediments.– At the beginning of the Paleogene, calcareous oozes are the dominant lithology found in deep-sea Southern Ocean sediments; however during the Eocene and the Oligocene, biosiliceous sedimentation appears locally in various regions south of 50°S (Lazarus & Caulet 1993). At the end of the Oligocene siliceous oozes have already a circumpolar distribution and during the Miocene become the dominant lithology south of the Polar Front. From the late Miocene onwards, the depth and latitude distribution of pelagic sediments is as follows: below 4000 meters depth, lies abiogenic pelagic clay; north of 40°S and above 4000 meters sediments are mainly composed of calcareous oozes; south of 50°S and between 2000 and 4000 meters depth sediments are almost entirely composed of biosiliceous oozes while above 2000 meters calcareous oozes are also sometimes present; finally, between 40°S and 50°S is a mixed zones in which both calcareous and siliceous oozes and clays are present (Lazarus & Caulet 1993).

Sites sampled in this study.– The samples studied in this study (see Chapter 2, Fig. 1 for the location of all the sites observed) come from various sites recovered by the ODP (Ocean Drilling Program) drilling campaign during legs 113 (Atlantic sector of the Southern Ocean), 119, 120 and 183 (all three from the Kerguelen-Heard Plateau region in the Indian Sector).

Site 689 (Leg 113) was drilled on Maud Rise in the Atlantic sector of the Southern Ocean (at 64°31 S and 3°06 E with a water depth of 2091 mbsl, i. e. meters below sea level).

Recovered sediments are composed from the Late Eocene to the Late Miocene of a mixture of siliceous and calcareous oozes followed, from the Late Miocene to the Quaternary, exclusively by siliceous oozes (Shipboard Scientific Party 1988a). The sedimentation is rather condensed with short hiatuses, including in the lowermost Miocene and the upper Pliocene. Radiolarians, diatoms and silicoflagellates are abundant and well preserved throughout the late Miocene to Quaternary sequence. In the Middle and Early Miocene, radiolarians and diatoms are still common but rarer while calcareous nannofossils are more and more abundant as depth increases. This site was sampled for taxonomy (Chapter 2), macroevolution study (Chapter 3) and biostratigraphy (Chapter 4).

Site 690 (Leg 113) was also drilled on Maud Rise, on the southwestern flank (at 65°10 S and 1°12 E with a water depth of 2925 mbsl). This site is very much comparable to site 689 in its sedimentation: from Miocene to upper Pliocene/Pleistocene, the pelagic sediments recovered are biosiliceous oozes while Early Miocene to Oligocene sediments are a mixture of siliceous and calcareous oozes with a decreasing abundance of radiolarians and diatoms coupled with an increase in calcareous nannofossil abundance in this lower part. The sequence is condensed (with a low sedimentation rate). The only noticeable differences in lithology with site 689 would be a somewhat higher terrigenous component (Scientific Shipboard Party 1988b).This site was sampled for taxonomy, macroevolution study and biostratigraphy in this study.

Site 693 (Leg 113) was drilled on the Weddell Sea continental slope of East Antarctica (at 70°50 S and 14°34 W with a water depth of 2359 mbsl). From the Oligocene to the upper Pliocene, mostly siliceous clays were recovered with the exception of some siliceous oozes in the Late Miocene (Shipboard Scientific Party 1988c). The Neogene sedimentation rate is fairly high, with some hiatuses in the Middle Miocene. This site is characterized by the presence of numerous terrigenous components (ice-rafted debris) after the Middle Miocene hiatuses. Diatoms are generally numerous and well-preserved in this site while radiolarians and silicoflagellates are rarer but as well preserved. Foraminifera are found commonly in the upper Pleistocene but not in the Neogene (Grobe et al. 1990; Shipboard Scientific Party 1988c). For this study, this site was sampled for taxonomy, macroevolution study and biostratigraphy.

Site 737 (Leg 119) was drilled on the northern part of the Kerguelen-Heard Plateau (at 50°14 S and 73°02 E with a water depth of 564 mbsl). Sediments from Late Miocene to the Quaternary are a siliceous ooze (with the uppermost part enriched in volcanic and glauconitic sand) while the Middle to Late Miocene sediments are a mixed siliceous and calcareous ooze (Shipboard Scientific Party 1989a). Radiolarians are fairly common and well preserved in the Late Miocene to Early Pliocene sequence, rarer afterwards and barren prior to that. In this study, this site was sampled for taxonomical exploration exclusively.

Site 738 (Leg 119) was drilled on the southernmost part of the Kerguelen Plateau (at 62°43 S and 82°47 E with a water depth of 2253 mbsl). The latest Miocene to Quaternary sequence consist of a siliceous ooze but below the latest Miocene is calcareous. The siliceous sequence is dominated by diatoms but radiolarians are fairly common and well-preserved (Shipboard Scientific Party 1989b). As for the previous site, site 738 was here sampled exclusively for taxonomy.

Site 744 (Leg 119) was drilled on the Southern Kerguelen Plateau (at 61° 35 S and 80° 35 E with a water depth of 2307 mbsl). The lithology is as follows: the latest Miocene to Quaternary sequence is a siliceous ooze with very abundant diatoms and relatively abundant radiolarians as well, while the Late Eocene to Late Miocene sequence is a calcareous nannofossil-dominated ooze with occasional siliceous components. Both sequences are separated by a hiatus and several other hiatuses occur in the Early and Middle Miocene (Shipboard Scientific Party 1989c). This site was studied here for taxonomy and macroevolution

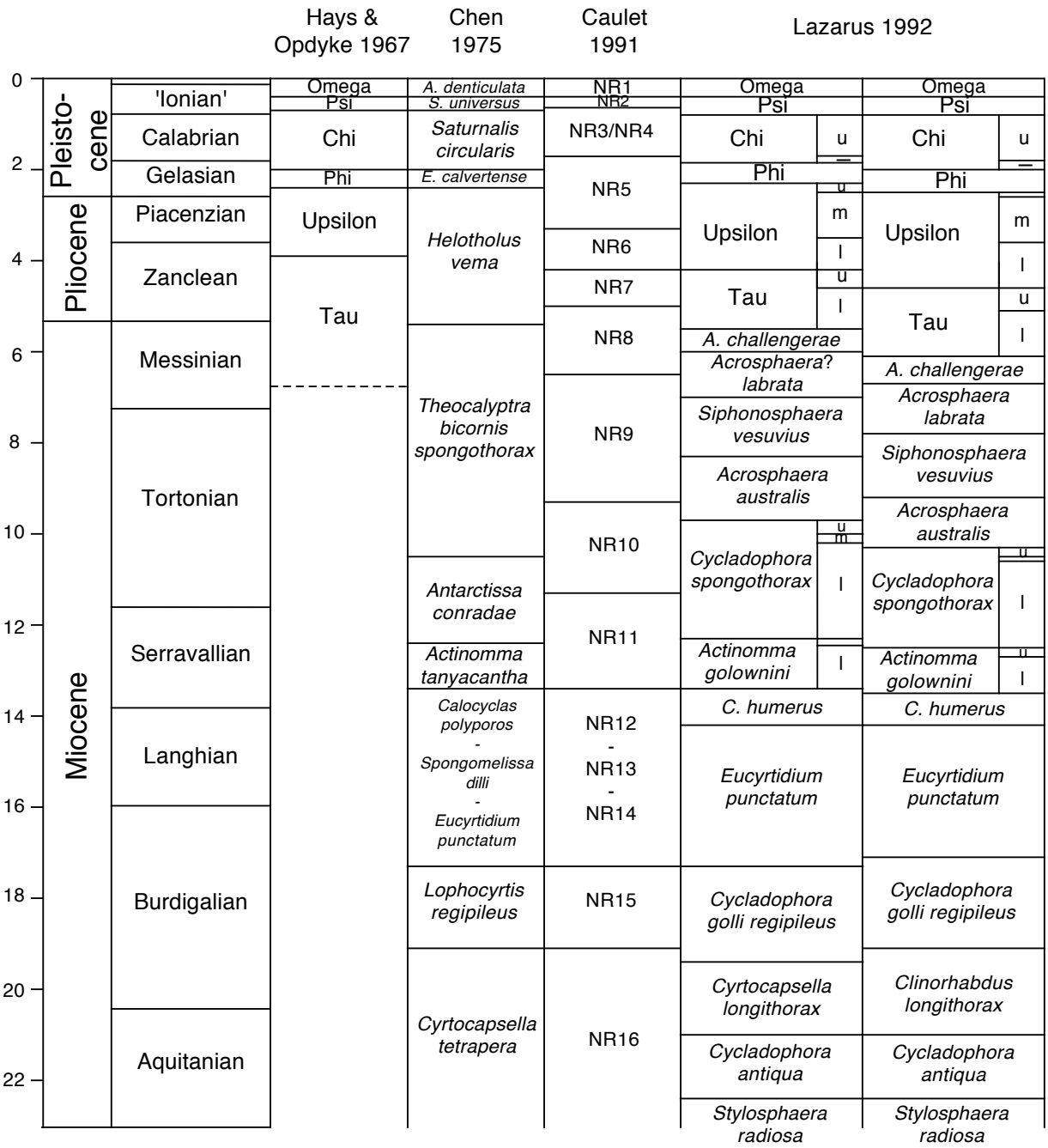

Figure 9.– History of Antarctic Neogene radiolarian zonation.
First two columns are Series and Stage of the Neogene and Quaternary (Gradstein et al. 2004 for current numerical ages), then follows zonation of Hays & Opdyke 1967, Chen 1975, Caulet 1991 and Lazarus 1992. For Lazarus 1992 zonation, first column has numerical age as given in original publication using the Berggren et al. 1985 scale and second column as modified by Spencer-Cervato 1999 to the Berggren et al. 1995 scale used in this study).
u: upper; m: middle; l: lower; *A. challengerae*: *Amphymenium challengerae*; *A. denticulata*: *Antarctissa denticulata*; *S. universus*: *Stylatractus universus*; *E. calvertense*: *Eucyrtidium calvertense*; *C. humerus*: *Cycladophora humerus*.

study.

Site 745 (Leg 119) was drilled in deep water at the base of the southeastern slope of the Kerguelen Plateau (at 59°36 S and 85°52 E with a water depth of 4083 mbsl). The sediments recovered on this site are for the most part a high sedimentation rate, diatom-rich siliceous clay with frequent and well-preserved radiolarians, running from the latest Miocene to the Pleistocene (Shipboard Scientific Party 1989d). This site was studied here for taxonomy only.

Site 746 (Leg 119) was drilled 5 km away from site 745 (at 59°33 S and 85°52 E with a water depth of 4060 mbsl). This site was drilled to continue the work on site 745, disrupted by the arrival of an iceberg (Shipboard Scientific Party 1989e). The sequence retrieved on this site is a succession of diatomaceous oozes and diatomaceous clay from the Late Miocene to the Early Pliocene, with common to frequent well-preserved radiolarians. The early Late Miocene is composed of a calcareous ooze with occasional diatoms and radiolarians (Shipboard Scientific Party 1989e). As for Site 745, this site was only sampled for taxonomical purposes.

Site 747 (Leg 120) was drilled on a terrace in the central Kerguelen Plateau at 54°48 S and 76°48 E, at a water depth of 1695 mbsl. Recovered sediments are composed from the latest Miocene to the Quaternary of a diatom-rich siliceous ooze with common foraminiferans and relatively frequent and well-preserved radiolarians, preceded from the Late Oligocene to the Late Miocene by a calcareous nannofossil ooze with rare diatoms and radiolarians. The recovery of the Neogene sequence for this site, in contrast with most other sites, is almost perfect (Shipboard Scientific Party 1989f) but the paleomagnetic signal is rather poor for the upper part of the sequence (Heider et al. 1992). It was sampled in this study for taxonomy, macroevolution study and biostratigraphy.

Site 748 (Leg 119) was drilled on the Southern Kerguelen Plateau at 58°26 S and 78°59 E, at a water depth of 1291 mbsl. The uppermost part of the retrieved sediments are an Early Pliocene to Late Pleistocene diatom ooze enriched in some intervals by foraminiferans and in other by radiolarians. This lithological unit is preceded by a Middle Eocene to Late Miocene sequence composed by a nannofossil ooze with occasional intervals enriched in diatom, radiolarians and silicoflagellates (Shipboard Scientific Party 1989g). The site was sampled for its rich, well-preserved Early Miocene sequence, for taxonomy and macroevolution study.

Site 751 (Leg 119) was drilled on the Southern Kerguelen Plateau at 57°44 S and 79°49 E, at a water depth of 1634 mbsl. Recovered sediments are an Early Pliocene to Late Pleistocene sequence of diatom-dominated siliceous ooze and an Early to Late Miocene sequence of mixed calcareous and siliceous oozes. Radiolarians are relatively abundant and well-preserved from the late Middle Miocene to the Pleistocene. As for Site 747 the recovery was almost perfect (98%, Shipboard Scientific Party 1989h) but the paleomagnetic signal is relatively poor above the middle Miocene (Heider et al. 1992). This site was here sampled for taxonomy, macroevolution study as well as biostratigraphy.

Site 1138 (Leg 183) was drilled 150 km north of site 747 on the Central Kerguelen Plateau, at 53°33 S and 75°58 E, at a depth of 1141 mbsl. The lithology consists of a Late Miocene to Late Pleistocene sequence of siliceous clays alternating with siliceous oozes and occasional ash layers and terrigenous clays, and an Early to Late Miocene sequence of calcareous clays alternating with calcareous oozes (Shipboard Scientific Party 2000). Radiolarians are well-preserved and relatively abundant between the late Middle Miocene and the Early Pliocene. This site was sampled for taxonomy, macroevolution study and biostratigraphy.

Geochronological framework.– As mentioned above, starting in the middle to late Miocene, calcareous oozes are almost totally absent below 50°S, hence the quasi-impossibility to apply

calcareous microfossil (foraminiferans and coccolithophores, mainly) zonations to the Neogene Southern Ocean. On the other hand, diatoms and radiolarians are very abundant and very diversified: however, because the Southern Ocean is biogeographically distinct from the rest of the World Ocean (e. g. Longhurst 1998), correlation with lower latitude zonations are difficult. The paleomagnetic record finally is sometimes rather good but rarely continuous on one single sites: numerous widespread hiatuses, occasional terrigenous input, changing rates of sedimentation are among the main issues that makes single-site continuous paleomagnetic records rare and therefore hinders our capacity to attribute a numerical age to bioevents data.

Antarctic Neogene radiolarian zonation.– A first zonation for the Antarctic Neogene fauna was established by Hays (1965) and Hays & Opdyke (1967), based on sediments recovered by the Robert Conrad and the Vema expeditions of the Lamont-Doherty Oceanographical observatory: the technical possibilities of these scientific vessels was such that only the uppermost part of the sediments could be cored hence this first biostratigraphy encompassed only the upper 5 Ma (i. e. from lowest Pliocene to the recent). It was composed of 6 zones (zones Omega to Tau; Figure 9) based on 18 species (Hays 1965; Hays & Opdyke 1967). As the DSDP (and later ODP) campaigns and the JOIDES Resolution research vessel allowed better recovery of the sediments drilled and older sediments to be extracted, the biostratigraphy improved. Petrushevskaya (1975) and, the same year, Chen (1975) came up respectively with 11 and 13 zones (both results overlapping substantially) ranging from late Oligocene to recent. With additional sites recovered, Abelmann (1990, 1992) and Lazarus (1990, 1992) developed, using Hays & Opdyke (1967) and Chen (1975) biostratigraphy as a starting point, a somewhat higher resolution stratigraphy with 25 zones (and subzones). In the same time, Caulet (1991) tried to create a biostratigraphy linking subtropical (Caulet 1982) and antarctic faunas for correlation purposes. All these zonations are summarized on Figure 9.

Species-level synthesis of Antarctic Neogene radiolarians

Introduction

Radiolarians from deep-sea sediments around Antarctica have been studied for over 50 years (Riedel 1958). They have been extensively used in studies of past Southern Ocean conditions, both to provide a biostratigraphical framework for dating sediments and to reconstruct environmental conditions in past geological intervals (e. g. Lazarus, 1990, 1992). Unfortunately, despite this body of prior work, even the most basic knowledge of these fossils – their descriptive species taxonomy – is still highly incomplete. Individual studies have documented many species as part of more general work on biostratigraphy (Chen 1975; Petrushevskaya 1975; Caulet 1986, 1991; Abelmann 1990, 1992b; Lazarus 1990, 1992) and the more common species encountered in the water column have been summarized by Abelmann (1992a). There have also been a small number of more purely taxonomic works for individual groups of taxa, such as the antarctissids (Petrushevskaya 1986), cycladophorids (Lombari & Lazarus 1988) and 'prunoid' spumellarians (Lazarus et al. 2005). None the less, the majority of forms encountered on typical radiolarian slides from the Antarctic Neogene have remained undescribed until now and, thus, unusable for biostratigraphical, palaeoenvironmental or palaeobiological research.

In an attempt to reduce this limit to research, this study aims at documenting exhaustively the species that constitute the Antarctic Neogene radiolarian fauna.

Material

All observed samples (ca. 300) come from Ocean Drilling Program (ODP) sediments, mostly from the Kerguelen-Heard Plateau (Leg 119 Sites 737, 738, 744, 745 and 746; Leg 120, Sites 747, 748 and 751 and Leg 183, Site 1138) with the addition of samples from the Atlantic sector (Leg 113 Sites 689, 690 and 693) (Figure 1). Prepared slides were drawn from David

Figure 1.– Location of sites studied for taxonomy.
Map created with R (R development core team 2011) along with package GEOmap (Lees, 2010).

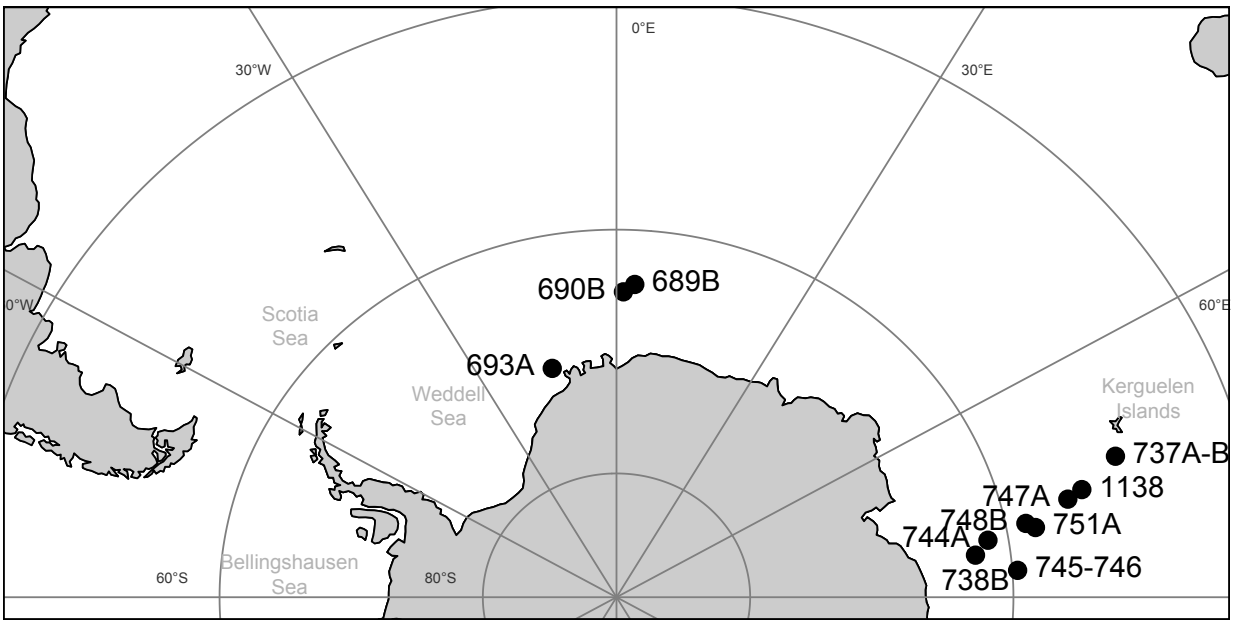

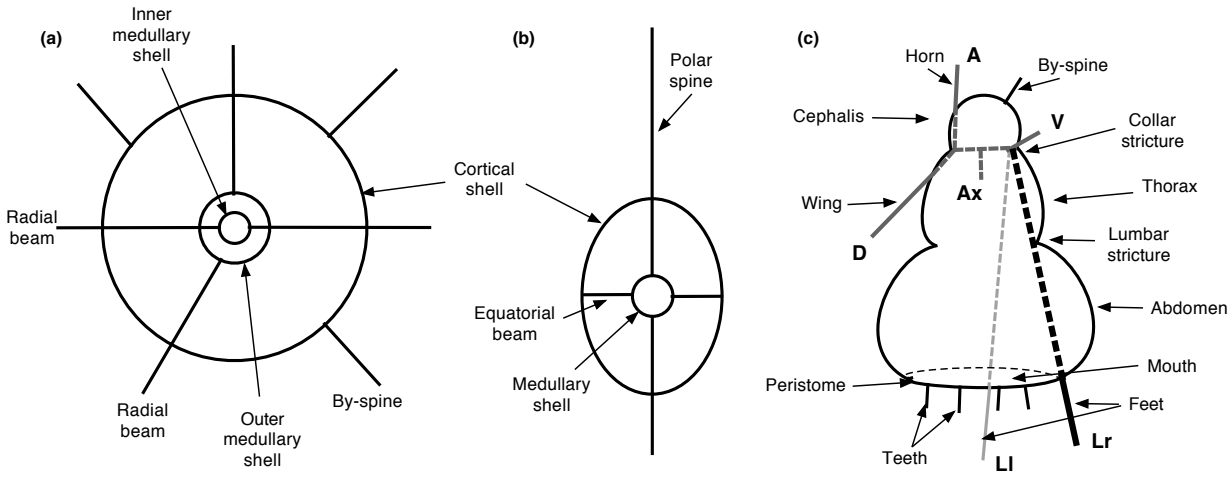

Figure 2.– Terminology for Polycystine radiolarian external features.
a. Spherical spumellarians; b. Heteropolar spumellarians; c. Multisegmented nassellarians.
A, **V**, **D**, **Ax**, **Lr** and **Ll**: see Fig. 3.

Lazarus' personal collection or the MRC radiolarian collection hosted by the Museum für Naturkunde in Berlin (Lazarus 2006). Samples were prepared on random strewn slides using standard methods (Moore 1973) using 45 µm (occasionally 38 µm and 63 µm) sieves.

The measurements given for the new forms were made on specimen pictures using ImageJ (Abramoff et al. 2004): the range of variation and the mean (between brackets) are both given in microns (µm) in the Dimensions paragraph for each species.

All holotypes are deposited in the micropaleontology collection of the Museum für Naturkunde, Berlin. ECO-xxx are the MfN accession numbers. Specimens are identified by a circle on the slide.

Terminology

Spumellarian external features.– In spherical spumellarians (Fig. 2a), the different concentric shells are called **cortical** or **medullary** depending if they are situated at the periphery of the skeleton or toward the center (in living spumellarians, medullary shells contain only the intracapsulum). The innermost shell, also seen in non-spherical spumellarians, is referred to as the **microsphere**. Some authors recognize spicular elements in those microspheres, but the terminology for those elements is not stable yet and therefore won't be used here to avoid confusing with that of the nassellarians. The same remarks apply to the entactinarians.

In spherical spumellarians, spines joining the different concentric shells together are called **radial beams** while spines projecting from the outermost shell are **by-spines** or **thorns** if they are short, needle-like projections arising from the bar nodes.

In non-spherical spumellarians, if the shell bears one aperture, it is referred to as the **pylome**.

In asymmetrical spumellarians, any element present at the extremity of the long axis is referred to as being **polar** while elements in the direction of the short axis are **equatorial** (Fig. 2b).

Nassellarian inner structure.– Nassellarians are characterized by the presence of a spicular

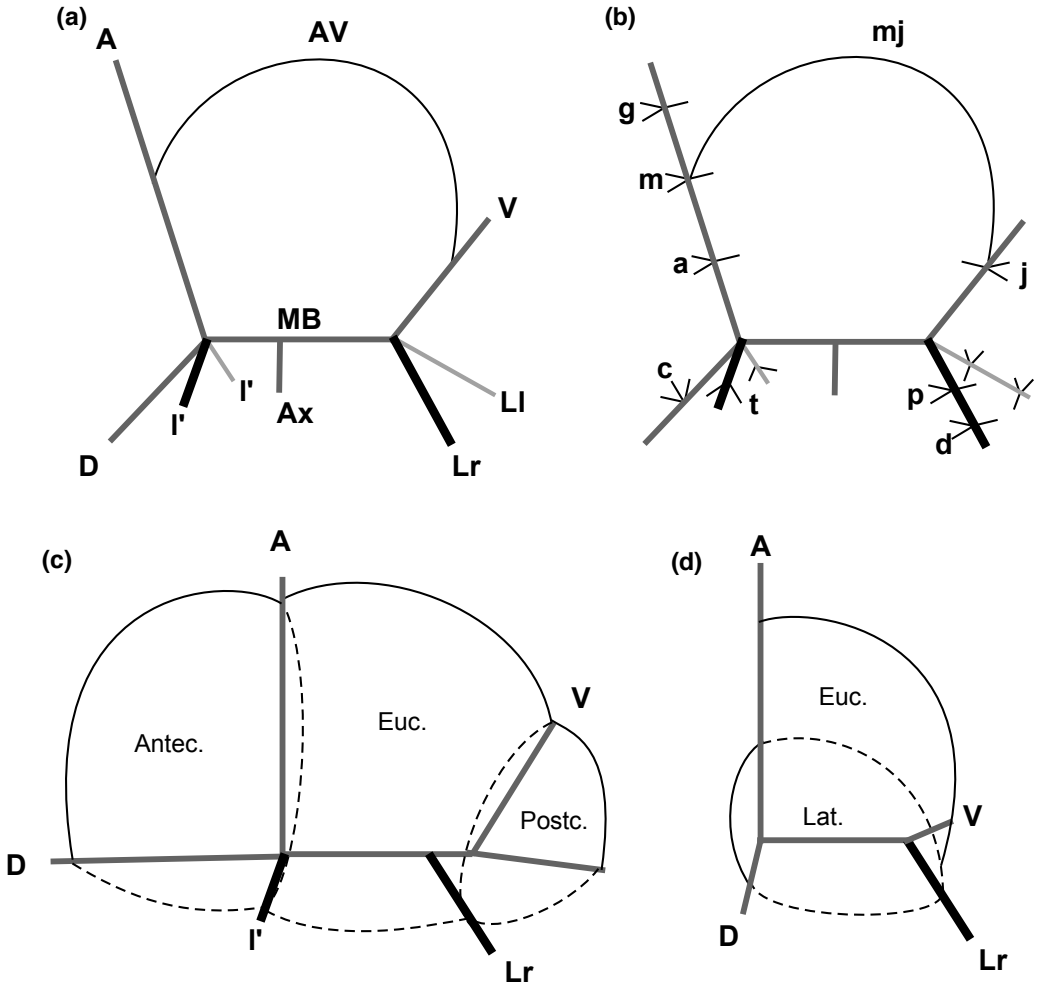

Figure 3.– Schematic illustrations of nassellarian cephalic inner structure.
a. Initial spicule (modified after Jörgensen, 1905). b. Apophyses (modified after Petrushevskaya, 1971). c and d. Cephalic chambers.
A, apical spine; **V**, ventral or vertical spine; **D**, dorsal spine; **Lr** and **Ll,** lateral spines; **l',** secondary lateral spine; **MB**, median bar; **Ax**, axobate; **AV**, arch connecting spine **A** and spine **V**.
Dark grey, spines in the sagittal plane; black, spines on our side of the sagittal plane; light grey, spines on the other side of the sagittal plane.
g, galear; *m*, mitral; *a*, anterior; *t*, tergal; *c*, cervical; *p*, pectoral; *j*, jugal; *d*, second serie of apophyses on spines **Ll** and **Lr;** *mj*, arch connecting apophyses *m* and *j*.
Antec.: Antecephalic lobe; Euc.: Eucephalic lobe; Postc.: Postcephalic lobe; Lat.: Lateral lobe.

element called the **inner structure** or the **initial spicule** since it is thought to be the first skeletal element to grow during the organism ontogenesis. The elements of this inner structure being considered homologies are all named (Fig. 3a; Jørgensen 1905; Petrushevskaya 1965, 1968): from the **median bar** (**MB**) arise on one side the **apical** (**A**) and the **dorsal** (**D**) spines and on the other side, on the same plane as **A**, **D** and **MB** (i.e. the **sagittal plane**), the **ventral** or **vertical** (**V**) spine and, projecting laterally from this plane, the **lateral** (**Ll** and **Lr**) spines. In some groups, two **secondary lateral (l')** spines project laterally from the junction of **A, D** and **MB**. A final element is the **axobate** or **axial rod** (**Ax**) which projects from the median bar, somewhere between spine **A** and spines **Ll** and **Lr**.

Apophyses project from these spicular elements. These apophyses can be connected by **arches**. Because apophyses have a non-negligible impact on the taxonomy of some groups, they are all named (Fig. 2b; Petrushevskaya 1965, 1968): the apophyses arising from spine **A** are, from the proximal-most to the distal-most, the **anterior** (*a*), the **mitral** (*m*) and the **galear** (*g*) apophyses; from spine **D**, the **cervical** (*c*) apophyses; from spine V, the **jugal** (*j*) apophyses;

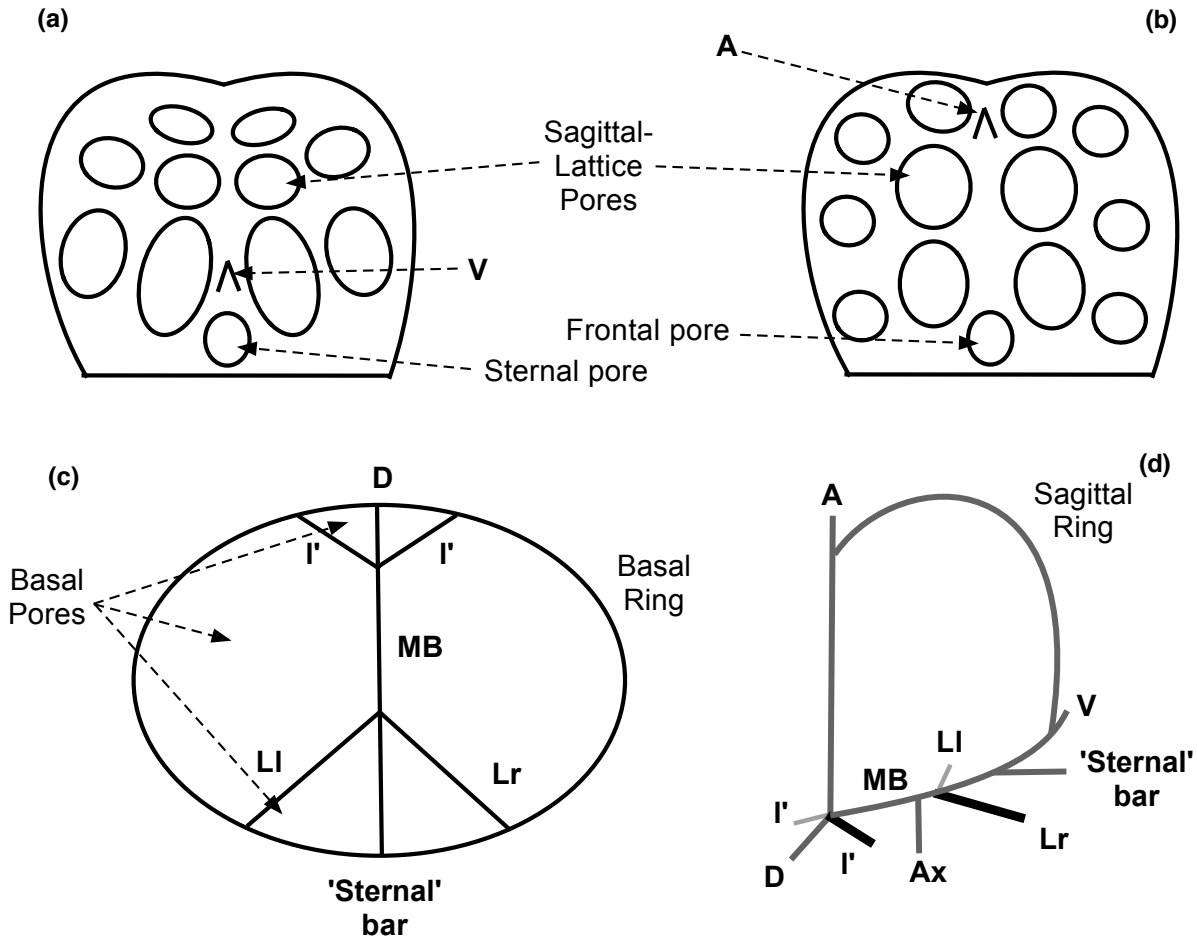

Figure 4.– Terminology for Trissocyclidae (redrawn and modified after Goll, 1968).
a. Back view (=ventral view). b. Front view (=dorsal view). c. Basal view. d. Schematic illustration of the sagittal ring.
A, **V**, **D**, **MB**, **Ax**, **Ll**, **Lr** and **l'**: see Fig. 2.

from spines Ll and Lr, the **pectoral** (*p*) and an unnamed second series (*d*) of apophyses and from spines l', the **tergal** (*t*) apophyses. Arches connecting those apophyses are either named after the two spines from which they arise (De Wever et al 1979; Dumitrica 1991; Funakawa 1995) or after the two apophyses they join (Petrushevskaya 1965, 1968): for example an arch connecting spines A and V by the mean of apophyses *m* and *j* would be either called arch **AV** or arch *mj*.

Some groups possess additional elements: in some species such as *Helotholus*? *vema* Hays 1965 or *Antarctissa ballista* Renaudie & Lazarus 2012, a ring structure (aka **proximal ring** [**PR**]; see Figs. 6 and 7; Sugiyama 1993) is present above the median bar. From this structure can arise **tertiary lateral** (**l''**) spines (directed upward), a **secondary apical** spine (**A'**) and a **secondary** and a **tertiary ventral** spine (**V'** and **V''**).

In addition to the **sagittal** view (mentionned above) of this structure, there is also a **dorsal view,** an **apical view**, a **ventral view** and a **basal view**. The first three views correspond to the view from the tip of spines **D, A** and **V** respectively and the fourth one is the view opposite to the apical view, from the thorax (if there is one).

Because of the complex arrangement of those spicular element and the arches connecting them, the cephalic cavity can be separated into different **chambers** or **lobes** (Fig. 2c-d). The main lobe, contained between spines **A, V** and **MB**, is the **eucephalic** lobe. The lobe contained between spines **A** and **D** (and both **l'** if they are present) is the **antecephalic** lobe while the one

contained between spine **V** and spines **Ll** and **Lr** is the **postcephalic** lobe. In such groups as Pterocorythidae, there is a cephalic lobe contained between arch **AL**, spines **D** and **MB**: it is called the **lateral** lobe.

Nassellarian external features.– In multisegmented nassellarians (Fig. 2c), the first segment (the one that usually contains the internal structure) is referred to as the **cephalis**. The second segment is the **thorax** and the third the **abdomen**. Any additional segments are called **postabdominal segments**. The separations between segments can be expressed externally by a constriction or stricture: the one separating the cephalis and the thorax is called the **collar** stricture and the one separating the thorax and the abdomen is the **lumbar** stricture. In some small dicyrtids (i.e two-segmented forms), the inner "cephalic" structure can partially sink into the thorax and the apparent collar stricture might be the external expression of specific arches: these external bumps at the collar stricture can be referred as **shoulders**. The last segment can be either open (and if this opening is surrounded by a specific structure, this structure is called a **peristome** and the aperture the **mouth**) or closed by a **sieve plate**.

Spines projecting from the shell but unconnected to the inner structure of the nassellarian are simply called **by-spines** or **supplementary spines**: if they project from the peristome, they are **teeth**. Spines connected to the inner structure are referred as **horns** if they project from the cephalis, **wings** if they project latterally from the thorax or any subsequent segment and **feet** if they project from the last segment termination. Horns, wings and feet can bear lateral **panels** in some species. Spines can be **conical**, **rod-like** or **tribladed**. As for spumellarians, small spines projecting from a bar node are **thorns**. In Artostrobiidae, the vertical spine, instead of projecting as an horn, projects as an hollow pipe called the **ventral tube** or **ventral pore** depending on its length.

Terminology specific to the family Trissocyclidae.– (Fig. 4; Goll 1968) The Trissocyclidae are characterized by a cephalis separated in two lobes by a ring consisting of spines **V**, **MB, A** and arch **AV** called the **sagittal ring** (Fig. 3d). Paired pores that are situated from one side and the other of the sagittal ring as referred to as **sagittal-lattice** pores (Fig. 4a). Unpaired pores situated on the dorsal side or the ventral side of the shell are called, respectively, **frontal** and **sternal** pores (respectively Fig. 4b and 4a). The ring joining, in basal view, spines **D, MB, Ll, Lr,** eventually **l'** and sometimes a secondary vertical spine (referred to by Goll 1968 as the **sternal bar**) is called the **basal ring** (Fig. 4c). Pores delimited by the various spines conencting to the basal ring are logically called **basal pores**.

Systematic Paleontology

Phylum **Rhizaria** Cavalier-Smith 2002

Class **Cercozoa** Cavalier-Smith 1998 emend. Adl et al. 2005

Subclass **Phaeodarea** Haeckel 1879

Family **Challengeridae** Murray 1876 emend. Takahashi 1991

Genus *Challengeron* Haeckel 1887

Type-species: *Challengeron bethelli* Murray 1885

Challengeron diodon (Haeckel 1887)

(Pl. 1, Fig. 1)

1887 *Challengeron diodon* Haeckel: p. 1654; pl. 99, fig. 6

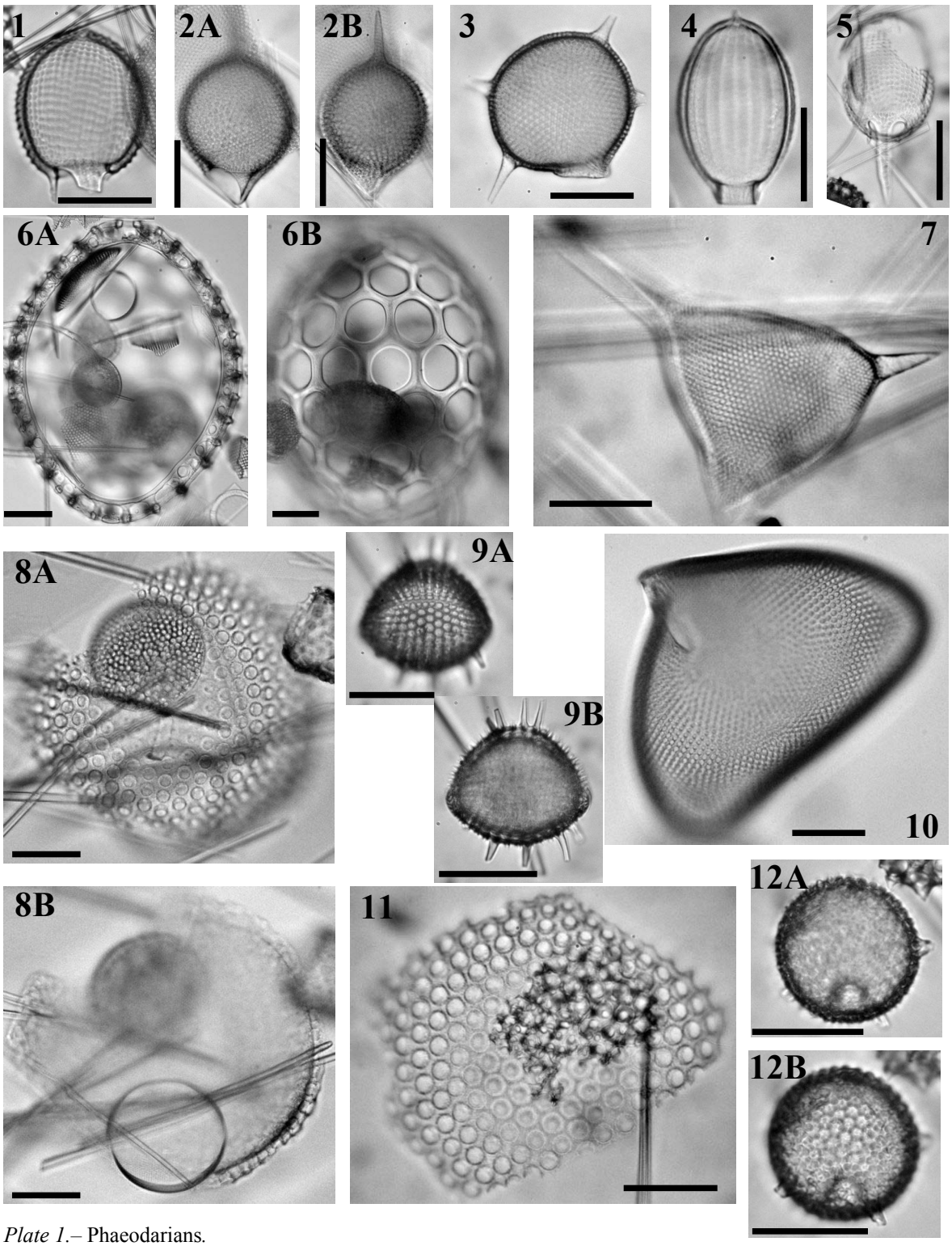

Plate 1.– Phaeodarians.
1. *Challengeron diodon* (Haeckel 1887), Sample 120-751A-3H-2 98-102cm, Late Pliocene.
2. *Challengeron lingi* Takahashi 1991, Sample 120-751A-1H-1 98-102cm, Pleistocene.
3. *Challengeron lingi*?, Sample 120-751A-4H-5 98-102cm, Early Pliocene.
4. *Lirella bullata* (Stadum & Ling 1969), Sample 120-751A-8H-6, 98-102cm, Late Miocene.
5. *Protocystis tritonis* (Haeckel 1887), Sample 120-751A-2H-3 98-102cm, Late Pliocene.
6. *Conchellium capsula* Borgert 1907, Sample 113-689B-3H-3 116-118cm, Late Miocene.
7. *Protocystis micropelecus*?, Sample 120-751A-11H-4 98-102cm, Middle Miocene.
8. *Conchellium* sp., Sample 120-751A-12H-3 98-102cm, Middle Miocene.
9. Phaeodarian gen. et sp. indet., Sample 119-745B-20H-6 53-55cm, Early Pliocene.
10. *Protocystis micropelecus* Haecker 1908, Sample 120-751A-3H-2 98-102cm, Late Pliocene.
11. *Conchellium* sp., Sample 120-751A-12H-6 98-102cm, Middle Miocene.
12. *Porospathis holostoma* (Cleve 1899), Sample 119-746A-7H-2 53-55cm, Late Miocene.
All scale bars 50 µm. Magnification x384 except for 6A-B, 8A-B and 10 (x192).

Challengeron lingi Takahashi 1991
(Pl. 1, Figs 2A-3)
1991 *Challengeron lingi* Takahashi: p. 138; pl. 48, figs 1-5

Genus *Protocystis* Wallich 1869 emend. Takahashi 1991
Type-species: *Protocystis aurita* Wallich 1869

Protocystis micropelecus Haecker 1908
(Pl. 1, Figs 7, 10)
1908 *Protocystis micropelecus* Haecker: p. 272; pl. 50, fig. 403

Protocystis tritonis (Haeckel 1887)
(Pl. 1, Fig. 5)
1887 *Challengeria tritonis* Haeckel: p. 1649; pl. 99, fig. 5
1901 *Challengeron tritonis* (Haeckel) – Borgert: p. 28; fig. 29
1991 *Challengeron tritonis* (Haeckel) – Takahashi: p. 143; pl. 52, figs 4-5

Family **Lirellidae** Loeblich & Tappan 1961

Genus *Lirella* Ehrenberg 1873a
Type-species: *Lirella baileyi* Ehrenberg 1873a

Lirella bullata (Stadum & Ling 1969)
(Pl. 1, Fig. 4)
1969 *Cadium bullatum* Stadum & Ling: p. 484; pl. 1, figs 9-14
1975 *Lirella bullata* (Stadum & Ling) – Ling: p. 732; pl. 13, fig. 29

Family **Porospathididae** Borgert 1901 emend. Campbell 1954

Genus *Porospathis* Haeckel 1879
Type-species: *Porospathis tabulata* Haeckel 1879

Porospathis holostoma (Cleve 1899)
(Pl. 1, Figs 12A-B)
1899 *Polypetta holostoma* Cleve: p. 32; pl. 3, figs 4a-b
1901 *Porospathis holostoma* (Cleve) – Borgert: p. 48; fig. 56
1991 *Porospathis holostoma* (Cleve) – Takahashi: p. 150; pl. 57, figs 1-8

Family **Conchariidae** Haeckel 1879

Genus *Conchellium* Haeckel 1887
Type-species: *Conchellium tridaena* Haeckel 1887

Conchellium capsula Borgert 1907
(Pl. 1, Figs 6A-B)
1907 *Conchellium capsula* Borgert: p. 208; pl. 17, figs 1-4
1991 *Conchellium capsula* Borgert – Takahashi: p. 157; pl. 61, figs 1-5, 7-8, 10

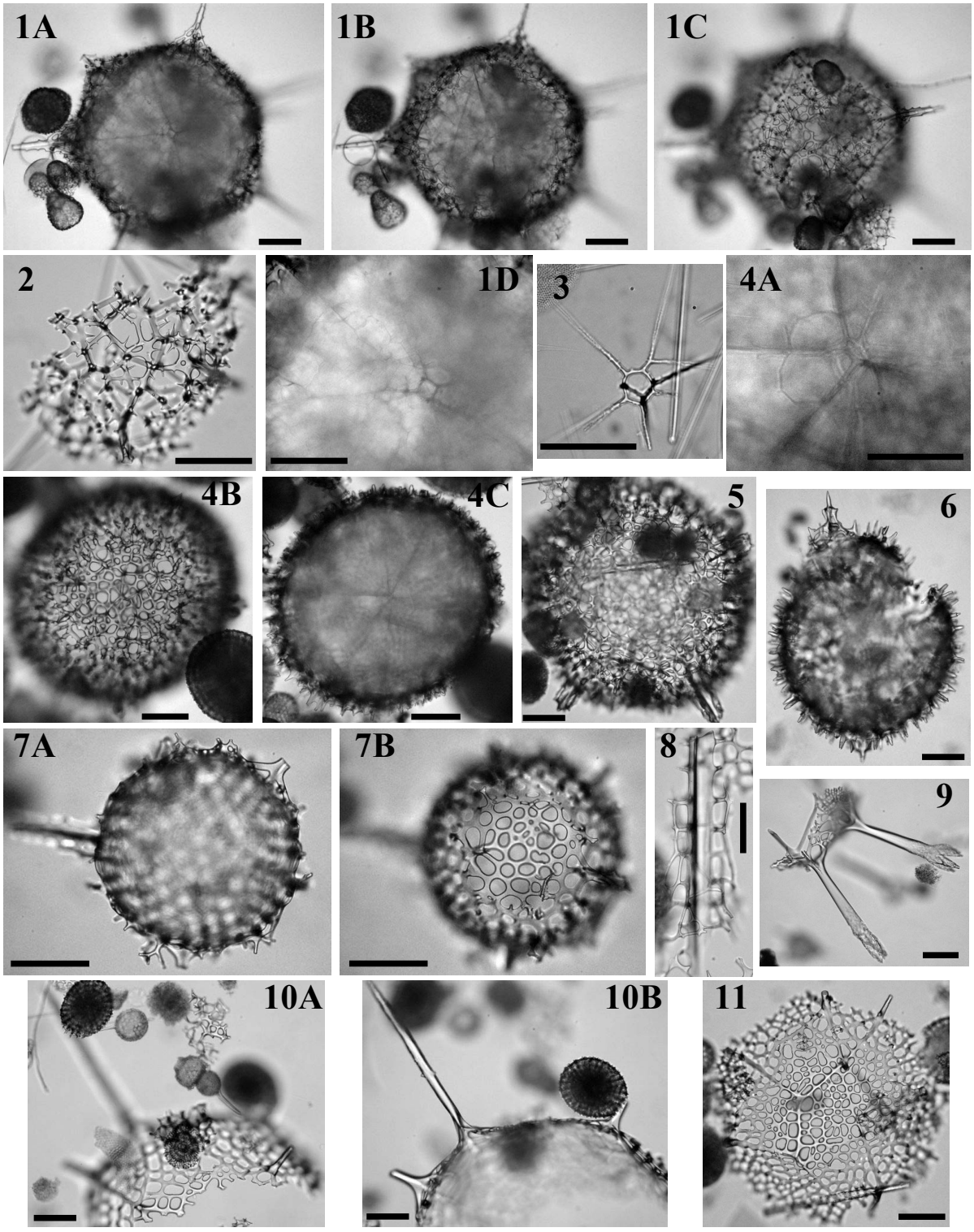

Plate 2.– Entactinarians.
1. *Orodapis*? *ferrealuma* Renaudie & Lazarus 2012, holotype, Sample 120-747A-2H-5 45-47 cm, Late Pliocene (A: view of cortical shell surface; B: view of intermediate meshwork; C: view of medullary shell; D: focus on medullary shell). 2. Fragment of *Orodapis*? *ferrealuma*, Sample 119-744A-2H-1 53-55cm, Late Pliocene. 3. *Gonosphaera primordialis* Jørgensen 1905, Sample 120-747A-1H-1 45-47cm, Pleistocene. 4. *Orodapis hericina* Renaudie & Lazarus 2012, holotype, Sample 120-748B-6H-CC, Early Miocene (A: view of cortical shell surface; B: view of medullary shell; C: focus on medullary shell). 5. *Orodapis hericina*, Sample 120-748B-6H-7 45-47 cm, Early Miocene. 6. Broken specimen of *Orodapis hericina*, Sample 113-690B-6H-4 22-24 cm, Early Miocene. 7. *Orodapis*? sp. A, Sample 113-690B-6H-4 22-24cm, Early Miocene. 8. Broken spine of *Orodapis*? sp. A, Sample 120-748B-6H-5 45-47cm, Early Miocene. 9. Spines of *Oroscena carolae* Friend & Riedel 1967, Sample 120-747A-8H-1 45-47cm, Middle Miocene. 10. *Oroscena carolae*, Sample 120-748B-6H-5 45-47cm, Early Miocene. 11. *Oroscena carolae*, Sample 119-744A-10H-7 16-18cm, Early Miocene.
All scale bars 100 µm except 3 and 4A where the scale bar is 50 µm. Magnification x96 except for 1D, 2, 7A-8 (x192) and for 3 and 4A (x384).

Conchellium? sp.
(Pl. 1, Figs 8A-B, 11)

Remarks. Fragments of large hemispherical shells have been found in the Middle Miocene of the Kerguelen Plateau. Because of their color and their texture they clearly belong to a Phaeodarian. They bear numerous small, closely-packed and regularly-arranged, round pore-like tubes. Their outer margin flares horizontally, giving, when seen sideways, the impression that the shell is double-layered (Pl. 1, fig. 8B).

Class **Radiolaria** Müller 1858
Superorder **Polycystinea** Ehrenberg 1838 emend. Riedel 1967
Order **Entactinaria** Kozur & Mostler 1982
Family **Excentroconchidae** Hollande & Enjumet 1960 emend. Dumitrica 2001

Genus *Gonosphaera* Jørgensen 1905
Type-species: *Gonosphaera primordialis* Jørgensen 1905

Gonosphaera primordialis Jørgensen 1905
1905 *Gonosphaera primordialis* Jørgensen: p. 133; pl. 14, figs 64-68
1976 *Gonosphaera primordialis* Jørgensen – Bjørklund: pl. 9, figs 7-10
2001 *Gonosphaera primordialis* Jørgensen – Dumitrica: p. 196; pl. 1, figs 1-4; pl. 2, fig. 1

Family **Orosphaeridae** Haeckel 1887

Genus *Orodapis* Friend & Riedel 1967
Type-species: *Orodapis spongiosa* Friend & Riedel 1967

Orodapis hericina Renaudie & Lazarus 2012
(Pl. 2, Figs 4A-6)

Derivation of name. *hericina* is Latin for "of the hedgehog".
Diagnosis. Spherical cortical shell with 6 large spines and thorns at each bar nodes; medullary spicule with arches joining each of the radial beam.
Holotype. Plate 2, figs. 4A-C; Sample 120-748B-6H-CC (Early Miocene); ECO-029.
Material. 328 specimens (including broken specimens) were observed from ODP Sites 690, 744, 748 and 751.
Description. Large, thick, spherical, latticed cortical shell. Pores are irregular in size and in shape, and irregularly-distributed. Each bar nodes bears a radially oriented, short, conical thorn. Medullary shell consists of a somewhat octahedral spicule from which arise six radial beams that reach the cortical shell and continue as more or less developed tri- or tetraradiate, serrated spine with a large basis. Arches link each of the radial beams a little further from the center of the medullary shell (ca. 40µ).
Dimensions. (based on 6 specimens) Shell diameter: 440-590 (515).
Occurrence. Common from the *C. antiqua* to the *C. golli regipileus* zone (early Miocene) and rare from the *E. punctatum* to the *A. golownini* Zone (early to middle Miocene).
Remarks. *Orodapis hericina* differs from *O. spongiosa* in the medullary spicule lying at the middle of the cortical shell cavity, in the arches joining the beams, in the lattice wall of the cortical shell being way more simple and in the shape of the main spines.

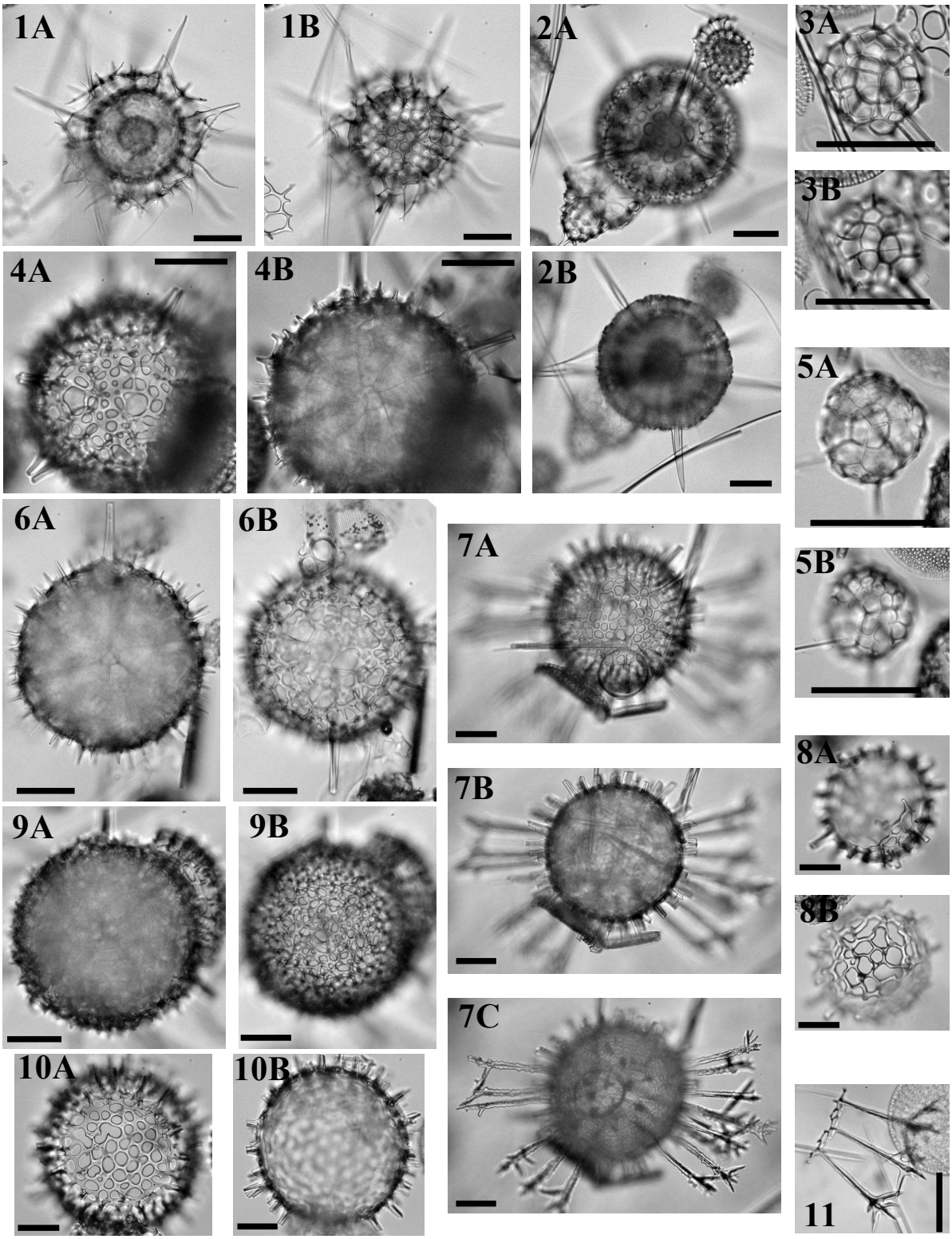

Plate 3.–
1. Actinommid sp. O, Sample 120-751A-4H-6 98-102cm, Early Pliocene. 2. Actinommid sp. O, Sample 120-751A-4H-4 98-102cm, Early Pliocene. 3. Actinommid sp. L, Sample 113-689B-3H-2 148-150cm, Late Miocene. 4. Actinommid sp. P, Sample 113-690C-3H-6 48-54cm, Late Miocene. 5. Actinommid sp. L, Sample 113-689B-3H-3 116-118cm, Late Miocene. 6. Actinommid sp. P, Sample 183-1138A-13R-2 20-22cm, Late Miocene. 7. *Cladococcus* sp. I, Sample 120-748B-5H-7 45-47cm, Middle Miocene (A: focus on cortical shell surface; B: focus on cortical shell outline; C: focus on spines). 8. *Cladococcus* sp. I?, Sample 113-690B-1H-1 126-132cm, Late Pliocene. 9. Actinommid sp. P, Sample 113-690C-3H-6 48-54cm, Late Miocene. 10. *Cladococcus* sp. I, Sample 119-744A-11H-3, Early Miocene. 11. Spines of *Cladococcus* sp. I, Sample 120-748B-5H-5 45-47cm, Middle Miocene.
All scale bars 50 µm. Magnification x 192 except on 3A-B, 4, 5A-B and 11 where it is x384.

Orodapis? *ferrealuma* Renaudie & Lazarus 2012
(Pl. 2, Figs 1A-2)

Derivation of name. The name derived from the Latin words *ferrea*, meaning "made of iron" and *luma*, "brambles": *ferrealuma* therefore stands for "iron brambles", i.e barbwires.
Diagnosis. Cortical meshwork made of spiny bars; twelve serrated spines.
Holotype. Plate 2, figs. 1A-D; Sample 120-747A-2H-5 45/47cm (Late Pliocene); ECO-031.
Material. 546 specimens (including identifiable fragments and broken specimens) were observed from ODP Sites 738, 744, 747, 748 and 751.
Description. Cortical shell is a nearly spherical icosahedron made of a meshwork of relatively thick, spiny anastomosed bars. The medullary shell is situated approximately at the center of the cortical shell cavity and is a somewhat octahedral spicule from which arises six thin radial beams that connects to the cortical shell at six of its vertices and continues outside as long, tribladed or conical, serrated spines. Between the medullary and the cortical shell lies a thin and sparse meshwork of anastomosed bars that diverged from those radial beams. There are six other radial spines, similar in shape and length to the six main radial spines, that arises from the six other vertices and that seem to root in the median meshwork. The base of the twelve spines are thickened by the cortical meshwork that is overgrowing along them.
Dimensions. (based on 5 specimens) Shell diameter: 430-600 (510).
Occurrence. Rare from the *A. golownini* to the Psi Zone (middle Miocene to Pleistocene); appears mostly as fragments.
Remarks. *Orodapis*? *ferrealuma* differs from *O. hericina* n.sp. and *O. spongiosa* in having this polyhedral outline instead of being nearly spherical as they are.

Orodapis? sp. A
(Pl. 2, Figs 7A-8)

Description. Large single-shelled skeleton (no medullary shell observed to date). Shell is rather smooth, with large irregularly-shaped pores. Some complex spines arises from this shell here and then: three or four bars join together to form the basis of the spine thus creating a tri- or quadribladed long spines. At regular interval, apophyses protrudes from each of the spine blades, extends perpendicularly to the spine axis and then branch to one another, thus forming a thin bar that runs alongside the spine (Pl. 2, fig. 8).
Remarks. No complete specimen was found to date (specimen from Pl. 2, figs 7A-B is the most complete specimen observed), meaning that the inner structure of this species is unknown and comparison with other Orosphaeridae (if this is indeed an Orosphaeridae) is limited. However the smoothness of the shell and the characteristic spines may be specific enough to identify this species. Furthermore the specimens is considerably smaller than the other Orosphaeridae presented here (the specimen from Pl. 2, figs 7A-B has a diameter of 265 µm, whereas *O.*? *ferrealuma* for example measures ~500 µm and *Oroscena carolae* more than 800 µm; Friend & Riedel 1967).

Genus *Oroscena* Haeckel 1887
Type-species: *Oroscena geganbauri* Haeckel 1887

Oroscena carolae Friend & Riedel 1967
(Pl. 2, Figs 9-11)
1967 *Oroscena carolae* Friend & Riedel: p. 225; pl. 2, figs 9-10; pl. 3, figs 1-2

Order **Spumellaria** Ehrenberg 1876

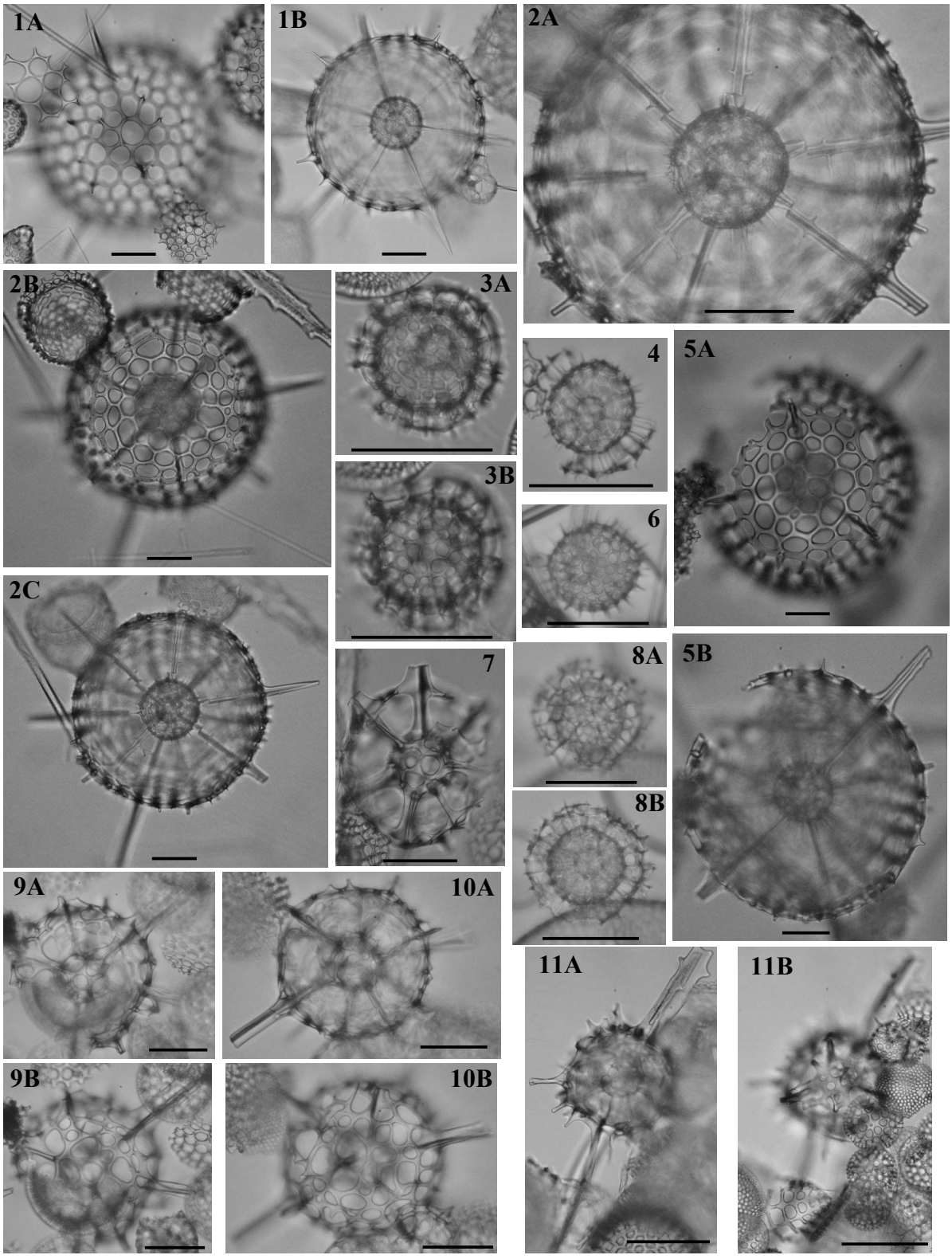

Plate 4.– 1. *Actinomma eldredgei* Renaudie & Lazarus in press, Sample 120-748B-6H-3 45-47cm, Early Miocene. 2. *Actinomma eldredgei*, holotype, Sample 120-748B-6H-3 45-47cm, Early Miocene (A: zoom on outer medullary shell; B: focus on cortical shell; C: focus on outer medullary shell). 3. *Actinomma cocles* Renaudie & Lazarus in press, holotype, Sample 113-689B-3H-2 148-150cm, Early Pliocene. 4. *Actinomma cocles*, specimen with cortical shell poorly developed, Sample 120-748B-7H-2 45-47cm, Early Miocene. 5. *Actinomma eldredgei*, Sample 120-751A-15H-CC, Early Miocene. 6. *Actinomma cocles*, specimen with cortical shell not developed, Sample 120-751A-11H-6 98-102cm, Early Miocene. 7. *Anomalacantha*? *jeapica* Renaudie & Lazarus in press, Sample 120-748B-8H-6 45-47cm, Early Miocene. 8. *Actinomma* cocles, Sample 120-751A-8H-3 98-102cm, Middle Miocene (A: focus on cortical shell; B: focus on outer medullary shell). 9. *Anomalacantha*? *jeapica*, Sample 120-748B-8H-6 45-47cm, Early Miocene. 10. *Anomalacantha*? *jeapica*, holotype, Sample 120-748B-8H-6 45-47cm, Early Miocene. 11. *Anomalacantha*? *jeapica*?, Sample 120-748B-8H-6 45-47cm, Early Miocene.
Scale bars are 50 µm. Magnification is x384 except for 1A-B, 2B-C, 5A-B and 11A-B (x192).

Family **Actinommidae** Haeckel 1862 emend. Sanfilippo & Riedel 1980

Actinommid sp. P
(Pl. 3, Figs 4A-B, 6A-B, 8A-B)

Description. Large, spherical cortical shell with rough surface and numerous pores that are irregular in size, shape and randomly arranged. Cortical shell bears numerous thorns. A small number (4, 6, 8?) of long, triangular (yet somewhat tribladed at the base) spines also protrudes from the cortical shell. They originated directly from the irregular polyhedral medullary shell, that evokes that of species of genus *Lonchosphaera*.

Genus *Acanthosphaera* Ehrenberg 1858
Type-species: *Acanthosphaera haliphormis* Ehrenberg 1861

Acanthosphaera actinota (Haeckel 1860)
1860 *Heliosphaera actinota* Haeckel: p. 803
1980 *Acanthosphaera actinota* (Haeckel) – Boltovskoy & Riedel: p. 107; pl. 1, fig. 19
1991 *Acanthosphaera actinota* (Haeckel) – Takahashi: p. 66; pl. 8, fig. 1

Acanthosphaera insignis (Hertwig 1879)
1879 *Heliosphaera insignis* Hertwig: p. 40; pl. 5, fig. 7
1887 *Acanthosphaera insignis* (Hertwig) – Haeckel: p. 212
1984 *Acanthosphaera insignis* (Hertwig) – Nishimura & Yamauchi: pl. 7, figs 3a-b; pl. 49, fig. 2

Genus *Actinomma* Haeckel 1862 emend. Bjørklund 1976b
TYpe-species: *Haliomma trinacrium* Haeckel 1860

Actinomma boreale Cleve 1899
1899 *Actinomma boreale* Cleve: p. 26; pl. 1, fig. 5
1905 *Cromyechinus borealis* (Cleve) – Jørgensen: p. 117-118; pl. 8, fig. 35; pl. 9, figs 36-37
1976 *Cromyechinus borealis* (Cleve) – Bjørklund: pl. 2, figs 7-15

Actinomma campilacantha Caulet 1991
1991 *Actinomma campilacantha* Caulet: p. 533; pl. 1, figs 3-4

Actinomma delicatulum (Dogiel & Reshetnyak 1952)
1952 *Heliosoma delicatulum* Dogiel & Reshetnyak: p. 7-8; fig. 2
1967 *Echinomma delicatulum* (Dogiel & Reshetnyak) – Petrushevskaya: p. 18-20; pl. 11, figs 1-3

Actinomma golownini Petrushevskaya 1975
(Pl. 8, Figs. 11, 12)
1975 *Actinomma golownini* Petrushevskaya: p. 569; pl. 2, fig. 16
1975 *Actinomma tanyacantha* Chen: p. 450; pl. 11, figs 5-6

Actinomma eldredgei Renaudie & Lazarus in press
(Pl. 4, figs. 1A-2C, 5A-B)

Derivation of name. Named after Niles Eldredge, early mentor to the junior author, and thereby early supporter of micropaleontological evolution research.

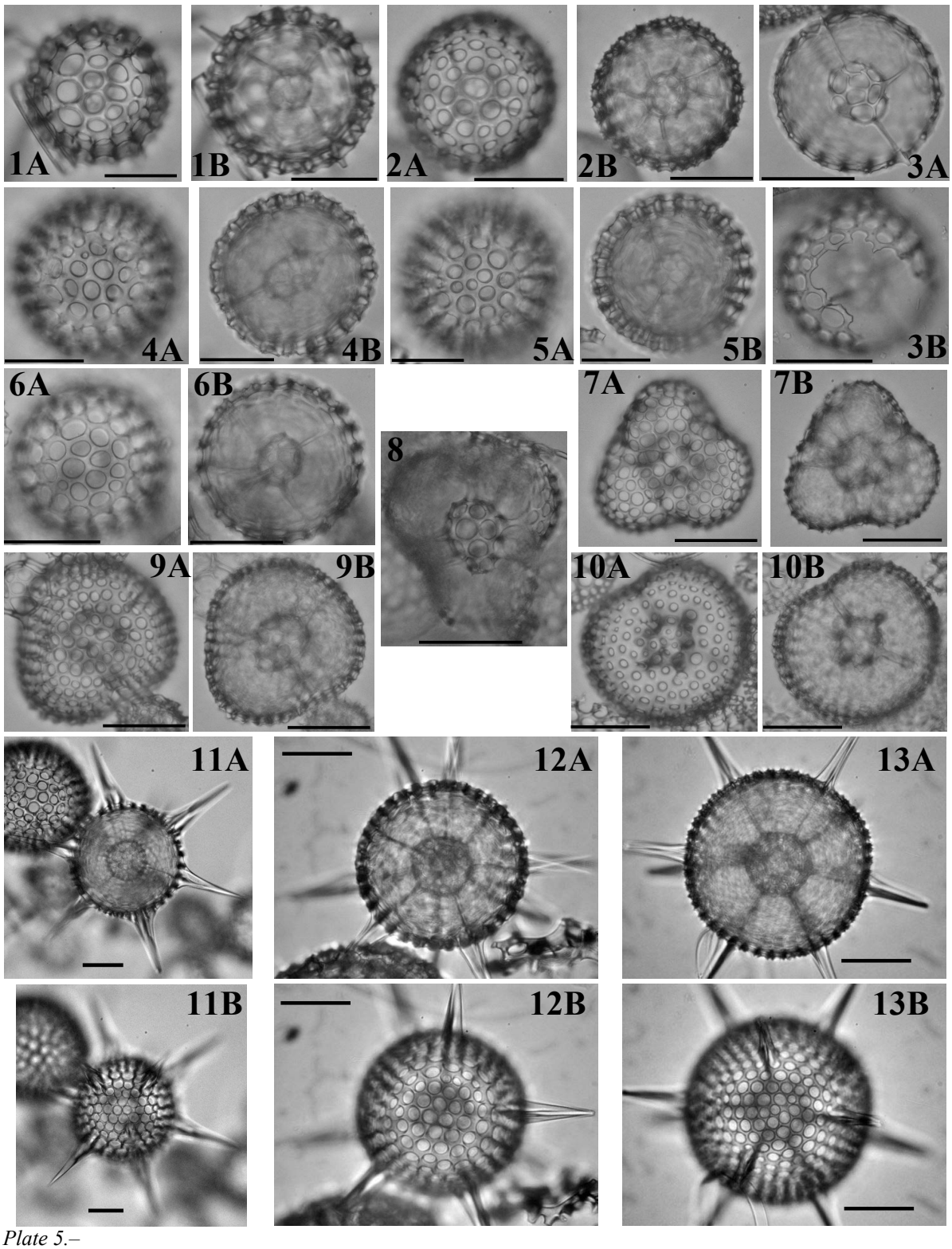

Plate 5.–
1. *Pentactinosphaera codonia* Renaudie & Lazarus in press, Sample 119-744A-4H-4 59-61cm, Late Miocene. 2. *Pentactinosphaera codonia,* Sample 119-744A-4H-2 59-61cm, Late Miocene. 3. *Pentactinosphaera codonia,* Sample 113-689B-3H-5 136-138cm, holotype, Late Miocene. 4. *Pentactinosphaera codonia,* Sample 113-689B-3H-5 136-138cm, Late Miocene. 5. *Pentactinosphaera codonia,* Sample 113-689B-3H-5 136-138cm, Late Miocene. 6. *Pentactinosphaera codonia,* Sample 113-689B-3H-5 136-138cm, Late Miocene. 7. *Sethodiscus*? *pravus* Renaudie & Lazarus in press, Sample 120-748B-8H-4 45-47cm, holotype, Early Miocene. 8. *Sethodiscus*? *pravus,* Sample 120-748B-8H-6 45-47cm, broken specimen, Late Oligocene/Early Miocene. 9. *Sethodiscus*? *pravus* Sample 120-748B-8H-6, 45-47cm, Late Oligocene/Early Miocene. 10. *Sethodiscus*? *pravus,* Sample 120-748B-8H-6 45-47cm, Late Oligocene/Early Miocene. 11. *Actinomma*? *nigriniae* Renaudie & Lazarus 2012, Sample 120-748B-6H-4 45-47cm, Early Miocene. 12. *Actinomma*? *nigriniae,* Sample 120-748B-6H-5 45-47cm, Early Miocene. 13. *Actinomma*? *nigriniae,* Sample 120-748B-6H-4 45-47cm, holotype, Early Miocene.
All sclae bars 50 µm. Magnification x384 except for 2A-B (x192).

Diagnosis. Shell ratio of 1:2:6; outer medullary shell bears numerous thin by-spines; twelve (?) tribladed radial beams; presence of apophyses branching from radial beams between outer medullary shell and cortical shell.
Holotype. Pl. 4, figs 2A-C; Sample 120-748B-6H-3, 45-47cm (Early Miocene); ECO-049.
Material. 62 specimens were observed from ODP Sites 744, 748 and 751.
Description. Three concentric shells. The innermost shell is globular to somewhat polyhedral and is constituted by a network of pentagonal and hexagonal pores separated by thin bars. The second shell, or outer medullary shell, is twice as large as the innermost medullary shell, spherical in most specimens, globular in the others, and bears numerous (7 to 10 on an half-equator), hexagonally-framed round pores of similar diameter as the ones on the inner medullary shell, as well as numerous thin, short spines (one at each bar node). The outermost shell, or cortical shell, is three times as large as the latter, hence six times as large as the innermost, and bears irregularly-distributed, circular to elliptical pores, of various size (but generally very large). The bars between the pores are here slightly crested and thickened at the nodes where, in some specimens, arise relatively long, conical, thick thorns. Twelve (or more?) tribladed radial beams arise from the innermost shell, connect the outer medullary shell and the cortical shell and protrude outside as fairly long spines (often broken). At the junction with each shell, the beams are thickened. Somewhere between the outer medullary shell and the cortical shell, in some specimens, these radial beams exhibit lateral apophyses (see Pl. 4, fig. 2A), all at the same height, suggesting the presence of yet another shell which was not preserved.
Dimensions. (based on 5 specimens) Diameter of inner medullary shell: 27-33 (30); diameter of outer medullary shell: 63-71 (67); diameter of cortical shell: 215-269 (233); diameter of pores on cortical shell: 12-31 (20); diameter of pores on outer medullary shell: 5-10 (8); diameter of pores on innermost shell: 5-7 (7).
Occurence. Rare from the *Stylosphaera radiosa* to the *Cycladophora golli regipileus* Zone (Late Oligocene to upper Early Miocene)
Remarks. *Actinomma eldredgei* differs from *Actinomma leptodermum* (Jørgensen) 1900 in the size of its cortical shell and in the spiny outer medullary shell. It is distinguised from *Actinomma golownini* Petrushevskaya, 1975 and *Hexalonche esmarki* Goll & Bjørklund, 1989 in its perfectly spherical cortical shell, its smaller, spiny outer medullary shell and its more numerous, weaker radial beams. It also differs from *Haliomma minor* Campbell & Clark, 1944 and from *H. schucherti* Campbell & Clark, 1944 in having three concentric shells, in the shell ratio and the cortical shell diameter and in the number of radial beams (8 for *minor* and *schucherti*); from *Haliomma echinaster* Haeckel, 1862 in the size, shape and arrangement of the cortical shell pores and in the presence of a latticed outer medullary shell; from *Haliomma beroes* Ehrenberg, 1854b, in the size of the cortical shell and in the size and shape of the cortical shell pores; from *Haliomma echinoides* Müller, 1858, in being larger, in having less numerous, tribladed radial beams and an outer medullary shell; from *Actinomma trinacrium* Haeckel, 1862, in its shell ratio, in having less numerous spines, and in its thorn-covered outer medullary shell; from *Actinomma plasticum* Goll & Bjørklund, 1989, in the beams, in the latter, being irregularly disposed, and the cortical shell, in the latter, being smaller, thicker and irregularly-shaped.

Actinomma kerguelensis Caulet 1991

1991 *Actinomma kerguelensis* Caulet: p. 531; pl. 1, figs 1-2

Actinomma leptoderma (Jørgensen 1900)

1900 *Echinomma leptoderma* Jørgensen: p. 57-58
1905 *Echinomma leptodermum* Jørgensen – Jørgensen: p. 116; pl. 8, figs 33a-b

1976a *Echinomma leptodermum* Jørgensen – Bjørklund: pl. 1, figs 13-14; pl. 2, figs 1-6
1976b *Actinomma leptodermum* (Jørgensen) – Bjørklund: pl. 1, figs I-L
1998 *Actinomma leptoderma leptoderma* (Jørgensen) – Cortese & Bjørklund: p. 153; pl. 2, figs 1-14; pl. 3, figs 4-5, 9-10, 15-16
1998 *Actinomma leptoderma* (Jørgensen) *longispina* Cortese & Bjørklund – Cortese & Bjørklund: p. 153; pl. 2, figs 15-22

Actinomma magnifenestra Lazarus 1992

1992 *Actinomma*? *magnifenestra* Lazarus: p. 795, pl. 3, figs 1-9

Actinomma popofskii (Petrushevskaya 1967)

1967 *Echinomma popofskii* Petrushevskaya: p. 20-22; pl. 12, figs 1-3
1995 *Actinomma popofskii* (Petrushevskaya) – Morley & Nigrini: p. 81; pl. 1, figs 4-5

Actinomma livae? Goll & Bjørklund 1989

? 1989 *Actinomma livae* Goll & Bjørklund: p. 728-729; pl. 1, figs 1-5

Remarks. The forms observed in our material differ somewhat from the ones described and illustrated in Goll & Bjørklund 1989 in the distance between the shell (shell ratio of 1:2:4:6) and the thickness of the outermost shell.

Actinomma? *nigriniae* Renaudie & Lazarus 2012
(Pl. 5, figs 11A-13B)

Derivation of name. Named in memory of Catherine Nigrini for her numerous contributions to radiolarian research.

Diagnosis. Spherical cortical shell; twelve evenly-distributed radial beams protruding as twelve tribladed spines.

Holotype. Plate 5, figs. 13A-B; Sample 120-751A-13H-2 98/102cm (Middle Miocene); ECO-032.

Material. 147 specimens (including identifiable fragments and broken specimens) were observed on sites 690, 738, 744, 747, 748 and 751.

Description. Three concentric shells linked together by twelve tribladed radial beams that continue outside the cortical shell as twelve strongly tribladed radial spines. The innermost shell is an irregular sphere that tends to have a regular icosahedral outline where each summit is linked to a radial beam. The median shell is approximately two times bigger and has the same outline as the latter, except that the edges are smoother and therefore the shell is closer to a sphere. Pores are numerous, polygonal (penta- or hexagonal) and separated by thin bars. The outermost shell is approximately three times bigger than the median one and has an almost perfectly spherical outline. Pores on this shell are rounded, approximately equal in size and in shape, distributed according to a hexagonal pattern and separated by thin, rough, crested bars with raised nodes.

Dimensions. (based on 5 specimens) Cortical shell diameter: 130-145 (140); outer medullary shell diameter: 45-60 (53); inner medullary shell diameter: 20-25 (22); length of spines: 50-95 (73).

Occurrence. Rare to common from the *S. radiosa* to the *C. humerus* Zone (early to middle Miocene), sporadic from the *A. golownini* to the Upsilon Zone (middle Miocene to late Pliocene).

Remarks. *Actinomma nigriniae* differs from *A. golownini* Petrushevskaya, 1975 in the spherical shape of its cortical shell and in its smaller, more numerous, smaller pores. Furthermore every

single one of the external spine is connected to the outer medullary shell whereas in *A. golownini* only 6 of them are connected.

Actinomma cocles Renaudie & Lazarus in press
(Pl. 4, figs. 3-4, 6, 8A-B)

Derivation of name. From the Latin *cocles,* meaning 'one-eyed'.
Diagnosis. Small three-shelled test with a small, eccentric innermost shell and a thin, spherical outermost shell close to the middle shell and linked to it by numerous thin radial bars.
Holotype. Pl. 4, figs 3A-B; Sample 113-689B-3H-2, 148-150cm (Late Miocene); ECO-050.
Material. 126 specimens were observed from ODP Sites 689, 693, 748, 751 and 1138.
Description. The innermost shell is polyhedral to spherical, with polygonal pores (3 to 4 on a half-equator). The middle shell is spherical to globular (even ovoid in some rare specimens). Those two shells are connected to one another by the mean of several thin beams that arise at the nodes of the innermost shell. The latter can be seen to be eccentrically placed in the middle shell cavity in most specimens. Pores on the middle shell are round to polygonal (7 to 9 on an half-equator). The outermost shell is a delicate meshwork of anastomosed bars branching from the numerous, thin beams that project from the middle shell. In most specimens, that meshwork is poorly developed. The resulting shell outline generally mimics the middle shell outline. The two latter shells are close to one another, while the innermost shell is less than half the size of the middle shell. The two sets of connecting beams seem unrelated to one another.
Dimensions. (based on 6 specimens) Diameter of medullary shell: 12-16 (15); diameter of inner cortical shell: 36-42 (38); diameter of outer cortical shell: 51-71 (58).
Occurence. Rare from the *Stylosphaera radiosa* to the *Cycladophora golli regipileus* Zone (Late Oligocene to Early Miocene) and from the *Siphonosphaera vesuvius* to the Tau Zone (Late Miocene to Early Pliocene); sporadic from the *Eucyrtidium punctatum* to the *Siphonosphaera vesuvius* Zone (Early to Late Miocene) and from the Tau to the Psi Zone (Early Pliocene to Late Pleistocene)
Remarks. It differs from *Echinomma sphaerechinus* Haeckel, 1887, *Helisoma dispar* Blueford, 1982 and *Drymyomma elegans* Jørgensen, 1900 in having three shells, in its thin, delicate outermost shell and in its eccentric innermost shell. *Excentrosphaerella sphaeroconcha* Dumitrica, 1978a and *Excentrodiscus japonicus* (Nakaseko & Nishimura) 1974 also possess an eccentric innermost shell: however the shell ratio and the thickness of the shell in these two species make them clearly distinguishable from this new species. Furthermore, although eccentric, the innermost shell in *A. cocles* is not fused to the next shell wall as in the two latter species (compare Pl. 4, fig. 3A with Pl. 3, fig. 7B in Nakaseko & Nishimura, 1974, or with Pl. 4, figs 19B-C in Kamikuri, 2010).

Actinomma? sp. O
(Pl. 3, Figs 1A-2B)

Diagnosis. Shell ratio of 1:2:6:7; 7/8? long, conical spines; thin, anastomed outermost cortical shell.
Description. Four-shelled actinommid with two medullary and two cortical shells. Innermost shell is polyhedral; outer medullary shell is globular. 3 or 4 (?) beams protrudes from the outer medullary shell, joins the cortical shells and protrudes outside as long, conical spines. 3 or 4 (?) additional by-spines, similar in shape and size to the beams, protrudes directly from the inner cortical shell. Inner cortical shell is spherical, thick and bears large circular pores surrounded by hexagonal frames with raised apices. Those raised apices extends as needle-like by-spines, diverges distally into several thin bars parallel to the inner cortical shell, and anastomose to form

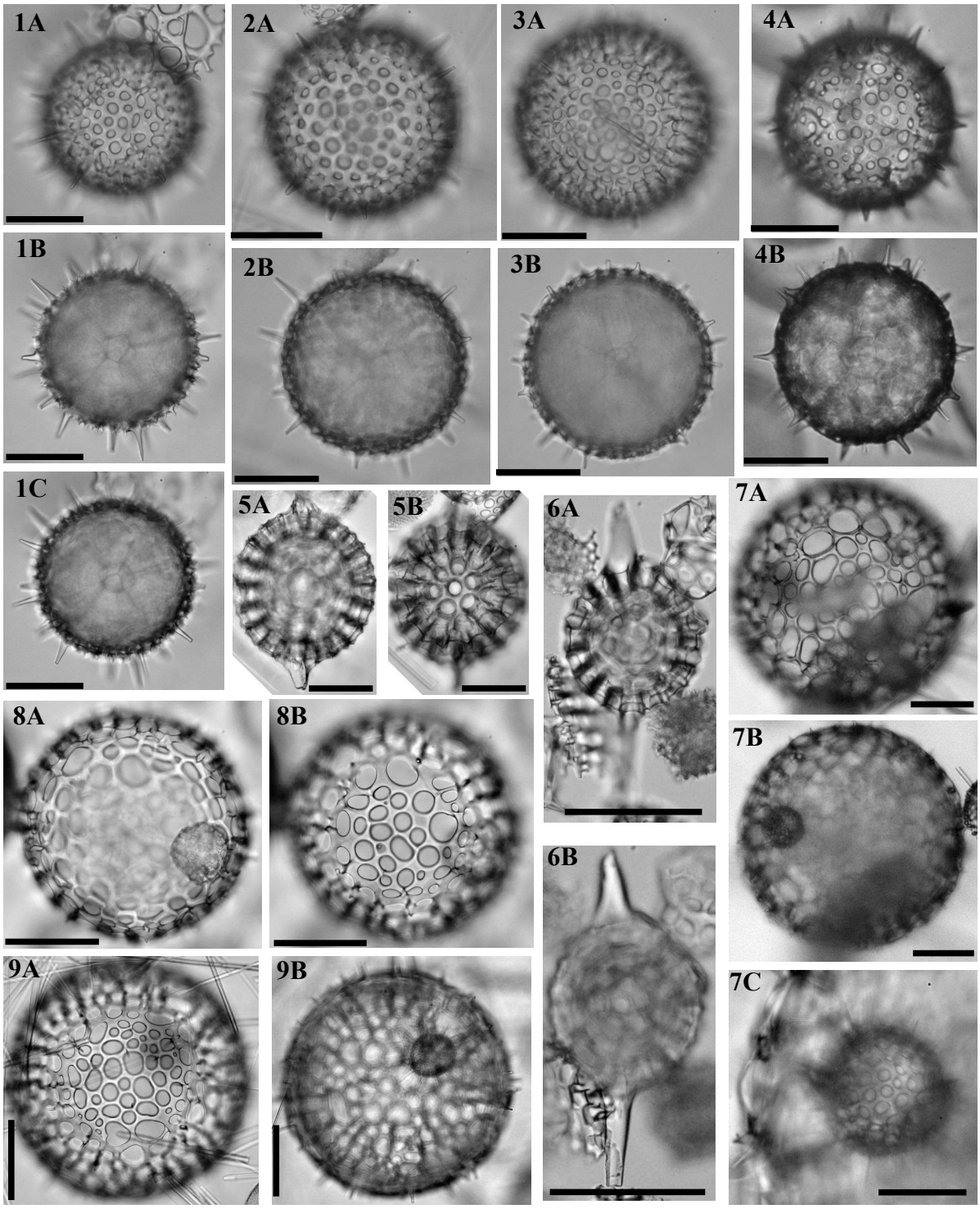

Plate 6.–
1. *Lonchosphaera suzukii* Renaudie & Lazarus in press, Sample 120-747A-2H-5 45-47cm, holotype, Pleistocene (A: Focus on cortical shell; B: Focus on back of medullary shell; C: Focus on front of medullary shell).
2. *Lonchosphaera suzukii,* Sample 120-747A-1H-1 45-47cm, Pleistocene.
3. *Lonchosphaera suzukii,* Sample 120-747A-3H-1 45-47cm, Late Pliocene.
4. *Lonchosphaera suzukii,* Sample 119-745B-22H-4, 53-55cm, smaller specimen with fewer pores, Early Pliocene.
5. *Stylatractus* sp. C, Sample 120-748B-8H-3 45-47cm, Early Miocene.
6. *Stylatractus* sp. C, Sample 120-748B-8H-3 45-47cm, Early Miocene.
7. *Carposphaera annikae* Renaudie & Lazarus 2012, holotype, Sample 120-751A-7H-2 98-102cm, Late Miocene (A: Focus on cortical shell; B: Focus on medullary shell; C: Zoom on medullary shell)
8. *Carposphaera annikae,* Sample 119-744A-4H-2 59-61cm, Late Miocene.
9. *Carposphaera annikae,* Sample 120-751A-11H-2 98-102cm, Middle Miocene.
All scale bars 50 µm except for 7A-B (100 µm). Magnification x192 except for 7A-B (x96) and for 1A-5B and 7C (x384).

the outer cortical shell.

Remarks. *Actinomma*? sp. O differs from *Actinomma kerguelensis* and *A. livae* in its long conical spines and its outermost shell being constituted of thin anastomed material. It also differs from those species in its shell ratio.

Genus *Anomalacantha* Loeblich & Tappan 1961

Type-species: *Heteracantha dentata* Mast 1910

Anomalocantha dentata (Mast 1910)

1910 *Heteracantha dentata* Mast: p. 159; pl. 37, fig. 47

1961 *Anomalacantha dentata* (Mast) – Loeblich & Tappan: p. 223

1976a *Heteracantha dentata* Mast – Bjørklund: pl. 14, figs 10-12

Anomalacantha? *jeapica* Renaudie & Lazarus in press

(Pl. 4, figs. 7, 9A-10B; ? Pl. 4, figs 11A-B)

Derivation of name. Named after Jean-Pierre Caulet.

Diagnosis. Shell ratio of 1:2.5 to 1:3; thick, crested medullary shell; latticed cortical shell; 7 to 10 strong, tribladed spines.

Holotype. Pl. 4, figs 10A-B; Sample 120-748B-8H-6, 45-47cm (Late Oligocene/Early Miocene); ECO-051.

Material. 15 specimens were observed from ODP Site 748.

Description. Medullary shell is a small sphere composed of narrow, thick, crested bars surrounding a few (usually three on a half-equator) large, circular to elliptical pores. Seven to ten strong tribladed beams arise from the medullary shell, join the cortical shell and protrudes as spines (almost always found broken). Near the junction between the beams and the cortical shell, they broaden and, in some cases, branch and therefore join the shell at several points (see Pl. 4, fig. 9A).

The cortical shell is subspherical and two and a half to three times larger than the medullary shell. Bars are somewhat thinner than the ones on the medullary shell, but still crested. Pores are circular or elliptical and irregular in size (yet rather large), in shape and in distribution. The cortical shell is slightly deformed near the spines. Some of the bar nodes bear small thorns.

Dimensions. (based on 6 specimens) Diameter of medullary shell: 39-51 (45); diameter of cortical shell: 100-133 (114); diameter of cortical shell pores: 5-29 (15); diameter of medullary shell pores: 8-13 (10).

Occurence. Rare in the *Stylosphaera radiosa* Zone (Late Oligocene to Early Miocene).

Remarks. *Anomalacantha*? *jeapica* has a medullary shell similar to that of *A. dentata* or *Cladococcus pinetum* Haeckel, 1887 but it differs from this species in having a latticed cortical shell. *A.*? *jeapica* also differs from *Haeckeliella macrodoras* (Haeckel) 1887 in Hollande & Enjumet, 1960 in the smaller shell ratio, in the medullary shell being smaller, less spherical with crested bars. No complete specimen of *A.*? *jeapica* has been found so far, thus it is not possible to determine the distal shape of the spines. One specimen (Pl. 4, figs 11A-B) that we assigned tentatively to *A.*? *jeapica,* however, possess spines that are serrated along their length, just as in *A. dentata*. This specimen differs from other specimens of our new species in its thinner medullary shell and in having numerous, well-developed thorns on its cortical shell.

Genus *Arachnosphaera* Haeckel 1862

Type-species: *Arachnosphaera oligacantha* Haeckel 1862

Arachnosphaera dichotoma Jørgensen 1900

1900 *Arachnosphaera dichotoma* Jørgensen: p. 60-61; pl. 3, fig. 18
1976a *Arachnosphaera dichotoma* Jørgensen – Bjørklund: pl. 3, figs 5-9

Genus *Carposphaera* Haeckel 1881

Type-species: *Carposphaera capillacea* Haeckel 1887

Carposphaera? *annikae* Renaudie & Lazarus 2012
(Pl. 6, figs 7A-9B)

? 1887 *Elatomma penicillus* Haeckel: p. 243.
? 1991 *Elatomma penicillus* Haeckel – Takahashi: p. 69; pl. 9, figs 9-10.

Derivation of name. Named after Annika Sanfilippo for her many contributions to radiolarian taxonomy and stratigraphy.

Diagnosis. Shell ratio of 1:4 to 1:6; inward-oriented, thin spines at each node of the cortical shell.

Holotype. Plate 6, figs. 7A-C; Sample 120-751A-7H-2 98/102cm (Late Miocene); ECO-033.

Material. 83 specimens were observed from ODP Sites 690, 744, 747, 748 and 751.

Description. Very large, thick cortical shell with large, irregularly shaped, unequal, randomly distributed pores. On the inner side of the cortical shell, numerous small spines are projecting inward at each node of the latticed shell. These projections are thin and slender; in rare specimens, they protrude on the outer side of the shell as relatively small, conical spines. A small medullary shell (4 to 6 times smaller than the cortical shell) is sometimes found free in the large cortical shell on unbroken specimens. Pores on this medullary shell are small, round and closely packed. The bars between the pores are crested and numerous thin spines are projecting outwardly from each of the node.

The number and the direction of the spines both on the medullary and on the cortical shell strongly suggest a connection between the two. The radial beams where probably too thin to be preserved.

Dimensions. (based on 6 specimens) Cortical shell diameter: 250-400 (310); medullary shell diameter: 60-75 (67); cortical shell pores diameter: 6-43 (23).

Occurrence. Sporadic from the *S. radiosa* to the *A.golownini* Zone (early to middle Miocene), rare from the middle *A. golownini* to the *S. vesuvius* Zone (middle to late Miocene) and fairly common from the *C. spongothorax* to the *A. australis* (late Miocene).

Remarks. *C.*? *annikae* differs primarily from *Liosphaera antarctica* Nakaseko, 1959 and the species of genus *Carposphaera* in its shell ratio and in the shape and size of its cortical shell pores. It also differs from other Actinommidae in its numerous thin radial beams. It finally differs from *Elatomma penicillus* in having larger elliptical pores, a thicker wall, a considerably smaller medullary shell (shell ratio of 1:4 to 1:6 instead of 1:2 for *E. penicillus*) and in lacking branching radial spines.

Carposphaera subbotinae Borisenko 1958

1958 *Carposphaera subbotinae* Borisenko: p. 85; pl. 5, figs 5-7
1973 *Carposphaera subbotinae* Borisenko – Riedel & Sanfilippo: p. 490; pl. 4, fig. 3; pl. 23, figs 4-5

Genus *Cenosphaera* Ehrenberg 1854

Type-species: *Cenosphaera plutonis* Ehrenberg 1854

Cenosphaera cristata Haeckel 1887 *sensu* Riedel 1958

? 1887 *Cenosphaera cristata* Haeckel: p. 66
1958 *Cenosphaera cristata* Haeckel – Riedel: p. 223; pl. 1, figs 1-2
1967 *Cenosphaera cristata* Haeckel – Petrushevskaya: p. 10-11; pl. 7, figs 1-2

Remarks. The species (or group of species) that we identified as *Cenosphaera cristata* is characterized by the absence of a medullary shell, and a thick, crested cortical shell with uneven, irregularly-placed round to elliptical pores.

Cenosphaera elysia Haeckel 1887

1887 *Cenosphaera elysia* Haeckel: p. 64; pl. 12, fig. 8
1980 *Cenosphaera elysia* Haeckel – Boltovskoy & Riedel: p. 106; pl. 1, fig. 14
1982 *Cenosphaera riedeli* Blueford: p. 193; pl. 1, figs 7-9

Remarks. This species is differenciated from the other single-shelled actinommids, in its aligned, large, circular pores.

Cenosphaera oceanica Clark & Campbell 1945

1945 *Cenosphaera*? *oceanica* Clark & Campbell: p. 7; pl. 1, fig. 4
1975 *Cenosphaera*? *oceanica* Clark & Campbell group – Petrushevskaya: p. 571; pl. 1, figs 12-13; pl. 31, fig. 5
1989 *Cenosphaera*? *oceanica* Clark & Campbell – Lazarus & Pallant: p. 365; pl. 7, figs 7-8

Remarks. This species is characterized by its considerable diameter (~450 µm) and the numerous, comparatively small (their diameter is almost equal to their depth), closely-packed, elliptical pores.

Cenosphaera reticulata (Haeckel 1860)

1860 *Cyrtidosphaera reticulata* Haeckel: p. 803
1862 *Cyrtidosphaera reticulata* Haeckel – Haeckel: p. 349; pl. 11, fig. 2
1887 *Cenosphaera reticulata* (Haeckel) – Haeckel: p. 66
2003 *Cyrtidosphaera reticulata* Haeckel – Itaki: pl. 1, fig. 6

Cenosphaera? sp. K

(Pl. 9, figs 10A-B; Pl. 26, figs 19-20)

Diagnosis. Single-shelled; double-contoured, elliptical pores.

Description. Single-shelled actinommid with a thick, sometimes bumpy (see Pl. 26, fig. 20), cortical shell with uneven, irregularly-placed and shaped pores. All pores are double-contoured: the width of the pores on the outermost, thin, layer of the shell is larger than on the innermost, thick, layer. Those two layers may be two cortical shells fused to one another.

Remarks. It differs from the other single-shelled actinomiids in its double-contoured pores. The specimen illustrated in Pl. 9, figs 10A-B seems to contained a broken, small medullary shell similar to that of genus *Spongoplegma.* However, since no connection between this fragment and the cortical shell have been seen and since only one specimen exhibited such a shell, we can not rule out the possibility that this fragment belong to another specimen and just happened to get stuck in the cavity of the studied specimen. The contouring of the pores might also have been a preservation artifact caused by dissolution however the specimen illustrated on Pl. 26, fig. 19 seems to indicate otherwise. In addition to this specimen, the coherency of the observed range of those forms is also a good argument to think that this is a real character and not an artifact.

Genus *Cladococcus* Müller 1857

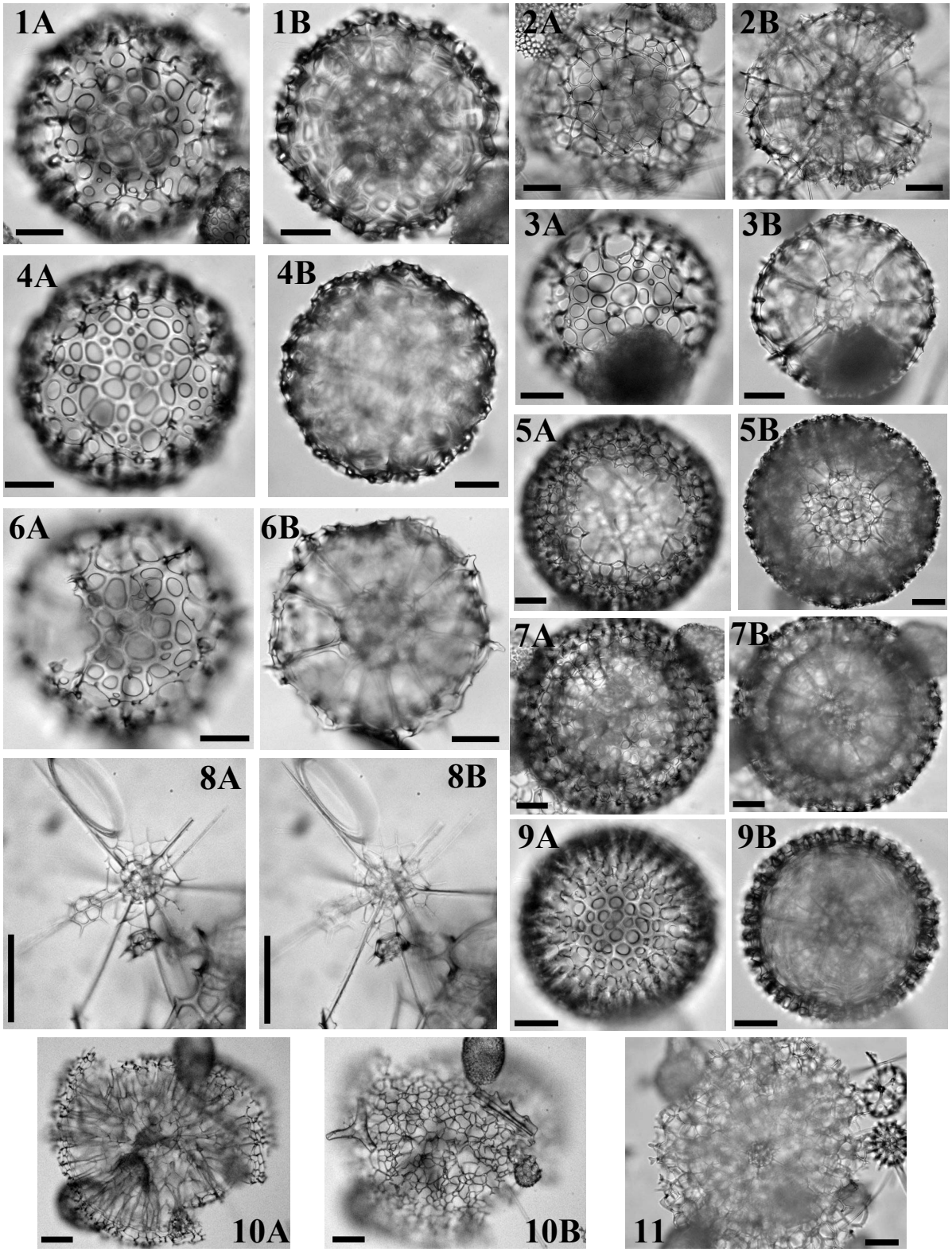

Plate 7.– 1. *Spongoplegma sp. D*, Sample 120-747A-1H-3 45-47cm, Pleistocene.
2. *Spongoplegma arcadophorum* (Haeckel 1887), Sample 120-747A-1H-1 45-47cm, Pleistocene.
3. *Spongoplegma medianum* (Nigrini 1967), Sample 120-747A-2H-7 45-47cm, Late Pliocene.
4. *Spongoplegma* sp. D, Sample 120-747A-1H-3 45-47cm, Pleistocene.
5. *Spongoplegma antarcticum* Haeckel 1887, Sample 120-747A-1H-3 45-47cm, Pleistocene.
6. *Spongoplegma* sp. D?, Sample 120-747A-3H-1 45-47cm, Late Pliocene.
7. *Spongoplegma holtedahli* (Bjørklund 1976), Sample 120-747A-1H-3 45-47cm, Pleistocene.
8. *Rhizoplegma boreale* Jørgensen 1905, Sample 120-751A-5H-3 98-102cm, Late Miocene.
9. *Spongoplegma variabile* Nakaseko, 1971 Sample 119-737A-27X-2, Late Miocene.
10. P*legmosphaera lepticali*? Renz 1976, Sample 120-748B-6H-2 45-47cm, Early Miocene.
11. *Styptosphaera spongiacea* Haeckel 1887, Sample 120-747A-2H-3 45-47cm, Pleistocene.
All scale bars are 50 µm. Magnification x192 except for 8A-B (x384) and 10A-B (x96).

Type-species: *Cladococcus arborescens* Müller 1858

Cladococcus sp. I
(Pl. 3, Figs 7A-8B, 10A-11)

Diagnosis. Irregularly-shaped pores; tribladed, somewhat serrated, by-spines ending in a tri- or quadrifurcation.

Description. Fairly large cortical shell with, somewhat irregularly arranged, irregularly shaped (elliptical, globular or irregular as in Pl. 3, fig. 8B) pores of various isze. Numerous, long, tribladed and sometimes even serrated (Pl. 3, fig. 7C) thorns projects from the cortical shell. Those thorns terminated with shorter projections branching from them (Pl. 3, fig. 11). No medullary shell was observed on any specimens.

Remarks. It differs from *Cladococcus leptus* Hülsemann 1963 in the latter having polygonal pores and in the divergence of the spines occurring in the later midways instead of being terminal.

Genus *Druppatractus* Haeckel 1887

Type-species: *Druppatractus hippocampus* Haeckel 1887

Druppatractus hastatus Blueford 1982

1982 *Druppatractus hastatus* Blueford: p. 206-208; pl. 6, figs 3-4
1990 *Druppatractus hastatus* Blueford – Abelmann: pl. 2, fig. 3

Druppatractus irregularis Popofsky 1912

1912 *Druppatractus irregularis* Popofsky: p. 114; text-figs 24-26

Genus *Drymosphaera* Haeckel 1881

Type-species: *Drymosphaera hexagonalis* Haeckel 1887

Drymosphaera? *pseudosagenoscena* Sugiyama 1992b

1992b *Drymosphaera*? *pseudosagenoscena* Sugiyama: p. 194; pl. 9, figs. 1a-4b

Genus *Drymyomma* Jørgensen 1900

Type-species: *Drymyomma elegans* Jørgensen 1900

Drymyomma elegans Jørgensen 1900

1900 *Drymyomma elegans* Jørgensen: p. 58-59
1905 *Drymyomma elegans* Jørgensen – Jørgensen: pl. 8, figs 34a-b
1976 *Drymyomma elegans* Jørgensen – Bjørklund: pl. 3, figs 1-4
1998 *Drymyomma elegans* Jørgensen – Cortese & Bjørklund: p. 154; pl. 3, figs 17-19

Genus *Echinomma* Haeckel 1882

Type-species: *Echinomma echinidium* Haeckel 1887

Echinomma sphaerechinus Haeckel 1887

1887 *Echinomma sphaerechinus* Haeckel: p. 258; pl. 29, fig. 2

Genus *Excentrodiscus* Hollande & Enjumet 1960

Type-species: *Excentrodiscus echinatus* Hollande & Enjumet 1960

Excentrodiscus japonicus (Nakaseko & Nishimura 1974)

1974 *Prunulum japonicum* Nakaseko & Nishimura: p. 52; pl. 3, figs 6a-7b; pl. 4, figs 2a-b

2010 *Excentrodiscus japonicus* (Nakaseko & Nishimura) – Kamikuri: p. 86-94 ; pl. 2, figs 2a-3b, 5a-6b, 8a-9b, 11a-b, 13a-14b; pl. 4, figs 19a-c

Excentrodiscus medusa (Ehrenberg 1844)

1844 *Haliomma medusa* Ehrenberg: p. 83

1975 *Actinomma medusa* (Ehrenberg) emend. group – Petrushevskaya: p. 568; pl. 2, figs 6-8

Genus *Excentrosphaerella* Dumitrica 1978a

Type-species: *Excentrosphaerella sphaeroconcha* Dumitrica 1978a

Excentrosphaerella sphaeroconcha Dumitrica 1978a

1978a *Excentrosphaerella sphaeroconcha* Dumitrica: p. 238; pl. 5, figs 17-18, 22

1992 *Excentrosphaerella sphaeroconcha* Dumitrica – Sugiyama & Furutani: p. 202; pl. 12, figs 1-2; pl. 16, fig. 3

Genus *Haeckeliella* Hollande & Enjumet 1960

Type-species: *Haliomma macrodoras* Haeckel 1887

Haeckeliella inconstans Dumitrica 1973

1973 *Haeckeliella inconstans* Dumitrica: p. 833; pl. 7, figs 1-2; pl. 18, figs 7-22

Haeckeliella macrodoras (Haeckel 1887)

1887 *Haliomma macrodoras* Haeckel: p. 238; pl. 28, fig. 6

1960 *Haeckeliella macrodoras* (Haeckel) – Hollande & Enjumet: p. 119-120; pl. 41, fig. 5; pl. 56, figs 1-6

Genus *Haliometta* Haeckel 1887

Type-species: *Haliomma circumtextum* Haeckel 1887

Haliometta miocenica (Campbell & Clark 1944)

1944 *Heliosphaera miocenica* Campbell & Clark: p. 16; pl. 2, figs 10-14

1972 *Haliometta miocenica* (Campbell & Clark) group – Petrushevskaya & Kozlova: p. 517; pl. 9, figs 8-9

Genus *Heliosoma* Haeckel 1881

Type-species: *Heliosoma radians* Haeckel 1887

Heliosoma dispar Blueford 1982

1982 *Helisoma* [sic] *dispar* Blueford: p. 202; pl. 6, figs 1-2b

Genus *Hexacontium* Haeckel 1881

Type-species: *Hexacontium phaenaxonium* Haeckel 1887

Hexacontium enthacanthum Jørgensen 1900

(Pl. 8, figs. 15A-B)

1900 *Hexacontium entacanthum* Jørgensen: p. 52; pl. 2, fig. 14
1976 *Hexacontium entacanthum* Jørgensen – Bjørklund: pl. 1, figs 1-3

Hexacontium laevigatum Haeckel 1887
(Pl. 8, figs. 16A-B)
1887 *Hexacontium laevigatum* Haeckel: p. 193; pl. 24, fig. 6
1955 *Hexacontium nipponicum* Nakaseko: p. 85; pl. 3, figs 5a-c
1974 *Hexacontium nipponicum* Nakaseko – Nakaseko & Nishimura: p. 50; pl. 2, figs 7a-b
1987 *Hexacontium laevigatum* Haeckel – Boltovskoy & Riedel: pl.1, fig. 28

Hexacontium pachydermum Jørgensen 1900
(Pl. 8, figs. 14A-B)
1900 *Hexacontium pachydermum* Jørgensen: p. 53
1976 *Hexacontium pachydermum* Jørgensen – Bjørklund: pl. 1, figs 4-9

Hexacontium sp. A
(Pl. 8, figs. 1-3)
Diagnosis. High shell ratio (1:2); 6 short, lanceolate spines.
Description. Two (three?; Pl. 8, fig. 3) concentric shells. Both are perfectly spherical and connected to one another by 6 radial beams, that prtrudes outside the cortical shell as 6 short, lanceolate spines that are tribladed at their base. Pores on both shells are even in size and shape and evenly distributed. Pores on medullary shell are smaller and almost polygonal.
Remarks. It differs from *Hexalonche philosophica* in its spherical outline and lanceolate spines; from *Hexacontium pachydermum* and *H. entacanthum* in its small diameter and its characteristic shell ratio.

Genus *Hexalonche* Haeckel 1881
Type-species: *Hexalonche phaenaxonia* Haeckel 1887

Hexalonche aristarchi Haeckel 1887
(Pl. 8, figs. 17A-B)
1887 *Hexalonche aristarchi* Haeckel: p. 186, pl. 22, fig. 3
1982 *Hexalonche aristarchi* Haeckel – Blueford: pl. 5, figs 1-2

Hexalonche philosophica Haeckel 1887
(Pl. 8, figs. 4A-B)
1887 *Hexalonche philosophica* Haeckel: p. 186; pl. 22, fig. 4
1992 *Hexalonche philosophica* Lazarus: pl. 4, figs 1-3, 5

Hexalonche sp. B cf *H. esmarki* Goll & Bjørklund 1989
(Pl. 8, figs. 5A-8)
Description. Large three-shelled actinommid with a shell ratio of approximately 1:2:6. Cortical shell is thick, covered with thorns, with a circular to somewhat oblong outline. Pores on the cortical shell are large and closely packed (see Pl. 8, fig. 5A). Outer medullary shell has a somewhat flattened spheroidal outline. Inner medullary shell is a polyhedron. Six radial beams arise from this polyhedron, joins the outer medullary shell and the cortical shell and then prtrudes as conical spines of same length and shape as the numerous thorns covering the cortical shell.

Dimensions. (based on 4 specimens) Diameter of cortical shell: 199-220 (213).
Remarks. This species shares many common features with *Actinomma golownini* such as the shape, size and porosity of their medullary shells and their cortical shell outline. However they differs in *Actinomma golownini* thinner cortical shell bearing four supplementary spines similar to the six radial ones and in *H.* sp. B thick cortical shell bearing numerous thorns. This species is also very similar to the arctic species *Hexalonche esmarcki* Goll & Bjørklund 1989 but differs in its larger, thicker and "thornier" cortical shell.

Hexalonche sp. G aff *H. philosophica* Haeckel 1887
(Pl. 8, figs. 7A-B, 13A-B)

Diagnosis. Square contour; crested wall; 6 tribladed spines.
Description. Three-shelled skeleton with a small polyhedral inner medullary shell, a larger spherical outer medullary shell with polygonal pores separated by thin bars, a rough, crested cortical shell with square outline and circular pores evenly arranged, and 6 radial beams projecting as short tribladed spines outside the cortical shell.
Dimensions. (based on 3 specimens) Diameter of cortical shell: 111-135; diameter of outer medullary shell: 41-51.
Remarks. It differs from *Hexalonche philosophica* in its size (~110 to 140 µm for *H.* sp. G vs ~70 to 80 µm for *H. philosophica*) and in its shell being thick and crested. Otherwise it shares with *H. philosophica* and *H. aristarchi* its characteristic square contour.

Hexalonche? sp. J
(Pl. 8, figs. 9-10B)

Diagnosis. Small, thick spherical cortical shell; 6 slender, conical spines.
Description. Two- (three-?) shelled skeleton with a spherical medullary shell and a spherical cortical shell, approximately twice as big as the medullary shell. Cortical shell is rather thick with closely-packed, large, round to elliptical pores. Six radial beams protrudes outside the cortical shell as fairly long, thin, conical spines.
Remarks. It differs from others species of *Hexacontium* and *Hexalonche* in its characteristic spines.

Genus *Hexastylus* Haeckel 1881
Type-species: *Hexastylus triaxonius* Haeckel 1881

Hexastylus triaxonius Haeckel 1887
1887 *Hexastylus triaxonius* Haeckel: p. 175; pl. 21, fig. 2
1991 *Hexastylus triaxonius* Haeckel – Takahashi: p. 71; pl. 12, figs 7-8

Genus *Joergensenium* Bjørklund et al. 2008
Type-species: *Joergensenium rotatile* Bjørklund et al. 2008

Joergensenium appolo Kamikuri 2010
2010 *Joergensenium appolo* Kamikuri: p. 99; pl. 3, figs 1a-3b, 5a-6b; pl. 4, figs 17a-c

Genus *Liosphaera* Haeckel 1882
Type-species: *Liosphaera hexagona* Haeckel 1887

Liosphaera antarctica Nakaseko 1959

1959 *Liosphaera (Craspedomma) antarctica* Nakaseko: p. 4; pl. 1, figs 1a-2c
1984 *Liosphaera antarctica* Nakaseko – Nishimura & Yamauchi: p. 31; pl. 6, figs 6-7; pl. 44, fig. 9

Genus *Lonchosphaera* Popofsky 1908

Type-species: *Lonchosphaera spicata* Popofsky 1908

Lonchosphaera spicata Popofsky 1908

1908 *Lonchosphaera spicata* Popofsky: p. 218; pl. 24, fig.2; pl. 25, figs 2, 7
1975 *Lonchosphaera spicata* Popofsky – Petrushevskaya: p. 567; pl. 17, figs 4-8
Remarks. See remarks of *Lonchosphaera*? *suzukii.*

Lonchosphaera? *suzukii* Renaudie & Lazarus in press
(Pl. 6, figs 1A-4B)

1975 *Lonchosphaera* sp. C Petrushevskaya: pl. 17, figs 11-15; non *Lonchosphaera* sp. C Petrushevskaya in Itaki et al., 2008: pl. 2, figs 4A-B.
Derivation of name. Named after Noritoshi Suzuki for his extensive contributions to radiolarian taxonomic synthesis.
Diagnosis. Cortical shell with numerous small pores and thorns; medullary shell polyhedral.
Holotype. Pl. 6, figs 1A-C; Sample 120-747A-2H-5, 45-47cm (Early Pleistocene); ECO-052, circle 1.
Material. 181 specimens were observed from ODP Sites 689, 690, 693, 744, 747, 748, 751 and 1138.
Description. The medullary shell is a simple, delicate polyhedron from which arise seven (eight?) beams that join the cortical shell and protrude as fairly long, conical spines. In some specimens, the beams seem to be connected to each other, somewhere between the medullary and the cortical shell, by arches.
The cortical shell is a rather thick sphere, with numerous small, subcircular, irregularly-distributed pores. The surface of the shell is crested and bears numerous conical by-spines often as long as the main spines and numerous small needle-like thorns. The main spines can, in some specimens, be tribladed at their base.
Dimensions. (based on 7 specimens) Diameter of the cortical shell: 110-137 (123); diameter of cortical shell pores: 3-10 (7).
Occurence. Rare from the *Stylosphaera radiosa* to the Omega Zone (Early Miocene to Holocene).
Remarks. It differs from *Lonchosphaera spicata* in its cortical shell being a spherical, latticed shell with small pores instead of an irregular, thin meshwork of anastomosed bars. It also differs from it in the presence of numerous conical by-spines and numerous thorns. It differs from *Actinomma delicatulum* (Dogiel in Dogiel & Reshetnyak, 1952) in their respective medullary shells, in the latter having a thicker wall and fewer, bigger pores and in the main spines being, in *Lonchosphaera*? *suzukii*, similar in shape and size to the by-spines. It also differs from the specimen illustrated as *Heliosoma* sp. in Takahashi, 1991 (Pl. 9, fig. 8) in that the spines, in the latter, are all connected to the medullary shell and in the bars between the pores being narrower. It finally differs from *Actinosphaera acanthophora* (Popofsky) 1912 in the radial beams being less numerous (ca. 20 in the latter vs ca. 7 in *L.? suzukii*), the number of faces of the polyhedral medullary shell, the size of the pores and the size of the spines.
Regarding the specimens of the genus *Lonchosphaera* illustrated in Petrushevskaya, 1975: the specimen identified as *Lonchosphaera* sp. B (Pl. 17, figs 9-10) shares some external similarities

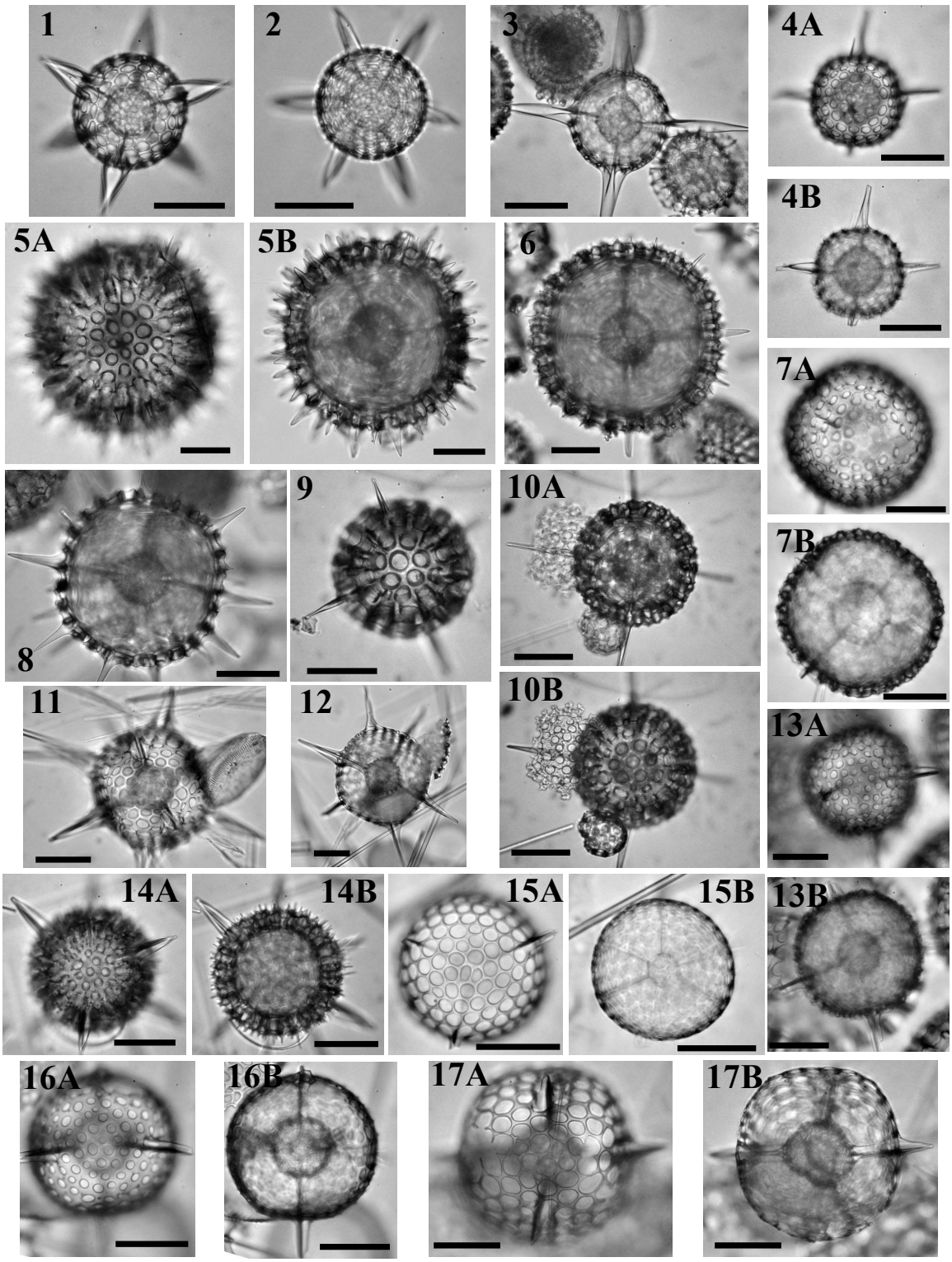

Plate 8.– 1. *Hexacontium* sp. A, Sample 119-744A-8H-1, Middle Miocene. 2. *Hexacontium* sp. A, Sample 119-744A-10H-7 16-18cm, Early Miocene. 3. *Hexacontium* sp. A, Sample 120-751A-15H-CC, Middle Miocene. 4. *Hexalonche philosophica* Haeckel 1887, Sample 120-748B-7H-6 45-47cm, Early Miocene. 5. *Hexacontium* spB, Sample 113-690B-6H-4 22-24cm, Early Miocene. 6. *Hexacontium* sp. B, Sample 119-744A-10H-1 60-62cm, Early Miocene. 7. *Hexacontium* sp. G, Sample 119-746A-11X-4 53-55cm, Late Miocene. 8. *Hexacontium* sp. B, Sample 119-744A-10H-7 16-18cm, Early Miocene. 9. *Hexacontium* sp. J, Sample 113-690B-7H-2 27-29cm, Early Miocene. 10. *Hexacontium* sp. J, Sample 113-690B-7H-2 27-29cm, Early Miocene. 11. *Actinomma golownini* Petrushevskaya 1975, Sample 119-744A-6H-4 53-55cm, Middle Miocene. 12. *Actinomma golownini*, Sample 119-744A-6H-1 53-55cm, Middle Miocene. 13. *Hexacontium* sp. G, Sample 120-748B-8H-2 45-47cm, Early Miocene. 14. *Hexacontium pachydermum* Jørgensen 1900 , Sample 119-744A-6H-1 53-55cm, Middle Miocene. 15. *Hexacontium enthacanthum* Jørgensen 1900, Sample 120-748B-6H-2 45-47cm, Early Miocene. 16. *Hexacontium laevigatum* Haeckel 1887, Sample 120-748B-6H-6 45-47cm, Early Miocene. 17. *Hexacontium aristarchi* Haeckel 1887, Sample 119-744A-6H-4 60-62cm, Middle Miocene.
All scale bars are 50 µm. Magnification x384 except for 5A-B, 6 and 12 (x192).

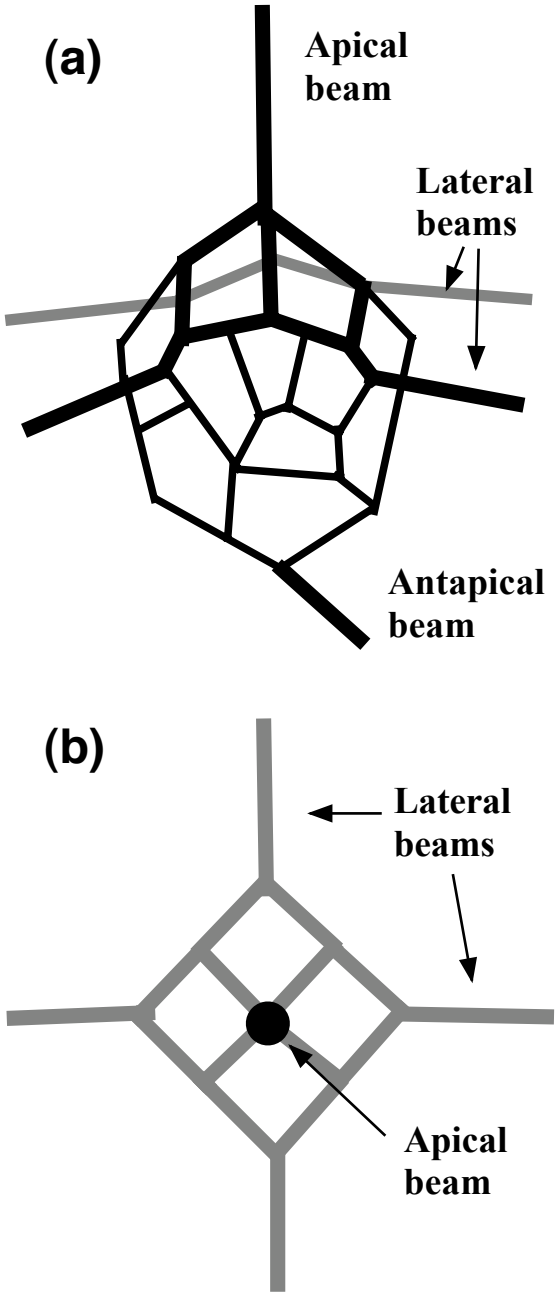

Figure 5.– Schematic illustration of *Pentactinosphaera codonia* medullary shell.
a. View from the front. Redrawn and modified after Nakaseko et al. (1983)'s illustration of *Pentactinosphaera hokurikuensis* medullary shell.
b. View of the apical structure from above.

with *L.*? *suzukii* but, because of the peculiar shape of the medullary shell in the latter, it is doubtful that they are conspecific; the specimen identified as *Lonchosphaera* sp. A (Pl. 17, fig. 3) and two of the specimens identified as *L. spicata* (Pl. 17, figs 4-5) differ from our new species in lacking additional by-spines and in their shell ratio, but they also differ from *L. spicata* in their thick latticed shell with small pores and large bars between them; the final specimen identified as *L. spicata* (Pl. 17, figs 7-8) differs from *L.*? *suzukii* in its thin cortical shell with large pores and in lacking additional by-spines as well. This specimen is closer to Popofsky's specimens but differs from them in its more regular cortical and medullary shell.

The cortical shell of *L.*? *suzukii* differs greatly from that described in Popofsky (1908)'s diagnosis of the genus; however, because of the similarities in their medullary shell and their spines, we feel that *L.*? *suzukii* and *L. spicata* are closely related, hence the tentative generic assignment. Petrushevskaya (1975)'s diagnosis for this genus varies from that of Popofsky (1908): our new species seems to fit better with her generic concept.

Lonchosphaera? sp. L
(Pl. 3, Figs 3A-B, 5A-B)

Description. Small globular cortical shell consisting of a meshwor of anastomosed bars diverging from the small, thin spines extending from the silicoflagellate-looking medullary shell. Shell ratio 1:2.

Remarks. It differs from *Lonchosphaera spicata* and *L.*? *suzukii* in its highly reduced size and its subsequently high shell ratio.

Genus *Pentactinosphaera* Nagata & Nishimura in Nakaseko et al. 1983

Type-species: *Melittosphaera hokurikuensis* Nakaseko 1955

Pentactinosphaera hokurikuensis (Nakaseko 1955)

1955 *Melittosphaera (Melittosphaera) hokurikuensis* Nakaseko: p. 70; pl. 1, figs 7a-b
1982 *Pentactinosphaera hokurikuensis* (Nakaseko) – Nakaseko et al.: p. 424; pl. 1, figs 1-3
1982 *Nanina hokurikuensis* (Nakaseko) – Kozur & Mostler: p. 409
1983 *Pentactinosphaera hokurikuensis* (Nakaseko) – Nakaseko et al.: p. 33; pl. 1, figs 1-3

Pentactinosphaera codonia Renaudie & Lazarus in press
(Pl. 5, figs 1A-6B; Fig. 4)

2001 *Hexalonche* sp. De Wever *et al.*: Pl. 133, figs 3, 8.

Derivation of name. From the Occitan *codonha* (the digraph *nh* being pronounced [ɲ]) meaning 'quince', after the shape of its medullary shell.

Diagnosis. Medullary shell as in genotype; cortical shell simple, spherical, with relatively large pores.

Holotype. Pl. 5, figs 3A-B; Sample 113-689B-3H-5, 136-138cm (Late Miocene); ECO-053.

Material. 1609 specimens were observed from ODP Sites 689, 693, 744, 751 and 1138.

Description. Relatively small cortical shell of various thickness (though, most specimens have a rather thick wall) with large, circular to subcircular pores, separated by narrow, crested bars. The pores are arranged in a rather irregular hexagonal pattern. Some additional smaller pores sometimes disturb this pattern.

The medullary shell is similar to that of *Pentactinosphaera hokurikuensis*: it consists of an ellipsoidal to pyriform meshwork with a few large, elliptical to subpolygonal pores separated by thin bars; on one end of this shell (the apical end) is a beam joining perpendicularly the apex, and four lateral beams (Pl. 5, fig. 3A; Fig. 4); on the other end (the antapical end) is a sixth beam joining the shell at an acute angle with its elongation axis. Some specimens exhibit additional beams either on the apical side or on the antapical side (see Pl. 5, fig. 2B). The beams connect the medullary and the cortical shells and, in some rare specimens, can protrude as short conical spines (see Pl. 5, fig. 1B).

Dimensions. (based on 8 specimens) Diameter of the cortical shell: 89-119 (102); length of medullary shell from apex to antapex: 28-42 (35); diameter of cortical shell pores: 4-19 (11).

Occurence. Common in the *Acrosphaera australis* and the lower part of the *Siphonosphaera vesuvius* Zone (Late Miocene) and then rare until the lower Upsilon Zone (Early Pliocene). Two specimens were also seen in the lower *Cycladophora spongothorax* Zone (Middle Miocene).

Remarks. *Pentactinosphaera codonia* differs from *P. hokurikuensis* in the latter having a typical very thick, double-layered outer shell. *P. codonia* is also noticeably smaller than *P. hokurikuensis*. It also differs from *Thecosphaera akitaensis* Nakaseko, 1972 in the shape and structure of the inner medullary shell and in lacking an outer medullary shell. *P. codonia* and *P. hokurikuensis* clearly share the same medullary shell structure, yet the cortical shell of the latter is so peculiar that it can render the assignment of our new species to genus *Pentactinosphaera* questionable.

P. hokurukuensis was previously described (Kozur & Mostler, 1982; Nakaseko et al., 1982, 1983) as belonging to the family Palaeoscenidiidae Riedel, 1967, however, as can be seen on Figure 4 and in Nakaseko et al., 1983 (Text-fig. 1), the four beams extending laterally from the medullary shell are not connected directly with the apical beam and are therefore not homologous with the Palaeoscenidiidae basal spines (see Dumitrica, 1978b; Furutani, 1982; Goodbody, 1986 for Palaeoscenidiidae morphology). Without this homology, the resemblance between the medullary shell of *P. hokurukuensis* or *P. codonia* and the shell of the members of the Palaeoscenidiidae seem to be, in our opinion, only superficial.

De Wever et al., 2001, and Dumitrica, 1985, relate the genus *Pentactinosphaera* to the family Hexalonchidae Haeckel, 1881, on the basis of the medullary shell structure described herein (refered to as a tetrapetaloid structure in De Wever et al, 2001). The only element of the structure they are describing that has not been recognized here is the element they referred to as being a 'median bar', by analogy (or homology) with the Nassellarian spicular element (Fig. 3), but it is possible that this element is either here reduced to a point, or simply that we were not able to see it due to the orientation of the specimens.

The specimen illustrated on Pl. 133, fig. 8 in De Wever et al, 2001 as *Hexalonche* sp. is very likely to be conspecific with our new species; however, since neither Haeckel's (1887) illustrations for genus *Hexalonche* (Pl. 22, 25) nor Haeckel's (1887) description of the type-species *Hexalonche phaenaxonia* Haeckel, 1887 mention this medullary shell structure, we preferred assigning this new species to genus *Pentactinosphaera* rather than to genus *Hexalonche*.

Genus *Rhizoplegma* Haeckel 1882
Type-species: *Rhizoplegma polyacanthum* Haeckel 1887

Rhizoplegma boreale (Cleve 1899)
(Pl. 7, figs 8A-B)
1899 *Hexadoras boreale* Cleve: p. 30; pl. 2, fig. 4
1900 *Rhizoplegma boreale* (Cleve) – Jørgensen: p. 61-62
1967 *Rhizoplegma*? *boreale* (Cleve) – Petrushevskaya: p. 12-14; pl. 8, figs 1-2

Genus *Sphaeropyle* Dreyer 1889
Type-species: *Sphaeropyle langii* Dreyer 1889

Sphaeropyle antarctica (Dreyer 1889) emend. Nishimura 2003
1889 *Prunopyle antarctica* Dreyer: p. 100-101; pl. 10, fig. 75
1967 *Cromyechinus antarctica* (Dreyer) – Petrushevskaya: p. 25-30; fig. 14
1975 *Prunopyle antarctica* Dreyer – Chen: p. 454; pl. 23, figs 5-6
2003 *Prunopyle antarctica* Dreyer – Nishimura: p. 197-198; pl. 1

Sphaeropyle langii Dreyer 1889
1889 *Sphaeropyle langii* Dreyer: p. 89, fig. 54
1973 *Sphaeropyle langii* Dreyer – Kling: p. 634; pl. 1, figs 5-10; pl. 13, figs 6-8
2006 *Sphaeropyle langii* Dreyer – Suzuki: p. 861-863; text-fig. 3

Sphaeropyle robusta Kling 1973
1973 *Sphaeropyle robusta* Kling: p. 634; pl. 1, figs 11-12; pl. 6, figs 9-13; pl. 13, figs 1-5
2006 *Sphaeropyle robusta* Kling – Suzuki: p. 863-865; pl. 3-4; pl. 10-12

Genus *Sphaerostylus* Haeckel 1882
Type-species: *Sphaerostylus zitteli* Rüst 1885

Sphaerostylus rosetta? Blueford 1982
(Pl. 9, figs 16A-B)
? 1982 *Sphaerostylus rosetta* Blueford: p. 202; pl. 7, figs 1-2

Genus *Spongoplegma* Haeckel 1881
Type-species: *Spongoplegma antarcticum* Haeckel 1887

Spongoplegma antarcticum Haeckel 1887
(Pl. 7, figs 5A-B)
1887 *Spongoplegma antarcticum* Haeckel: p. 90
1958 *Diploplegma banzare* Riedel: p. 223; pl. 1, figs 3-4

1967 *Actinomma antarcticum* (Haeckel) – Nigrini: p. 26-27; pl. 2, figs 1a-d
1985 *Rhizosphaera antarcticum* (Haeckel) – Caulet: p. 853

Spongoplegma holtedahli (Bjørklund 1976a)
(Pl. 7, figs 7A-B)

1976a *Actinomma holtedahli* Bjørklund: p. 1121; pl. 20, figs 8-9
1990 *Actinomma holtedahli* Bjørklund – Abelmann: pl. 1, figs 4a-b

Spongoplegma arcadophorum (Haeckel 1887)
(Pl. 7, figs 2A-B)

1887 *Actinomma arcadophorum* Haeckel: p. 225; pl. 29, figs 7-8
1967 *Actinomma arcadophorum* Haeckel – Nigrini: p. 29; pl. 2, fig. 3

Spongoplegma medianum (Nigrini 1967)
(Pl. 7, figs 3A-B)

1959 *Actinomma (Actinommilla) capillaceum* Nakaseko: p. 11-12; pl. 3, figs 2a-b non *Actinomma capillaceum* Haeckel 1887
1967 *Actinomma medianum* Nigrini: p. 27; pl. 2, figs 2a-b
1979 *Actinomma medianum* Nigrini – Nigrini & Moore: p. S31-32; pl. 3, figs 5-6

Spongoplegma variabile Nakaseko 1971
(Pl. 7, figs 9A-B)

1971 *Spongoplegma variabilium* Nakaseko: p. 54; pl. 1, figs 1a-3
1974 *Spongoplegma variabile* Nakaseko – Nakaseko & Nishimura: p. 49; pl. 2, figs 4a-b

Spongoplegma sp. D
(Pl. 7, figs 1A-B, 4A-B, 6A-B)

Diagnosis. Dense medullary meshwork; shell ratio of 1:2; thick latticed cortical shell with large, irregular pores.

Description. Two concentric shells consisting of a thick, latticed cortical shell and a medullary meshwork both connected by a fairly high number of rather thin, cylindrical (rarely bladed) radial beams. There is a depression on the cortical shell where each radial beam fuses with the shell, thus creating a "bumpy" surface. Pores on the cortical shell are rounded to elliptical, of variable size (but somewhat large) and unevenly distributed. They are separated by thick, cylindrical bars. The medullary meshwork is two times smaller than the cortical shell and is somewhat dense. It has a general spherical shape but has a cupola-shaped extension where the radial beams arise. It seems that the very center of this medullary meshwork is denser and has a more regular geometrical pattern; but, due to the already substantial density of the meshwork, it is difficult to observe it.

Remarks. *S.* spD differs from *S. antarticum, S. medianum* and *S. holtedahli* in having a thick, latticed cortical shell (compared to a thin meshwork of anastomed bars). It also differs from *S. variabile* in having a thicker wall, bigger, unequal pores, a smaller but denser medullary meshwork and a "bumpy" surface.

Genus *Stauroxiphos* Haeckel 1887

Type-species: *Stauroxiphos gladius* Haeckel 1887

Stauroxiphos communis Carnevale 1908

1908 *Stauroxiphos communis* Carnevale: p. 15; pl. 2, fig. 9
1944 *Lithatractus timmsi* Campbell & Clark: p. 18; pl. 2, figs 18-19
1982 *Druppatractus nanus* Blueford; p. 204; pl. 7, figs 3a-4
1990 *Stauroxiphos communis* Carnevale – Abelmann: p. 692; pl. 2, fig. 12
1992 *Lithatractus timmsi* Campbell & Clark – Lazarus: pl. 4, figs 10-12

Remarks. The two species *S. communis* and *L. timmsi* were lumped into one species here because middle to late Miocene specimens assignment to one or the other species was problematic; however early to middle Miocene specimens are all clearly *S. communis* (large thick shell, with three thick tribladed spines on one pole and one long sword-like spine on the other) while late Miocene specimens are all clearly *L. timmsi* (smaller shell with one middle-lengthed tribladed spine on one pole and one to three small spines on the other and a pyriform medullary shell).

Genus *Stylacontarium* Popofsky 1912

Type-species: *Stylacontarium bispiculum* Popofsky 1912

Stylacontarium acquilonium (Hays 1970)

1970 *Druppatractus acquilonius* Hays: p. 214; pl. 1, figs 4-5
1973 *Stylacontarium acquilonium* (Hays) – Kling: p. 634; pl. 1, figs 17-20; pl. 14, figs 1-4

Stylacontarium bispiculum Popofsky 1912

1912 *Stylacontarium bispiculum* Popofsky: p. 91; pl. 2, fig. 2
1975 *Stylacontarium bispiculum* Chen: pl. 21, figs 1-2

Genus *Stylatractus* Haeckel 1887

Type-species: *Amphistylus neptunus* Haeckel 1878

Stylatractus neptunus (Haeckel 1878)

1878 *Amphistylus neptunus* Haeckel
1887 *Stylatractus neptunus* (Haeckel) – Haeckel: p. 328; pl. 17, fig. 6
1958 *Stylatractus neptunus* (Haeckel) – Riedel: p. 226; pl. 1, fig. 9
1990 *Stylatractus neptunus* (Haeckel) – Abelmann: pl. 2, figs 8-9

Stylatractus santaeannae (Campbell & Clark 1944)

1944 *Lithatractus santaeannae* Campbell & Clark: p. 19; pl. 2, figs 20-22
1972 *Stylatractus santaeannae* (Campbel & Clark) – Petrushevskaya & Kozlova: p. 510; pl. 11, fig. 10
1975 *Amphisphaera santaeannae* (Campbell & Clark) – Petrushevskaya: p. 570; pl. 2, fig. 2
1990 *Stylatractus santaeannae* (Campbell & Clark) – Abelmann: pl. 2, fig. 6

Stylatractus universus Hays 1970

1965 *Stylatractus* sp. Hays: p. 167; pl. 1, fig. 6
1970 *Stylatractus universus* Hays: p. 215; pl. 1, figs 1-2
1975 *Stylatractus universus* Hays – Chen: p. 455; pl. 21, fig. 5-9

Stylatractus sp. C

(Pl. 6, figs 5A-6B)

Description. Large prunoid cortical shell with very thick wall and large, relatively closely-

packed (five to six pores at the equator of the shell) circular pores, that are quincuncially arranged. Two large, smooth, conical polar spines with broad bases are present. No medullary shell was observed to date.

Remarks. This species differs from the Eocene species *Stylosphaera coronata coronata* Ehrenberg 1873a in its elliptic outline and its conical spines (instead of the characteristics sword-like spines of *S. c. coronata*).

Stylatractid sp. A
(Pl. 27, figs 11, 14)

Description. Three-shells: an ellipsoidal cortical shell bearing a multitude of needle-like thorns projecting from bar nodes, a thin, ellipsoidal outer medullary shell and a polyhedral inner medullary shell. Two polar spines (one smaller than the other) are present: these are conical, yet can be tribladed at their base.

Remarks. It differs from *Druppatractus hastatus* in being covered with thorns and in the later having usually a deformed cortical shell where the equatorial radial beams join the shell.

Genus *Stylosphaera* Ehrenberg 1847

Type-species: *Stylosphaera hispida* Ehrenberg 1854

Stylosphaera angelina Campbell & Clark 1944

1944 *Stylosphaera angelina* Campbell & Clark: p. 12; pl. 1, figs 14-20
1973 *Axoprunum angelinum* (Campbell & Clark) – Kling: p. 634; pl. 6, fig. 18, non figs 14-17
1975 *Amphystylus angelinus* (Campbell & Clark) – Chen: pl. 21, figs 3-4

Stylosphaera laevis Ehrenberg 1873a

1873a *Stylosphaera laevis* Ehrenberg: p. 259
1875 *Stylosphaera laevis* Ehrenberg – Ehrenberg: pl. 25, fig. 6
1973 *Stylosphaera coronata laevis* (Ehrenberg) – Sanfilippo & Riedel: p. 520; pl. 1, fig. 19; pl. 25, figs 5-6

Stylosphaera minor Clark & Campbell 1942

1942 *Stylosphaera minor* Clark & Campbell: p. 16; pl. 1, figs 13-14
1972 *Stylosphaera minor* Clark & Campbell – Petrushevskaya & Kozlova: p. 520; pl. 10, fig. 4

Stylosphaera radiosa Ehrenberg 1854

1854 *Stylosphaera radiosa* Ehrenberg: p. 256
1875 *Stylosphaera radiosa* Ehrenberg – Ehrenberg: pl. 24, fig. 5
1975 *Amphisphaera radiosa* Ehrenberg – Petrushevskaya: p. 570; pl. 2, figs 18-20
1990 *Stylosphaera radiosa* Ehrenberg – Abelmann: p. 692; pl. 2, figs 4a-c

Genus *Thecosphaera* Haeckel 1881

Type-species: *Thecosphaera unica* Rüst 1885

Thecosphaera inermis (Haeckel 1860)

1860 *Haliomma inerme* Haeckel: p. 815
1862 *Actinomma inerme* (Haeckel) – Haeckel: p. 440; pl. 24, fig. 5
1887 *Thecosphaera inermis* (Haeckel) – Haeckel: p. 80
1980 *Thecosphaera inermis* (Haeckel) – Boltovskoy & Riedel: p. 114; pl. 3, fig. 6

Thecosphaera japonica Nakaseko 1971
1971 *Thecosphaera japonica* Nakaseko: p. 61; pl. 1, figs 3a-b
1996 *Thecosphaera japonica* Nakaseko – Motoyama: p. 252; pl. 2, figs 3a-b

Thecosphaera miocenica Nakaseko 1955
1955 *Thecosphaera (Thecosphaera) miocenica* Nakaseko: p. 73; pl. 2, figs 1a-b
1971 *Thecosphaera miocenica* Nakaseko – Nakaseko: p. 60; pl. 1, figs 1a-b
1996 *Thecosphaera miocenica* Nakaseko – Motoyama: p. 252; pl. 2, figs 4a-b

Thecosphaera pseudojaponica Nakaseko 1971
1971 *Thecosphaera pseudojaponica* Nakaseko: p. 62; pl. 1, figs 8a-b
1996 *Thecosphaera pseudojaponica* Nakaseko – Motoyama: p. 252; pl. 2, figs 5a-b

Thecosphaera sanfilippoae Blueford 1982
1982 *Thecosphaera sanfilippoae* Blueford: p. 199; pl. 5, figs 5-6

Family **Ethmosphaeridae** Haeckel 1862

Genus *Plegmosphaera* Haeckel 1881
Type-species: *Plegmosphaera maxima* Haeckel 1887

Plegmosphaera lepticali? Renz 1976
(Pl. 7, figs 10A-B)
? 1976 *Plegmosphaera lepticali* Renz: p. 115; pl. 1, fig. 14
? 1981 *Plegmosphaera lepticali* Renz – Takahashi & Honjo: p. 146; pl. 1, figs 15-16

Genus *Styptosphaera* Haeckel 1881
Type-species: *Styptosphaera spumacea* Haeckel 1887

Styptosphaera spongiacea Haeckel 1887
(Pl. 7, fig. 11)
1887 *Styptosphaera spongiacea* Haeckel 1887
1991 *Styptosphaera spongiacea* Haeckel – Takahashi: p. 63; pl. 6, figs 6-7, 9

Family **Coccodiscidae** Haeckel 1862 emend. Sanfilippo & Riedel 1980

Genus *Circodiscus* Kozlova in Petrushevskaya & Kozlova 1972
Type-species: *Trematodiscus microporus* Stöhr 1880

Circodiscus ellipticus (Stöhr 1880)
1880 *Trematodiscus ellipticus* Stöhr: p. 108; pl. 4, fig. 16
1887 *Porodiscus ellipticus* (Stöhr) – Haeckel: p. 494
1975 *Circodiscus ellipticus* (Stöhr) – Petrushevskaya: p. 575; pl. 6, figs 1-6

Genus *Diartus* Sanfilippo & Riedel 1980
Type-species: *Ommatocampe hughesi* Campbell & Clark 1944

Diartus hughesi (Campbell & Clark 1944)

1944 *Ommatocampe hughesi* Campbell & Clark: p. 23; pl. 3, fig. 12
1980 *Diartus hughesi* (Campbell & Clark) – Sanfilippo & Riedel: p. 1010; text-fig. 1i
1983 *Diartus hughesi* (Campbell & Clark) – Weaver: pl. 5, fig. 1

Genus *Didymocyrtis* Haeckel 1860 emend. Riedel 1967

Type-species: *Haliomma didymocyrtis* Haeckel 1862

Didymocyrtis laticonus (Riedel 1959)

1959 *Cannartus laticonus* Riedel: p. 291; pl. 1, fig. 5
1980 *Didymocyrtis laticonus* (Riedel) – Sanfilippo & Riedel: text-fig. 1e

Didymocyrtis violina (Haeckel 1887)

1887 *Cannartus violina* Haeckel: p. 538; pl. 39, fig. 10
1959 *Cannartus violina* Haeckel – Riedel: pl. 1, fig. 3
1980 *Didymocyrtis violina* (Riedel) – Sanfilippo & Riedel: text-fig. 1d

Genus *Heliodiscus* Haeckel 1862

Type-species: *Haliomma phacodiscus* Haeckel 1860

Heliodiscus asteriscus Haeckel 1887

1887 *Heliodiscus asteriscus* Haeckel: p. 445; pl. 33, fig. 8
1991 *Heliodiscus asteriscus* Haeckel – Takahashi: p. 89; pl. 23, figs 1-3

Heliodiscus decorus (Ehrenberg 1873a)

1873a *Periphaena decora* Ehrenberg: p. 246
1875 *Periphaena decora* Ehrenberg – Ehrenberg: pl. 28, fig. 6
1973 *Periphaena decora* Ehrenberg – Sanfilippo & Riedel: p. 523; pl. 8, figs. 8-10; pl. 27, figs. 2-5

Genus *Sethodiscus* Haeckel 1881

Type-species: *Haliomma radiatum* Ehrenberg 1854b

Sethodiscus? *pravus* Renaudie & Lazarus in press

(Pl. 5, figs 7A-10B)

Derivation of name. From the latin *pravus* meaning 'misshaped'.

Diagnosis. Pyriform medullary shell from which thick beams project; cortical shell outline reniform or trilobate.

Holotype. Pl. 5, figs 7A-B; Sample 120-748B-8H-4 45-47cm (Early Miocene); ECO-054.

Material. 43 specimens were observed from ODP Site 748.

Description. Flattened ellipsoid (see Remarks) with a medullary and a cortical shell. The medullary shell is somewhat pyriform with a few large, circular to polygonal pores and narrow, crested bars (see Pl. 2, fig. 8). One or several thick beams on each side of the medullary shell and one or two at one of the apex projects to join the cortical shell. Several other shorter beams also seem to project from the upper and the lower side (i.e. in the direction of the shell flattening; see pl. 2, figs 7A, 10A-B) of the medullary shell and also connect to the cortical shell. The junction of these beams with the cortical shell creates, in most cases, a depression on the latter, thus deforming its outline from subcircular to clover-shaped (see Pl. 5, figs 7A-8). In

some specimens, the depth of the depression is irregular, in which case the outline can be reniform (see Pl. 5, figs 10A-B). Pores on the cortical shell are circular, somewhat irregular in size (generally moderately small) and regularly placed, except in the areas of shell depression where their placement becomes irregular (see Pl. 5, figs 7A and 10A). Bars between the pores are of various thickness and generally crested.

Dimensions. (based on 8 specimens) Maximum diameter of the cortical shell: 70-105 (93); length of the internal beams: 15-34 (24); length of the medullary shell: 32-40 (36).

Occurence. Rare to common in the *Stylosphaera radiosa* Zone (Late Oligocene to Early Miocene).

Remarks. This species has been tentatively assigned to the genus *Sethodiscus* because of the flattening of the shell and the several short radial beams joining the medullary and the cortical shells. However there are many differences between this species, *S. macrococcus* Haeckel, 1887 and *S. lenticularis* Haeckel, 1887 which includes a deformed cortical shell, pyriform medullary shell and radial beams in the equatorial plane as well as in the direction of the shell flattening. As was shown in Suzuki *et al*., 2009, the type-species of the genus, *Sethodiscus radiatum,* is in fact a sponge spicule and not a radiolarian which renders the genus improper for these forms. Pending a full revision of this group we however use *Sethodiscus*.

No specimen was seen in profile view, so the extant of the shell flattening cannot be assessed with certainty; however, under the microscope, the distance between the focal plane of the outer shell wall and that of the medullary shell wall seems very short (probably ca. 5 µm).

Family **Litheliidae** Haeckel 1862

Prunoid? sp. D
(Pl. 9, figs 8-9B)

Description. Globular, deformed shell with a thin cortical shell with round to elliptical pores that are irregular in size and disposition. Inside the cortical shell, the medullary shell seems to be composed of a random meshwork of cylindrical bars (Pl. 9, fig. 9B).

Prunoid sp. G
(Pl. 9, figs 5A-C, 11A-12B)

Description. Large spherical to elliptical shell with a small hyaline cylindrical to truncated-conical pylome. Pores on the shell are regularly-arranged, small and round. They are surrounded by a pore frame with raised apices thus giving the shell a rough, crested aspect. One specimen (Pl. 9, figs 5A-C) shows a double-layer of thinner material overgrowing this structure. Pores on this other layer are smaller, more irregular both in shape and in arrangement.

Remarks. The overall shape of this species (in particular for the specimen illustrated on Pl. 9, figs 5A-C) resembles *Enamelon imemmestrum* Sugyama 1992b and *Prunopyle frakesi* Chen 1975 but their peculiar inner structure have not been observed in any of the specimens of Prunoid sp. G.

Genus *Larcopyle* Dreyer 1889 emend. Lazarus et al. 2005

Type-species: *Larcopyle buetschlii* Dreyer 1889

Larcopyle augusti Lazarus et al. 2005

1975 Sponguridae gen. sp. D Petrushevskaya: p. 577; pl. 4, fig. 1

2005 *Larcopyle augusti* Lazarus et al.: p. 113-115; pl. 8, figs 1-13

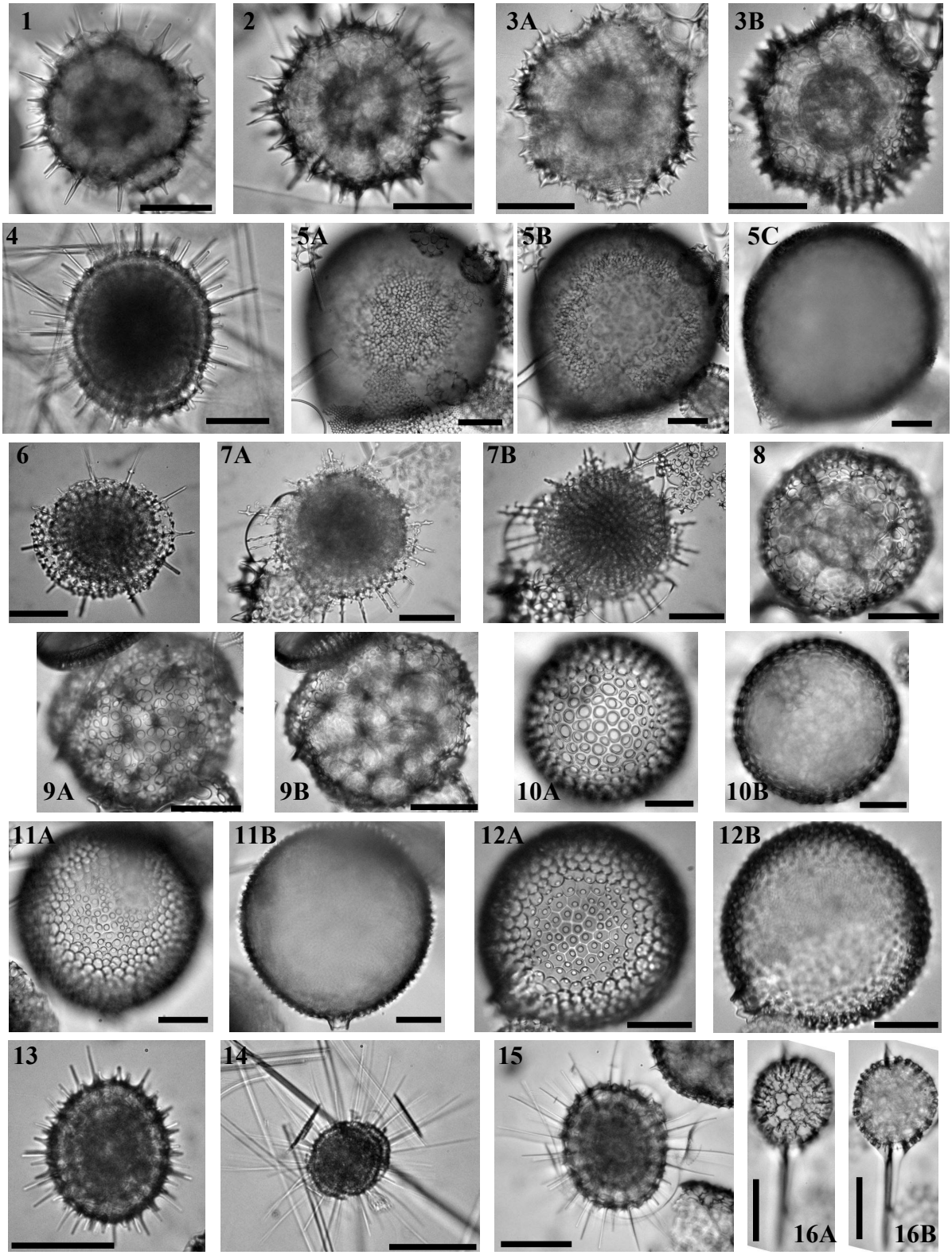

Plate 9.–
1. Spumellarian sp. A, Sample 119-746A-6H-2 53-55cm, Late Miocene. 2. Spumellarian sp. A, Sample 120-751A-17H-CC, Early Miocene. 3. Spumellarian sp. A, Sample 119-744A-8H-1, Middle Miocene. 4. Spongodiscid sp. G, Sample 119-744A-6H-4 53-55cm, Middle Miocene. 5. Prunoid sp. G, Sample 120-748B-8H-3 45-47cm, Early Miocene. 6. Spongodiscid sp. A, Sample 120-747A-7H-7 45-47cm, Middle Miocene. 7. Spongodiscid sp. A, Sample 120-751A-13H-2 98-102cm, Middle Miocene. 8. Prunoid sp. D, Sample 119-744A-2H-4 53-55cm, Late Pliocene. 9. Prunoid sp. D, Sample 119-746A-14X-1 53-55cm, Late Miocene. 10. *Cenosphaera*? sp. K, Sample 119-744A-4H-4 59-61cm, Late Miocene. 11. Prunoid sp. G, Sample 120-751A-9H-5 98-102cm, Late Miocene. 12. Prunoid sp. G, Sample 119-744A-7H-2 53-55cm, Middle Miocene. 13. Spongodiscid sp. H, Sample 119-738B-2H-3 53-55cm, Late Pliocene. 14. Spongodiscid s. pH, Sample 120-747A-1H-1 45-47cm, Pleistocene. 15. Spongodiscid sp. H, Sample 120-747A-2H-2 45-47cm, Pleistocene. 16. *Sphaerostylus rosetta*? Blueford 1982, Sample 119-744A-8H-3 53-55cm, Middle Miocene.
All scale bars 50 µm. Magnification x384 except for 5A-C and 10A-11B (x192).

Larcopyle buetschlii Dreyer 1889

1889 *Larcopyle Bütschlii* Dreyer: p. 124; pl. 5, fig. 70
2005 *Larcopyle buetschlii* Dreyer – Lazarus et al.: pl. 1, figs 10-14

Larcopyle eccentricum Lazarus et al. 2005

1990 *Prunopyle titan* Campbell & Clark – Abelmann: p. 693; pl. 3, fig. 16
2005 *Larcopyle eccentricum* Lazarus et al.: p. 111; pl. 6, figs 1-15

Larcopyle hayesi (Chen 1975)

1975 *Prunopyle hayesi* Chen: p. 454; pl. 9, figs 3-5
2005 *Larcopyle hayesi* (Chen) – Lazarus et al.: p. 119-120; pl. 11, figs 1-21

Larcopyle labyrinthusa Lazarus et al. 2005

1989 *Lithelius*? spp. group A Lazarus & Pallant: p. 367; pl. 8, fig. 5 non pl. 8, figs. 6, 11-12
2005 *Larcopyle labyrinthusa* Lazarus et al.: p. 111; pl. 5, figs 14-24

Larcopyle nebulum Lazarus et al. 2005

1975 *Lithocarpium polyacantha* Campbell & Clark – Petrushevskaya: p. 572; pl. 3, fig. 6; non pl. 3, figs 7-8; pl. 29, fig. 6
2005 *Larcopyle nebulum* Lazarus et al.: p. 111; pl. 5, figs 1-13

Larcopyle peregrinator Lazarus et al. 2005

2005 *Larcopyle peregrinator* Lazarus et al.: p. 111-113; pl. 7, figs 1-16

Larcopyle polyacantha polyacantha (Campbell & Clark 1944)

1944 *Larnacantha polyacantha* Campbell & Clark: p. 30-31; pl. 5, figs 4-7
1975 *Lithocarpium polyacantha* (Campbell & Clark) – Petrushevskaya: p. 572; pl. 3, figs 6-8
2005 *Larcopyle polyacantha* (Campbell & Clark) – Lazarus et al.: p. 106-108; pl. 2, figs 8-9, 13

Larcopyle polyacantha (Campbell & Clark 1944) *amplissima* Lazarus et al. 2005

1975 *Lithocarpium fragilis* (Stöhr) – Petrushevskaya: p. 572; pl. 4, fig. 4
1990 *Prunopyle* sp. D Abelmann: p. 693-694; pl. 4, fig. 1a-b
2005 *Larcopyle polyacantha amplissima* Lazarus et al.: p. 108; pl. 4, figs 1-10

Larcopyle polyacantha (Campbell & Clark 1944) *titan* Lazarus et al. 2005

1975 *Prunopyle titan* Campbell & Clark – Chen: p. 454; pl. 23, figs 1-2
1990 *Prunopyle titan* Chen – Lazarus: p. 717; pl. 5, figs 1, 3-4
2005 *Larcopyle polyacantha titan* Lazarus et al.: 108; pl. 3, figs 1-12

Larcopyle pylomaticus (Riedel 1958)

1958 *Spongurus pylomaticus* Riedel: p. 226; pl. 1, figs 10-11
1975 *Spongurus pylomaticus* Riedel – Petrushevskaya: p. 577; pl. 7, fig. 4
2005 *Larcopyle pylomaticus* (Riedel) – Lazarus et al.: p. 115-117; pl. 9, figs 1-12

Larcopyle titan (Campbell & Clark 1944)

1944 *Prunoyple titan* Campbell & Clark: p. 20-21; pl. 3, figs 1-3
2005 *Larcopyle titan* (Campbell & Clark) – Lazarus et al.: p. 108-111; pl. 4, figs 11-17

Larcopyle weddelium Lazarus et al. 2005

2005 *Larcopyle weddelium* Lazarus et al.: p. 117-118; pl. 10, figs 1-14

Genus *Larcospira* Haeckel 1887

Type-species: *Larcospira quadrangula* Haeckel 1887

Larcospira moschkovskii Kruglikova 1978

1978 *Larcospira moschkovskii* Kruglikova: p. 88-89; pl. 27, figs 3-6
2009 *Larcospira moschkovskii* Kruglikova – Kamikuri et al.: pl. 8, fig. E

Larcospira quadrangula Haeckel 1887

1887 *Larcospira quadrangula* Haeckel:p. 696; pl. 49, fig. 3
1978 *Larcospira quadrangula* Haeckel – Kruglikova: pl. 27, fig. 1
1981 *Larcospira quadrangula* Haeckel – Takahashi & Honjo: p. 150; pl. 6, fig. 2

Genus *Lithelius* Haeckel 1862

Type-species: *Lithelius spiralis* Haeckel 1862

Lithelius hexaxyphophorus (Clark & Campbell 1942)

1942 *Stylosphaera hexaxyphophora* Clark & Campbell: p. 28, pl. 6, figs 4-5, 7, 11-12
1973 *Lithelius hexaxyphophorus* (Clark & Campbell) – Sanfilippo & Riedel: p. 522; pl. 7, figs. 7-9; pl. 26, figs. 6-7
2005 *Lithelius hexaxyphophorus* (Clark & Campbell) – Funakawa et al.: pl. P17, figs 7a-9

Lithelius minor Jørgensen 1900

1900 *Lithelius minor* Jørgensen: p. 65-66; pl. 5, fig. 24

Lithelius nautiloides Popofsky 1908

1908 *Lihelius nautiloides* Poposfky: p. 230-231; pl. 27, fig. 2-4
1958 *Lihelius nautiloides* Poposfky – Riedel: p. 228-229; pl. 2, figs 3-4; text-fig. 2

Family **Porodiscidae** Haeckel 1881

Genus *Perichlamydium* Ehrenberg 1847

Type-species: *Flustrella praetexta* Ehrenberg 1844

Perichlamydium praetextum (Ehrenberg 1844)

1844 *Flustrella praetexta* Ehrenberg: p. 81
1854 *Perichlamydium praetextum* (Ehrenberg) – Ehrenberg: pl. 22, fig. 20
1975 *Perichlamydium praetextum* (Ehrenberg) group – Petrushevskaya: p. 575; pl. 6, fig. 10

Genus *Stylochlamidium* Haeckel 1881

Type-species: *Stylochlamydium asteriscus* Haeckel 1887

Stylochlamydium venustum (Bailey)

1856 *Perichlamydium venustum* Bailey: p.5; pl. 1, figs 16-17
1887 *Stylochlamydium venustum* (Bailey) – Haeckel: p. 515
1980 *Stylochlamydium venustum* (Bailey) – Boltovskoy & Riedel: p. 118; pl. 4, fig. 3

Genus *Stylodictya* Ehrenberg 1847
Type-species: *Stylodictya gracilis* Ehrenberg 1854

Stylodictya aculeata Jørgensen 1905
1905 *Stylodictya aculeata* Jørgensen: p. 119-120; pl. 10, figs 41a-c
1967 *Stylodictya aculeata* Jørgensen – Petrushevskaya: p. 32; pl. 17, figs 1-3

Stylodictya ocellata Ehrenberg 1873a
1873a *Stylodictya ocellata* Ehrenberg: p. 258
1875 *Stylodictya ocellata* Ehrenberg – Ehrenberg: pl. 23, fig. 7
1975 *Xiphospira ocellata* (Ehrenberg) – Petrushevskaya: p. 576; pl. 7, fig. 11

Stylodictya validispina Jørgensen 1905
1905 *Stylodictya validispina* Jørgensen: p. 119; pl. 10, fig. 40
1967 *Stylodictya validispina* Jørgensen – Petrushevskaya: p. 30-31; pl. 17, figs 4-5

Family **Pyloniidae** Haeckel 1881 emend. Dumitrica 1989

Genus *Dipylissa* Dumitrica 1988
Type-species: *Dipylissa bensoni* Dumitrica 1988

Dipylissa bensoni Dumitrica 1988
1966 *Spirema* sp. Benson: p. 268; pl. 18, figs 9-10.
1988 *Dipylissa bensoni* Dumitrica: p. 190-192; pl. 3, figs 1-7; pl. 4, figs 11-15; pl. 6, figs 1-15.

Genus *Hexapyle* Haeckel 1881
Type-species: *Hexapyle triangula* Haeckel 1887

Hexapyle dodecantha Haeckel 1887
1887 *Hexapyle dodecantha* Haeckel: p. 569; pl. 48, fig. 16
1981 *Hexapyle dodecantha* Haeckel – Takahashi & Honjo: p. 150; pl. 6, fig. 3
2008 *Hexapyle dodecantha* Haeckel – Kamikuri et al.: pl. 2, fig. 29

Genus *Octopyle* Haeckel 1881
Type-species: *Octopyle ovulina* Haeckel 1887

Octopyle stenozona Haeckel 1887
1887 *Octopyle stenozona* Haeckel: p. 652; pl. 9, fig. 11
1981 *Octopyle stenozona* Haeckel – Takahashi & Honjo: p. 150; pl. 6, fig. 7

Genus *Pentapylonium* Dumitrica 1991
Type-species: *Pentapylonium implicatum* Dumitrica 1991

Pentapylonium implicatum Dumitrica 1991
1991 *Pentapylonium implicatum* Dumitrica: p. 37-46; pl. 2, figs 1-7; pl. 3, figs 1-3; pl. 5, figs 1-9; pl. 6, figs 1-9; pl. 7, figs 1-7
1992 *Pentapylonium implicatum* Dumitrica – Nigrini & Caulet: p. 146; pl. 1, figs 9-10

Genus *Phorticium* Haeckel 1881

Type-species: *Phorticium pylonium* Haeckel 1887

Phorticium clevei (Jørgensen)

1899 *Phorticium pylonium* Haeckel – Cleve: p. 31; pl. 3, fig. 2a-b non fig. 2c

1900 *Tetrapylonium clevei* Jørgensen: p. 64

1967 *Phorticium clevei* (Jørgensen) – Petrushevskaya: p. 58; pl. 32, figs 1-2; pl. 33, figs 1-3; pl. 34, figs 1-5

Genus *Streblacantha* Haeckel 1887

Type-species: *Streblacantha siderolina* Haeckel 1887

Streblacantha circumtexta (Jørgensen 1900)

1900 *Sorolarcus circumtexta* Jørgensen: p. 65

1905 *Streblacantha circumtexta* (Jørgensen) – Jørgensen: p. 121-122; pl. 11, figs 46a-e; pl. 12, figs 46g-k

1976a *Streblacantha circumtexta* (Jørgensen) – Bjørklund: pl. 5, figs 9-12

Genus *Tetrapyle* Müller 1858

Type-species: *Tetrapyle octacantha* Müller 1858

Tetrapyle octacantha Müller 1858

1858 *Tetrapyle octacantha* Müller: p. 33; pl. 2, figs 12-13; pl. 3, figs 1-12

1979 *Tetrapyle octacantha* Müller – Nigrini & Moore: p. S125; pl. 16, figs 3a-b

1981 *Tetrapyle octacantha* Müller – Takahashi & Honjo: p. 150; pl. 6, figs 5-6

Family **Saturnalidae** Deflandre 1953

Genus *Saturnalis* Haeckel 1881 emend. Nigrini 1967

Type-species: *Saturnalis circularis* Haeckel 1887

Saturnalis circularis Haeckel 1887

1887 *Saturnalis circularis* Haeckel: p. 131

1967 *Saturnalis circularis* Haeckel – Nigrini: p. 25; pl. 1, fig. 9

Family **Spongodiscidae** Haeckel 1862

Spongodiscid sp. G

(Pl. 9, fig. 4)

Remarks. This species resembles *Larcopyle hayesi* in the shell layers' disposition and the numerous radial beams. It differs however from it in that the radial beams extend outside as fairly long conical spines. The shell seems also to be more spherical than prunoid.

Spongodiscid sp. A

(Pl. 9, figs 6-7B)

Description. Lenticular shell consisting of numerous concentric, closely-packed layers joined together by a multitude of radial beams extending outside the outermost shell as thin spines.

Remarks. It differs form the various species of genus *Spongodiscus* in possessing radial spines, in species of genus *Spongotrochus* in lacking additional, stronger spines and in species of genus *Stylodictya* in being lenticular and in the layers being closely-packed.

Spongodiscid sp. H
(Pl. 9, figs 13-15)

1979 *Lithelius minor* Jørgensen – Nigrini & Moore: pl. 17, fig. 3.
1980 *Lithelius* sp. aff *L. spiralis* Boltovskoy & Riedel: 118-119; pl. 4, fig. 6.
? 1987 *Lithelius* spp. Boltovskoy & Riedel: pl. 3, fig. 7
? 2002 *Lithelius minor* Jørgensen – Cortese & Abelmann: pl. 2, fig. 2.

Description. The elliptical shell is composed on several concentric layers closely linked together by numerous thin radial beams extending outside the outermost layer as long, thin spines. The shell is usually rather small (~50 μm) but the spines can be as long as the shell itself (see Pl. 9, fig. 14).

Remarks. The innermost part of the shell has not been observed to date: the assignment of this species to the Spongodiscidae is therefore purely tentative (the species could indeed be a Pyloniidae). Indeed, this species appeared frequently in the literature as belonging to genus *Lithelius* (see synonymy list). It differs from *Lithelius minor* Jørgensen 1900 in lacking a spiral arrangment of the different layers and in being smaller.

Genus *Amphirhopalum* Haeckel 1881

Type-species: *Amphirhopalum ximorphum* Haeckel 1887

Amphirhopalum ypsilon Haeckel 1887

1887 *Amphirhopalum ypsilon* Haeckel: p. 522
1967 *Amphirhopalum ypsilon* Haeckel – Nigrini: p. 35; pl. 3, figs 3a-d

Genus *Amphymenium* Haeckel 1881

Type-species: *Amphymenium zygartus* Haeckel 1887

Amphymenium amphystylium Haeckel 1887 emend. Morley & Nigrini 1995

1887 *Amphymenium amphystylium* Haeckel: p. 520; pl. 44, fig. 9
1975 *Amphymenium*? *splendiarmatum* Clark & Campbell – Petrushevskaya: p. 577; pl. 7, fig. 1; pl. 37, figs 1-3
1985 *Amphymenium splendiarmatum* Clark & Campbell – Westberg-Smith & Riedel: p. 488; pl. 6, fig. 17
1995 *Amphymenium amphystylium* Haeckel – Morley & Nigrini: p. 78; pl. 1, figs 8-9

Amphymenium challengerae Weaver 1983

1983 *Amphymenium challengerae* Weaver: p. 675; pl. 6, figs 1-2
1992 *Amphymenium challengerae* Weaver – Lazarus: pl. 6, figs 4-7

Genus *Dictyocoryne* Ehrenberg 1861

Type-species: *Dictyocoryne profunda* Ehrenberg 1861

Dictyocoryne profunda Ehrenberg 1861

1861 *Dictyocoryne profunda* Ehrenberg: p. 767
1873b *Dictyocoryne profunda* Ehrenberg – Ehrenberg: p. 288; pl. 7, fig. 23

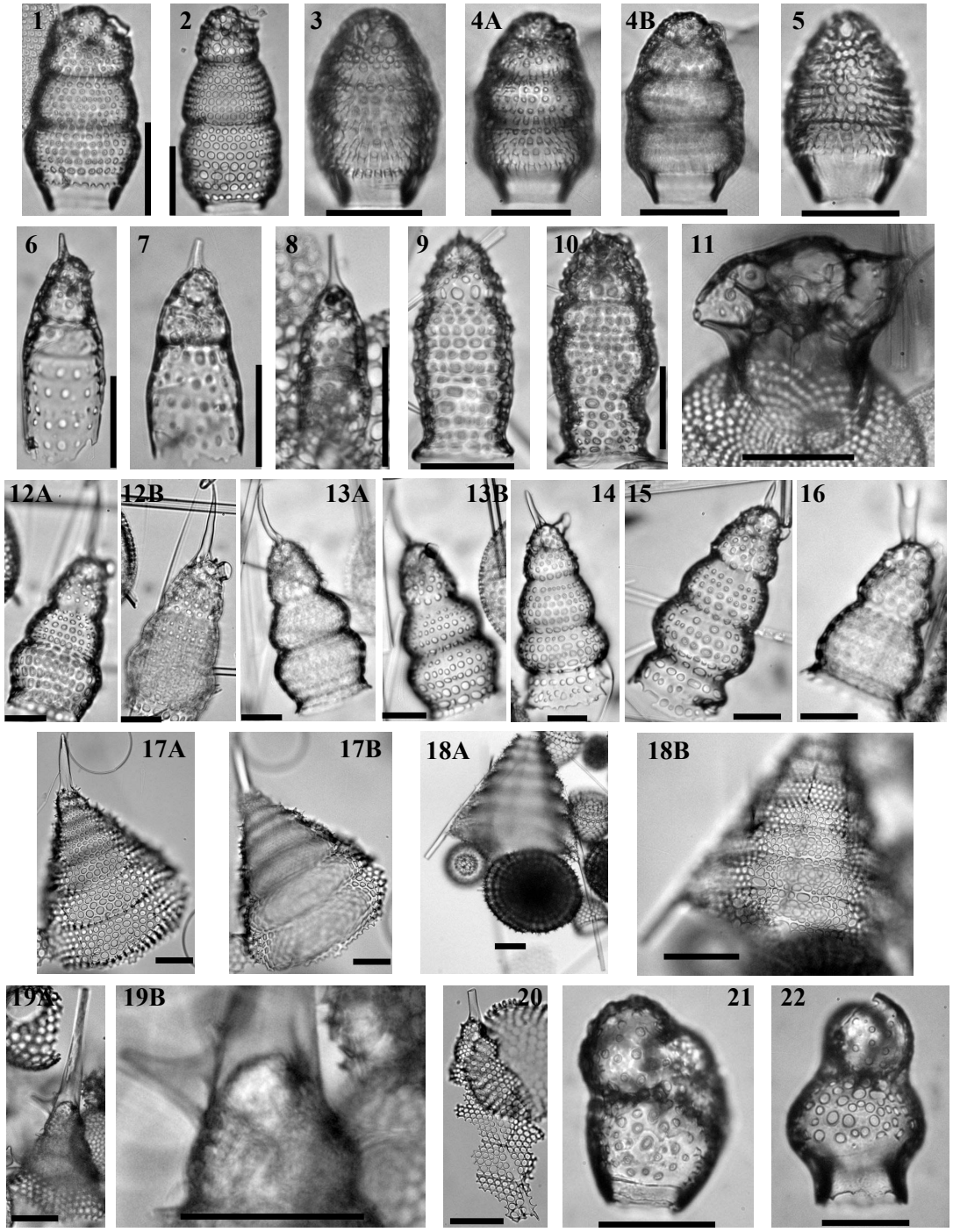

Plate 10.– 1. *Phormostichoartus corbula* (Harting 1863), Sample 119-737A-27X-2, Late Miocene. 2. *Phormostichoartus fistula* Ngrini 1977, Sample 119-744A-8H-1, Middle Miocene. 3. *Phormostichoartus* sp. G, Sample 119-746A-5H-1 53-55cm, Late Miocene. 4. *Phormostichoartus* sp. G, Sample 119-746A-5H-3 53-55cm, Late Miocene. 5. *Phormostichoartus* sp. G, Sample 120-747A-4H-3 45-47cm, Early Pliocene. 6. *Siphocampe* sp. D, Sample 113-690B-6H-2 22-24cm, Early/Middle Miocene. 7. *Siphocampe* sp. D, Sample 113-690B-6H-2 22-24cm, Early/Middle Miocene. 8. *Siphocampe* sp. D, Sample 120-748B-8H-6 45-47cm, Late Oligocene/Early Miocene. 9. Artostrobiid sp. B Sample 119-745B-19H-5 46-48cm, Early Pliocene. 10. Artostrobiid sp. B, Sample 119-745B-23H-2 53-55cm, Late Miocene. 11. Undetermined Cannobotryidae, Sample 120-751A-12H-2 98-102cm, Middle Miocene. 12. *Siphostichartus jahnae* Renaudie & Lazarus 2012, Sample 119-744A-5H-3 53-55cm, Late Miocene. 13. *Siphostichartus jahnae*, Sample 120-751A-11H-4 98-102cm, Middle Miocene. 14. *Siphostichartus jahnae*, Sample 120-751A-12H-1 98-102cm, Middle Miocene. 15. *Siphostichartus jahnae*, Sample 120-748B-5H-5 45-47cm, Middle Miocene. 16. *Siphostichartus jahnae*, Sample 120-751A-12H-3 98-102cm, Middle Miocene. 17. *Spirocyrtis*? *hollisi* Renaudie & Lazarus 2012, holotype, Sample 119-744A-5H-2 53-55cm, Late Miocene. 18. *Spirocyrtis*? *hollisi*, Sample 120-748B-6H-2 45-47cm, Early Miocene. 19. *Spirocyrtis*? *hollisi*, Sample 119-744A-8H-2 60-62cm, Middle Miocene. 20. *Spirocyrtis*? *hollisi*, Sample 120-748B-6H-1 45-47cm, Middle Miocene. 21. *Botryopyle* sp. A, Sample 119-744A-11H-3, Early Miocene. 22. *Botryopyle* sp. A, Sample 120-747A-4H-1 45-47cm, Early Pliocene. All scale bars 50 µm. Magnification x384 except for 19B (x576), for 18B, 19A and 20 (x192) and for 18A (x96).

1980 *Dictyocoryne profunda* Ehrenberg – Boltovskoy & Riedel: p. 115; pl. 3, fig. 10

Dictyocoryne truncatum (Ehrenberg 1861)

1861 *Rhopalodictyum truncatum* Ehrenberg: p. 301
1979 *Dictyocoryne truncatum* (Ehrenberg) – Nigrini & Moore: p. S88, pl. 2, figs 2a-b

Genus *Spongaster* Ehrenberg 1861

Type-species: *Spongaster tetras* Ehrenberg 1861

Spongaster cruciferus (Clark & Campbell 1942)

1942 *Spongasteriscus (Spongasteriscinus) cruciferus* Clark & Campbell: p.50; pl. 1, figs. 1-6, 8, 10, 11, 16-18
1973 *Spongodiscus cruciferus* (Clark & Campbell) – Sanfilippo & Riedel: p. 524; pl. 11, figs 14-17; pl. 28, figs. 10-11

Spongaster tetras Ehrenberg 1861

1861 *Spongaster tetras* Ehrenberg: p. 833
1873b *Spongaster tetras* Ehrenberg – Ehrenberg: p. 299; pl. 6, fig. 8
1967 *Spongaster tetras tetras* Ehrenberg – Nigrini: p. 41; pl. 5, figs 1a-b

Genus *Spongocore* Haeckel 1887

Type-species: *Spongocore velata* Haeckel 1887

Spongocore puella Haeckel 1887

1887 *Spongocore puella* Haeckel: p. 347; pl. 48, fig. 6
1979 *Spongocore puella* Haeckel – Nigrini & Moore: p. S69; pl. 8, figs 5a-c

Genus *Spongodiscus* Ehrenberg 1854

Type-species: *Spongodiscus resurgens* Ehrenberg 1854

Spongodiscus craticulatus (Stöhr 1880)

1880 *Spongotrochus craticulatus* Stöhr: p. 118; pl. 6, fig. 12
1975 *Spongodiscus craticulatus* (Stöhr) – Petrushevskaya: p. 574; pl. 5, figs 9-10

Spongodiscus favus Ehrenberg 1861

1861 *Spongodiscus favus* Ehrenberg: p. 301
1887 *Spongodiscus favus* Ehrenberg – Haeckel: p. 57
1908 *Spongodiscus favus* Ehrenberg var. *maxima* Popofsky: p. 216-217; pl. 26, fig. 4
1975 *Schizodiscus favus* (Ehrenberg) *maxima* Popofsky – Petrushevskaya: p. 574; pl. 5, figs 6-7; pl. 34, figs 1-2

Spongodiscus osculosus (Dreyer 1889)

1889 *Spongopyle osculosa* Dreyer: p. 118-119; pl. 11, figs 99-100
1889 *Spongopyle setosa* Dreyer; p. 119; pl. 11, figs. 97-98
1967 *Spongodiscus*? *osculosus* (Dreyer) – Petrushevskaya: p. 39-40; pl. 20, figs 1-2
1967 *Spongodiscus*? *setosus* (Dreyer) – Petrushevskaya: p. 36-39; pl. 20, figs 3-4

Spongodiscus spatangus (Dogiel in Dogiel & Reshetnyak 1952)

1952 *Schizodiscus spatangus* Dogiel in Dogiel & Reshetnyak: p. 10-11; fig. 4

Genus *Spongotrochus* Haeckel 1860

Type-species: *Spongotrochus brevispinus* Haeckel 1862

Spongotrochus glacialis Popofsky 1908

1908 *Spongotrochus glacialis* Popofsky: p. 228; pl. 26, fig. 8; pl. 27, fig. 1; pl. 28, fig. 2
1958 *Spongotrochus glacialis* Popofsky – Riedel: p. 227; text-fig. 1; pl. 2, figs 1-2

Family **Tholoniidae** Haeckel 1887

Genus *Amphitholus* Haeckel 1887

Amphitholus spp.

Remarks. The taxonomy of family Tholoniidae seems, to this day and particularly at a specific level, very artificial. Because of the scarcity of specimens belonging to this family in the material from the Southern Ocean, it was not possible here, with this material, to revise this group. Members from this family were divided into two sub-groups: *Amphitholus* spp. and *Cubotholus* spp. In the first one, I placed specimens with an inner medullary shell composed of five cupolas (in a star-shaped disposition) and in the second specimens with an inner medullary shell composed of four cupolas (arranged in a cross with one pair of opposite cupolas larger than the other). Other characters (other outer shells, porosity, spines, ...) varied significantly from one specimen to the other and were therefore not considered here.

Genus *Cubotholus* Haeckel 1887

Cubotholus spp.

Remarks. See remarks for *Amphitholus* spp.

Family ***Incertae sedis***

Genus *Spongopylidium* Dreyer 1889 emend. Suzuki et al. 2009

Type-species: *Spongopyle ovata* Dreyer 1889

Spongopylidium pyloma Reynolds 1980

1980 *Collosphaera*? *pyloma* Reynolds: p. 761; pl. 1, figs 5-9
1995 Gen. et sp. indet. Morley & Nigrini: p. 81; pl. 1, fig. 1

Spumellarian sp. A

(Pl. 9, figs 1-3B)

Description. Three-shelled spumellarian with an angular (often hexagonal) cortical shell, a spherial to globular outer medullary shell and an eccentric inner medullary shell that is stuck on the inner wall of the outer medullary shell. Numerous radial beams extend from the outer medullary shell to the cortical shell and protrude outside as short conical spines. The cortical shell also bears numerous short triangular thorns. In some specimens (Pl. 9, fig. 1) a fourth shell seems to develop by joining these thorns.

Remarks. This species shares a fair amount of characteristics with the species recognized here as *Actinomma medusa*: the eccentric inner medullary shell and the deformed cortical shell in particular. However the hexagonal shape of the shell and the numerous thorns seem sufficient to differentiate these two species.

Spumellarian sp. B
(Pl. 31, figs 3A-5B)

Description. Small (usually <50 µm) two-shelled skeleton from which arises four (six?) very long (usually >150 µm), conical spines. Cortical shell is spherical to ellipsoidal, with small, regularly-arranged circular pores and a fair amount of medium-length by-spines. The medullary shell has an oblong outline and seems to be a Pyloniid medullary shell (Pl. 31, figs 4A-B). Radial beams extend from it and protrude outside the cortical shell as long conical spines with a thickened base.

Order **Nassellaria** Ehrenberg 1876
Family **Artostrobiidae** Riedel 1967 emend. Foreman 1973

Artostrobiid sp. B
(Pl. 10, figs 9-10)

Diagnosis. Wavy post-thoracic segment(s) with numerous pore rows; row of wider pores at the lumbar stricture.

Description. Number of segments not clear. Cephalothorax is separated from the post-thoracic segment(s) by a clear constriction. The row of pores above the constriction is larger than both the cephalothoracic and the post-thoracic pores. Shell globally spindle-shaped although the last segment termination flares moderately wide. Post-thoracic outline is somewhat wavy. Numerous pore rows of various sizes are present on the post-thoracic segment(s). Cephalis bears both a short, thin apical horn and an upwardly-directed ventral tube (Pl. 10, fig. 10).

Genus *Botryostrobus* Haeckel 1887 emend. Nigrini 1977
Type-species: *Lithostrobus botryocyrtis* Haeckel 1887

Botryostrobus aquilonaris (Bailey 1856)
1856 *Eucyrtidium aquilonaris* Bailey: p. 4; pl. 1, fig. 9
1856 *Eucyrtidium tumidulum* Bailey: p. 5; pl. 1, fig. 11
1971 *Siphocampe aquilonaris* (Bailey) – Ling et al.: p. 716; pl. 2, fig. 12
1977 *Botryostrobus aquilonaris* (Bailey) – Nigrini: p. 246; pl. 1, fig. 1

Botryostrobus auritus (Ehrenberg 1844)
1844a *Lithocampe aurita* Ehrenberg: p. 84
1844b *Lithocampe australe* Ehrenberg: p. 187
1854 *Eucyrtidium auritum* (Ehrenberg) – Ehrenberg: pl. 22, fig. 25
1854 *Eucyrtidium australe* (Ehrenberg) – Ehrenberg: pl. 35A-21, fig. 18
1972 *Botryostrobus auritus* (Ehrenberg) group – Petrushveskaya & Kozlova: p. 539; pl. 24, figs 15-18
1972 *Botryostrobus australis* (Ehrenberg) group – Petrushveskaya & Kozlova: p. 539; pl. 24, figs 12-14
1977 *Botryostrobus auritus-australis* (Ehrenberg) group – Nigrini: p. 246-248; pl. 1, figs 2-5

Botryostrobus bramlettei (Campbell & Clark 1944)
1944 *Lithomitra bramlettei* Campbell & Clark: p. 53; pl. 7, figs 10-14
1977 *Botryostrobus bramlettei* (Campbell & Clark) – Nigrini: p. 248-249; pl. 1, figs 7-8

Botryostrobus joides Petrushevskaya 1975

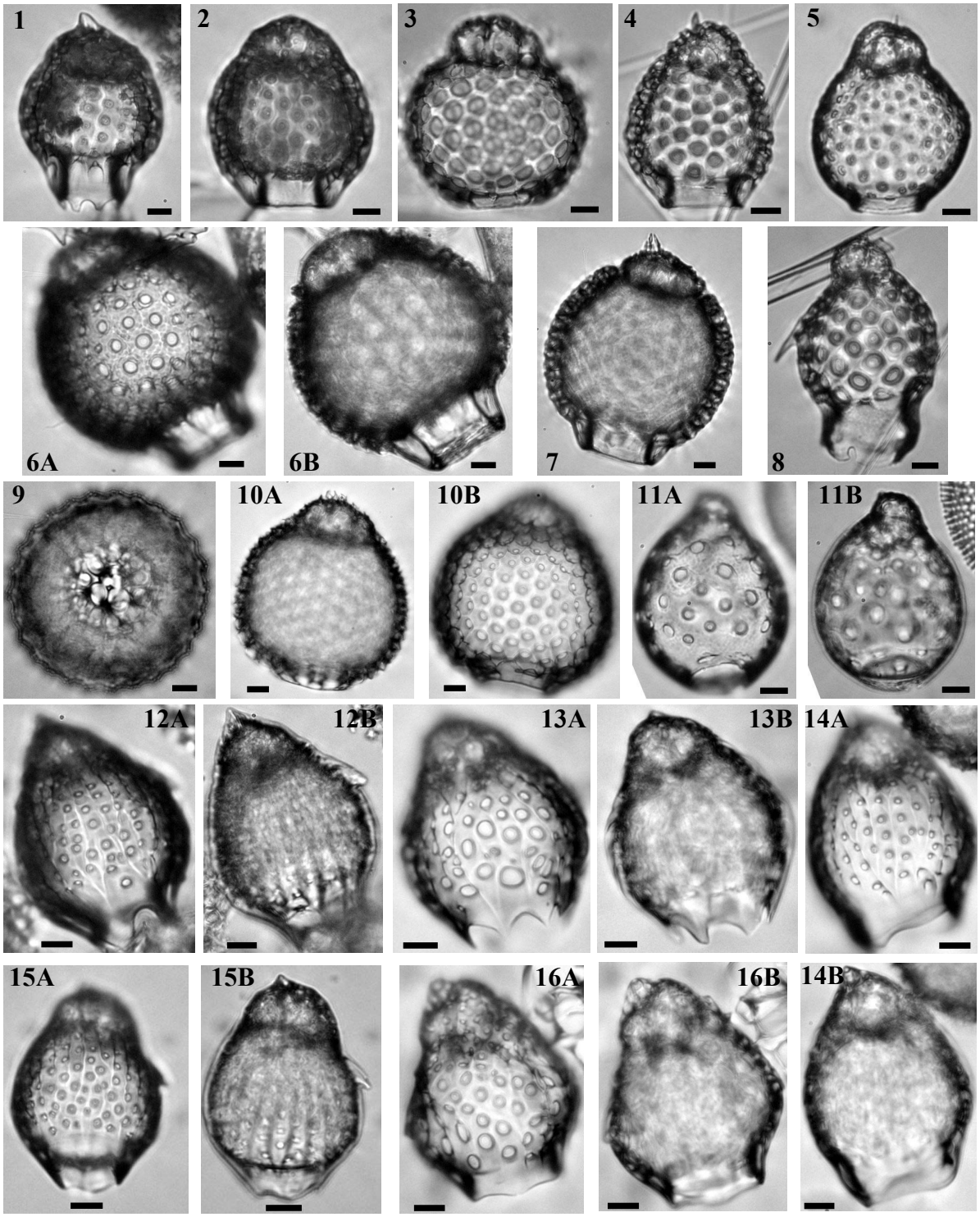

Plate 11.–
1. *Cystophormis pulchrum* (Carnevale 1901), Sample 119-737B-6R-2 54-56cm, Middle Miocene. 2. *Cystophormis brevispina*? Vinassa de Regny 1899, Sample 119-737AB-6R-2 54-56cm, Middle Miocene. 3. *Cystophormis ob* Petrushevskaya 1975, Sample 119-744A-7H-5 53-55cm, Middle Miocene. 4. *Plannapus mauricei* O'Connor 1997, Sample 119-744A-6H-4 53-55cm, Middle Miocene. 5. *Plannapus hornibrooki* O'Connor 1997, Sample 120-748B-6H-1 45-47cm, Middle Miocene. 6. *Cystophormis gargantua* Renaudie & Lazarus 2012, Sample 120-748B-6H-1 45-47cm, Early/Middle Miocene. 7. *Cystophormis gargantua*, holotype, Sample 120-748B-6H-3 45-47cm, Early Miocene. 8. *Plannapus papillosus* (Ehrenberg 1873a), Sample 119-737B-5H-2, Late Miocene. 9. *Cystophormis gargantua*, Sample 120-748B-6H-1 45-47cm, Early/Middle Miocene. 10. *Cystophormis gargantua*, Sample 119-744A-11H-3, Early Miocene. 11. *Plannapus microcephalus* (Haeckel 1887), Sample 119-745B-20H-6 53-55cm, Early Pliocene. 12. *Plannapus uburex* (Renaudie & Lazarus 2012), Sample 119-738B-1H-3 53-55cm, Pleistocene. 13. *Plannapus uburex*, Sample 119-744A-2H-2 53-55cm, Pleistocene. 14. *Plannapus uburex*, holotype, Sample 119-744A-2H-2 53-55cm, Pleistocene. 15. *Plannapus uburex*, Sample 119-744A-2H-1 53-55cm, Pleistocene. 16. *Plannapus uburex*, Sample 120-747A-2H-2 45-47cm, Pleistocene.
All scale bars are 10 µm. Magnification x384.

1972 *Botryostrobus* sp. Petrushevskaya & Kozlova: p. 539; pl. 24, figs 8-11
1975 *Botryostrobus joides* Petrushevskaya: p. 585; pl. 10, fig. 37
1976a *Botryostrobus joides* Petrushevskaya – Bjørklund: pl. 23, figs 7-14
1996 *Botryostrobus joides* Petrushevskaya group – Hull: p. 137; pl. 4, figs 5-6, 20

Genus *Phormostichoartus* Campbell 1951 emend. Nigrini 1977
Type-species: *Cyrtophormis cylindrica* Haeckel 1887

Phormostichoartus corbula (Harting 1863)
(Pl. 10, fig. 1)
1863 *Lithocampe corbula* Harting: p. 12; pl. 1, fig. 21
1967 *Siphocampe corbula* (Harting) – Nigrini: p. 85; pl. 8, fig. 5; pl. 9, fig. 3
1977 *Phormostichoartus corbula* (Harting) – Nigrini: p. 252; pl. 1, fig. 10

Phormostichoartus fistula Nigrini 1977
(Pl. 10, fig. 2)
1977 *Phormostichoartus fistula* Nigrini: p. 253; pl. 1, figs 11-13

Phormostichoartus furcaspiculata (Popofsky 1908)
1908 *Lithamphora furcaspiculata* Popofsky: p. 295; pl. 36, figs 6-8
1913 *Lithamphora furcaspiculata* Popofsky – Popofsky: p. 408-413; text-fig 131-140
1967 *Lithamphora*? *furcaspiculata* Popofsky – Petrushevskaya: p. 127-133; pl. 73, figs 1-3; pl. 74, figs 1-4
1985 *Phormostichoartus furcaspiculata* (Popofsky) – Caulet: p. 853

Phormostichoartus marylandicus (Martin 1904)
1904 *Lithocampe marylandica* Martin: p. 450; pl. 130, fig. 4
1972 *Theocamptra marylandica* (Martin) – Petrushevskaya & Kozlova: p. 538; pl. 23, figs 20-21
1977 *Phormostichoartus marylandicus* (Martin) – Nigrini: p. 253; pl. 2, figs 1-3

Phormostichoartus pitomorphus Caulet 1985
1985 *Phormostichoartus pitomorphus* Caulet: p. 850; pl. 3, figs 3-4, 9-10, 12
1995 *Phormostichoartus pitomorphus* Caulet – Morley & Nigrini: pl. 6, fig. 9

Phormostichoartus sp. G
(Pl. 10, figs. 3-5)
Diagnosis. Spindle-shaped; four segments; downward-directed ventral tube; 3 to 4 pore rows per segments.
Description. Four-segmented, spindle-shaped, thick-walled artostrobiid with a short downward-directed ventral tube (in some specimens it appears as a ventral pore; Pl. 10, fig. 5). No externally expressed stricture, although both lumbar and post-abdominal strictures are marked internally. Relatively long, hyaline, inverted-truncated conical peristome. Abdomen and post-abdominal segment are of nearly equal length (peristome exluded) and breadth. The inflexion of the shell outline is on the abdomen. Thorax, abdomen and post-abdominal segemnts with 3 or 4 pore rows. Pores of equal diameter on all segments except on cephalis (smaller).
Remarks. It differs from *Phormostichoartus corbula* and *P. fistula* in its shell outline, in the smaller number of pore rows per segment and in the length and breadth ratio of the abdomen vs

the post-abdominal segment. It differs from other artostrobiids, and in particular from *Botryostrobus aquilonaris*, in its number of segments and the direction of its ventral tube.

Genus *Siphocampe* Haeckel 1887

Type-species: *Siphocampe annulosa* Haeckel 1887

Siphocampe acephala (Ehrenberg 1875)

1875 *Eucyrtidium acephalum* Ehrenberg: p. 70; pl. 11, fig. 5
1882 *Lithomitra acephala* (Ehrenberg) – Bütschli: p. 529
1977 *Siphocampe acephala* (Ehrenberg) – Nigrini: p. 254-255; pl. 3, fig. 5

Siphocampe arachnea (Ehrenberg 1861)

1861 *Eucyrtidium lineatum* (Ehrenberg) *arachneum* Ehrenberg: p. 299
1958 *Lithomitra arachnea* (Ehrenberg) – Riedel: p. 242; pl. 4, figs 7-8
1977 *Siphocampe arachnea* (Ehrenberg) group – Nigrini: p. 255; pl. 3, figs 7-8

Siphocampe pachyderma (Ehrenberg 1873a)

1873a *Eucyrtidium pachydermum* Ehrenberg: p. 231
1875 *Eucyrtidium pachydermum* Ehrenberg – Ehrenberg: pl. 11, fig. 21
1991 *Siphocampe pachyderma* (Ehrenberg) – Caulet: pl. 3, fig. 12

Siphocampe quadrata (Petrushevskaya & Kozlova 1972)

1972 *Lithamphora sacculifera* (Clark & Campbell) *quadrata* Petrushevskaya & Kozlova: p. 539; pl. 30, figs 4-6
1977 *Siphocampe*? *quadrata* (Petrushevskaya & Kozlova) – Nigrini: p. 257; pl. 3, fig. 12

Siphocampe sp. D

(Pl. 10, figs 6-8)

Diagnosis. Thin, apical horn; abdomen long, smooth, with a few pores rows.

Description. Three-segmented shell. Truncated-conical cephalothorax. No ventral tube has been observed, though one specimen (Pl. 10, fig. 6) bears what seems to be a ventral horn, in addition to its thin, long apical horn (which is tribladed at the base and conical thereafter). Abdomen is long, thin, slightly barrel-shaped, with a few rather widely separated rows of pores. Those rows are transversal to almost diagonal. Abdominal pores are relatively large and elongated longitudinally.

Remarks. It differs from *Siphocampe arachnea* in its apical horn, its clearly marked lumbar stricture and its wider abdomen.

Genus *Siphostichartus* Nigrini 1977

Type-species: *Cystophormis corona* Haeckel 1887

Siphostichartus corona (Haeckel 1887)

1887 *Cystophormis (Acanthocyrtis) corona* Haeckel: p. 1462; pl. 77, fig. 15
1971 *Phormostichoartus corona* (Haeckel) – Riedel & Sanfilippo: p. 1600; pl. 1I, figs 13-15; pl. 2J, figs 1-5
1977 *Siphostichartus corona* (Haeckel) – Nigrini: p. 257-258; pl. 2, figs 5-6

Siphostichartus jahnae Renaudie & Lazarus 2012

(Pl. 10, fig. 12A-16)

Derivation of name. Named after Regine Jahn for her efforts to preserve and restore the Ehrenberg Collection.

Diagnosis. Duck-billed vertical tube, long apical horn.

Holotype. Plate 10, figs. 12A-B; Sample 119-744A-5H-3 53/55cm (Late Miocene); ECO-028.

Material. 229 specimens were observed from ODP Sites 744, 746, 748 and 751.

Description. Spindle-shaped four- to five-segmented shell.

The cephalis bears a duck-billed, upward-directed vertical tube and a long, slender apical horn (at least as long as cephalis but most of the time as long as cephalothorax). This horn is very variable in shape: it can be either straight, rod-like, blade-shaped, strongly curved or even bifurcated. The axobate is a cluster of several thin rods extending straight down toward the lumbar stricture. The pores on the thick cephalic wall are few, small and rounded.

Collar stricture is slightly indented dorsally. The pores on thorax are bigger, rounded and arranged randomly. Lumbar stricture is marked by a strong indentation and a wide poreless area below. Abdomen is barrel-shaped or truncated-conical and bears four to six transversal rows of rounded to elliptical pores increasing in size distally (pores on the first row are smaller than the thoracic pores while pores in the final row are only slightly smaller than the pores on the fourth segment). The fourth segment is either barrel-shaped or inverted truncated-conical and bears four to five more or less regular transversal rows of large, transversally-elongated (elliptical to quadrangular) pores. When present, fifth segment is thinner, flares distally and bears irregular rows of irregularly-shaped (but mostly quadrangular) pores. The largest segment is invariably the fourth and the longest is either the abdomen or the fourth segment.

Dimensions. (based on 7 specimens) Length of apical horn: 22-59 (35); of vertical tube: 10-13 (12); of cephalothorax: 36-42 (40); of third segment: 32-41 (35); of fourth segment: 30-40 (35); of fifth segment: 16-41 (27).

Occurrence. Rare from the *A. golownini* to the Tau Zone (middle Miocene to early Pliocene).

Remarks. *Siphostichartus jahnae* differs from *S. corona* and *S. praecorona* Nigrini, 1977 in its peculiar apical horn and in having a considerably shorter fourth segment. It also differs from *Botryostrobus auritus-australis* (Ehrenberg) group Nigrini, 1977 in the apical horn and in the post-thoracic segments that are, in *B. auritus-australis*, more or less uniform whereas, in *S. jahnae,* the segments that follow the thorax differ in width, length, shape, thickness (fifth segment) as well as in the shape of their pores.

Genus *Spirocyrtis* Haeckel 1881 emend. Nigrini 1977

Type-species: *Spirocyrtis scalaris* Haeckel 1887

Spirocyrtis subscalaris Nigrini 1977

1977 *Spirocyrtis subscalaris* Nigrini: p. 259-260; pl. 3, figs 1-2

Spirocyrtis? *hollisi* Renaudie & Lazarus 2012

(Pl. 10, figs 17A-20)

1999a Cyrtida fam., genn. et spp. indet O'connor: 500, pl. 4, fig. B.

2002 *Spirocyrtis*? aff *gyroscalaris* Hollis: 301, pl. V, figs. 7a-c.

Derivation of name. Named after Christopher J. Hollis, who first described this species.

Diagnosis. Strong apical horn; seven to eight segments with transverse pore rows; at least two strong ribs.

Holotype. Plate 10, figs. 17A-B; Sample 119-744A-5H-2 53/55cm (Late Miocene); ECO-034.

Material. 18 specimens were observed from ODP Sites 690, 744, 747, 748 and 751.

Description. Large conical shell with 7 or 8 segments.
Cephalis and thorax are only separated externally by shallow furrows. Apical horn is conical, long (2 to 3 times the length of the cephalothorax) and robust (ca. as wide as cephalis). The cephalis also bears a triangular ventral horn (no vertical tube or vertical pore have been recognized though) and a dorsal horn (downward-directed and smaller than the ventral one). Several small, additional horn are also present on both the cephalis and the thorax, and some specimens show small thorns on other segments as well. Pores on cephalis and thorax are small, numerous, closely-packed, rounded to subhexagonal and loosely arranged in transverse rows.
The following segments (from the abdomen to the seventh segment) are barrel-shaped and expanding distally both in width and in length (but considerably more in width than in length). The final segment (generally the eight) is tapering inward (no specimen has a complete enough final segment to show the presence or absence of a mouth or any other feature). Pores on those segments are elliptical to hexagonal, arranged in transverse rows (3 to 6 per segment) and increasing in size distally.
Two (?) strong ribs arise from the thoracic wall and continue as feet after the penultimate segment (generally the seventh). Some specimens show several weaker additional ribs.
Dimensions. (based on 6 specimens) Length of apical horn: 37-140 (89); of cephalothorax: 31-50 (42); of third segment: 15-33 (25). Only two specimens were found complete: total length 270 and 310; maximum width 250 and 270.
Occurrence. Sporadic from the *S. radiosa* to the lower Chi Zone (early Miocene to early Pleistocene). This species has been reported by Hollis (2002) in Zone RP6 (Late Paleocene).
Remarks. The assignment of *Spirocyrtis*? *hollisi* to the genus *Spirocyrtis* is questionable since no vertical tube or vertical pore have been seen and no other *Spirocyrtis* (or no other Artostrobiidae) bear ribs. However the structure of the cephalothorax, the alignment of the pores and the number of segments tend to indicate a close link between *S.*? *hollisi* and the other *Spirocyrtis* species (*S. scalaris, S. subtilis* Petrushevskaya in Petrushevskaya & Kozlova ,1972, *S. subscalaris* Nigrini, 1977*, S. gyroscalaris* Nigrini, 1977*, S. proboscis* O'Connor, 1994 and *S. greeni* O'Connor, 1999b).

Family **Cannobotryidae** Haeckel 1881 emend. Riedel 1967

Genus *Amphimelissa* Jørgensen 1905
Type-species: *Botryopyle setosa* Cleve 1899

Amphimelissa? *hibernifortuna* Renaudie & Lazarus 2012
(Pl. 15, figs. 16-18B)
Derivation of name. From the Latin, *Hibernus* meaning "the Irish" and *fortuna* meaning "luck"; *hibernifortuna* therefore stands for "the luck of the Irish", for its ressemblance to a shamrock clover.
Diagnosis. Three cephalic chambers approximately spherical and equal in size, arranged triradiately instead of laterally.
Holotype. Plate 15, figs. 18A-B; Sample 119-744A-4H-2 59/61cm (Late Miocene); ECO-037, circle 1.
Material. 134 specimens were observed from ODP Sites 737, 744, 746, 747, 748 and 751.
Description. Small, two-segmented shell with rough, crested, thorny surface.
The thorax is cylindrical, short - approximately equal in length and width to the cephalis. Its termination is ragged. Thoracic pores are rounded, unequal in size and distributed randomly.

The cephalis is trilobate with two chambers equal in size and an eucephalic lobe somewhat smaller. The three lobes are spherical and are arranged triradiately around spine A (see pl. 15, fig. 17B). Cephalic pores are small and sparser than the thoracic ones. The internal spines don't seem to protrude outside the cephalic wall with the notable exception of spine A that can continue as a small, thorn-like spine. In apical view (see pl. 17, fig. 18B; to be compared with Petrushevskaya, 1971, pl. 10, fig. 8), eucephalic chamber inner structure can be seen: spine V crosses the eucephalic chamber longitudinally while two wide, flat arches pj - according to Petrushevskaya (1971)'s terminology - join spine V and spines L. The two other cephalic chambers are separated by spine D: therefore it is not an antecephalic and postcephalic chambers but an antecephalic chamber split in two lobes.

Dimensions. (based on 4 specimens on apical view) Thorax maximum width: 64-100 (80); cephalic chambers diameter: 29-44 (35).

Occurrence. Rare from the *C. humerus* to the Tau Zone (middle Miocene to early Pliocene).

Remarks. The cephalic lobe arrangement seems to be unique to this species amongst other Cannobotryidae. Because of this peculiar layout where the three lobes are not ante-, eu- and postcephalic but rather an eucephalic and two antecephalic lobes, the affinity with the genus *Amphimelissa* remains putative.

Genus *Botryometra* Petrushevskaya 1975

Type-species: *Lithomelissa heros* Campbell & Clark 1944

Botryometra poljanskii Petrushevskaya 1975

(Pl. 23, figs 18A-B)

1975 *Botryometra poljanskii* Petrushevskaya: p. 590; pl. 13, figs 9-10; pl. 21, fig. 7; pl. 26, fig. 13

Genus *Botryopyle* Haeckel 1881 emend. Petrushevskaya 1965

Type-species: *Botryopyle dictyocephalus* Haeckel 1887

Botryopyle cribosa (Popofsky 1913)

1913 *Acrobotrissa cribosa* Popofsky: p. 322; text-fig. 29

1971 *Botryopyle cribosa* (Popofsky) – Petrushevskaya: p. 163-164; pl. 84, figs 1-3

Botryopyle dionisii Petrushevskaya 1975

1975 *Botryopyle*? *dionisii* Petrushevskaya: p.589; pl. 13, fig. 18; pl. 26, fig. 10

Botryopyle? sp. A

(Pl. 10, figs 21-22)

Diagnosis. Large antecephalic lobe; thorax ending with a hyaline peristome.

Description. Cannobotryid with a large kidney-shaped antecephalic lobe, a smaller eucephalic lobe, an even smaller postcephalic lobe and a thorax tapering downward with a hyaline peristome. In some specimens, the thorax is barrel-shaped (Pl. 10, fig. 22). Pores on the thorax are irregular in shape, size and disposition but pores on the antecephalic and eucephalic lobes are regularly disposed, small and circular.

Remarks. It differs from *Botryopyle dionisii* in lacking the characteristic post-cephalic downward-directed 'tube' of the latter and in its thoracic porosity. It however shares with the latter the shape of its antecephalic and eucephalic lobes and the shape of its thorax.

Genus *Saccospyris* Haecker 1908

Type-species: *Saccospyris antarctica* Haecker 1908

Saccospyris antarctica Haecker 1908

1908 *Saccospyris antarctica* Haecker: p. 447, pl. 84, figs 584, 589-590
1958 *Botryopyle*? *antarctica* (Haecker) – Riedel: p. 244; pl. 4, fig. 12; text-fig. 13
1967 *Saccospyris antarctica* Haecker – Petrushevskaya: p. 149; pl. 85, fig. 2
1983 *Saccospyris antarctica* Haecker – Weaver: pl. 1, fig. 4

Saccospyris conithorax Petrushevskaya 1965

1965 *Saccospyris conithorax* Petrushevskaya: p. 98-99; fig. 11
1967 *Saccospyris conithorax* Petrushevskaya – Petrushevskaya: p. 150; pl. 85, fig. 1
1971 *Botryocampe conithorax* (Petrushevskaya) – Petrushevskaya: pl. 79, fig. 4
1975 *Botryocampe conithorax* (Petrushevskaya) group – Petrushevskaya: p. 588; pl. 13, figs 26-27

Saccospyris preantarctica Petrushevskaya 1975

1975 *Saccospyris preantarctica* Petrushevskaya: p. 589; pl. 13, figs 19-20
1983 *Saccospyris preantarctica* Petrushevskaya – Weaver: pl. 1, fig. 8

Saccospyris victoria Renaudie & Lazarus in press

(Pl. 15, figs. 10A-15)

Derivation of name. Named after the 'Winged Victory of Samothrace', for the resemblance between the holotype and the shape of this statue; the latin word *victoria* being a generic name for statues of the goddess Victory.

Diagnosis. Cephalis with two equal chambers; long, truncated-conical thorax.

Holotype. Pl. 15, fig. 14; Sample 120-751A-9H-1, 98-102cm (Late Miocene); ECO-065.

Material. 122 specimens observed from ODP Sites 689, 693, 748, 751 and 1138.

Description. Two-segmented shell. The cephalis is separated into the antecephalic and eucephalic chambers (some specimens show a small, reduced postcephalic chamber: Pl. 15, figs 12A-B). These two chambers are equal in size and shape (hemispherical). Spine **A** separate the two chambers and protrudes outside as a thin, short apical horn (some specimens have a stronger apical horn; Pl. 15, figs 13 and 15). The collar shows a more or less marked stricture.

The thorax is fairly long and truncated-conical. Pores on the thorax are small, numerous, usually round, but vary in size and shape. They are randomly disposed. Pores on the cephalis are similar to that of the thorax, yet somewhat smaller. Cephalis and upper thoracic wall bear numerous small, thin thorns that, in some specimens (Pl. 15, figs 12A-15), connect distally to form a thin peripheral feltwork.

Dimensions. (based on 7 specimens) Total length: 50-94 (75); cephalis width: 38-66 (42).

Occurence. Rare from the *Actinomma golownini* to the *Siphonosphaera vesuvius* Zone (Middle to Late Miocene). Sporadic from the *Siphonosphaera vesuvius* to the lower Tau Zone (Late Miocene).

Remarks. *Saccospyris victoria* differs from *Saccospyris antarctica* and *S. praeantarctica* Petrushevskaya, 1975 in its long, flaring thorax, which is wider than the two cephalic chambers, in the presence of a peripheral spongiose meshwork on the upper thorax of some specimens and in the numerous small pores covering the entire test.

Saccospyris victoria shares with *Lophophaena apiculata* Ehrenberg, 1874 (see Ogane et al., 2009; pl. 19, figs 3a-d) the presence of a bilobed cephalis separated by a free spine **A** and a skirt-

looking thorax but differs in the apical constriction being stronger, the smaller size of the cephalis compared to the thorax and the lack of longitudinal lineation in the thoracic pores.
Despite the fact that the typical cannobotryid cephalic structure (Petrushevskaya, 1965, 1971) was not observed clearly in any of the specimens, *Saccospyris victoria* is assigned to this family on the basis of the presence of a bilobed cephalis and, in the specimens illustrated in pl. 15, figs 12A-B and 15, of a possible vestigial post-cephalic lobe, similar to the one seen in *Saccospyris antarctica*.

Family **Carpocaniidae** Haeckel 1881 emend. Riedel 1967

Genus *Cystophormis* Haeckel 1887
Type-species: *Cystophormis pyla* Haeckel 1887

Cystophormis brevispina? (Vinassa de Regny 1900)
(Pl. 11, fig. 2)

? 1900 *Carpocanistrum brevispina* Vinassa de Regny: p. 579; pl. 2, fig. 23
1972 *Carpocanistrum* sp. aff. *Sethocorys odysseus* (Haeckel) – Petrushevskaya & Kozlova: pl. 22, fig. 16
1975 *Cystophormis brevispina* (Vinassa de Regny) group – Petrushevskaya: p. 588; pl. 13, figs 3-7; pl. 44, figs 1-2
1989 *Cystophormis brevispina*? (Vinassa de Regny) – Lazarus & Pallant: p. 363; pl. 5, figs 14-15

Remarks. This species is characterized by its cephalis/thorax ratio and its short hyaline peristome. Both the specimens observed during this study and those illustrated by Petrushevskaya 1975 and Lazarus & Pallant 1989 differs from the species described and illustrated by Vinassa de Regny in lacking the numerous, small spine-like teeth around the peristome ("*Appendici basali numerose, piccolissime, simili a minute spine*", p.580 in Vinassa de Regny 1900). The species identified here and in the various sources above-mentioned therefore doubtfully belongs to that described by Vinassa de Regny. The name is kept here for continuity with the other authors that used this species name, but a new name for this species would be necessary in the future.

Cystophormis gargantua Renaudie & Lazarus 2012
(Pl. 11, figs 6A-7, 9-10B)

? 1992 *Carpocanistrum* spp Sugiyama et al: pl. 27, fig. 8 (non fig. 7 and 9).

Derivation of name. Named after the giant Gargantua in Rabelais eponymous novel.

Diagnosis. Large (ca. 130 µm long and ca. 110 µm wide) Carpocaniid with a short trilobate cephalis.

Holotype. Plate 11, fig. 7; Sample 120-748B-6H-3 45/47cm (Early Miocene); ECO-048, circle 1.

Material. 846 specimens were observed from ODP Sites 690, 744 and 748.

Description. Large two-segmented shell with a trilobate dome-shaped cephalis and a barrel-shaped to spherical thorax ending with a wide hyaline peristome of variable length.
The three lobes of the cephalis are not marked externally. The eucephalic lobe is slightly wider and taller than the two others. In some specimens, a small tribladed apical spine arise at the junction between the eucephalic and the antecephalic lobe. Externally, the collar stricture is marked by an indentation and, in some specimens, by a slight change in contour. Internally, the cephalis and the thorax are marked by a plate pierced by four adjacent collar pores (two large

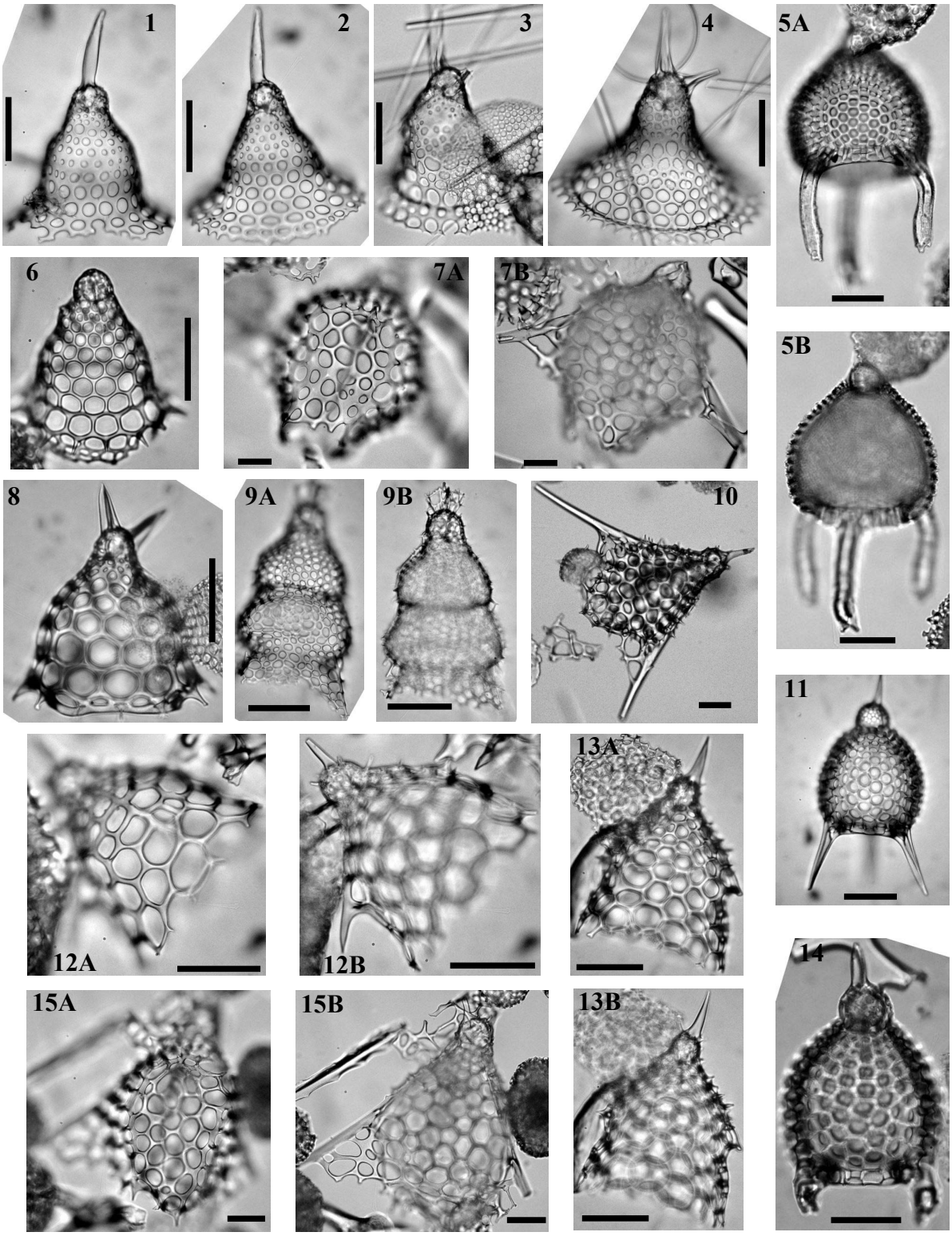

Plate 12.–
1. *Cycladophora* sp. A, Sample 120-751A-12H-6, 98-102cm, Middle Miocene. 2. *Cycladophora* sp. A, Sample 120-751A-12H-6, 98-102cm, Middle Miocene. 3. *Cycladophora* sp. A, Sample 120-748B-5H-7 45-47cm, Middle Miocene. 4. *Cycladophora* sp. A, Sample 120-748B-5H-4 45-47cm, Middle Miocene. 5. *Lychnocanium* sp. C, Sample 120-747A-4H-3 45-47cm, Early Pliocene. 6. *Cycladophora* sp. B?, Sample 113-690B-7H-2 27-29cm, Early Miocene. 7. *Dictyophimus larus* Renaudie & Lazarus 2012, Sample 120-747A-10H-4 45-47cm, Early/Middle Miocene. 8. *Cycladophora* sp. B, Sample 113-690B-7H-2 27-29cm, Early Miocene. 9. *Artophormis* sp cf. *A. gracilis* Riedel 1959, Sample 120-748B-8H-4 45-47cm, Early Miocene. 10. *Dictyophimus larus*, holotype, Sample 120-748B-6H-1 45-47cm, Early Miocene. 11. *Lychnocanium* sp. B, Sample 120-747A-8H-3 45-47cm, Middle Miocene. 12. *Dictyophimus kiwi* Renaudie & Lazarus 2012, Sample 120-748B-6H-4 45-47cm, Early Miocene. 13. *Dictyophimus kiwi*, holotype, Sample 120-748B-6H-1 45-47cm, Early Miocene. 14. *Lychnocanium* sp. B, Sampl 119-737B-10R-2 53-55cm, Middle Miocene. 15. *Dictyophimus larus*, Sample 119-744A-8H-3 53-55cm, Early Miocene. All scale bars 50 µm. Magnification x384 except for 3, 5A-B, 7A-B and 15A-B (x192) and for 10 (x96).

and two small). The cephalic wall is thick, crested and bears only a few, small, rounded pores.
The thoracic wall is also thick and crested. It bears larger, round pores that are aligned longitudinally (on half the equator, 8 to 11 rows of 7 to 10 pores). Transversally, they are arranged according to a hexagonal pattern. Because of the crests on the wall, each pore seems to be framed. The longitudinal alignment is not strict: it particularly tends to be irregular near the peristome.
The peristome is thick, smooth and hyaline, internally cylindrical and externally cylindrical to inverted truncated-conical. The pore frames of the pores closest to the peristome sometimes extend to its base.
Dimensions. (based on 6 specimens) Total length: 109-140 (128); maximum width: 93-121 (111); length of cephalis: 16-25 (20); of thorax: 77-95 (87).
Occurrence. Common from the *S. radiosa* to the *E. punctatum* Zone (early to middle Miocene).
Remarks. *Cystophormis gargantua* differs from other carpocaniids primarily in its size. It also differs from *Sethocorys odysseus* Haeckel, 1887 in its cephalis being flat and distinctly trilobed, and in the collar stricture being less marked; from *Carpocanopsis favosa* (Haeckel) 1887 in the peristome being cylindrical or inverted conical rather than widening distally and in having a smooth termination.

Cystophormis ob Petrushevskaya 1975
(Pl. 11, fig. 3)
1975 *Cystophormis ob* Petrushevskaya: p. 488; pl. 13, figs 1-2
1981 *Cystophormis ob* Petrushevskaya – Petrushevskaya: p. 260; fig. 389

Cystophormis pulchrum (Carnevale 1908)
(Pl. 11, fig. 1)
1908 *Carpocanium pulchrum* Carnevale: p. 30; pl. 4, fig. 15
1981 *Cystophormis pulchrum* (Carnevale) – Petrushevskaya: p. 260
Remarks. This species is easily identifiable and distinguishable from the other Carpocaniid by its cephalis/thorax ratio, its apical horn, and more importantly, by its long peristome with teeth that are directed inwards. *Cystophormis brevispina*?, *C. pulchrum, C. ob* and *C. gargantua* are clearly related to one another because of their characteristic three-lobed cephalis, with a higher eucephalic chamber. *C. brevispina*?*, C. gargantua* and *C. pulchrum* also share the presence of longitudinal rows of pores separated by wavy ridges and a well-expressed hyaline peristome. Finally, *C. pulchrum* and *C. gargantua* also shares the presence of a small, triangular apical spine stuck between the antecephalic and the eucephalic lobe.

Genus *Plannapus* O'Connor 1997a
Type-species: *Dicolocapsa microcephala* Haeckel 1887

Plannapus hornibrooki O'Connor 1999a
(Pl. 11, fig. 5)
1999a *Plannapus hornibrooki* O'Connor: p. 7-8; pl. 1, figs 7a-10; pl. 5, figs 8a-11
2002 *Plannapus hornibrooki* O'Connor – Apel et al.: pl. P10, fig. 12

Plannapus mauricei O'Connor 1999a
(Pl. 11, fig. 4)
1999a *Plannapus mauricei* O'Connor: p. 8; pl. 1, figs 11-14; pl. 5, figs 12a-15
2002 *Plannapus mauricei* O'Connor – Apel et al.: pl. P10, fig. 13

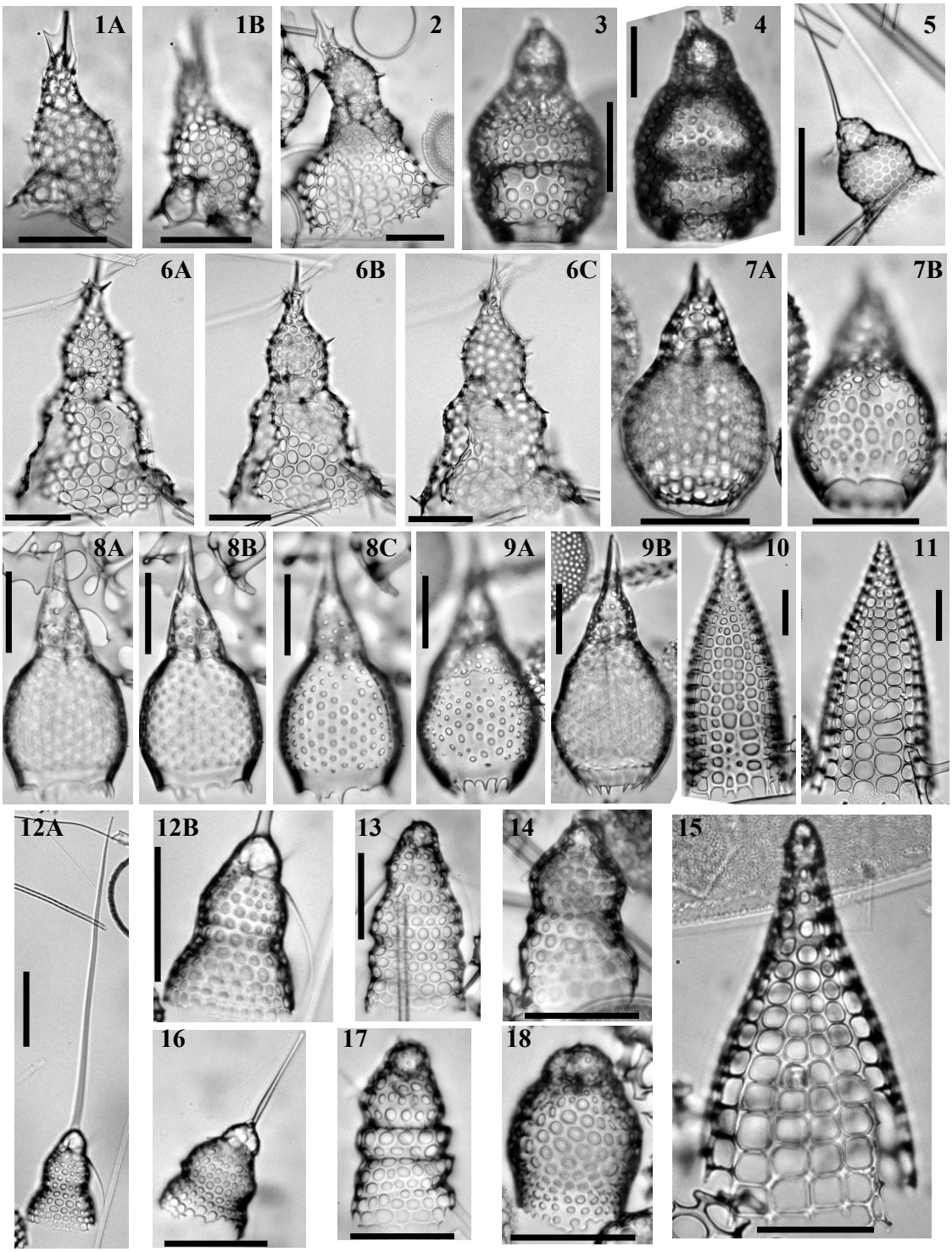

Plate 13.– 1. *Lamprocyrtis*? *datureacornis* Renaudie & Lazarus in press, Sample 120-751A-12H-2 98-102cm, Middle Miocene. 2. *Lamprocyrtis*? *datureacornis*, Sample 120-751A-12H-1 98-102cm, Middle Miocene. 3. *Lamprocyclas* spE, Sample 119-746A-6H-2 53-55cm, Late Miocene. 4. *Lamprocyclas* sp. E, Sample 119-737A-26X-1, Late Miocene. 5. *Artostrobus semazen* Renaudie & Lazarus 2012, Sample 120-751A-6H-698-102cm, Late Miocene. 6. *Lamprocyrtis*? *datureacornis*, holotype, Sample 120-751A-12H-3 98-102cm, Middle Miocene. 7. *Anthocyrtidium* sp. B?, Sample 120-751A-14H-CC, Early/Middle Miocene. 8. *Anthocyrtidium* spB, Sample 120-751A-14H-CC, Early/Middle Miocene. 9. *Anthocyrtidium* sp. B, Sample 120-751A-14H-CC, Early/Middle Miocene. 10. *Cornutella* sp. A, Sample 120-748B-6H-7 45-47cm, Early Miocene. 11. *Cornutella* spA, Sample 119-744A-10H-2 60-62cm, Early Miocene. 12. *Artostrobus semazen*, holotype, Sample 120-748B-5H-7 45-47cm, Middle Miocene. 13. *Artostrobus* sp. B, Sample 120-751A-12H-3 98-102cm, Middle Miocene. 14. *Artostrobus* sp. B, Sample 120-751A-12H-3 98-102cm, Middle Miocene. 15. *Cornutella* sp. A, Sample 119-744A-10H-2 60-62cm, Early Miocene. 16. *Artostrobus semazen*, Sample 120-751A-6H-698-102cm, Late Miocene. 17. *Artostrobus* sp. B, Sample 120-751A-12H-3 98-102cm, Middle Miocene. 18. Undetermined cornutellid, Sample 120-748B-8H-6 45-47cm, Late Oligocene/Early Miocene. All scale bars 50 µm. Magnification x384, except for 6A-C and 10-12A (x192).

Plannapus microcephalus (Haeckel 1887)
(Pl. 11, figs 11A-B)

1887 *Dicolocapsa microcephala* Haeckel: p. 1312; pl. 57, fig. 1
1990 *Dictyocephalus microcephalus* (Haeckel) – Nishimura: p. 163; pl. 35, fig. 5
1997a *Plannapus microcephalus* (Haeckel) – O'Connor: p. 70; pl. 1, figs 10-14; pl. 5, figs 10-12; pl. 6, figs 1-5

Plannapus papillosus (Ehrenberg 1873a)
(Pl. 11, fig. 8)

1873a *Eucyrtidium papillosum* Ehrenberg: p. 310
1873b *Eucyrtidium papillosum* Ehrenberg – Ehrenberg: p. 293; pl. 7, fig. 10
1958 *Dictyocephalus papillosus* (Ehrenberg) – Riedel: p. 236; text-fig. 8; pl. 3, fig. 10
1967 *Dictyocryphalus papillosus* (Ehrenberg) – Nigrini: p. 63; pl. 6, fig. 6
1971 *Tricolocapsa papillosa* (Ehrenberg) – Petrushevskaya: pl. 91, fig. 10
1991 *Carpocanarium papillosum* (Ehrenberg) – Takahashi: p. 132; pl. 45, figs 16-17
1999a *Plannapus papillosus* (Ehrenberg) – O'Connor: p. 7

Plannapus uburex (Renaudie & Lazarus 2012)
(Pl. 11, fig. 12A-14B)

2012 *Carpocanium*? *uburex* Renaudie & Lazarus: p. 41-42; pl. 3, figs 3A-B, 7A-B, 15A-B, 17A-B.

Derivation of name. Named after Alfred Jarry's play 'King Ubu', for the ressemblance of the specimen on pl. 11, fig. 16A-B with the eponymous character.

Diagnosis. Spindle-shaped shell; large cephalis; large peristomial teeth.

Holotype. Plate 11, figs. 14A-B; Sample 120-747A-2H-2 45/47cm (Pleistocene); ECO-038.

Material. 41 specimens were observed from ODP Sites 738, 744, 747 and 751.

Description. Spindle-shaped two-segmented shell. Cephalis is wide and separated externally into three lobes by a more or less pronounced furrow near spine A and another near spine V(?). Spine A is free in the cephalis and often continues outside as a small, tribladed apical horn. Post-cephalic lobe seems on some specimens to open on a vertical tube. The axobate wasn't observed. The collar stricture is marked outside by a furrow and a more or less pronounced shoulder. Some specimens bear a small triangular wing as a continuation of spine D.

Cephalic wall is crested and bears a few small, rounded, unevenly distributed pores. Pores on the thoracic wall however are bigger (but of variable size), often elongated in the longitudinal direction and somewhat aligned longitudinally. This alignment is not strict and tends to be very irregular near the peristome. Ridges can be seen in most specimens between the longitudinal row; they follow the irregularity of the pore alignment. The peristome is hyaline and is composed of a variable number of inward-oriented teeth. The teeth can be either shovel-shaped or triangular or simply a wavy aperture. There is rarely a change in contour between the thorax and the peristome.

Dimensions. (based on 5 specimens) Total length: 92-105 (99); maximum width: 69-76 (72); length of cephalis: 15-27 (22); of thorax: 60-75 (65).

Occurrence. Rare from the Phi to the Psi Zone (Pleistocene).

Remarks. *Plannapus uburex* differs from *Plannapus microcephalus* (Haeckel) 1887*, P. papillosus* (Ehrenberg) 1873a*, P. mauricei* O'Connor, 1999 and *P. hornibrooki* O'Connor, 1999 in the presence of large teeth around the peristome, its cephalis/thorax ratio and the presence of ridges. It also differs from *Carpocanium kinugasense* Nishimura, 1990 in the cephalis being clearly separated externally from the thorax and in the inner structure of the cephalis; and from

Carpocanium rubyae O'Connor, 1997 for the same reasons as the latter and in the pore alignment being far more irregular in *P. uburex*.

Family **Collosphaeridae** Müller 1858

Collosphaerid sp. D
(Pl. 15, figs. 4A-5)

Diagnosis. Large ellipsoidal shell with a thin wall delimiting numerous irregular polygonal pores.

Genus *Acrosphaera* Haeckel 1881

Type-species: *Acrosphaera echinoides* Haeckel 1887

Acrosphaera australis Lazarus 1990

1990 *Acrosphaera australis* Lazarus: p. 712; pl. 1, figs 1-6; pl. 2, fig. 6

Acrosphaera cyrtodon (Haeckel 1887)

1887 *Odontosphaera cyrtodon* Haeckel: p. 102; pl. 5, fig. 6
1971 *Acrosphaera cyrtodon* (Haeckel) – Strelkov & Reshetnyak: p. 344; pl. 7, fig. 51; pl. 8, fig. 54; text-fig. 24

Acrosphaera labrata Lazarus 1992

1979 Collosphaerid sp. Keany: pl. 1, fig. 5
1990 *Acrosphaera* sp. - "ringed" collosphaerid Lazarus: p. 713; pl. 2, fig. 5
1992 *Acrosphaera*? *labrata* Lazarus: p. 793; pl. 1, figs 1-10

Acrosphaera lappacea (Haeckel 1887)

1887 *Xanthiosphaera lappacea* Haeckel: p. 120; pl. 8, figs 10-11
1967 *Polysolenia lappacea* (Haeckel) – Nigrini: p. 16, pl. 1, figs 3a-b
1980 *Acrosphaera lappacea* (Haeckel) – Johnson & Nigrini: p. 119; pl. 1, fig. 2

Acrosphaera? *mercurius* Lazarus 1992

1992 *Acrosphaera*? *mercurius* Lazarus: p. 794; pl. 1, figs 11-16

Acrosphaera murrayana (Haeckel 1887)

1887 *Choenicosphaera murrayana* Haeckel: p. 102; pl. 8, fig. 4
1906 *Acrosphaera murrayana* (Haeckel) – Hilmers: p. 63
1917 *Acrosphaera murrayana* (Haeckel) – Popofsky: p. 259; figs 22-23
1968 *Polysolenia murrayana* (Haeckel) – Nigrini: p. 52, pl. 1, figs 1a-b
1990 *Acrosphaera murrayana* (Haeckel) – Lazarus: p. ; pl. 2, figs 3-4

Acrosphaera cuniculiauris Renaudie & Lazarus 2012
(Pl. 15, figs. 1A-3)

1979 *Cenosphaera* sp. Chen – Keany: p. 51; pl. 1, fig. 3; pl. 5, fig. 1; non *Cenosphaera* sp. Chen, 1975, p. 453; pl. 6, fig. 9; pl. 7, figs 1-2
2002 *Cenosphaera* sp. Keany – Vigour & Lazarus: p. 4; pl. P1, figs 4-13

Derivation of name. *Cuniculus* is Latin for bunny and *auris* for ears; therefore *cuniculiauris* stands for bunny ears, for the shape of the lamellar projections.

Diagnosis. Large pores surrounded by up to three forked lamellar projections.
Holotype. Plate 15, figs. 1A-B; Sample 120-747A-4H-3 45/47cm (late Miocene/early Pliocene); ECO-047.
Material. 133 specimens (including identifiable fragments and broken specimens) were observed from ODP Sites 747 and 751.
Description. Large latticed sphere made of thin lamellar bars separating large subcircular pores. Each pore bears, at its margin, up to three appendices. Those projections are lamellar, of the same width as the bars of the latticed shell, and bi- or trifurcate distally. There are a few smaller pores between the large ones, but those do not bear appendices.
Dimensions. (based on 4 specimens) Pore diameter: 34-63 (50); bar width: 8-18 (12).
Occurrence. Rare to common from the *A. australis* to the *A. challengerae* Zone (late Miocene), appears mostly as fragments.
Remarks. *Acrosphaera cuniculiauris* differs from *A. murrayana* (Haeckel) 1887 primarily in the width of the pores and the appendages surrounding them being several forked lamellar projections instead of one single tubular projection. It also differs from *A. trepanata* (Haeckel) 1887 as illustrated by Goll (1980) in the shape of the appendages and the absence of a rim around the apertures.

Acrosphaera spinosa (Haeckel 1861)

1861 *Collosphaera spinosa* Haeckel: p. 845
1887 *Acrosphaera spinosa* (Haeckel) – Haeckel: p. 100
1967 *Polysolenia spinosa* (Haeckel) – Nigrini: pl. 1, fig. 1
1971 *Acrosphaera spinosa* (Haeckel) – Strelkov & Reshetnyak: pl. 5, figs 33-38; pl. 6, figs 39-41
1979 *Acrosphaera spinosa spinosa* (Haeckel) – Bjørklund & Goll: p. 1308-1311; pl. 1, figs. 8-9

Genus *Collosphaera* Müller 1855

Collosphaera huxleyi Müller 1855

1855 *Collosphaera huxleyi* Müller: p. 238
1917 *Collosphaera huxleyi* Müller – Popofsky: p. 241; text-figs 2-3; pl. 13, figs 1-9
1980 *Collosphaera huxleyi* Müller – Boltovskoy & Riedel: p. 103; pl. 1, fig. 5

Collosphaera macropora Popofsky 1917

1917 *Collosphaera macropora* Popofsky: p. 247; text-figs 5-6; pl. 14, figs 2a-c
1971 *Collosphaera macropora* Popofsky – Strelkov & Reshetnyak: p. 337; pl. 4, figs. 30-31
1982 *Collosphaera planca* Su: p. 275-276, p. 281; pl. 1, figs 7-10

Collosphaera reynoldsi Kamikuri 2010

1980 *Collosphaera* sp. A Reynolds: p. 761; pl. 1, figs. 1-4
2010 *Collosphaera reynoldsi* Kamikuri: p. 97; pl. 3, figs. 18-25

Genus *Siphonosphaera* Müller 1858

Type-species: *Collosphaera tubulosa*? Müller 1855

Siphonosphaera abelmannae Renaudie & Lazarus 2012

(Pl. 15, figs. 6A-9)

1990 *Disolenia* spp. group Abelmann: p. 690; pl. 1, figs 3A-B
Derivation of name. Named after Andrea Abelmann, who first illustrated this species.

Diagnosis. Poreless sphere; a few external tubes ending irregularly.
Holotype. Plate 15, figs. 6A-B; Sample 113-690B-6H-6 22/24cm (Early Miocene); ECO-046.
Material. 37 specimens were observed from ODP Sites 690, 744, 748 and 751.
Description. Small, smooth, hyaline sphere with two to seven large external tubes of variable diameter. Each tube is generally subcylindrical and as long as the diameter of the aperture. These tubes end with thin, irregularly-shaped, filamentous appendices which can be twice as long as the tube itself.
Dimensions. (based on 9 specimens) Shell diameter: 84-125 (107); tube diameter: 21-80 (40).
Occurrence. Rare from the *S. radiosa* to the *C. golli regipileus* Zone (early Miocene).
Remarks. *Siphonosphaera abelmannae* differs from *A. murrayana* in having fewer apertures and in being considerably smaller (its diameter is approximately three times smaller). It also differs from species of the genus *Trisolenia* in having a poreless, hyaline wall; from *S. hyalina* Caulet, 1986 in having more numerous, larger tubes; from *S. chonopora* Haeckel, 1887 in the tubes widely expanding distally in the latter; and from the subspecies *S. socialis* Haeckel, 1887 *tubuliloba* Strelkov & Reshetnjak, 1971 in the shell being totally poreless and lacking crests and in the tubes being larger.

Siphonosphaera magnisphaera Takahashi 1991

? 1982 *Siphonosphaera arkys* Su: p. 276, p. 281-282; pl. 2, figs 3-4
1991 *Siphonosphaera magnisphaera* Takahashi: p. 59; pl. 4, figs 1, 3
1992 *Siphonosphaera magnisphaera* Takahashi – Lazarus: p. 795; pl. 2, figs 9-10; pl. 5, figs 11-14

Siphonosphaera martensi Brandt 1905

1905 *Siphonosphaera martensi* Brandt: p. 339; pl. 9, figs 9-12
1971 *Siphonosphaera martensi* Brandt – Strelkov & Reshetnyak: 9. 356; fig. 28
1980 *Siphonosphaera martensi* Brandt – Boltovskoy & Riedel: p. 104; pl. 1, fig. 8
1991 *Siphonosphaera martensi* Brandt – Takahashi: p. 59; pl. 4, figs 4-5, 7-8

Siphonosphaera vesuvius Lazarus 1992

1979 Collosphaerid sp. Keany: pl. 1, fig. 4
1990 *Acrosphaera* sp. - "conical pore" collosphaerid Lazarus: p. 713; pl. 2, figs 1-2
1992 *Siphonosphaera vesuvius* Lazarus: p. 794-795; pl. 2, figs 1-8

Genus *Trisolenia* Ehrenberg 1861

Type-species: *Trisolenia megalactis* Ehrenberg 1861

Trisolenia megalactis Ehrenberg 1861 emend. Bjørklund & Goll 1979

1861 *Trisolenia megalactis* Ehrenberg: p. 833
1873b *Trisolenia megalactis* Ehrenberg – Ehrenberg: pl. 8, fig. 19
1979 *Trisolenia megalactis* Ehrenberg – Bjørklund & Goll: p. 1318-1321; pl. 5, figs. 1-21

Family **Pterocorythidae** Haeckel 1881 emend. Riedel 1967 emend. Moore 1972

Genus *Anthocyrtidium* Haeckel 1881

Type-species: *Anthocyrtis ophirensis* Ehrenberg 1873a

Anthocyrtidium ehrenbergi (Stöhr 1880)

1880 *Anthocyrtis ehrenbergi* Stöhr: p. 100; pl. 3, figs 21a-b
1887 *Anthocyrtidium ehrenbergi* (Stöhr) – Haeckel: p. 1277
1988 *Anthocyrtidium ehrenbergi* (Stöhr) – Nigrini & Caulet: p. 345-349; pl. 1, figs 3-4

Anthocyrtidium sp. B

(Pl. 13, figs. 7A-9B)

Description. Two-segmented shell. Cephalis elongated, tapering upwards toward a large, tribladed apical horn. Two lateral lobes at the base of the cephalis. Collar stricture marked externally by a change in contour. Thorax barrel-shaped to almost spindle-shaped (Pl. 13, figs 9A-B) with well-spaced longitudinal rows of tiny circular pores. Thorax termination is a thin, hyaline peristome with several triangular projections directed inwards. Pores on cephalis are of same diameter and shape as pores on thorax.

Remarks. It differs from other two-segmented Pterocorythidae in having a smaller, less numerous pores, in having a single row of inward-directed teeth and a long thorax.

Genus *Lamprocyclas* Haeckel 1881

Type-species: *Lamprocyclas nuptialis* Haeckel 1887

Lamprocyclas aegles (Ehrenberg 1854)

1854 *Podocyrtis aegles* Ehrenberg: pl. 35B-4, fig. 18
1887 *Lamprocyclas aegles* (Ehrenberg) – Haeckel: p. 1391
1972 *Lamprocyclas aegles* (Ehrenberg) – Petrushevskaya & Kozlova: pl. 36, fig. 13

Lamprocyclas hannai (Clark & Campbell 1944)

1944 *Calocyclas (Calocycletta) hannai* Clark & Campbell: p. 48; pl. 6, figs 21-22
1986 *Lamprocyclas hannai* (Clar & Campbell) – Caulet: p. 852

Lamprocyclas maritalis Haeckel 1887

1887 *Lamprocyclas maritalis* Haeckel: p. 1390; pl .74, figs 13-14
1967 *Lamprocyclas maritalis maritalis* Haeckel – Nigrini: p. 74; pl. 7, fig. 5

Lamprocyclas? sp. E

(Pl. 13, figs. 3-4)

Description. Thick-walled, three-segmented pterocorythid with an almost spherical cephalis, a campanulate thorax and a barrel-shaped to inverted-truncated conical abdomen shorter and narrower than the thorax. The abdomen ends with a short hyaline, toothless peristome. Lumbar stricture slightly expressed externally by a constriction.

Remarks. It differs from *Lamprocyclas maritalis* and *L. aegles* in its short, narrow abdomen, its small pores and its toothless peristome.

Genus *Lamprocyrtis* Kling 1973

Type-species: *Lamprocyclas heteroporos* Hays 1965

Lamprocyrtis heteroporos (Hays 1965)

1965 *Lamprocyclas heteroporos* Hays: p. 179; pl. 3, fig. 1
1973 *Lamprocyrtis heteroporos* (Hays) – Kling: p. 639; pl. 5, figs 19-21; pl. 15, fig. 6
1986 *Lamprocyrtis heteroporos* (Hays) – Mullineaux & Westberg-Smith: p. 58

Lamprocyrtis? *datureacornis* Renaudie & Lazarus in press
(Pl. 13, figs. 1A-2, 6A-C)

Derivation of name. Named after its apical horn that looks like a *Datura* flower: *datureacornis* is composed of *datura* with the suffix *-eus* denoting a resemblance and *cornis*, horn.

Diagnosis. Hood-shaped cephalis with an open apex surrounded by a cluster of thorns; lateral lobes; flaring thorax with longitudinally-aligned pores.

Holotype. Pl. 4, figs 15A-C; Sample 120-751A-12H-3, 98-102cm (Middle Miocene); ECO-055.

Material. 11 specimens were observed from ODP Sites 748 and 751.

Description. Two-segmented shell with a cephalis that is elongated apically on the dorsal side and a thorax that is, first, truncated-conical, then cylindrical and, finally, truncated-conical again. The cephalis has a large eucephalic chamber and two lateral chambers (i.e. chambers situated laterally below the arches **AL**; Pl. 4, figs 11A and 15B). The collar stricture is marked by a furrow following arches **AL** and **VL**. Spine **A** is free in the eucephalic cavity and continues as a complex horn disposed around an apical opening (Pl. 4, fig. 15B). This horn has several vertices (at least three): each pair of adjacent vertices are joined by a hyaline plate (sometimes perforated at its base; Pl. 4, fig. 12) whose upper boundary trace an elliptical arc between the two vertices. At its widest, the cephalis often bears additional small thorns which do not seem to be connected to inner spines.

Pores on the cephalis are round, relatively large, closely packed and arranged according to a more or less regular hexagonal pattern. Pores on thorax are larger; they are round, elliptical or subpolygonal and are aligned longitudinally. The thorax flares distally and seems to bear a few laterally projecting, spine-like teeth at its termination (Pl. 4, fig. 12 and 15B).

Dimensions. (based on 3 specimens) Length of cephalis (including horns): 118-122 (121); length of thorax: 217-224 (221).

Occurence. Rare from the *Actinomma golownini* to the lower *Cycladophora spongothorax* Zone (Middle Miocene).

Remarks. *Lamprocyrtis*? *datureacornis* was assigned to the family Pterocorythidae on the basis of the presence of lateral lobes. However, the shape of its thorax in particular is very uncommon in this family. Because of its open-ended apex, this species was assigned tentatively to the genus *Lamprocyrtis* but there are dissimilarities with the other members of the genus: the two principal being an hood-shaped instead of a cylindrical cephalis and externally-expressed lateral lobes. The open-ended apex and the elongated cephalis are also a character found in some lophophaenids such as *Amphiplecta acrostoma* Haeckel, 1887, or *Lophophaena buetschlii* (Haeckel) 1887; so an alternative hypothesis would be that *L.*? *datureacornis* is indeed a lophophaenid.

Lamprocyrtis? *datureacornis* differs from *Lampromitra sinuosa* Popofsky, 1913, in its elongated cephalis, its apical opening, its lateral lobes and the shape of its upper thorax.

Genus *Pterocorys* Haeckel 1881

Type-species: *Pterocorys campanula* Haeckel 1887

Pterocorys clausus (Popofsky 1913)

1913 *Lithornithium clausum* Popofsky: p. 393-395; text-fig. 111
1913 *Theoconus zancleus* Popofsky: p. 397-398; pl. 38, figs 6-7
1972 *Pterocorys clausus* Popofsky group – Petrushevskaya & Kozlova: p. 545; pl. 36, figs 16-18
1988 *Pterocorys clausus* Popofsky – Caulet & Nigrini: p. 229; pl. 1, figs 6-10

Genus *Theocorythium* Haeckel 1887

Type-species: *Theocorys dianae* Haeckel 1887

Theocorythium trachelium (Ehrenberg 1873a)

1873a *Eucyrtidium trachelius* Ehrenberg: p. 312
1873b *Eucyrtidium trachelius* Ehrenberg – Ehrenberg: pl. 7, fig. 8
1887 *Theocyrtis trachelius* (Ehrenberg) – Haeckel: p. 1405
1967 *Theocyrtidium trachelium trachelium* (Ehrenberg) – Nigrini: p. 79-81; pl. 8, fig. 2; pl. 9, fig. 2
1971 *Theocyrtidium trachelium* (Ehrenberg) – Petrushevskaya: p. 232; pl. 117, fig. 4; pl. 118, fig. 1-2

Genus *Theocyrtis* Haeckel 1887

Type-species: *Eucyrtidium barbadense* Ehrenberg 1873

Theocyrtis diabolensis Clark & Campbell 1942

1942 *Theocyrtis diabolensis* Clark & Campbell: p. 90; pl. 8, fig. 13
1975 *Theocyrtis diabolensis* Clark & Campbell – Chen: pl. 5, figs 4-7

Family **Sphaeozoidae** Haeckel 1862

Genus *Sphaerozoum* Meyen 1834

Type-species: *Sphaerozoum fuscum* Meyen 1834

Sphaerozoum punctatum (Huxley 1851)

1851 *Thalassicola punctata* Huxley: p. 434; pl. 16, figs 1-3
1858 *Sphaerozoum punctatum* (Huxley) – Müller: p. 54; pl. 8, figs 1-2
1980 *Sphaerozoum punctatum* (Huxley) – Goll: pl. 1, figs 1-2

Family **Theoperidae** Haeckel 1887 emend. Riedel 1967

Genus *Anthocyrtella* Haeckel 1887

Type-species: *Anthocyrtella mespilus* Ehrenberg 1854

Anthocyrtella callospima Caulet 1986

1975 *Anthocyrtella* sp. A Petrushveskaya: pl. 15, fig. 2; pl. 16, fig. 5
1986 *Anthocyrtella*? *callospima* Caulet: p. 227; pl. 1, figs 1-2

Anthocyrtella kruegeri (Popofsky 1908)

1908 *Corocalyptra kruegeri* Popofsky: p. 289; pl. 35, fig. 8
1972 Eucyrtidioidea gen. sp. Petrushevskaya & Kozlova: pl. 25, fig. 3
1975 *Anthocyrtella*? *kruegeri* (Popofsky) - Petrushevskaya: pl. 25, figs 9-10

Genus *Artobotrys* Petrushevskaya 1971

Type-species: *Theocorys borealis* Cleve 1899

Artobotrys auriculaleporis (Clark & Campbell 1942)

1942 *Lophophaena auriculaleporis* Clark & Campbell: p. 89; pl. 8, figs 20, 27-29

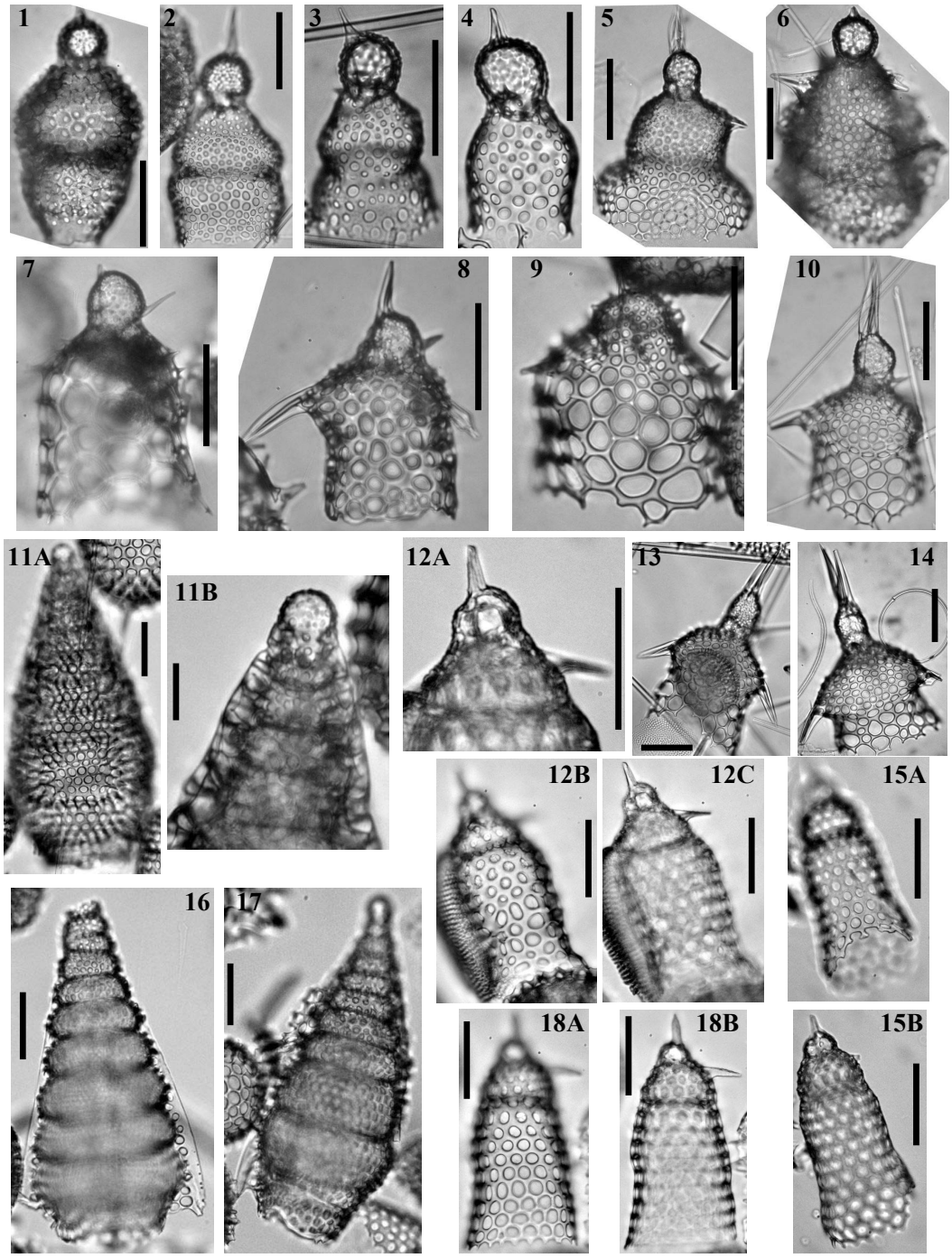

Plate 14.– 1. *Theocorys redondoensis* (Campbell & Clark 1944), Sample 119-737A-27X-2 53-55cm, Late Miocene. 2. *Gondwanaria deflandrei* Petrushevskaya 1975, Sample 120-748B-6H-3 45-47cm, Early Miocene. 3. *Gondwanaria japonica* (Nakaseko 1963), Sample 120-748B-5H-7 45-47cm, Middle Miocene. 4. *Gondwanaria hister* Petrushevskaya 1975, Sample 119-744A-8H-1, Early Miocene. 5. *Gondwanaria nigriniae* Petrushevskaya & Kozlova 1979, Sample 119-744A-10H-2 60-62cm, Early Miocene. 6. *Lipmanella dictyoceras* (Haeckel 1860), Sample 120-747A-1H-5 45-47cm, Pleistocene. 7. *Gondwanaria campanulaeformis* (Campbell & Clark 1944), Sample 119-745B-12H-4 53-55cm, Late Pliocene. 8. *Gondwanaria cylindrica* Funakawa 2000, Sample 120-748B-6H-3 45-47cm, Early Miocene. 9. *Gondwanaria reschetnjakae* (Petrushsvakya 1967), Sample 120-747A-2H-3 45-47cm, Pleistocene. 10. *Gondwanaria clarae* Renaudie & Lazarus 2012, holotype, Sample 120-748B-5H-5 45-47cm, Middle Miocene. 11. *Stichophormis*? *cheni* Renaude & Lazarus 2012, holotype, Sample 119-744A-8H-1 60-62cm, Early Miocene. 12. *Lophocyrtis pallantae* Renaudie & Lazarus in press, holotype, Sample 120-748B-8H-6 45-47cm, Late Oligocene/Early Miocene. 13. *Gondwanaria clarae*, Sample 120-751A-12H-2 98-102cm, Middle Miocene. 14. *Gondwanaria clarae*, Sample 120-751A-10H-2 98-102cm, Middle Miocene. 15. L*ophocyrtis pallantae*, Sample 120-748B-8H-4 45-47cm, Early Miocene. 16. *Stichophormis*? *cheni* , Sample 120-751A-15H-CC, Early Miocene. 17. *Stichophormis*? *cheni* , Sample 120-751A-16H-CC, Early Miocene. 18. *Lophocyrtis pallantae*, Sample 120-748B-8H-6 45-47cm, Late Oligocene/Early Miocene. All scale bars 50 µm except for 11B where it is 10 µm. Magnification x384 except for 2, 11A, 13, 16 and 17 (x192), and for 11B (x576).

1979 *Artobotrys* aff. *auriculaleporis* (Clark & Campbell) – Petrushevskaya & Kozlova: fig. 397

Artobotrys biaurita (Ehrenberg 1873)

1873 *Eucyrtidium biauritum* Ehrenberg: p. 226
1875 *Eucyrtidium biauritum* Ehrenberg – Ehrenberg: pl. 10, figs 7-8
1979 *Artobotrys* aff. *biaurita* (Ehrenberg) – Petrushevskaya & Kozlova: p. 136; fig. 396

Artobotrys borealis (Cleve 1899)

1899 *Theocorys borealis* Cleve: p. 33; pl. 3, fig. 5
1971 *Artobotrys borealis* (Cleve) – Petrushevskaya: p. 238; pl. 82, figs 7-12
1976a *Artobotrys borealis* (Cleve) – Bjørklund: pl. 11, figs 24-27

Genus *Artophormis* Haeckel 1881

Type-species: *Artophormis horrida* Haeckel 1887

Artophormis sp. cf *A. gracilis* Riedel 1959
(Pl. 12, figs. 9A-B)

cf 1959 *Artophormis gracilis* Riedel: p. 300; pl. 2, figs 12-13
1990 *Artophormis gracilis* Riedel – Abelmann: p. 697; pl. 7, fig. 5

Remarks. The specimens found here and those illustrated by Abelamnn (1990) differs from the species described by Riedel (1959) in the fourth segment being developed in the same fashion as the thorax and the abdomen instead of being arranged around several longitudinal ribs and in the apical horn being indifferentiable from the other spines that the characteristic apical cluster consists of.

Genus *Artostrobus* Haeckel 1887

Type-species: *Cornutella*? *annulata* Bailey 1856

Artostrobus annulatus (Bailey 1856)

1856 *Cornutella*? *annulata* Bailey: p. 3; pl. 1, figs 5a-b
1862 *Eucyrtidium annulatum* (Bailey) – Haeckel: p. 327-328
1887 *Artostrobus annulatus* (Bailey) – Haeckel: p. 1481
1958 *Artostrobus annulatus* (Bailey) – Riedel: p. 239-242; pl. 4, fig. 6
1967 *Artostrobus annulatus* (Bailey) – Petrushevskaya: p. 98-99; pl. 56, figs 1-5
2006 *Cornutella*? *annulata* Bailey – Itaki & Bjørklund: p. 451; pl. 1, figs 9-17

Artostrobus joergenseni Petrushevskaya 1967

1967 *Artostrobus jörgenseni* Petrushevskaya: p. 99-101; pl. 57, figs 1-10
1976a *Artostrobus joergenseni* Petrushevskaya – Bjørklund: pl. 11, figs 12-13

Artostrobus pretabulatus Petrushevskaya 1975

1975 *Artostrobus*? *pretabulatus* Petrushevskaya: p. 580; pl. 10, figs 2-3
1986 "*Artostrobus*" *pretabulatus* Petrushevskaya – Ashby: pl. 30, fig. 15

Artostrobus quadriporus Bjørklund 1976a

1976a *Artostrobus quadriporus* Bjørklund: p. 1125; pl. 23, figs 15-21

Artostrobus tabulatus (Ehrenberg 1873)

1873 *Cycladophora tabulatus* Ehrenberg: pl. 4, fig. 18
1899 *Sethoconus tabulatus* (Ehrenberg) – Cleve: p. 33; pl. 4, fig. 2
1967 *Sethoconus*? *tabulatus* (Ehrenberg) – Petrushveskaya: p. 94-96; pl. 54, figs 1-5

Artostrobus? sp. B
(Pl. 13, figs 13-14 17)

Description. Spherical cephalis with thin, apical horn and downward-directed dorsal and lateral wings. Campanulate thorax with two to four transversal rows of pores. Post-thoracic segment(s) are irregularly shaped, of various width and height, giving the shell a wavy outline. Each of the post-thoracic segments bears two to four transversal rows of pores. All pores are more or less equal in size and shape except for the tiny cephalic pores. Stricture between the post-thoracic segments is more or less expressed (compare Pl. 13, fig. 13 and Pl. 13, fig. 17).
Remarks. It differs from *A.*? *semazen* in its shorter apical horn, its shorter thorax and in the latter having a flared abdomen and no post-abdominal segments.

Artostrobus? *semazen* Renaudie & Lazarus 2012
(Pl. 13, figs 5, 12A-B, 16)

Derivation of name. *Semazen* is Turkish for a Whirling Dervish.
Diagnosis. Long apical horn; mid-thorax constriction; lower thorax flares distally; pores aligned in transverse rows.
Holotype. Plate 4, figs. 5A-B; Sample 120-748B-5H-7 45/47cm (Middle Miocene); ECO-045.
Material. 11 specimens were observed from ODP Sites 748 and 751.
Description. Two-segmented shell with a small hemispherical cephalis and a thorax divided into an upper and a lower thorax by a change in contour at mid-height and a slight constriction.
Cephalis has a poreless wall. Spine A runs in the cephalic wall as a rib from the collar stricture to the apex where it continues outside as a long (generally as long as the whole shell but can be longer), slender conical horn. Spines D, Ll and Lr protrudes outside the cephalic wall at the collar stricture at first as ribs on the uppermost part of the thorax and then as curved, downward-directed, thin, slender wings. Spine V also continues as a short, thin and slender horn that forms a ca. 50° angle with the apical horn. Arches AL form small ribs on the cephalic wall (see Pl. 4, fig. 10). A small axobate can be seen at the junction between spines V, Ll and Lr.
The upper thorax is somewhat barrel-shaped whereas the lower thorax forms a short flaring skirt. Both have thin, smooth walls with transverse rows of circular to hexagonal or quadrangular pores. Some of these pores are infilled on the uppermost part of the thorax. Some specimens shows a differentiation in the size of the upper and lower thorax pores; but, most generally, pores are approximately even in size.
Dimensions. (based on 4 specimens) Shell length (without horn): 54-70 (61); apical horn length: 54-226 (68); lower thorax maximum width: 45-50 (48); width at constriction: 33-37 (35).
Occurrence. Sporadic to rare from the lower *C. spongothorax* to the *A. australis* Zone (Middle to Late Miocene).
Remarks. *Artostrobus semazen* differs from *A. annulatus*, *A. joergenseni* Petrushveskaya, 1967, *A. quadriporus* Bjørklund ,1976a and *A.*? *pretabulatus* Petrushevskaya, 1975 in its thorax being differentiated into an upper thorax and a flaring lower thorax. It also differs from *Cycladophora davisiana* Ehrenberg, 1873a, *C. conica* Lombari & Lazarus, 1988, *C. cosma* Lombari & Lazarus, 1988 and *C. robusta* Lombari & Lazarus, 1988 in its pore size and disposition, in the constriction and change in contour between the upper and lower thorax, in the apical and ventral horns being slender and conical and in the presence of dorsal and lateral wings.

Genus *Clinorhabdus* Sanfilippo & Caulet 1998
Type-species: *Clinorhabdus anantomus* Sanfilippo & Caulet 1998

Clinorhabdus anantomus Sanfilippo & Caulet 1998
1998 *Clinorhabdus anantomus* Sanfilippo & Caulet: p. 20; pl. 1, figs 14-25; pl. 8, figs 1a-b, 3a-b

Clinorhabdus longithorax (Petrushevskaya 1975) emend. Sanfilippo & Caulet 1998
1975 *Theocorys longithorax* Petrushevskaya: p. 580; pl. 8, figs 17-18; pl. 22; fig. 2
1975 *Cyrtocapsella isopera* Chen: p. 460; pl. 11, figs 7-9
1990 *Cyrtocapsella longithorax* (Petrushevskaya) – Abelmann: p. 696; pl. 5, figs 12a-b
1998 *Clinorhabdus longithorax* (Petrushevskaya) – Sanfilippo & Caulet: p. 22; pl. 1, figs 1-5; pl. 8, figs 1-8c

Clinorhabdus robusta (Abelmann 1990) emend. Sanfilippo & Caulet 1998
1990 *Cyrtocapsella robusta* Abelmann: p. 696; pl. 5, figs 10-11
1992 *Cyrtocapsella robusta* Abelmann – Takemura: p. 746; pl. 1, figs 5-6
1998 *Clinorhabdus robusta* (Abelmann) – Sanfilippo & Caulet: p. 22; pl. 1, figs 7-10; pl. 8, figs 9-14

Genus *Cornutella* Ehrenberg 1838
Type-species: *Cornutella clathrata* Ehrenberg 1838

Cornutella clathrata Ehrenberg 1838
1838 *Cornutella clathrata* Ehrenberg: p. 129
1854 *Cornutella clathrata* Ehrenberg – Ehrenberg: pl. 22, figs 39a-c
1887 *Cornutella curvata* Haeckel: p. 1183
1990 *Cornutella clathrata* Ehrenberg – Abelmann: pl. 8, fig. 8

Cornutella profunda Ehrenberg 1854
1854 *Cornutella clathrata profunda* Ehrenberg*:* pl. 35, fig. 21
1958 *Cornutella profunda* Ehrenberg – Riedel: pl. 3, figs 1-2
1976a *Cornutella profunda* Ehrenberg – Bjørklund: pl. 11, fig. 15

Cornutella sp. A
(Pl. 13, figs. 10-11, 15)

Description. Large cornutellid with a thorax flaring quickly after the cephalis and then stopping fairly soon. Subquadrangular pores arranged in longitudinal rows and, almost, in transversal rows. Some longitudinal rows sometimes split in two. The cephalis is very small, hyaline and spherical, and bears no apparent horns.

Genus *Cycladophora* Ehrenberg 1861 emend. Lombari & Lazarus 1988
Type-species: *Cycladophora davisiana* Ehrenberg 1873a

Cycladophora antiqua Abelmann 1990
1990 *Cycladophora antiqua* Abelmann: p. 698; pl. 7, figs 13a-b

Cycladophora bicornis (Popofsky 1908)
1908 *Pterocorys bicornis* Popofsky: p. 288; pl. 34, figs 7-8

1958 *Theocalyptra*? *bicornis* (Popofsky) – Riedel: p. 240; pl. 4, fig. 4
1972 *Clathrocyclas bicornis* (Popofsky) – Petrushevskaya & Kozlova: p. 540; pl. 33, figs 11-12
1988 *Cycladophora bicornis bicornis* (Popofsky) – Lombari & Lazarus: p. 106-108; pl. 5, figs 9-12
1988 *Cycladophora bicornis amphora* (Popofsky) – Lombari & Lazarus: p. 110-114; pl. 4, figs 6-12

Cycladophora campanula Lombari & Lazarus 1988

1988 *Cycladophora campanula* Lombari & Lazarus: p. 123-124; pl. 10, figs 1-12

Cycladophora conica Lombari & Lazarus 1988

1913 *Clathrocyclas alcmenae* Haeckel – Popofsky: pl. 37, fig. 4 non pl. 38 fig. 5
1988 *Cycladophora conica* Lombari & Lazarus: p. 105-106; pl. 3, figs 1-16

Cycladophora cornutoides Petrushveskaya 1967

1967 *Cycladophora davisiana* Ehrenberg var. *cronutoides* Petrushevskaya: p. 124; pl. 70, figs 1-3
1989 *Cycladophora davisiana* Ehrenberg var. *cronutoides* Petrushevskaya – Goll & Bjørklund: p. 728
1991 *Theocalyptra davisiana* Ehrenberg *cornutoides* Petrushevskaya – Takahashi: p. 123; pl. 42, figs 12-16
1997 *Cycladophora cornutoides* Petrushevskaya – Motoyama: p. 56

Cycladophora cosma Lombari & Lazarus 1988

1988 *Cycladophora cosma cosma* Lombari & Lazarus: p. 104-105; pl. 1, figs 1-6
1988 *Cycladophora cosma irregularis* Lombari & Lazarus: p. 105; pl. 2, figs 1-12

Cycladophora davisiana Ehrenberg 1862

1862 *Cycladophora*? *davisiana* Ehrenberg: p. 297
1873 *Cycladophora*? *davisiana* Ehrenberg – Ehrenberg: pl. 2, fig. 11
1958 *Theocalyptra davisiana* Riedel: p. 239; pl. 4, figs 2-3; text-fig. 10
1967 *Cycladophora davisiana* Ehrenberg – Petrushevskaya: p. 120-122; pl. 69
1976a *Cycladophora davisiana* Ehrenberg – Bjørklund: pl. 11, figs 9-10

Cycladophora golli golli (Chen 1975)

1975 *Lophocyrtis golli* Chen: p. 461; pl. 12, figs 4-5
1988 *Cycladophora golli golli* (Chen) – Lombari & Lazarus 1988: p. 124; pl. 11, figs 1-5, 10-12
1990 *Cycladophora golli golli* (Chen) – Abelmann: pl. 8, figs 1a-b

Cycladophora golli regipileus (Chen 1975)

1975 *Lophocyrtis regipileus* Chen: p. 461; pl. 12, figs 6-7
1988 *Cycladophora golli regipileus* (Chen) – Lombari & Lazarus 1988: p. 124; pl. 11, figs 6-9
1990 *Cycladophora golli regipileus* (Chen) – Abelmann: pl. 8, figs 2a-b

Cycladophora humerus (Petrushevskaya 1975)

1975 *Clathrocyclas humerus* Petrushevskaya: p. 586; pl. 15, figs 22-23; pl. 43, figs 1-2 non pl. 15, fig. 7
1988 *Cycladophora humerus* (Petrushevskaya) – Lombari & Lazarus: p. 123; pl. 9, figs 1-6

1990 *Cycladophora humerus* (Petrushevskaya) – Lazarus: p. 715-716; pl. 4, fig. 8

Cycladophora pliocenica (Hays 1965)

1965 *Clathrocyclas bicornis* Hays: p. 179; pl. 2, fig. 3
1988 *Cycladophora pliocenica* (Hays) – Lombari & Lazarus: p. 104
1990 *Cycladophora pliocenica* (Hays) – Lazarus: pl. 4, figs 6-7

Cycladophora robusta Lombari & Lazarus 1988

1984 *Theocalyptra davisiana davisiana* (Ehrenberg) – Nigrini & Lombari: p. N139; pl. 26, fig. 2
1988 *Cycladophora robusta* Lombari & Lazarus: p. 105; pl. 2, figs 1-14

Cycladophora rosetta Lombari & Lazarus 1988

1988 *Cycladophora rosetta* Lombari & Lazarus: p. 114-116; pl. 6, figs 1-10

Cycladophora spongothorax (Chen 1975)

1975 *Theocalyptra bicornis* (Popofsky) *spongothorax* Chen: p. 462; pl. 12, figs 1-3
1988 *Cycladophora spongothorax* (Chen) – Lombari & Lazarus: p. 122-123; pl. 9, figs 7-12
1990 *Cycladophora spongothorax* (Chen) – Lazarus: pl. 4, figs 1-3

Cycladophora sp. A
(Pl. 12, figs 1-4)

Description. Large two-segmented shell with a small spherical cephalis bearing a strong, smooth, blade-like apical horn and, in some specimens (Pl. 12, figs 3-4), a short tribladed ventral horn. The upper part of the thorax is campanulate with small, spaced, circular pores. The lower part of the thorax flares widely and bears large elliptical pores. In some specimens (Pl. 12, figs 3-4), the horizontal-most part of the thorax seems to be separated from the rest of the thorax by an inner circular ring (lumbar stricture?).
Remarks. Easily distinguishable from the other cycladophorids by its characteristic apical horn and its flaring lower thorax.

Cycladophora sp. B
(Pl. 12, figs 6, 8)

Diagnosis. Small cycladophorid characterized by large, closely-packed, subpolygonal to polygonal pores and a row of spines above the thorax termination.

Genus *Cyrtocapsella* Haeckel 1887

Type-species: *Cyrtocapsa (Cyrtocapsella) tetrapera* Haeckel 1887

Cyrtocapsella japonica (Nakaseko 1963)

1963 *Eusyringium japonicum* Nakaseko: p. 184; text-fig. 15; pl. 3, figs 1-3
1970 *Cyrtocapsella japonica* (Nakaseko) – Sanfilippo & Riedel: p. 452; pl. 1, figs 13-15
1980 *Cyrtocapsella japonica* (Nakaseko) – Sakai: p. 709; pl. 8, figs 7a-b

Cyrtocapsella tetrapera (Haeckel 1887)

1887 *Cyrtocapsa (Cyrtocapsella) tetrapera* Haeckel: p. 1512; pl. 78, fig. 5
1970 *Cyrtocapsella tetrapera* (Haeckel) – Sanfilippo & Riedel: p. 453; pl. 1, figs 16-18

Genus *Cyrtopera* Haeckel 1882

Type-species: *Cyrtopera thoracoptera* Haeckel 1887

Cyrtopera laguncula Haeckel 1887

1887 *Cyrtopera laguncula* Haeckel: p. 1451; pl. 75, fig. 10
1971 *Cyrtolagena laguncula* (Haeckel) – Petrushevskaya: pl. 89, fig. 1-3
1984 *Cyrtolagena laguncula* (Haeckel) – Nishimura & Yamauchi: p. 55; pl. 41, figs 5, 8
1991 *Cyrtopera laguncula* Haeckel – Takahashi: p. 119; pl. 40, figs 3-6

Genus *Dictyophimus* Ehrenberg 1847 *sensu* Nigrini 1967

Type-species: *Dictyophimus crisiae* Ehrenberg 1854

Dictyophimus archipilium Petrushevskaya 1975

1975 *Dictyophimus archipilium* Petrushevskaya: p. 538; pl. 25, figs 1-2

Dictyophimus crisiae Ehrenberg 1854

1854 *Dictyophimus crisiae* Ehrenberg: p. 241
1967 *Dictyophimus crisiae* Ehrenberg – Nigrini: p. 66; pl. 6, figs 7a-b
1979 *Dictyophimus crisiae* Ehrenberg – Nigrini & Moore: pl. 22, figs 1a-b
1991 *Dictyophimus crisiae* Ehrenberg – Takahashi: p. 115; pl. 37, fig. 2

Dictyophimus hirundo (Haeckel 1887)

1887 *Pterocorys hirundo* Haeckel: p. 1318; pl. 71, fig. 4
1958 *Pterocorys hirundo* Haeckel – Riedel: p. 238; pl. 3, fig. 1; pl. 4, fig. 1; text-fig. 9
1967 *Pterocorys*? *hirundo* Haeckel – Petrushevskaya: p. 114-116; pl. 67
1979 *Dictyophimus hirundo* (Haeckel) group – Nigrini & Moore: pl. 22, figs 2-4

Dictyophimus infabricatus Nigrini 1968

1968 *Dictyophimus infabricatus* Nigrini: p. 56; pl. 1, fig. 6
1991 *Dictyophimus infabricatus* Nigrini – Talahashi: pl. 37, figs 3-5
1992 *Dictyophimus infabricatus* Nigrini – Nigrini & Caulet: p. 146; pl. 2, figs, figs 3-5

Dictyophimus macropterus (Ehrenberg 1873)

1873 *Lithomelissa macroptera* Ehrenberg: p. 241
1875 *Lithomelissa macroptera* Ehrenberg – Ehrenberg: pl. 3, figs 9-10 non fig. 8
1887 *Lithomelissa macroptera* Ehrenberg – Haeckel: p. 1204
1991 *Dictyophimus macropterus* (Ehrenberg) – Takahashi: p. 116; pl. 39, figs 8-11

Dictyophimus? *planctonis* Popofsky 1908

1908 *Dictyophimus planctonis* Popofsky: p. 275; pl. 32, fig. 6
1974 *Pseudodictyophimus gracilipes* (Bailey) *tetracanthus* (Popofsky) – Renz: pl. 18, fig. 2

Dictyophimus larus Renaudie & Lazarus 2012

(Pl. 12, figs 7A-B, 10, 15A-B)

1975 *Pterocanium* sp Benson – Chen: pl. 13, fig. 9.
1992 *Pterocanium*(?) sp Takemura: p. 747; pl. 1, fig. 7.

Derivation of name. *Larus* is Latin for a sea-gull.

Diagnosis. Large pyriform thorax; wings widely flaring; rough, thick cephalis.

Holotype. Plate 12, fig. 10; Sample 120-748B-6H-1 45/47cm (Early Miocene); ECO-040.

Material. 22 specimens were observed from ODP Sites 744, 747 and 748.
Description. Two-segmented shell with a small, spherical cephalis and a very large pyriform thorax.
The cephalis is thick, rough, bumpy and poreless. It bears a conical, fairly long horn in relation with spine A which is free in the cephalic cavity. The cephalis also bears also many thorns that could be almost as long as the apical horn. Spines D, Ll and Lr continues in the thoracic wall as thick, cylindrical ribs that protrudes at mid-length outside the wall as long, widely (up to 80°) flaring wings.
Pores on thorax are large, unequal in size, circular to polygonal. The bars between the pores are relatively thin (compared to the pores), slightly crested and they bear spine-like thorns on the upper thorax at each node. At mid-length the thorax begins to taper inwards, to the closure which is a large peristome with the same lattice wall as the rest of the thorax. Bars often connect the wings with the upper part of this peristome.
Dimensions. (based on 4 specimens) Length (without the horns): 199-288 (247); maximum width: 134-220 (180); wings length: 244-345 (290).
Occurrence. Very rare from the *S. radiosa* to the *E. punctatum* Zone (early to middle Miocene). According to Takemura (1992), this species originates in the Eocene or earlier.
Remarks. *Dictyophimus larus* differs primarily from the other Pterocanids in its size. It also differs from *D. crisiae, D. hirundo* (Haeckel) 1887 and *D. infabricatus* Nigrini, 1968 in its thick, rough, thorn-bearing cephalis. The thorax termination seems to be also typical of this species.

Dictyophimus? *kiwi* Renaudie & Lazarus 2012
(Pl. 12, figs 12A-13B)

Derivation of name. Named after the kiwi bird.
Diagnosis. Short wings; large flaring thorax.
Holotype. Plate 12, figs. 13A-B; Sample 120-748B-6H-1 45/47cm (Early Miocene); ECO-043.
Material. 23 specimens were observed from ODP Sites 744, 748 and 751.
Description. Two-segmented shell with a small spherical cephalis and a large, long, flaring thorax.
The cephalis bears several, scattered, very small circular pores, along with a long (nearly 2 times the length of the cephalis), conical apical horn, a small and thin ventral horn and several additional thin and short horns, unconnected to any internal spines. Spine A and V are free in the cephalic cavity. Spines D, Ll and Lr extends as thin, cylindrical ribs on the upper part of the thorax and ends up protruding outside the thoracic wall as very short and thin conical wings.
The thoracic pores are polygonal and get bigger along a gradient from the cephalis to the flaring termination of the thorax. The angle formed by the lower thorax (i.e. the part below the wings) is somewhat smaller than the angle formed by the upper thorax. The thin bars between the upper thoracic pores are crested and often bear thorns.
Dimensions. (based on 3 specimens) Length (without the horns): 123-148 (138); maximum width: 110-126 (120).
Occurrence. Very rare from the *C. antiqua* to the *A. golownini* Zone (early to middle Miocene).
Remarks. *Dictyophimus*? *kiwi* differs from the other species of the genus *Dictyophimus* in its short wings and its long thorax extending well below the wings.

Dictyophimus splendens (Campbell & Clark 1944)

1944 *Pterocorys (Pterocyrtidium) splendens* Campbell & Clark: p. 46; pl. 6, figs 16, 19-20
1986 *Dictyophimus splendens* (Campbell & Clark) – Caulet: p. 852
1995 *Dictyophimus splendens* (Campbell & Clark) – Morley & Nigrini: p. 79; pl. 7, figs 3-4

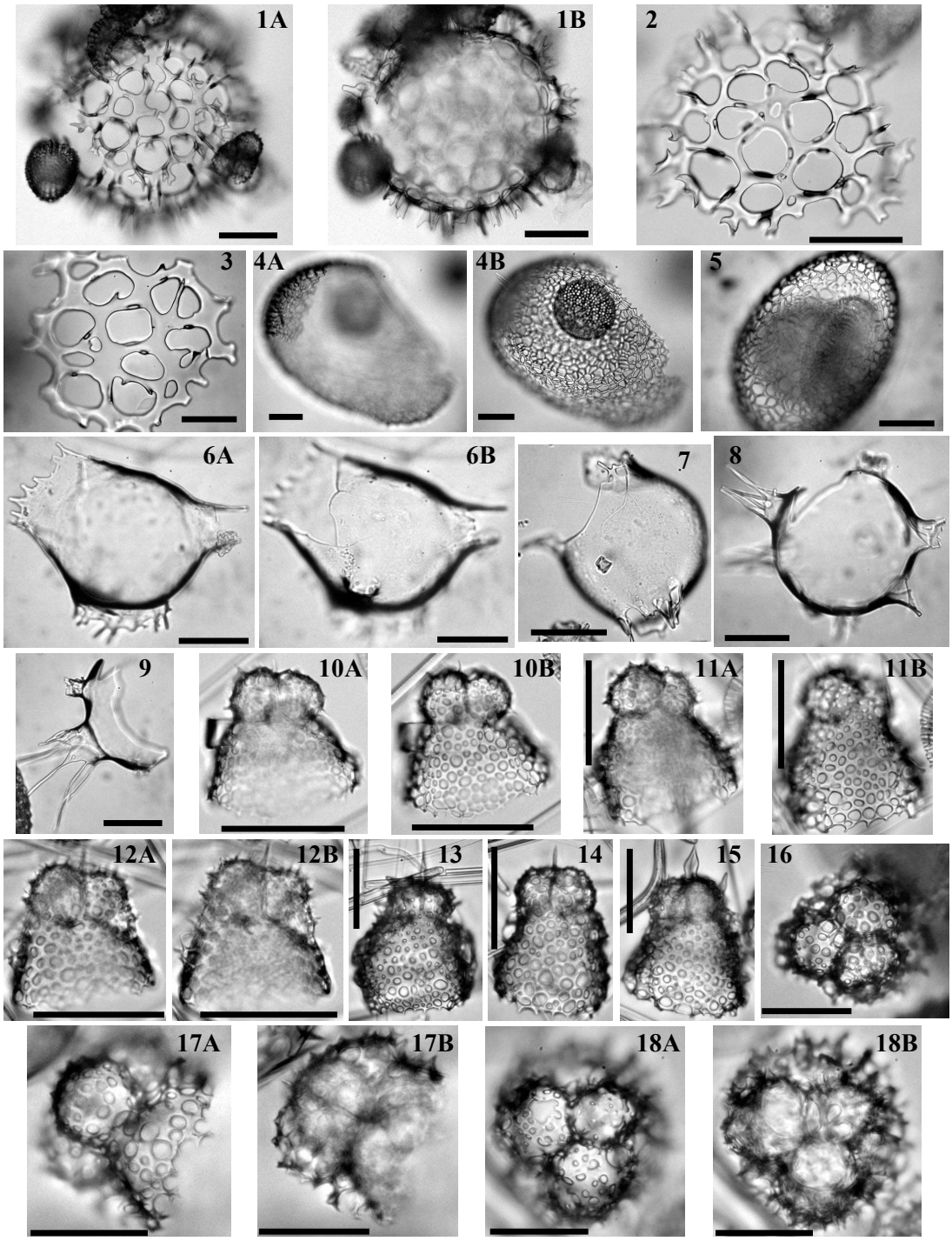

Plate 15.– 1. *Acrosphaera cuniculiauris* Renaudie & Lazarus 2012, holotype, Sample 120-747A-4H-3, 45-47cm, Late Miocene. 2. Fragment of *Acrosphaera cuniculiauris*, Sample 120-751A-5H-5 98-102cm, Late Miocene. 3. Fragment of *Acrosphaera cuniculiauris*, Sample 120-751A-5H-5 98-102cm, Late Miocene. 4. *Collosphaera*? spD, Sample 120-748B-5H-7 45-47cm, Middle Miocene. 5. *Collosphaera*? spD, Sample 120-748B-5H-4 45-47cm, Middle Miocene. 6. *Siphonosphaera abelmannae* Renaudie & Lazarus 2012, holotype, SSample 113-690B-6H-6 22-24cm, Early Miocene. 7. *Siphonosphaera abelmannae*, Sample 119-744A-10H-1 60-62cm, Early Miocene. 8. *Siphonosphaera abelmannae*, Sample 120-748B-6H-5 45-47cm, Early Miocene. 9. Fragment of *Siphonosphaera abelmannae*, Sample 120-748B-6H-5 45-47cm, Early Miocene. 10. *Saccospyris victoria* Renaudie & Lazarus in press, Sample 120-751A-8H-3 98-102cm, Late Miocene. 11. *Saccospyris victoria*, Sample 120-751A-9H-1 98-102cm, Late Miocene. 12. *Saccospyris victoria*, Sample 120-751A-9H-1 98-102cm, Late Miocene. 13. *Saccospyris victoria*, Sample 120-751A-9H-1 98-102cm, Late Miocene. 14. *Saccospyris victoria*, holotype, Sample 120-751A-9H-1 98-102cm, Late Miocene. 15. *Saccospyris victoria*, specimen with landeolate apical horn and a ventral (?) horn, Sample 120-751A-10H-4 98-102cm, Middle Miocene. 16. *Amphimelissa*? *hibernifortuna* Renaudie & Lazarus 2012, Sample 119-746A-13X-2 53-55cm, Late Miocene. 17. *Amphimelissa*? *hibernifortuna*, Sample 119-744A-4H-2 59-61cm, Early Pliocene. 18. *Amphimelissa*? *hibernifortuna*, holotype, Sample 119-744A-4H-2 59-61cm, Early Pliocene. All scale bars 50 µm except for 1A-B where it is 100 µm. Magnification x384 except for 4A-B (x192) and for 1A-B (x96).

Genus *Eucyrtidium* Ehrenberg 1847
Type-species: *Lithocampe acuminata* Ehrenberg 1844

Eucyrtidium acuminatum (Ehrenberg 1844)
1844 *Lithocampe acuminata* Ehrenberg: p. 84
1967 *Eucyrtidium acuminatum* (Ehrenberg) – Nigrini: p. 81; pl. 8, figs 3a-b

Eucyrtidium calvertense Martin 1904
1904 *Eucyrtidium calvertense* Martin: p. 450-451; pl. 120, fig. 5
1965 *Eucyrtidium calvertense* Martin – Hays: pl. 3, fig. 4
1975 *Eucyrtidium calvertense* Martin – Chen: p. 460; pl. 15, fig. 9

Eucyrtidium cienkowskii Haeckel 1887
1887 *Eucyrtidium cienkowskii* Haeckel: p. 1493; pl. 80, fig. 9
1975 *Eucyrtidium cienkowskii* Haeckel – Chen: pl. 15, fig. 7
1976 *Eucyrtidium cienkowskii* Haeckel – Weaver: pl. 4, figs 3-5; pl. 8, figs 7-9
1990 *Eucyrtidium cienkowskii* Haeckel – Lazarus: pl. 6, figs 1-3

Eucyrtidium inflatum Kling 1973
1973 *Eucyrtidium inflatum* Kling: p. 636; pl. 11, figs 7-8; pl. 15, figs 7-10
1980 *Eucyrtidium inflatum* Kling – Sakai: pl. 7, figs 11a-b
1988 *Eucyrtidium inflatum* Kling – Funayama: pl. 3, figs 1-2, 12

Eucyrtidium pseudoinflatum Weaver 1983
1983 *Eucyrtidium pseudoinflatum* Weaver: p. 675-676; pl. 5, figs 8-9
1990 *Eucyrtidium pseudoinflatum* Weaver – Lazarus: pl. 6, figs 12-14

Eucyrtidium punctatum (Ehrenberg 1844)
1844 *Lithocampe punctata* Ehrenberg: p. 84
1854 *Eucyrtidium punctatum* (Ehrenberg) – Ehrenberg: pl. 22, fig. 24
1990 *EUcyrtidium punctatum* (Ehrenberg) – Abelmann: pl. 6, figs 6a-b

Eucyrtidium teuscheri Haeckel 1887
1887 *Eucyrtidium teuscheri* Haeckel: p. 1491; pl. 77, fig. 5
1967 *Eucyrtidium*? *teuscheri* Haeckel – Petrushevskaya: pl. 68, figs 1-2
1986 *Eucyrtidium teuscheri* Haeckel – Caulet: pl. 5, figs 1-8

Genus *Eurystomoskevos* Caulet 1991
Type-species: *Eurystomoskevos petrushevskaae* Caulet 1991

Eurystomoskevos petrushevskaae Caulet 1991
1972 *Diplocyclas* sp. A Petrushevskaya & Kozlova: p. 541; pl. 33, figs 14-16
1975 *Diplocyclas* sp. A Petrushevskaya & Kozlova – Petrushevskaya: p. 587; pl. 24, fig. 4
1991 *Eurystomoskevos petrushevskaae* Caulet: p. 536; pl. 3, figs 14-15

Genus *Inversumbrella* Nigrini & Caulet 1992
Type-species: *Acanthocorys macroceras* Haeckel 1887

Inversumbrella? sp. 15
(Pl. 20, fig. 14)

Description. Dome-shaped to conical shell with a small cephalis and a large flaring thorax. Both are separated by furrows, but no constriction or change in contour. Spines **V**, **D**, **Ll**, **Lr** and the two spines **l'** join the thoracic wall near the collar structure, continue in the wall as ribs and after the ragged thorax termination as fairly long, downward-directed feet (conical or tribladed in one specimen, not illustrated here). Pores on the cephalis are usually smaller than pores on thorax. Both are round to elliptical. Upper thorax and cephalis usually bear numerous small thorn on bar nodes. Spine **A** join the apex on the cephalis and sometimes protrude as an horn.

Remarks. The generic assignment is doubtful: indeed the cephalis of *Inversumbrella*? sp. 15 evokes that of a plagoniid and not, as other *Inversumbrella*, that of a theoperid.

Genus *Litharachnium* Haeckel 1860

Type-species: *Litharachnium tentorium* Haeckel 1862

Litharachnium tentorium Haeckel 1862

1862 *Litharachnium tentorium* Haeckel: p. 281; pl. 4, figs 7-10
1971 *Litharachnium tentorium* Haeckel – Petrushevskaya: p. 227; pl. 108, figs 1-3; pl. 109, figs 1-4
1991 *Litharachnium tentorium* Haeckel – Takahashi: p. 114; pl. 35, figs 14-18

Genus *Lophocyrtis* Haeckel 1887

Type-species: *Eucyrtidium stephanophorum* Ehrenberg 1874 (=*Thyrsocyrtis jacchia* Ehrenberg 1874)

Lophocyrtis aspera (Ehrenberg 1873)

1873 *Eucyrtidium asperum* Ehrenberg: p. 226
1875 *Eucyrtidium asperum* Ehrenberg – Ehrenberg: pl. 8, fig. 15
1972 *Calocyclas asperum* (Ehrenberg) – Petrushevskaya & Kozlova: p. 548; pl. 28, figs 16-18
1998 *Lophocyrtis (Apoplanius) aspera* (Ehrenberg) – Sanfilippo & Caulet: p. 14-15; pl. 3A, figs 5-10; pl. 3B, figs 1-2, 5-9; pl. 6, figs 6-8

Lophocyrtis semipolita (Clark & Campbell 1942)

1942 *Calocyclas (Calocycletta) semipolita semipolita* Clark & Campbell: p. 83, pl. 8, figs 12, 14, 17-19, 22-23
1942 *Calocyclas (Calocycletta) semipolita robusta* Clark & Campbell: p. 84, pl. 8, figs 21
1998 *Lophocyrtis (Lophocyrtis?) semipolita* (Clark & Campbell) – Sanfilippo & Caulet: p. 9-10; pl. 4, figs 2-6, 8

Lophocyrtis milowi (Riedel & Sanfilippo 1971)

1971 *Cyclampterium milowi* Riedel & Sanfilippo: p. 1593; pl. 3B, fig. 3; pl. 7, figs 8-9
1975 *Cyclampterium*? *longiventer* Chen: p. 459; pl. 10, fig. 7
1975 *Cyclampterium*? *milowi* Riedel & Sanfilippo – Chen: pl. 2, figs 4-5
1990 *Cyclampterium milowi* Riedel & Sanfilippo – Abelmann: pl. 7, fig. 8

Lophocyrtis pallantae Renaudie & Lazarus in press
(Pl. 14, figs 12A-C, 15A-B, 18A-B)

1992b *Calocyclas* cf. *semipolita* Abelmann; pl. 5, fig. 8.
cf. 2009 '*Pterocanium graecum*' Ehrenberg in Ogane *et al.*; pl. 25, fig. 4a-d.
Derivation of name. Named after Amy Pallant for her contributions to radiolarian research.
Diagnosis. Lophocyrtid with transversally-aligned abdominal pores and a short dorsal wing.
Holotype. Pl. 14, figs 12A-C; Sample 120-748B-8H-6 45/47cm (Late Oligocene /Early Miocene); ECO-036, circle 2.
Material. 104 specimens observed from ODP Site 748.
Description. Three-segmented shell with a small, subspherical, thick, crested cephalis, a short, campanulate thorax and a long, subcylindrical abdomen. Some rare, small, round pores can be seen on the cephalis. The thorax bears three to four transverse rows of hexagonally-framed, regularly shaped and sized, round pores while the pores on the abdomen, also arranged in transversal rows, are larger and somewhat irregular in shape, generally elliptical but ranging from round to subpolygonal. The upper abdominal pores of some highly-silicified specimens are infilled with a thin, cobweb-shaped feltwork (see Pl. 4, fig. 3B).
The collar stricture is marked by rather deep furrows in the upper thorax. Near the collar, spine **D** protrudes as a short, hyaline, conical wing, directed perpendicularly to the shell main axis. A few specimens also bear two additional, shorter wings originating from spines **Ll** and **Lr** but in most specimens those were not seen. Spine **A** is attached to the cephalic wall by one or two apophyses and protrudes subapically as a rather thick, blade-like horn with, in some specimens, a somewhat tribladed base. Two arches **AL** can be clearly seen on the inner side of the cephalic wall in most specimens. Spine **V** joins the cephalic wall above the collar stricture but does not protrude outside.
The lumbar stricture is marked by a constriction but there is only a slight change in contour. The abdomen flares distally and has a ragged termination.
Dimensions. (based on 5 specimens) Length of cephalis: 13-18 (18); length of thorax: 24-31 (28); length of abdomen: 96-113 (99); width of abdomen: 59-66 (61).
Occurence. Common in the *Stylosphaera radiosa* Zone (Late Oligocene to Early Miocene). Its LO seems to be in the earlier *Cycladophora antiqua* Zone (Early Miocene).
Remarks. The cephalic structure of *Lophocyrtis pallantae* is similar to that described and illustrated for the genus in Sanfilippo & Caulet, 1998, hence the generic assignment, however it differs from the other lophocyrtids, and from the specimens illustrated as *Pterocyrtidium barbadiense* (Ehrenberg) in Petrushevskaya & Kozlova, 1972, mainly in its short thorax and the transversal alignement of the abdominal pores. It also differs in its **D** spine protruding as a short wing. The specimens illustrated as Nassellarian gen. et sp. #8 in Lazarus & Pallant, 1989, appear conspecific with *Pterocodon apis* Ehrenberg, 1874 (see Ogane *et al.*, 2009; pl. 5, figs 8a-d): they differ from our species in the presence of long, thin, dorsal and lateral wings, in the shape of the thorax, in the depth and width of the lumbar stricture, in the width ratio of the three segments and in the size and shape of the apical horn.
Ehrenberg's unpublished species '*Pterocanium graecum*' (Pl. 25, figs 4a-d in Ogane et al., 2009) differs from our species in having more numerous, smaller thoracic and abdominal pores, more numerous rows of thoracic pores and a deeper lumbar stricture.

Genus *Lophocorys* Haeckel 1881

Type-species: *Lophocorys cribrosa* Rüst 1885

Lophocorys polyacantha Popofsky 1913

1913 *Lophocorys polyacantha* Popofsky: p. 400-401; text-fig. 122
1984 *Lophocorys polyacantha* Popofsky – Nishimura & Yamauchi: p. 59; pl. 33, figs 13-14

2009 *Lophocorys polyacantha* Popofsky – Itaki: pl. 21, figs 19a-b

Genus *Lychnocanium* Ehrenberg 1847

Type-species: *Lychnocanium falciferum* Ehrenberg 1854

Lychnocanium amphitrite (Foreman 1973)

1973 *Lychnocanoma amphitrite* Foreman: p. 437; pl. 11, fig. 10
1975 *Lychnocanoma amphitrite* Foreman – Chen: p. 462; pl. 2, fig. 7

Lychnocanium conicum Clark & Campbell 1942

1942 *Lychnocanium conicum* Clark & Campbell: p. 71; pl. 9, fig. 38
1975 *Lychnocanella conica* (Clark & Campbell) – Petrushevskaya: p. 583; pl. 12, figs 2, 11-15
1990 *Lychnocanoma conica* (Clark & Campbell) – Abelmann: pl. 6, fig. 8; pl. 7, figs 1a-b

Lychnocanium elongata (Vinassa de Regny 1900)

1900 *Tetrahedrina elongata* Vinassa de Regny: p. 581; pl. 2, fig. 31
1973 *Lychnocanoma elongata* (Vinassa de Regny) – Sanfilippo et al.: p. 221; pl. 5, figs 19-20
1990 *Lychnocanium elongata* (Vinassa de Regny) – Nishimura: p. 133; pl. 27, figs 4a-6
1992 *Lychnocanoma elongata* (Vinassa de Regny) – Sugiyama & Furutani: p. 210; pl. 17, figs 2a-b

Lychnocanium grande Campbell & Clark 1944

1944 *Lychnocanium (Lychnocanella) grande* Campbell & Clark: p. 42; pl. 6, figs 3-4, 6
1976a *Lychnocanium grande* Campbell & Clark – Bjørklund: pl. 15, fig. 5
1990 *Lychnocanium grande* Campbell & Clark – Lazarus: p. 717; pl. 7, fig. 9
1995 *Lychnocanium grande* Campbell & Clark – Morley & Nigrini: p. 80

Lychnocanium magnacornuta (Sakai 1980)

1973 *Lychnocanium* sp. Ling: p. 781; pl. 2, figs 10-11
1980 *Lychnocanoma nipponica* (Nakaseko) *magnacornuta* Sakai: p. 710; pl. 9, figs 3a-b
1995 *Lychnocanoma nipponica* (Nakaseko) *magnacornuta* Sakai – Morley & Nigrini: p. 81, pl. 5, figs 1-2
1996 *Lychnocanoma magnacornuta* Sakai – Motoyama: p. 248; pl. 5, figs 10a-11

Lychnocanium sphaerothorax Weaver 1976

1975 *Lychnocanoma sphaerothorax* Weaver: p. 581-582; pl. 5, figs 4-5

Lychnocanium sp. B

(Pl. 12, figs 11, 14)

Remarks. It differs from *L. grande, L. magnacornuta, L. conicum* and *L. nipponicum* Nakaseko in Kanaseko & Sugano 1973 in its elongated barrel-shaped thorax and its short feet.

Lychnocanium sp. C

(Pl. 12, figs 5A-B)

1992 *Lychnocanoma* spC Abelmann: Pl. 5, figs 1-2.

Diagnosis. No external collar constriction; thick, campanulate thorax; three inward-directed blade-like feet.

Description. Two-segmented form with a spherical, poreless cephalis with a short apical horn

and a thick-walled campanulate thorax. No constriction or change in contour at the collar stricture. Thorax wall bears longitudinal rows of small, circular pores. Three feet extends beyond the thorax rim. They are medium-length (approximately same size as thorax), blade-shaped, incurved inwards and ends bluntly.

Remarks. This species differs from *Lychnocanium amphitrite* Foreman 1973 in lacking an abdomen, and in its short apical horn.

Genus *Periarachnium* Haeckel 1881

Type-species: *Periarachnium periplectum* Haeckel 1887

Periarachnium periplectum Haeckel 1887

1887 *Periarachnium periplectum* Haeckel: p. 1297; pl. 55, fig. 11
1984 *Periarachnium periplectum* Haeckel – Nishimura & Yamauchi: p. 53; pl. 33, fig. 8
1990 *Periarachnium periplectum* Haeckel – Nishimura: p. 97; pl. 17, figs 4a-6c

Genus *Peripyramis* Haeckel 1881 emend. Riedel 1958

Type-species: *Peripyramis circumtexta* Haeckel 1887

Peripyramis circumtexta Haeckel 1887

1887 *Peripyramis circumtexta* Haeckel: p. 1162; pl. 54, fig. 5
1967 *Peripyramis circumtexta* Haeckel – Petrushevskaya: p. 113-114; pl. 64-65

Genus *Plectopyramis* Haeckel 1881

Type-species: *Plectopyramis magnifica* Haeckel 1887

Plectopyramis dodecomma Haeckel 1887

1887 *Plectopyramis dodecomma* Haeckel: p. 1258; pl. 54, fig. 6
1979 *Plectopyramis dodecomma* Haeckel – Nigrini & Moore: p. N31; pl. 21, fig. 5

Genus *Pterocanium* Ehrenberg 1847 emend. Petrushevskaya 1971

Type-species: *Podocyrtis charybdea* Müller 1855

Pterocanium trilobum (Haeckel 1861)

1861 *Dictyopodium trilobum* Haeckel: p. 839
1862 *Dictyopodium trilobum* Haeckel – Haeckel: p. 340; pl. 8, figs 6-10
1913 *Pterocanium trilobum* (Haeckel) – Popofsky: p. 390-392; text-figs 104-109
1985 *Pterocanium charybdeum* (Müller) *trilobum* (Haeckel) – Lazarus et al.: p. 195; pl. 10, figs 1-4

Pterocanium korotnevi (Dogiel in Dogiel & Reshetnyak 1952)

1952 *Pterocorys korotnevi* Dogiel in Dogiel & Reshetnyak: p. 17; fig. 11
1970 *Pterocanium korotnevi* (Dogiel in Dogiel & Reshetnyak) – Nigrini: pl. 3, figs 10-11
1985 *Pterocanium korotnevi* (Dogiel in Dogiel & Reshetnyak) – Lazarus et al.: p. 201-202; pl. 18

Pterocanium praetextum (Ehrenberg 1873a)

1873a *Lychnocanium praetextum* Ehrenberg: p. 316
1873b *Lychnocanium praetextum* Ehrenberg – Ehrenberg: p. 297; pl. 10, fig. 2

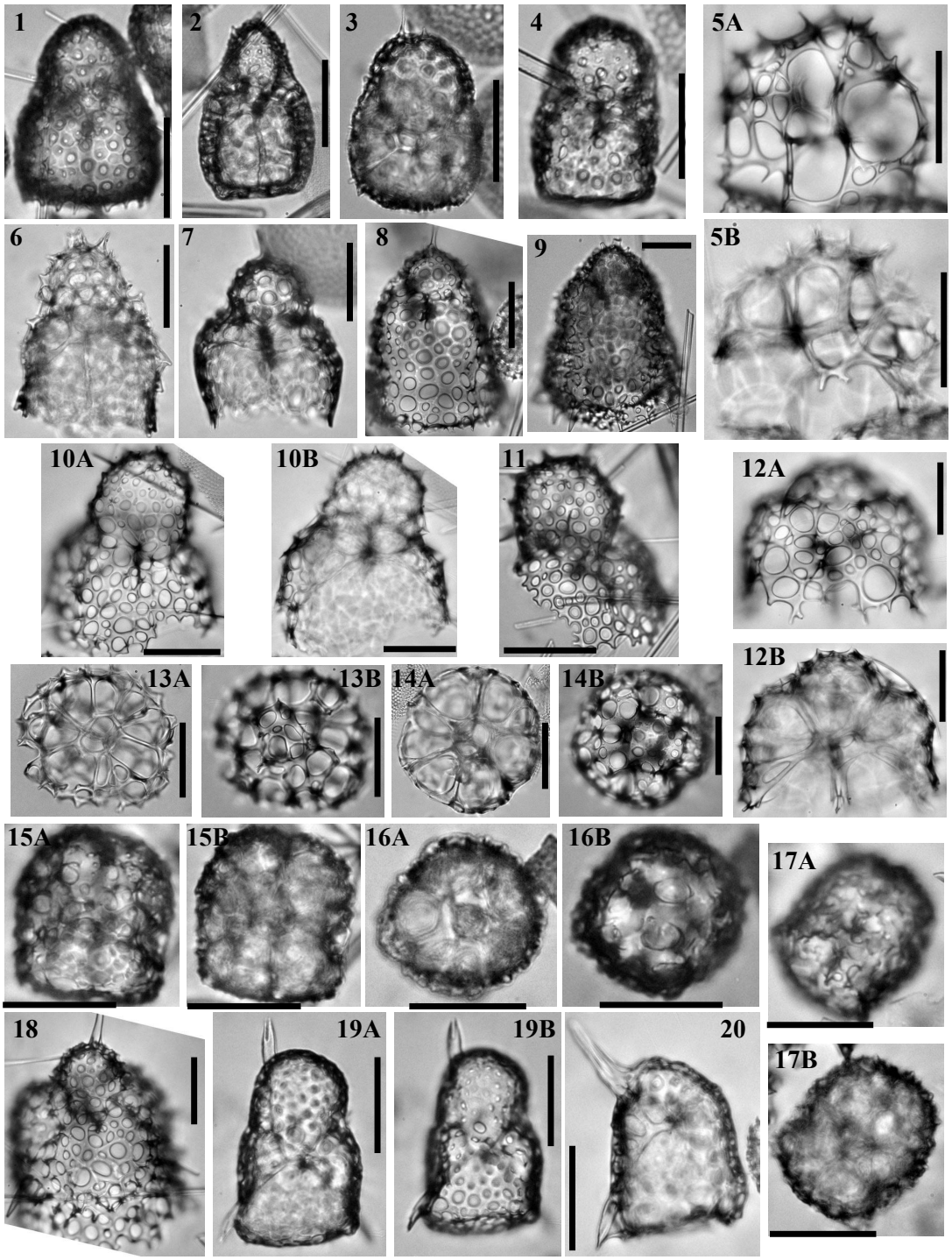

Plate 16.– 1. *Antarctissa denticulata* (Ehrenberg 1844b), Sample 120-747A-1H-1 45-47cm, Pleistocene. 2. *Antarctissa deflandrei* (Petrusveskaya 1975), Sample 119-746A-14X-1 53-55cm, Late Miocene. 3. *Antarctissa cylindrica* Petrushevskaya 1967, Sample 119-744A-4H-1 53-54cm, Late Miocene. 4. *Antarctissa robusta* (Petrusveskaya 1975), Sample 119-744A-5H-4 36-38cm, Middle/Late Miocene. 5. *Helotholus*? *warreni* (Goll 1980), Sample 120-747A-1H-4 45-47cm, Pleistocene. 6. *Antarctissa strelkovi,* Sample 119-744A-2H-1 53-55cm, Pleistocene. 7. *Helotholus*? *praevema* Weaver 1983, Sample 119-746A-4H-1 53-55cm, Late Miocene. 8. *Lithomelissa*? sp. 11, Sample 119-745B-18H-2 53-55cm, Early Pliocene. 9. *Lithomelissa*? sp. 11, Sample 120-751A-4H-2 98-102cm, Early Pliocene. 10. *Lithomelissa*? sp. T, Sample 120-751A-1H-1 98-102cm, Pleistocene. 11. *Lithomelissa*? sp. T, Sample 120-747A-1H-1 45-47cm, Pleistocene. 12. *Helotholus*? *vema* Hays 1970, Sample 120-751A-2H-CC, Late Pliocene. 13. *Helotholus*? *haysi* Lazarus 1990, Sample 119-746A-7H-4 53-55cm, Late Miocene. 14. *Helotholus*? *vema*, Sample 119-744A-3H-1 53-55cm, Late Pliocene. 15. *Antarctissa ballista* Renaudie & Lazarus 2012, Sample 119-746A-8H-1 53-55cm, Late Miocene. 16. *Antarctissa ballista*, Sample 119-746A-8H-CC, Late Miocene. 17. *Antarctissa ballista*, Sample 120-751A-6H-1 98-102cm, Late Miocene. 18. *Lithomelissa*? sp. 11, Sample 120-751A-4H-2 98-102cm, Early Pliocene. 19. *Botryopera chippewa* Renaudie & Lazarus in press, holotype, Sample 120-747A-9H-8 45-47cm, Early/Middle Miocene. 20. *Botryopera chippewa*?, unusual specimen with reduced cephalis, Sample 120-751A-12H-6 98-102cm, Middle Miocene. All scale bars 50 µm. Magnification x384 except for 9 (x192).

1887 *Pterocanium praetextum* (Ehrenberg) – Haeckel: p. 1330; pl. 73, fig. 6
1967 *Pterocanium praetextum praetextum* (Ehrenberg) – Nigrini: p. 68-70 ; pl. 7, fig. 1
1985 *Pterocanium praetextum* (Ehrenberg) – Lazarus et al.: p. 198-200; pl. 15-16

Pterocanium prismatium Riedel 1957

1957 *Pterocanium prismatium* Riedel: p. 87-88; pl. 3, figs 4-5
1985 *Pterocanium prismatium* Riedel – Lazarus et al.: p. 200; pl. 17

Genus *Stichocorys* Haeckel 1881

Type-species: *Stichocorys wolffii* Haeckel 1887

Stichocorys delmontensis (Campbell & Clark 1944)

1944 *Eucyrtidium delmontense* Campbell & Clark: p. 56; pl. 7, fig. 21
1955 *Eucyrtidium delmontense* Campbell & Clark *nipponicum* Nakaseko: p. 109; pl. 10, fig. 8
1970 *Stichocorys delmontense* (Campbell & Clark) – Sanfilippo & Riedel: p. 451; pl. 1, fig. 9
1980 *Stichocorys delmontense* (Campbell & Clark) – Sakai: p. 711; pl. 8, fig. 3

Stichocorys peregrina (Riedel 1953)

1953 *Eucyrtdium elongatum* Stöhr *peregrinum* Riedel: p. 812; pl. 85, fig. 2
1970 *Stichocorys peregrina* (Riedel) – Sanfilippo & Riedel: p. 451; pl. 1, fig. 10
1986 *Stichocorys peregrina* (Riedel) – Caulet: pl. 6, fig. 4

Genus *Stichophormis* Haeckel 1881

Type-species: *Stichophormis cornutella* Haeckel 1887

Stichophormis cheni Renaudie & Lazarus 2012
(Pl. 14, figs 11A-B, 16-17)

1975 ?*Lithostrobus*(?) *clava* (Ehrenberg); Petrushevskaya: 14, fig. 1-2 (non *Lithocampe clava* Ehrenberg, 1874 in Ogane et al., 2009, pl. 22, fig. 2a-c).
1975 *Stichophormis* sp. Chen: 462-463, pl. 13, fig. 8.
1990 *Stichophormis* sp. Chen; Abelmann: 698, pl. 8, fig. 9.
1992 *Cyrtolagena aglaogena* (Takahashi) *(sic)*; Wang & Yang: pl. 2, fig. 11 (non *Cyrtopera aglaolampa* Takahashi, 1991, p.119, pl. 40, fig. 7).
1999b *Cyrtolagena* cf. *aglaolampa* (Takahashi); O'Connor: 500, pl. 4, figs. L-M (not N).

Derivation of name. Named after Pei-Hsin Chen who first described this species.

Diagnosis. Numerous segments; thick wall; last segment tapering to a mouth; no apical horn.

Holotype. Plate 14 figs. 11A-B; Sample 119-744A-8H-1 60/62cm (Early/Middle Miocene); ECO-027.

Material. 23 specimens were observed from ODP Sites 744, 748 and 751.

Description. Spindle-shaped shell consisting of usually eleven thick-walled segments (ten to twelve). Up to the nine first segments, the shell is conical and the segments barrel-shaped. The two last segments are inverted truncate-conical. The change in contour occurs either on the lower part of the ninth segment or on the upper part of the tenth.

The hyaline cephalis consists of two parts: an upper part which is spherical and a cylindrical lower part. The two parts are separated by a constriction (see pl. 14, fig. 11B). None of the internal spines were observed in our material. The upper part of the cephalis is rough and poreless while the lower part bears a few randomly distributed, small pores.

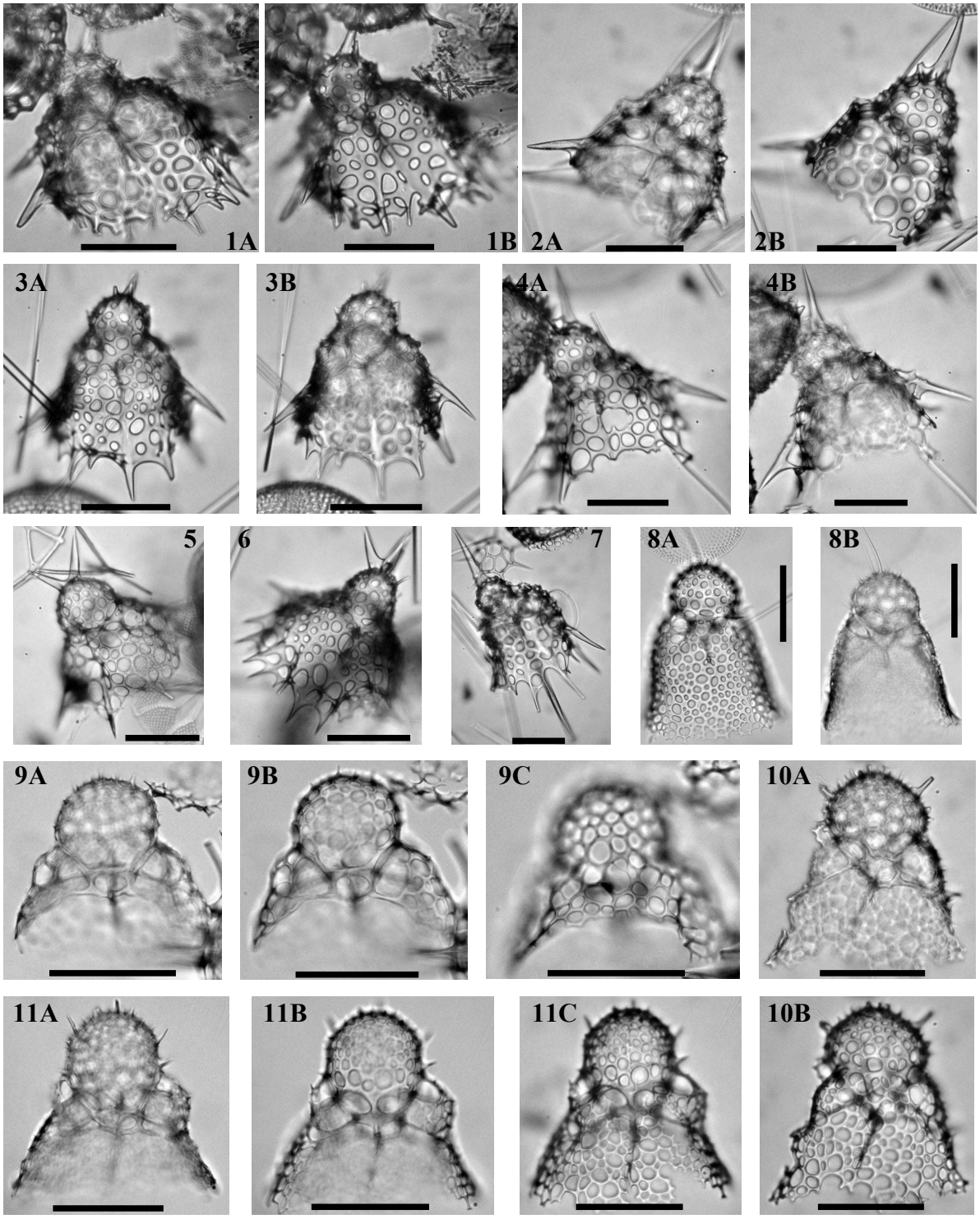

Plate 17.– 1. *Antarctissa evanida* Renaudie & Lazarus in press, Sample 120-747A-4H-1 45-47cm, Early Pliocene. 2. *Antarctissa evanida*, Sample 120-751A-4H-2 98-102cm, Early Pliocene. 3. *Antarctissa evanida*, Sample 120-751A-4H-2 98-102cm, Early Pliocene. 4. *Antarctissa evanida*, Sample 120-751A-4H-4 98-102cm, Early Pliocene. 5. *Antarctissa evanida*, holotype, Sample 120-751A-4H-4 98-102cm, Early Pliocene. 6. *Antarctissa evanida*, Sample 120-751A-6H-1 98-102cm, Late Miocene. 7. *Antarctissa evanida*? Sample 120-751A-4H-2 98-102cm, Early Pliocene. 8. *Botryopera*? *daleki* Renaudie & Lazarus in press, specimen with long thorax, Sample 120-748B-6H-3 45-47cm, Early Miocene. 9. *Botryopera*? *daleki*, specimen in ventral view, Sample 120-748B-6H-3 45-47cm, Early Miocene (A: Focus on dorsal side; B: Focus on ventral side; C: Focus on shell wall). 10. *Botryopera*? *daleki*, specimen in sagittal view, Sample 120-748B-6H-5 45-47cm, Early Miocene. 11. *Botryopera*? *daleki*, holotype, specimen in dorsal view, Sample 120-748B-6H-5 45-47cm, Early Miocene (A: Focus on ventral side; B: Focus on dorsal side; C: Focus on shell wall).
All scale bars 50 µm. Magnification x384.

Pores on the following segments are relatively small, rounded and aligned transversally. The second through the eighth segments are approximately equal in length and have three to five rows of pores. The ninth and the tenth segments are usually longer and therefore have more pore rows. The last segment has somewhat larger pores that are loosely aligned transversally too. This segment ends in a distal opening or mouth with a poreless rim that may have some small poreless teeth.

Most specimens have three wings that are flat and end with a conical Large rounded pores can sometimes be observed on the panel that connects the wings with the main body. They arise from the third or fourth segment.

Dimensions. (based on 4 specimens) Length: 304-326 (314); width:119-145 (132).

Occurrence. Very rare from the *C. golli regipileus* to the lower *A. golownini* Zone (early to middle Miocene).

Remarks. *Stichophormis? cheni* differs from *Cyrtolagena laguncula* Haeckel, 1887 in having a thick wall, in ending on a differentiated mouth and in the shape of the cephalis; and from *Cyrtopera aglaolampa* Takahashi, 1991 in the last segment, in the latter, being globular and accounting for more than a third of the total height, and in the absence of apical horn. The cephalis of *S.*? *cheni* seems rather similar to that of the cretaceous *Amphipyndax* but, since the internal spines where not actually seen on any of the specimens, the two cannot be efficiently compared. The lack of apical horn or any discernable apical spine makes the affinity with *S. cornutella* and therefore the generic assignment to *Stichophormis* doubtful. Petrushevskaya's tentative assignment of her form to *L. clava* Ehrenberg, 1874 is clearly incorrect, as the newly figured type series material in Ogane et al., 2009 shows. *L. clava* has much longer segments, fewer in number, lacks wings and is more similar to the modern concept of *Stichocorys*. We are not sure if Petrushevskaya's specimens are conspecific with ours, as the photographs are of poor quality. The number of segments and development of external wings however appear to differ from our material. Petrushevskaya's material is of Paleocene age.

Genus *Theocorys* Haeckel 1881

Type-species: *Theocorys morchellula* Rüst 1885

Theocorys redondoensis (Campbell & Clark 1944)

1944 *Theocyrtis (Theocorusca) redondoensis* Campbell & Clark: p. 49-50; pl. 7, fig. 4
1973 *Theocorys redondoensis* (Campbell & Clark) – Kling: pl. 11, figs 26-28
1975 *Theocorys redondoensis* (Campbell & Clark) – Chen: pl. 20, figs 2-3

Theocorys veneris Haeckel 1887

1887 *Theocorys veneris* Haeckel: p. 1415; pl. 69, fig. 5
1913 *Theocorys veneris* Haeckel – Popofsky: p. 399; text-fig. 119
1974 *Theocorys veneris* Haeckel – Renz: p. 738; pl. 16, fig. 18
1991 *Theocorys veneris* Haeckel – Takahashi: p. 120; pl. 40, figs 11-14

Genus *Thyrsocyrtis* Ehrenberg 1847

Type-species: *Thyrsocyrtis rhizodon* Ehrenberg 1873

Thyrsocyrtis clausa Chen 1975

1975 *Thyrsocyrtis clausa* Chen: p. 463; pl. 14, figs 1-2

Family **Plagiacanthidae** Hertwig 1879 emend. Petrushevskaya 1971

Genus *Archipilium* Haeckel 1881
Type-species: *Archipilium orthopterum* Haeckel 1887

Archipilium macropus (Haeckel 1887)
1887 *Sethpilium macropus* Haeckel: p. 1203; pl. 97, fig. 9
1972 *Archipilium* spp. aff. *A.macropus* (Haeckel) - Petrushevskaya and Kozlova: pl. 29, fig. 14
1981 *Archipilium macropus* (Haeckel) – Petrushevskaya: p. 249

Archipilium orthopterum Haeckel 1887
1887 *Archipilium orthopterum* Haeckel: p. 1138; pl. 98, fig. 7
1981 *Archipilium orthopterum* Haeckel – Petrushevskaya: p. 249; figs 368-369
1991 *Archipilium* sp. aff. *A. orthopterum* Haeckel - Takahashi: pl. 36, figs 5, 7

Subfamily **Clathromitrinae** Petrushevskaya 1971

Genus *Archiscenium* Haeckel 1881
Type-species: *Archiscenium quadrispinum* Haeckel 1887

Archiscenium quadrispinum Haeckel 1887
(Pl. 20, figs 11A-B)
1887 *Archiscenium quadrispinum* Haeckel: p. 1150; pl. 53, fig. 11

Genus *Clathromitra* Haeckel 1881 emend. Petrushevskaya 1971
Type-species: *Clathromitra pterophormis* Haeckel 1887

Clathromitra pentacantha Haeckel 1887
(Pl. 20, fig. 3)
1887 *Clathromitra pentacantha* Haeckel: p. 1219
1971 *Clathromitra pentacantha* Haeckel – Petrushevskaya: p. 75; pl. 37, figs 1-3

Clathromitra pterophormis Haeckel 1887
(Pl. 20, figs 10A-B)
1887 *Clathromitra pterophormis* Haeckel: p. 1219; pl. 57, fig. 8
1983 *Clathromitra pterophormis* Haeckel – Benson: p. 501; pl. 9, fig. 8
1991 *Clathromitra pterophormis* Haeckel – Takahashi: p. 94; pl. 24, fig. 8

Clathromitra lemi Renaudie & Lazarus in press
(Pl. 21, figs 1-3B, 5-8B)
Derivation of name. The broadly splayed basal feet and roughly equidimensional main shell resemble NASA's Lunar Excursion Module (LEM), hence the name lemi.
Diagnosis. Small tetrahedral to hemispherical clathromitrid with a thin inner spicule and short, sometimes serrated, external projections.
Holotype. Pl. 21, fig. 2; Sample 119-744A-10H-2, 60-62cm (Early Miocene); ECO-060.
Material. 50 specimens were observed from ODP Sites 744, 748 and 751.
Description. Tetrahedral to hemispherical one-segmented shell. The shell wall is a random meshwork of irregularly disposed, sized and shaped pores. In hemispherical specimens, the wall is usually thicker and crested (Pl. 21, figs 3A-B, 7A-B).

The inner spicule is rather thin and delicate and consists of spines **A**, **D**, **Ll** and **Lr**, plus an axobate formed by a cluster of small lumps on the median bar. Most of the apophyses drawn in text-fig. 3B are expressed here as rod-like spines that join the wall: on spine **A**, the three apophyses a are slightly directed upward (Pl. 21, figs 3B and 7A), while the three short apophyses *m* are perpendicular to spine **A** (Pl. 21, fig. 2); on spine **D,** the two apophyses *c* can be seen (Pl. 21, figs 2, 5, 7A); on spines **Ll** and **Lr**, apophyses *p* can be quite long and robust (the upper one look a lot like a spine **V**; Pl. 21, figs 3B, 6A, 7A-B) while apophyses d are short and perpendicular to spines **Ll** and **Lr** (Pl. 21, fig. 2). The wall tapers distally toward spines **A**, **D**, **Ll** and **Lr**. Spines **A**, **D**, **Ll** and **Lr** all continue as short, tribladed, sometimes serrated (Pl. 21, fig. 6) horn and feet (respectively). The feet are curved downwardly.

Dimensions. (based on 5 specimens) Height of shell (excluding the feet): 109-147 (133).

Occurence. Rare from the *Stylosphaera radiosa* to the *Cycladophora humerus* Zone (Early to Middle Miocene); sporadic from the *Actinomma golownini* to the *Siphonosphaera vesuvius* Zone (Middle to Late Miocene).

Remarks. *Clathromitra lemi* differs from *Archiscenium quadrispinum* Haeckel, 1887 and from *Clathromitra pentacantha* Haeckel, 1887 in its smaller size, short horn, feet, thinner inner spicule and in the overall tetrahedral shape of the shell. It is also distinguishable from *C. pterophormis* in the latter having a large axobate, robust, laterally-projected feet and a paneled apical horn.

Clathromitra? *fulgureanubes* Renaudie & Lazarus in press
(Pl. 21, figs 4A-B, 11A-12B)

Derivation of name. From the Latin nubes (cloud) and fulgureus (charged with lighting).

Diagnosis. Bilobate cephalis with large angular arches *mc* and *mp*, and serrated feet.

Holotype. Pl. 21, figs 4A-B; Sample 120-751A-5H-3, 98-102cm (Late Miocene); ECO-061.

Material. 48 specimens were observed from ODP Sites 689, 690, 748, 751 and 1138.

Description. Shell consists of a single segment: a large angular cephalis covered by a tenuous meshwork of anastomosed bars and three divergent basal feet.

Spine **A** divides the cephalic chamber in two equal parts: in some specimens though (Pl. 7, figs 7A-B), spine **A** is slightly closer to spine **D**. It is directed upward, perpendicularly to the median bar, and continues as a tribalded horn. Spines **D**, **Ll** and **Lr** are first directed laterally and then turn downward as long (for a distance approximately equal to the height of the cephalis), tribladed feet, serrated at their extremities. The axobate is a cluster of small lumps situated at the junction between spine **A** and the median bar. Large angular arches *mc* and *mp* form the two lobes of the cephalic chamber. Each lobe has a pentagonal outline.

The shell wall is thinner than the arches or the spines. The pores delimited by the anastomosed bars are irregularly disposed, irregularly shaped and sized. The shell wall is, in some specimens (Pl. 7, figs 8A-B), linked to apophyse *g* on spine **A** by several bars.

Dimensions. (based on 6 specimens) Height of cephalic chamber: 39-65 (49); width of cephalis: 83-97 (92); length of apical horn: 32-70 (49); length of feet: 42-129 (94).

Occurence. Very sporadic from the *Cycladophora golli regipileus* to the lower *Cycladophora spongothorax* zone; rare from the *Cycladophora spongothorax* to the Upsilon zone.

Remarks. *Clathromitra*? *fulgureanubes* differs from *Clathromitra pterophormis*, *A. quadrispinum*, *C. pentacantha* and *C. lemi* primarily in its strongly marked arches. Similar arches are present in species of the genus *Semantis* such as *S. gracilis* Popofsky, 1908, but *C.*? *fulgureanubes* differs from those species in its size and in the presence of a shell wall.

Genus *Corythomelissa* Campbell 1951

Type-species: *Lithomelissa corythium* Ehrenberg 1873

Corythomelissa horrida Petrushevskaya 1975
(Pl. 20, figs. 2A-B)

1975 *Corythomelissa horrida* Petrushevskaya: p. 589-590; pl. 11, figs 14-15; pl. 21, fig. 9
1994 *Corythomelissa horrida* Petrushevskaya – Funakawa: p. 476-477; pl. 14, figs 1a-b

Genus *Pteroscenium* Haeckel 1881

Type-species: *Pteroscenium arcuatum* Haeckel 1887

Pteroscenium pinnatum Haeckel 1887
(Pl. 20, figs. 9A-B)

1887 *Pteroscenium pinnatum* Haeckel: p. 1152; pl. 53, fig. 14-16
? 1913 *Verticillata hexacantha* Popofsky: p. 282-283; text-fig. 11
1984 *Verticillata pinnatum* (Haeckel) – Nishimura & Yamauchi: pl. 29, figs 1a-2
1991 *Pteroscenium pinnatum* Haeckel – Takahashi: pl. 36, figs 8-9

Genus *Spongomelissa* Haeckel 1887

Type-species: *Lithomelissa spongiosa* Bütschli 1882

Spongomelissa dilli Chen 1975
(Pl. 20, figs. 1A-B)

1975 *Spongomelissa dilli* Chen: p. 458; pl. 13, figs 6-7
1992a *Spongomelissa dilli* Chen – Abelmann: pl. 5, figs 5-6
? 1995a *Corythomelissa omoprominentia* Funakawa: p. 212-213; pl. 5, fig. 1a-2b

Genus *Tripophaenoscenium* Clark & Campbell 1944

Type-species: T*ripophaenoscenium laimingi* Clark & Campbell 1944

Tripophaenoscenium laimingi Clark & Campbell 1944
(Pl. 20, fig. 4)

1944 *Tripophaenoscenium laimingi* Clark & Campbell: p. 38; pl. 5, fig. 19

Subfamily **Lophophaeninae** Haeckel 1881 emend. Petrushevskaya 1971

Plagoniid sp. P
(Pl. 21, fig. 9)

Description. Dicyrtid with a more or less spherical cephalis bearing large circular to elliptical pores and a long, thinner, bent, cylindrical thorax with randomly-arranged, small circular to elliptical pores. Apophyse *a* on spine **A** as well as spines **Ll** and **Lr** join the thoracic wall at the same height as **MB**, respectively dorsally and ventrally. Spine **D** is long, downward projected and terminates in a dendritic multifurcation above the thorax end. None of the branches of spine **D** protrude outside the wall. Thorax is closed.

Remarks. The shape of the cephalis evokes that of species *Arachnocorallium calvata* but the very unique shape of spine **D** and the presence of a thoracic wall distinguish clearly the two species.

Genus *Amphiplecta* Haeckel 1881 emend. Petrushevskaya 1971

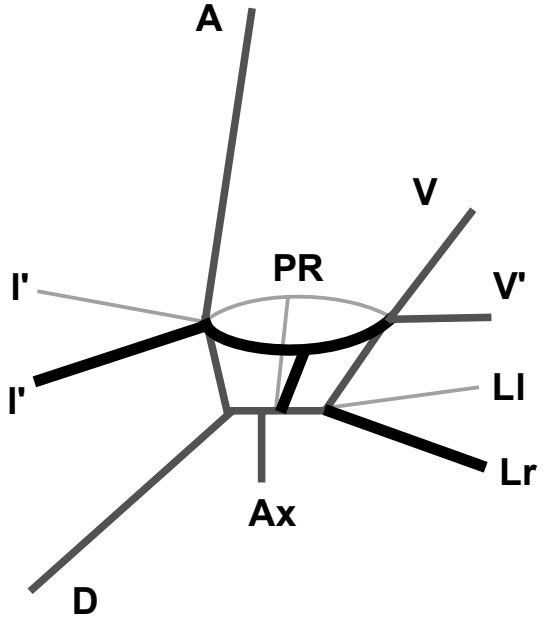

Figure 6.– Schematic illustration of *Antarctissa ballista* Renaudie & Lazarus 2012 inner structure.
Terminology after Sugiyama, 1993.
PR, proximal ring; **V'**, secondary vertical spine.

Type-species: *Amphiplecta acrostoma* Haeckel 1887

Amphiplecta acrostoma Haeckel 1887

1887 *Amphiplecta acrostoma* Haeckel: p. 1223-1224; pl. 97, fig. 10
1971 *Amphiplecta acrostoma* Haeckel – Petrushevskaya: p. 103; pl. 54, figs 2.7

Amphiplecta tripleura Funakawa 1995a

1971 *Amphiplecta* sp. Petrushevskaya: pl. 54, fig. 1
1995a *Amphiplecta tripleura* Funakawa: p. 18-20; text-fig. 5; pl. 1, figs 1-3

Amphiplecta? sp. R
(Pl. 26, figs 13-15B)

Diagnosis. Large, elongated cephalis; dorsal shoulder; short flaring thorax.
Description. Dicyrtid with a long, apically-elongated cephalis (some specimens have a somewhat flattened apex; Pl. 26, figs 13-14) and a short, largely flaring thorax. Shell wall is smooth with randomly-arranged, well-spaced, small, circular to elliptical pores. A large amount of small thorns connected to one another are present at the apex of the cephalis but do not seem related to spines **A** or **V**. Spine **V** is short, and can protrude at the collar stricture as a very short triangular horn (Pl. 26, fig. 13). Spine **A** is fused to the dorsal part of the cephalic wall. An arch **AD** is well-developed, thus creating a small shoulder.
Remarks. It differs from *Amphiplecta tripleura* in the elongated shape of its cephalis, in having less numerous, smaller pores and a smoother shell wall and in the dorsal shoulder being less developed but covered by the shell wall.

Genus *Antarctissa* Petrushevskaya 1967

Type-species: *Lithobotrys denticulata* Ehrenberg 1844b

Antarctissa cylindrica Petrushevskaya 1967
(Pl. 16, fig. 3)

1967 *Antarctissa denticulata* var. *cylindrica* Petrushevskaya: p. 86; pl. 49, fig. 5; pl. 50, fig. 1
1975 *Antarctissa ewingi* Chen: p. 457; pl. 16, figs 5-9
1975 *Antarctissa cylindrica* Petrushevskaya – Petrushevskaya: p. 591; pl. 11, figs 19-20

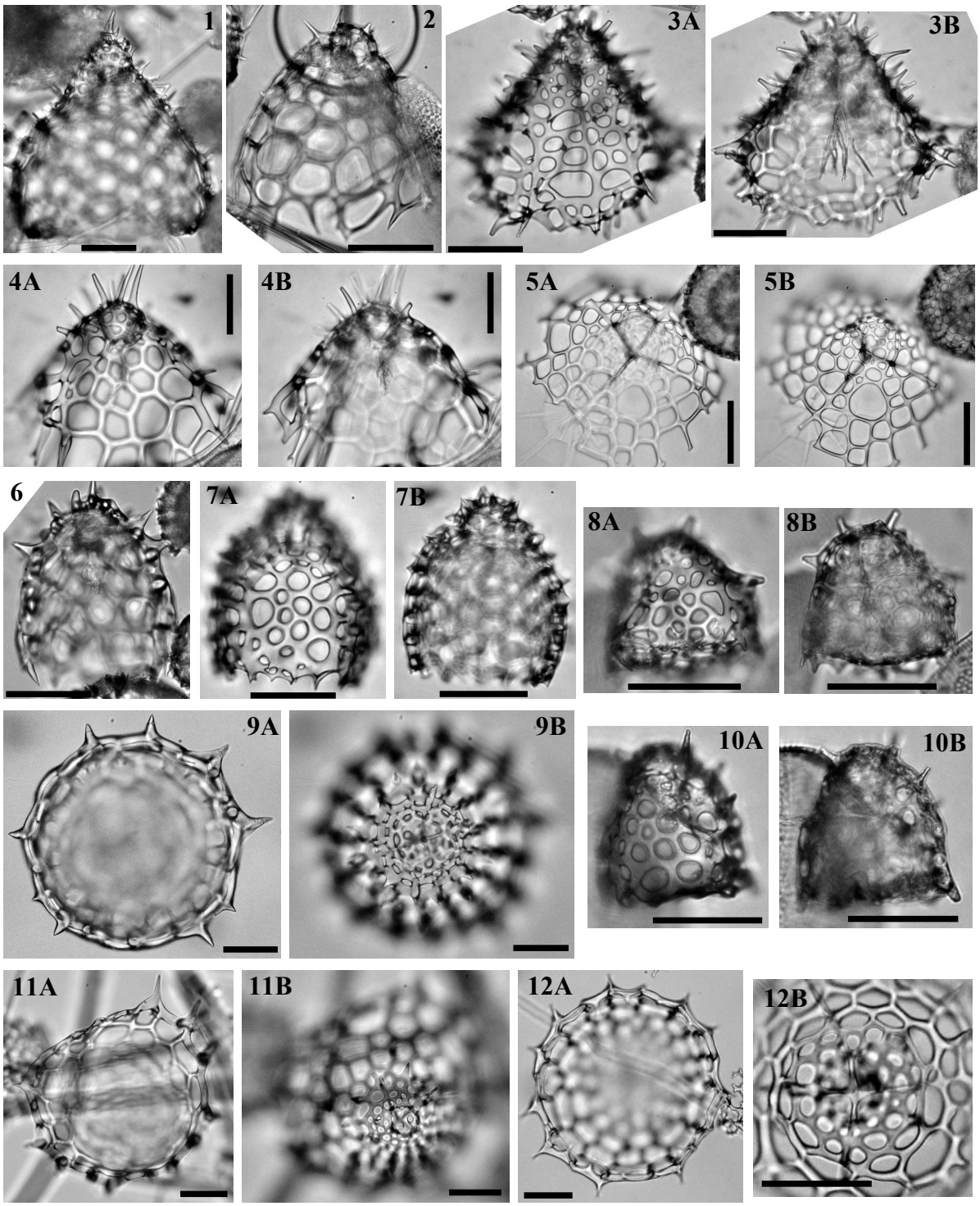

Plate 18.–
1. *Ceratocyrtis cuccularis* Bütschli 1882, Sample 120-748B-6H-5 45-47cm, Early Miocene.
2. *Ceratocyrtis histricosa*, Sample 119-744A-5H-3 53-55cm, Late Miocene.
3. *Ceratocyrtis robustus* Bjorklund 1976, Sample 120-747A-3H-1 45-47cm, Late Pliocene.
4. *Ceratocyrtis galeus*, Sample 120-747A-1H-1 45-47cm, Pleistocene.
5. *Ceratocyrtis dolvenae* Renaudie & Lazarus 2012, Sample 120-748B-6H-3 45-47cm, Early Miocene.
6. *Ceratocyrtis mashae*, Sample 119-744A-2H-4 53-55cm, Pleistocene.
7. *Ceratocyrtis stoermeri*, Sample 120-751A-15H-CC, Early Miocene.
8. *Ceratocyrtis* sp. F, Sample 119-737A-25X-3 53-55cm, Late Miocene.
9. *Ceratocyrtis*? sp. K, Sample 119-744A-8H-1 53-55cm, Middle Miocene.
10. *Ceratocyrtis* sp. F, Sample 119-745B-18H-2 53-55cm, Early Pliocene.
11. *Ceratocyrtis*? sp. K, Sample 119-744A-7H-3 53-55cm, Middle Miocene.
12. *Ceratocyrtis*? sp. K, Sample 119-744A-8H-1 53-55cm, Middle Miocene.
All scale bars 50 µm. Magnification x384 except for 1, 9A-B, 11A-12B (x192).

1990 *Antarctissa cylindrica* Petrushevskaya – Lazarus: p. 713; pl. 3, figs 8-12

Antarctissa deflandrei (Petrushevskaya 1975)
(Pl. 16, fig. 2)

1975 *Botryopera deflandrei* Petrushevskaya: p. 592; pl. 11, figs 30-32
1975 *Antarctissa conradae* Chen: p. 457; pl. 17, figs 1-5
1990 *Antartcissa deflandrei* (Petrushevskaya) – Lazarus: p. 713; pl. 3, figs 18-19

Antarctissa denticulata (Ehrenberg 1844b)
(Pl. 16, fig. 1)

1844b *Lithobotrys denticulata* Ehrenberg: p. 203
1873b *Lithopera denticulata* (Ehrenberg) – Ehrenberg: pl. 12, fig. 7
1958 *Peromelissa denticulata* (Ehrenberg) – Riedel: p. 236; pl. 3, fig. 9; text-fig. 7
1967 *Antarctissa denticulata* (Ehrenberg) – Petrushevskaya: p. 87-89; pl. 49, figs 1-5 non fig. 6
1990 *Antarctissa denticulata* (Ehrenberg) – Lazarus: p. 713-714; pl. 3, figs 1-4

Antarctissa robusta Petrushevskaya 1975
(Pl. 16, fig. 4)

? 1944 *Dictyocephalus equiceps* Campbell & Clark: p. 46; pl. 6, fig. 15
1975 *Antarctissa robusta* Petrushevskaya: p. 591; pl. 11, figs 21-22
1975 *Antarctissa antedenticulata* Chen: p. 484; pl. 2, figs 8-9
? 1986 *Botryopera equiceps* (Campbell & Clark) – Petrushevskaya: p. 193
1990 *Antarctissa robusta* Petrushevskaya – Lazarus: p. 714-715; pl. 3, figs 6-7

Antarctissa ballista Renaudie & Lazarus 2012
(Pl. 16, figs 15A-17B; Fig. 6)

2001 *Antarctissa* "bullet" Lazarus: 21, pl. P1, figs. 5-8
Derivation of name. *Ballista* is Latin for projectile.
Diagnosis. Cephalis and thorax undifferentiated; internal ring with six lateral beams; robust spine A free in the cephalis.
Holotype. Plate 16, fig. 17A-B; Sample 120-751A-6H-1 98/102cm (Late Miocene); ECO-041.
Material. 236 specimens were observed from ODP Sites 746, 747 and 751.
Description. Two-segmented shell with a cephalis and a thorax that are not distinguishable externally by any constriction, furrow or shoulder. The thorax is short and closed in most specimens. The cephalis apex is slightly rounded (just a little less squarred than the thorax termination).
Spine **A** is robust (as are the other spines) and free in the cephalic cavity; it reaches the wall approximately at mid-width (slightly closer to the dorsal side than to the opposite side) and thus creates a furrow, in most specimens, that can make the cephalis look bilobate. The axobate is just below spine **A** and is almost long enough to reach termination of the thorax. Spine **D** is directed downward - very similar to that of *A. denticulata* and *A. cylindrica* Petrushevskaya, 1975 - and reaches the wall near the thorax closure. Specimens seen from below or above (see Pl. 16, fig. 16A) show the presence of an internal ring, similar to that of *Helotholus vema* Hays, 1965. The ring structure is supported by six beams: five horizontal or sub-horizontal (**Ll**, **Lr**, **V'** and two **l'** according to Sugiyama, 1993's terminology, see Fig. 6), plus the downward-directed **D** spine. This structure is almost at the equator of the shell; the cephalic chamber and the thorax are thus of almost the same length as well as the same width.

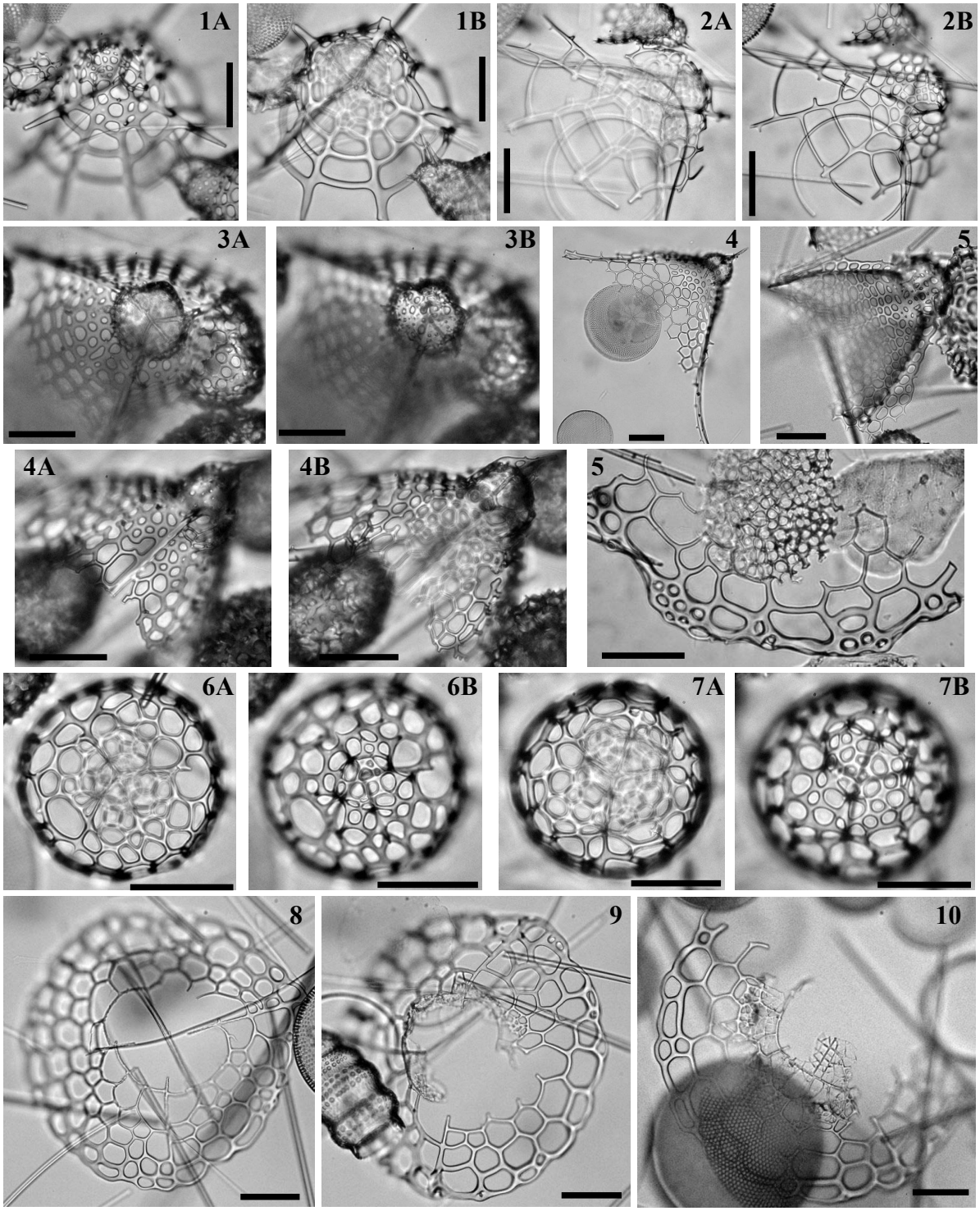

Plate 19.–
1. *Ceratocyrtis dolvenae*, holotype, Sample 120-751A-3H-4 98-102cm, Early Pliocene.
2. *Ceratocyrtis dolvenae*, Sample 120-751A-7H-2 98-102cm, Late Miocene.
3. *Clathrocorys sugyiamai* Renaudie & Lazarus in press, Sample 119-738B-2H-3 53-55cm, Late Pliocene.
4. *Clathrocorys sugyiamai,* Sample 120-747A-2H-3 45-47cm, Pleistocene.
5. *Clathrocorys sugyiamai*, Sample 120-751A-4H-4 98-102cm, Early Pliocene.
6. *Clathrocorys sugyiamai*, holotype, Sample 119-744A-2H-1 53-55cm, Late Pliocene.
7. *Enneaphormis* sp. Renaudie & Lazarus in press, Sample 119-738B-2H-5 53-55cm, Early Pliocene.
8. *Lampromitra*? sp. V, Sample 119-744A-2H-1 53-55cm, Pleistocene.
9. *Lampromitra*? sp. V, Sample 119-738B-1H-3 53-55cm, Pleistocene.
10. *Enneaphormis* sp., Sample 120-751A-3H-1 98-102cm, Late Pliocene.
11. *Enneaphormis* sp., Sample 120-751A-3H-1 98-102cm, Late Pliocene.
12. *Enneaphormis* sp., Sample 120-751A-3H-2 98-102cm, Early Pliocene.
All scale bars 50 µm. Magnification x384 except for 4-5, and 10-12 (x192).

The wall is rough, crested and bears only a few pores, unequal in size and arranged randomly. No other ornamentation (such as horns) have been seen on any specimens.

Dimensions. (based on 6 specimens) Length: 66-83 (74); width: 58-70 (66); length of cephalis: 36-44 (40).

Occurrence. Rare from the *C. spongothorax* to the Upsilon Zone (middle Miocene to early Pliocene), common in the *A. australis* and *S. vesuvius* Zone (late Miocene).

Remarks. *Antarctissa ballista* differs from all other members of the genus *Antarctissa* mostly in its median, free, robust spine **A**. Its overall shape is rather similar to that of *Botryopera pseudoantarctissa* Petrushevskaya in Petrushevskaya & Kozlova, 1979 and *A. whitei* Bjørklund, 1976a, yet the length and width ratio of the two segments, the closed thorax and the lack of any external spine or spongy meshwork make it unique.

Antarctissa strelkovi Petrushevsakya 1967

(Pl. 16, fig. 6)

1967 *Antarctissa strelkovi* Petrushevsakya: p. 88; pl. 51, figs 3-6

1990 *Antarctissa strelkovi* Petrushevsakya – Lazarus: p. 713; pl. 3, figs 13-15

Antarctissa evanida Renaudie & Lazarus in press

(Pl. 17, fig. 1A-7;)

Derivation of name. From the latin adjective *evanidus,* meaning ephemeral.

Diagnosis. Dicyrtid with flaring thorax; double apically-located horn unrelated to spine **A** or spine **V**; three wings and numerous small "feet"; internal skeletal structure similar to that of the genotype.

Holotype. Pl. 17, fig. 6; Sample 120-751A-4H-4, 45-47cm (Early Pliocene); ECO-056.

Material. 1079 specimens were observed from ODP Sites 689, 693, 747, 751 and 1138.

Description. Two-segmented shell with a subspherical to slightly ovoid cephalis and a flaring thorax.

Cephalic inner structure is made of robust spines. Spine **A** and spine **V** join the cephalic wall at the collar stricture and, generally, do not continue outside: some rare specimens though exhibit a very small, triangular horn as continuation of both spines (Pl. 17, fig. 3B). Spine **D** is directed downward and reach the thoracic wall near its middle. An apophyse *c* branches from spine **D** to join the upper thorax wall (Pl. 17, fig. 2A;) and so is an apophyse *a* on spine **A** (Pl. 17, fig. 3B;). The axobate branches from the median bar close to the junction of spines **A** and **D**. It is fairly long, rod-shaped and ends with a cluster of thin branches (Pl. 17, fig. 2A). Spines **Ll** and **Lr** are fairly similar to spine **D** in shape and direction. Those three spines (**Ll**, **Lr** and **D**) protrude outside the thoracic wall as long, conical wings. In some specimens, bars connect these wings with the lower thorax (Pl. 17, fig. 3B).

The cephalis bears additional horns unconnected to inner spines: in particular, a strong, double (or even triple in some rare specimens; Pl. 17, fig. 6) horn is situated at the apex. Each branch of this horn is conical to blade-shaped and somewhat tribladed near the base. The other additional horns are small, needle-like and irregularly disposed. The cephalic wall is rough and bears several large, circular to subcircular pores, more or less regular in size and disposition, separated by crested bars.

The thoracic wall is rough and bears somewhat larger pores that are more irregularly sized, shaped and distributed than the ones on the cephalis. Some ribs are present on the lower half of the thorax: they continue as feet at the thorax end. Most specimens (such as the ones in Pl. 17, figs 1A-B and 6) also bears on the lower half of the thorax, an extra ring of "feet" made of

thorns projecting from the bar nodes. In some specimens (Pl. 17, figs 1A-B), furrows follow spines **D**, **Ll** and **Lr**, thus making the thorax trilobate in apical view.

Dimensions. (based on 10 specimens) Length of cephalis: 31-43 (37); total length: 98-163 (119); final width of thorax: 82-108 (97); width of cephalis: 32-43 (38).

Occurence. Common in the Tau and the lower Upsilon Zone (Early Pliocene); two specimens were encountered in the *Siphonosphaera vesuvius* Zone (Late Miocene).

Remarks. *Antarctissa evanida* differs from *Antarctissa strelkovi* Petrushevskaya, 1967, and *Helotholus praevema* Weaver, 1983, in its flaring thorax and in the presence of numerous "feet" at its termination*;* from *Lithomelissa? kozoi* n. sp.*, Ceratocyrtis morawanensis* Funakawa, 1995, and *Ceratocyrtis cantharoides* Sugiyama & Furutani, 1992, in the apical and ventral horn being, in these species, well-developed; from *Lophophaena simplex* Funakawa, 1994, in its flaring thorax, its wings and its typical *Antarctissa* inner structure; from *Lampromitra huxleyi* (Haeckel, 1879) and from *L. sinuosa* Popofsky, 1913, in the shape and size of the cephalis, in the presence of wings and in the thoracic pores, in the latter, being polygonal.

Antarctissa? sp. 3

(Pl. 23, figs 19-20B)

Diagnosis. Strawberry-shaped cephalis with, apically, a cluster of supplementary horns; characteristic thorax termination with numerous ridges prolonged as feet, and an large hemispherical, thin sieve plate.

Description. Large dicyrtid with a cephalis elongated toward its somewhat blunt apex and a long thorax with an short flaring upper part and a lower part in the shape of a pinched cylinder (i. e. an hyperboloid). Thorax end with several ribs projecting as long, thin teeth. Below this termination a large, thin, largely concave sieve plate, perforated by numerous, closely packed elliptical to polygonal pores. Spines **A** and **V** join the wall at the collar stricture. The cephalis however exhibits a cluster of apically situated horns (unrelated to any internal spines or apophyses). Spine **D** is projected downward and bears an upward-directed apophyse ***c*** (evoking a similar disposition typical of genus *Antarctissa*). Spines **D**, **Ll** and **Lr** joins the thoracic wall between the upper and the lower thorax and continue outside as short needle-like wings. Spine **Ax** is situated at the middle of **MB** and is fairly long and straight.

Remarks. Although the overall shape of the species as well as the thorax termination are very uncharacteristic of genus *Antarctissa*: the fact that spine **A**, in particular, join the cephalis wall at the level of the external collar stricture and the shape and direction of spine **D** seem to be chracters strong enough to justify the assignment of this species to the genus. This species differs from *Antarctissa strelkovi* in the shape of the cephalis, the length of the thorax and its specific termination. Although *Antarctissa strelkovi* and *A. evanida* also have clusters of apical horns (systematic in *evanida* but rarer in *strelkovi*), they are, in those two species, conical whereas in *A.*? sp. 3 they are linked together by blade-shaped connections.

Genus *Arachnocorallium* Heckel 1887 emend. Petrushevskaya 1971

Type-species: *Arachnocorys hexaptera* Haeckel 1887 (=*Psilomelissa calvata* Haeckel 1887)

Arachnocorallium calvata (Haeckel 1887)

1887 *Psilomelissa calvata* Haeckel: p. 1205; pl. 56, fig. 6

1887 *Arachnocorys hexaptera* Haeckel: p. 1265

1971 *Arachnocorallium calvata* (Haeckel) – Petrushevskaya: p. 136-137; pl. 70

Arachnocorallium sp. 5

(Pl. 26, figs 2-4)

Diagnosis. Large, almost spherical, cephalic chamber; strong spines **D, Ll** and **Lr** that branch irregularly in their distal part; several long, subapical by-spines.

Description. Monocyrtid whose cephalis is in two distinct parts: a large, spherical upper part that bears regularly-arranged, relatively large circular pores and whose wall is rough and crested and a more or less cylindrical, narrow lower part with a few large circular pores and a rather smooth wall. Spine **A** is embedded in the wall of the lower and the upper part and eventually, in some specimens, protrudes as a fairly long conical spines (Pl. 26, fig. 4). Spines **D**, **Ll** and **Lr** are rather strong, relatively long and bifurcate distally. **Ax** can be seen near the junction of **MB**, **Ll** and **Lr** as a triangular dent on **MB**. Several supplementary thin, long, conical horns can be also present subapically.

Remarks. It differs from *Peridium sphaerum* Funakawa 1995b in the presence of the long by-spines and in the robustness, length and shape of the basal spines.

Arachnocorallium sp. 17

(Pl. 26, figs 9-10)

Diagnosis. Elongated cephalis; few irregularly-arranged pores, numerous spine-like thorns on upper cephalis.

Description. Monocyrtid with apically elongated cephalis. Pores are circular to elliptical, generally large, irregularly-arranged. Shell wall is rough and numerous spine-like thorns arise from bar nodes. Spines **A** and **V** (Pl. 26, fig. 9) are incorporated in the shell wall but do not seem to protrude as horns (at least distinguishable from the numerous thorns). Spines **D**, **Ll** and **Lr** are fairly long, conical and can bifurcate close to their base (Pl. 26, fig. 9). **Ax** is not noticeable.

Remarks. It differs from *Peridium infundibulum* (Funakawa 1995b) in the latter possessing numerous thorns on the lower cephalis while in *A*. sp. 17 there are situated on the very upper cephalis. They also differs in this new species having few, large pores and in spines **D, Ll** and **Lr** being more robust and longer than in *P. infundibulum*.

Arachnocorallium? sp. A

(Pl. 26, figs 11-12B)

Diagnosis. Cephalis wall is a loose meshwork attached to a sagittal ring; spines **D**, **Ll** and **Lr** are long and conical.

Description. Monocyrtid with a cephalis arranged on both side of a clearly developed sagittal ring (i. e. **A**, **V** and arch **AV**). This sagittal ring apex is oriented ventrally. Spines **D**, **Ll** and **Lr** are well-developed, long and conical. A supplementary spine projects from spine **A** dorsally as a short conical horn. Ventrally, a triangular dent can be seen high on spine **V**. Shell wall is loose, constituted by a few large, elliptical pores separated by crested bars.

Remarks. Despite having a sagittal ring, this species is not a Trissocyclidae due to the absence of a basal ring. It differs from members of genus *Zygocircus* Bütschli 1882 in possessing a shell wall and in its well-developed spines **D**, **Ll** and **Lr**. It differs from members of genus *Arachnocorallium* in possessing a sagittal ring.

Genus *Arachnocorys* Haeckel 1860 emend. Petrushevskaya 1971

Type-species: *Arachnocorys circumtexta* Haeckel 1862

Arachnocorys circumtexta Haeckel 1862emend. Petrushevskaya 1971

1862 *Arachnocorys circumtexta* Haeckel: p. 304; pl. 6, figs 9-11

1862 *Arachnocorys circumtexta* Haeckel – Petrushevskaya: p. 125-128; pl. 65, figs 3-5; pl. 67

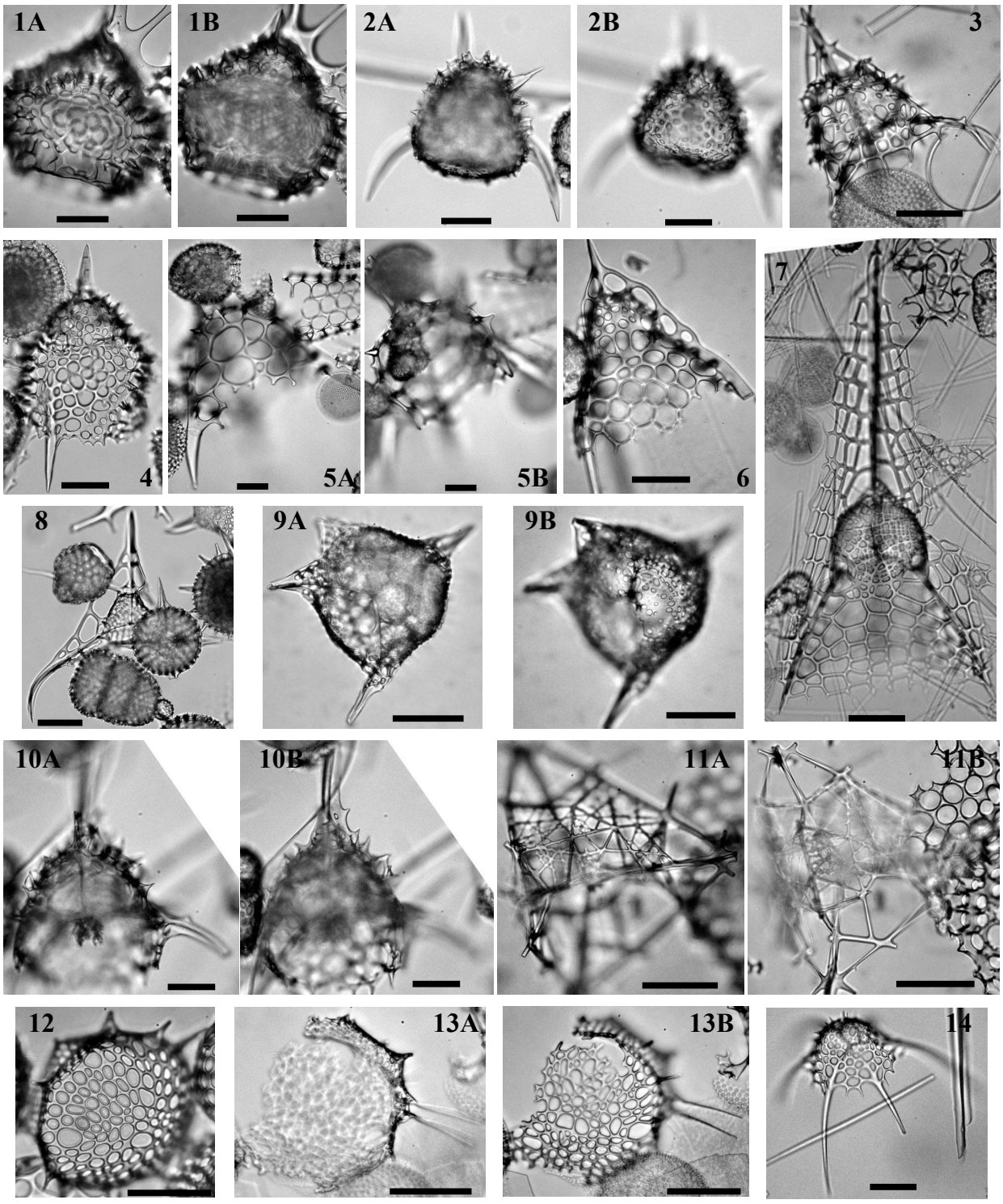

Plate 20.– 1. *Spongomelissa dilli* Chen 1975, Sample 119-744A-7H-2 53-55cm, Middle Miocene. 2. *Corythomelissa horrida* Petrushevskaya 1975, Sample 119-744A-7H-3 53-55cm, Middle Miocene. 3. *Clathromitra pentacantha* Haeckel 1887, ample 120-751A-7H-4 98-102cm, Late Miocene. 4. *Tripophaenoscenium laimingi* Clark & Campbell 1944, Sample 120-748B-6H-1 45/47cm, Early Miocene. 5. *Lamprotripus mawsoni* Riedel 1959, Sample 120-747A-2H-5 45-47cm, Pleistocene. 6. *Genetrix petrushevskaae* Sugiyama 1994, Sample 119-744A-10H-2 60-62cm, Early Miocene. 7. *Callimitra solicicribata* Takahashi 1991, Sample 120-747A-1H-2 82-89cm, Pleistocene. 8. *Clathrocorys murrayi* Haeckel 1887, Sample 120-748B-6H-1 45-47cm, Early Miocene. 9. *Pteroscenium pinnatum* Haeckel 1887, Sample 120-747A-7H-5 45-47cm, Middle Miocene. 10. *Clathromitra pterophormis* Haeckel 1887, Sample 119-745B-15H-4 53-55cm, Late Pliocene. 11. *Archiscenium quadrispinum* Haeckel 1887, Sample 119-744A-7H-4 60-62cm, Middle Miocene. 12. *Lampromitra*? sp. E, Sample 119-744A-8H-1 53-55cm, Early/Middle Miocene. 13. *Lampromitra*? sp. E, Sample 120-748B-7H-2 45-47cm, Early Miocene. 14. *Inversumbrella*? sp. 15, Sample 120-751A-13H-2 98-102cm, Middle Miocene.
All scale bars 50 µm. Magnification x384 except for 2A-B, 4-5B, 7-8, 10A-B and 14 (x192).

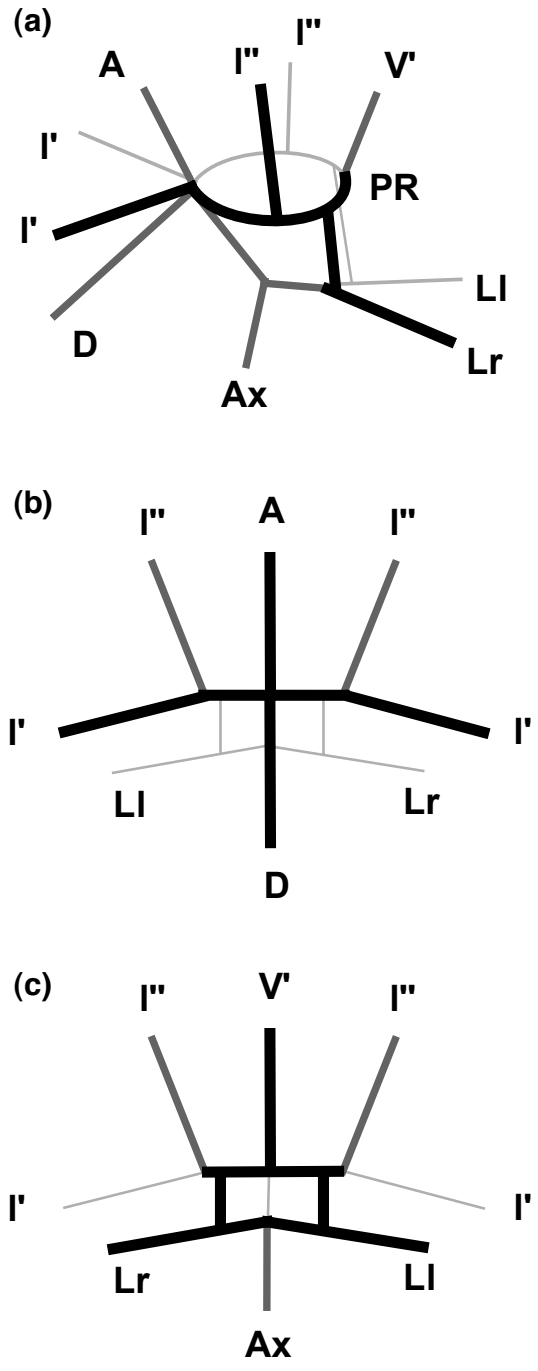

Figure 7.– Schematic illustration of *Botryopera*? *daleki* cephalic inner structure.
a. Sagittal view (tilted). b. Dorsal view. c. Ventral view.
Dark grey: spines in the plane of the paper; black: spines on the viewer side of the plane; light grey: spines on the opposite side of the plane.
Terminology after Sugiyama, 1993.
PR: proximal ring; **V'**: secondary vertical spine, arising from **PR**; **l''**: tertiary lateral spine, arising from **PR**.

Genus *Botryopera* Haeckel 1887
Type-species: *Botryopera cyrtoloba* Haeckel 1887

Botryopera chippewa Renaudie & Lazarus in press
(Pl. 16, figs 19A-20, Pl. 26, figs 8-9, 17A-18B)
1971 *Dimelissa sp. P* Petrushevskaya: pl. 46, fig. 12.
? 1975 *Pseudodictyophimus* (?) sp. Petrushevskaya: pl. 11, fig. 18.
? 1975 *Lithomelissa* sp. B aff *L. mitra* Bütschli – Chen: p. 458, pl. 8, figs 4-5 (as *Lithomelissa mitra*?).

Derivation of name. Named after the resemblance of the shoulders and apical horn to portraits of Chippewa and other northeast American Indian peoples.

Diagnosis. Small dicyrtid with cephalis and thorax almost similar in size, with a strong apical horn on the dorsal side of the cephalis.

Holotype. Pl. 16, figs 19A-B, Sample 120-747A-9H-8, 45-47cm (Middle Miocene); ECO-057.

Material. 38 specimens were observed from ODP Sites 744, 747, 748 and 751.

Description. Two-segmented shell with a subspherical cephalis with two approximately equal cephalic horns projecting vertically-laterally and a cylindrical thorax of approximately the same size as the cephalis, separated by a collar stricture marked by shoulders along arches **AL** and **VL**. In most specimens the stricture is more pronounced ventrally than dorsally.

Spine **A** is free in the cephalic cavity and protrudes outside subapically as a strong, smooth, blade-like horn, sometimes tribladed at its base. Spine **V** extends outside the wall as a short, triangular horn at the collar stricture. Spines **D**, **Ll** and **Lr** often continue as short blade-like wings/feet. An apophyse on spine **D** joins the thoracic wall. Some specimens have a long, slim axobate. The median bar is generally situated below the upper third of the thorax.

The crested, thick cephalis wall bears few, rounded pores while the thoracic pores are increasingly numerous and big as they reach the thorax closure, which consists of a thinner meshwork with numerous small, irregular pores separated by thin

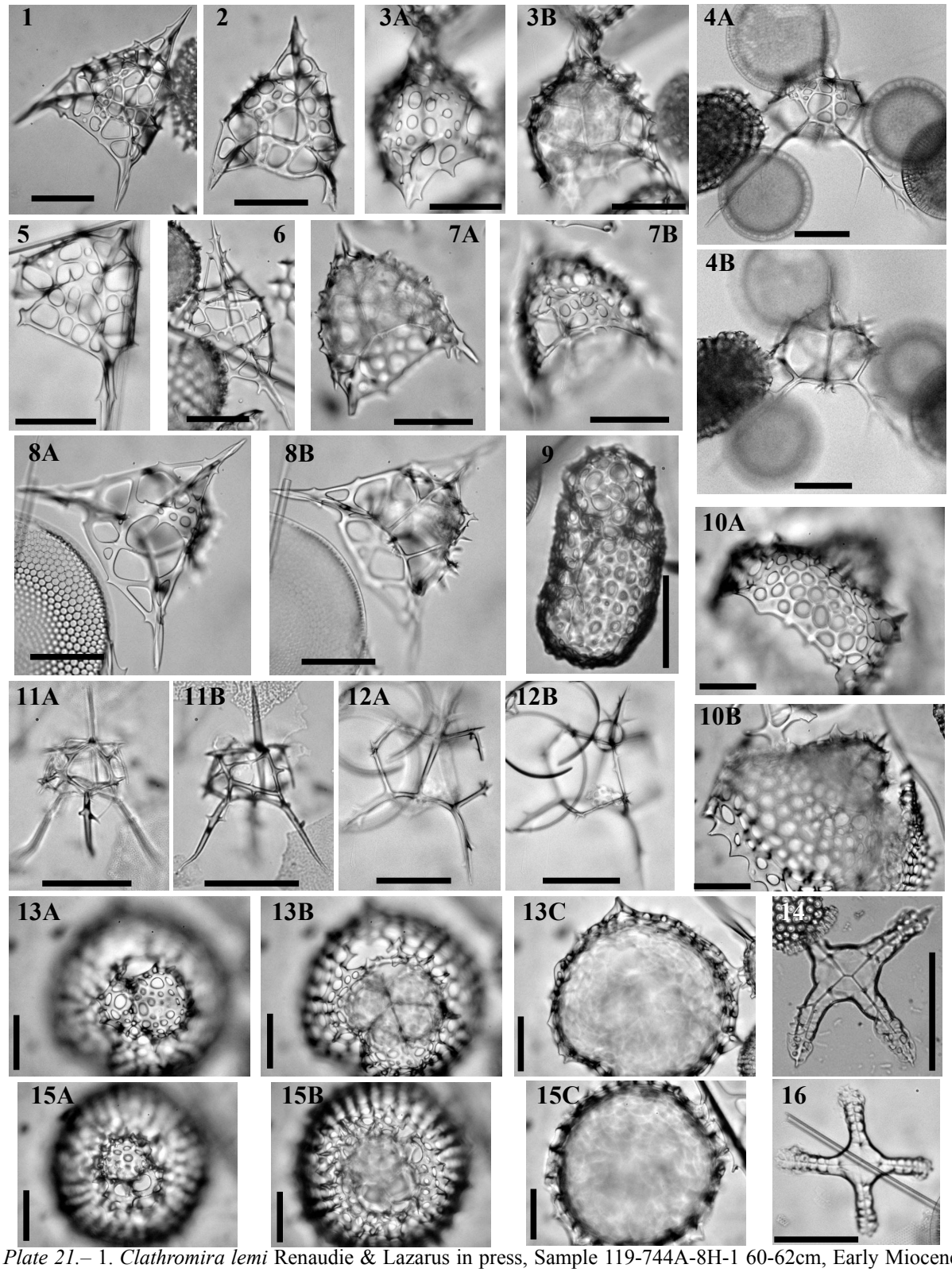

Plate 21.– 1. *Clathromira lemi* Renaudie & Lazarus in press, Sample 119-744A-8H-1 60-62cm, Early Miocene. 2. *Clathromira lemi*, holotype, Sample 119-744A-10H-2 60-62cm, Early Miocene. 3. *Clathromira lemi*, Sample 120-748B-6H-CC, Early Miocene. 4. *Clathromitra*? *fulgureanubes* Renaudie & Lazarus in press, holotype, Sample 120-748B-6H-3 45-47cm, Early Miocene. 5. *Clathromira lemi*, Sample 120-751A-4H-6 98-102cm, Early Pliocene. 6. *Clathromira lemi*, Sample 120-748B-8H-2 45-47cm, Early Miocene. 7. *Clathromira lemi*, Sample 120-748B-6H-CC, Early Miocene. 8. *Clathromira lemi,* Sample 120-748B-6H-5 45-47cm, Early Miocene. 9. Plagoniid sp. P, Sample 119-746A-10H-1 53-55cm, Late Miocene. 10. *Ceratocyrtis*? sp. 12, Sample 120-748B-8H-2 45-47cm, Early Miocene 11. *Clathromitra*? *fulgureanubes*?, Sample 113-690B-6H-6 22-24cm, Early Miocene. 12. *Clathromitra*? *fulgureanubes*, Sample 120-751A-13H-2 98-102cm, Middle Miocene. 13. *Ceratocyrtis*? sp. 12, Sample 120-748B-8H-2 45-47cm, Early Miocene. 14. *Plectagonidium deflandrei* Cachon et al. 1969, 113-689B-3R-5 136-138cm, Late Miocene. 15. *Ceratocyrtis*? sp. 12, Sample 120-748B-8H-2 45-47cm, Early Miocene 16. *Plectagonidium deflandrei* Cachon et al. 1969, Sample 120-751A-12H-2 98-102cm, Middle Miocene. All scale bars 50 µm. Magnification x384 except for 4A-B (x192).

bars.

Dimensions. (based on 5 specimens) Total height (without horn and feet): 77-107 (87); height of cephalis (from apex to collar): 32-51 (46); length of apical horn: 22-47 (36).

Occurence. Sporadic from the *Cycladophora golli regipileus* to the Tau Zone (Early Miocene to Early Pliocene).

Remarks. It differs from *Antarctissa robusta* Petrushevskaya, 1975 and *Botryopera oceanica* (Ehrenberg) 1873a primarily in the strong spine **A** which protrudes subapically as a robust horn. It also differs from *B. braevispicula* (Popofsky) 1908 in having less numerous pores, in the clearer demarcation of the two segments and the stronger horns; from *Dimelissa apis* (Haeckel) 1887 (as illustrated in Petrushevskaya, 1971; p.134-135; pl.69, figs I-IV) in its longer thorax, its less numerous and smaller pores, its stronger horns and in the relative position of the median bar and the collar stricture; from *Lithomelissa macroptera* Ehrenberg, 1874 (see Ogane *et al.*, 2009) in the latter having stronger, tribladed lateral and dorsal wings and in the relative position of the median bar and the collar stricture. The specimens illustrated in Chen (1975) as *L. mitra?* seem to be conspecific with *Botryopera chippewa*: they differ however from our specimens in being narrower and in having a less marked collar stricture.

Botryopera? *gibbera* Renaudie & Lazarus 2012

(Pl. 24, figs 11A-14B)

Derivation of name. *Gibbera* is Latin for hunchback.

Diagnosis. Characterized by a large hump between spine A and spine D.

Holotype. Plate 24, figs. 14A-B; Sample 120-751A-10H-4 98/102cm (Middle Miocene); ECO-039.

Material. 160 specimens were observed from ODP Sites 744, 747, 748 and 751.

Description. Two-segmented shell with a thorax slightly longer (ca. 1.2 times) than the cephalis which is separated into two chambers: an antecephalic "hump" between spine **A** and spine **D** and an eucephalic chamber between spine **A** and spine **V**. Externally, the two chambers are separated by a furrow along **AL** while the eucephalic chamber wall and the thoracic wall are separated by a furrow along **VL**. Spine **A** and spine **V** both continue outside as small triangular horns. The wall of both cephalic chambers also bears numerous thorns. The antecephalic chamber is variable in size: it can be only 0.25 times the volume of the eucephalic chamber (see Pl. 7, figs. 4A-B and 6A-B) as well as up to 0.75 times (see Pl. 7, figs. 3A-B).

The thorax is short and somewhat barrel-shaped. Its termination is ragged; it bears no specific ornamentation nor does it flare. Pores on both segments are circular to elliptical and irregular both in size and in disposition.

Dimensions. (based on 6 specimens) Length: 69-86 (78); width at collar: 43-56 (49); length of eucephalic chamber: 33-47 (41); width of antecephalic chamber: 17-29 (22).

Occurrence. Very rare from the *A. golownini* to the *S. vesuvius* Zone (middle to late Miocene).

Remarks. *Botryopera*? *gibbera* differs from other small Lophophaenids by its fairly large antecephalic chamber. Because of this peculiar character, the assignment to genus *Botryopera* remains uncertain.

Botryopera? daleki Renaudie & Lazarus in press

(Pl. 17, figs 8A-11C; Fig. 7;)

Derivation of name. Named after the Daleks in the UK science-fiction TV series 'Doctor Who'.

Diagnosis. Large spherical cephalic chamber with a thorn-bearing wall; thin-walled thorax loosely connected to cephalis; complex ring structure.

Holotype. Pl. 17, figs 11A-C; Sample 120-748B-6H-5, 45-47cm (Early Miocene); ECO-058.

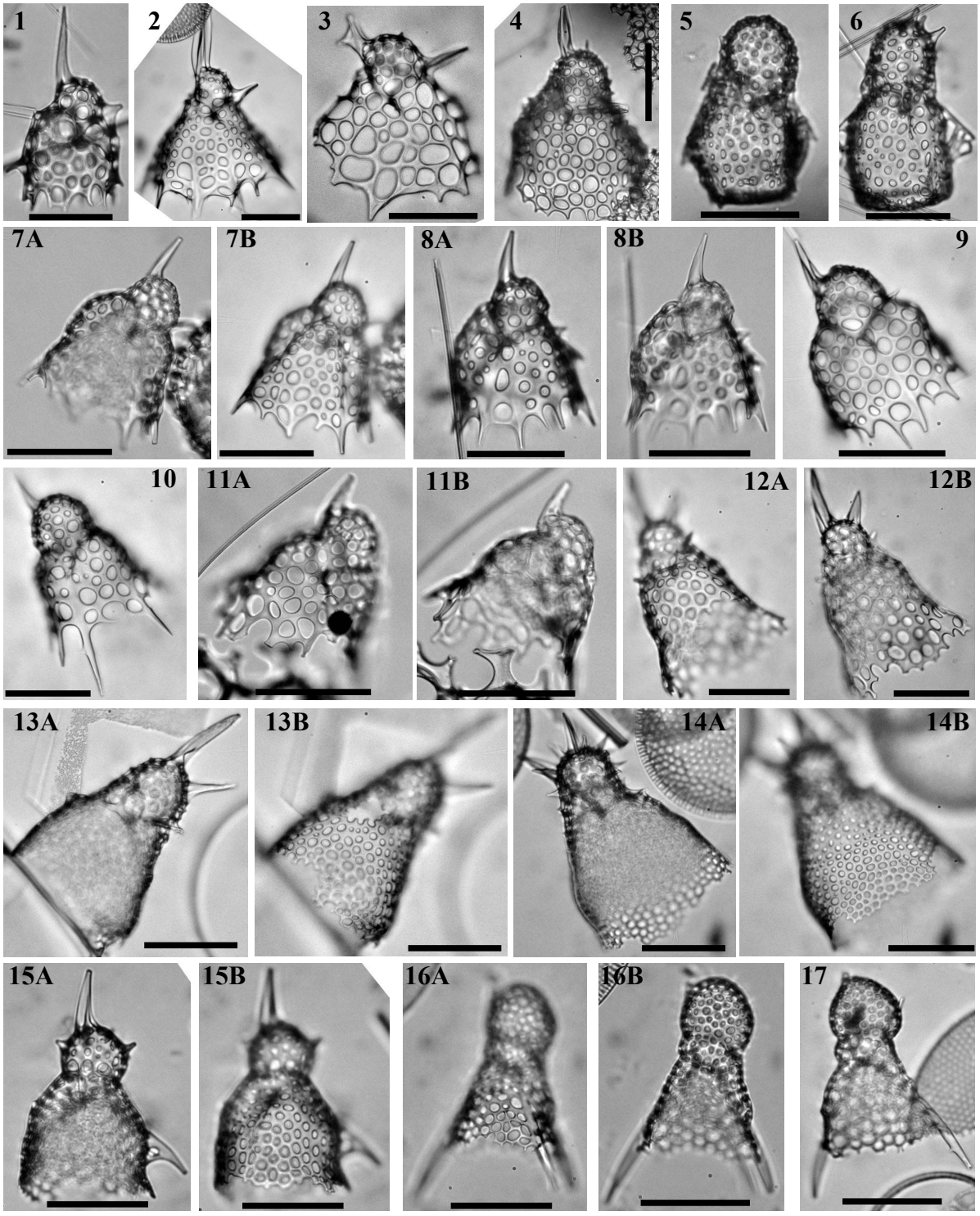

Plate 22.– 1. *Lithomelissa*? *stigi* Bjorklund 1976, Sample 119-744A-5H-3 53-55cm, Late Miocene. 2. *Ceratocyrtis*? *morawanensis* Funakawa 1995b, Sample 120-751A-12H-6 98-102cm, Middle Miocene. 3. *Ceratocyrtis*? *cantharoides* Sugiyama & Furutani 1992, Sample 120-748B-6H-1 45-47cm, Early/Middle Miocene. 4. *Lophophaena*? *thaumasia* Caulet 1991, Sample 120-748B-6H-5 45-47cm, Early Miocene. 5. *Botryopera* spB, Sample 119-737A-27X-2 53-55cm, Late Miocene. 6. *Botryopera* spB, Sample 120-751A-8H-3 98-102cm, Late Miocene. 7. *Lithomelissa*? *kozoi* Renaudie & Lazarus in press, Sample 120-747A-2H-5 45-47cm, Pleistocene. 8. *Lithomelissa*? *kozoi*, holotype, Sample 120-747A-2H-5 45-47cm, Pleistocene. 9. *Lithomelissa*? *kozoi*, Sample 120-747A-2H-5 45-47cm, Pleistocene. 10. *Lithomelissa*? *kozoi*?, Sample 120-747A-4H-7 45-47cm, Late Miocene. 11. *Lithomelissa*? *kozoi*, Sample 120-747A-2H-5 45-47cm, Pleistocene. 12. *Lophophaena leberu* Renaudie & Lazarus 2012, Sample 120-751A-16H-CC, Early Miocene. 13. *Lophophaena leberu*, holotype, Sample 120-748B-7H-2 45-47cm, Early Miocene. 14. *Lophophaena leberu*, Sample 120-751A-18H-CC, Early Miocene. 15. *Lophophaena* spX, Sample 119-737A-27X-4 53-55cm, Late Miocene. 16. *Lophophaena* spU, Sample 119-744A-2H-4 53-55cm, Pleistocene. 17. *Lophophaena* spU, Sample 119-746A-7H-2 53-55cm, Late Miocene. All scale bars 50 µm. Magnification x384.

Material. 69 specimens were observed from ODP Sites 744, 746, 748 and 751.
Description. Two-segmented shell with a spherical cephalis and a truncate conical thorax, loosely connected to the lower third of the cephalis.
The inner cephalic structure is quite complex. It is composed of a proximal ring from which arise, on its upper side, four similar and regularly-spaced spines: spine **A**, spine **V'** and two spines **l''**. On the lower side of the proximal ring, spine **D** and the median bar are connected at the junction with spine **A**. The median bar bears an axobate (Pl. 17, figs 10A-B;) and bifurcates, on the ventral side, into spines **Ll** and **Lr**. These two spines are furthermore connected to the proximal ring by two vertical apophyses (called **L-R** in Sugiyama, 1993). Finally, two spines **l'** extends laterally from the proximal ring, close to the junction with spine **A** (see Fig. 7;).
The eucephalic chamber is entirely supported by the arches connecting the four spines **A**, **V'** and **l''** (i.e. what is referred in Sugiyama, 1993, as the distal ring, **DR**). The thorax is connected to the cephalis on those arches as well. Above this collar stricture, the cephalic wall is rather thick, crested, bears numerous thorns and numerous circular to elliptical small pores: there is a increasing pore size gradient from the apex to the collar stricture.
The upper part of the thorax (i.e. between the collar stricture and the junction of spines **l'**, **Ll** and **Lr** with the thoracic wall) is cylindrical in outline whereas the lower part (i.e. below the level at which spines **l'**, **L1** and **Lr** penetrate the shell wall) is truncated-conical. The thoracic wall is thin and bears numerous circular to subpolygonal relatively large pores, irregularly-disposed and separated by thin bars. The thorax termination is ragged.
Furrows at the junctions with spines **l'**, **Ll**, **Lr** and **D** and the thoracic wall are often seen (Pl. 17, fig. 8A).
Dimensions. (based on 5 specimens) Total height: 97-124 (107); height of cephalis: 34-47 (44); width of cephalis: 42-51 (46); width of thorax (at collar): 57-69 (66).
Occurence. Rare in the *Cycladophora golli regipileus* Zone (Early Miocene); sporadic from the *Eucyrtidium punctatum* to the *Siphonosphaera vesuvius* Zone (Middle to Late Miocene).
Remarks. *Botryopera? daleki* differs from *Antarctissa cylindrica* Petrushevskaya, 1975 in the shape, thickness and porosity of the thorax and the way it is attached to the cephalis; from *Steganocubus subtilis* Sugiyama, 1993*, S. lipus* Sugiyama, 1993, *S. incrassatus* Funakawa, 1995 and *Antarctissa*? *whitei* Bjørklund, 1976a primarily in the clear external differentiation between the two segments; from *Botryopera*? *leptostraca* Sugiyama, 1993 in the loose attachment of the thorax to the cephalis and the width of the thorax.
This new species has been assigned tentatively to genus *Botryopera* because of the shape and size of the eucephalic chamber and the fact that the collar is situated in its lower third. However the length and width of the thorax relative to that of its cephalis is uncommon for the genus. Internally, this species shares common characteristics with species of the genus *Steganocubus* Sugiyama, 1993 (such as the presence of a relatively narrow proximal ring with connecting spines **l''**) however, externally, they are very dissimilar.

Botryopera sp. C
(Pl. 23, figs 11-14B)

Description. Dicyrtid with an hemispherical cephalis (ca. a third of the shell height) and a truncated conical thorax. Both segments are separated externally by furrows following arches **AL** and **VL**. Spine **A** is fused to the dorsal side of the cephalic wall and protrudes subapically as a short triangular, tribladed, slightly incurved, robust horn. Spine **V** protrudes at the collar stricture as a shorter, triangular and tribladed horn. Spine **D, Ll** and **Lr** join the thoracic wall, are directed downwards (and eventually form furrows on the thoracic wall; Pl. 23, fig. 11) and continues after the thorax termination as small feet. These feet are short and conical and are

undifferenciated from the fairly numerous teeth that also project at the thorax termination. Mouth is closed by a sieve plate, relatively thick, perforated by a few, randomly distributed, small circular pores. Additional robust spines can be present on the cephalis. Shell wall is generally rather thick. Pores on the cephalis are small and circular while pores on thorax are somewhat larger.

Remarks. This species is easily differentiable from other species of genus *Botryopera* because of the presence of basal teeth and of a sieve plate closing the basal aperture. The thickness of the shell and the short, robust horns are also characteristic of this species.

Botryopera sp. B
(Pl. 22, figs 5-6)

Description. Dicyrtid with an hemispherical to ellipsoidal (elongated toward the apex) cephalis and a cylindrical to barrel-shaped thorax. Both are separated externally by furrows along **AL** and **VL.** Spine **A** is fused to the dorsal side of the cephalic wall while spine **V** joins the wall at the collar stricture. Both can protrudes (when they do) as very small, bearly noticeable needle-like spines. Spines **D, Ll** and **Lr** on the contrary always protrude as long needle-like, downward-directed wings. Some bars can occasionally link the distal part of the wings to the rest of the thorax (see Pl. 22,. fig. 6). Thorax termination is closed. Pores on the cephalis and on the thorax are small, circular to elliptical, and randomly-distributed. Cephalis can bear additional small spines.

Remarks. This species is characterized by its wings and its more or less cylindrical, closed thorax. The furrows along arches **AL** and **VL,** the shape of the cephalis and the disposition of spines **A** and **V** relatively to the shell wall seem to be very characteristic of this group of small dicyrtid, here regrouped inside the genus *Botryopera* (with the exclusion of *Botryopera*? *daleki*).

Genus *Ceratocyrtis* Bütschli 1882
Type-species: *Cornutella*? *cucullaris* Ehrenberg 1873

Ceratocyrtis cucullaris (Ehrenberg 1873)
(Pl. 18, fig. 1)

1873 *Cornutella*? *cucullaris* Ehrenberg: p. 221
1875 *Cornutella cucullaris* Ehrenberg – Ehrenberg: pl. 2, fig. 7
1882 *Ceratocyrtis cucullaris* (Ehrenberg) – Bütschli: p. 536; fig. 36

Ceratocyrtis galeus (Cleve 1899)
(Pl. 18, figs 4A-B)

1899 *Sethoconus galea* Cleve: p. 33; pl. 4, fig. 3
1976a *Ceratocyrtis galeus* (Cleve) – Bjørklund: pl. 11, figs 1-3

Ceratocyrtis histricosus (Jørgensen 1905)
(Pl. 18, fig. 2)

1905 *Helotholus histricosa* Jørgensen: p. 137; pl. 16, figs 86-88
1971 *Ceratocyrtis histricosa* (Jørgensen) – Petrushevskaya: p. 98-101; pl. 52, figs 2-4
1976a *Ceratocyrtis histricosus* (Jørgensen) – Bjørklund: pl. 8, figs 19-24; pl. 11, figs 4-5

Ceratocyrtis mashae Bjørklund 1976
(Pl. 18, fig. 6)

1976a *Ceratocyrtis mashae* Bjørklund: p. 1125; pl. 17, figs 1-5

Ceratocyrtis robustus Bjørklund 1976
(Pl. 18, figs 3A-B)
1976a *Ceratocyrtis robustus* Bjørklund: p. 1125; pl. 17, figs 6-10

Ceratocyrtis stoermeri Goll & Bjørklund 1979
(Pl. 18, figs 7A-B)
1979 *Ceratocyrtis stoermeri* Goll & Bjørklund: p. 731; pl. 5, figs 5-9
1992 *Ceratocyrtis stoermeri* Goll & Bjørklund – Sugiyama & Furutani: p. 205
1993 *Ceratocyrtis stoermeri* Goll & Bjørklund – Sugiyama: p. 69; pl. 20, figs 4-6

Ceratocyrtis? *morawanensis* Funakawa 1995b
(Pl. 22, fig. 2)
1994 *Pseudodictyophimus* sp. B O'Connor: p. 62; pl. 6, figs 14-15
1995b *Ceratocyrtis morawanensis* Funakawa: p. 20; pl. 1, figs 4-5
1997a *Lophophaena tekopua* O'Connor: p. 73; pl. 2, fig. 11-14; pl. 7, figs 7-10

Ceratocyrtis? *cantharoides* (Sugiyama & Furutani 1992)
(Pl. 22, fig. 3)
1992 *Ceratocyrtis*? *cantharoides* Sugiyama & Furutani; p. 205; pl. 13, figs 1-2; pl. 20, figs 1-2

Ceratocyrtis dolvenae Renaudie & Lazarus 2012
(Pl. 18, figs 5A-B; pl. 19, figs 1A-2B)
Derivation of name. Named after Jane K. Dolven for her support of radiolarian research via radiolaria.org.
Diagnosis. Large, more or less aligned, quadrangular, thoracic pores; cephalis and thorax not distinguishable externally; spines **Ll, Lr** and **D** extend laterally at cephalic suture.
Holotype. Plate 5, figs. 5A-B; Sample 120-748B-6H-3 45/47cm (Early Miocene); ECO-048, circle 2.
Material. 33 specimens were observed from ODP Sites 690, 744, 747, 748 and 751.
Description. Two-segmented, conical shell with a cephalis and a thorax that are not separated externally by any furrow, constriction, shoulder or even change in contour. The cephalis is considerably smaller than the thorax. The angle formed by the shell is obtuse.
The cephalis is dome-shaped. Spine **V**, **Ll**, **Lr**, **A** and **D** are usually all protruding outside as thin, conical spines. Spines **Ll**, **Lr** and **D** are roughly in the same plane as the median bar (pl. 5, fig. 2B) whereas spine **A** is orthogonal to it. The axobate is also present as a relatively short, simple, downward-oriented, cylindrical spines approximately at the junction between **Ll**, **Lr**, **V** and the median bar.
The cephalic wall is thorny and bears small, circular to subelliptical, irregularly distributed pores. Pores on the thoracic wall are rectangular with rounded angles and becoming larger and aligned along thin longitudinal bars as they are further from the cephalis.
Dimensions. (based on 4 specimens) Diameter of cephalic pores: 2-15 (7); of thoracic pores: 18-47 (28).
Occurrence. Sporadic from the *C. golli regipileus* to the lower Upsilon Zone (early Miocene to early Pliocene).
Remarks. *Ceratocyrtis dolvenae* differs from *C. galeus* (Cleve) 1899 in the pattern, the size and the shape of its thoracic pores. It also differs from *C. morawanensis* Funakawa, 1995 in the latter having a cephalis distinct from the thorax by a collar stricture, and having a tribladed apical

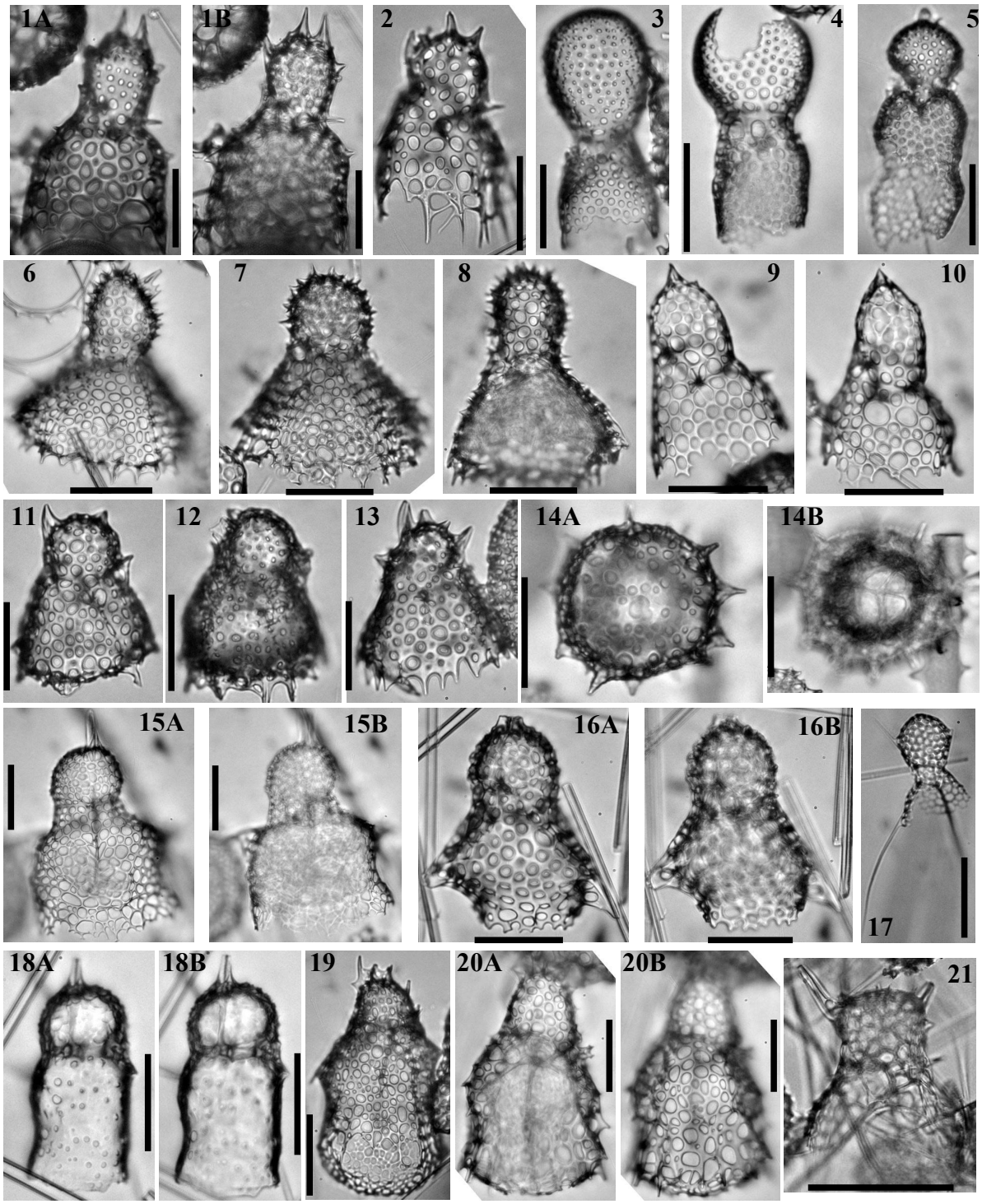

Plate 23.– 1. *Lophophaena nadezdae* Petrushevskaya 1971, Sample 120-747A-2H-1 45-47cm, Pleistocene. 2. *Lophophaena simplex* Funakawa 1995a, Sample 119-744A-9H-1 60-62cm, Early Miocene. 3. *Lophophaena* sp. S, Sample 120-748B-6H-6 45-47cm, Early Miocene. 4. *Lophophaena* sp. S, Sample 120-748B-7H-2 45-47cm, Early Miocene. 5. *Lophophaena macrencephala*?, Sample 119-737B-5R-2 53-55cm, Late Miocene. 6. *Lophophaena* sp14, Sample 120-751A-12H-1 98-102cm, Middle Miocene. 7. *Lophophaena* sp. 14, Sample 120-751A-12H-2 98-102cm, Middle Miocene. 8. *Lophophaena* sp14, Sample 120-751A-12H-2 98-102cm, Middle Miocene. 9. *Lophophaena* sp. Q, Sample 120-747A-2H-5 45-47cm, Pleistocene. 10. *Lophophaena* sp. Q, Sample 120-747A-2H-5 45-47cm, Pleistocene. 11. *Botryopera* sp. C, Sample 120-748B-6H-3 45-47cm, Early Miocene. 12. *Botryopera* sp. C, Sample 120-748B-6H-7 45-47cm, Early Miocene. 13. *Botryopera* sp. C, Sample 119-744A-10H-2 60-62cm, Early Miocene. 14. *Botryopera* sp. C, Sample 120-751A-6H-1 53-55cm, Late Miocene. 15. *Lithomelissa*? sp. 25, Sample 120-748B-7H-4 45-47cm, Early Miocene. 16. *Lithomelissa*? sp. 25, Sample 120-751A-3H-1 98-102cm, Late Pliocene. 17. *Lophophaena clevei* Petrushevskaya 1971, Sample 119-744A-6H-1 53-55cm, Middle Miocene. 18. *Botryometra poljanskii* Petrushevskaya 1975, Sample 120-751A-11H-4 98-102cm, Middle Miocene. 19. *Antarctissa*? sp. 3, Sample 120-747A-2H-5 45-47cm, Pleistocene. 20. *Antarctissa*? sp. 3, Sample 120-747A-2H-5 45-47cm, Pleistocene. 21. *Lophophaena witjazkii* Petrushevskaya 1971, sample 120-747A-1H-2 82-89cm, Pleistocene. All scale bars 50 µm. Magnification x384.

horn. It finally differs from other known members of *Ceratocyrtis* in having prominent lateral spines extending from the cephalic suture.

Ceratocyrtis? sp. 12

(Pl. 21, figs 10A-B, 13A-C, 15A-C)

Description. Large dicyrtid with a large bell-shaped thorax that ends at a short poreless rim with several short triangular teeth. No visible constriction or change in contour at the collar stricture. Spine **A** is free in the cephalic cavity and protrudes apically as a short tribladed horn. Cephalic wall, in apical view, is separated in three sectors: one is latticed, with round to elliptical pores and thick bar nodes with thorns and the two others are each one large pore delimited by a strong, thick circular arch extending from apophyses *g*. **MB** is reduced. Apophyses *m* can be seen joining **A** with the shell wall (Pl. 21, fig. 10B). Still in apical view, the thorax contour is irregular with a few (5-6?) triangular supplementary spines extending laterally from the largest part of the bell-shaped thorax. Pores on thorax are numerous, large, regularly arranged and spaced, and elliptical. Spines **D, V, Ll** and **Lr** are all in the same horizontal plane and do not seem to extend as horns, wings or feet.

Remarks. The peculiar cephalic structure of this species distinguishes it from the other lophophaenids or clathromitrids present in the Southern Ocean, rendering the generic assignment problematic. This structure evokes that of the specimens illustrated by Sanfilippo & Riedel 1973 as *Velicucullus* sp. (Pl. 20, figs 5-6; Pl. 34, fig. 14) but the rest of the skeleton differs widely from our new species (specifically the shell flattening and the thorax termination).

Ceratocyrtis? *spF*

(Pl. 18, figs 8A-B, 10A-B)

Description. Small dicyrtid with a cephalis and a thorax indiscernable externally. Thorax seems to be closed by a sieve plate. Pores on the shell wall are irregular in size, shape (though usually polygonal) and disposition. **MB** is reduced to a point from where all spines project upwards and protrude outside the wall as short conical horns. Some additional spines are present on the cephalis and some of them may be related to apophyses (see Pl. 18, 10B). The point where all spines converge, i. e. **MB**, is situated halfway down the shell cavity, meaning that, technically, the cephalis and the thorax are of equal length.

Remarks. Because of the thorax termination and the cephalis length and because the axobate wasn't observed, the generic assignment of this species to *Ceratocyrtis* is still very much putative.

Ceratocyrtis? *spK*

(Pl. 18, figs 9A-B, 11A-12B)

Description. Large dicyrtid with a reduced cephalis and a long, conical thorax. The collar stricture is not marked externally. Thorax terminated with a rim that bears between 10 and 20 downward-directed, short, conical spines. Pores on the thorax are large and polygonal. There is a size gradient from the cephalis to the thorax rim for these pores. They seem to be distributed randomly. Numerous thorns arise from bar nodes on the cephalis and the upper thorax. Spines **D, V, Ll** and **Lr** are of equal length and in the same plane, as a cross (see Pl. 18, fig. 12B), while **MB** is reduced to a point. **A** and **Ax** were not observed (maybe due to the fact that most of the specimens were observed in apical view). Spines **D, V, Ll** and **Lr** protrude outside the wall as horns that are similar in shape and size to the numerous thorns that the wall already bears.

Remarks. The possible absence of an axobate, the thorax termination and the 'cross' disposition of spines **D, V, Ll** and **Lr** make the assignment to genus *Ceratocyrtis* questionable. All those

characters would fit rather well with species of genus *Lampromitra*: however, the reduced size of the cephalis, and the fact that the spines protrudes outside as horns do not fit with this genus.

Genus *Dimelissa* Campbell 1951 emend. Petrushevskaya 1971

Type-species: *Lithomelissa thoracites* Haeckel 1862

Dimelissa thoracites (Haeckel 1862)

1862 *Lithomelissa thoracites* Haeckel: p. 301; pl. 6, figs 2-8
1971 *Dimelissa thoracites* (Haeckel) – Petrushevskaya: p. 134; pl. 69, figs 7-8
1995 *Peromelissa thoracites* forma *thoracites* (Haeckel) – van de Paverd: p. 224; pl. 66, figs 9-10

Genus *Gondwanaria* Petrushevskaya 1975

Type-species: *Lithomelissa campanulaeformis* Campbell & Clark 1944 (=*Sethoconus dogieli* Petrushevskaya 1967)

Gondwanaria campanulaeformis (Campbell & Clark 1944)
(Pl. 14, fig. 7)

1944 *Lithomelissa campanulaeformis* Campbell & Clark: p. 41; pl. 6, fig. 1
1967 *Sethoconus*? *dogieli* Petrushevskaya: p. 95; pl. 53, figs 1-2
1971 *Pterocyrtidium dogieli* (Petrushevskaya) – Petrushevskaya: pl. 110, fig. 2
1972 *Lipmanella*? *dogieli* (Petrushevskaya) – Petrushevskaya & Kozlova: p. 542; pl. 37, fig. 10
1975 *Gondwanaria dogeli* (Petrushevskaya) – Petrushevskaya: p. 585
1992 *Gondwanaria campanulaeformis* (Campbell & Clark) – Sugiyama et al.: p. 23; pl. 21, figs 8-9b
2000 *Gondwanaria campanulaeformis* (Campbell & Clark) – Funakawa: p. 100-101; pl. 1, figs 1a-d; pl. 7, figs 1a-b; text-fig. 4

Gondwanaria cylindrica Funakawa 2000
(Pl. 14, fig. 8)

2000 *Gondwanaria cylindrica* Funakawa: p. 101; pl. 1, figs 2a-3b; pl. 7, figs 2a-c; text-fig. 5
2000 *Gondwanaria kiroroensis* Funakawa: p. 105; pl. 2, figs 1a-2d; pl. 7, fgs 3a-c; text-fig. 6

Gondwanaria deflandrei Petrushevskaya 1975
(Pl. 14, fig. 2)

1975 *Gondwanaria deflandrei* Petrushevskaya: p. 584-585; pl. 9, figs 8-9
1990 *Gondwanaria deflandrei* Petrushevskaya – Abelmann: pl. 7, fig. 7

Gondwanaria hister Petrushevskaya 1975
(Pl. 14, fig. 4)

1972 *Lipmanella*? sp. M Petrushevskaya & Kozlova: pl. 37, fig. 2-3
1975 *Gondwanaria hister* Petrushevskaya: p. 585; pl. 9, fig. 19; pl. 21, fig. 3
1992 *Lipmanella hister* (Petrushevskaya) – Sugiyama & Furutani: p. 209; pl. 13, figs 7-8

Gondwanaria japonica (Nakaseko 1963)
(Pl. 14, fig. 3)

1963 *Sethocyrtis japonica* Nakaseko: p. 176; pl. 1, fig. 10; text-fig. 9
1975 *Gondwanaria japonica* (Nakaseko) – Petrushevskaya: pl. 8, fig. 15; pl. 19, figs 2-7; pl. 12,

fig. 1
1976a *Gondwanaria japonica* (Nakaseko) – Bjørklund: pl. 18, figs 22-27
1990 *Gondwanaria japonica* (Nakaseko) – Abelmann: pl. 7, figs 3a-b

Gondwanaria nigriniae Petrushevskaya & Kozlova 1979
(Pl. 14, fig. 5)
1976a *Lipmanella xiphephorum* (Jørgensen) – Bjørklund: pl. 16, figs 11-13
1976 *Gondwanaria dogieli* (Petrushevskaya) group – Dzinoridze et al.: pl. 41, fig. 13
1979 *Gondwanaria nigriniae* Petrushevskaya & Kozlova: p. 140-141; figs 402-403, 532-534
1990 *Gondwanaria* sp. A Abelmann: p. 697; pl. 7, fig. 6

Gondwanaria reschetnjakae (Petrushevskaya 1967)
(Pl. 14, fig. 9)
1967 *Sethoconus*? *reshetnjakae* Petrushevskaya: p. 92; pl. 53, figs 3-4
1971 *Pterocyrtidium reshetnjakae* (Petrushevskaya) – Petrushevskaya: pl. 110, fig. 1
1976 *Pseudodictyophimus*? *reshetnjakae* (Petrushevskaya) – Dzinoridze et al: pl. 41, figs 6-7
1981 *Gondwanaria reshetnjakae* (Petrushevskaya) – Petrushevskaya: p. 110; fig. 117

Gondwanaria clarae Renaudie & Lazarus 2012
(Pl. 14, fig. 10, 13-14)

Derivation of name. Named after Clara Ehrenberg who devoted much of her life to supporting the study of radiolaria and other micro-organisms.

Diagnosis. Apically-elongated cephalis with a strong lanceolate apical horn; three strong tribladed wings; median constriction of the thorax.

Holotype. Plate 14, fig. 10; Sample 120-748B-5H-5 45/47cm (Middle Miocene); ECO-044.

Material. 104 specimens were observed from ODP Sites 737, 744, 748 and 751.

Description. Two-segmented shell with a narrow, apically-elongated, ellipsoidal (almost 2 times as long as wide in some specimens) cephalis and a large (at least 3 times the width of the cephalis) thorax with a conical, quickly flaring, upper thorax with three long, tribladed wings and a broadly cylindrical lower thorax.

The cephalis and the thorax are separated by a marked collar stricture. The cephalis is rough, crested and poreless. It bears a strong, lanceolated, tribladed, apical horn (up to 2 times the length of the cephalis) at the apex and a short, tribladed, ventral horn at the collar stricture, slightly directed upward.

Spine A is free in the cephalic cavity. Arches AL are clearly seen at approximately the first quarter of the length of the cephalis and appear parallel to MB; they are not however expressed externally by any furrows or strictures. Spines D, Ll and Lr protrude outside the upper thorax wall as three long (as long as the apical horn), tribladed spines.

The upper and the lower thorax are separated by a superficial constriction below the wings. The pores on the upper thorax are rather small and increase in size from the collar stricture to the mid-thorax constriction; on the lower thorax, the pores are large, rounded and somewhat aligned longitudinally.

Dimensions. (based on 5 specimens) Length of apical horn: 62-69 (67); of cephalis: 41-53 (46); of thorax: 102-153 (110); width of upper thorax: 102-127 (109).

Occurrence. Sporadic from the *C. antiqua* through the *E. punctatum* Zone (early to middle Miocene); rare from the *C. humerus* to the *C. spongothorax* Zone (Middle to Late Miocene).

Remarks. *Gondwanaria clarae* differs from *G. cylindrica* Funakawa, 2000 in the shape of the cephalis (ellipsoidal in *G. clarae* and hemispherical in *G. cylindrica*) and the presence in *G.*

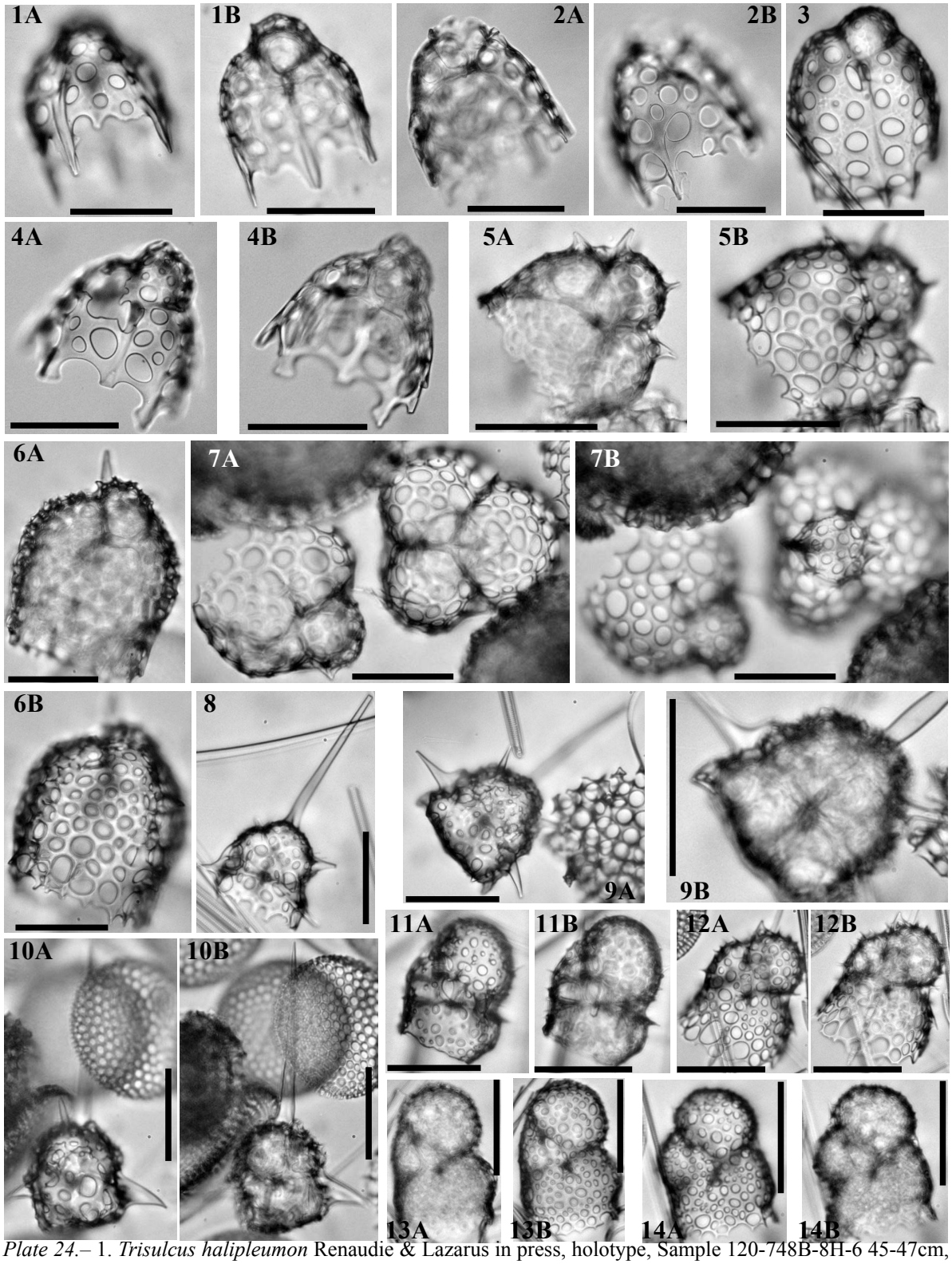

Plate 24.– 1. *Trisulcus halipleumon* Renaudie & Lazarus in press, holotype, Sample 120-748B-8H-6 45-47cm, Late Oligocene/Early Miocene. 2. *Trisulcus halipleumon*, Sample 120-748B-8H-6 45-47cm, Late Oligocene/Early Miocene. 3. *Trisulcus halipleumon*?, Sample 120-748B-8H-4 45-47cm, Early Miocene. 4. *Trisulcus halipleumon*, Sample 120-748B-8H-6 45-47cm, Late Oligocene/Early Miocene. 5. *Trisulcus pinguiculus* Renaudie & Lazarus 2012, Sample 120-748B-8H-4 45-47cm, Early Miocene. 6. *Trisulcus pinguiculus*, Sample 120-748B-8H-4 45-47cm, Early Miocene. 7. *Trisulcus pinguiculus*, specimen on the right is holotype, , Sample 120-748B-8H-6 45-47cm, Late Oligocene/Early Miocene. 8. *Lithomelissa vespa* Renaudie & Lazarus 2012, Sample 120-751A-9H-6 98-102cm, Middle Miocene. 9. *Lithomelissa vespa*, Sample 120-751A-6H-6 98-102cm, Late Miocene. 10. *Lithomelissa vespa*, holotype, Sample 119-744A-4H-2 56-61cm, Late Miocene. 11. *Botryopera gibbera* Renaudie & Lazarus 2012, Sample 119-744A-6H-4 60-62cm, Middle Miocene. 12. *Botryopera gibbera*, Sample 120-751A-6H-3 98-102cm, Late Miocene. 13. *Botryopera gibbera,* Sample 120-751A-9H-6 98-102cm, Middle Miocene. 14. *Botryopera gibbera*, holotype, Sample 120-751A-10H-4 98-102cm, Middle Miocene.
All scale bars 50 µm. Magnification x384 except 9B (x576).

clarae of both a clear, strong collar stricture and a constriction of the thorax below the wings. It differs from *G. nigriniae* Petrushevskaya in Petrushevskaya & Kozlova, 1979 in having three long, subhorizontal, tribladed wings and in the lower part of the thorax being approximately the same width as the upper part. It differs from the specimens illustrated in Caulet, 1991 as *Pteropilium contiguum* (Ehrenberg) (pl. 2, fig. 11) and in Petrushevskaya & Kozlova, 1972 as *Pteropilium*? sp aff *Pterocanium contiguum* (Ehrenberg) group (pl. 29, figs. 8-10) in the absence of longitudinal alignment of the thoracic pores (which are also larger in *G. clarae*) and the postcephalic part of the shell being, in Caulet's specimen, seemingly separated into a thorax and an abdomen by a lumbar septum whereas in *G. clarae* there is no separation between the upper and the lower thorax. It also differs from *Stichopilium campanulatum* Haeckel, 1887 for the same reasons as from the latter, in the wings being longer and tribladed and in the cephalis being longer. The specimen illustrated as *S. campanulatum* in Nishimura & Yamauchi, 1984 (pl. 35, fig. 7) also seems to have a somewhat pyramidal thorax whereas *G.clarae* has a campanulate upper thorax.

Genus *Helotholus* Jørgensen 1905

Type-species. *Helotholus histricosa* Jørgensen 1905

Helotholus? *haysi* Lazarus 1992

(Pl. 16, figs 13A-B)

1992 *Helotholus*? *haysi* Lazarus: p. 797; pl. 8, figs 1-17

Helotholus? *praevema* Weaver 1983

(Pl. 16, fig. 7)

1983 *Helotholus praevema* Weaver: p. 677-678; pl. 3, figs 1, 5-15

Helotholus? *vema* Hays 1965

(Pl. 16, figs 12A-B, 14A-B)

1965 *Helotholus vema* Hays: p. 176; pl. 2, fig. 3
1971 *Pseudocubus vema* (Hays) – Petrushevskaya: pl. 24, figs 1-4
1975 *Helotholus vema* Hays – Chen: pl. 16, figs 1-4
1983 *Helotholus vema* Hays – Weaver: pl. 3, figs 2-4
1990 *Helotholus vema* Hays – Lazarus: pl. 7, figs 1-5

Helotholus? *warreni* (Goll 1980)

(Pl. 16, figs 5A-B)

1980 *Pseudocubus warreni* Goll: p. 437; pl. 3, figs 5-6
1992 *Pseudocubus warreni* Goll – Nigrini & Caulet: p. 146; pl. 2, figs 1-2

Genus *Lampromitra* Haeckel 1881

Type-species: *Lampromitra coronata* Haeckel 1887

Lampromitra dodecaster (Haeckel 1887)

1887 *Sethophormis dodecaster* Haeckel: p. 1248; pl. 56, fig. 12
1991 *Tetraphormis dodecaster* (Haeckel) – Takahashi: p. 108; pl. 32, fig. 7

Lampromitra huxleyi (Haeckel 1879)

1879 *Eucecryphalus huxleyi* Haeckel: pl. 16, fig. 9

1887 *Lampromitra huxleyi* (Haeckel) – Haeckel: p. 1215; pl. 59, fig. 1
1992 *Lampromitra* spp. Sugiyama et al: pl. 16, figs 1-3

Lampromitra quadricuspis Haeckel 1887

1887 *Lampromitra quadricuspis* Haeckel: p. 1214-1215; pl. 58, fig. 7
1984 *Lampromitra quadricuspis* (Haeckel) – Nishimura & Yamauchi: p. 52; pl. 28, figs 4a-c
1990 *Lampromitra quadricuspis* (Haeckel) – Nishimura: p. 103; pl. 19, figs 1a-3b

Lampromitra sp. E
(Pl. 20, figs 12-13B)

Remarks. Only a few fragments of this species' thoracic rim have been found, thus hindering a meaningful description. However the thin, needle-like teeth regularly-disposed around the circular rim and the large, concave sieve plate, perforated by numerous, closely-packed, large elliptical pores, closing the mouth seem to be found in no other species encountered in this study and thefore seem to justify these fragments being included in a new, yet unkown, species.

Lampromitra? sp. V
(Pl. 19, figs 8A-9B)

Description. Shell dome-shaped. Cephalis and thorax do not seem to be distinguished externally by any constriction or change in contour. Pores are randomly distributed and variable in size: there is a clear size gradient from small circular cephalic pores to large elliptical to almost polygonal lower thoracic pores. The thorax termination is a circular (in apical view) rim. Spines **V, D, Ll** and **Lr** are all more or less in the same plane, and all protruding as very short, barely noticeable spines. Some bar nodes on the cephalis are slightly raised and are easily mistaken with those very small spines. Because all specimens were seen in apical view, spine **A** was not observed to this date.

Remarks. The genera *Ceratocyrtis* and *Lampromitra* are very close to one another morphologically. According to Petrushevskaya (1971), they differ "in having a downwardly widened cephalis and a differentiated margin of the thorax" so *L.*? sp. V would be a *Lampromitra* according to those criteria. However other species of *Lampromitra* (such as the four species mentioned above) are classically flattened, and generally have a clearly expressed segmentation which neither of which is the case here. *L.*? sp. V looks very similar to *Ceratocyrtis* species such as *C. mashae* or *C. stoermeri* to which it differs in lacking cephalic by-spines and horns, in its thinner cephalic wall and its thoracic rim. The generic assignment remain therefore putative until specimens can be observed in sagittal view.

Genus *Lamprotripus* Haeckel 1881

Type-species: *Lamprotripus squarrosus* Haeckel 1887

Lamprotripus mawsoni (Riedel 1958)
(Pl. 20, figs. 5A-B)

1958 *Dictyophimus mawsoni* Riedel: p. 234, pl. 3, figs 6-7
1972 *Lamprotripus mawsoni* (Riedel) – Petrushevskaya & Kozlova: p. 534; pl. 29, fig. 15
1975 *Dictyophimus mawsoni* (Riedel) – Chen: pl. 19, figs 1-2

Genus *Lipmanella* Loeblich & Tappan 1961

Type-species: *Lithornithium dictyoceras* Haeckel 1860

Lipmanella dictyoceras (Haeckel 1860)
(Pl. 14, fig. 5)

1860 *Lithornithium dictyoceras* Haeckel: p. 840
1973 *Lipmanella dictyoceras* (Haeckel) – Kling: p. 636; pl. 4, figs 24-26
1980 *Lipmanella dictyoceras* (Haeckel) – Boltovskoy & Riedel: p. 100; pl. 5, fig. 6

Lipmanella? *melitta* Haeckel 1887

1887 *Dictyoceras melitta* Haeckel: p. 1325; pl. 71, fig. 9
1987 ?*Dictyoceras mellitta* (sic) Haeckel – Boltovskoy & Riedel: p. 100; pl. 4, fig. 24

Genus *Lithomelissa* Ehrenberg 1847 *sensu* Petrushevskaya 1971

Type-species: *Lithomelissa microptera* Ehrenberg 1854

Lithomelissa brevispicula Popofsky 1908

1908 *Lithomelissa brevispicula* Popofsky: p. 279; pl. 32, figs 7-8
1967 *Lithomelissa brevispicula* Popofsky – Petrushevskaya: p. 74-76; fig. 44
1992 *Lithomelissa brevispicula* Popofsky – Abelmann: pl. 3, fig. 13

Lithomelissa cheni Caulet 1991

1975 *Lithomelissa* sp. A aff. *L. ehrenbergi* Chen: p. 458; pl. 11, figs 1-2
1991 *Lithomelissa cheni* Caulet: p. 533; pl. 2, figs 1-2

Lithomelissa ehrenbergi Butschli 1882

1875 *Lithomelissa macroptera* Ehrenberg – Ehrenberg: pl. 3, fig. 8 non figs 9-10
1882 *Lithomelissa ehrenbergi* Bütschli: p. 517; pl. 33, figs 21a-b
1973 *Lithomelissa*? *ehrenbergi* Bütschli – Dumitrica: p. 837; pl. 25, figs 6-7

Lithomelissa mitra Bütschli 1882

1882 *Lithomelissa mitra* Bütschli: p. 520; pl. 3, fig. 24
2009 *Lithomelissa* aff. *mitra* Bütschli – Suzuki et al.: pl. 21, figs 11a-b

Lithomelissa robusta Chen 1975

1975 *Lithomelissa robusta* Chen: p. 457; pl. 9, figs 1-2
1990 *Lithomelissa robusta* Chen – Abelmann: pl. 5, figs 2a-b

Lithomelissa setosa Jørgensen 1900

1900 *Lithomelissa setosa* Jørgensen: p. 81-82; pl. 4, figs 21-22
1976a *Lithomelissa setosa* Jørgensen – Bjørklund: pl. 8, figs 1-13; pl. 11, figs 19-23

Lithomelissa? *kozoi* Renaudie & Lazarus in press
(Pl. 22, figs 7A-11B)

1987 *Lithomelissa setosa* Jørgensen; Takahashi: p. 230, pl. 5, fig. e.
2008 *Lithomelissa sp. D* Itaki et al: p. 213, pl. 1, fig. 6.
2009 *Lithomelissa sp. D* Itaki et al; Itaki: pl. 17, figs 15-23.

Derivation of name. Named after Kozo Takahashi, who first illustrated the species.

Diagnosis. Little lophophaenid with shoulders and five ribs extending as small, thin feet.

Holotype. Pl. 22, fig. 8A-B; Sample 120-747A-2H-5 45-47cm (Early Pleistocene); ECO-052 circle 2.

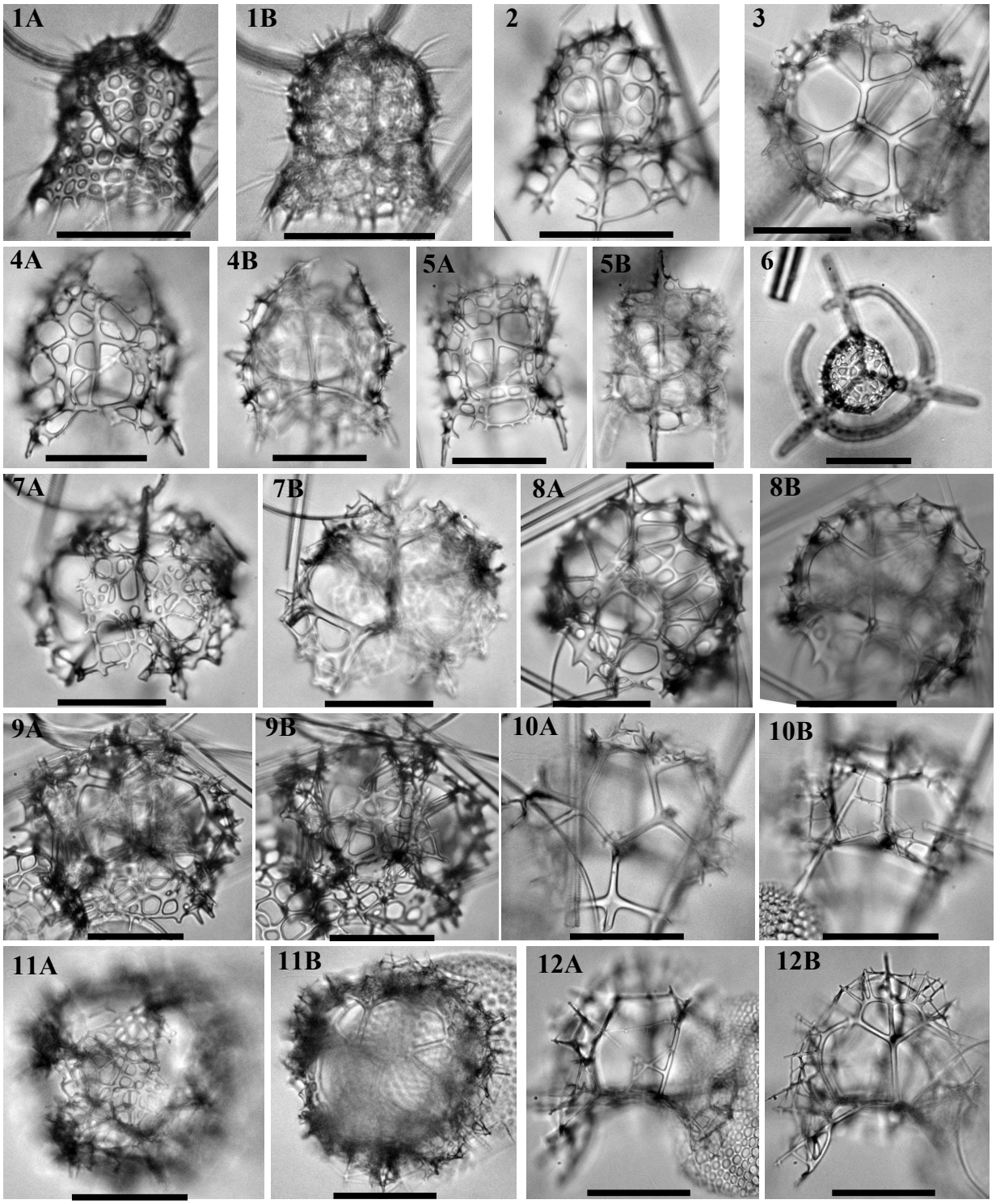

Plate 25.– 1. *Protoscenium*? sp. 8, Sample 120-748B-5H-7 45-47cm, Middle Miocene. 2. *Protoscenium*? sp. 8?, Sample 120-751A-11H-6 98-102cm, Middle Miocene. 3. *Protoscenium pantarhei* Renaudie & Lazarus in press, Sample 120-751A-3H-2 98-102cm, Late Pliocene. 4. *Protoscenium*? sp. 23, sample 120-748B-5H-4 45-47cm, Middle Miocene. 5. *Protoscenium*? sp. 23, sample 120-748B-5H-7 45-47cm, Middle Miocene. 6. *Enneaphormis*? sp. I, Sample 119-746A-5H-1 53-55cm, Late Miocene. 7. *Protoscenium pantarhei*, Sample 120-747A-5H-3 45-47cm, Late Miocene. 8. *Protoscenium pantarhei*, holotype, Sample 120-751A-3H-2 98-102cm, Late Pliocene. 9. *Protoscenium pantarhei*, Sample 120-751A-8H-3 98-102cm, Late Miocene. 10. *Protoscenium pantarhei,* Sample 120-751A-3H-2 98-102cm, Late Pliocene. 11. *Protoscenium pantarhei*, Sample 120-748B-5H-4 45-47cm, Middle Miocene. 12. *Protoscenium pantarhei*?, Sample 120-748B-5H-4 45-47cm, Middle Miocene.
All scale bars 50 µm. Magnification x384.

Material. 81 specimens were observed from ODP Sites 689, 693, 745, 747, 751 and 1138.
Description. The shell consists of two segments: a short cephalis and a flaring thorax. The collar stricture is marked by shoulders (that can be strongly expressed in some specimens) and furrows following arches **AL** and **VL**.
Spine **A** is fused to the dorsal side of the cephalis and protrudes subapically as a slightly ventrally-curved horn (approximately as long as the cephalis), the base of which is weakly tribladed while the rest of the horn is conical. Spine **V** protrudes at the collar stricture or a little below as a short triangular horn (Pl. 8, fig. 5). The axobate can sometimes be seen as a small knob near the junction between spine **V** and the median bar. Spines **Ll** and **Lr** reach the thoracic wall and continue as (primary) ribs to the thorax termination where they go on as short, thin, conical tooth-like feet while spine **D** reaches the thoracic wall very close to its end so that it extends effectively as a foot. Both spines **l'** follows the same pattern as spines **Ll** and **Lr**: they continue as secondary ribs and terminate as small feet comparable to the previous ones. A short apophyse on each spine **l'** sometimes protrudes, at the point where the spines join the thoracic wall, as very short and thin wings (Pl. 5, figs 11, 13A). An apophyse on spine **D**, comparable to that typical of genus *Antarctissa,* can also be seen, joining spine **D** and the thoracic wall halfway down (Pl. 5, fig. 10A; Pl. 8, fig. 5).
Pores on the cephalic wall are elliptical, closely packed and rather large. Pores on the thorax are somewhat larger but less densily packed and are randomly sized, shaped and arranged. Pores near thorax termination are downwardly-elongated so that the bars between them appear in some specimens as additional small teeth.
Dimensions. (based on 6 specimens) Height of cephalis (from apex to collar): 23-36 (27); length of apical horn: 18-50 (28); length of thorax: 62-90 (74); final width of thorax: 58-82 (73).
Occurence. Rare from the Tau to the Chi Zone (Early Pliocene to Early Pleistocene). One specimen was also seen in the Omega Zone (Holocene) of ODP Site 747 and two specimens in the *Acrosphaera australis* Zone (Late Miocene) of ODP Site 747 were also tentatively assigned to this species (Pl. 5, fig. 15). This species was reported in Takahashi, 1987, Itaki et al., 2008 and Itaki, 2009 in the Holocene of the Japan Sea and the North Pacific.
Remarks. This species together with others like *Lithomelissa stigi* Bjørklund, 1976a, *Ceratocyrtis morawanensis* Funakawa, 1995 (=*Lophophaena tekopua* O'Connor, 1997), *C. cantharoides* Sugiyama & Furutani, 1992, *Lophophaena*? *thaumasia* Caulet, 1991, *Lophophaena leberu* Renaudie & Lazarus, in press, or even *Pseudodictyophimus tanythorax* Funakawa, 1994, despite being scattered in several genera, all share some common morphological features such as the separation of the two segments by shoulders along arches **AL** and **VL**, a well-developed apical horn protruding subapically and a vertical horn protruding at the collar. The taxonomy of this group needs to be resolved, but in the meantime, we are tentatively assigning this new species to the genus *Lithomelissa*. *L.*? *kozoi* differs from *L. stigi, L. thaumasia*, *L. leberu,* and *Trisulcus nanus* Popofsky, 1913 in its flaring thorax and its ribs/feet; from *C. morawanensis* and *C. cantharoides* in lacking the longitudinal pore alignment and in having only five ribs/feet: three primary derived from spines **D**, **Ll** and **Lr** and two secondary derived from the two spines **l'**. It finally differs from *Pseudodictyophimus hexaptesimus* Sugiyama *et al.*, 1992, in that the ribs in the latter protrude as tribladed feet and wings originating from the three primary spines and the three secondary spines respectively.

Lithomelissa sphaerocephalis Chen 1975

1975 *Lithomelissa sphaerocephalis* Chen: p. 457; pl. 8, figs 1-2
1983 *Lithomelissa sphaerocephalis* Chen – Weaver: p. 678

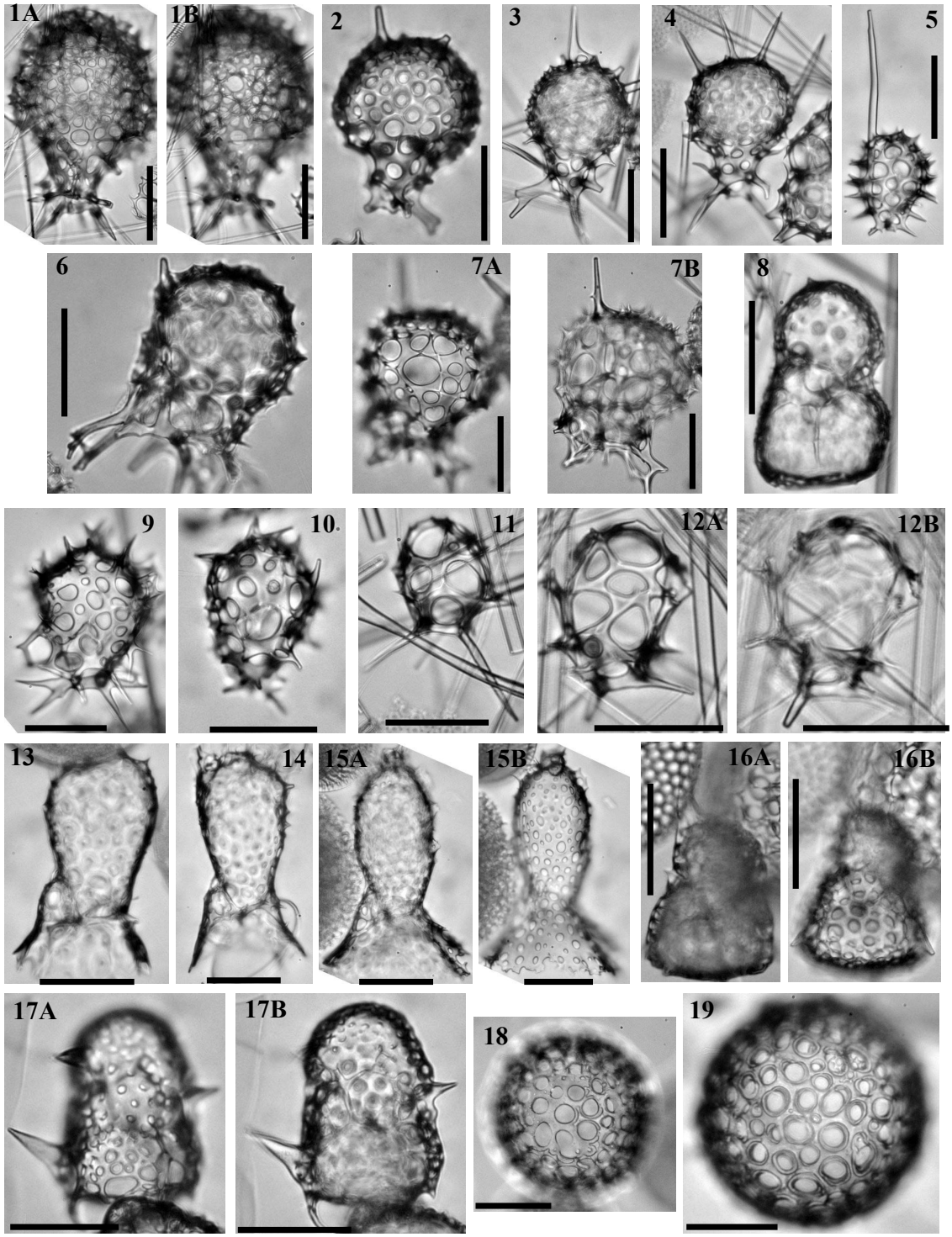

Plate 26.– 1. *Mitrocalpis araneafera* Popofsky 1908, Sample 120-747A-1H-1 45-47cm, Pleistocene. 2. *Arachnocorallium* sp. 5, Sample 120-747A-4H-1 45-47cm, Early Pliocene. 3. *Arachnocorallium* sp. 5, Sample 120-751A-4H-4 98-102cm, Early Pliocene. 4. *Arachnocorallium* sp. 5, Sample 120-751A-4H-4 98-102cm, Early Pliocene. 5. *Peridium longispinum* Jørgensen 1900, Sample 120-747A-2H-2 45-47cm, Pleistocene. 6. *Peridium*? sp. L, Sample 119-744A-5H-1 53-55cm, Middle/Late Miocene. 7. *Peridium*? sp. L, Sample 119-744A-5H-1 53-55cm, Middle/Late Miocene. 8. *Botryopera chippewa*, Sample 120-751A-9H-CC, Middle/Late Miocene. 9. *Arachnocorallium* sp. 17, Sample 119-745B-14H-6 53-55cm, Late Pliocene. 10. *Arachnocorallium* sp. 17, Sample 119-746A-7H-2 53-55cm, Late Miocene. 11. *Arachnocorallium*? sp. A, Sample 120-751A-9H-1 98-102cm, Middle/Late Miocene. 12. *Arachnocorallium*? sp. A, Sample 120-751A-9H-1 98-102cm, Middle/Late Miocene. 13. *Amphiplecta*? sp. R, Sample 120-751A-12H-6 98-102cm, Middle Miocene. 14. *Amphiplecta*? sp. R, Sample 120-751A-12H-6 98-102cm, Middle Miocene. 15. *Amphiplecta*? sp. R, Sample 120-751A-12H-6 98-102cm, Middle Miocene. 16. *Botryopera chippewa*, Sample 119-744A-4H-2 59-61cm, Late Miocene. 17. *Botryopera chippewa*, Sample 120-747A-4H-7 45-47cm, Late Miocene. 18. *Cenosphaera*? sp. K, Sample 113-693A-18R-4 101-107cm, Late Miocene. 19. *Cenosphaera*? sp. K, Sample 119-744A-4H-4 59-61cm, Late Miocene. All scale bars 50 µm. Magnification x384.

Lithomelissa? sp. T
(Pl. 16, 10A-11)

Remarks. This species differs from *Antarctissa strelkovi* and *Helotholus praevema* in the shape of its cephalis and its collar stricture (see Pl. 16, fig. 11): indeed the two segments are separated here by a sulcus on arches **AL** and **VL** (as is common in genus *Lithomelissa* and *Lophophaena*).

Lithomelissa? *stigi* Bjørklund 1976a
(Pl. 22, fig. 1)

1975 *Lithomelissa* sp. C Chen: p. 458; pl. 11, figs 4-5
1976a *Lithomelissa stigi* Bjørklund: p. 1125; pl. 15, figs 12-17
? 1979 *Ceratocyrtis panicula* Petrushevskaya in Petrushevskaya & Kozlova: p. 115; fig. 289
1990 *Ceratocyrtis stigi* (Bjørklund) – Abelmann: pl. 4, fig. 12

Remarks. See remarks on *Lithomelissa*? *kozoi*.

Lithomelissa sp. 11
(Pl. 16, figs 8-9, 18)

Description. Large dicyrtid with a flattened hemispherical cephalis. Spine **A** forms apically a rather robust horn. Spine **Ax** is well-developed and spines **D**, **Ll** and **Lr**, in some specimens, protrude outside the thoracic wall near the collar stricture as short ribs/wings. Thorax is truncated-conical, long, thick and crested with irregularly-placed, elliptical, large pores. Near the thorax termination a ring of numerous, short, conical teeth are projected downward.

Remarks. It differs from *Antarctissa strelkovi* and *Helotholus praevema* in its size (length of 150 to 200 µm), its truncated-conical thorax termination (ring of subterminal teeth) and its simple collar structure (both the above-mentioned species have complex, thick inner spines while *L.* sp. 11 seems to have a classic simple, thin structure).

Lithomelissa tricornis Chen 1975

1975 *Lithomelissa tricornis* Chen: p. 458; pl. 8, figs 6-7
1990 *Lithomelissa tricornis* Chen – Abelmann: pl. 5, fig. 3

Lithomelissa vespa Renaudie & Lazarus 2012
(Pl. 24, figs 8-10B)

Derivation of name. *Vespa* is Latin for wasp.

Diagnosis. One long, slender apical horn; three short wings; two (three?) short, thin, subapical horns; cephalis and thorax undifferentiated.

Holotype. Plate 24, figs. 10A-B; Sample 119-744A-4H-2 59/61cm (Late Miocene); ECO-037, circle 2.

Material. 56 specimens were observed on site 744 and 751.

Description. Two-segmented shell with a cephalis and a thorax that are not distinguishable externally by any constriction, furrow or shoulder. The cephalis is longer than the thorax.

Spine A is free in the cephalic cavity and protrudes as a long (1.5 to 2 times longer than the shell itself), slender, cylindrical horn. Spines D, Ll and Lr protrude as short, triangular (with a thick base) wings from the thoracic wall, slightly lower than the level of the median bar. The axobate is short. Spine V joins the cephalic wall subhorizontally and doesn't seem to extend outside the wall. Two (three?) short, thin, conical, upward-directed spines appear to extend subapically from apophyses branching from spine A: apophyses *a*, according to Petrushevskaya (1971)'s terminology.

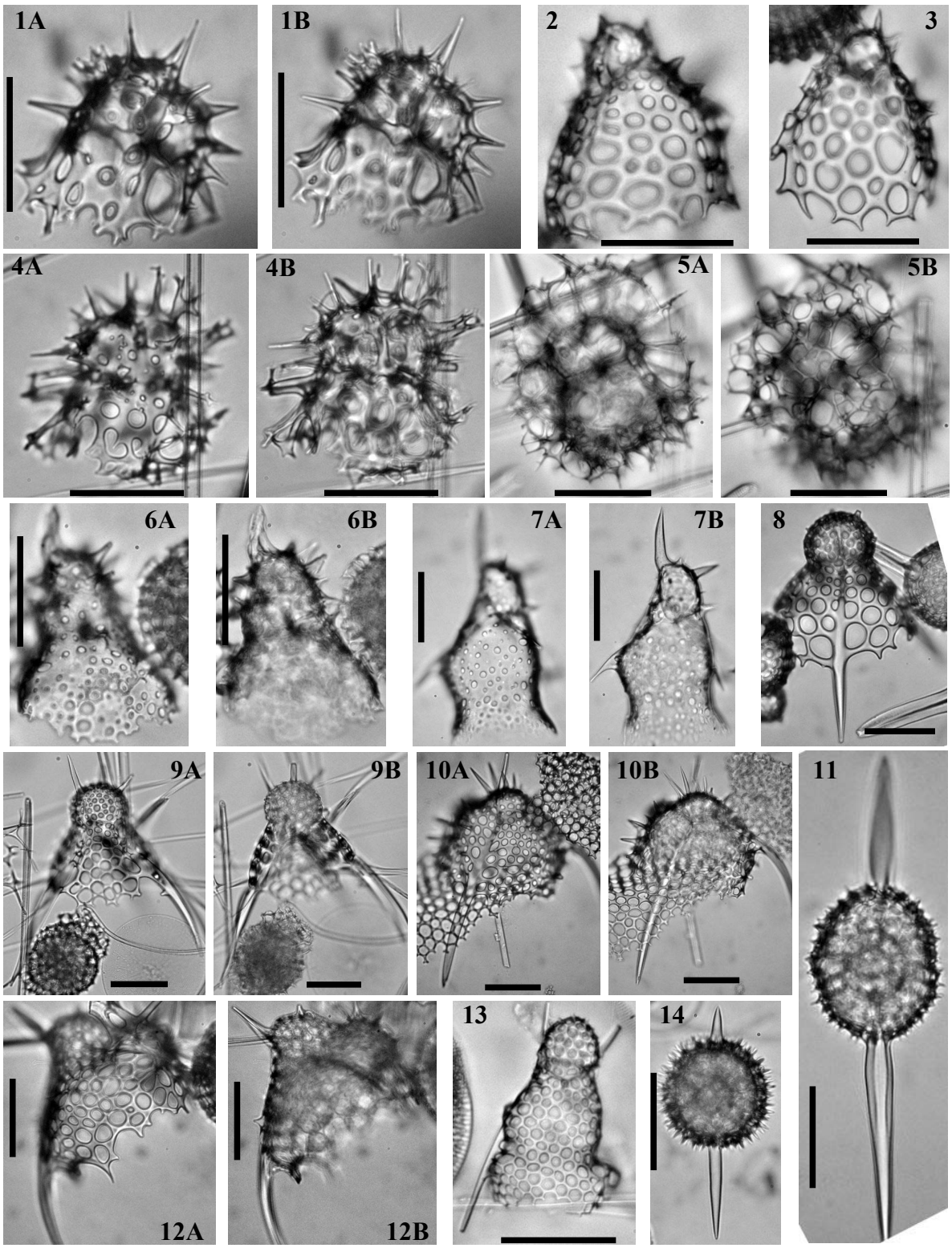

Plate 27.– 1. *Syscioscenium wabisabi* Renaudie & Lazarus 2012, Sample 119-746A-7H-6 53-55cm, Late Miocene. 2. Nasselarian sp. D, Sample 120-748B-6H-7 45-47cm, Early Miocene. 3. Nasselarian sp. D, Sample 120-748B-6H-7 45-47cm, Early Miocene. 4. *Syscioscenium wabisabi*, holotype, Sample 120-751A-7H-4 98-102cm, Late Miocene. 5. *Syscioscenium wabisabi*, Sample 120-751A-9H-5 98-102cm, Middle Miocene. 6. Nassellarian sp. B, Sample 120-748B-8H-2 45-47cm, Early Miocene. 7. Nassellarian sp. B, Sample 747A-9H-8 45-47cm, Early/Middle Miocene. 8. *Lophophaena* sp. 7, Sample 120-747A-7H-5 45-47cm, Middle Miocene. 9. *Lophophaena* sp. 7, Sample 120-748B-5H-7 45-47cm, Middle Miocene. 10. *Pseudodictyophimus* sp. Y, Sample 120-751A-13H-2 98-102cm, Middle Miocene. 11. *Druppatractus*? sp. A, Sample 119-744A-11H-3, Early Miocene. 12. *Pseudodictyophimus* sp. Y, Sample 120-748B-5H-7 45-47cm, Middle Miocene. 13. *Lophophaena undulatum* (Popofsky 1913), Sample 120-751A-12H-2 98-102cm, Middle Miocene. 14. *Druppatractus*? sp. A, Sample 113-690B-6H-6 22-24cm, Early Miocene.
All scale bars 50 µm. Magnification x384, except for 9A-B (x192).

Some specimens have a thick, crested wall (see Pl. 7, figs 7A-B and 9A-B) but commonly the wall is thin and smooth (see Pl. 7, fig. 10). Specimens with a thick wall have their thorax closed by a sieve plate. In both cases, pores on thorax are somewhat bigger than the cephalic ones; but, on both segments, they are randomly distributed, uneven in size and subelliptical.

Dimensions. (based on 4 specimens) Length (without apical horn): 54-70 (61); of cephalis: 30-35 (34); of apical horn: 71-110 (97); width: 46-58 (53).

Occurrence. *L. vespa* is sporadic in the *A. golownini* and the lower *C. spongothorax* Zone (middle Miocene); rare in the middle and upper *C. spongothorax* and in the *A. australis* Zone (late Miocene).

Remarks. *Lithomelissa vespa* differs from most Lophophaenidae in its horn combination: A, D, Ll, Lr and two more branching from spine A. This combination, however, is shared by *L. tricornis* Chen, 1975. *L. vespa* differs from the latter in its unusually long apical horn, in its cephalis/thorax ratio and in the overall shape of the shell. Furthermore, the horns of *L. tricornis* are all of rather similar size and shape whereas each set of horns in *L. vespa* are different from one another.

Lithomelissa? sp. 25

(Pl. 23, figs. 15A-16B)

? 1971 *Lophophaenoma* sp. G Petrushevskaya: pl. 56, fig. 17 non fig. 16

Description. Large dicyrtid with a spherical to globular cephalis and a thorax whose upper part is deformed by three, almost horizontal in some specimens, short, robust wings derived from spines **D**, **Ll** and **Lr**. Spine **A** is free in the cephalic cavity and protrudes subapically as a tribladed horn. Arches *ap* are clearly marked. The collar stricture on the dorsal side is situated at the level of apophyse *a*. Pores vary widely in size and shape and are randomly distributed. Pores on the cephalis are smaller than on the thorax. Thorax termination is ragged.

Remarks. It differs from *Lithomelissa ehrenbergi* in possessing three wings and in being generally larger; however it shares with this species its peculiar cephalis structure.

Genus *Lophophaena* Ehrenberg 1847 *sensu* Petrushevskaya 1971

Type-species: *Lophophaena galeaorci* Ehrenberg 1854

Lophophaena capito Ehrenberg 1873

1873 *Lophophaena capito* Ehrenberg: p. 242

1875 *Lophophaena capito* Ehrenberg – Ehrenberg: pl. 8, fig. 6

2005 *Lophophaena capito* Ehrenberg group – Funakawa et al.: pl. P3, figs 3a-4b

Lophophaena clevei Petrushevskaya 1971

(Pl. 23, fig. 17)

1899 *Dictyocephalus* sp. Cleve: p. 20; pl. 2, fig. 1

1971 *Lophophaena clevei* Petrushevskaya: p. 107-109; pl. 57, fig. 1

1996 *Lophophaena clevei* Petrushevskaya – Hull: pl. 6, fig. 6

2003 *Lophophaena clevei* Petrushevskaya – Bjørklund & Kruglikova: pl. 7, figs 15-16 non pl. 6, fig. 19

Lophophaena macrencephala? Clark & Campbell 1945

(Pl. 23, fig. 5)

? 1945 *Lophophaena (Lophophaenula) macrencephala* Clark & Campbell: p. 41; pl. 7, figs 6-9

? 1978 *Lophophaena macrencephala* Clark & Campbell group – Dzinoridge et al.: pl. 29, fig. 20

Lophophaena nadezdae Petrushevskaya 1971
(Pl. 23, figs 1A-B)
1971 *Lophophaena nadezdae* Petrushevskaya: p. 11-115; pl. 60, figs 1-4

Lophophaena simplex Funakawa 1994
(Pl. 23, fig. 2)
1994 *Lophophaena simplex* Funakawa: p. 465-466; pl. 8, figs 1-2

Lophophaena thaumasia Caulet 1991
(Pl. 22, fig. 4)
1991 *Lophophaena*? *thaumasia* Caulet: p. 534; pl. 2, figs 5-6

Lophophaena undulatum (Popofsky 1913)
(Pl. 27, fig. 13)
1913 *Artopilium undulatum* Popofsky: p. 405; pl. 36, figs 4-5
1991 *Lophocorys undulata* (Popofsky) – Takahashi: p. 120; pl. 40, figs 9-10
1995 *Peromelissa undulata* (Popofsky) – van de Paverd: p. 224; pl. 71, figs 12-13
2003 *Lophophaena clevei* Petrushevskaya – Bjørklund & Kruglikova: pl. 6, fig. 19

Lophophaena witjazii (Petrushevskaya 1971)
(Pl. 23, fig. 21)
1971 *Lophophaenoma witjazii* Petrushevskaya: p. 118; pl. 62, figs 3-7

Lophophaena? *leberu* Renaudie & Lazarus, 2012
(Pl. 22, fig. 12A-14B)
Derivation of name. Named after the Mythical creature Leberou, whose name derives from the Occitan *lèbre* (hare).
Diagnosis. Long apical horn; long secondary horn halfway between spine **A** and **V**; no feet; no ribs.
Holotype. Plate 22, figs. 13A-B; Sample 120-748B-7H-2 45/47cm (Early Miocene); ECO-030.
Material. 25 specimens were observed from ODP Sites 747, 748 and 751.
Description. Two-segmented shell with a long, truncated-conical thorax, approximately twice as long as the ellipsoidal cephalis. The shell tilts on the ventral side. The cephalis and the thorax are separated by a shoulder along **AL** and a furrow following **VL**.
Spine **A** is fused to the cephalic wall and protrudes outside the wall apically as a robust, blade-shaped horn (ca. 1-1,5 time the height of the cephalis). Spine **V** protrudes at the junction of the cephalis and the thorax as a short triangular horn. Spines **D, Ll** and **Lr** join the thoracic wall and, sometimes, spine **D** extends outside as a very short wing. There is a change in contour of the thorax where those spines join the wall (concave for spine **D**, convex for spines **Ll** and **Lr**). The cephalis bears an additional horn halfway between the apical and the ventral horn: it is rather similar in shape to the apical horn but smaller; it doesn't seem to be linked to any internal spine. Some rare specimens also bear numerous small additional horns scattered on the cephalis (see pl.5, figs. 11A-B).
The thoracic wall is smooth, with numerous small pores, more or less arranged in a hexagonal pattern, but somewhat irregular in size. The cephalic wall is similar to the thoracic wall, yet some specimens have a crested cephalis. Thorax termination is ragged.

Dimensions. (based on 5 specimens) Length (without horns): 102-132 (119); of cephalis: 37-45 (41); of apical horn: 30-54 (42); of additional horn: 25-30 (28).
Occurrence. Rare from the *C. antiqua* Zone to the *E. punctatum* Zone (early Miocene); sporadic from the *E. punctatum* to the *A. australis* Zone (middle to late Miocene).
Remarks. *Lophophaena*? *leberu* differs from other Lophophaenidae, and in particular from the otherwise similar *L. thaumasia* Caulet, 1991, in its long, robust, additional horn.

Lophophaena? sp. S
(Pl. 23, figs. 3-4)

Remarks. This species has a neck structure very similar to that of the species here recognized as *Lophophaena macrencephala*?, however the rough, club-shaped cephalis and the thorax porosity seem sufficient to distinguish the two species.

Lophophaena sp. U
(Pl. 22, figs 16A-17)

Description. Spines **A** and **V** are free in the cephalic cavity and are both projected upwards (they form together an angle of ~45°). They both protrude as short conical horns. **MB** is short are inclined toward spines **V**, **Ll** and **Lr**. Spines **D, Ll** and **Lr** project downwards, reach the thorax wall at its midst, continue on the wall as ribs until the become, at the thorax termination, conical feet. Cephalis is globular and covered by randomly distributed, round pores of various size (usually smaller than thoracic pores). Cephalis and thorax are distinctly separated by a 'turtleneck'-looking structure, delimited on top by arches **AV** and on the bottom by a fold that follows **MB.**
Remarks. This species differs from the species here recognized as *Lophophaena macrencephala*? primarily in possessing three well-developed feet.

Lophophaena? sp. 7
(Pl. 27, figs 8-9B)

Diagnosis. Characterized by its three blade-like feet, its large spherical cephalis and its three horns.
Description. Large dicyrtid with a flattened, almost spherical cephalis and a truncated-conical to tetrahedral thorax. Both segments are separated by a clear collar stricture, above **MB** (following arches **DL** and **LL** maybe). Thorax termination is ragged. Spine **A** is free in the cephalic cavity and protrudes subapically as a curved, conical horn. Two other supplementary horns that are very similar in shape and size to the apical horn are also present subapically on the cephalis. They do not seem to be connected with any internal spine or apophyse. Spine **V** reaches the wall at the cephalic stricture but does not seem to continue outside as a horn. Spines **D**, **Ll** and **Lr** are projected downward, reach the thoracic wall at the third of its height and continue after the thorax termination as fairly long, blade-like, smooth feet. Pores on cephalis are smaller than pores on thorax. Both are round to elliptical. Pores on thorax are more or less quincuncially arranged.
Remarks. It differs from species of genus *Pseudodictyophimus* and from Theoperidae in the shape of its cephalis and the disposition of its collar stricture: in Theoperidae, the collar stricture is systematically situated at the same height as **MB**, while in genus *Pseudodictyophimus* the separation between the two external segments follows furrows along arches **AL** and **VL** (Funakawa 1995a).

Lophophaena? sp. Q

(Pl. 23, figs 9-10)

Description. Dicyrtid with an ellipsoid cephalis elongated toward the apex where a short triangular, tribladed horn is present. This horn does not seem connected to any internal spine or apophyse. Indeed spine **A** is fused to the dorsal side of the cephalic wall and does not seem to protrude outside of it. Nor do spines **V** (which join the wall on the ventral side of the collar stricture) or **D**. Spines **Ll** and **Lr** are almost perpendicular to **MB** and join the wall in an intermediate position between the dorsal and the ventral side where, in some specimens (Pl. 23, fig. 9), they can protrude as very short wings. Thorax and cephalis are separated externally by furrows along arches **AL** and **VL**: because spines **Ll** and **Lr** are relatively close to spine **D**, the furrow along **AL** forms a smaller angle with the one along **VL** thus forming a more or less marked dorsal shoulder. The thorax is more or less conical in outline. Pores on both segments are numerous, circular of various size but generally relatively large (smaller toward the apex of the cephalis) and randomly arranged. Thorax termination is ragged.

Remarks. The apical triangular horn unconnected to spine **A** seem characteristic of this species.

Lophophaena? sp. X

(Pl. 22, figs 15A-B)

Remarks. Few specimens of this species were observed and the variability between them was strong enough to prevent a clear description of all the characters. However a combination of two characters seem to be significant enough to separate this species from the other lophophaenids: the presence of blade-like wings derived from spines **D**, **Ll** and **Lr** and a spine **A** free in the cephalic cavity protruding subapically as a tribladed apical horn.

Lophophaena? sp. 14

(Pl. 23, figs 6-8)

Description. Dicyrtid with a spherical to apically-elongated cephalis and a largely flaring truncated-conical thorax. Thorax ends at a circular rim where numerous small triangular teeth project. Spine **A** is fused to the dorsal side of the cephalic wall and can protrude outside the wall as a short triangular spine that can be hardly differentiated from the multitude of conical thorns projecting from the bar nodes of the cephalic wall and the upper thoracic wall. Spines **D**, **Ll** and **Lr** joins the upper thoracic wall and continue as ribs. Some specimens (Pl. 23, fig. 6) exhibit a more or less marked pore alignment following these ribs. Pores on the thorax are more or less even in size, circular to elliptical and numerous. Pores on the cephalis are slightly smaller than those on the thorax in general. Cephalic wall can be rough and crested in some specimens (Pl. 23, fig. 6)

Remarks. This species differs from *Lophophaena nadezdae* and *Lophophaena simplex* in its flaring thorax, in its whole shell being covered by tiny, needle-like thorns and its thorax terminating with a ring of small triangular teeth, slightly above the rim. It also differs from *Lophophaena hispida* (Ehrenberg) 1873a in the cephalic pores and the cephalic thorns being considerably smaller and in the flaring thorax of *L.*? sp. 14. Even if *L.*? sp. 14 differs from Petrushevskaya (1971)'s generic concept for *Lophophaena,* because of the numerous similarities with the three species mentioned here, this species was still tentatively assigned to this genus.

Genus *Mitrocalpis* Haeckel 1881

Type-species: *Mitrocalpis palliata* Haeckel 1887

Mitrocalpis aranaefera Popofsky 1908

(Pl. 26, figs 1A-B)
1908 *Mitrocalpis aranaefera* Popofsky: p. 273-274; pl. 30, fig. 11
1958 *Mitrocalpis aranaefera* Popofsky – Riedel: pl. 3, figs 3-4

Genus *Peridium* Haeckel 1887
Type-species: *Peridium lasanum* Haeckel 1887

Peridium longispinum Jørgensen 1900
(Pl. 26, fig. 5)
1900 *Peridium longispinum* Jørgensen: p. 75-76
1905 *Peridium longispinum* Jørgensen – Jørgensen: p. 135; pl. 15, figs 75-79; pl. 16, fig. 80
1976a *Peridium longispinum* Jørgensen – Bjørklund: pl. 7, figs 9-15

Peridium? sp. L
(Pl. 26, figs 6-7B)
Description. Large monocyrtid with large, globular cephalis. The cephalic wall is rough and crested with pores of various size and shape, and irregularly arranged. Spine **A** is strong and runs free in the cephalic cavity until it reaches the wall subapically: it then protrudes as a conical apical horn. Spine **V** is short and doesn't protrude outside the wall. Spine **D** is strong and linked to **A** by a robust arch **AD** (Pl. 26, fig. 6B). Spines **Ll** and **Lr** seems to be very much identical to spine **D** with possibly arches joining them with the cephalic wall (Pl. 26, fig. 7B).
Remarks. This species differs from *Arachnocorallium* sp. 5 in the latter having a cephalis differentiated into a lower and an upper part, in spine **A** being free in *P.*? sp. L in the cephalic chamber and in the pores' size and arrangment (compare Pl. 26, fig. 2 and fig. 7A). It also differs from *P. longispinum* in its size (almost twice as big) and its shape. The free spine **A** is a problematic character for the assignment of this new species to genus *Peridium*, hence the doubtful assignment.

Genus *Phormacantha* Jørgensen 1905
Type-species: *Peridium hystrix* Jørgensen 1900

Phormacantha hystrix (Jørgensen 1900)
1900 *Peridium hystrix* Jørgensen: p. 76
1905 *Phormacantha hystrix* (Jørgensen) – Jørgensen: p. 132; pl. 14, figs 59, 61
1971 *Phormacantha hystrix* (Jørgensen) – Petrushevskaya: p. 129; pl. 68, figs 1.5

Genus *Pseudodictyophimus* Petrushevskaya 1971
Type-species: *Dictyophimus gracilipes* Bailey 1856

Pseudodictyophimus gracillipes (Bailey 1856)
1856 *Dictyophimus gracilipes* Bailey: p. 4; pl. 1, fig. 8
1861 *Lithomelissa bicornis* Ehrenberg 1861: p. 300
1967 *Dictyophimus bicornis* (Ehrenberg) – Petrushevskaya: p. 72-74; pl. 41, fig. 1-5
1971 *Pseudodictyophimus gracilipes* (Bailey) – Petrushevskaya: p. 93-95; pl. 47-48 non pl.. 49

Pseudodictyophimus platycephalus (Haeckel 1887)
1887 *Dictyophimus platycephalus* Haeckel: p. 1198; pl. 60, figs 4-5
1971 *Pseudodictyophimus platycephalus* (Haeckel) – Petrushevskaya: p. 91

1983 *Pseudodictyophimus platycephalus* (Haeckel) – Benson: p. 502; pl. 8, fig. 7

Pseudodictyophimus tanythorax Funakawa 1994

1994 *Pseudodictyophimus tanythorax* Funakawa: p. 473; pl. 12, figs 2a-3b

Pseudodictyophimus sp. Y

(Pl. 27, figs 10A-B, 12A-B)

Description. Large dicyrtid with a dome-shaped cephalis, bearing small rounded pores, an apical and a ventral horn (usually tribladed at least at their base) and, often, numerous additional horns. The thorax is at least two times wider and longer than the cephalis. Both segments are separated by furrows along arches **AL** and **VL**. Spines **D**, **Ll** and **Lr** join the wall at the collar stricture, continue on at least half the length of the thorax, in the thoracic wall as ribs and then protrude as fairly-long, downward-directed, conical to blade-like wings. Pores on the thorax are round to elliptical, relatively large (somewhat larger next to the ribs). Additional spines on the upper part of the thorax are frequent.

Remarks. This species differs from *P. tanythorax* and *P. gracilipes* in the flaring of its thorax, its size and the presence of additional horns. It differs from *P. platycephalus* primarily in the latter having a collar stricture barely marked externally.

Genus *Syscioscenium* Sugiyama 1992a

Type-species: *Syscioscenium velamen* Sugiyama 1992a

Syscioscenium? *wabisabi* Renaudie & Lazarus 2012

(Pl. 27, figs 1A-B, 4A-5B)

Derivation of name. Named after the Japanese aesthetic concept *wabi-sabi*: the beauty that is imperfect, impermanent and incomplete.

Diagnosis. Numerous thorns branching together distally; bilobed cephalis.

Holotype. Plate 27, figs. 4A-B; Sample 120-751A-7H-4 98/102cm (Late Miocene); ECO-042.

Material. 298 specimens were observed from ODP Sites 744, 746, 747, 748 and 751.

Description. Two-segmented shell with a short (up to ca. 1.2 times the length of the cephalis) flaring thorax and a cephalis with an approximately median indentation where spine A joins the wall.

Spine **A** is free in the cephalis and continues outside as a small, tribladed at least at the base, apical horn. Spines **D**, **Ll** and **Lr** extends approximately horizontally and sometimes continues outside as slender downward-directed horns. The median bar bears a very small axobate (most often just an indentation, see Pl. 27, fig. 1B). Spine **V** is present and is almost horizontal too; it sometimes protrudes outside the wall as a very short, upward-directed tribladed horn. All the internal spines are rather thick. Collar stricture is marked by a small constriction externally.

The cephalic wall is thick, it can be smooth or rough depending on the specimen, and is almost poreless: some specimens have a few small, rounded pores. The thoracic wall is smooth and bears some larger, circular to elliptical pores of variable size and uneven distribution. The thorax ends with upward directed small thorns. Both the cephalis and the thorax bear a fairly large amount of slender thorns (that can be as long as the apical horn). Those thorns branch distally to form ultimately on some specimens a secondary 3D meshwork made of thin anastomosed bars.

Dimensions. (based on 8 specimens) Length: 62-78 (70); of cephalis: 26-34 (31); of projections: 16-37 (24); collar width: 42-53 (47).

Occurrence. Rare from the *C. humerus* to the *A. challengerae* Zone (middle to late Miocene).

Remarks. *Syscioscenium? wabisabi* differs from *S. velamen* in the thorns branching to form a secondary meshwork and in having a spine **V**. The sethophormid structure described by Sugiyama (1992a) on *S. velamen* was not observed here. The assignment to the genus *Syscioscenium* is therefore questionable.

Genus *Trisulcus* Popofsky 1913 emend. Petrushevskaya 1971
Type-species: *Trisulcus triacanthus* Popofsky 1913

Trisulcus halipleumon Renaudie & Lazarus in press
(Pl. 24, figs 1A-4B)

Derivation of name. *halipleumon* is Greek for a jellyfish (literally 'sea-lungs').
Diagnosis. Cephalis partially sunken into the thoracic cavity; five downwardly-directed, tribladed feet.
Holotype. Pl. 24, figs 1A-B; Sample 120-748B-8H-6, 45/47cm (Late Oligocene/Early Miocene); ECO-036, circle 3.
Material. 39 specimens were observed from ODP Site 748.
Description. Small dicyrtid with a relatively small cephalis subhemispherical externally and a cupola-shaped thorax. The two segments are separated by shoulders and furrows that can be more or less pronounced. There is a small change in contour between the two segments, that tend to disappear in some specimens.
Spine **A** is fused to the dorsal side of the cephalic wall and protrudes subapically as a small, barely noticeable, triangular horn. Spine **V** is short and joins the wall at the collar: it protrudes outside in some specimens as a small triangular horn similar to the apical one (Pl. 5, fig. 9B). Spines **D**, **Ll**, **Lr** and the two **l'** reach the thoracic wall at its widest point and become strong ribs that continue as medium-length, tribladed, downward-directed feet at the termination of the thorax. Two apophyses can be seen joining spine **D** and the thoracic wall in the upper thorax. Arches **AL** can be clearly seen in some specimens on the inner side of the shoulders (Pl. 5, fig. 6B). The axobate appears in some specimens as a stubby, triangular spine. The median bar and the other inner spines are all relatively thick compared to the size of the total shell.
Cephalic pores are rather small, irregular in size and pattern and generally rounded. The cephalic wall between the pores is crested. Thoracic pores are larger, also irregular in size and pattern and elliptical. There is somewhat of a size gradient toward thorax ragged end.
Some rare specimens exhibit supplementary ribs in their lower part.
Dimensions. (based on 5 specimens) Length of shell: 75-98 (88); width of thorax: 63-78 (71); width of cephalis (at collar): 28-33 (32); height of cephalis (from median bar to apex): 28-36 (30).
Occurence. Rare to common in the *Stylosphaera radiosa* Zone (Late Oligocene to Early Miocene).
Remarks. It differs from *Trisulcus triacanthus* Popofsky, 1913 and *T. pinguiculus* Renaudie & Lazarus, in press, in its five tribladed feet and in the relative width of the thorax compared to the cephalis. It also differs from *Lithomelissa? kozoi* n. sp. in its porosity, the size and degree of immersion of the cephalis in the thorax and the shape of the thorax itself.

Trisulcus nanus (Popofsky 1913) emend. Petrushevskaya 1971
1913 *Lithomelissa nana* Popofsky: p. 336; pl. 31, fig. 7
1971 *Trisulcus nana* (Popofsky) – Petrushevskaya: p. 144-145; pl. 73, fig 1-3

Trisulcus pinguiculus Renaudie & Lazarus 2012

(Pl. 24, figs 5A-7B)

Derivation of name. *pinguiculus* is Latin for chubby.

Diagnosis. Three large thoracic lobes; small cephalis with a short apical horn; thorax with large pores.

Material. 107 specimens were observed from ODP Sites 744, 748 and 751.

Holotype. Plate 24, figs. 7A-B (specimen on the right); Sample 120-748B-8H-6 45/47cm (Late Oligocene/Early Miocene); ECO-036.

Description. Two-segmented shell with a trilobate thorax, ca. three times wider than the cephalic chamber. The lobes are separated by short, rather shallow furrows formed by the junction of spines **D**, **Ll** and **Lr** with the thoracic wall. Those spines protrude outside the wall as really small, slender spines on most specimens. Thorax termination is ragged and of nearly the same width as its upper part. In some specimens, the dorsal side of the upper thorax (ie the two lobes separated by the dorsal furrow) is slightly bigger than the lateral one.

The cephalic chamber is approximately hemispherical; spine **A** is fused to the wall and protrude outside subapically as a very short three-bladed horn. There is a furrow between the cephalis and the thorax, where spine **V** joins the wall. None of the specimens bears a ventral horn, but some rare specimens (see Pl. 7, figs 12A-B) bear some short (nearly equal to the apical horn in length and width), additional horns at the apex and on the thoracic lobes. The axobate has never been observed.

The cephalic pores are small and roundish, but somewhat larger and downwardly elongated near the furrow between the cephalis and the thorax. The thoracic pores are larger yet unequal in size, elliptical and randomly distributed. Pores on the lower part of the thorax are larger than the ones on the upper part. The cephalic wall is rougher than the thoracic wall (some specimens have a slightly crested cephalic wall).

Dimensions. (based on 7 specimens) Width of cephalis: 32-40 (36); of thorax at shoulders: 66-94 (82); total length (without apical horn): 72-112 (89).

Occurrence. *T. pinguiculus* is common in samples from the *S. radiosa* to the *C. golli regipileus* Zone (early Miocene) and rare from the *E. punctatum* to the *A. golownini* Zone (early to middle Miocene).

Remarks. *Trisulcus pinguiculus* differs from *T. triacanthus* in having a rougher surface, larger pores and smaller apophyses. The thorax in *T. pinguiculus* is shorter and does not taper downward. The furrows between the thoracic lobes are deeper than in *T. triacanthus*. It also differs from other small dicyrtids such as species of the genera *Antarctissa, Botryopera* or *Lithomelissa* in that the cephalis is partially sunken into the thorax cavity, in the cephalis/thorax width ratio and in the three distinctive shoulders present in the genus *Trisulcus.*

Trisulcus triacanthus Popofsky 1913 emend. Petrushevskaya 1971

1913 *Trisulcus triacanthus* Popofsky: p. 354-355; text-figs 59-60
1971 *Trisulcus triacanthus* Popofsky – Petrushevskaya: p. 141-143; pl. 72, figs 8-13
1987 *Trisulcus triacanthus* Popofsky – Boltovskoy & Riedel: p. 100; pl. 4, fig. 18
1995 *Trisulcus triacanthus* Popofsky – van de Paverd: pl. 65, fig. 9

Subfamily **Plagicanthinae** Hertwig 1879 emend. Petrushevskaya 1971

Genus *Dumetum* Popofsky 1908

Type-species: *Dumetum rectum* Popofsky 1908

Dumetum rectum Popofsky 1908

1908 *Dumetum rectum* Popofsky: p. 265-167; pl. 29, figs 4-5; pl. 36, pl. 1
1967 *Dumetum rectum* Popofsky – Petrushevskaya: p. 60-61; fig. 35

Genus *Neosemantis* Popofsky 1913
Type-species: *Semantis distephanus* Haeckel 1887

Neosemantis bjoerklundi Goll 1979 *mimicus* Goll 1979
1979 *Neosemantis bjoerklundi mimicus* Goll: p. 383-384; pl. 3, figs 1-2

Neosemantis distephanus (Haeckel 1887)
1887 *Semantis distephanus* Haeckel: p. 957; pl. 83, fig. 7
1913 *Neosemantis distephanus* (Haeckel) – Popofsky: p. 229; pl. 29, fig. 2
1979 *Neosemantis distephanus* (Haeckel) – Goll: p. 384; pl. 4, figs 1-15

Neosemantis hofferti Goll 1980
1980 *Neosemantis hofferti* Goll: p. 438; pl. 3, figs 1-3
1989 *Neosemantis hofferti* Goll – Alexandrovitch: pl. 1, fig. 12

Genus *Plagiacantha* Claparède 1855
Type-species: *Plagicantha arachnoides* Claparède 1855

Plagiacantha panarium Dumitrica 1973
1966 *Plectacantha*? sp. Benson: p. 356-357; pl. 23, figs 21-23
1973 *Plagiacantha*? *panarium* Dumitrica: p. 835; pl. 22, figs 1, 3 5
1983 *Plagiacantha*? *panarium* Dumitrica – Benson: p. 506

Genus *Plectacantha* Jørgensen 1905
Type-species: *Plectacantha oikiskos* Jørgensen 1905

Plectacantha cresmatoplegma Nigrini 1968
1968 *Plectacantha cresmatoplegma* Nigrini: p. 55; pl. 1, figs 3a-c; text-fig. 2

Plectacantha oikiskos Jørgensen 1905
1905 *Plectacantha oikiskos* Jørgensen: p. 131-132; pl. 13, figs 50-58
1976 *Plectacantha oikiskos* Jørgensen – Bjørklund: pl. 6, figs 8-10

Genus *Plectagonidium* Cachon & Cachon 1969
Type-species: *Plectagonidium deflandrei* Cachon & Cachon 1969

Plectagonidium deflandrei Cachon & Cachon 1969
(Pl. 21, figs 14, 16)
1969 *Plectagonidium deflandrei* Cachon & Cachon: p. 236-239; text-fig. 1; pl. 39
2005 *Plectagonidium deflandrei* Cachon & Cachon – Okazaki et al.: pl. 12, fig. 47

Genus *Pseudocubus* Haeckel 1887
Type-species: *Pseudocubus obeliscus* Haeckel 1887

Pseudocubus obeliscus Haeckel 1887

1887 *Pseudocubus obeliscus* Haeckel: p. 1010; pl. 94, fig. 11
1913 *Obeliscus pseudocuboides* Popofsky: p. 280-281; pl. 29, figs 4-5
1971 *Pseudocubus obeliscus* Haeckel – Petrushevskaya: p. 150; pl. 76
1995b *Pseudocubus obeliscus* Haeckel – Funakawa: p. 23-25; pl. 4, figs 2-3

Subfamily **Sethoperinae** Haeckel 1881 emend. Petrushevskaya 1971

Genus *Callimitra* Haeckel 1881
Type-species: *Callimitra carolatae* Haeckel 1887

Callimitra solocicribrata Takahashi 1991
(Pl. 20, fig. 7)
1991 *Callimitra solocicribrata* Takahashi: p. 100; pl. 27, figs 10-11
1992b *Callimitra solocicribrata* Takahashi – Abelmann: pl. 4, fig. 10

Genus *Chitascenium* Sugiyama 1994
Type-species: *Chitascenium cranites* Sugiyama 1994

Chitascenium cranites Sugiyama 1994
1994 *Chitascenium cranites* Sugiyama: p. 5; pl. 1, figs 4a-d, 6a-b

Genus *Cladoscenium* Haeckel 1881
Type-species: *Cladoscenium ancoratum* Haeckel 1887

Cladoscenium ancoratum Haeckel 1887
1887 *Cladoscenium ancoratum* Haeckel: p. 1149; pl. 53, fig. 13
1991 *Cladoscenium ancoratum* Haeckel – Takahashi: p. 94; pl. 24, figs 9-14

Cladoscenium tricolpium (Haeckel 1887)
1887 *Euscenium tricolpium* Haeckel: p. 1147; pl. 53, fig. 12
1900 *Cladoscenium tricolpium* (Haeckel) – Jørgensen: p. 78-79
1905 *Cladoscenium tricolpium* (Haeckel) – Jørgensen: p. 134; pl. 15, figs 71-73
1976a *Cladoscenium tricolpium* (Haeckel) – Bjørklund: pl. 7, figs 5-8

Genus *Clathrocanium* Ehrenberg 1861
Type-species: *Clathrocanium squarrosum* Ehrenberg 1861

Clathrocanium coarctatum Ehrenberg 1861 emend. Petrushevskaya 1971
1861 *Clathrocanium coarctatum* Ehrenberg: p. 767
1873b *Clathrocanium coarctatum* Ehrenberg – Ehrenberg: p. 287; pl. 7, fig. 6
1971 *Clathrocanium coarctatum* Ehrenberg – Petrushevskaya: p. 81; pl. 39, figs 1-4

Genus *Clathrocorys* Haeckel 1881
Type-species: *Clathrocorys murrayi* Haeckel 1887

Clathrocorys murrayi Haeckel 1887
(Pl. 20, fig. 8)
1887 *Clathrocorys murrayi* Haeckel: p. 1219-1220; pl. 64, fig. 8

1991 *Clathrocorys murrayi* Haeckel – Takahashi: p. 101; pl. 27, figs 4-8

Clathrocorys? *sugiyamai* Renaudie & Lazarus in press
(Pl. 19, fig. 3A-6B)

1992 *Euscenarium* sp. B Sugiyama et al.: p. 21; pl. 15, figs 6a-b.
1998 Sethophormid gen. et sp. indet. A Sugiyama: p. 236; pl. 3, figs 3-4b.
Derivation of name. Named after Kazuhiro Sugiyama who first illustrated this species.
Diagnosis. Tetrahedral shell with three weakly-paneled ribs/feet; apical horn has three small projections at its base.
Holotype. Pl. 19, figs 6A-B; Sample 119-744A-2H-1, 53-55cm (Middle Pleistocene); ECO-059.
Material. 230 specimens have been observed from ODP Sites 689, 693, 738, 744, 747, 751 and 1138.
Description. Two-segmented shell with a tetrahedral outline. The globular cephalis is four to five times shorter than the flaring thorax.
Spine **A** is free in the cephalic cavity and extends subapically outside the wall as a tribladed horn that can be as long as the cephalis and that is commonly bearing panel-like projections at its base between the cephalic wall and the horn. Spine **V** protrudes as a shorter horn. The angle between spine **A** and spine **V** is approximately 70°. Spines **D**, **Ll** and **Lr** are directed downward, join the wall at the collar stricture and extend below as ribs on the thoracic wall. The median bar is short, subhorizontal, and has not been observed to bear an axobate. None of the spines mentioned above seem to bear any additional apophyses. Pores on the generally crested cephalic wall are few, randomly distributed, uneven in size and globular.
The upper part of the thorax bears subelliptical, relatively small, sparse pores whereas the lower part bears large, polygonal pores separated by thin bars and somewhat longitudinally aligned in some specimens. The three ribs extend below the ragged thorax termination as short diverging feet. Most specimens bear some projections along the ribs, that, in some specimens, end up forming a poorly-developed panel, bearing up to three longitudinal rows of large subelliptical pores.
Dimensions. (based on 5 specimens) Length of cephalis: 37-51 (46); length of feet (from collar to end): 152-286 (225); height of apical horn: 28-44 (37); maximum width of thorax: 186-288 (218).
Occurence. Rare from the *Eucyrtidium punctatum* to the Omega Zone (Early Miocene to Holocene).
Remarks. *Clathrocorys*? *sugiyamai* differs from *Clathrocorys murrayi* and from *Callimitra atavia* Goll, 1979 primarily in having a fully-developed thorax and from *Callimitra solocicribrata* Takahashi, 1991 in its overall shape and in the poorly-developed panel along the thoracic ribs. It also differs from *Genetrix petrushevskayae* Sugiyama, 1994 in its spine **A** lacking apophyses *a*, in the shape of the thorax and in the latter having a somewhat spongy upper thorax. It finally differs from the specimen illustrated as *Clathrocorys* (?) sp. in Funakawa, 1994 in lacking the external ribs on the cephalis along arches **AL**.

Genus *Euscenarium* Haeckel 1887 emend. Petrushevskaya 1981
Type-species: *Euscenium tricolpium* Haeckel 1887

Euscenarium joergenseni (Dumitrica 1978a)

1905 *Cladoscenium tricolpium* (Haeckel) – Jørgensen: p. 134; pl. 15, figs 71-73
1978a *Clathromitra joergenseni* Dumitrica: p. 240; pl. 7, fig. 1
1992 *Eucenarium* (sic) *joergenseni* (Dumitrica) – Sugiyama & Furutani: p. 206; pl. 18, figs 1a-b

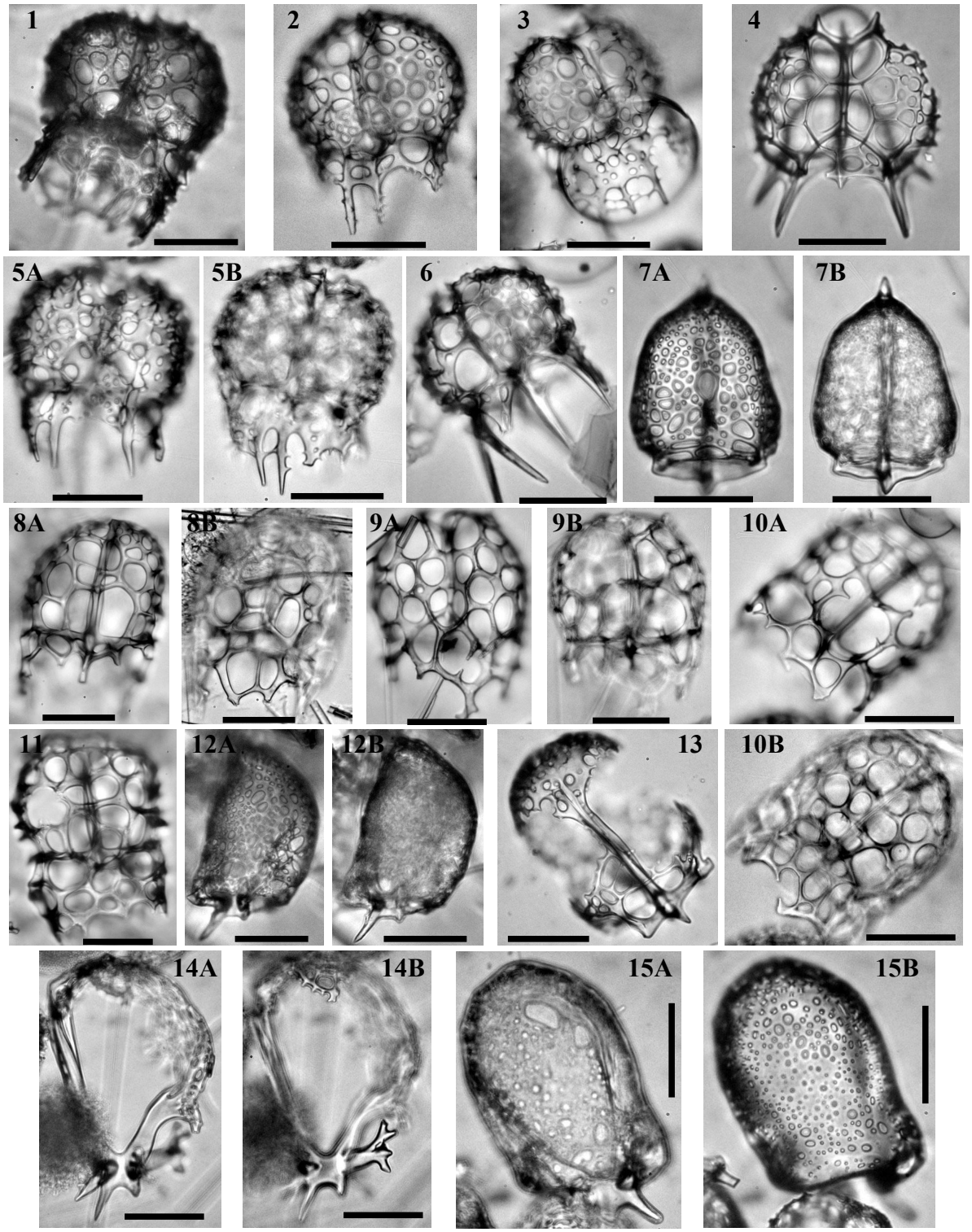

Plate 28.– 1. *Phormospyris loliguncula* Renaudie & Lazarus in press, Sample 119-746A-9H-4 48-50cm, Late Miocene. 2. *Phormospyris loliguncula*, Sample 120-751A-5H-2 49-51cm, Early Pliocene. 3. *Phormospyris loliguncula*, Sample 120-751A-5H-2 49-51cm, Early Pliocene. 4. *Ceratospyris laventaensis* Clark & Campbell, Sample 120-751A-13H-2 98-102cm, Middle Miocene. 5. *Phormospyris loliguncula*, holotype, Sample 120-751A-6H-1 98-102cm, Late Miocene. 6. *Phormospyris loliguncula*, Sample 183-1138A-14R-1 20-22cm, Late Miocene. 7. *Platybursa harpoi* Renaudie & Lazarus in press, Sample 120-747A-2H-3 45-47cm, Pleistocene. 8. *Dendrospyris jobstae* Renaudie & Lazarus 2012, Sample 119-745B-14H-6 53-55cm, Late Pliocene. 9. *Dendrospyris jobstae*, Sample 120-747A-3H-5 45-47cm, Early Pliocene. 10. *Dendrospyris jobstae*, Sample 120-747A-3H-5 45-47cm, Early Pliocene. 11. *Dendrospyris jobstae*, holotype, Sample 119-745B-14H-6 53-55cm, Late Pliocene. 12. *Platybursa harpoi*, Sample 120-747A-2H-1 45-47cm, Pleistocene. 13. *Platybursa harpoi*, Sample 120-747A-2H-1 45-47cm, Pleistocene. 14. *Platybursa harpoi*, holotype, Sample 120-747A-2H-1 45-47cm, Pleistocene. 15. *Platybursa harpoi*, Sample 119-744A-2H-2 53-55cm, Pleistocene.
All scale bars 50 µm. Magnification x384.

1994 *Euscenarium joergenseni* (Dumitrica) – Sugiyama: pl. 2, figs 8a-b

Euscenarium? sp. 2
(Pl. 31, figs 1-2A, 6)

Description. Dicyrtid with a thorax often reduced to a very short cylindrical extension of the shell wall below **MB**. Cephalic wall is thick and almost poreless but often crested. Spines **A, D, Ll** and **Lr** protrude outside the wall as, respectively, a lanceolate, tribladed apical horn and three tribladed, downward bent wings. Spine **V** is a very short spine which joins the wall without extending outside. Apophyses *m* extend from **A** to reach the wall whereas apophyses *a* are present but only as short denticles of **A**. **Ax** was not observed. Apophyse *c* extends upwards from **D** and joins the shell wall.

Remarks. This species differs from *E. joergenseni* in its almost poreless wall and its reduced thorax. It differs from *C. coarctatum* in the apical horn lacking the anchor-shaped extensions and, again, in lacking a proper thorax.

Genus *Genetrix* Sugiyama 1994

Type-species: *Genetrix petrushevskayae* Sugiyama 1994

Genetrix petrushevskayae Sugiyama 1994
(Pl. 20, fig. 6)

1994 *Genetrix petrushevskayae* Sugiyama: p. 5-6; pl. 3, figs 1a-3

Genus *Tetraplecta* Haeckel 1881 emend. Takahashi 1991

Type-species: *Tetraplecta pinigera* Haeckel 1887

Tetraplecta pinigera Haeckel 1887

1887 *Tetraplecta pinigera* Haeckel: p. 924; pl. 91, fig. 9

1991 *Tetraplecta pinigera* Haeckel – Takahashi: p. 93; pl. 24, figs 1-5

Subfamily **Sethophormidinae** Haeckel 1881 emend. Petrushevskaya 1971

Genus *Enneaphormis* Haeckel 1881 emend. Petrushevskaya 1971

Type-species: *Enneaphormis rotula* Haeckel 1881

Enneaphormis rotula Haeckel 1881

1881 *Enneaphormis rotula* Haeckel: pl. 8, fig. 9

1887 *Sethophormis rotula* (Haeckel) – Haeckel: p. 1246; pl. 57, fig. 9

1971 *Enneaphormis rotula* Haeckel – Petrushevskaya: p. 68; pl. 31, figs 1-3

Enneaphormis? sp. I
(Pl. 25, fig. 6)

Remarks. Very few specimens of this species have been seen to date, preventing a complete description: however, its strong, circular ring formed by arches **DL** and **LL** and its hemispherical to spherical latticed cephalic cap seem enough to differenciate it from *Enneaphormis rotula, E.* sp. Renaudie & Lazarus in press or *Sethophormis aurelia.*

Enneaphormis sp. Renaudie & Lazarus in press
(Pl. 19, figs 7, 10-12)

Diagnosis. Flat, circular thorax with large pores and some smaller pores close to the smooth, spineless margin.
Material. 21 specimens (including margin fragments) were observed from ODP Sites 689, 693, 738, 747 and 751.
Description. Large, flat (slightly convex) shell consisting of two segments. The cephalis is a third the diameter of the shell. A few specimens have been found with at least a small part of the cephalis remaining and none with a complete cephalis. It seems to be a very delicate 'velum' consisting of a feltwork of thin, anastomosed bars delimiting numerous polygonal pores. The cephalis encroaches on to the thorax and attaches to the rim of some of the large thoracic pores (Pl. 7, figs 10, 14). The inner spicule was not observed in any of the specimens, however three ribs originating from the cephalic structure are clearly distinguishable on the thorax of most specimens (Pl. 7, figs 10, 12, 14) and most probably represent extensions of spines **D**, **Ll** and **Lr**. The thorax consists of a network of large polygonal pores of various sizes and a very irregular 'honey-comb' disposition. The thorax ends with an irregular but not ragged, almost circular, rim. On most specimens (Pl. 7, figs 10, 13-14), several small, circular pores can be seen adjacent to the rim: in some specimens they are aggregated in small clusters (Pl. 7, fig. 13).
Dimensions. (based on 4 specimens) Diameter of the shell: 271-381 (301); diameter of the cephalis: 102-166 (115); diameter of the large pores: 15-51 (32); diameter of the small pores close to margin: 2-20 (10).
Occurence. Rare to sporadic from the Upsilon to the Chi Zone (Late Pliocene to Early Pleistocene).
Remarks. Since a specimen with a completely preserved cephalis is yet to be found, the generic assignment of this species is problematic: indeed, the cephalic 'velum', coupled with the three radial ribs seem characteristic of genus *Enneaphormis*; yet the porosity of the thorax and its rim are morphological features that seem more coherent with genus *Lampromitra* Haeckel, 1881.
This species differs from *Sethophormis aurelia* (Haeckel) 1879 in possessing three radial ribs instead of four, in the size and shape of its thoracic pores and in the thorax ending with a rim. It is distinguished from *Lampromitra coronata* Haeckel, 1887 in its velum-shaped cephalis, in the size of the thoracic pores, the flatness of the shell and the absence of spines on the rim. It finally differs from *Velicucullus oddgurneri* Bjørklund, 1976a in the size and shape of the thoracic pores and in the latter having its cephalis and thorax raised with regard to the lower thorax.
Because a complete specimen is yet to be found, we leave this species in open nomenclature.

Genus *Protoscenium* Jørgensen 1905
Type-species: *Plectacantha simplex* Cleve 1900

Protoscenium simplex (Cleve 1900) emend. Petrushevskaya 1971
1900 *Plectacantha simplex* Cleve: p. 32; pl. 3, fig. 3
1971 *Protoscenium simplex* (Cleve) – Petrushevskaya: p. 69; pl. 32, figs 1-3

Protoscenium pantarhei Renaudie & Lazarus, in press
(Pl. 25, figs 3, 7A-12B)
Derivation of name. Named after the Greek expression 'panta rhei' (παντα ρει: literaly, 'everything flows'), employed by Simplicius to characterize Heraclitus' theory of impermanence.
Diagnosis. Spicular Plagiacanthidae with an anastomosed shell wall; apophyses *m, c* and *p* well developed.
Holotype. Pl. 25, figs 8A-B; Sample 120-751A-3H-2, 98-102cm (Late Miocene); ECO-063.
Material. 253 specimens were observed from ODP Sites 689, 693, 747, 748, 751 and 1138.

Description. Skeleton consists almost entirely of the initial spicule, comprising spines **A**, **D**, **Ll** and **Lr**. Spines **D**, **Ll** and **Lr** are identical in shape and size; they are also more or less in the same plane. In apical view (Pl. 6, figs 8A-B), they are separated from each other by a 120° angle. Apophyses *c* and *p* bifurcate from spines **D**, **Ll** and **Lr** in their distal half; they are also situated more or less in the basal plane. The median bar is extremely reduced but is more than just a point since spine **A** join the spicule 1 or 2 µm away from the junction of spines **Ll** and **Lr**. The axobate, when present, is a short cluster of lumps (Pl. 6, fig. 8B). Spine **A** is almost perpendicular to the basal plane. Three apophyses *m* bifurcate from it in its distal third and are upwardly directed. Arches *mc* and *mp* are usually present and can be strongly expressed in some specimens (Pl. 6, figs 14A-B). Some specimens also exhibit arches *mg* (Pl. 6, fig. 12B).
The shell wall rests on the arches and is connected to the distal end of all spines and apophyses, with the exception of spine **A** which protrudes apically. The wall consists of randomly distributed anastomosing thin bars, branching from a multitude of small, needle-like thorns arising from the arches (Pl. 6, fig. 12B). When complete, the shell wall has a somewhat hemispherical outline. In some specimens (Pl. 6, figs 12A-B and 14A-B), the wall extends sightly below the basal plane.
Dimensions. (based on 6 specimens) Total width: 92-105 (103); total height: 70-101 (88).
Occurence. Sporadic from the *Cycladophora golli regipileus* to the *Eucyrtidium punctatum* Zone (Early to Middle Miocene); Rare to common from the *Cycladophora humerus* to the *Acrosphaera*? *labrata* Zone (Middle to Late Miocene); Sporadic again from the *Acrosphaera*? *labrata* to the Tau Zone (Late Miocene to Early Pliocene) and then rare again in the Upsilon Zone (Early to Late Pliocene).
Remarks. *Protoscenium pantarhei* and *P. simplex* exhibits more or less the same skeletal pattern, however the presence of a wall, the size of the specimen and the thickness of the spines differentiate *P. pantarhei* from the latter.

Protoscenium? sp. 8
(Pl. 25, figs 1A-2)

Description. Globular, dome-shaped cephalis and short truncated-conical, flaring thorax. Spine **A** is free inside the cavity until it reaches subapically the shell wall. Spines **D**, **Ll** and **Lr** extend more or less horizontally in the plane of the collar stricture (which is marked externally only by a change in contour). Several arches seem to extend as ribs on the wall from the collar to the apex of the cephalis. The cephalic wall is somewhat of a latticed wall and not a random meshwork of anastomosed bars (as in *P.*? sp. 23 and *P. pantarhei*), but it still seems to extend from these arches (see Pl. 25, fig. 2). Pores are somwhat polygonal, small and randomly arranged. Needle-like thorns on the cephalic wall are frequent.
Remarks. The number of observed specimens for this species is still too low to recognize and identify every arches and apophyses making the genus assignment problematic. In particular a specimen observed in apical view might be useful to observe the typical sethophormid structure (e.g. Sugyama 1992a).

Protoscenium? sp. 23
(Pl. 25, figs 4A-5B)

Description. Apically-elongated, almost cylindrical, cephalic wall consisting of a chaotic meshwork of bars of various thicknesses. Bar nodes often bear tiny thorns from which new, thinner, bars extend. Spine **A** and spine **V** both join the cephalic wall and continue as upward-directed ribs (and eventually as conical horns). Spines **D**, **Ll** and **Lr** (each separated by an equal angle) extend to the bottom of the cephalic wall where they then continue downwardly (in a

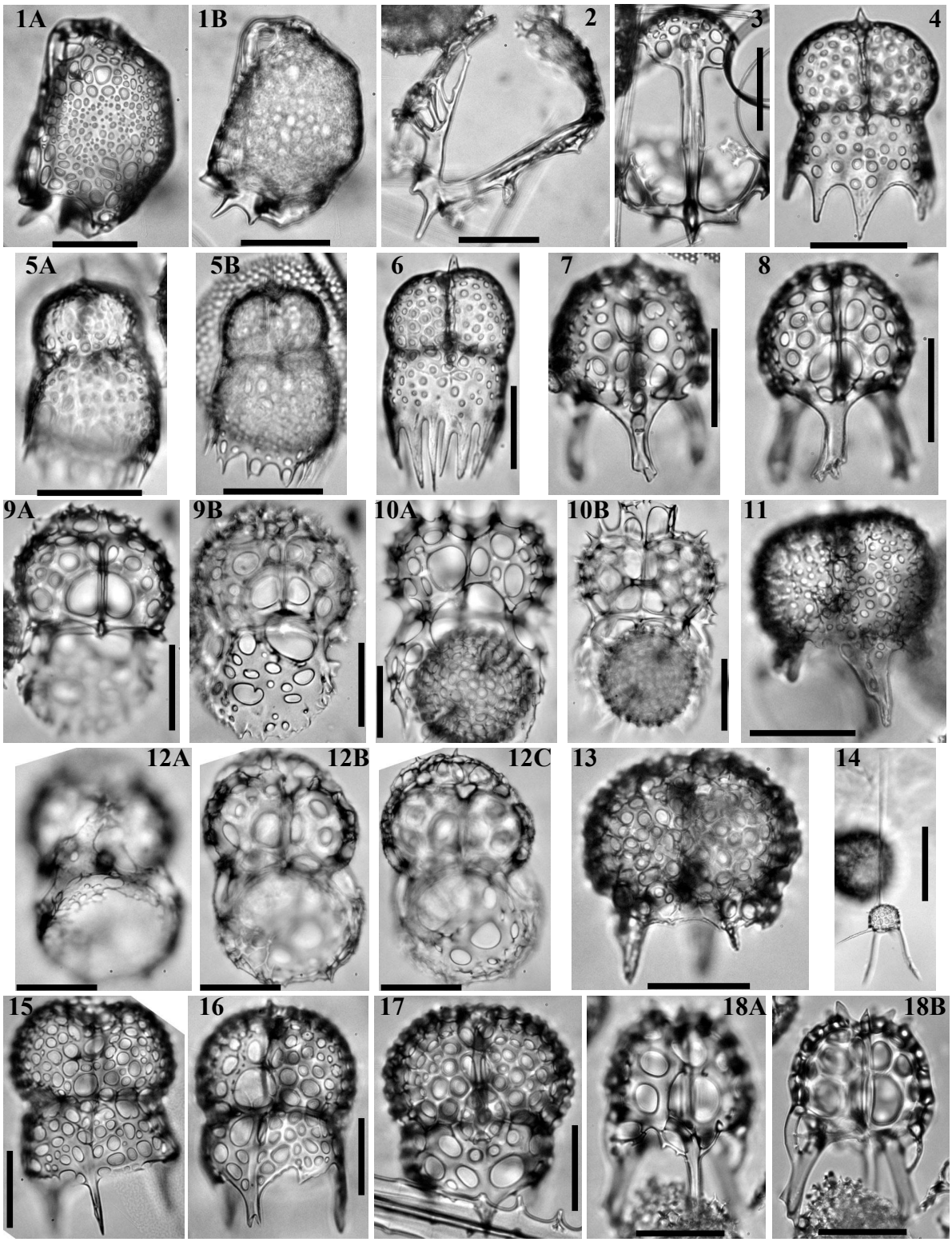

Plate 29.– 1. *Platybursa harpoi*, Sample 120-747A-2H-3 45-47cm, Pleistocene. 2. *Platybursa harpoi*, Sample 120-747A-2H-1 45-47cm, Pleistocene. 3. *Platybursa harpoi*, Sample 120-747A-2H-1 45-47cm, Pleistocene. 4. *Rhodospyris* sp. N, Sample 119-744A-10H-2 60-62cm, Early Miocene. 5A-B. *Rhodospyris* sp. N, Sample 120-748B-7H-4 45-47cm, Early Miocene. 6. *Rhodospyris* sp. N, Sample 119-744A-10H-2 60-62cm, Early Miocene. 7. *Dendrospyris* sp. C, Sample 119-737A-26X-1, Late Miocene. 8. *Dendrospyris* sp. C, Sample 119-744A-7H-4 60-62cm, Middle Miocene. 9. T*holospyris* sp. O, Sample 120-747A-9H-8 45-47cm, Early/Middle Miocene. 10. *Tholospyris* sp. O?, Sample 120-747A-9H-5 45-47cm, Early/Middle Miocene. 11. *Phormospyris*? sp. J, Sample 119-746A-6H-2 53-55cm, Late Miocene. 12. *Tholospyris* sp. O, sample 120-748B-6H-1 45-47cm, Early Miocene. 13. *Phormospyris*? sp. J, Sample 119-746A-6H-2 53-55cm, Late Miocene. 14. *Tetraspyris tetracorethra* Haeckel 1887, Sample 120-747A-2H-1 45-47cm, Pleistocene. 15. *Phormospyris* sp. L, Sample 119-744A-10H-2 60-62cm, Early Miocene. 16. *Phormospyris* sp. L, Sample 119-744A-10H-2 60-62cm, Early Miocene. 17. *Phormospyris* sp. L, Sample 120-748B-6H-5 45-47cm, Early Miocene. 18. *Dendrospyris*? sp. C?, Sample 119-744A-3H-1 53-55cm, Late Pliocene. All scale bars 50 µm. Magnification x384.

direction almost parallel to that of the cephalic wall) as conical feet. Cephalic wall bars randomly connect to these feet in several places. The shell wall does not seem to be properly closed apically.

Remarks. The fact that this species belongs to genus *Protoscenium* is very improbable (because of the presence of spine **V** in particular). Yet, it still seems to be the closest genus to this species (based mostly on external characters.)

Genus *Sethophormis* Haeckel 1881 *sensu* Petrushevskaya 1971

Type-species: *Sethophormis cruciata* Haeckel 1887

Sethophormis aurelia Haeckel 1887

1887 *Sethophormis aurelia* Haeckel: pl. 55, figs 3-4

Genus *Velicucullus* Riedel & Campbell 1952

Type-species: *Soreuma magnificum* Clark & Campbell 1942

Velicucullus altus Abelmann 1990

1990 *Velicucullus altus* Abelmann: p. 698; pl. 8, figs 5a-c

1992 *Lampromitra coronata* Haeckel group – Lazarus: p. 797

Remarks. This species includes a wide range of morphotype going from forms with high shells and poorly developed basal fringe (as illustrated in Abelmann 1990) to flat forms with well-developed fringe. No morphological gap have been seen between those forms, hence those forms were gathered here into one single species. In the specimen of *Lampromitra coronata* described and illustrated in Haeckel 1887, spines **V**, **D**, **Ll** and **Lr** join the shell near the fringe, while in all specimens observed in our material those spines are horizontal and join the shell near the collar stricture: as a consequence, the name *Lampromitra coronata* was not retained for the species observed here.

Velicucullus oddgurneri Bjørklund 1976a

1976a *Velicucullus oddgurneri* Bjørklund: p. 1126; pl. 19, figs 6-9

Family **Trissocyclidae** Haeckel 1881 emend. Goll 1968

Genus *Acanthodesmia* Müller 1856

Type-species: *Lithocircus viniculatus* Müller 1856

Acanthodesmia micropora (Popofsky 1908)

1908 *Semantis micropora* Popofsky: p. 268; pl. 30, fig. 4

1971 *Acanthodesmia micropora* Petrushevskaya: p. 279; pl. 135, figs 1-9

Genus *Ceratospyris* Ehrenberg 1847 *sensu* Nigrini 1967

Type-species: *Haliomma radicatum* Ehrenberg 1844

Ceratospyris borealis Bailey 1856

1856 *Ceratocyrtis borealis* Bailey: p. 3; pl. 1, fig. 3

2006 *Ceratocyrtis borealis* Bailey – Itaki & Bjørklund: p. 450-451; pl. 1, figs 3-8; text-fig. 2

2009 *Ceratocyrtis borealis* Bailey – Itaki: pl. 13, figs 10-11b

Ceratospyris laventaensis Campbell & Clark 1944
(Pl. 28, fig. 4)
1944 *Ceratospyris (Lophospyris) laventaensis* Campbell & Clark: p. 36; pl. 8, fig. 15

Ceratospyris? sp. M
(Pl. 30, figs 14A-15B)
Description. Bilobed cephalis with a weak sagittal constriction and a loose latticed shell wall that appears to be asymmetrical on both sides of the sagittal ring. Pores are randomly distributed and of various size and shape. Spine **A** and spine **D** both extend as fairly significant horns, one near the apex of the sagittal ring, the other near the antapex.

Ceratospyris? sp. A
(Pl. 30, figs 7, 9-10, 16A-18)
? 1944 *Tristylospyris (Tristylospyrula) lunadae* Campbell & Clark: p. 34; pl. 5, fig. 19
Diagnosis. No sagittal constriction and apical horn near the apex of the sagittal ring; large pairs of sagittal-lattice pores (specifically on the dorsal side); thorax is a short extension of the shell wall below the basal ring.
Description. Shell divided in two lobes by a sagittal ring which is not marked by any external constriction. The apex of the shell is the apex of the sagittal ring, where spine **A** forms a small apical horn. On the dorsal side, the two pairs of sagittal-lattice pores can be seen, the lowermost being the larger, and being elliptical, elongated in the direction of the sagittal ring. On the ventral side, three pairs of sagittal-lattice pores are present. Other pores present on the cephalic wall are smaller, quite numerous, more or less circular and irregularly-distributed. The shell wall continues below the basal ring to form a very short thorax.
Remarks. The species described herein differs from *Tristylospyris lunadae* Campbell & Clark 1944 in lacking three distinct feet, and in possessing large pairs of sagittal-lattice pores.

Genus *Corythospyris* Haeckel 1881 emend. Goll 1978
Type-species: *Elaphrospyris damaecornis* Haeckel 1887

Corythospyris fiscella Goll 1978
1978 *Corythospyris fiscella* Goll: p. 178; pl. 5, figs 1-21

Corythospyris jubata Goll 1978
1978 *Corythospyris jubata* Goll: p. 177-178; pl. 4, figs 1-2, 4-5, 7-17
1990 *Corythospyris fiscella* Goll – Abelmann: pl. 4, fig. 9

Genus *Dendrospyris* Heackel 1881 emend. Goll 1968
Type-species: *Ceratospyris stylophora* Ehrenberg 1874

Dendrospyris haysi Chen 1975
1975 *Dendrospyris haysi* Chen: p. 455; pl. 15, figs 3-5

Dendrospyris megalocephalis Chen 1975
1975 *Dendrospyris megalocephalis* Chen: p. 455; pl. 14, figs 3-5
1990 *Dendrospyris megalocephalis* Chen – Abelmann: pl. 5, fig. 15

Dendrospyris rhodospyroides (Petrushevskaya 1975)

1975 *Desmospyris rhodopyroides* Petrushevskaya: pl. 10; figs. 27-29, 31, 32
1992 *Desmospyris rhodopyroides* Petrushevskaya – Lazarus: pl. 7, fig. 4 non fig. 3

Dendrospyris? *sakaii* Sugiyama & Furutani 1992
1992 *Dendrospyris*? *sakaii* Sugiyama & Furutani: p. 205; pl. 13, figs 3, 6,; pl. 20, figs 3-4c

Dendrospyris? *jobstae* Renaudie & Lazarus 2012
(Pl. 28, figs 8A-11)

Derivation of name. Named after Anne Jobst, for her long effort in curating and databasing the Ehrenberg Collection.
Diagnosis. Characterized by its large pores, its relatively thin bars and its longitudinally-elongated shell.
Holotype. Plate 28, fig. 11; Sample 119-745B-14H-6 53/55cm (Late Pliocene); ECO-035.
Material. 73 specimens were observed from ODP Sites 745, 747 and 751.
Description. The latticed shell is made of few large, circular to subelliptical pores that are loosely arranged according to a hexagonal pattern and are separated by relatively thin, crested bars. Some smaller pores are sometimes intercalated between the larger ones, and the pores at the apex are also usually smaller. The latticed shell continues below the basal ring as a cylindrical thorax. Some specimens show a slight constriction at the basal and the sagittal ring. The latticed shell is linked to the D-shaped sagittal ring by 8(?) pairs of bars and, on front view, by the frontal bar. The two sagittal-lattice pores just above this frontal bar are generally larger than the others (see Pl. 4, figs. 8A, 11A and 12B).
The shell outline is somewhat narrow (laterally) but elongated (longitudinally).
Dimensions. (based on 6 specimens) Length of sagittal ring: 79-90 (85); width of basal ring: 76-99 (88); maximum width of cephalic lobes: 82-109 (98).
Occurrence. Rare to common from the Tau to the lower Upsilon Zone (early Pliocene).
Remarks. *Dendrospyris*? *jobstae* differs from *D. stabilis* Goll, 1968 and *D. haysi* Chen, 1975 in its outline being narrower but longer, in its sagittal and basal constriction being slighter (and even absent in some most specimens) and in its pores being larger with smaller crested bars.

Dendrospyris sp. C
(Pl. 29, figs 7-8, 18A-B)

Description. Relatively narrow, bilobed cephalis with a weak sagittal constriction. Spines **D**, **Ll** and **Lr** extend below the basal ring as feet. The feet are conical to triangular in section and, at their distal end, branch irregularly. Dorsally, the lowermost pair of sagittal-lattice pores and the two basal pores surrounding spine **D** link together to form what seem to be one large pore. Eventually, as in several species of *Phormospyris* described herein, some secondarily-grown feltwork can spread over this pore. Two other pairs of smaller sagittal-lattice pores are also present on the dorsal side. Other lattice pores on the shell wall are more or les even in size and regularly arranged.
One specimen (Pl. 29, figs 18A-B) shows some additional feautres: several subapical, triangular spines and arches joining feet **Ll** and **Lr** with the shell wall. This specimen also exhibits larger pores and a deeper sagittal constriction.
Remarks. This species differs primarily from *Dendrospyris pododendros* (Carnevale 1908) sensu Goll 1968 in possessing only three feet and in the feet, in the latter, being widely divergent.

Dendrospyris? sp. K

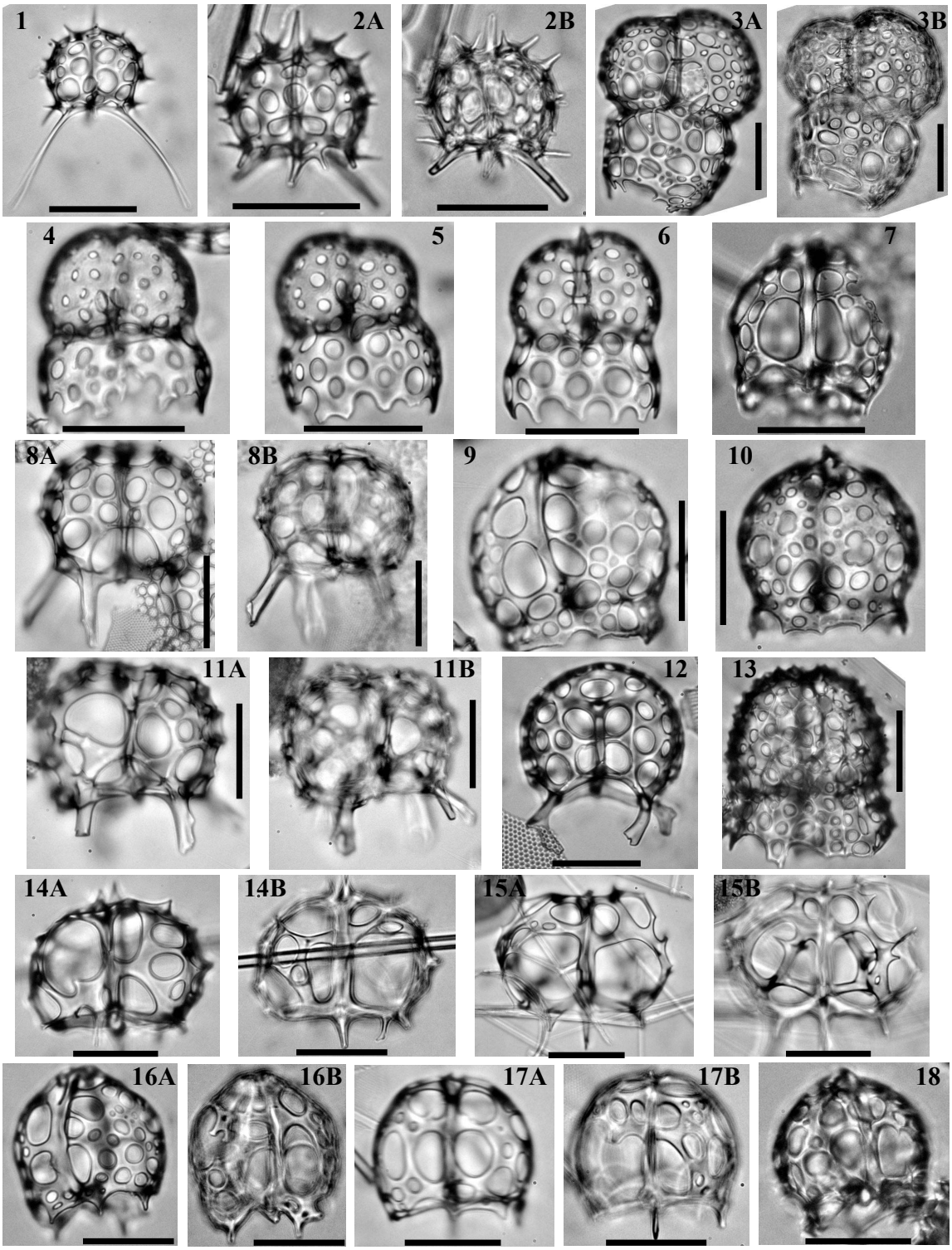

Plate 30.– 1. *Dorcadospyris*? sp. P, Sample 120-748B-8H-2 45-47cm, Early Miocene. 2. *Dorcadospyris*? sp. P, Sample 120-748B-6H-1 45-47cm ,Early Miocene. 3. *Phormospyris*? sp. I, Sample 119-744A-8H-1, Early Miocene. 4. *Rhodospyris*? sp. D, Sample 120-748B-8H-2 45-47cm, Early Miocene. 5. *Rhodospyris*? sp. D, Sample 120-751A-13H-CC, Early/Middle Miocene. 6. *Rhodospyris*? sp. D, Sample 120-751A-15H-CC, Early Miocene. 7. *Ceratospyris*? sp. A, Sample 119-744A-9H-1 60-62cm, Early Miocene. 8. *Dendrospyris* sp. K, Sample 120-748B-8H-6 76-83cm, Late Oligocene/Early Miocene. 9. *Ceratospyris*? sp. A, Sample 120-751A-15H-CC, Early/Middle Miocene. 10. *Ceratospyris*? sp. A?, Sample 120-748B-6H-3 45-47cm, Early Miocene. 11. *Dendrospyris* sp. K, Sample 120-748B-8H-6 76-83cm, Late Oligocene/Early Miocene. 12. Unidentified Trissocyclidae, Sample 119-737A-26X-1, Late Miocene. 13. *Desmospyris*? sp. H, Sample 120-747A-3H-5 45-47cm, Early Pliocene. 14. *Ceratospyris*? sp. M, Sample 119-744A-6H-4 60-62cm, Middle Miocene. 15. *Ceratospyris*? sp. M, Sample 120-748B-5H-5 45-47cm, Middle Miocene. 16. *Ceratospyris*? sp. A, Sample 120-751A-13H-2 98-102cm, Middle Miocene. 17. *Ceratospyris*? sp. A?, Sample 120-748B-6H-5 45-47cm, Early Miocene. 18. *Ceratospyris*? sp. A, Sample 119-744A-9H-1 60-62cm, Early Miocene.
All scale bars 50 µm. Magnification x384.

(Pl. 30, figs 8A-B, 11A-B)

Description. Cephalis with two lobes separated by a weak sagittal constriction and a flattened apex. Cephalic wall bears a few large, framed, elliptical pores. Several pairs of sagittal-lattice pores are present including a large basal one on the dorsal side (Pl. 30, fig. 8A) and another large one at mid-height on the ventral one (surrounding the barely visible ventral spine). Four feet, triangular in section, protrude from the basal ring following spines **Ll, Lr** (on the ventral side) and the two **l'** (on the dorsal side). The two feet extending from spines **l'** are directed straight downward while the two feet extending from spines **Ll** and **Lr** are directed somewhat sideways. All feet branch irregularly at their distal end.

Dendrospyris? sp. J

(Pl. 29, figs 11, 13)

Description. Bilobed cephalis with a clear sagittal constriction. No sagittal-lattice pores. Shell wall bears numerous small, circular pores, separated by rather strongly crested bars. The shell wall continues a little below the basal ring and, sometimes, along the three sconical feet.

Genus *Desmospyris* Haeckel 1881

Type-species: *Desmospyris mamillata* Haeckel 1887

Desmospyris spongiosa Hays 1965

1965 *Desmospyris spongiosa* Hays: p. 173; pl. 2, fig. 1

1975 *Desmospyris spongiosa* Hays – Chen: pl. 15, figs 1-2

Desmospyris? sp. H

(Pl. 30, fig. 13)

Remarks. This species differs primarily from *Desmoypris spongiosa* in its short, flaring thorax being truncated-conical instead of tapering toward the mouth.

Genus *Dorcadospyris* Haeckel 1881 emend. Goll 1969

Type-species: *Dorcadospyris dentata* Haeckel 1887

Dorcadospyris alata? (Riedel 1959)

? 1959 *Brachiospyris alata* Riedel: p. 293; pl. 1, figs 10-12

? 1970 *Dorcadospyris alata* (Riedel) – Riedel & Sanfilippo: pl. 14, fig. 5

Dorcadospyris? sp. P

(Pl. 30, figs 1-2B)

Description. Hemispherical to spherical cephalis separated in two chambers by a sagittal ring. No sagittal constriction whatsoever. Ventral side of the cephalis shows several unpaired sagittal-lattice pores but dorsal side does not have any sagittal-lattice pore. The other pores on the shell wall are large, round to elliptical and more or less regularly arranged. Spine **A** extends as a short, conical apical horn. Spines **D**, **Ll** and **Lr** continue as fairly long, thin, conical feet that are bent downwards. Numerous thorns arise from bar nodes as thin, needle-like supplementary horns slightly shorter than the apical horn.

Remarks. This species differs from the two Oligocene morphotypes illustrated as Do2 and Do4 in Goll 1969 (Text-Fig. 2) in being covered by needle-like thorns and in having fewer, larger pores.

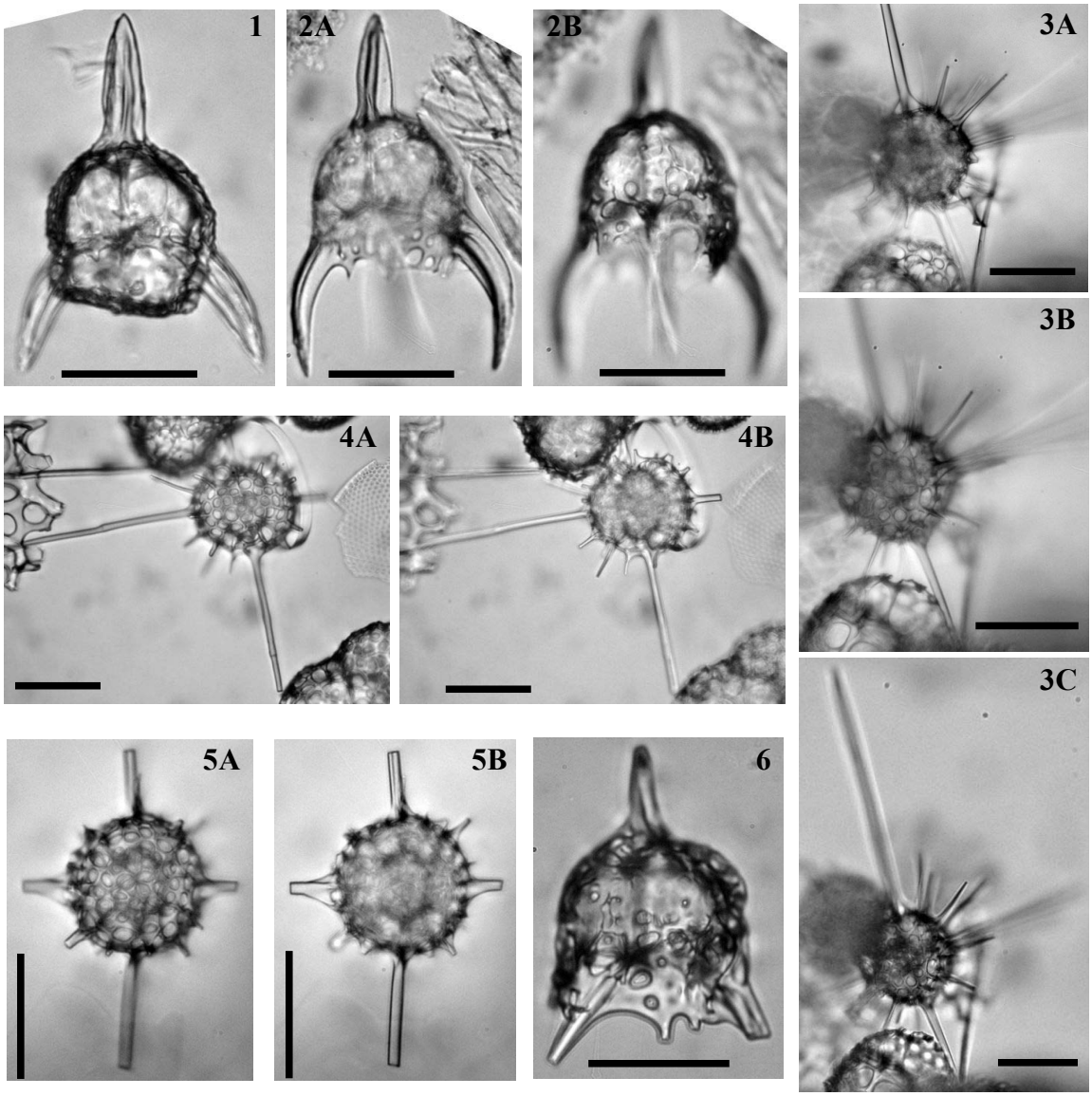

Plate 31.– 1. *Euscenarium*? sp2, Sample 119-744A-8H-1 53-55cm, Early/Middle Miocene. 2. *Euscenarium*? sp2, Sample 120-747A-9H-2 40-42cm, Early/Middle Miocene. 3. Spumellarian spB, Sample 120-747A-2H-5 45-47cm, Pleistocene. 4. Spumellarian spB, Sample 120-747A-2H-5 45-47cm, Pleistocene. 5. Spumellarian spB, Sample 120-747A-3H-1 45-47cm, Late Pliocene. 6. *Euscenarium*? sp2, Sample 120-748B-6H-3 45-47cm, Early Miocene. All scale bars 50 µm. Magnification x384 except for 3C (x192).

Genus *Giraffospyris* Haeckel 1881 emend. Goll 1969

Type-species: *Ceratospyris heptaceros* Ehrenberg 1873a

Giraffospyris circumflexa Goll 1969

1969 *Giraffospyris circumflexa* Goll: p. 332; pl. 60, figs 1-4; text-fig. 2

Genus *Gorgospyris* Haeckel 1881

Type-species: *Gorgospyris medusa* Haeckel 1887

Gorgospyris quinquespine Goll 1978

1978 *Gorgospyris quinquespine* Goll: p. 179; pl. 1, figs 11-12, 15

Genus *Liriospyris* Haeckel 1881 emend. Goll 1968

Type-species: *Liriospyris hexapoda* Haeckel 1887

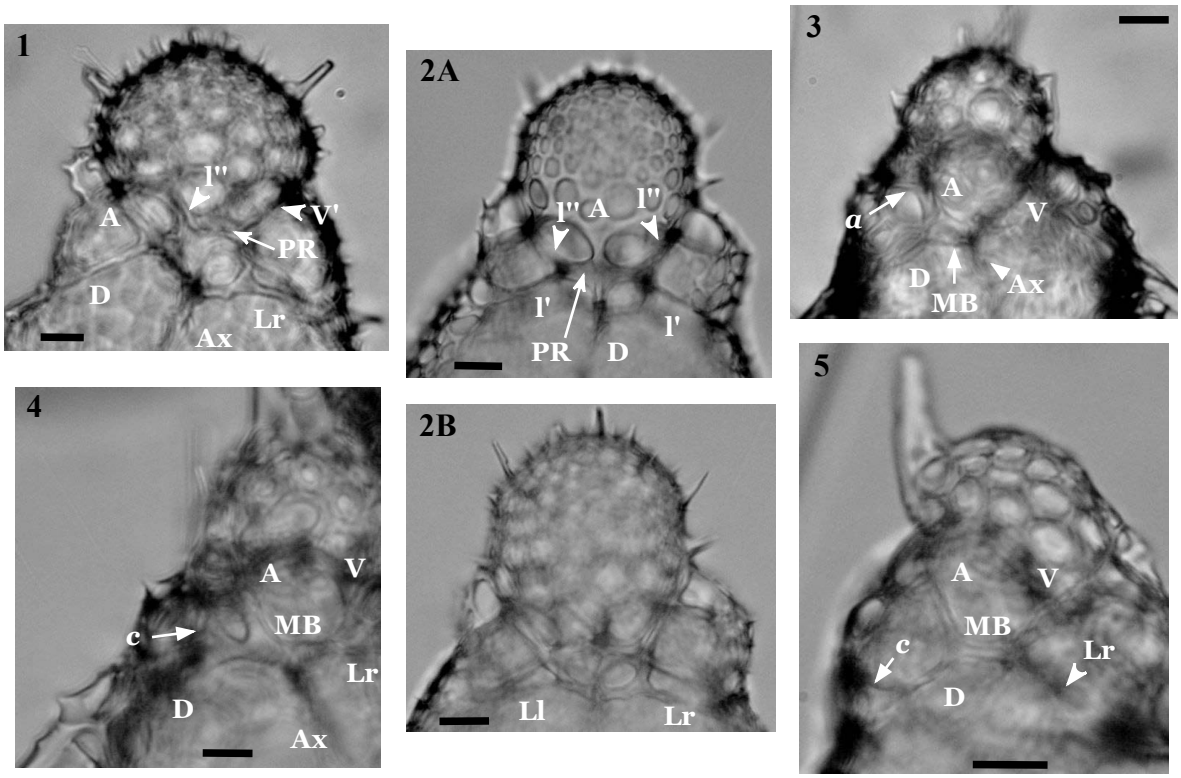

Plate 32.– Details of the inner structure of some of the specimens illustrated on plates 17 and 22.
1. *Botryopera*? *daleki* n. sp. Zoom on specimen from Pl. 17, fig. 10A-B. 2. *Botryopera*? *daleki* n. sp. Zoom on specimen (holotype) from Pl. 17, fig. 11A-C. 3. *Antarctissa evanida* n. sp. Zoom on specimen from Pl. 17, fig. 3A-B. 4. *Antarctissa evanida* n. sp. Zoom on specimen from Pl. 17, fig. 4A-B. 5. *Lithomelissa*? *kozoi* n. sp. Zoom on specimen from Pl. 22 fig. 11A-B.
Scale bars are 10 µm. Magnification is x384.

Liriospyris elevata Goll 1968

1968 *Liriospyris elevata* Goll: p. 1426-1427; pl. 175, figs 4-5, 8-9; text-fig. 9

Liriospyris mutuaria Goll 1968

1968 *Liriospyris mutuaria* Goll: p. 1428-1429; pl. 175, figs 6, 10-11,14; text-fig. 9

Genus *Lophospyris* Haeckel 1881 emend. Goll 1977

Type-species: *Ceratocyrtis polygona* Haeckel 1887

Lophospyris pentagona (Ehrenberg)

1976 *Lophospyris pentagona pentagona* (Ehrenberg) – Goll: p. 398; pl. 10; pl. 11, figs 1-3, 5

Genus *Phormospyris* Haeckel 1881 emend. Goll 1976

Type-species: *Phormospyris tricostata* Haeckel 1887

Phormospyris tricostata Haeckel 1887

1887 *Phormospyris tricostata* Haeckel: p. 1087; pl. 83, fig. 15
1966 *Phormospyris tricostata* Haeckel – Benson: p. 334-336; pl. 23, fig. 9

Phormospyris antarctica Haecker 1907

1907 *Phormospyris antarctica* Haecker: p. 124; fig. 9
1908 *Triceraspyris antarctica* (Haecker) – Haecker: p. 445; pl. 84, fig. 586

1976 *Phormospyris stabilis* (Goll) *antarctica* Haecker – Goll: p. 394; pl. 3; pl. 4; pl. 5, figs 3-6
1992 *Triceraspyris antarctica* (Haecker) – Abelmann: pl. 3, fig. 12

Phormospyris scaphipes (Haeckel 1887)

1887 *Tristylospyris (Tristylospyrula) scaphipes* Haeckel: p. 1033; pl. 84, fig. 13
1969 *Tholospyris scaphipes* (Haeckel) – Goll: p. 328-329; pl. 58, figs 1-8, 13-14; text-fig. 1
1976 *Phormospyris stabilis* (Goll) *scaphipes* (Haeckel) – Goll: p. 394-395; pl. 8, pl. 9

Phormospyris stabilis (Goll 1968)

1968 *Dendrospyris stabilis* Goll: p. 1422-1423; pl. 173, figs 16-18, 20; text-fig. 8

Phormospyris coronata (Weaver 1976)

1976 *Triceraspyris coronatus* Weaver: p.580; pl. 2, figs 4-5; pl. 6, figs 8-9
1992 *Triceraspyris coronata* Weaver – Lazarus: pl. 7, figs 5-9

Phormospyris sp. L
(Pl. 29, figs 15-17)

Remarks. This species differs from *P. coronata* in its deeply-set sagittal-lattice pores on the dorsal side and by its well-developed thoracic wall joining its three feet together.

Phormospyris loliguncula Renaudie & Lazarus in press
(Pl. 28, figs 1-3, 5A-6)

Derivation of name. *loliguncula* is Latin for a 'little squid'.
Diagnosis. Large lattice-sagittal pores on dorsal side; five or more thin, spine-like feet; latticed thorax.
Holotype. Pl. 28, figs 5A-B; Sample 120-751A-6H-1, 98-102cm (Late Miocene); ECO-041, circle 2.
Material. 56 specimens were observed from ODP Sites 689, 693, 746, 751 and 1138.
Description. The cephalis is bilobate, slightly constricted in its median part by a sagittal ring. The shell wall is rather thick, crested, with a highly variable pore pattern. The pores are usually rather small and elliptical, sometimes densely packed. Three pairs of large sagittal-lattice pores (the apical-most being usually the smaller and the basal-most the larger) are seen in dorsal view (Pl. 4, figs 4, 6 and 8). In some specimens, a thin secondary feltwork covers the basalmost pair of dorsal sagittal-lattice pores (Pl. 4, figs 6 and 8). In ventral view, the sagittal-lattice pores are small, of variable number and hardly discernable from the other lattice pores. An upward-directed ventral spine can be seen at the third of the height of the sagittal ring in ventral view. From the basal ring, several more or less robust feet extend (at least five: probably spines **D**, **Ll**, **Lr** and the two spines **l'**, but, because of the thickness of the shell and because we use mounted slides which do not allow us to rotate the specimens, the connections have not been precisely observed). They are shorter than the height of the cephalis. A thoracic latticed shell, in most specimens, grow between these feet: it is usually thin and perforated by circular to elliptical pores, irregular in size.
Dimensions. (based on 6 specimens) Total length: 126-141 (133); width of cephalis: 99-122 (105).
Occurence. Rare from the *Siphonosphaera vesuvius* to the Tau Zone (Late Miocene to Early Pliocene).
Remarks. *Phormospyris loliguncula* differs from *Triceraspyris antarctica* (Haecker, 1907), *T. pacifica* Campbell & Clark, 1942 and *T. coronata* Weaver, 1976 in its large dorsal sagittal-lattice

pores and having five or more feet. It also differs from *Ceratospyris laventaensis* Clark & Campbell, 1942 in its other pores being small and round, in the overall shape of the cephalis, in the latticed thorax and in the absence of spines on the cephalis.

Phormospyris sp. I
(Pl. 30, figs 3A-B)

Remarks. This species differs from such species as *Phormospyris* sp. L, *P. loliguncula*, *P. coronata* and *P. pacifica* Campbell & Clark 1944 in lacking feet and in its characteristic curved, barrel-shaped thorax consisting of a web-like anastomosed shell. Otherwise the cephalic shell itself and its deeply-set sagittal-lattice pores (along with the occasional secondary feltwork covering the basalmost pair of dorsal sagittal-lattice pores) are very similar to that of *P.* sp. L and *P. loliguncula*.

Genus *Platybursa* Haeckel 1881 emend. Petrushevskaya 1971
Type-species: *Cantharospyris platybursa* Haeckel 1887

Platybursa harpoi Renaudie & Lazarus in press
(Pl. 28, figs 7A-B, 12A-16)

? 1975 *Platybursa* sp. Petrushevskaya: pl. 8, fig. 5.

Derivation of name. Named after Harpo Marx, because the species, in profile view, looks like a harp.

Diagnosis. Trissocyclid with a thick, apically-elongated sagittal ring; numerous apophyses link spine **V** and the latticed shell.

Holotype. Pl. 28, figs 14A-B; Sample 120-747A-2H-1, 45-47cm (Middle Pleistocene); ECO-064.

Material. 145 specimens were observed from ODP Sites 738, 744, 747 and 751.

Description. D-shaped, thick, apically-elongated sagittal ring with a shorter, conical, downward-directed spine **D**. Spines **l'** are similar in size and shape to spine **D** but project laterally. Spines **Ll** and **Lr** also project laterally and terminate in several short bifurcations (Pl. 2, fig. 16B). A short, triangular axobate can also be seen below the junction of the median bar and spines **Ll** and **Lr**.

The latticed shell is connected to spine **A**, spines **Ll** and **Lr**, spines **l'**. It is also connected to spine **V** by numerous small apophyses (Pl. 2, figs 14, 16A).

The latticed shell has no sagittal constriction and bears numerous circular, elliptical or sometimes polygonal, irregularly-disposed generally small pores of various sizes. The width of the bars between the pores varies widely between the specimens or even on one single specimen (Pl. 2, fig. 13A). Typically, the shell outline is semi-ellipsoidal with a rounded apex but it can be more irregularly-shaped in some rare specimens (Pl. 2, figs 11A-B, 13A-B). Some specimens exhibit a small, conical apical horn (Pl. 3, figs 10A-B).

Dimensions. (based on 6 specimens) Height of shell: 117-151 (147); maximum width of shell in sagittal view: 72-104 (97); length of spine D: 23-39 (25).

Occurence. Common in the Chi Zone (Early Pleistocene); four specimens have also been found in the lower Upsilon Zone (Early Pliocene).

Remarks. *Platybursa harpoi* differs from *Platybursa cancellata* (Haeckel, 1887) and from the specimen illustrated in pl. 62, fig. 8 of van de Paverd, 1995 as *Lophospyris dictyopus* (Haeckel, 1881) in the apex being rounded, the sagittal ring being considerably thicker and the pores being larger and irregular in size and shape, *Platybursa clathrobursa* (Haeckel, 1887) and *Platybursa platybursa* (Haeckel, 1887) in being elongated apically and having a thicker sagittal ring.

Platybursa platybursa (Haeckel 1887)

1887 *Cantharospyris platybursa* Haeckel: p. 1051; pl. 53, fig. 7
1974 *Cantharospyris platybursa* Haeckel – Renz: pl. 19, figs 19a-b
1991 *Cantharospyris platybursa* Haeckel – Takahashi: pl. 31, fig. 5

Genus *Rhodospyris* Haeckel 1881

Type-species: *Rhodospyris tricornis* Haeckel 1887

Rhodospyris? sp. D

(Pl. 30, 4-6)

Description. Dicyrtid with bilobed cephalis. Thorax has ca. same height and same width as cephalis. Sagittal constriction is weaker than basal constriction. Thorax is barrel-shaped with open, ragged termination, bearing large, circular to elliptical pores. Cephalis bears few, relatively widely-spaced small, round to elliptical pores. One pair of sagittal-lattice pores around spine **V**. Apical horn is short and conical.

Rhodospyris sp. N

(Pl. 29, figs 4-6)

Description. Bilobed cephalis with no sagittal-lattice pores and a short conical apical horn. Pores on the cephalis are circular, evenly distributed and even in size (all relatively small). Shell wall extends below the basal ring as a cylindrical to inverted-truncated conical thorax with larger, more randomly-arranged pores. Thorax ends with a crown of several long, triangular teeth. Basal ring is marked by a constriction.

Remarks. This species differs from *Rhodospyris tricornis* Haeckel 1887 in having only one short apical horn instead of three long ones, in the thorax length (from basal ring to the beginning of the teeth) being somewhat equal to the cephalic length and in the sagittal constriction being relatively weak.

Genus *Tetracorethra* Haeckel 1887 emend. Petrushevskaya 1971

Type-species: *Tetraspyris tetracorethra* Haeckel 1887

Tetracorethra tetracorethra (Haeckel 1887)

(Pl. 29, fig. 14)

1887 *Tetraspyris (Tetracorethra) tetracorethra* Haeckel: p. 1044; pl. 53, figs 19-20
1971 *Tetracorethra tetracorethra* (Haeckel) – Petrushevskaya: p. 145; pl. 121, figs 1-4
1976 *Tetracorethra tetracorethra* (Haeckel) – Renz: p. 145; pl. 6, fig. 23

Genus *Tholospyris* Haeckel 1881 emend. Goll 1969

Type-species: *Tholospyris tripodiscus* Haeckel 1887

Tholospyris kantiana (Haeckel 1887)

1887 *Tricolospyris kantiana* Haeckel: p. 1098; pl. 88, fig. 10
1887 *Tricolospyris baconiana* Haeckel: p. 1098; pl. 88, fig. 8
1887 *Tricolospyris newtoniana* Haeckel: p. 1098; pl. 88, fig. 11
1969 *Tholospyris kantiana* (Haeckel) – Goll: p. 327; pl. 58, figs 17-19, 23; text-fig. 1

Tholospyris cortinisca (Haeckel 1887)

1887 *Tripospyris (Tripospyrantha) cortiniscus* Haeckel: p. 1026; pl. 84, fig. 6
1969 *Tholospyris cortinisca* (Haeckel) – Goll: p. 325; pl. 56, figs 3, 5-6, 8; text-fig. 1

Tholospyris gephyristes Hülsemann 1963

1963 *Tholospyris gephyristes* Hülsemann: p. 24-25; figs 14-15
1998 *Tholospyris gephyristes* Hülsemann – Bjørklund et al.: pl. 2, figs 20-21
2003 *Tholospyris*? *gephyristes* Hülsemann – Bjørklund & Kruglikova: pl. 6, fig. 18

Tholospyris sp. O
(Pl. 29, figs 9A-10B, 12A-C)

? 1969 "T4" Goll: 324, text-fig. 1.
? 1994 *Tholospyris* sp. "T4" Goll in Maharapatra and Sharma: 164, pl. 3, fig. 15-16.
Diagnosis. *Tholospyris* with unequal pairs of sagittal-lattice pores in front view; latticed shell extends below basal ring but not above apex; constriction at basal ring.
Material. 24 specimens were observed from ODP Sites 744, 747 and 748.
Remarks. *Tholospyris* sp. O differs from *T. kantiana* (Haeckel, 1887), *T. baconiana* (Haeckel, 1887) and *T. newtoniana* (Haeckel, 1887) primarily in the latticed shell extending below the basal ring but not above the apex. It also differs from the specimens illustrated as "T4" in Goll, 1969 and *T. sp* "T4" Goll in Mahapatra and Sharma, 1994 in the two pairs of sagittal-lattice pores in front view being unequal in size and in the latticed shell below the basal ring lacking a large aperture just below the latter. It finally differs from *Dendrospyris(?) sakaii* Sugiyama and Furutani, 1992 mostly in its peculiar apical structure and in the pattern of the lattice shell below the basal ring.

Family ***Incertae sedis***

Nassellarian sp. B
(Pl. 27, figs 6A-7B)

Remarks. This species (or group of species) has a large variability however five elements seem characteristic: a large incurved apical horn, numerous supplementary cephalic horns, a dorsal shoulder (stuck under arches **AL**), a wavy thorax and very few, widely spaced small pores on both thorax and cephalis.

Nassellarian sp. D
(Pl. 27, figs 2-3)

Description. Small dicyrtid with a tiny, very thick, poreless, hemispherical cephalis bearing numerous conical horns (among which an apical and a ventral horn but also numerous additional horns) and a conical thorax with ragged end. Spines **D**, **Ll** and **Lr** can be clearly seen forming ridges on the thoracic wall of one specimen (Pl. 27, fig. 2). Pores on the thorax increase in size from the upper part to the lower part: they are round to elliptical and more or less aligned longitudinally. The upper thorax also bears numerous spines that echo the ones on the cephalis.
Remarks. Because of the very small size of the cephalis (diameter ≤ 10 µm) and its thickness, the inner spicule organization and its relationship with the rest of the skeleton is hard to assess, rendering the familial assignment of this species problematic: it seems reasonable to think that this species is either a Theoperidae (because of the size and the shape of the cephalis and the fact that the collar stricture seems to be indeed at the same level as **MB**) but can as well be a Plagiacanthidae (specifically a Lophophaenidae). The longitudinal alignment of the pores on the thorax is recurrent in Theoperidae and rarer in Lophophaenidae (though still known to exist:

e. g. *Ceratocyrtis*? *morawanensis*, *C.*? *cantharoides* or *Velicucullus oddgurneri*).

Genus *Lithostrobus* Bütschlii 1882

Type-species: *Eucyrtidium argus* Ehrenberg 1875

Lithostrobus hexagonalis Haeckel 1887

1887 *Lithostrobus hexagonalis* Haeckel: p. 1475; pl. 79, fig. 20
1968 *Lithostrobus hexagonalis* Haeckel – Nigrini: p. 58; pl. 1, fig. 10
1972 *Stichocapsa hexagonalis* (Haeckel) – Petrushevskaya & Kozlova: p. 546; pl. 25, fig. 1
1991 *Lithostrobus hexagonalis* Haeckel – Takahashi: p. 122; pl. 41, figs 1-3

Genus *Stichopilium* Haeckel 1881

Type-species: *Stichopilium bicorne* Haeckel 1887

Stichopilium bicorne Haeckel 1887

1887 *Stichopilium bicorne* Haeckel: p. 1437; pl. 77, fig. 9
1976 *Stichopilium bicorne* Haeckel – Renz: p. 125-126; pl. 4, fig. 9
1992 *Stichopilium bicorne*? Haeckel – Lazarus: pl. 9, figs 9-10, 12-17

Stichopilium variabile Popofsky 1908

1908 *Stichopilium variabile* Popofsky: p. 290; pl. 35, figs 4-7
1958 *Stichopilium variabile* Popofsky – Riedel: p. 240; pl. 4, fig. 5; text-fig. 11
1967 *Stichopilium variabile* Popofsky – Petrushevskaya: p. 116; pl. 68, fig. 3
1984 *Stichopilium variabile* Popofsky – Nishimura & Yamauchi: pl. 39, figs 8a-b

Testing the accuracy of paleodiversity reconstitutions using whole-fauna data

Introduction

Reconstructing paleodiversity has become a major theme in paleobiology. To circumvent the numerous biases caused by the incompleteness and misrepresentativity of most fossil records (varying sample size, differential preservation among species, habitat or environment, etc [Bush et al. 2004; Smith & McGowan 2011]), a large number of statistical methods to produce such reconstructions have arisen in the literature. Subsampling procedures in particular (e.g. Shinozaki 1963; Alroy 1996, 2000; Foote 2000) have been designed to compensate heterogenous sampling effort.

Because of the nature of its extraordinary fossil record (very large number of individuals, relatively constant and widespread biogeographic and sedimentary regions, organisms with a wide variety of biological properties or ecological niches found together in the same samples), marine micropaleontology offers a unique resource for paleobiology (Lipps 1981; Lazarus 2011). Yet, it is only recently that this potential has started to be exploited with macroevolutionary studies based on large, global datasets (Rabosky & Sorhannus 2009; Kaminski et al. 2010; Liow et al. 2010; Kiessling & Danelian 2011; Lloyd et al. 2011; Ezard et al. 2011), thanks to the creation and the use of fossil occurrence databases such as the Paleobiology Database (Alroy et al. 2001), mostly for Mesozoic microfossil data, and the Neptune database (Lazarus 1994; Spencer-Cervato 1999), the latter containing much of the (largely Cenozoic) microfossil occurrence data published in the context of the DSDP/ODP drilling campaigns.

Neogene radiolarians offer material for an interesting case study: with the exception of the skeletonless members of the Thalasicollidae, all living families of radiolarians are recorded in the fossil record (De Wever et al. 2001) and more than 90% of the species are considered to be preserved (Lazarus 2011). Samples from more than 100 Neogene radiolarian-bearing sections recovered by DSDP and ODP deep drilling campaigns usually contain ~103 to 105 specimens

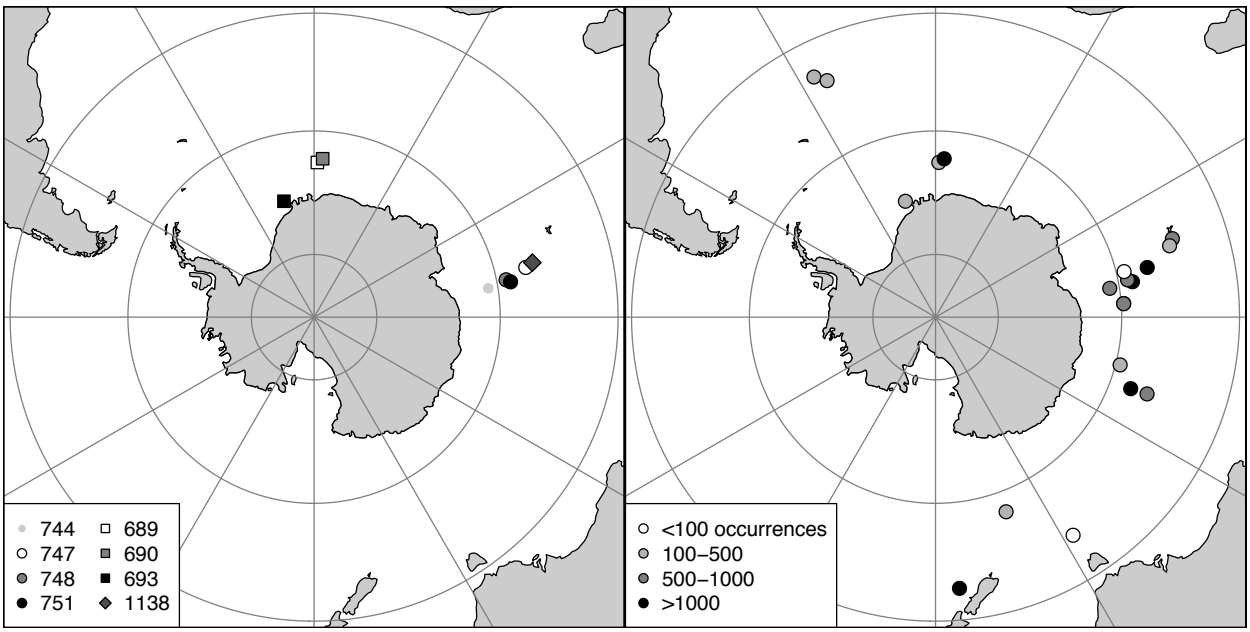

Figure 1.– Location of studied sites.
a. Location of sites in the whole-fauna dataset.
b. Location of sites in the Neptune dataset. (Color correspond to the number of occurrences for each site)

per gram of dry sediment, thus allowing uniform, large sample sizes (Lazarus 2011).

The biggest bias in this material is therefore the recording effort. This has been historically low, compared to what the material actually allows (Lazarus 2011). Thus the available published data, compiled in databases like Neptune, are only a subset of the preserved diversity and are similar to the, also incomplete, diversity data for other groups of fossil organisms more commonly studied for paleodiversity (e.g., Alroy 2010a). It should therefore be possible to collect taxonomically complete data from deep-sea sediment samples, and compare the diversity found to that reconstructed using standard paleobiologic methods from the incomplete published data, as has been implemented in this study.

We have chosen a single Neogene biogeographic province - the Southern Ocean, which has had a largely endemic radiolarian fauna since the mid-Paleogene (Lazarus & Caulet 1994). We collected a quantitative, taxonomically-complete dataset on the occurrences of Antarctic radiolarian species in numerous samples ranging from ca. 23 to 0 Ma (i.e., Neogene and Quaternary samples). Lastly, we have compared the diversity trend retrieved by our dataset and the ones produced using "classical" diversity reconstructions from the more incomplete published data in the Neptune database, as an empirical test of these methods' accuracy.

Material

1. Whole-fauna dataset:

For this work we used many of the same microscope slides used in earlier published studies (i.e., Lazarus 1990, 1992; Vigour & Lazarus 2002), but, unlike these earlier studies, where time and manpower constraints restricted data collection to a limited number of (primarily biostratigraphic or paleoenvironmental marker) taxa, we documented all taxa seen, including many rare species, and species of no known biostratigraphic or paleoenvironmental significance. Other previously prepared slides were drawn from a library of pre-made slides not yet previously examined for their content that are held in the MRC radiolarian collection hosted by the Museum für Naturkunde in Berlin (Lazarus 2006). Our taxonomic survey resulted in a Neogene Southern Ocean species list of 492 species, nearly double the number previously known from this region, and including nearly 100 species new to science (see Chapter 2).

Samples were chosen for whole-fauna analysis (Fig. 1) from the Atlantic sector of the Southern Ocean (ODP Leg 113 Sites 689, 690 and 693) and from the Kerguelen Plateau (ODP Leg 119 Site 744, Leg 120 Sites 747, 748 and 751 and Leg 183 Site 1138). Although there are regional differences in species' abundances in different sectors of the Southern Ocean, and strong gradients in species distributions as one crosses the frontal systems that mark the northern boundary of the province, the strong circumpolar circulation maintains the entire Southern Ocean as a single biogeographic province (e.g. Hays 1965; Boltovskoy 1995; Longhurst 1995), and our sampling distribution is sufficient to recover all species present in this biogeographic region.

The MRC slides, and additional new samples taken for this study, were prepared to random strewn slides using standard methods (Moore 1973) using 45 µm sieves. Although we did not encounter any species in our study that was completely absent in larger size fractions, use of 45 µm sieves improves the recovery of smaller radiolarian species, including many smaller nassellarian taxa that appear less abundantly or only rarely using the more commonly used 63 µm sieves. Larger sieve sizes concentrate larger, more easily identified specimens and reduces the amount of non-radiolarian material (e.g., diatoms), and 63 µm was the most common size used in many older studies (e.g., Chen 1975; Weaver 1976, 1983; Lazarus 1990, 1992) that are compiled in the Neptune database, although some previous published studies of

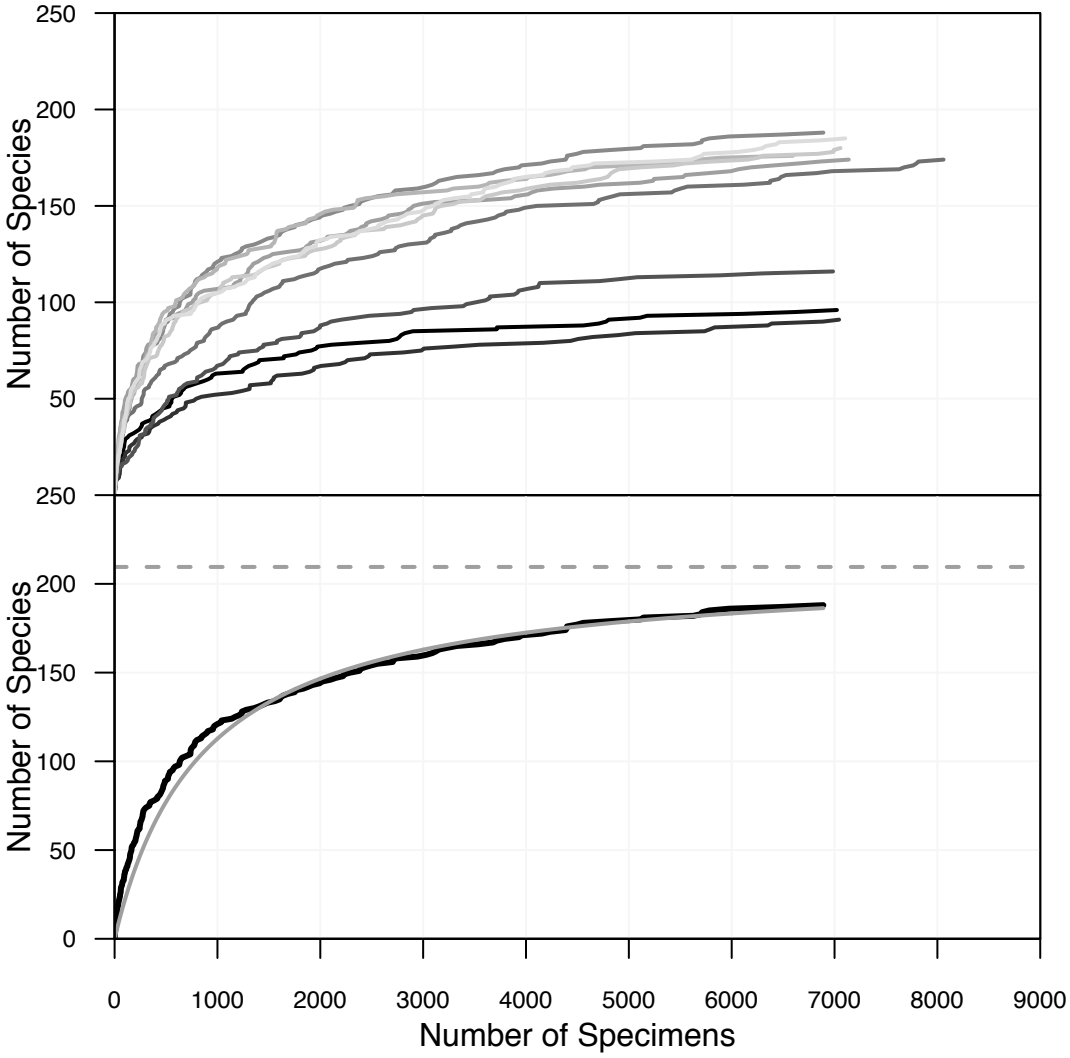

Figure 2.– Completeness metrics.
A. Several species accumulation curves from samples of various ages.
B. Species-accumulation curve on a typical sample (sample 120-751A-6H-6, 98/102cm, Late Miocene). Bold black curve is the species accumulation curve; light grey curve and dashed light grey line are, respectively, the de Caprariis et al. (1976, 1981) curve-fitting and its asymptote.

Antarctic Neogene sediments have used a variety of other sieve sizes, from 38 to 80 µm. Although the use of different sieve sizes can complicate comparisons between quantitative datasets, it should not affect basic presence-absence data on species occurrences, so long as the taxon is recorded at all.

The Neogene record of Southern Ocean radiolarians, while having distinct advantages over numerous other possible microfossil materials, also has some disadvantages, most notably an unusually (for deep-sea sedimentation) dynamic depositional history, which has created a substantial number of hiatuses, and made it difficult to develop highly accurate age models for many sections. All sample ages were assigned based on the age models used in the Neptune database (Lazarus et al. 1995). As Leg 183 Site 1138 is absent in the database, its age model was drawn from Bohaty et al. (2003). For many of our sections age errors for individual samples may be as high as 1 My, although the mean error is likely to be less than 0.5 My. Sampling within each of our sections was not uniform, due to the presence in several sections of hiatuses, and, within the early Miocene of some sections, of a short interval of generally poor radiolarian preservation. All of our age models use the Berggren et al. (1995) geochronologic scale. While

the age model quality is moderate to good for newer sites, particularly those also used for our whole fauna data collection, the age model quality for some of the older sites used in the Neptune data is only fair. We include these older sites to improve the taxonomic scope of the Neptune data and to include a larger amount of data from a wider variety of authors. Inclusion of larger numbers of authors in compiled micropaleontology literature data improves sampling of diversity (see Discussion). For our whole-faunal data we took 98 samples, providing an average sample density of ~4 per My.

Approximately 7,000 specimens were recorded for each sample, using a stratified procedure in which, in a first step, all taxa are counted on a certain number of tracks until the count reaches ca. 2,000 specimens; then, countings are resumed but the species that accounts for more than five percent of the assemblages in the first step (usually the two to six most abundant species) are not counted anymore but estimated using the mean number of specimens per track observed in the previous step. The number counted in each sample varied somewhat and was based on the behavior of the cumulative specimen-diversity curve that was computed dynamically during counting. Counting continued until the specimen-diversity curve began to flatten. In some cases more than one complete 45 µm slide was examined per sample in order to obtain the required number of specimens. As can be seen on Figure 2, a typical species accumulation curve for even our most diverse, early Late Miocene samples usually begins to flatten between 4000 and 6000 specimens. The high amount of specimens recorded per sample thus assures us a taxonomical coverage close to completeness: Good (1953)'s coverage estimator (u) for our samples range from 0.992 to 0.999, while, if we are to believe diversity estimators such as ACE (Chao & Lee 1992; Colwell & Coddington 1994) or curve-fitting extrapolation (de Caprariis et al. 1976, 1981), we are recovering in most individual samples more than 80% of the species present. In all more than 700,000 individual specimens were recorded.

2. Neptune database:

The Neptune database contains species occurrences as reported in the scientific publications of the Deep Sea Drilling Project and Ocean Drilling program. Only occurrences for sections where a reasonable (if often still imperfect, see above) age model is available were included (Lazarus 1994; Spencer-Cervato 1999). For our current study we used the latest implementation of this database - Neptune Sandbox Berlin (NSB) which is managed by the junior author. A dataset consisting of the majority of Neogene radiolarian bearing sections drilled in the Southern Ocean, and including all the dated occurences in the database below 40°S was retrieved from Neptune. The dataset consists of 12,749 occurences of 286 species taken from 956 samples: 524 from the Kerguelen Plateau (ODP Legs 119 and 120), 209 from the Atlantic sector of the Southern Ocean (DSDP Leg 71 and ODP Leg 113) and 223 from the easternmost part of the Indian sector of the Southern Ocean (DSDP Legs 28, 29 and 90). A pacman trim of 5% of the youngest and 3% of the oldest occurrences for each species was applied, following values established in Lazarus et al. (2012). Results for raw data were virtually identical, suggesting that erroneous data in this Neptune dataset are minimal, which is more generally confirmed, at least for radiolarian data, by the analyses of Lazarus et al. (2012).

Methods

1. Subsamplings

The dataset retrieved from the Neptune dataset was processed using several types of subsampling procedures: classical rarefaction (CR, with a quota of 100 occurences) (Sanders 1968), unweighted by-list (UW, with a quota of 10 collections) (Shinozaki 1963), occurence-

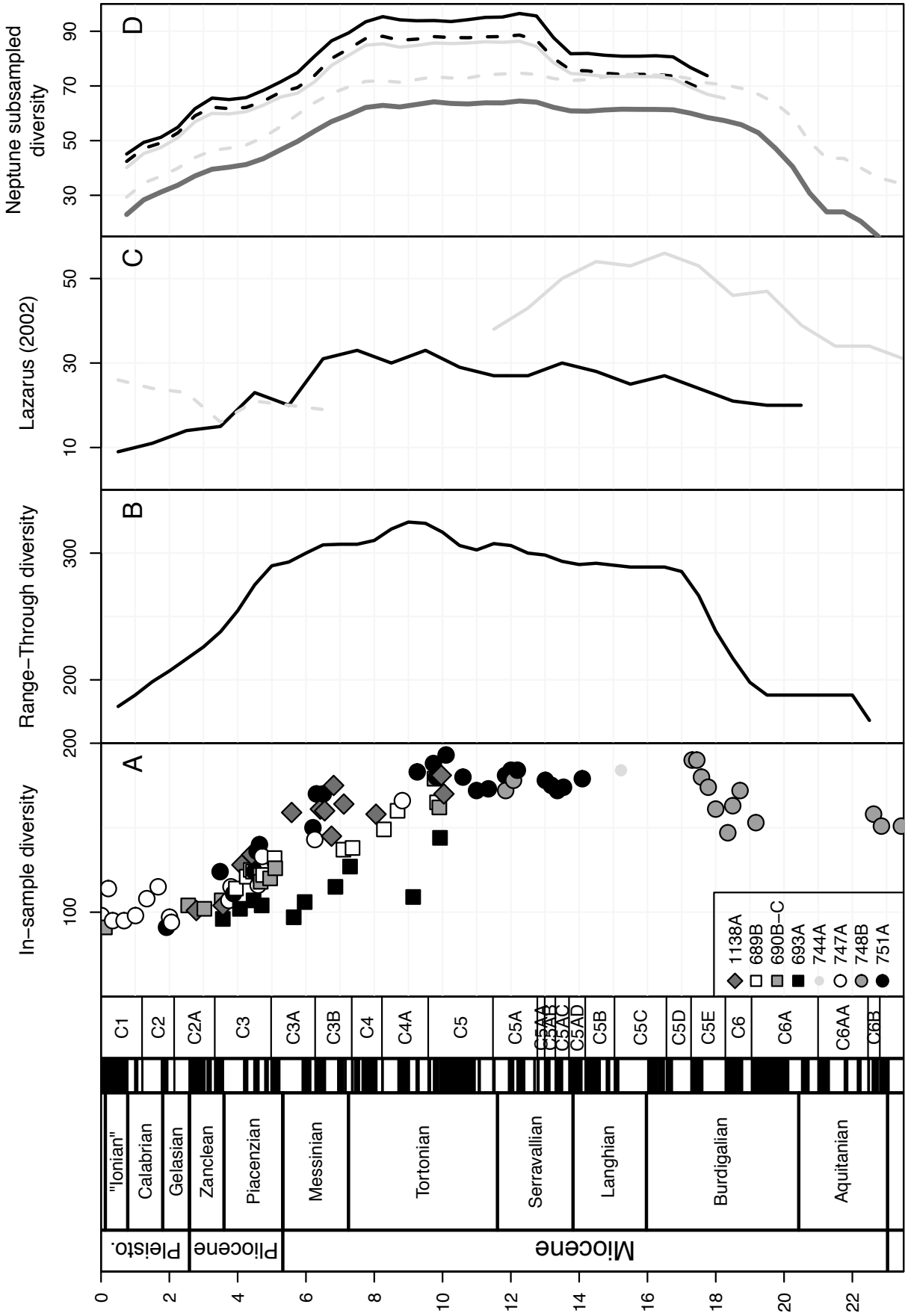
In−sample diversity
Range−Through diversity
Lazarus (2002)
Neptune subsampled diversity
A
B
C
D
1138A
689B
690B−C
693A
744A
747A
748B
751A
C1
C2
C2A
C3
C3A
C3B
C4
C4A
C5
C5A
C5AA
C5AB
C5AC
C5AD
C5B
C5C
C5D
C5E
C6
C6A
C6AA
C6B
"Ionian"
Calabrian
Gelasian
Zanclean
Piacenzian
Messinian
Tortonian
Serravallian
Langhian
Burdigalian
Aquitanian
Pleisto.
Pliocene
Miocene

Figure 3.– Antarctic Neogene radiolarian diversity.
A and B: Respectively, in-sample species richness and range-through diversity in our whole-fauna dataset. C: Diversity curves previously published in Lazarus (2002) where Caulet (1991)'s (dashed grey line), Lazarus (1992)' (black line) and Abelman (1992)'s (grey line) datasets were processed independently from one another. D: Diversity computed from the Neptune dataset with five different type of subsampling: UW (black line), OW (dashed black line), CR (light grey line), O2W (dashed light grey line) and SQS (bold dark grey line).
Magnetostratigraphy from Berggren et al. (1995).

weighted by-list (OW, with a quota of 100 occurences) (Alroy 1996), occurence-squared-weighted by-list (O2W, with a quota of 500 squared-occurences) (Alroy 2000) and the 'Shareholder Quorum' method (SQS, with a quota of 0.60 and dominant taxa included) (Alroy 2010a, b). These subsampling procedures were scripted and computed in R (R Development Core Team 2011).

As a point of comparison, we also show the results of a previously published study (Lazarus 2002). This study synthesised three independent previously published datasets focusing on ODP Legs 119 and 120 Kerguelen Plateau Sites (Caulet 1991; Abelmann 1992; Lazarus 1992) and consisted of data for 168 species. The data had been collected by a group of workers who cross-correlated taxonomies and methods, were carefully cleaned by elimination of potentially reworked specimens, utilisation of an uniform taxonomy, and other measures. No subsampling was used and diversity was calculated solely on species' first and last occurences in each dataset.

2. Diversity metrics

Standing mean diversities based on boundary crossers (Foote 2000) were computed using 0.5 My time bins on our new whole-fauna dataset and on each of the five subsampled versions of the Neptune dataset (Fig. 3). Extinction and origination rates (Foote 2000) were also computed on our dataset and on the UW and the SQS-subsampled Neptune dataset (Fig. 4). Diversity, extinction and origination metrics for the Lazarus (2002) study are shown as previously published (i.e., classic range-through diversity using 1My bins, and percentage of species going extinct -or appearing- in the bin scaled to the bin total diversity; Fig. 3 and 4).

3. Ecological metrics

The ecological pattern present in our dataset is summarized here (Fig. 5) using Shannon's evenness index (Boltzmann 1872; Shannon 1948) and a sample-by-sample Morisita-Horn similarity index (Morisita 1959; Horn 1966).

Lazarus (2011) noted that much previously published deep-sea micropaleontology data may have been compiled using fixed-list methods, and in particular, biostratigraphic marker taxa. We have calculated the proportion of occurences belonging to the 40 species classically used and preferentially recorded as biostratigraphical markers in the literature (Table 1; Lazarus 1992; Spencer-Cervato 1999) for both our new whole-fauna dataset and the Neptune dataset (Fig. 6).

Finally, the Pacman trimming procedure (Lazarus et al. 2012) was applied on our whole fauna dataset, with several sets of quotas (3, 5 and 12% of the abundances for the top of the ranges were trimmed and 1, 3 and 8% for the bottom), to study the effect of a possible (respectively) moderate, strong and very strong specimen displacement (upsection and downsection) in the stratigraphic column on the diversity pattern (Fig. 7).

Results

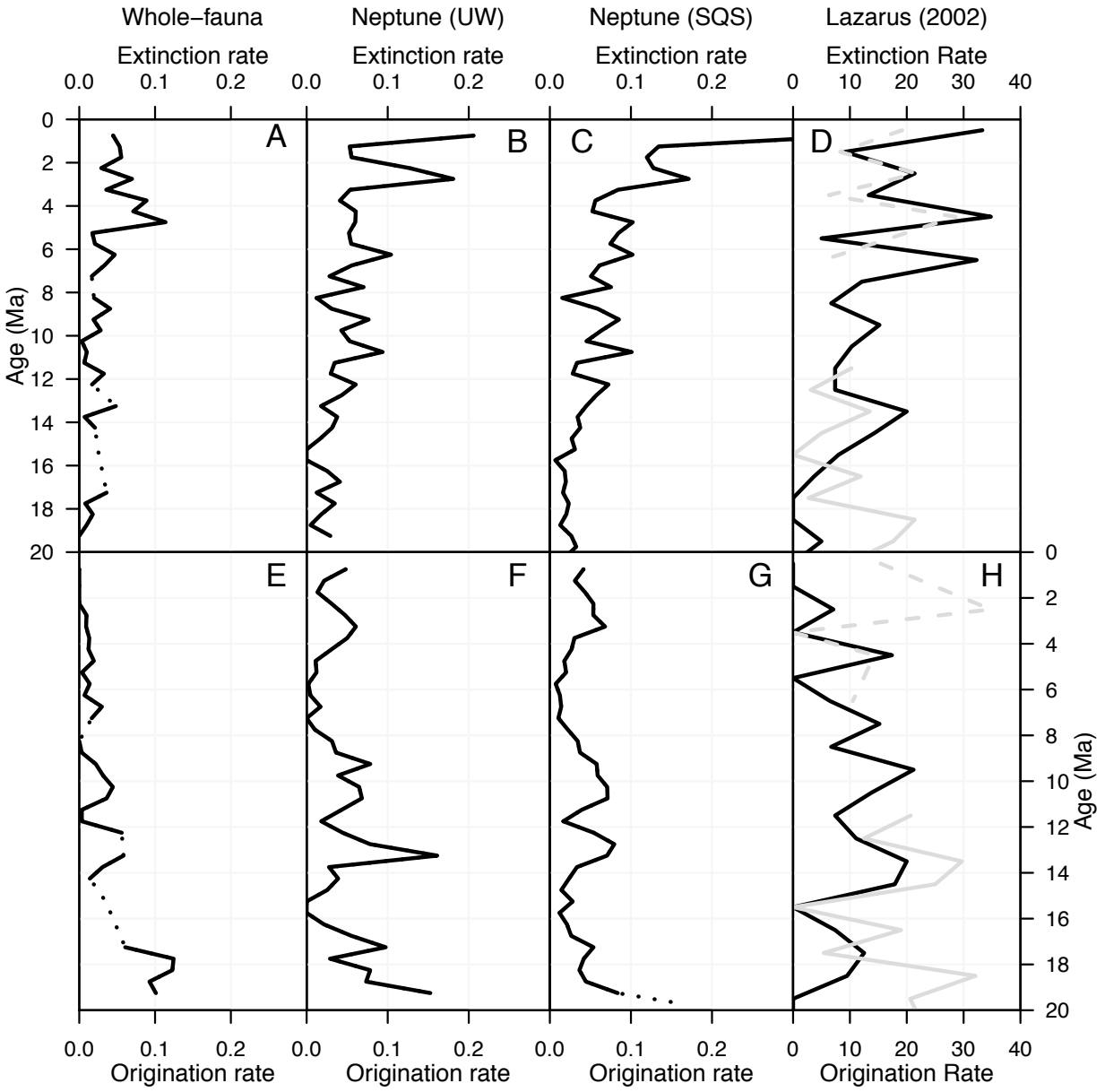

Figure 4.– Extinction and origination rates for our whole-fauna dataset (A and E, respectively), the UW (B and F) and the SQS (C and G) subsampled Neptune dataset. Extinction and origination rates previously published in Lazarus (2002) are also shown (D and H).

1. Observed diversity trend

The general trend in our data (Fig. 3A-B) show an increase in diversity at the end of the Early Miocene (between 19 and 17Ma), after which it reaches a plateau, followed by a slight increase in the early late Miocene and an equally slight decrease in the late late Miocene. Diversity then begins to drop quite rapidly at ca. 5 Ma. Depending on whether the within-sample or range-through results are used, this diversity drop ends ca 1.5 My later (Fig. 3A) or continues, at a slightly reduced rate of decrease, to the end Pleistocene and top of our dataset (Fig. 3B).

The Neptune dataset subsampled with classical rarefaction, occurence-weighted or unweighted by-list subsampling (Fig. 3D) shows the same main diversity trend as our whole fauna dataset. Diversity increases in the early Miocene, becomes fairly stable in the mid to late Miocene, and declines to lower values in the Pliocene and Pleistocene. However two significant

differences can be seen between those reconstructions and our whole-fauna dataset diversity. First a rather abrupt, if fairly modest increase in diversity at ca. 13 Ma is shown by several of the subsampled diversity curves. More significantly, while the Late Miocene diversity drop begins at ca. 5 Ma on our curve, it starts to occur at ca. 8 Ma in the subsampled curves: there is a 3 My lag between the two otherwise similar patterns.

Both the occurence-squared weighted by-list subsampling and the 'shareholder quorum' subsampling show another lag in comparison to the whole-fauna dataset in the early Miocene, where the subsampled Neptune data indicates an increase in diversity between 21 and 19 Ma, vs. an increase only 2 My later in the whole-fauna data. However, the whole-fauna data from the lower Miocene is based on a single site and is not stratigraphically complete, so this difference may simply reflect differences in sample coverage.

Finally, as shown on Figure 3C, the diversity pattern described in Lazarus (2002) peaks at ca. 16 Ma to decrease, first, at ca. 13 Ma and then at ca. 6.5Ma. It then increased again in the Plio-Pleistocene. Though this pattern exhibits the late Miocene drop in diversity observed in our material, in most respects it does not follow either our whole-fauna main diversity trend, or the trend seen in the subsampled Neptune data.

Reworking, age model errors and, to a lesser extent, other stratigraphic displacement mechanisms are recurring problem when dealing with deep-sea microfossils (Lazarus 2011), and although these problems are most common in compilations of data from different sources, they can in principle affect our data as well. We have chosen sites with reasonably good age models but these are not perfect, and for the Miocene, can still have age errors of 1 My or more. Further, because of the large numbers of specimens we counted in each sample, the likelihood of counting a displaced specimen (reworking, mis-identification) is higher in our dataset than in most published datasets. Since these mechanisms displace occurrences in time they could in principle affect our diversity pattern. Pacman style trimming of species occurrences from the ends of ranges is designed to remove such errors from datasets, and can be used to test, and if neccessary, remove the effects of these range distortions on our diversity calculations. Figure 7 shows however that even a strong trimming of each taxon range doesn't noticeably affect the observed trend. Only the early Late Miocene bump seen on our range-through diversity curve seen to be accentuated by this occurence trimming. The timing of diversity drop at ca 5 Ma is not affected, even with a very strong trim of species ranges.

2. Diversity dynamics

Our whole-fauna dataset shows, for the extinction rate (Fig. 4A), a somewhat random, noisy pattern and very low average extinction rates until the Miocene-Pliocene boundary where an abrupt, substantially higher extinction rate develops at ca. 5 Ma. Average extinction rates in our whole fauna data are noticably lower than in any of the other datasets analysed. Whole fauna origination rates (Fig. 4E) show relatively high values in the Early Miocene followed by a less high yet somewhat sustained Mid-Miocene interval with two origination peaks at around 13 and 10 Ma. Origination rates decline to very low values in the late Neogene and Quaternary.

The pattern shown by the UW-subsampled Neptune dataset follow the first-order trend seen in the whole fauna data with a few major exceptions: a much stronger peak at ca. 13 Ma (corresponding obviously to the increase in diversity observed on Fig. 3D) and a substantial increase at ca. 3.5 Ma of the origination rate (Fig. 4F), where the whole faunal data shows low and constant rates of origination. The extinction rate in the UW-subsampled Neptune dataset, though following a the first-order increasing trend seen in the whole-fauna data, does not show a clear acceleration of this trend during near the Miocene-Pliocene boundary as in the whole

faunal data. A large extinction rate peak is also noticeable around 2.5 Ma in the UW-subsampled dataset (Fig. 4B) which is entirely absent in the whole-fauna data.

The SQS-subsampled Neptune dataset exhibits a pattern very similar to that of the UW-subsampled except for one clear improvement: the reduction of the 13 Ma origination peak. The resulting origination rate (Fig. 4G) is therefore very comparable to that seen in our whole-fauna dataset, at least as far as the Miocene is concerned. However the ca. 3.5 Ma increase in origination is still a noteworthy difference with the pattern we retrieved with our whole-fauna dataset.

The Lazarus (2002) study, finally, showed a very noisy pattern for both the extinction and origination rates (Fig.s 4D-H). The only noteworthy event, which was also stressed by Lazarus (2002) is an increased extinction rate starting at ca. 6.5 Ma.

3. Ecological metrics

A self-similarity recurrence plot (Fig. 5A) shows the overall pattern of similarity (using Morisita-Horn overlap index) between each couple of samples based on the abundances of all species, here arranged by geologic age. In this index, the presence or absence of extremely rare species has almost no effect on the similarity value. The index is affected by change in abundances (at the extreme, extinction) of more common forms. Similarity ranges from 1 (identical taxa and relative abundances) to 0 (no similarity, e.g., no taxa at all in common). As is to be expected in a time series with substantial origination and extinction, samples of similar age are more similar to each other, with low values of similarity between samples of very different age. If change over time in species abundances were continuous and uniform, the plot would show a diagonal of maximum similarity and uniform decreases in similarity moving directly away from the diagonal. Change in similarity of abundances however has not been uniform over time. The largest change in similarity over the Neogene occurs rather abruptly between 8 and 9 Ma. Other secondary, less significant dissimilarity events are also shown by this plot, such as one at ca. 13 Ma and another one between 4 and 5 Ma which leads to a very stable Plio-Pleistocene community (all samples from ca. 4 to ca. 1 Ma being almost identical to one another with a Mosita-Horn index higher than 0.8). Characteristics of the faunal composition that influence the similarity result are shown in Fig. 5B-C. The evenness pattern observed in our whole-fauna dataset shows a very clear pattern of change (Fig. 5B): there is a shift from very equitable to highly dominated assemblages which occurs over the interval between 10 and 8 Ma. This is caused in large part by the dramatic increase in the relative abundance of a few species, particularly those within the nassellarian genus *Antarctissa*, which increase from <20% before 10 Ma to >40% by 8 Ma (Fig. 5C). The impact of these shifts are reflected on the sample-by-sample similarity plot (Fig. 5A) e.g., the abrupt dissimilarity event between 9 and 8 Ma.

4. Environmental context

We cannot here attempt a full review of Southern Ocean paleoceanography, nor at the moment do we have much information on the ecologic preferences of most radiolarian species, particularly extinct ones. Thus a functional understanding of the mechanisms driving the

Figure 5.– Ecological metrics.
A: Sample-by-sample self-similarity plot, using here the Morisita-Horn index (Morisita 1959; Horn 1966): the color key represents the value of the index, while the x and y-axis both represents time (in Ma).
B: Evenness (here, Shannon H' index) for studied samples.
C: Mean relative abundance in each time bin of the species of genus *Antarctissa* (*Antarctissa cylindrica* Petrushevskaya 1975, *A. ballista* Renaudie and Lazarus 2012, *A. deflandrei* Petrushevskaya 1975, *A. denticulata* (Ehrenberg) 1844, *A. evanida* Renaudie and Lazarus *in press*, *A. robusta* Petrushevskaya 1975 and *A. strelkovi* Petrushevskaya 1967).

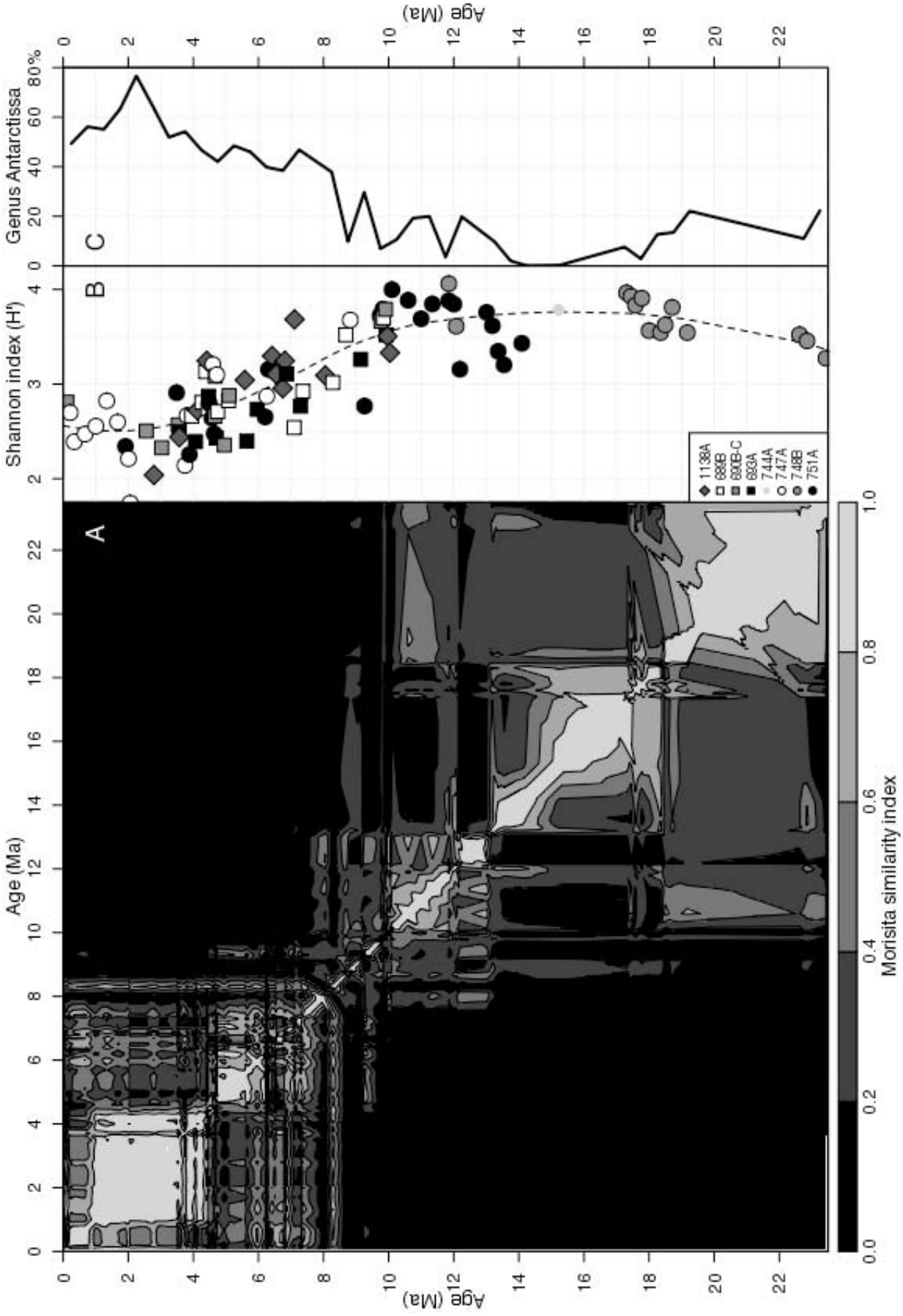
A
B
C
Age (Ma)
Shannon index (H')
Genus Antarctissa
Morisita similarity index
1138A
689B
690B-C
693A
744A
747A
748B
751A

evolutionary patterns observed is not yet possible. Here we wish simply to explore if there is any obvious pattern in the known record of Southern Ocean environmental change that might correlate to our radiolarian diversity pattern. Figure 8 summarizes a few aspects of the Neogene paleoenvironmental history of the Southern Ocean. The benthic signal of carbon isotope ratios (from Mackensen et al. [1992], Wright & Miller [1992] and Billups [2002]) shows an increase between ca. 18 and 15 Ma, followed by a steady decline until ca. 8 Ma where its value shifts

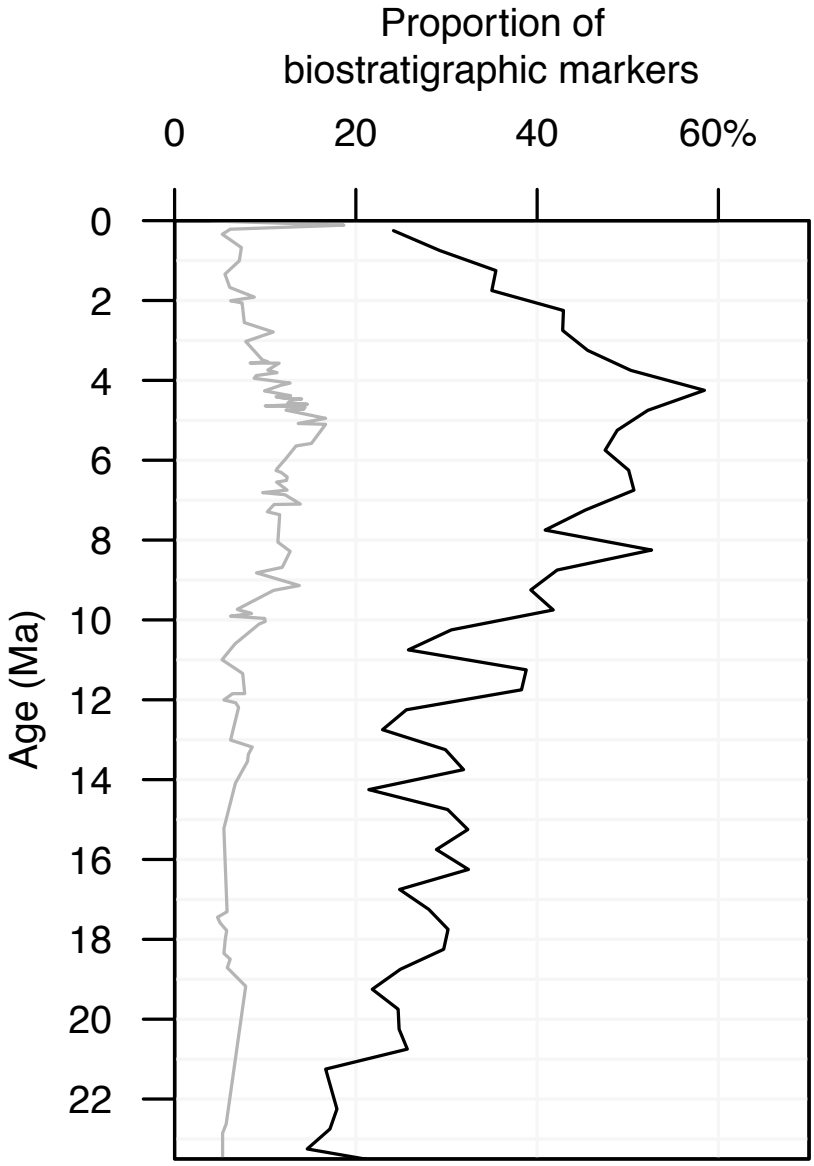

Figure 6.– Proportion of the 40 species classically used as biostratigraphic markers in Southern Ocean sediments among total occurences in our whole-fauna dataset (grey line) and the Neptune dataset (black line).

toward negative values quite abruptly. This event is known as the Late Miocene Carbon Shift (Haq et al. 1980; Tedford & Kelly 2004; Waddell et al. 2009): although widespread, it is thought to have occured earlier and with greater intensity in the Southern Ocean (Billups 2002; Hodell & Venz-Curtis 2006). Though poorly understood, it is thought to be linked to the development of a modern interbasinal $\partial^{13}C$ gradient and, to some extent, to the growth of the West Antarctic Ice Sheet and the initiation of the modern bottom water formation process (Hodell & Venz-Curtis 2006; Waddell et al. 2009).

The record of fossilisable primary producer abundances in the studied sites (calcareous nannofossils and diatoms, Fig. 8B-C) broadly shows a temporal pattern: until ca. 16 Ma, microfloras are dominated by coccoliths; after that, diatoms become more abundant. Between 16 and 8 Ma both diatoms and coccolithophores are both abundant in individual samples. At ca. 8 Ma, the abundance of the coccoliths drops dramatically and, except for a short peak around 6Ma, never really recovers. Since then, diatoms appear to have been the dominating component of the Southern Ocean phytoplankton. The pattern of strong inverse co-variation in relative abundance seen between these two components in the earlier Miocene also breaks down at around 8 Ma. This shift from carbonate to silica primary producers seen in the sedimentary record may have also been affected by changes in the preservability of calcite, particularly by changes in bottom water carbon chemistry at ca 8 Ma as indicated by the carbon isotope record, but the basic pattern is likely to be correct, and fits with the true absolute dominance of diatoms vs coccolithophores known from the modern Southern Ocean plankton (e.g. Gregg & Casey 2007).

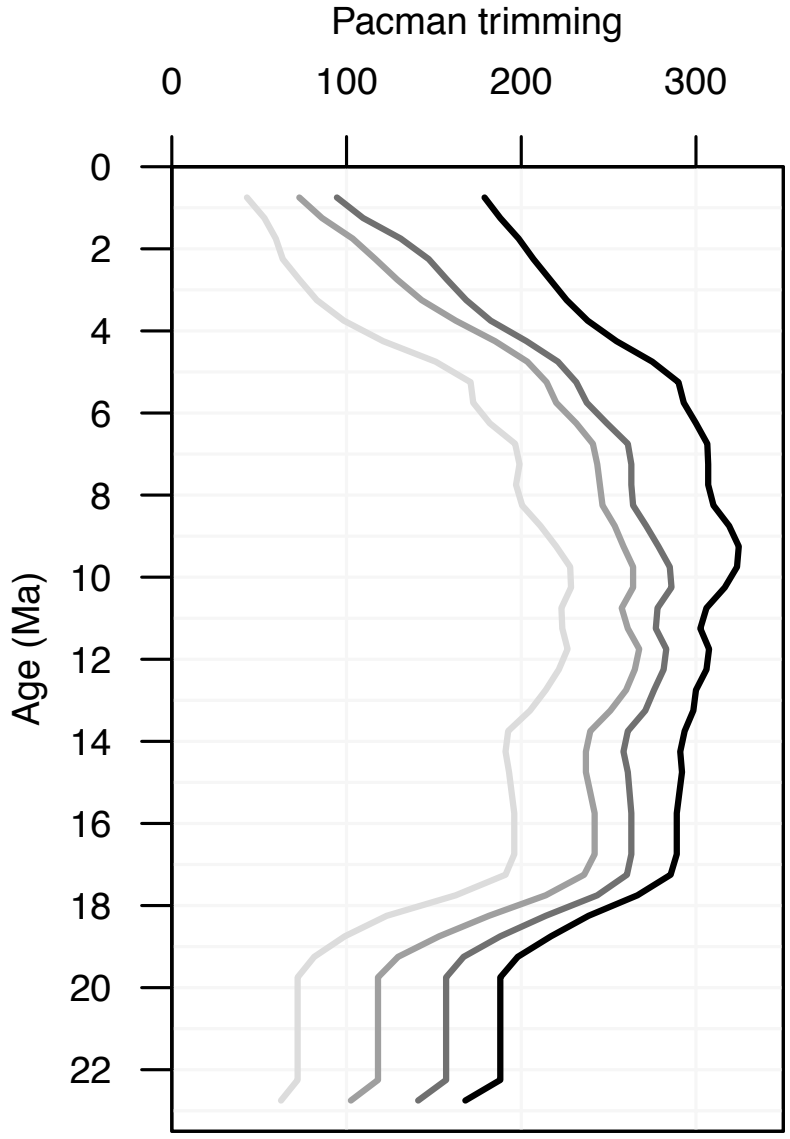

Figure 7.– Effect of range-trimming on diversity. Black line is without any trimming, dark grey line with a light trimming (3% at the top, 1% at the bottom), grey line with a moderate trimming (5 and 3%) and light grey line with a very strong trimming (12 and 8%).

Discussion

In the following it should be noted that, in comparison to most paleobiologic diversity data, the published data we have extracted from the Neptune database and analysed here as a proxy for "typical" paleobiologic data is in many ways untypical in that it is of unusually good quality (see review in Lazarus 2011). The deep-sea microfossil data is recorded at species level, rather than at the level of genera or families. The sedimentary sections are, if not continuous, at least much more so at most time scales than those typical of shallow water invertebrates, or terrestrial records. Our chronology, while still poor compared to the potential of the deep-sea sediment record, is still an order of magnitude more precise than is typical of many other studies (0.5 My time bins in our study vs ca 10 My bins in many other studies). Although there are numerous unresolved problems with radiolarian taxonomy, species-level taxonomy has been to a substantial degree standardised by direct cross-comparison between workers for most biostratigraphic marker taxa, and for many of the more commonly occuring other taxa in the Southern Ocean Neogene. This has been possible as the data is all relatively recently collected by a comparatively small number of cooperating workers. The species level taxonomy has been further standardised by the use of extensive synonym lists within Neptune. Surely, if the literature compilation with subsampling approach to reconstructing biodiversity should work at all, it should work in this test case.

1. Selection biases

As noted in the introduction, the main defect (as a source of biodiversity information) in published marine micropaleontology data is the incompleteness and systematic bias with which the preserved biodiversity of samples is recorded. Cataloging is not the primary focus of faunal description in micropaleontology, and, to some extent, in invertebrate paleontology (e.g., Koch 1978): biostratigraphy and paleoenvironmental analysis are (Lazarus 2011). Hence the data found in the literature and therefore in a database such as Neptune are not an unbiased inventory of the more abundant species, but to a very substantial degree checklists of only a subset of biostratigraphically, biogeographically or ecologically significant species. It is important to note that, at least for biostratigraphic species, they will be recorded, within time/manpower limits, regardless of their abundances. Most marine micropaleontologists can attest to the need on many occasions to search intensively in samples to determine the presence or absence of unfortunately rare stratigraphic markers. In addition to biostratigraphic species, some number of 'non-significant' species are typically added to the occurrence data, depending mostly on each paleontologist's own interest. The quasi-systematic use of checklists during faunal inventories creates an important selection bias in the diversity data: each checklist is not a random but a pre-screened sample. Subsamplings do not, in this context, draw occurrences from a random subset of the fossil assemblages, let alone the living community. The use of data from numerous

Figure 8.– Environmental proxies for Neogene Southern Ocean.
A: $\partial^{13}C$ *Cibicidoides* spp. (benthic foraminifera) from Leg 120 Site 747A (Wright & Miller 1992) and Site 751A (Mackensen et al. 1992) on the Kerguelen Plateau and from Leg Site 1088 (Billups 2002) in the subantarctic Atlantic, in per mil.
B and C: Relative abundance of, respectively, calcareous nannofossils and diatoms in smear slides, as reported in the core descriptions of Leg 113 Sites 689, 690 and 693 (Shipboard Scientific Party 1988a, 1988b, 1988c) and Leg 120 Sites 747, 748 and 751 (Shipboard Scientific Party 1989f, 1989g, 1989h). Bold black line represents the median value, the dark grey area encompasses the range between the first to the third quartiles of the values and the light grey area the range between the smallest and the highest value.
Magnetostratigraphy from Berggren et al. (1995).

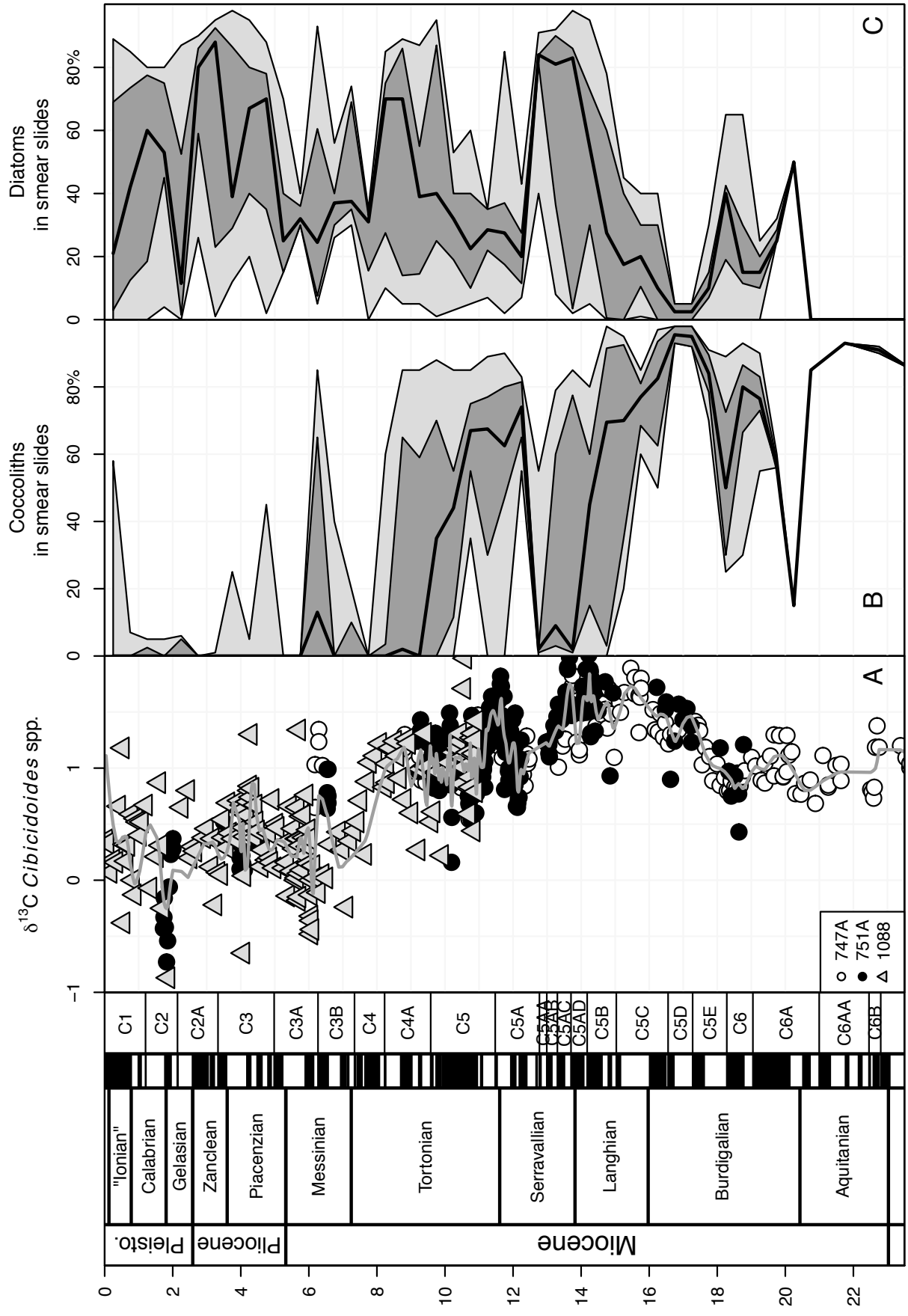
Diatoms
in smear slides
Coccoliths
in smear slides
$\delta^{13}C$ *Cibicidoides* spp.
A
B
C
747A
751A
1088
Pleisto.
Pliocene
Miocene
"Ionian"
Calabrian
Gelasian
Zanclean
Piacenzian
Messinian
Tortonian
Serravallian
Langhian
Burdigalian
Aquitanian
C1
C2
C2A
C3
C3A
C3B
C4
C4A
C5
C5A
C5AA
C5AB
C5AC
C5AD
C5B
C5C
C5D
C5E
C6
C6A
C6AA
C6B

Table 1.- List of classically used biostratigraphical markers.

Acrosphaera australis
Acrosphaera? *labrata*
Acrosphaera murrayana
Actinomma golownini
Amphymenium challengerae
Antarctissa cylindrica
Botryostrobus aquilonaris
Calocyclas disparidens
Ceratocyrtis stigi
Cycladophora antiqua
Cycladophora campanula
Cycladophora davisiana
Cycladophora golli
Cycladophora humerus
Cycladophora pliocenica
Cycladophora spongothorax
Cyrtocapsella longithorax
Cyrtocapsella tetrapera
Dendrospyris megalocephalis
Desmospyris spongiosa
Eucyrtidium calvertense
Eucyrtidium pseudoinflatum
Eucyrtidium punctatum
Helotholus praevema
Pseudocubus vema
Lamprocyrtis heteroporos
Lampromitra coronata
Gondwanaria hister
Lithelius nautiloides
Lychnocanoma conica
Lychnocanoma elongata
Lychnocanoma grande
Phormostichoartus pitomorphus
Prunopyle titan
Pterocanium charybdeum trilobum
Siphonosphaera vesuvius
Spongomelissa dilli
Stichocorys peregrina
Stylatractus universus
Triceraspyris antarctica

sources counteracts to some extent this selection bias: because of the addition of multiple individual investigator randomly-selected species to the checklist, the composite sampling converges toward being actually random and comprehensive. The biostratigraphical or ecological markers however still weight heavily in these datasets since their occurrences, and only theirs, are recorded systematically (Fig. 6). This significantly decreases the evenness of the population being sampled, and by reducing the number of non-biostratigraphic individuals drawn in any fixed-size subsample, reduces the subsampled diversity. The cumulative proportion of the biostratigraphic markers in the Neptune dataset used in this study not only reaches values as high as ca. 60% but varies also widely from the Early Miocene to the Late Pliocene. In particular, the relative abundance of fixed-list biostratigraphic markers increases gradually throughout the late Miocene, and may have contributed, by this masking effect, to subsampling procedures finding fewer of the other taxa in this time interval than they otherwise would have. That the subsampled curve is not entirely, or even primarily, controlled by this mechanism can however be seen by the lack of correlation between biostratigraphic marker values and subsampled diversity in the Plio-Pleistocene. Further work, not attempted here, is needed to determine to what degree biostratigraphic fixed list data has distorted the diversity signal recovered by subsampling the published dataset.

2. Impact of ecological change in assemblages on subsampled diversity

A second, and possibly more important factor affecting subsampled diversity is the change in true evenness of assemblages over time, and the consequent masking of relatively rarer taxa from subsampling estimates of diversity. As can be seen on Figure 5, our whole-fauna dataset record a significant ecological turnover around 8 Ma: the evenness starts shifting (Fig. 5B) and the self-similarity plot shows a strong break (Fig. 5A). This event is clearly linked to the rise to dominance of the genus *Antarctissa* (specifically of three species - A. denticulata, A. cylindrica and A. strelkovi, which can each account for up to 50% of the Pliocene and the Pleistocene assemblages, Fig. 5C). No drop of diversity seems to be directly linked to this event in our whole fauna dataset. Yet, all subsampled diversities start dropping during this event (Fig. 3D).

The shareholder quorum (SQS) subsampling method was designed by Alroy (2010) in part as an attempt to compensate for changes in evenness. Its failure to do so in this case is unclear, although it may be a combined effect of using fixed-list taxonomy and non-fixed sample sizes in individual sample occurrence lists. The Neptune database, like many other occurrence databases, contains few numerical abundance data but instead mostly either incidence data (presence-absence of a species) or semi-quantitative data, where the taxon is assigned a discrete categorical estimate of its abundance (the most common being 'abundant', 'frequent', 'common', 'rare' and 'trace'). The meaning of these categories, unfortunately, varies greatly from one source to the other, thus preventing us from translating it into true, numerical abundance data. Subsampling thus treats all data as binary data, instead of abundance data, so that SQS or other subsampling methods actually are responding to taxa ubiquity in the data instead of taxa evenness (Fig. 9). Here the most ubiquitous taxa are obviously those that were systematically looked for, but not necessarily the most abundant: the selection bias caused by the database containing many biostratigraphic checklists is therefore amplified.

Our results show that orgination rates have declined and extinction rates have increased in the Southern Ocean radiolarian fauna over the Neogene, but not in a uniform way. There are substantial fluctuations in rates, including a substantial step-like increase in extinction rates at ca 5 Ma. While some features of our observed evolutionary dynamics are correctly retained in the subsampled Neptune data (e.g., changes in origination rates in the mid Miocene, Fig. 3E-G), others are incorrectly represented (origination rates in the Plio-Pleistocene, Fig. 3E-G), and displacements in time of 2 My or more are found for changes in dynamics (e.g., Neptune subsampled extinction rate shifts in the mid Miocene and mid Pliocene, not at ca 5 Ma, Fig. 4A-C). Thus, there is both a substantial degree of distortion in the subsampled dynamics reconstructions, as well as shifts in timing by 2-3 My or more.

3. Mechanisms of evolutionary change

Paleoceanographic research has over the last decades continuously pushed towards higher temporal resolution (e.g., by drilling high sedimentation rate sections) in attempt to study ocean-climate dynamics at scales appropriate to understand mechanisms. These are in turn controlled by mean response times for the main ocean and atmosphere components of the system and are often within, or below, milankovitch climate frequencies (Zachos et al. 2001). Other paleoceanographic events appear over very much longer scales (tens of My), e.g., those driven by very long term processes such as continental drift (e.g. Barker & Thomas 2004). This is significant in so far as we wish to correlate observed changes in diversity to possible causal mechanisms - data on evolutionary change should in principle be matched in temporal scale to that of mechanisms whose records we wish to compare to. This is true not only for extinctions, which can be in principle virtually instantaneous on geologic time scales, but also for originations which have an inherent internal biologic response lag. Yet even origination responses in plankton on the largest of scales, e.g., recovery from the K/Pg mass extinction appear to be on scale of only a few My. All this suggests that diversity and its derivative - diversity dynamics - need to be measured at, and be accurate at temporal scales of at least 1 My, or better, and that for more complete understanding, diversity data, particularly to study extinction, should be collected at scales of better than 100 kyr.

As noted above, there are significant differences between the whole-fauna and Neptune subsampled reconstructed history of diversity and diversity dynamics. This includes distortion of primary signals in several intervals, and temporal discrepancies even at scales of 2-3 My. To compare evolutionary history to paleoceanographic history we need accuracy and precision significantly better than this. For this reason, we do not attempt to compare the subsampled

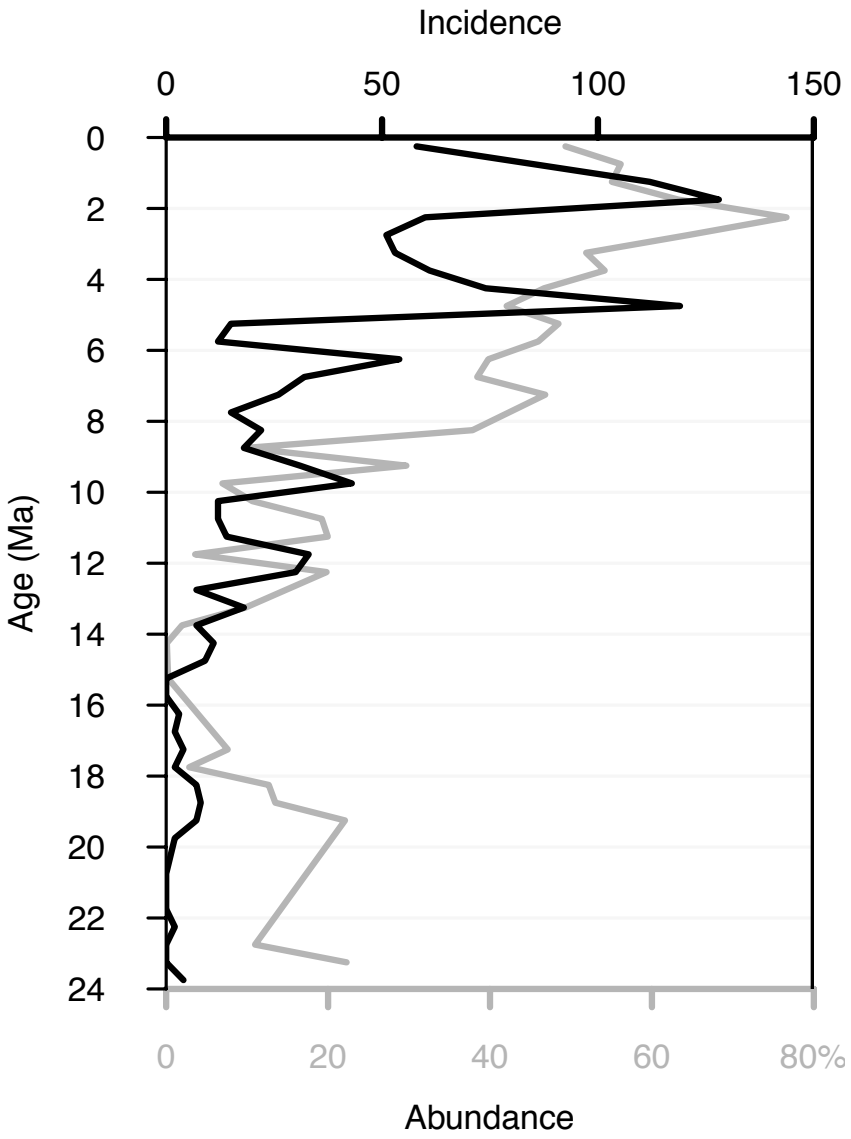

Figure 9.– Abundance (in percent) of species of genus *Antarctissa* in our whole-fauna dataset (in grey) compared with the incidence (in number of occurences) of the same set of species in the Neptune dataset (in black).

Neptune reconstructions of diversity to paleoceanographic history, and use only the more accurate and precise whole-faunal results. These too are still rather limited, by low numbers of samples in some time intervals, and a still fairly high degree of error in age estimation. The data is however sufficient to make an initial comparison to the environmental history of the region. Given the various uncertainties in our own data, the limited scope of paleoceanographic synthesis, and our very limited understanding of radiolarian ecology, what follows can only be labeled speculation, but is nonetheless useful in helping frame questions for future research.

Stable isotope and bulk sediment microfossil content, as summarised in Figure 8, suggests two major changes in the Southern Ocean Neogene environment. The first occurred in the mid Miocene with the development of the modern bottom water circulation pattern, bringing older, carbon isotope negative containing bottom waters into the Southern Ocean, correlated with a shift to more mixed phytoplankton communities. The second occurred in the early Late Miocene, coincident with a further decline in deep water carbon isotope values and a shift to diatom dominated phytoplankton. These two events lead us to suggest two possible hypotheses: either the radiolarian community was reshaped directly by the modifications in the bottom water

regime, or, and it is the more likely scenario, it was affected by the changes in the primary producer components. In this scenario, species which were feeding preferentially on calcareous nannoplankton decreased in relative abundance with the decrease of the latter, only to let species more specialized in diatom grazing take over the community. Species of the genus *Antarctissa* (Fig. 5C) began their rise to dominance of the radiolarian fauna during this event, suggesting they are most likely diatom grazers: unfortunately, to our knowledge, no studies on living *Antarctissa* feeding behaviour exist to date, to confirm or disprove this. Of course, those two hypotheses are not mutually exclusive. In fact, they have already been attempt to link changes in plankton productivity with the Late Miocene Carbon Shift (Vincent et al. 1980; Grant & Dickens 2002; Diester-Haass et al. 2005).

What the environmental summary of Figure 8 does not show is any major environmental change in the parameters plotted between 5.5 and 5 Ma, the time interval in which the radiolarian fauna undergoes a substantial increase in extinction rate (Fig. 4A). This time interval corresponds on a global scale to the Messinian event (Adams et al. 1977), and several deep-sea sections in the Southern Ocean show evidence of change at this time (Hillenbrand & Fütterer 2001). Other changes thought to have occurred at this time include the stabilisation of the West Antarctic ice sheet (Cieselski et al. 1982; Kennett & Barker 1990) and changes in the sea-ice extent, with consequent changes in the seasonality and geographic distribution of primary productivity (Hillenbrand & Fütterer 2001; Grützner et al. 2005). However, age models and paleoceanographic synthesis of Antarctic deep-sea sections are, particularly for this specific time interval, still in an early state of development and it is not yet possible to develop a clearer picture of Southern Ocean environmental history which could be compared to our evolutionary results. Our evolutionary data, as noted above, also may still be at too low a temporal resolution to use for study of the extinction event.

4. The decoupling of the ecological and the macroevolutionary patterns

Despite the abruptness and the strength of the ecological turnover observed at ca. 8 Ma, no significant changes in diversity, extinction or origination rates are observed at this time. Instead, changes in the diversity pattern occur 3 My later, at ca. 5.5-5 Ma. Ecological and evolutionary responses thus appear to be significantly decoupled in time: extinction does not seem to be a direct, immediate consequence of changing environments and ecology, or at least those that we have examined here. However, it is plausible that the reshaping of the community, with increasing dominance of *Antarctissa* starting at ca. 8 Ma, increased the extinction susceptibility to a subsequent unknown environmental change, by substantially reducing many species' relative abundances in the plankton. It is worth noting here that, without a thorough compilation of even the rarest taxa, the survival of many rare species after the 8 Ma event would have gone unnoticed and, hence, they would have appeared to have gone extinct earlier, e.g., closer to the environmental event at 8 Ma, masking this aspect of the evolution of this fauna.

Conclusions

1. The accuracy of paleodiversity reconstructions

This case study suggests that, even in the absence of systematic biases in preservation and even using subsampling methods, there are significant limits to our ability to reconstruct diversity history from existing published data on taxa occurrences in the (micro)fossil record. Standard paleobiologic methods do provide useful information, and in our study the main trend found in our whole-fauna data is seen in reconstructions from incomplete published data. This is a positive result which suggests that the existing published literature as contained in databases

such as Neptune can indeed be used to obtain at least a first-order impression of diversity history. Certainly, database compilations with subsampling perform much better than a literal reading of the fossil record provides (e.g., Lazarus 2002). However, it appears that it will be difficult to go beyond the most general of trends, and to extract patterns suitable for detailed study, e.g., comparison to paleoenvironmental data. The pattern recovered from incomplete data is distorted by artifactual secondary trends and by a significant offset in time. Our study is only a single example, and plankton data may be sufficiently different from other data (e.g., the frequency in use of fixed lists) that our conclusions cannot be generalised, or can only be applied within deep-sea marine micropaleontology. They should nonetheless suggest caution in using compilations of incomplete fossil occurrence data and subsampling, without at least considering the possible presence of these types of biases. Our study also does not address other types of potential error, such as systematic bias in preservation, or changing numbers of biogeographic provinces and the development of endemic biotas. All these also exist in the history of deep-sea plankton but are not significantly present in our specific dataset and are thus beyond the scope of this study.

Our results also underline the importance, and illustrate the feasibility, of collecting whole-fauna (or flora) data as the basis for detailed diversity history study of the plankton.

2. The macroevolutionary pattern of Antarctic Neogene radiolarians

Antarctic Neogene radiolarian faunas underwent a major ecological turnover at ca. 8 Ma, resulting from a change from a relatively equitable fauna to one heavily dominated by species of the nassellarian genus *Antarctissa*. This turnover was not associated with any extinction or origination event. A significant diversity drop, however, occured 3 My later, at ca. 5 Ma, for reasons as yet unknown. We speculate here that the ecological turnover is linked to changes in the relative abundance of primary producers which changed at ca 8 Ma from a coccolith dominated to a diatom-based flora.

Toward an high-resolution biostratigraphy for Antarctic Neogene radiolarians

Introduction

As was pointed out in Chapter 1, the global thermohaline circulation as well as the global climate Cenozoic evolution are directly linked to the paleoceanographic evolution of the Southern Ocean: the Cenozoic global cooling is linked to Antarctic glaciation, which is in turn linked to Antarctic thermal isolation caused by the presence of the Antarctic Circumpolar Current. To understand these events, a robust geochronological framework is needed. Indeed, while tectonic-driven events such as the opening of the Drake Passage and the Tasmanian Gateway take several million years to occur, paleoceanographically and climatically-induced events happen in less than 1 My (Zachos et al. 2001). Similarly, macroevolutionary studies also need a better accuracy. Yet, the accuracy of the current geochronological framework lies above 1 My.

Because of the peculiar sedimentary conditions of the Neogene Southern Ocean (see Chapter 1 §3.4) that prevents the reliable use of calcareous microfossils for biostratigraphy and because of the widespread hiatuses and the poor paleomagnetic polarity record in many sections, the Antarctic Neogene stratigraphic framework relies heavily of siliceous microfossils.

Current radiolarian biostratigraphy for the Antarctic Neogene is based on a total of 40 species (Hays 1970; Caulet 1991; Lazarus 1992; Spencer-Cervato 1999; see Table 1 in Chapter 3). However, as was shown in the two previous chapters, ca. 500 species are present in the Neogene Southern Ocean: the radiolarian fossil record for this time time interval and that region has a huge potential that previous studies didn't make use of.

The aim of this preliminary study is to uncover this potential by using our full fauna dataset in the context of a quantitative biostratigraphic analysis. Although still preliminary due to a too small number of samples, this study underlines the feasibility of improving biostratigraphic analysis using whole fauna data.

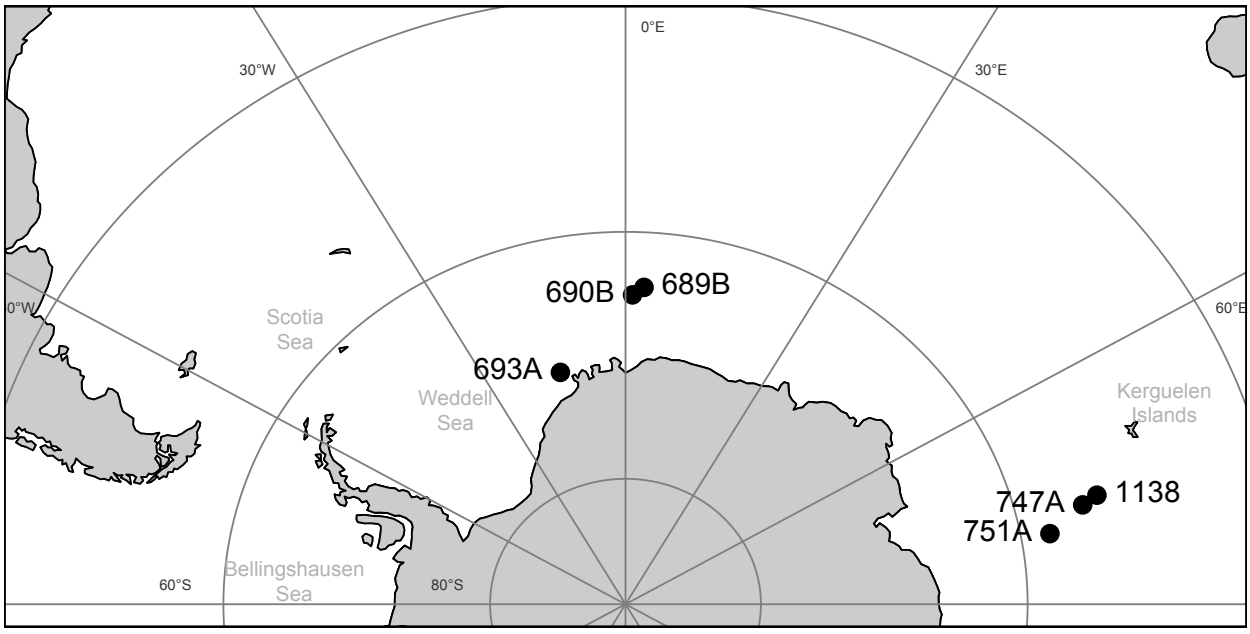

Figure 1.– Map of the sites used for the biostratigraphic analysis.

Material

Eighty-three samples from six of the studied sites were considered for this study: ODP Leg 113 Sites 689 (11 samples), 690 (10 samples) and 693 (10 samples), ODP Leg 120 Sites 747 (15 samples) and 751 (24 samples) and ODP Leg 183 Site 1138 (13 samples). The remaining sixteen samples from ODP Leg 119 Site 744 and ODP Leg 120 Site 748 were discarded in order to focus on the Late Miocene to Early Pleistocene sequence (11 to 3Ma).

From these sites the presence and abundance of radiolarian species were recorded following the processes described in the previous chapter. 447 species were present and therefore followed in the 83 samples considered in this chapter, hence a total of 894 events (first and last occurrences) in theory (indeed, ca. 100 species are still living and ca. 200 were already present at the beginning of the sequence, hence a real number of events of ca. 600).

CONOP analysis was done with CONOP9 (Sadler 2007) and all other computation were scripted and processed in R 2.14 (R development core team 2011; see Appendix B for the functions and scripts created for this study).

All ages referred to in this chapter are scaled on the Berggren et al. 1995 timescale to allow direct comparison with the formerly developed age scale (Figs 6A-F; Lazarus et al. 1995).

Methodology

Constrained Optimization (CONOP).– The Constrained Optimization (CONOP, Kemple et al. 1995; Sadler 2007) procedure is a computationally intensive biostratigraphy method that consists of optimizing the sequence of events in order to reduce the misfit between the observed sequence of events from each sites and the composite sequence of events. The optimization is

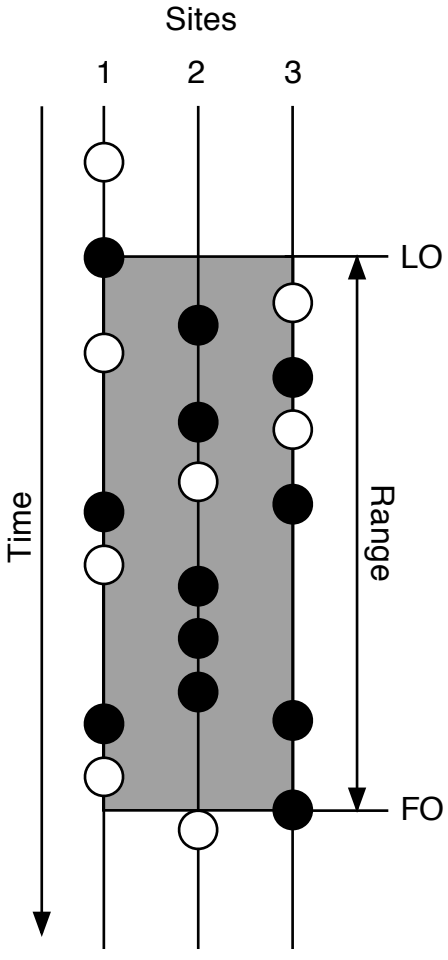

Figure 2.– Illustration of the Gap ratio metric.
Black dots are samples where the species is present and white dots samples where the species is absent.
The gap ratio is the ratio of samples where the species is absent on total number of samples in the species range.
Here the species is present in 3 sites, the range of the species covers 18 samples including 12 in which the species is actually present. The gap ratio is therefore of 33.3%.

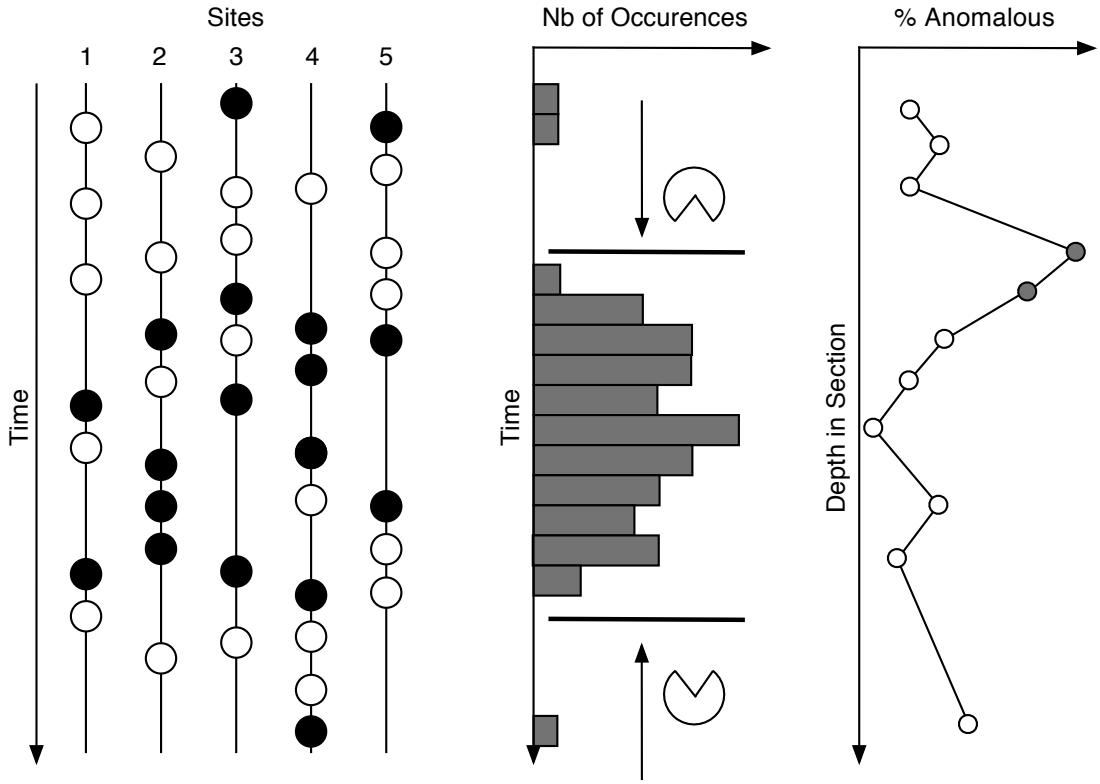

Figure 3.– Illustration of the pacman profiling concept.
Left panel: Occurences of a given species in several sites (white: absent; back: present).
Middle panel: Compilations of occurences on all sites. Pacman routine flags a given percentage of occurences at the top and the bottom of the species range as anomalous.
Right panel: Anomalous data for all species are compiled for each sites and problematic samples are hence spotted. (redrawn after Lazarus et al. 2012)

constrained by the observed co-occurences.

Dealing with full fauna data.– Using the full number of species in the fauna in a biostratigraphic analysis means improving the number of events obviously but also, given the nature of the abundance distributions of speices in a given ecosystem, adding mostly rare species to the analysis. A species that is scarce combined to the incompleteness of the fossil record produces truncated local ranges and therefore, the initial impression is that using a full fauna dataset should be more a source of noise than a tool for increasing resolution. However, even if the probability of finding a non-truncated range for a rare species in any given section is low, the first (FO) and last occurences (LO) for a section stil help constraining the true solution for the "line of correlation" (Shaw 1964): all FO, by definition, plot on or above the line of correlation and all LOs on or below. This cloud of points can, over a number of sample levels, siginificantly constrain the solution even if at any level no point is directly on the atual correlation line. Furthermore, the co-occurences of species (rare or abundant) with other species are additional constraints (see previous paragraph) that narrow the field of possible solutions.

Parameters of the run.– The chosen measure of misfit was the one on the number of level (i. e. samples): indeed the sample-per-meter ratio in such sites as 693 (10 samples took between 47.58 mbsf and 236.41 mbsf) and 690 (10 samples between 1.26 mbsf and 28.57 mbsf), for instance, is so radically different, that choosing a depth-based measure of misfit would add a strong weight on sites with high sedimentation rate (such as site 693); as for the event-based misfit (i. e. the misfit between the observed event order on each site and the order on the composite sequence),

because the number of events (894) is so high compared to the number of samples (83) that many events occur at the same level hence creating an artificially increased misfit. Misfit based on pairwise contradictions in the order of events (Sadler 2007) are better fitted for predictive biostratigraphy than for establishing an age scale and were therefore discarded here. No secondary misfit (such as 'smoother', 'squeezer', 'shrinker' or 'teaser' which penalizes departure from a straight LOC or events seen only in the bottom or top level of one section; Sadler 2007) were applied.

The simulated annealing heuristic that computes the optimization (Kirkpatrick et al. 1983; Kemple et al. 1995) was configured with an initial temperature of 200 and 500 cooling steps (at a 0.98 rate) of 1000 trials. According to Sadler (2007), a problem consisting of 10 sections and 100 taxa needs 500 steps of 1000 trials, cooling from an initial temperature of 50-100 while a problem consisting of 100 sections and 400 taxa needs 500 steps of 5000 trials from an initial temperature of 100-200: an intermediate configuration as been chosen here since our problem consists of 6 sections and 447 taxa.

Outlier detection.– A preliminary raw CONOP run was processed. In order to flag the events which were showing systematically the highest misfit, the results were analysed and statistics on the misfit for each events computed. Events with outlying misfit (i. e. here a mean per-site misfit over 4 levels) were flagged as unreliable events. Pacman profiling (Fig. 3) was conducted on abundance data, using the preliminary composite depth as a timescale. Samples bearing a statistically disproportionate amount of outlying occurences were flagged as possibly misdated or reworked samples. The gap ratio metric used to identify species with discontinuous ranges is very straightforward: it is the number of samples that fall in the range of the species in which the species was not seen divided by the total number of samples that constitute the range (Fig. 2). Species with high gap ratio (i. e. here gap ratios over 50%) were also flagged. For the final CONOP analysis, events, samples and species that were flagged as outliers were accorded a cumulative weight of 0.5 (i. e. an entry flagged by one method only is given a weight of 0.5 while an entry flagged by two methods has a weight of 0.25 and by three methods 0.125).

Building an age model based on the composite sequence.– The output of the CONOP analysis, as mentioned above, is a scaled composite sequence of events. To derive an age model from this composite sequence (see Fig. 4), in a first step, reliable magnetostratigraphic and diatom-based biostratigraphic data were gathered from the literature for some of the sites (sites 689 and 690, Censarek & Gersonde 2002; site 1138, Bohaty et al. 2003; Fig. 4B). By cross-correlating these "age-depth (mbsf)" datums to the line-of-correlation observed in the "depth (mbsf)-composite depth" plot (Fig. 4A) after the CONOP run, "age-composite depth" data are obtained. An age model accomodating each sites (Fig. 4C) data was then calculated and used to create a conversion table from composite depth to numerical age. Age-depth plots were then plotted for each site and compared to the previous age models (Fig. 4D and Figs 6A to F).

Criteria for the selection of potential marker species.– Several criteria can be used *a posteriori* to select usable bioevents, a good bioevents being widespread (number of sites in which the events was observed and total number of observed specimens will be here relevant), synchronic (hence a low misfit between the observed event and the event as placed by the CONOP analysis) and clearly marked (the range leading to the event need to be consistent, hence a relatively low gap ratio, and unlikely to be caused by misidentification or reworking, hence robust to a pacman profiling).

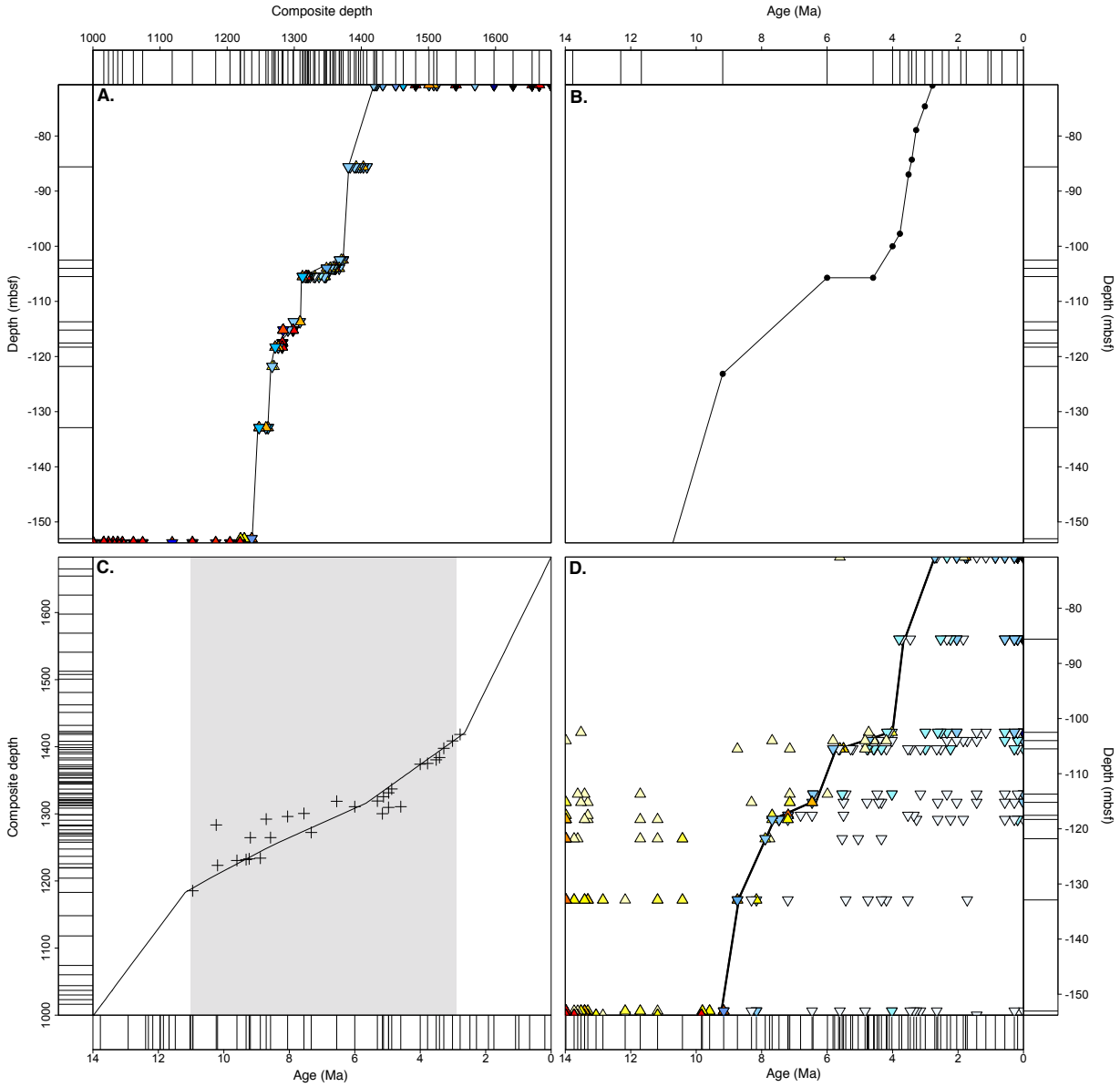

Figure 4.– Steps from composite depth to numerical age.
A. Depth vs Composite depth plot for site 1138: events represented are adjusted according to CONOP results. Blue, downward-directed triangle are LOs while red, upward-directed triangle are FOs. Intensity of color corresponds to the number of events superposed (see Fig. 6A-F for scale).
B. Line of correlation for site 1138 from Bohaty et al. 2003, based on magnetostratigraphic reversal, ash layers and diatom FOs and LOs.
C. Age models in term of composite depth: crosses are tie-points of lines-of-correlation for sites 689, 690 and 1138. Grey zone is interval of focus of this study (3 to 11 Ma).
D. Age vs depth plot for site 1138: events represented are observed (not adjusted).

Results

The Composite sequence of events.– The result of the CONOP run ended with a total level misfit of 2525.67 for the best sequence (the decimals are due to the use of weights: a 2 levels misfit on an event in a sample with a weight of 0.25 would be indeed counted as 0.5, etc.). The mean misfit per event on each site varied from 0.46 (site 747) to 0.92 (site 693) level (the mean on all sites being 0.696 level per observed event). The unweighted mean misfit per event in all sections is however 4.77 levels (5.81 levels if we exclude the singletons; Fig. 5). The sequence is composed of 78 levels: from 83 samples, the sequence only recognize 78 levels probably

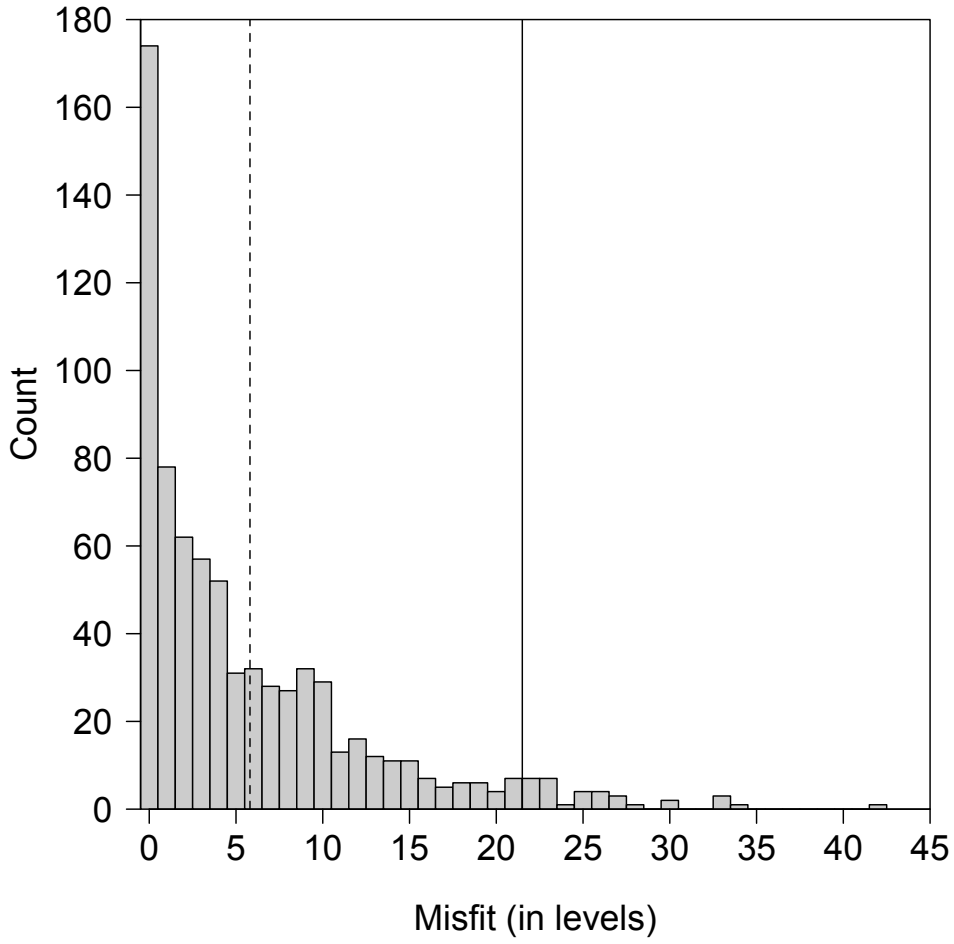

Figure 5.– Histogram of the total misfit of each event (singletons put aside).
Dotted vertical line is the mean. Misfit on the right of the straight vertical line are outliers. Here the misfit is shown unweighted: it is the actual number of samples the events need to be displaced to respect the composite sequence.

because some pairs of samples were not distinguishable temporally due to almost identical faunal composition. Out of the 1771 local events (i. e. one event in one site) that were adjustable (i. e. events that were observed in more than one site and that were not observed in the first or last sample of the site), 1266 (hence 71.49% of them) had to be indeed moved to find the optimal permutation.

Site by site.– Site 689 has a total level misfit of 409.32 levels with a mean misfit per event of 0.75. 548 events were observed in this site. The resulting age model for this site is largely conformable with that of Leg 113 Synthesis (Gersonde et al. 1990). Sediments from ca. 18 to 20 mbsf however seem to be 1 to 2 My younger than expected.

Site 690 has a total level misfit of 439.50 levels with a mean misfit per event of 0.80. 546 events were observed on this site. The age model resulting from the analysis conforms with the Neptune age model for a large part, with a few important distinctions. The top sample used in this study (113-690B-1H-1 126-132cm at 1.26 mbsf) was considered to be of upper Pleistocene age (0.1 Ma), however it appears to be of Pliocene age (3 Ma) and indeed both the presence of *Helotholus vema* and *Helotholus praevema*, for instance, are indeniable indicators of Pliocene age. The ca. 3My hiatus seen in our age model at ca. 24 mbsf (instead of being at ca. 19 mbsf) is most probably largely imputable to the poor sampling in that part of the site while the 1My lag between both age model prior to this hiatus (at ca. 18 mbsf) is poorly constrained here. The discrepancies between both age models between 18 and 25 mbsf are therefore unlikely to be

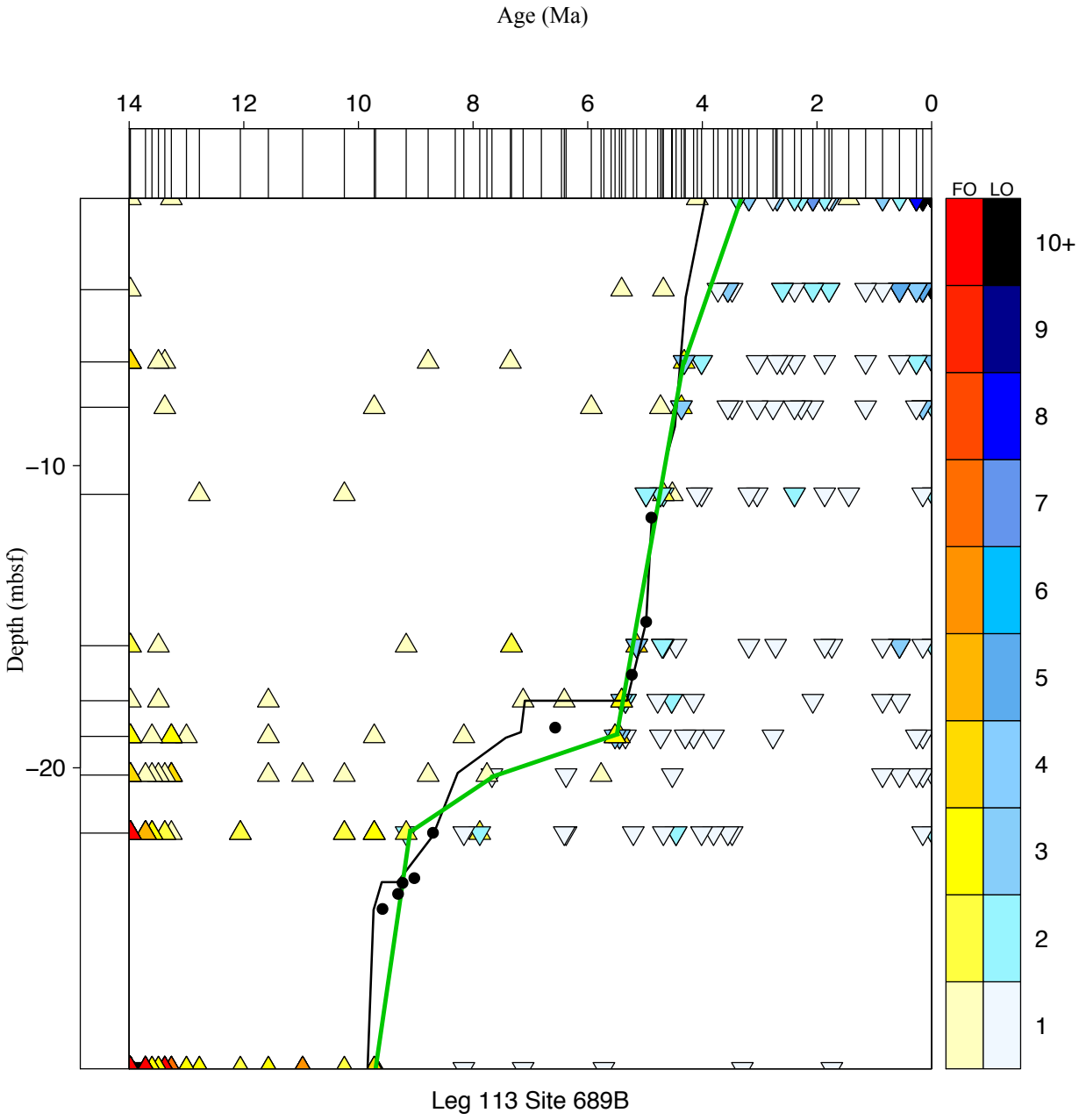

Figure 6A.– Age-Depth plot for Leg 113 site 689.
Lines on the left side represent the samples. Lines on the upper side represent each level of the composite sequence. Upwardly-directed triangles are observed FO of radiolarian species while downwardly-directed are observed LO of radiolarian species. Their colour is linked to the number of LO or FO present on this sample at this level (see chart on the right side for the equivalence). Bold black line is the former age model embedded in the Neptune database (Lazarus et al. 1995) while the green bold line is the age model deriving from the CONOP analysis. Black dots are the magnetostratigraphic datum.

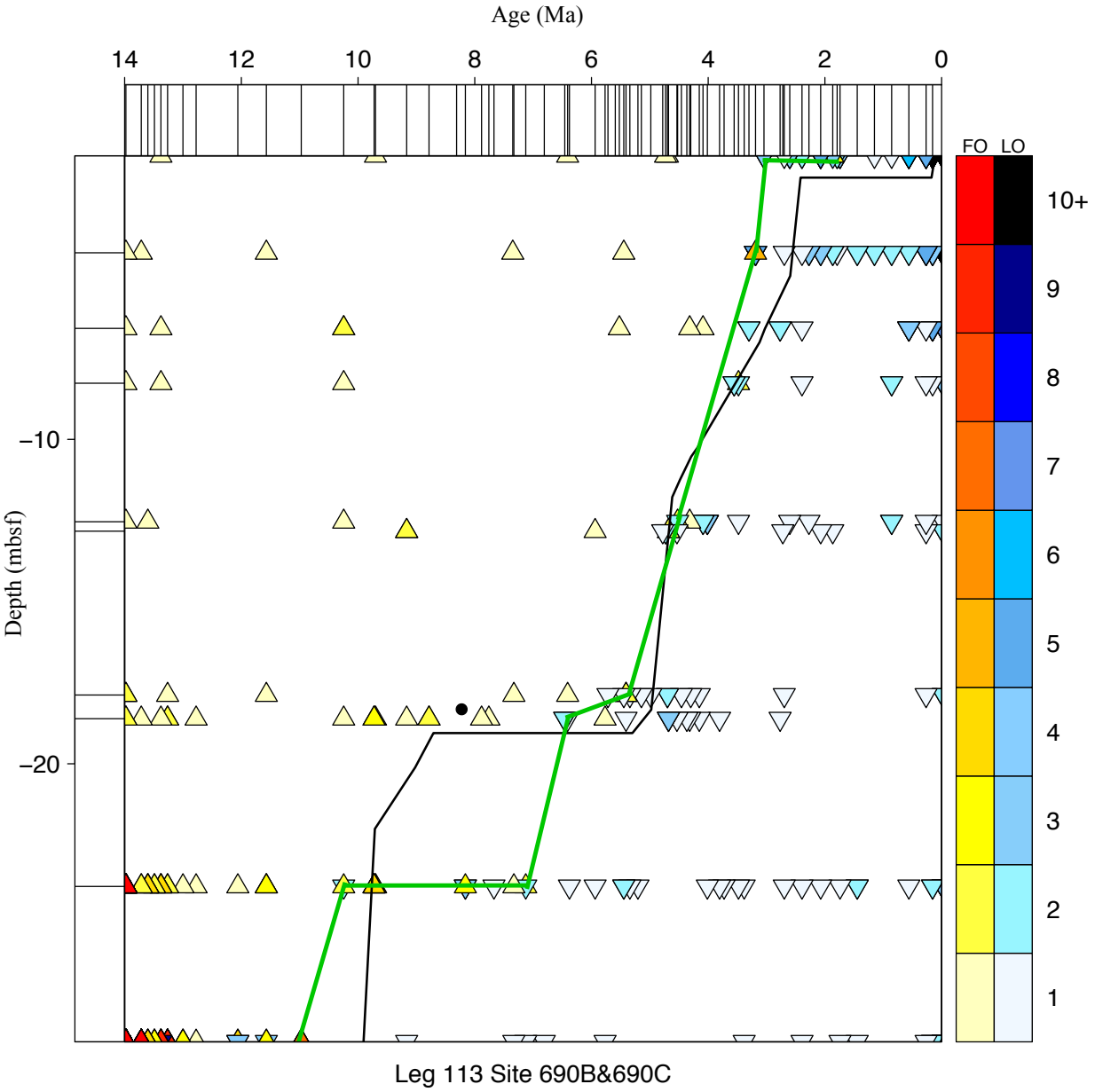

Figure 6B.– Age-depth plot for Leg 113 Site 690.
See caption of Fig. 6A for explanations.

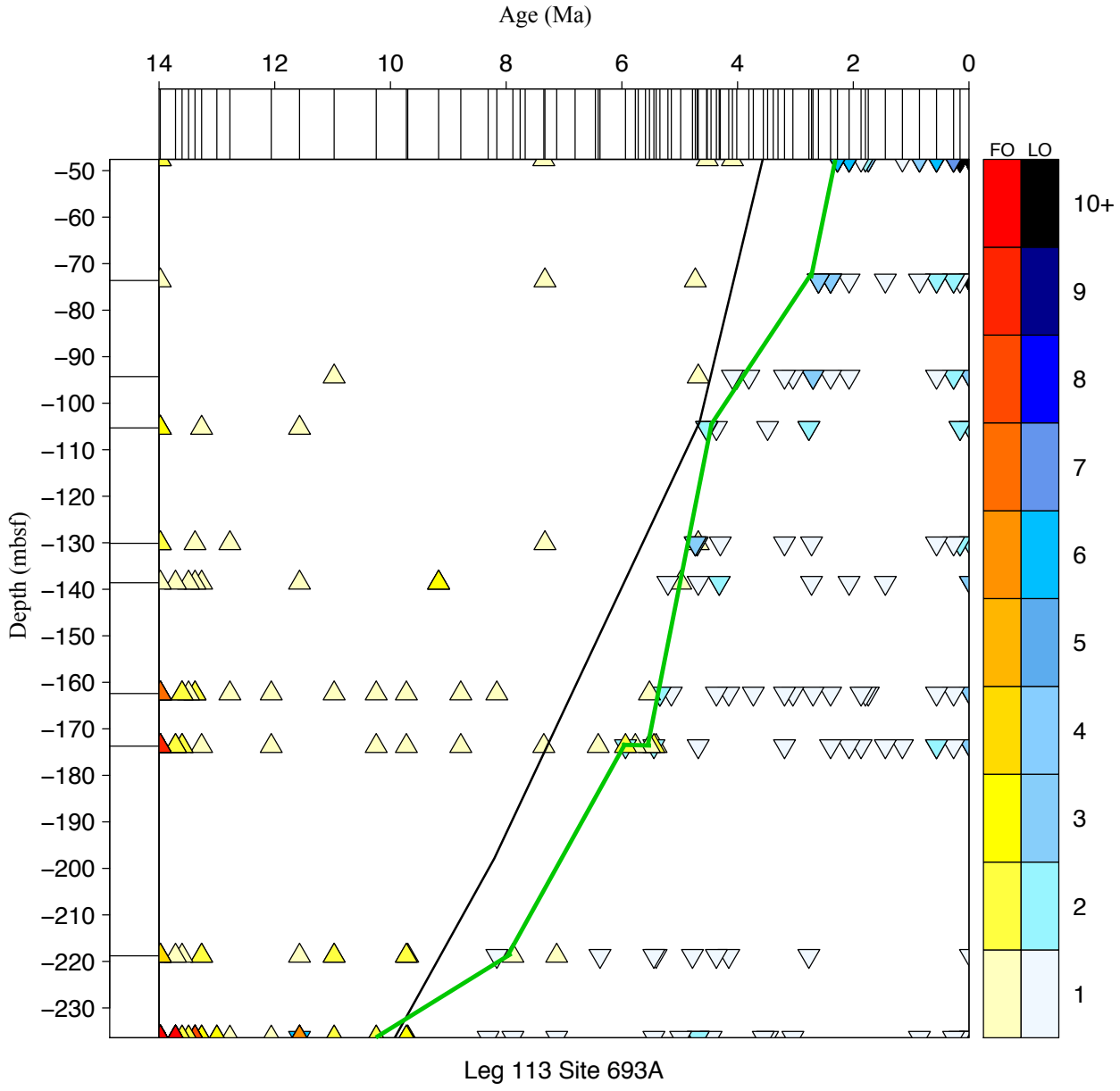

Figure 6C.– Ade-depth plot for Leg 113 Site 693.
See caption of Fig. 6A for explanations.

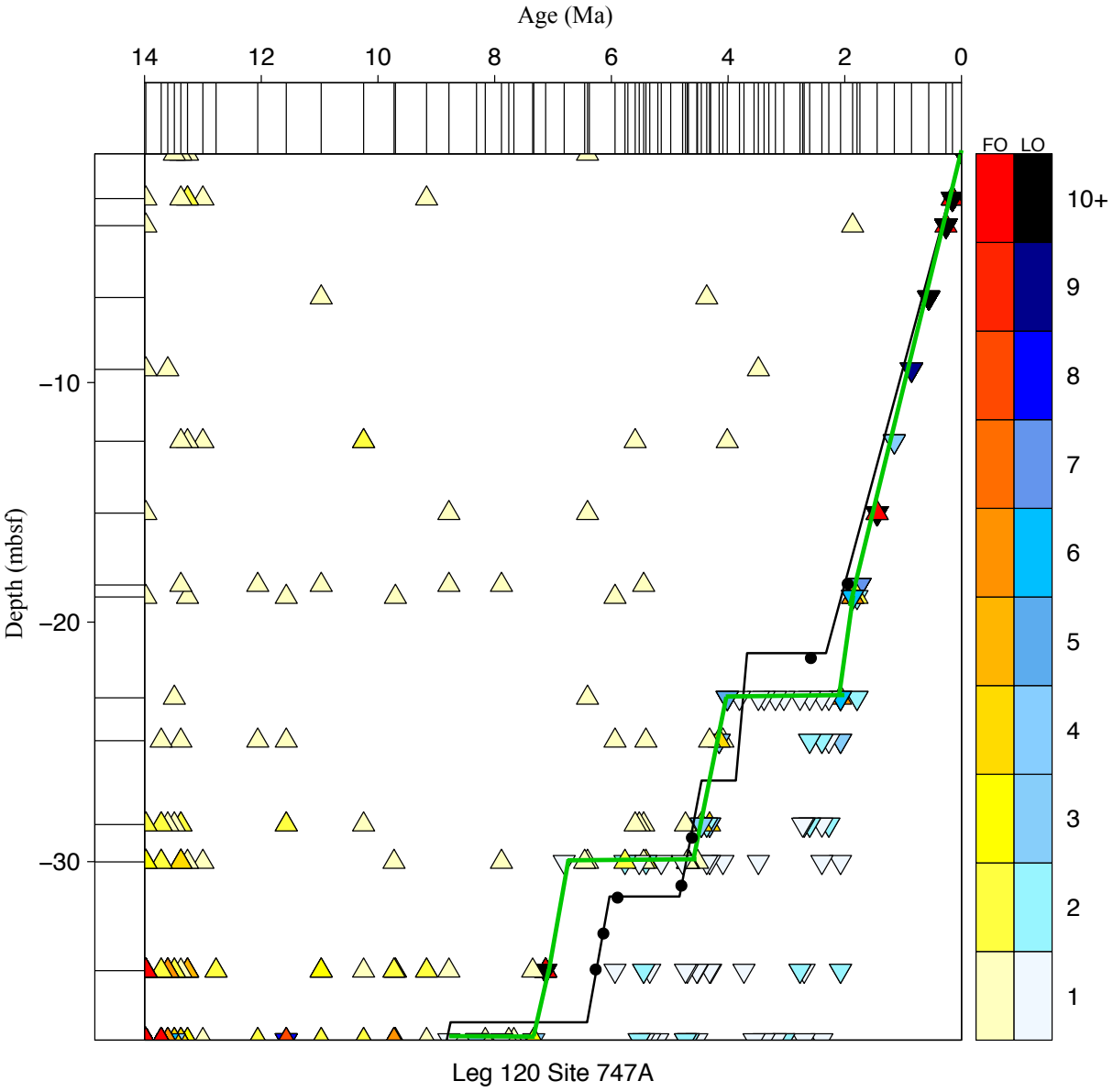

Figure 6D.– Age-depth plot for Leg 120 Site 747.
See captions of Fig. 6A for explanations.

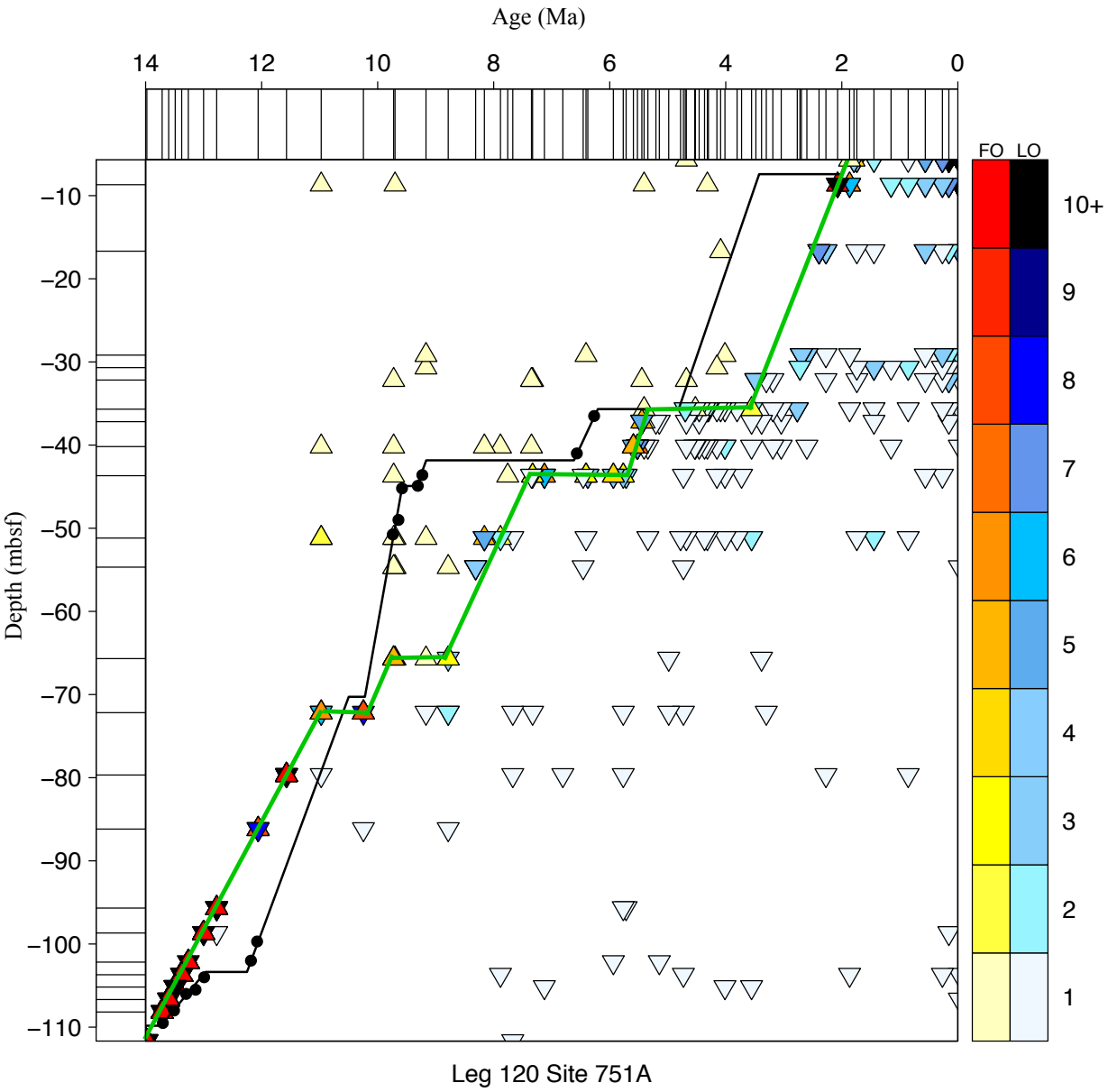

Figure 6E.– Age-depth plot for Leg 120 Site 751.
See captions of Fig. 6A for explanations.

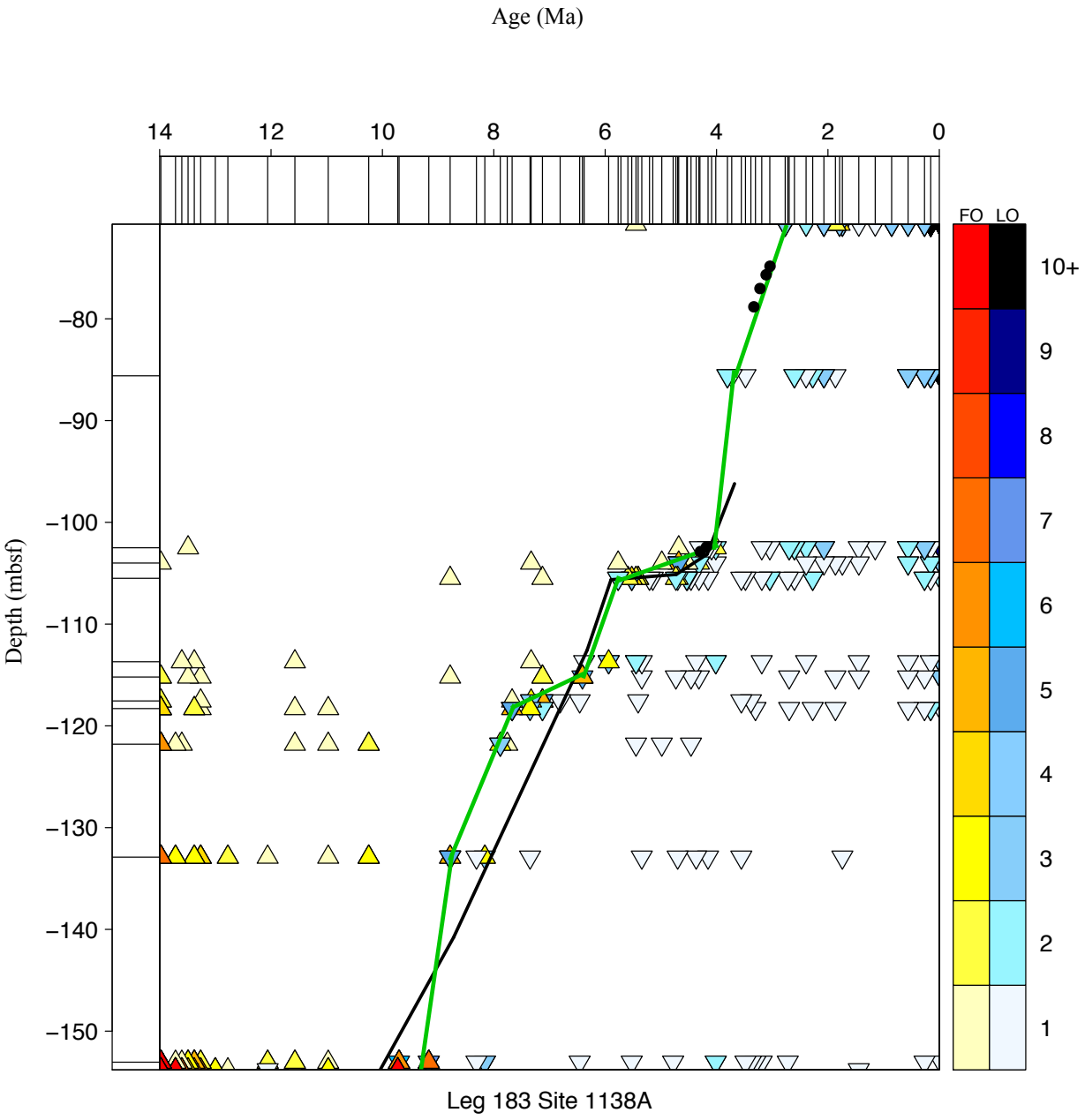

Figure 6F.– Age-depth plot for Leg 183 Site 1138.
See captions of Fig. 6A for explanations.

meaningful.

Site 693 has a total level misfit of 435.50 levels with a mean misfit per event of 0.92. 472 events were observed on this site. Globally the age model resulting from the CONOP analysis is 0.5 to 1 My younger than the previous age model. Sample 693A-26R-2 61-67cm at 236.41mbsf however was considered in the earlier age model as of upper Miocene age (ca. 7.8 Ma): in the CONOP-based age model it appears to be considerably older (9.8 Ma) and indeed the abundance of *Pentactinosphaera codonia*, *Acrosphaera murrayana* and *Larcopyle augusti* along with the absence of *Stichocorys peregrina*, *Siphonosphaera vesuvius* or *Lychnocanium grande* (to name a few) tend to confirm this age.

Site 747 has a total level misfit of 294.91 levels with a mean misfit per event of 0.46. 636 events were observed on this site. The published age model for site 747 and our CONOP-based age model are almost totally in perfect accordance. The only noticeable discrepancy is the age of the samples between ca. 30 and 35 mbsf that are, in the new age model, ca. 0.5 My older. This difference may be due to the difficulty of interpreting the poorly polarized magnetostratigraphic signal of that interval (see Heider et al. 1992).

Site 751 has a total level misfit of 473 levels with a mean misfit per event of 0.59. 804 events were observed on this site. The hiatuses spotted in the original age model are seen in the CONOP result as well. However their starting ages and their durations differ here somewhat, commonly 1 My to 1.5 My younger here. The reason for such a difference is the rather poor polarity signal in this interval (Heider et al. 1992) which therefore may be unreliable, if we are to believe the radiolarian-based results. The sequence below 80 mbsf (i. e. older than 12 Ma) being exclusively based on this single site is therefore totally unconstrained in this analysis. The differences or the similarities with the older age model for that interval are therefore purely artifactual. It is interesting to notice that, with the age model proposed herein, the sedimentation rates between each hiatus are very close to one another, when they were very dissimilar in the old age model.

Site 1138 has a total level misfit of 473.44 levels with a mean misfit per event of 0.76. 622 events were observed on this site. The Neptune database does not contain samples from leg 183, but the radiolarian-based age model does not diverge widely from that of Bohaty et al. 2003, granted that site 1138 was, along with sites 689 and 690 (Censarek & Gersonde 2002), used to calibrate the timescale in this study.

Event density.– Eighty-three samples is still too low to resolve the permutation of 894 events (605 if we sustract the LO of the 99 species present in the youngest sample and the FO of the 190 species present in the oldest). Despite being heavily sampled (55 samples out of the 83), the interval between 3 and 11 Ma is constituted, in the composite sequence, of 50 event levels for 245 events: although some levels represent indeed one single event, some levels aggregate up to 14 events (the median being 4 events per level in this interval). As can be seen in Figures 7 and 8, the distribution of these event levels is not even in this interval. Between 3 and 6 Ma, 31 event levels, for 127 events (with a median value of 3 events per level), can be seen on the composite sequence while, between 6 and 11 Ma, 19 levels for 118 events (with a median value of 6 events per level) are found. This disparity can be explained by two facts: on one hand the presence in several sites of hiatuses in the 6 to 11 Ma interval preventing the sampling of sediments from this age in these sites (see Figs 6B and 6E), and on the other hand the observed diversity drop (see Chapter 3) in the 6 to 3 Ma interval increasing the number of LO observed in this interval.

The interval between 0 to 3 Ma and the interval below 11 Ma being less densely sampled are much less resolved, with event levels gathering routinely more than 20 events (the median being 10.5 events per level).

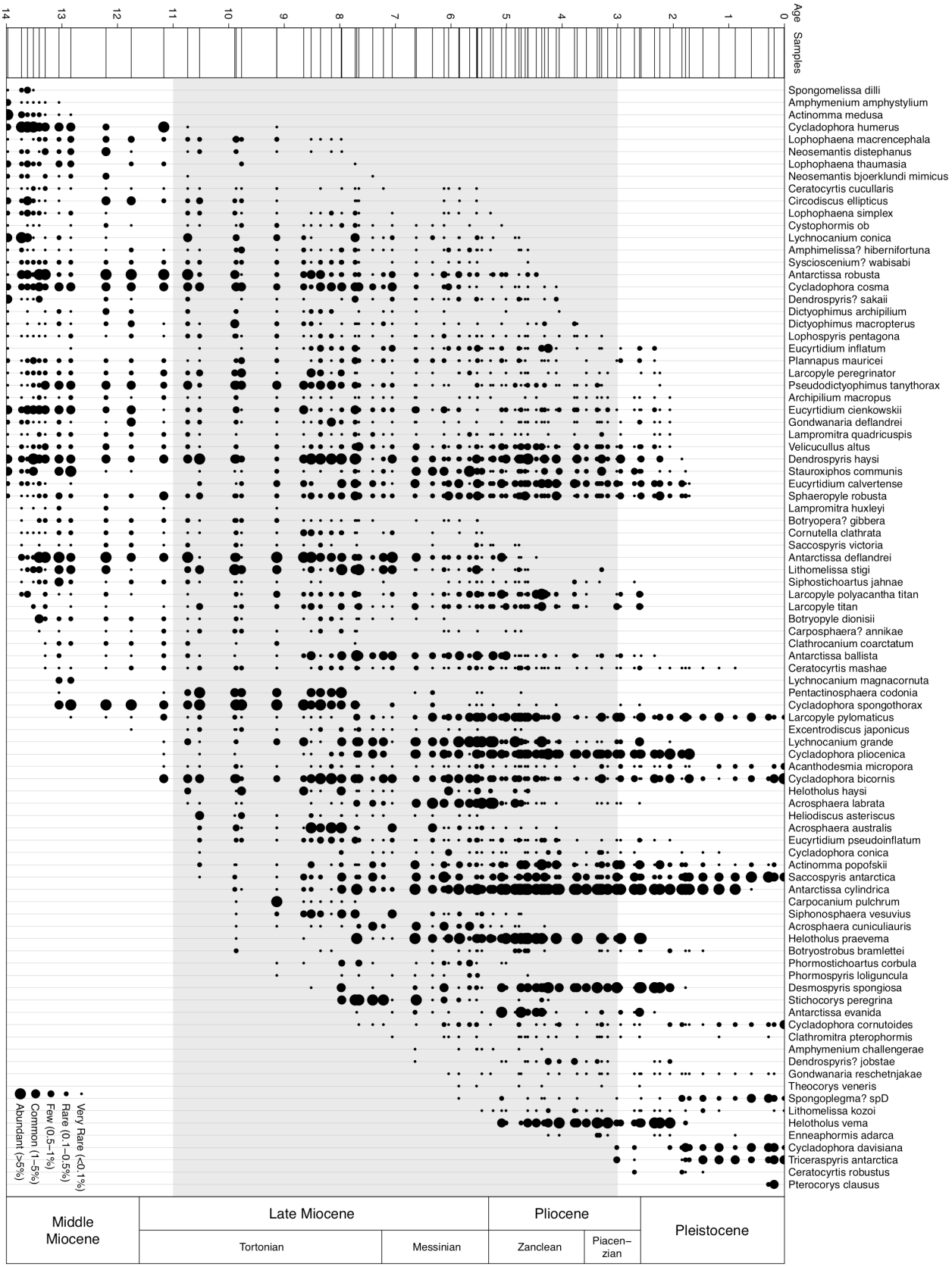
Age
Samples
14
13
12
11
10
9
8
7
6
5
4
3
2
1
0
Spongomelissa dilli
Amphymenium amphystylium
Actinomma medusa
Cycladophora humerus
Lophophaena macrencephala
Neosemantis distephanus
Lophophaena thaumasia
Neosemantis bjoerklundi mimicus
Ceratocyrtis cucullaris
Circodiscus ellipticus
Lophophaena simplex
Cystophormis ob
Lychnocanium conica
Amphimelissa? hibernifortuna
Sysciosceniumʔ wabisabi
Antarctissa robusta
Cycladophora cosma
Dendrospyris? sakaii
Dictyophimus archipilium
Dictyophimus macropterus
Lophospyris pentagona
Eucyrtidium inflatum
Plannapus mauricei
Larcopyle peregrinator
Pseudodictyophimus tanythorax
Archipilium macropus
Eucyrtidium cienkowskii
Gondwanaria deflandrei
Lampromitra quadricuspis
Velicucullus altus
Dendrospyris haysi
Stauroxiphos communis
Eucyrtidium calvertense
Sphaeropyle robusta
Lampromitra huxleyi
Botryopera? gibbera
Cornutella clathrata
Saccospyris victoria
Antarctissa deflandrei
Lithomelissa stigi
Siphostichoartus jahnae
Larcopyle polyacantha titan
Larcopyle titan
Botryopyle dionisii
Carposphaera? annikae
Clathrocanium coarctatum
Antarctissa ballista
Ceratocyrtis mashae
Lychnocanium magnacornuta
Pentactinosphaera codonia
Cycladophora spongothorax
Larcopyle pylomaticus
Excentrodiscus japonicus
Lychnocanium grande
Cycladophora pliocenica
Acanthodesmia micropora
Cycladophora bicornis
Heliotholus haysi
Acrosphaera labrata
Heliodiscus asteriscus
Acrosphaera australis
Eucyrtidium pseudoinflatum
Cycladophora conica
Actinomma popofskii
Saccospyris antarctica
Antarctissa cylindrica
Carpocanium pulchrum
Siphonosphaera vesuvius
Acrosphaera cuniculiauris
Heliotholus praevema
Botryostrobus bramlettei
Phormostichoartus corbula
Phormospyris loliguncula
Desmospyris spongiosa
Stichocorys peregrina
Antarctissa evanida
Cycladophora cornutoides
Clathromitra pterophormis
Amphymenium challengerae
Dendrospyris? jobstae
Gondwanaria reschetnjakae
Theocorys veneris
Spongoplegma? spD
Lithomelissa kozoi
Heliotholus vema
Enneaphormis adarca
Cycladophora davisiana
Triceraspyris antarctica
Ceratocyrtis robustus
Pterocorys clausus
Abundant (>5%)
Common (1–5%)
Few (0.5–1%)
Rare (0.1–0.5%)
Very Rare (<0.1%)
Middle Miocene
Late Miocene
Tortonian
Messinian
Pliocene
Zanclean
Piacen–zian
Pleistocene

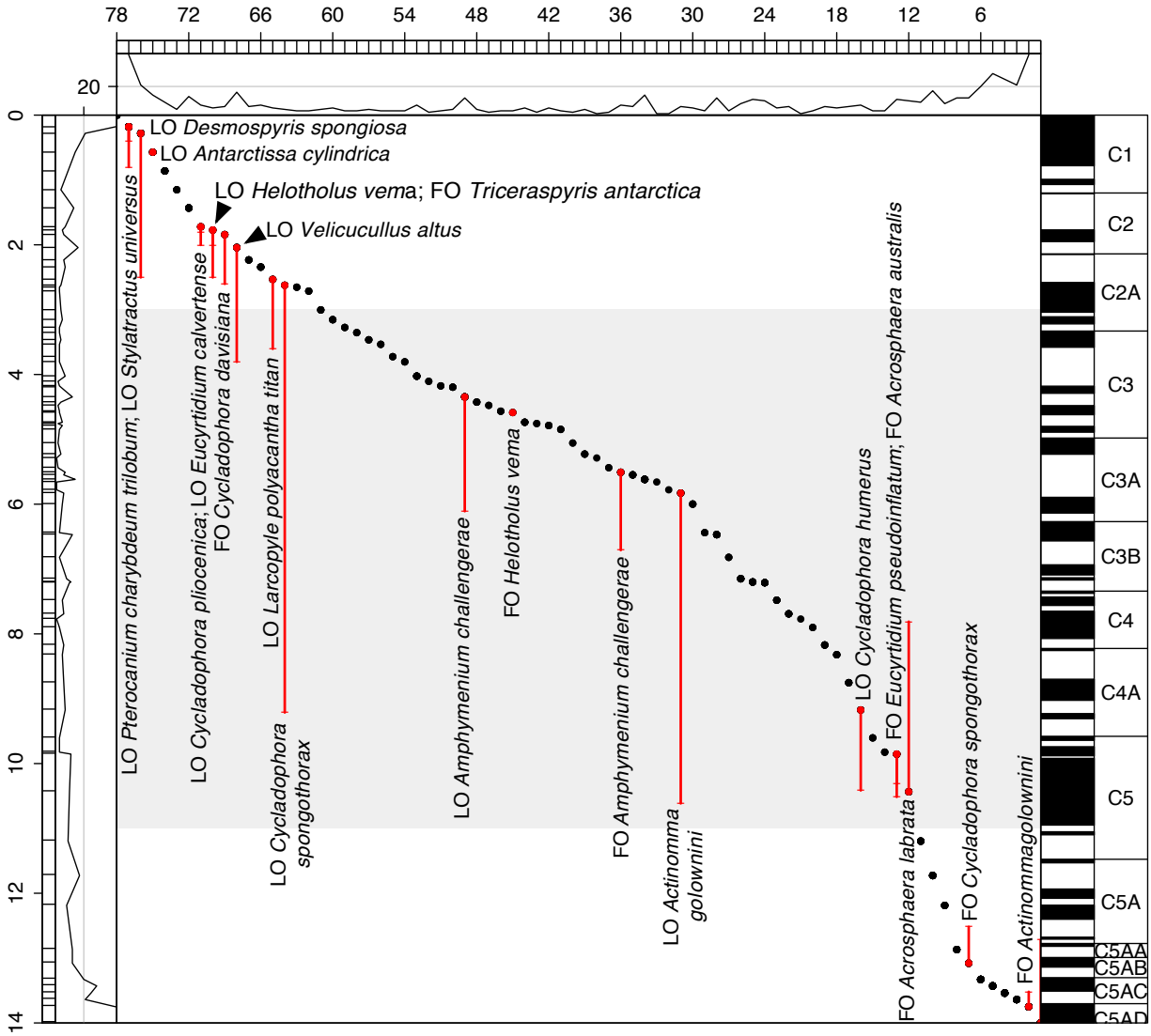

Figure 8.– Discrepancies between the published age for radiolarian bioevents and their age after the CONOP analysis on a graph comparing ranked event horizons to the age model implied by the analysis.
The classic radiolarian bioevents are spotted as red dots. Red segments show the time difference between their published age and their place in the composite sequence. Curves on the x and y axes show the density of events in each event horizon. Grey zone is the interval of focus of this study (3 to 11 Ma).

Figure 7.– Range-chart for a selection of species with usable LO, FO, LCO or FCO.
Occurrences of each species in samples (represented on the composite sequence of event on the side) by a black dot whose size increases with abundance (categorical; see legend). Taxa are arranged in order of first appearances. Highlighted grey area is the area of focus of the study (3 to 11 Ma).

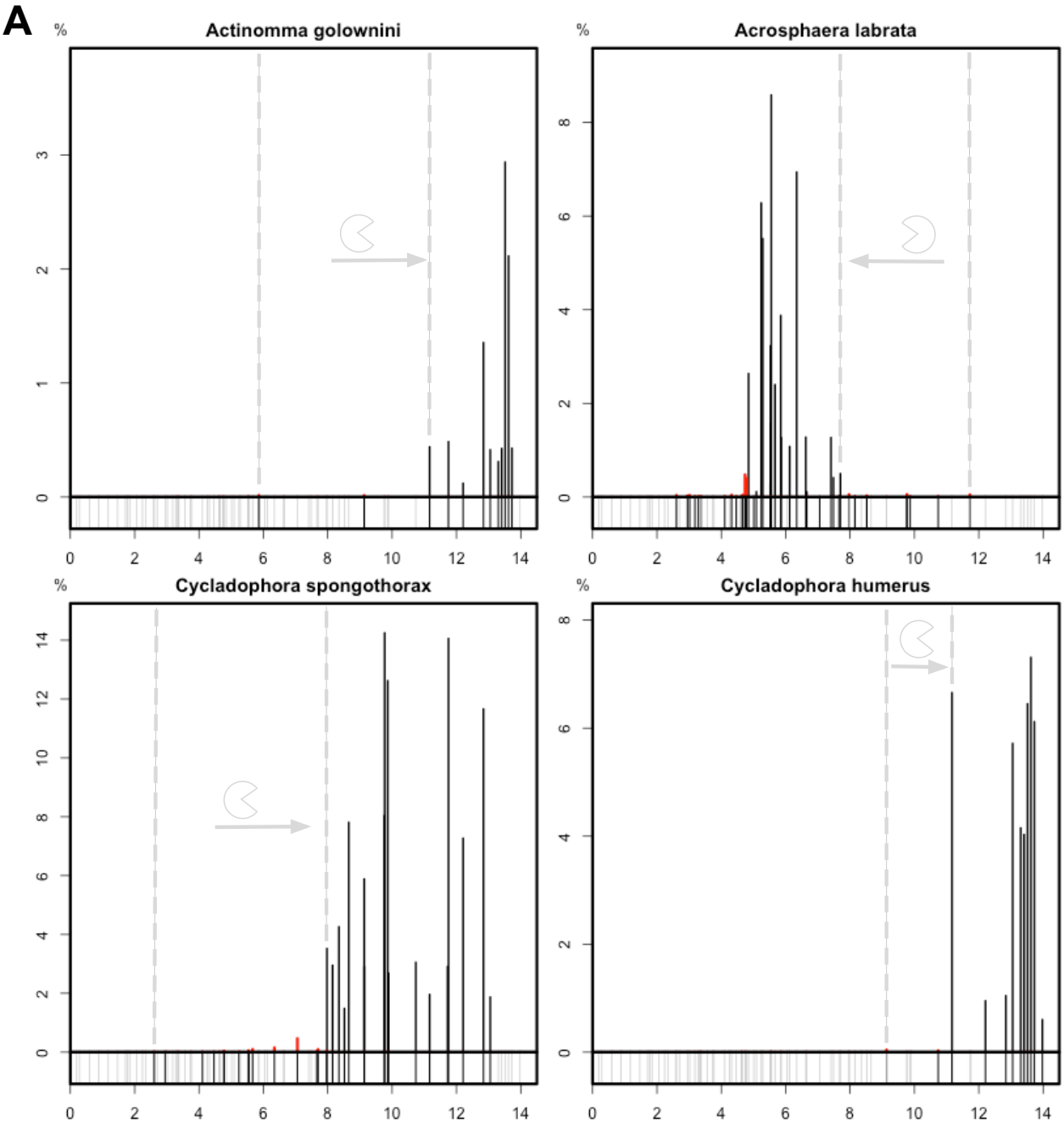

Figure 9A.– Abundance plots of various species classically used for biostratigraphy.
Abundances are expressed in percentage. Ages in Ma. Red bars are samples trimmed by a pacman profiling (with 3% and 1% trimmed for, respectively, the top and the bottom of the range. At the bottom of the plots, black bars correspond to samples where the species is present and grey bars samples where the species is absent.

Reassessment of classically used events.– Figure 8 shows the discrepancies between the published ages and those derived from this study for the formerly used radiolarian bioevents. Several events have a relatively significant dissimilarity here with their published age (a difference higher than 1My).

The LO of *Actinomma golownini* has a published age of 10.6 Ma: here it appears in the CONOP composite sequence at 5.8 Ma. However, when applying a moderate Pacman trimming (3% for the top of the range and 1% for the bottom; Fig. 9A), it appears that the occurrences (1 single specimen in sample 1138A-12R-3 20-22cm and 1 single specimen in sample 1138A-17R-2 105-107cm) above 11.2 Ma are clearly outlying. A LO at 11.2 Ma would therefore

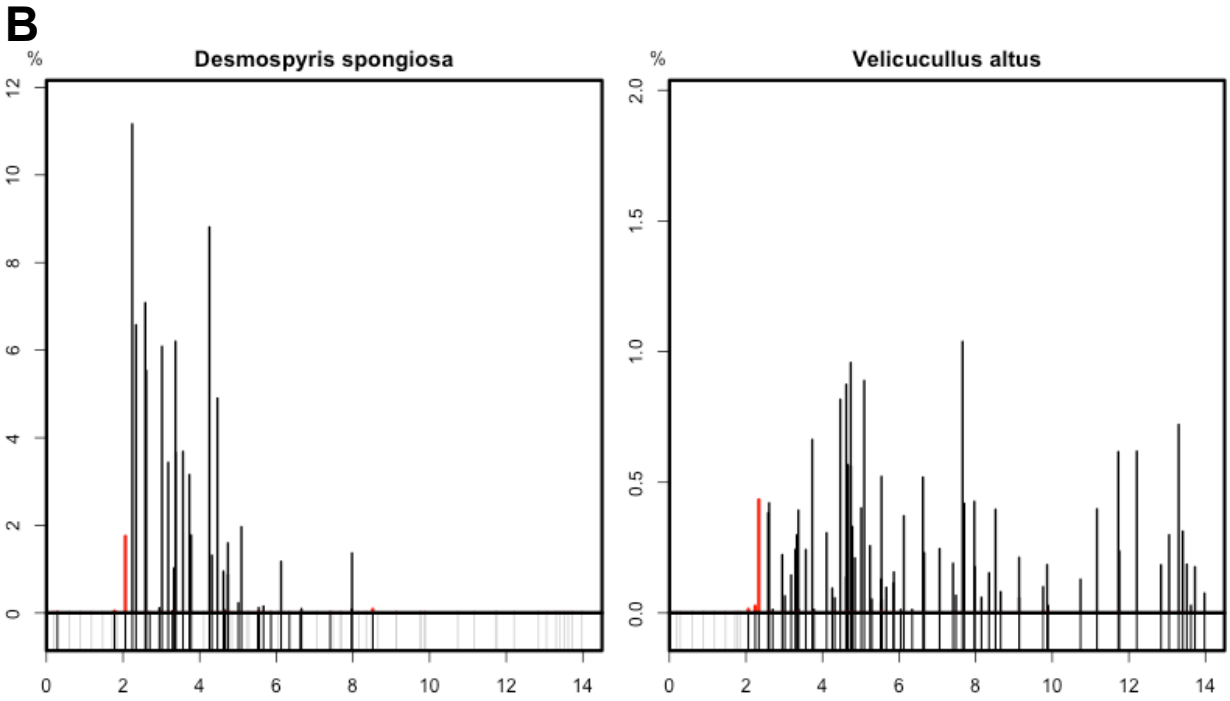

Figure 9B.– Abundance plots of various species classically used for biostratigraphy. See captions for Figure 9A for explanations.

be compliant with the published age considering that only one other sample lies between 11.2 Ma and 10.6 Ma in our dataset. In a similar way, the LO of *Cycladophora spongothorax* has a published age of 9.2 Ma but lies at 2.6 Ma in the composite sequence: after elimination of the oultying occurrences, this LO falls at 8.0 Ma. This age is still significantly different than the published age yet more credible than the original age output by the analysis. Three other events can be improved by the same treatment: the FO of *Acrosphaera labrata*, the LO *Desmospyris spongiosa* and the LO of *Cycladophora humerus*. The first one happens at 10.4 Ma on the composite sequence, and 7.7 Ma after Pacman trimming, to be compared to the published age of 7.8 Ma, the second appears at 0.3 Ma (2 Ma after Pacman trimming), still 0.5 My younger than the published 2.5 Ma while the third one occurs at 9.1 Ma (11.2 Ma after trimming), instead of the published 10.4 Ma (same remark as for the LO of *Actinomma golownini*). Those five events are therefore largely conformable to the already published age, if outlying specimens (mainly reworked or misidentified) are accounted for.

On the other hand, the LO and FO of *Amphymenium challengerae* lie at, respectively, 4.3 and 5.5 Ma instead of the published ages of 6.1 and 6.7 Ma. Because of the extreme scarcity of this species, a Pacman trimming does not spot any outlier to this range and indeed the range seems coherent (see Fig. 7). This species is furthermore very unlikely to be mistaken for another one present in the Southern Ocean, hence discarding a possible misidentification hypothesis. As this species' range defines the *A. challengerae* zone and is critical for age models crossing the Miocene-Pliocene boundary, this is an interesting preliminary result. A more abundant species, *Velicucullus altus* has a LO at 2 Ma instead of the published 3.8 Ma (for LO *Lampromitra coronata* group, see taxonomic notes in chapter 2). A Pacman trimming would lower this LO to 2.6 Ma however the trimmed occurrences do not seem to be properly outliers (see Fig. 9B). The discrepancy between the two ages, in this case, might be linked to the span of the taxonomic concept. Finally the LO of *Larcopyle polyacantha titan* (at 2.5 Ma instead of 3.6 Ma) seems equally robust to a Pacman trimming.

Considering events with a more modest age difference with the former literature: the LO

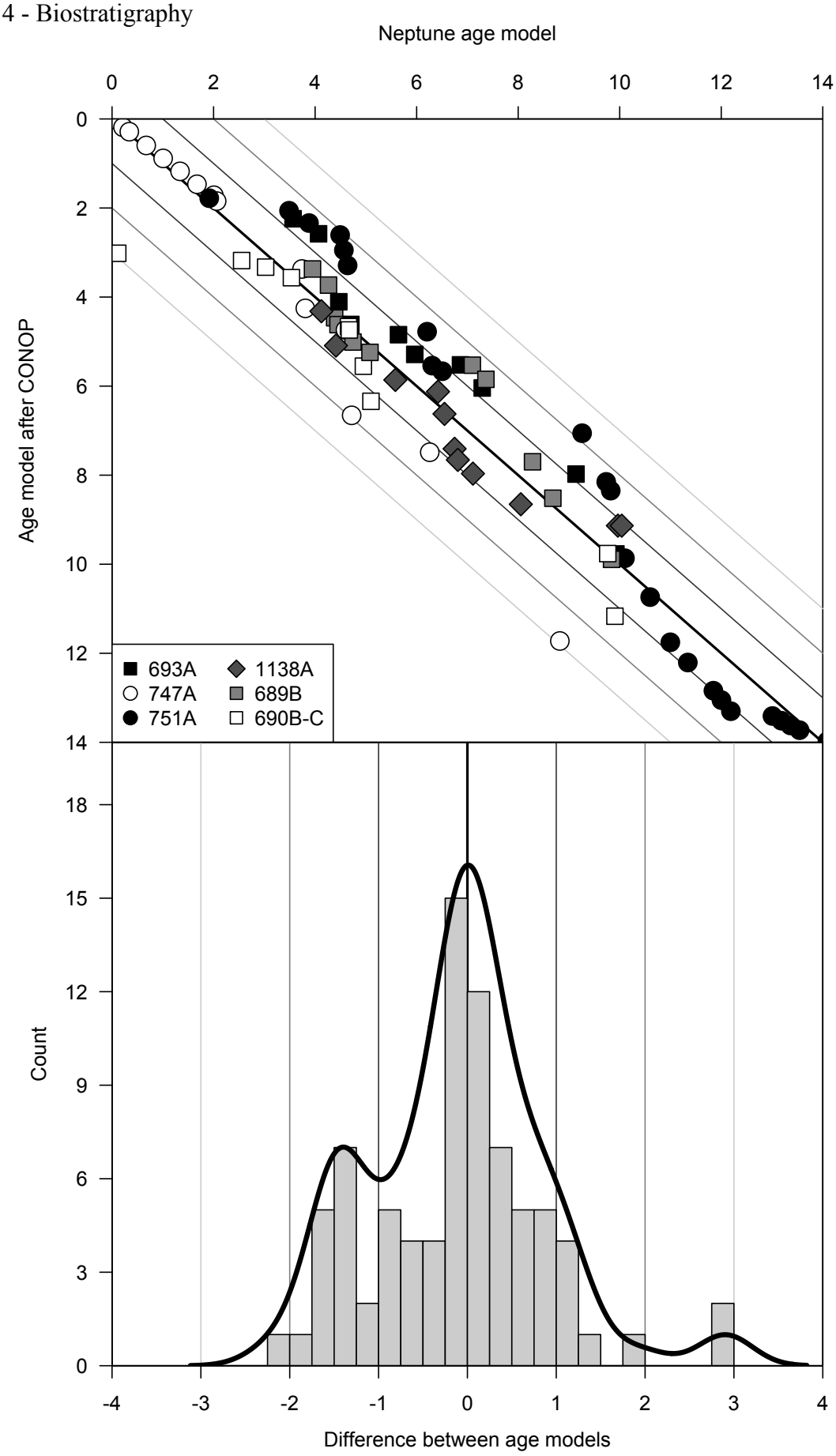

Figure 10.– Comparison (top) between the published age model and the age model resulting from this study and histogram (bottom) of the age models differences. Bold straight line correspond to equivalent age model, dark grey to age models with 1My differences, medium grey 2My and light grey 3My.

of *Pterocanium charybdeum trilobum* is observed here at 0.2 Ma instead of 0.8 Ma, the LO of *Helotholus vema* occurs at 1.8 Ma instead of 2.5 Ma, the FO of *Acrosphaera australis* at 9.8 Ma instead of 10.3 Ma and the FO of *Cycladophora spongothorax* at 13.1 Ma instead of 12.5 Ma.

Finally the following events have an observed age in this study similar to the published age (or have an age difference falling within the sampling uncertainty): the LO of *Stylatractus universus* (0.2 Ma vs the published 0.4 Ma), the LO of *Antarctissa cylindrica* (at 0.6 Ma), the LO of *Cycladophora pliocenica* (observed at 1.7 Ma instead of 1.8 Ma), the FO of *Triceraspyris antarctica* (1.8 Ma observed and 2 Ma published), the LO of *Eucyyrtidium calvertense* (1.7 Ma instead of 2 Ma) and the FO of *Helotholus vema* at 4.6 Ma.

Usable events.– Figure 7 and Table 1 show a selection of 87 potentially useful biostratigraphic species and events. These events have robust ranges (continuous and without trailing range ends; Fig. 7), a low mean misfit (2.5 levels, i. e. less than half the total mean misfit, was considered here a correct threshold) and are widespread (observed at, at least, half the sites, here 3 out of 6). Out of those 87 events, 50 lie between 3 and 11 Ma (i. e. the time span that particularly lacks a solid geochronologic framework as of this date). Although it is a considerable improvement, the interval between 6 and 9 Ma only has 9 potentially usable events: the FO of *Gondwanaria reschetnjakae* at 6 Ma, the LO of *Botryopyle dionisii* at 6.1 Ma, the FO of *Clathromitra pterophormis* at 7.1, of *Phormostichoartus* spG at 7.4 and of *Cycladophora cornutoides* at 7.7 Ma, the LO of *Carpocanium pulchrum* and *Lophophaena macrencephala*? at 8 Ma and the LO of *Lophophaena thaumasia* and the FO of *Stichocorys peregrina* at 8.3 Ma.

In addition to these first and last occurrences, Figure 7 also highlights the usability of some abundance-based events: the first common occurrence (FCO) of *Antarctissa evanida* is indeed clearly identifiable at 4.5 Ma while the last common occurrence (LCO) of *Acrosphaera labrata* lies around 4.7 Ma. The FCO and LCO of *Pentactinosphaera codonia* are, respectively, at 11.2 and 8 Ma; while the LCO of *Circodiscus ellipticus* occurs at 9.8 Ma and that of *Neosemantis bjoerklundi mimicus* happens around 12.2 Ma.

Discussion

The problem with hiatuses.– As shown in the age-depth plots, hiatuses are fairly common both in the published age model and the CONOP-based ones. When an event is displaced by the algorithm from one end to the other of a hiatus, the misfit is the same as the one for an event which is moved between two samples in a continuous section (and this is the case no matter what kind of misfit measure is used obviously). Evidently, if in the next site the hiatus is filled by numerous samples this effect will be countered; however some hiatuses are widespread in the studied sites (e. g. very few sites contain a continuous sequence between 5.5 and 6 Ma or between 3 and 3.5 Ma, see Figs 6A-F). Unfortunately the only solutions would be to define *a priori* the duration of the hiatuses and use that information to develop a secondary measure of misfit superimposed to the other one but, as can be seen when comparing published age models and the new one, the exact extent of those hiatuses is unkown *a priori*. This is probably a potentially significant source of mistake in the CONOP analysis shown here.

Age model coherency with published data.– As can be seen in Figure 10, the difference between the published age model and the (highly preliminary) radiolarian-based age model developed in this study is in half of the samples greater than 0.6 My. A fair number of samples are between 1 and 2 My younger in the new model than in the old one: they are mainly imputable to samples from sites 747 and 751. In both cases it is presumably due, in the original age model, to a difficulty to interpret the paleomagnetic signal.

Conclusion

Although a considerable sampling effort is still needed to achieve an higher resolution biostratigraphy and to resolve this particular seriation problem, the advances made by this study are already noticeable and not negligeable: it seems indeed that 94 bioevents are reliable enough to be used to correlate Southern Ocean sites together. Assigning a numerical age to these events seems however somewhat premature considering the lack of reliability of the magnetostratigraphic polarity signal in most of the studied sites (specifically sites from leg 120 and to some extent leg 113).

Despite the highly preliminary nature of the data and thus analytic results, some interesting features are apparent, such as the adjustment of age models for some sites by more than 1 My, and the tentative recalibration of the *A. challengerae* zone to the basal Pliocene instead of the latest Miocene. This latter, if confirmed by additional data, would reinforce similar tentative inferences from stratigraphic studies of other sites (e.g. Lazarus 2001) and support a substantial re-calibration of many Southern Ocean age-models near the Miocene-Pliocene boundary.

Table 1.– Bioevents with low misfit, widespread and with robust range (see Fig. 7).
Numerical age, number of sites where the species is seen, mean and maximum misfit for the event are given for each of those FO and LO.

Events	Age	# Sites	Mean misfit	Max misfit
LO *Ceratocyrtis mashae*	0.9	6	0.17	1
LO *Cycladophora conica*	1.2	6	2.5	7
LO *Botryostrobus bramlettei*	1.5	5	0.8	2
LO *Ceratocyrtis robustus*	1.5	3	0	0
LO *Sphaeropyle robusta*	1.7	6	0	0
LO *Arachnocorallium* sp5	1.8	6	1.33	6
LO *Stauroxiphos communis*	1.8	6	0.33	1
LO *Dendrospyris haysi*	1.9	6	0.5	2
LO *Archipilium macropus*	2.1	6	1.5	5
LO *Dendrospyris*? *jobstae*	2.1	6	0.33	1
LO *Eucyrtidium cienkowskii*	2.1	6	0	0
LO *Gondwanaria deflandrei*	2.1	6	0.5	1
LO *Lampromitra quadricuspis*	2.1	6	1.33	4
LO *Enneaphormis* sp.	2.1	5	0.4	1
LO *Desmospyris*? spH	2.2	5	1.4	4
LO *Larcopyle peregrinator*	2.2	6	0	0
LO *Antarctissa ballista*	2.3	6	0.5	3
LO *Antarctissa evanida*	2.3	6	1.17	3
LO *Eucyrtidium inflatum*	2.3	6	1.17	3
LO *Eucyrtidium pseudoinflatum*	2.6	6	0.67	2
LO *Helotholus praevema*	2.6	6	0.83	2
LO *Lychnocanium grande*	2.6	6	0.67	2
LO *Botryopera*? spB	2.6	6	1.5	4

LO *Theocorys veneris*	2.6	3	2	4
LO *Pseudodictyophimus* spY	2.7	6	0.67	2
LO *Siphostichoartus jahnae*	2.7	6	1.83	4
FO *Ceratocyrtis robustus*	2.7	3	0	0
LO *Lophospyris pentagona*	3.3	6	1.17	7
LO *Pseudodictyophimus tanythorax*	3.3	6	0.83	3
FO *Enneaphormis* sp.	3.4	5	2	4
LO *Dictyophimus macropterus*	3.7	6	2.5	4
LO *Cycladophora cosma*	4.1	6	0.67	4
LO *Dendrospyris*? *sakaii*	4.1	6	0.67	2
LO *Acrosphaera cuniculiauris*	4.3	6	1.83	5
LO *Antarctissa robusta*	4.5	6	0.83	3
LO *Amphimelissa*? *hibernifortuna*	4.6	6	0.67	2
LO *Helotholus haysi*	4.6	6	1.33	4
LO *Lithomelissa stigi*	4.6	6	0.17	1
LO *Syscioscenium*? *wabisabi*	4.6	6	1.5	2
LO *Phormospyris loliguncula*	4.6	6	1.67	3
LO *Carposphaera*? *annikae*	4.7	6	1	4
LO *Excentrodiscus japonicus*	4.7	6	1.33	3
LO *Phormostichoartus corbula*	4.8	5	1.2	3
LO *Lychnocanium conica*	4.8	6	0.5	1
LO *Saccospyris victoria*	5	5	1.6	6
FO *Dendrospyris*? *jobstae*	5.1	6	0.5	3
LO *Phormostichoartus* spG	5.1	5	0	0
FO *Spongoplegma*? spD	5.2	5	2	5
LO *Lophophaena simplex*	5.3	6	1.17	3
LO *Botryopera*? *gibbera*	5.5	6	1.33	3
LO *Ceratocyrtis cucullaris*	5.5	6	0.67	2
LO *Cornutella clathrata*	5.5	6	1.17	5
LO *Heliodiscus asteriscus*	5.5	6	1	3
LO *Stichocorys peregrina*	5.5	5	1.8	5
FO *Desmospyris*? spH	5.5	5	1.2	4
FO *Theocorys veneris*	5.9	3	0.33	1
FO *Gondwanaria reschetnjakae*	6	6	1.33	5
LO *Botryopyle dionisii*	6.1	5	0.2	1
FO *Clathromitra pterophormis*	7.1	6	1.5	5
FO *Phormostichoartus* spG	7.4	5	2.2	5
FO *Cycladophora cornutoides*	7.7	6	2.5	7
LO *Lophophaena macrencephala*	8	5	0.2	1
LO *Carpocanium pulchrum*	8	4	0	0
LO *Lophophaena thaumasia*	8.3	4	0	0
FO *Stichocorys peregrina*	8.3	5	0.4	1

LO *Lampromitra huxleyi*	9.1	3	0	0
FO *Phormostichoartus corbula*	9.1	5	2	4
FO *Acrosphaera cuniculiauris*	9.9	6	0.83	3
FO *Actinomma popofskii*	9.9	6	0.17	1
FO *Antarctissa cylindrica*	9.9	6	0.67	2
FO *Carpocanium pulchrum*	9.9	4	0.25	1
FO *Eucyrtidium pseudoinflatum*	9.9	6	0.17	1
FO *Heliodiscus asteriscus*	9.9	6	0.33	1
FO *Saccospyris antarctica*	9.9	6	0.33	1
FO *Siphonosphaera vesuvius*	9.9	6	0.5	1
FO *Arachnocorallium* sp5	10.7	6	1.17	3
FO *Helotholus haysi*	10.7	6	1.33	4
FO *Botryopera*? spB	10.7	6	2	5
FO *Acanthodesmia micropora*	11.2	6	1.33	7
FO *Cycladophora bicornis*	11.2	6	0	0
FO *Lychnocanium grande*	11.2	6	0.5	3
FO *Excentrodiscus japonicus*	11.8	6	0.17	1
FO *Larcopyle pylomaticus*	12.8	6	0.17	1
FO *Antarctissa ballista*	13.3	6	0.5	3
FO *Ceratocyrtis mashae*	13.3	6	0.17	1
FO *Clathrocanium coarctatum*	13.3	5	2	10
FO *Botryopyle dionisii*	13.4	5	0.8	2

Conclusions

This study demonstrates the feasability and the utility of whole-fauna analysis. Indeed, despite being studied regularly since the 1950s, the Antarctic Neogene radiolarian fauna was still largely unknown: one species out of four present in the collected material from this region is new to science (Chapter 2). Even with a database such as Neptune containing occurence data for most of the known taxa and for a very large number of samples collected extensively during the past 45 years by the DSDP and ODP campaigns, the macroevolutionary history of this fauna is shown here to have been still inaccurately recorded (Chapter 3). Regardless of the fact that the primary goal of the large majority of studies made on this fauna to date was biostratigraphy, thanks to the use of full-fauna data, the number of potentially usable biostratigraphic events has been multiplied by five for the late Miocene-Early Pliocene sequence in this study (Chapter 4).

Although the complete species-level taxonomy of this fauna has been reassessed in this study, the genus and family-level taxonomy used today for Cenozoic radiolarians is still largely based on the taxonomical framework developed by Haeckel (1862, 1881, 1887), even though is is believed to be highly artificial. Hopefully, the description and illustration of 120 previously unknown or undescribed species will help clarify the phylogenetic relationships between the various groups that constitute this fauna.

It has been shown that the Antarctic Neogene radiolarian fauna underwent important changes in the structure of its community at ca. 8 Ma followed by a drop in diversity at ca. 5 Ma. However, until we have the ability to correlate precisely and accurately these changes with known, global climatic and oceanographic events we can not fully understand their triggering mechanisms.

The biostratigraphy presented in this study, though promising, is still largely preliminary: heavy sampling is still required in order to develop a high resolution radiolarian biostratigraphy in the late Neogene. Once this is achieved, reconsidering the macroevolutionary history unveiled in this study in the light of a new, reliable and precise age model will allow us to understand the mechanisms behind macroevolutionary changes in planktonic protista.

References

Abelmann, A. 1990. Oligocene to middle Miocene radiolarian stratigraphy of southern high latitudes from Leg 113, Sites 689–690, Maud Rise. *In* P. F. Barker et al. (Eds), *Proceedings of the Ocean Drilling Program, Scientific Results*, College Station, TX (Ocean Drilling Program), 113: 675–708.

——. 1992a. Radiolarian taxa from Southern Ocean sediment traps (Atlantic sector). *Polar Biology*, 12: 373-385.

——. 1992b. Early to Middle Miocene radiolarian stratigraphy of the Kerguelen Plateau, leg 120. *In* S. W. Wise Jr et al. (Eds), *Proceedings of the Ocean Drilling Program, Scientific Results*, College Station, TX (Ocean Drilling Program), 120: 757-783.

Abelmann, A., U. Brathauer, R. Gersonde, R. Sieger & U. Zielinski. 1999. Radiolarian-based transfer function for the estimation of sea surface temperatures in the Southern Ocean (Atlantic sector). *Paleoceanography*, 14(3): 410-421.

Abramoff, M. D., P. J. Magelhaes & S. J. Ram. 2004. Image Processing with ImageJ. *Biophotonics International*, 11(7): 36-42.

Adams, C. G., R. H. Benson, R. B. Kidd, W. B. F. Ryan & R. C. Wright. 1977. The Messinian Salinity Crisis and evidence of Late Miocene eustatic changes in the world ocean. *Nature,* 269: 383-386.

Alroy, J. 1996. Constant extinction, constrained diversification, and uncoordinated stasis in North American mammals. *Palaeogeography, Palaeoclimatology, Palaeoecology*, 127: 285-311.

——. 2000. New methods for quantifying macroevolutionary patterns and processes. *Paleobiology*, 26(4): 707-733.

——. 2010a. Geographical, environmental and intrinsic biotic controls on Phanerozoic marine diversification. *Palaeontology*, 53(6): 1211-1235.

——. 2010b. Fair sampling of taxonomic richness and unbiased estimation of origination and extinction rates. *In* J. Alroy and G. Hunt (Eds), Quantitative methods in paleobiology. *The Paleontological Society Papers*, 16: 55-80.

Alroy, J., C. R. Marshall, R. K. Bambach, K. Bezusko, M. Foote, F. T. Fürsich, T. A. Hansen, S. M. Holland, L. C. Ivany, D. Jablonsky, D. K. Jacobs, D. C. Jones, M. A. Kosnik, S. Lidgard, S. Low, A. I. Miller, P. M. Novack-Gottshall, T. D. Olszewski, M. E. Patzkowsky, D. M. Raup, K. Roy, J. J. Sepkoski Jr, M. G. Sommers, P. J. Wagner & A. Webber. 2001. Effects of sampling standardization on estimates of Phanerozoic marine diversification. *Proceedings of the National Academy of Sciences*, 98(11): 6261-6266.

Apel, M., W. Kiessling, F. Böhm & D. Lazarus. 2002. Radiolarian faunal characteristics in Oligocene sediments of the Kerguelen Plateau, Leg 183, Site 1138. *In* F. A. Frey et al. (Eds), *Proceedings of the Ocean Drilling Program, Scientific Results*, College Station, TX (Ocean Drilling Program), 183: 48pp.

Anderson, J. B. & S. S. Shipp. 2001. Evolution of the West Antarctic Ice Sheet. *In* R. B: Alley & R. A. Bindschadler (Eds), The West Antarctic Ice Sheet: Behavior and Environment, *Antarctic Research Series,* 77: 45-58.

Anderson, O. R. 1976. A cytoplasmic fine-structure study of two spumellarian Radiolaria and their symbionts. *Marine micropaleontology,* 1: 81-99.

———. 1977. A cytoplasmic fine-structure study of nassellarian Radiolaria. *Marine micropaleontology,* 2: 251-264.

——. 1978. Light and electron microscopic observation sof feeding behavior, nutrition and reproduction in laboratory cultures of *Thalassicolla nucleata*. *Tissue & Cell*, 10(3): 401-412.

——. 1983. *Radiolaria*. Springer-Verlag, New York, 355pp.

Anderson, O. R. & A. Matsuoka. 1992. Endocytoplasmic microalgae and bacteroids within the central capsule of the radiolarian *Dictyocoryne truncatum*. *Symbiosis*, 12: 237-247.

Anderson, O. R., N. S. Swanberg & P. Bennett. 1984. An estimate of predation rate and relative preference for algal versus crustacean prey by a spongiose skeletal radiolarian. *Marine biology*, 78: 205-207.

Bailey, J. W. 1856. Notice of microscopic forms found in the soundings of the Sea of Kamtschatka. *American Journal of Science and Arts*, 2nd Series, 22: 1-6.

Barker, P. F. & E. Thomas. 2004. Origin, signature and palaeoclimatic influence of the Antarctic Circumpolar Current. *Earth-Science Reviews*, 66: 143-162.

Barron, E. J. & W. H. Peterson. 1991. The Cenozoic ocean circulation based on ocean General Circulation Model results. *Palaeogeography, Palaeoclimatology, Palaeoecology,* 83: 1-28.

Barron, J. A., J. G. Baldauf, E. Barrera, J.-P. Caulet, B. T. Huber, B. H. Keating, D. B. Lazarus, H. Sakai, H. R. Thierstein & W. Wei. 1991. Biochronologic and Magnetochronologic synthesis of leg 119 sediments from the Kerguelen Plateau and Prydz Bay, Antarctica. *In* J. Barron & B. Larsen (Eds), *Proceedings of the Ocean Drilling Program, Scientific Results*, College Station, TX (Ocean Drilling Program), 119: 813-847.

Bass, D. D. Moreira, P. López-García, S. Polet, E. E. Chao, S. von der Heyden, J. Pawlowski & T. Cavalier-Smith. 2005. Polyubiquitin insertions and the phylogeny of Cercozoa and Rhizaria. *Protist,* 156: 149-161.

Benson, R. N. 1966. *Recent Radiolaria from the Gulf of California.* PhD Thesis, University of Minnesota, Minneapolis.

——. 1983. Quaternary radiolarians from the mouth of the Gulf of California, Deep Sea Drilling Project Leg 65. *In* B. T. R. Lewis et al. (Eds), *Initial Reports of the Deep Sea Drilling Project,* Washington (U. S. Govt Printing Office), 65: 491-523.

Berggren, W. A., D. V. Kent, J. F. Flynn & J. A. van Couvering. 1985. Cenozoic geochronology. *Geological Society of America, Bulletin,* 96: 1407-1418.

Berggren, W. A., D. V. Kent, C. C. Swisher III & M.-P. Aubry. 1995. A revised Cenozoic geochronology and chronostratigraphy. *In* W. A. Berggren et al. (Eds), Geochronology time scales and global stratigraphic correlation, *SEPM Special Publication*, 54: 129-212.

Bernstein, R. E., R. H. Byrne & J. Schijf. 1998. Acantharians: a missing link in the oceanic biogeochemistry of barium. *Deep-Sea Research I,* 45: 491-505.

Billups, K. 2002. Late Miocene through early Pliocene deep water circulation and climate change viewed from the sub-antarctic South Atlantic. *Palaeogeography, Palaeoclimatology, Palaeoecology*, 185: 287-307.

Billups, K., C. Kelly & E. Pierce. 2008. The late Miocene to early Pliocene climate transition in the Southern Ocean. *Palaeogeography, Palaeoclimatology, Palaeoecology*, 267: 31-40.

Bjørklund, K. R. 1976a. Radiolaria from the Norwegian Sea, Leg 38 of the Deep Sea Drilling Project. *In* M. Talwani et al. (Eds), *Initial Reports of the Deep Sea Drilling Project*, Washington (U.S. Govt. Printing Office), 38: 1101-1168.

——. 1976b. *Actinomma haysi*, n. sp., its Holocene distribution and size variation in Atlantic Ocean sediments. *Micropaleontology*, 23(1): 114-126.

Bjørklund, K. R. & R. M. Goll. 1979. Internal skeletal structures of Collosphaera and Trisolenia: A case of repetitive evolution in the Collosphaeridae (Radiolaria). *Journal of Paleontology*, 53(6): 1293-1326.

Bjørklund, K. R. & S. B. Kruglikova. 2003. Polycystine radiolarians in surface sediments in the Arctic Ocean basins and marginal seas. *Marine Micropaleontology,* 49(3): 231-273.

Bjørklund, K. R., G. Cortese, N. Swanberg & H. J. Schrader. 1998. Radiolarian faunal provinces in surface sediments of the Greenland, Iceland and Norwegian (GIN) Seas. *Marine Micropaleontology,* 35: 105-140.

Blanc, P.-L. & J.-C. Duplessy. 1982. The deep-water circulation during the Neogene and the impact of the Messinian Salinity Crisis. *Deep-Sea Research,* 29(12A): 1391-1414.

Blueford, J. R. 1982. Miocene actinommid Radiolaria from the Equatorial Pacific. *Micropaleontology*, 28(2): 189-213.

Bohaty, S. M., S. W. Wise Jr, R. A. Duncan, C. L. Moore & P. J. Wallace. 2003. Neogene diatom biostratigraphy, tephra stratigraphy, and chronology of ODP Hole 1138A, Kerguelen Plateau. *In* F. A. Frey et al. (Eds), *Proceedings of the Ocean Drilling Program, Scientifc Results*, College Station ,TX (Ocean Drilling Program), 183: 53pp.

Boltzmann, L. 1872. Weitere studien über das wärmegleichgewicht unter gasmolekülen. *Sitzungsberichte der Akademie der Wissenschaften*, Wien, 66: 275-370.

Boltovskoy, D. 1995. Pelagic biogeography: background, gaps and trends. *In* A. C. Pierrot-Bults & S. van der Spoel (Eds.), *Pelagic Biogeography ICoPB II: Proceedings of the 2nd International Conference. Final reports of SCOR/IOC Working Group 93. IOC Workshop Report*, 142: 53-64

——. 1998. Classification and Distribution of South Atlantic recent Polycystine Radiolaria. *Palaeontologica Electronica*, 1(2): 116pp.

Boltovskoy, D. & W. R. Riedel. 1980. Polycystine Radiolaria from the southwestern Atlantic Ocean plankton. *Revista Española de Micropaleontologia*, 12: 99-146.

——. 1987. Polycystine Radiolaria of the California Current region: seasonal and geographic patterns. *Marine Micropaleontology,* 12: 65-104.

Boltovskoy, D., S. A. Kling, K. Takahashi & K. R. Bjørklund. 2010. World atlas of distribution of recent Polycystina (Radiolaria). *Palaeontologia Electronica*, 13(3): 230pp.

Borgert, A. 1901. Die nordische Tripyleen-Arten. *Nordisches Plankton*, 15: 1-52.

Borgert, A. 1907. Die Tripyleen Radiolarien der Plankton-Expedition. Concharidae. *Ergebnisse der Plankton-Expedition der Humboldt-Stiftung,* 3(5): 195-237.

Borisenko, N. N. 1958. Radiolyarii paleotsena zapadnoi Kubani. *In* A. P. Krylov (Ed), Voprosy geologii, bureniya i ekspluatatsii skvashin, *Trudy Vsesoyuzni Neftegazovyi Nauchno-Issledovaleskii Institut, Krasnodarskii Filial*, 17: 81-100.

Boyden, J., R. D. Müller, M. Gurnis, T. Torsvik, J. Clark, M. Turner, H. Ivey-Law. J. Farrow & R. Watson. 2011. Next-generation plate-tectonic reconstructions using GPlates. *In* G. R. Keller & C. Baru (Eds), *Geoinformatics: Cyberinfrastructure for the Solid Earth Sciences*, London (Cambridge University Press), 95-113.

Brandt, K., 1905. Zur Systematik der koloniebildenden Radiolarien. *Zoologische Jarbucher, Jena,* 21(8): 311-352.

Broecker, W. S. 1987. The biggest chill. *Natural History,* 97: 74-82.

Bush, A. M., M. J. Markey and C. R. Marshall. 2004. Removing bias from diversity curves: the effect of spatially organized biodiversity on sampling-standardization. *Paleobiology*, 30(4): 666-686.

Bütschli, O. 1882. Beiträge zur Kenntnis der Radiolarienskelette, insbesondere der Cyrtida. *Zeitschrift für wissenschaftliche Zoologie*, 36: 485-540.

Cachon, J. & M. Cachon. 1969. Révision systématique des Nassellaires *Plectoidea* à propos de la description d'un nouveau représentant, *Plectagonidium deflandrei* nov. gen. nov. sp. *Archiv für Protistenkunde*, 111: 236-251.

——. 1971. Le système axopodial des Radiolaires Nassellaires. *Archiv für Protistenkunde*, 113: 80-97.

——. 1972a. Le système axopodial des Radiolaires Sphaeroïdés. 1. Les Centroaxoplastidiés. *Archiv für Protistenkunde,* 114: 51-64.

——. 1972b. Le système axopodial des Radiolaires Sphaeroïdés. 2. Les Périaxoplastidiés. 3. Les Cryptoaxoplastidiés (Anaxoplastidiés). 4. Les fusules et le système rhéoplasmique. *Archiv für Protistenkunde,* 114: 291-307.

Calkins, G. N. 1901. The Protozoa. *Columbia University Biological Series,* New York (MacMillan Company), 6: 347pp.

Campbell, A. S. 1951. New genera and subgenera of Radiolaria. *Journal of Paleontology*, 25(4): 527-530.

Campbell, A. S. & B. L. Clark. 1942. Eocene radiolarian faunas from the Mt. Diablo area, California. *Geological Society of America, Special Papers*, 39: 1-112.

——. 1944. Miocene Radiolarian faunas from Southern California. *Geological Society of America, Special Papers*, 51: 1-76.

Cande, S. C., J. M. Stock, R. D. Müller & T. Ishihara. 2000. Cenozoic motion between East and West Antarctica. *Nature,* 404: 145-150.

Cane, M. A. & P. Molnar. 2001. Closing of the Indonesian seaway as a precursor to east African aridification around 3-4 million years ago. *Nature*, 411: 157-162.

Caridroit, M., P. De Wever & P. Dumitrica. 1999. Un nouvel ordre, une nouvelle famille et un nouveau genre de Radiolaires du Paléozoïque: Latentifistularia, Caulettidae et *Cauletella*. *Comptes Rendus de l'Académie des Sciences, Series IIa: Science de la Terre et des Planètes,* 329: 603-608.

Carnevale, P. 1908. Radiolarie e Silicoflagellati di Bergonzano (Reggio Emilia). *Memorie del Reale Istituo Veneto di Scienze, Lettere ed Arti,* 28(3): 1-46.

Caulet, J.-P. 1982. Faunes de radiolaires et fluctuations climatiques dans les sédiments de l'Océan Indien austral: une nouvelle biozonation. *Bulletin de la société géologique de France*, 24: 555-562.

——. 1986. Radiolarians from the Southwest Pacific. *In* J. P. Kennett et al. (Eds), *Initial Reports of the Deep Sea Drilling Project*, Washington (U.S. Govt. Printing Office), 90: 835-861.

——. 1991. Radiolarians from the Kerguelen Plateau, ODP Eg 119. *In* J. Barron & B. Larsen (Eds.), *Proceedings of the Ocean Drilling Program, Scientific Results*, College Station, TX (Ocean Drilling Program), 119: 513-546.

Caulet, J.-P. & C. Nigrini. 1988. The genus *Pterocorys* (Radiolaria) from the late Neogene of the Indian and Pacific Oceans. *Micropaleontology*, 34(3): 217-235.

Cavalier-Smith, T. 1993. Kingdom Protozoa and its 18 Phyla. *Microbiological Reviews,* 57(4): 953-994.

——. 1998. A revised Six Kingdom of Life. *BIological Reviews,* 73: 203-266.

——. 1999. Principles of protein and lipid targeting in seconday symbiogenesis: euglenoid, dinoflagellates, and sporozoan plastid origins and the Eukaryote Family Tree. *Journal of Eukaryotic Microbiology,* 46(4): 347-366.

——. 2002. The phagotrophic origin of eukaryotes and phylogenetic classification of Protozoa. *International Journal of Systematic and Evolutionary Microbiology*, 52: 297–354.

Cervato, C. & L. Burckle. 2003. Pattern of first and last appearance in diatoms: oceanic circulation and the position of polar fronts during the Cenozoic. *Paleoceanography*, 18(2): PA000805.

Chao, A. & S.-M. Lee. 1992. Estimating the number of classes via sample coverage. *Journal of the American Statistical Association*, 87(417): 210-217.

Chatton, E. 1920. Les péridiniens parasites: morphologie, reproduction, éthologie. *Archives de zoologie expérimentale et générale,* 59: 1-475.

Chen, P.H. 1975. Antarctic Radiolaria. *In* D. E. Hayes et al. (Eds), *Initial Reports of the Deep Sea Drilling Project*, Washington (US Govt Printing Office), 28: 437–513.

Clark, B. L. & A. S. Campbell. 1942. Eocene radiolarian faunas from the Monte Diablo area, California. *Geological Society of America, Special Paper*, 39: 1-112.

Cleve, P. T. 1899. Plankton collected by the Swedish Expedition to Spitzbergen in 1898. *Kongliga Svenska Vetenskaps-Akademiens Handlingar*, 32: 25-51

——. 1900. Notes on some Atlantic plankton organisms. *Kongliga Svenska Vetenskaps-Akademiens Handlingar*, 34(1): 1-22.

Cody, R., R. H. Levy, D. M. Harwood & P. M. Sadler. 2008. Thinking outside the zone: High-resolution quantitative diatom biochrnology for the Antarctic Neogene. *Palaeogeography, Palaeoclimatology, Palaeoecology,* 260: 92-121.

Colwell, R. K. & J. A. Coddington. 1994. Estimating terrestrial biodiversity through extrapolation. *Philosophical transactions of the Royal Society of London, B*, 345: 101-118.

Cooke, P. J. C. S. Nelson, M. P. Crundwell & D. Spiegler. 2002. *Bolboforma* as monitors of Cenozoic palaeoceanographic changes in the Southern Ocean. *Palaeogeography, Palaeoclimatology, Palaeoecology,* 188: 73-100.

Cortese, G. & A. Abelmann. 2002. Radiolarian-based paleotemperatures during the last 160kyr at ODP Site 1089 (Southern Ocean, Atlantic Sector).

Cortese, G. & K. R. Bjørklund. 1998. The taxonomy of boreal Atlantic Ocean Actinommida (Radiolaria). *Micropaleontology,* 44(2): 149-160.

Deacon, G. E. R. 1933. A general account of the hydrology of the South Atlantic Ocean. *Discovery Reports,* 7: 171-238.

De Caprariis, P., R. H. Lindemann & C. M. Collins. 1976. A method for determining optimum sample size in species diversity studies. *Mathematical Geology*, 8(5): 575-581.

De Caprariis, P., R. H. Lindemann & R. Haimes. 1981. A relationship between sample size and accuracy of species richness predictions. *Mathematical Geology*, 13(4): 351-355.

De Conto, R. M. & D. Pollard. 2003. Rapid Cenozoic glaciation of Antarctica induced by declining atmospheric CO_2. *Nature,* 421: 245-249.

De Conto, R. M., D. Pollard, P. A. Wilson, H. Pälike, C. H. Lear & M. Pagani. 2008. Thresholds for Cenozoic bipolar glaciation. *Nature,* 455: 652-656.

Deflandre, G. 1953. Radiolaires fossiles. *Traité de Zoologie*, 1(2): 389-436.

De Wever, P., A. Sanfilippo, W. R. Riedel & B. Gruber. 1979. Triassic radiolarians from Greece, Sicily and Turkey. *Micropaleontology*, 25(1): 75-110.

De Wever, P., P. Dumitrica, J.-P. Caulet, C. Nigrini & M. Caridroit. 2001. *Radiolarians in the sedimentary record*. Gordon and Breach, Amsterdam.

De Wever, P., L. O'Dogherty, M. Caridroit, P. Dumitrica, J. Guex, C. Nigrini & J.-P. Caulet. 2003. Diversity of radiolarian families through time. *Bulletin de la Société Géologique de France,* 174(5): 453-469.

Diester-Haass, L. C. Robert & H. Chamley. 1996. The Eocene-Oligocene preglacial-glacial transition in the Atlantic sector of the Southern Ocean (ODP Site 690). *Marine Geology,* 131: 123-149.

Diester-Haass, L., K. Billups & K. C. Emeis. 2005. In search of the late Miocene - early Pliocean "biogenic bloom" in the Atlantic Ocean (Ocean Drilling Program Sites 982, 925, 1088). *Paleoceanography*, 20: PA4001.

Dogiel, V. A. & V. V. Reshetnyak. 1952. Materialy po radiolyariyam severo-zapadnoy chasti tikhogo okeana. *Issledovanya Dalnevostochnykh Morei SSSR*, 3: 5-36.

Dolven, J. K., C. Lindqvist, V. A. Albert, K. R. Bjørklund, T. Yuasa, O. Takahashi & S. Mayama. 2007. Molecular diversity of alveolates associated with neritic North Atlantic radiolarians. *Protist*, 158: 65-76.

d'Orbigny, A. D. 1826. Tableau méthodique de la classe des Céphalopodes. *Annales des Sciences Naturelles*, 7: 96-314.

Dreyer, F. 1889. Die Pylombildungen in vergleichend-anatomischer und entwicklungsgeschichtlicher Beziehung bei Radiolarien und bei Protisten überhaupt, nebst System und Beschreibung neuer und der bis jetzt bekannten pylomatischen Spumellarien. *Jenaische Zeitschrift für Naturwissenschaft*, Jena, 23: 77-214.

Dujardin, F. 1835. Observations sur les rhizopodes et les infusoires. *Comptes Rendus hebdomadaires des scéances de l'Académie des Sciences,* 1: 338-340.

Dumitrica, P. 1973. Cretaceous and Quaternary Radiolaria in deep sea sediments from the Northwest Atlantic Ocean and Mediterranean Sea. *In* Ryan et al. (Eds.), *Initial Reports of the Deep Sea Drilling Project*, Washington (U.S. Govt Printing Office), 13: 829-901.

——. 1978a. Badenian Radiolaria from central Paratethys. *In* E. Brestenska (Ed), Chronostratigraphie und Neostratotypen Miozän der Zentralen Paratethys, *Verlag der Slowakischen Academie der Wissenschaften, Bratislava*, 6: 231-261.

——. 1978b. Triassic Palaeoscenidiidae and Entactiniidae from the Vicentinian Alps (Italy) and Eastern Carpathians (Romania). *Dàri de seamà ale sedintelor*, 64: 39-54.

——. 1985. Internal morphology of the Saturnalidae (Radiolaria): systematic and phylogenetic consequences. *Revue de Micropaléontologie*, 28(3): 181-196.

–––. 1988. New families and subfamilies of Pyloniacea (Radiolaria). *Revue de Micropaléontologie*, 31(3): 178-195.

———. 1989. Internal skeletal structures of the Superfamily Pyloniacea (Radiolaria), a basis of a new systematics. *Revista española de Micropaleontologia*, 21(2): 207-264.

——. 1991. Middle Triassic Tripedurnulidae, n. fam. (Radiolaria) from the eastern Carpathians (Romania) and Vicentinian Alps (Italy). *Revue de Micropaléontologie,* 34(4): 261-278.

——. 2001, On the status of the radiolarian genera *Gonosphaera* Jörgensen and *Excentroconcha* Mast. *Revue de Micropaléontologie*, 44(3): 191-198.

Dumitrica, P., N. Caridroit & P. De Wever. 2000. Archaeospicularia, ordre nouveau de radiolaires: une nouvelle étape pour la classification des radiolaires du Paléozoïque inférieur. *Comptes Rendus de l'Académie des Sciences, Séries IIa: Sciences de la Terre et des Planètes*, 330: 563-569.

Dzinoridze, R. N., A. P. Jousé, G. S. Koroleva-Golikova, G. E: Kozlova, G. S. Nagaeva, M. G. Petrushevskaya & N. I. Strelnikova. 1978. Diatom and radiolarian Cenozoic stratigraphy, Norwegian Basin; DSDP Leg 38. *In* M. Talwani et al. (Eds), *Initial Reports of the Deep Sea Drilling Project*, Washington (U. S. Govt Printing Office), Sup. to Vol. 38, 39, 40 & 41: 289-427.

Ehrenberg, C. G. 1839. Über die Bildung der Kreidefelsen und des Kreidemergels durch unsichtbare Organismen. *Königlichen Preußischen Akademie der Wissenschaften zu Berlin, Abhandlungen, Jahre 1838*, 59-147.

——. 1844a. Über 2 neue Lager von Gebirgsmassen aus Infusioren als Meeres-Absatz in Nord-Amerika und eine Vergleichung derselben mit den organischen Kreide-Gebirgen in Europa und Afrika. *Monatsberichte der Königlich Preußischen Akademie der Wissenschaften zu Berlin, Jahre 1844*, 57-97.

——. 1844b. Einige vorlaufige Resultate seiner Untersuchungen der ihm von der Sudpolreise des Captain Ross, so wie von den Herren Schayerund Darwin zugekommenen Materialien über das Verhalten des kleinsten Lebens in den Oceanen und den grossten Bisher zuganglichen Tiefen des Weltmeeres. *Königlichen Preußischen Akademie der Wissenschaften zu Berlin, Bericht, Jahre 1844*, 182-207.

——. 1847. Über die mikroskopischen kieselschaligen Polycystinen als mächtige Gebirgsmasse von Barbados und über das Verhältniss deraus mehr als 300 neuen Arten bestehenden ganz eigenthümlichen Formengruppe jener Felsmasse zu den jetzt lebenden Thieren und zur Kreidebildung. *Königlichen Preußischen Akademie der Wissenschaften zu Berlin, Bericht, Jahre 1847*, 40-60.

——. 1854a. Die systematische Charakteristik der neuen Mikroskopischen Organismen des Tiefen Atlantischen Oceans. *Königlichen Preußischen Akademie der Wissenschaften zu Berlin, Bericht, Jahre 1854*, 236-250.

——. 1854b. *Mikrogeologie*. Voss, Leipzig, 374pp.

——. 1861. Über den Tiefgrund des stillen Oceans zwischen Californien und des Sandwich-Inseln. *Königlichen Preußischen Akademie der Wissenschaften zu Berlin, Monatsbericht, Jahre 1860*, 819-833.

——. 1873a. Mikrogeologische Studien als Zusammenfassung seiner Beobachtungen des kleinsten Lebens der Meeres-Tiefgrunde aller Zonen und dessen geologischen Einfluss. *Konigliche Preußischen Akademie der Wissenschaften zu Berlin, Monatsbericht, Jahre 1872*, 265-322.

——. 1873b. Mikrogeologische Studien über das kleinste Leben der Meeres-Tiefgründe aller Zonen und dessen geologischen Einfluss. *Monatsberichte der Königlich Preußischen Akademie der Wissenschaften zu Berlin*, *Jahre 1872,* 131-399.

——. 1874. Grössere Felsproben des Polycystinen-mergels von Barbados mit weiteren Erläuterungen. *Monatsberichte der Königlich Preußischen Akademie der Wissenschaften zu Berlin, Jahre 1873,* 213-263.

——. 1876. Fortsetzung der mikrogeologischen Studien als Gesammt übersicht der mikroskopischen Paläontologie gleichartig analysirter Gebirgsarten der Erde, mit specieller Rücksicht auf den Polycystinen-mergel Von Barbados. *Königlichen Preußischen Akademie der Wissenschaften zu Berlin, Abhandlungen, Jahre 1875*, 1-225.

Ehrmann, W. U. & A. Mackensen. 1992. Sedimentological evidence for the formation of an East Antarctic ice sheet in Eocene/Oligocene time. *Palaeogeography, Palaeoclimatology, Palaeoecology,* 93: 85-112.

Ezard, T. H. G., T. Aze, P. N. Pearson & A. Purvis. 2011. Interplay between changing climate and species' ecology drives macroevolutionary dynamics. *Science*, 332: 349-351.

Fils, D., C. Cervato, J. Reed, P. Diver, X. Tang, G. Bohling & D. Greer. 2009. CHRONOS architecture: experiences with an open-source services-oriented architecture for geoinformatics. *Computers & Geosciences*, 35: 774-782.

Flower, B. P. 1999. Cenozoic deep-sea temperatures and polar glaciation: the oxygen isotope record. *Terra Antarctica Reports,* 3: 27-42.

Flower, B. P. & J. P. Kennett. 1994. The middle Miocene climatic transition: East Antarctic ice sheet development, deep ocean circulation and global carbon cycling. *Palaeogeography, Palaeoclimatology, Palaeoecology,* 108: 535-555.

Fol, H. 1883. Sur le *Sticholonche zanclea* et un nouvel ordre de Rhizopodes. *Memoires de l'Institut National Genevois,* 15: 1-35.

Foreman, H. P. 1973. Radiolaria of Leg 10 with systematics and ranges for the families Amphipyndacidae, Artostrobiidae, and Theoperidae. *In* J. L. Worzel et al. (Eds), *Initial Reports of the Deep Sea Drilling Project*, Washington (U.S. Govt. Printing Office), 10: 407- 474.

Foote, M. 2000. Origination and extinction components of taxonomic diversity: general problems. *Paleobiology*, 26(sp4): 74-102.

Friend, J. K. & W. R. Riedel. 1967. Cenozoic orosphaerid radiolarians from tropical Pacific sediments. *Micropaleontology*, 13(2): 217-232.

Funakawa, S. 1994. Plagiacanthidae (Radiolaria) from the Upper Miocene of Eastern Hokkaido, Japan. *Transactions and Proceedings of the Palaeontological Society of Japan, New Series*, 174: 458-483.

——. 1995a. Intrageneric variation and temporal change in the internal skeletal structure of plagiacanthids (Radiolaria) from Hokkaido, Japan. *Transactions and Proceedings of the Palaeontological Society of Japan, New Series,* 180: 208-225.

——. 1995b. Lophophaeninae (Radiolaria) from the upper Oligocene to lower Miocene and intrageneric variation in their internal skeletal structures. *Journal of Geosciences, Osaka City University*, 38: 13-59.

——. 2000. Internal skeletal structures of the Cenozoic genera *Gondwanaria, Lipmanella* and *Lithomelissa* (Plagiacanthidae, Nassellaria) and their taxonomy. *Micropaleontology*, 46(2): 97-121.

Funakawa, S. & H. Nishi. 2005. Late middle Eocene to late Oligocene radiolarian biostratigraphy in the Southern Ocean (Maud Rise, ODP Leg 113, Site 689). *Marine Micropaleontology*, 54: 213-247.

Funakawa, S., H. Nishi, T. C. Moore & C. Nigrini. 2005. Data report: Late Eocene- Early Oligocene radiolarians, ODP Leg 199 Holes 1218A, 1219A and 1220A, Central Pacific. *In* P. A. Wilson, M. Lyle & J. V. Firth (Eds), *Proceedings of the Ocean Drilling Program, Scientific Results*, College Station, TX (Ocean Drilling Program), 199: 74pp.

Furutani, H. 1982. Skeletal construction and phylogeny of Palaeoscenidiidae. *News of Osaka Micropaleontologists, Special Volume*, 5: 11-16.

Gast, R. J. & D. A. Caron. 2001. Photosymbiotic associations in planktonic Foraminifera and Radiolaria. *Hydrobiologia*, 461: 1-7.

Gersonde, R., A. Abelmann, L. H. Burckle, N. Hamilton, D. B. Lazarus, K. McCartney, P. O'Brien, V. Spieß & S. W. Wise Jr. 1990. Biostratigraphic synthesis of Neogene siliceous microfossils from the Antarctic Ocean, ODP Leg 113 (Weddell Sea). *In* P. F. Barker et al. (Eds), *Proceedings of the Ocean Drilling Program, Scientific Results*, College Station, TX (Ocean Drilling Program), 113: 915-936.

Gill, A. E. 1973. Circulation and bottom water production in the Weddell Sea. *Deep-Sea Research,* 20: 111-140.

Goll, R. M. 1968. Classification and phylogeny of Cenozoic Trissocyclidae (Radiolaria) in the Pacific and Caribbean Basins, Part I. *Journal of Paleontology*, 42(6): 1409-1432.

——. 1969. Classification and phylogeny of Cenozoic Trissocyclidae (Radiolaria) in the Pacific and Caribbean Basins, Part II. *Journal of Paleontology*, 43(2): 322-339.

——. 1976. Morphological intergradation between modern populations of *Lophospyris* and *Phormospyris* (Trissocyclidae, Radiolaria). *Micropaleontology*, 22(4): 379-418.

——. 1978. Five trissocyclid Radiolaria from Site 338. *In* M. Talwani et al. (Eds), *Initial Reports of the Deep Sea Drilling Project*, Washington (U. S. Govt Printing Office), Sup. to Vol. 38, 39, 40 & 41: 177-191.

——. 1979. The Neogene evolution of *Zygocircus, Neosemantis* and *Callimitra*: their bearing on nassellarian classification. *Micropaleontology*, 25(4): 365-396.

——. 1980. Pliocene-Pleistocene radiolarians from the East Pacific Rise and the Galapagos spreading, Deep Sea Drilling Project Leg 54. *In* B. R. Rosendahl et al. (Eds), *Initial Reports of the Deep Sea Drilling Project*, Washington (U.S. Govt. Printing Office), 54: 425-453.

Goll, R. M. & K. R. Bjørklund. 1974. Radiolaria in surface sediments of the South Atlantic. *Micropaleontology*, 20(1): 38-75.

——. 1989. A new radiolarian biostratigraphy for the Neogene of the Norwegian Sea: ODP Leg 104. *In* O. Eldholm et al. (Eds), *Proceedings of the Ocean Drilling Project, Scientific Results*, College Station, TX (Ocean Drilling Program), 104: 697-737.

Good, I. J. 1953. The population frequencies of species and the estimation of population parameters. *Biometrika*, 40(3-4): 237-264.

Goodbody, Q. H. 1986. Wenlock Palaeoscenidiidae and Entactiniidae (Radiolaria) from the Cape Phillips Formation of the Canadian Arctic Archipelago. *Micropalaeontology*, 32(2): 129-157.

Gowing, M. M. 1986. Trophic biology of phaeodarian radiolarians and flux of living radiolarians in the upper 2000 m of the North Pacific central gyre. *Deep-Sea Research*, 33(5): 655-674.

Gradstein, F. M., J. G. Ogg & A. G. Smith. 2004. *A Geological Time Scale 2004*. Cambridge University Press, Cambridge, 589pp.

Grant, K. M. & G. R. Dickens. 2002. Coupled paleoproductivity and carbon isotope records in the southwest Pacific Ocean during the late Miocene - early Pliocene biogenic bloom. *Palaeogeography, Palaeoclimatology, Palaeoecology*, 187: 61-82.

Gregg, W. W. & N. W. Casey. 2007. Modeling coccolithophores in the global oceans. *Deep-Sea Research II*, 54: 447-477.

Grobe, H., D. K. Fütterer & V. Spieß. 1990. Oligocene to Quaternary sedimentation processes on the Antarctic continental margin, ODP Leg 113, Site 693. *In* P. F. Barker et al. (Eds), *Proceedings of the Ocean Drilling Program, Scientific Results*, 113: 121-131.

Grützner, J., C.-D. Hillenbrand & M. Rebesco. 2005. Terrigenous flux and biogenic silica deposition at the Antarctic continental rise during the late Miocene to early Pliocene: implications for ice sheet stability and sea ice coverage. *Global and Planetary Change*, 45: 131-149.

Haeckel, E. 1860. Über neue, lebende Radiolarien des Mittelmeeres und die dazu gehörigen Abbildungen. *Monatsberichte der Königlich Preußischen Akademie der Wissenschaften zu Berlin, Jahre 1860*, 794-817.

——. 1862. *Die Radiolarien (Rhizopoda Radiaria)*. Reimer, Berlin, 572pp.

——. 1866. *Generelle Morphologie der Organismen.* Reimer, Berlin, 462pp.

——. 1879. *Naturliche Schopfungsgeschichte*. Reimer, Berlin, 718pp.

——. 1881. Entwurf eines Radiolarien-systems auf grund von studien der Challenger-Radiolarien. *Jenaische Zeitschrift für Naturwissenschaft*, 15: 418-472.

——. 1887. Report on the Radiolaria collected By H.M.S. Challenger during the years 1873-1876. *Report on the Scientific Results of the voyage of H.M.S. Challenger during the years 1873-1876, Zoology*, 18.

Haecker, V. 1907. Altertümliche Spharellarien und Cyrtellarien aus grossen Meerestiefen. *Archiv für Protistenkunde*, 10: 114-126.

——. 1908. Tiefsee-Radiolarien. Spezieller Teil. Die Tripyleen, Collodarien und Mikroradiolarien der Tiefsee. *Wissenschaftliche Ergebnisse der deutschen Tiefsee-Expedition auf dem Dampfer "Valdivia" 1898-1899*, 14: 336-476.

Harada, A., S. Ohtsuka & T. Horiguchi. 2007. Species of the parasitic genus *Duboscquella* are members of the enigmatic Marine Alveolate Group I. *Portist*, 158: 337-347.

Harding, G. C. H. 1974. The food of deep-sea copepods. *Journal of the Marine Biological Association of the United Kingdom,* 54: 141-155.

Harting, P. 1863. Bijdrage tot de kennis der mikroskopische fauna en flora van de Banda-Zee. *Verhandelung, Koninklijke Akademie van Wetenschappen*, *Amsterdam*, 10(1): 1-34.

Harwood, D. M., D. B. Lazarus, A. Abelmann, M.-P. Aubry, W. A. Berggren, F. Heider, H. Inokuchi, T. Maruyama, K. McCartney, W. Wei & S. W. Wise Jr. 1992. Neogene integrated Magnetobiostratigraphy of the central Kerguelen Plateau, leg 120. *In* S. W. Wise Jr et al. (Eds), *Proceedings of the Ocean Drilling Program, Scientific Results*, College Station, TX (Ocean Drilling Program), 120: 1031-1052.

Haug, G. H. & R. Tiedemann. Effect of the formation of the Isthmus of Panama on Atlantic Ocean thermohaline circulation. *Nature*, 393: 673-676.

Haq, B. U., T. R. Worsley, L. H. Burckle, R. G. Douglas, L. D. Keigwin Jr, N. D. Opdyke, S. M. Savin, M. A. Sommer II, E. Vincent & F. Woodruff. 1980. Late Miocene marine carbon-isotopic shift and synchroneity of some phytoplanktonic biostratigraphic events. *Geology*, 8: 427-431.

Hays, J. D. 1965. Radiolaria and late Tertiary and Quaternary history of Antarctic Seas. In G. A. Llano (Ed), Biology of the Antarctic Seas II. *Antarctic Research Series*, 5: 125-184.

——. 1970. Stratigraphy and evolutionary trends of Radiolaria in North Pacific Deep-Sea Sediments. *Geological Society of America, Memoir* 126: 185-218.

Hays, J. D. & N. D. Opdyke. 1967. Antarctic Radiolaria, magnetic reversals and climate change. *Science*, 158(3804): 1001-1011.

Hays, J. D., J. A. Lozano, N. J. Shackleton & G. Irving. 1976. Reconstruction of the Atlantic and western Indian Ocean sectors of the 18,000BP Antarctic Ocean. *Geological Society of America Memoir*, 145: 337-372.

Heider, F., B. Leitner & H. Inokuchi. 1992. High Southern latitude magnetostratigraphy and rock magnetic properties of sediments from sites 747, 749 and 751. *In* S. W. Wise Jr et al. (Eds), *Proceedings of the Ocean Drilling Program, Scientific Results,* College Station, TX (Ocean Drilling Program), 120: 225-245.

Hertwig, R. 1877. Studien über Rhizopoden. *Jenaische Zeitschrift für Naturwissenschaft,* Jena, 11: 324-348

——. 1879. *Der organismus der Radiolarien.* Jena, G.Fischer, 149pp.

Hillenbrand, C.-D. & D. K. Fütterer. 2001. Neogene to Quaternary deposition of opal on the continental rise west of the Antarctic Peninsula, ODP Leg 178, sites 1095, 1096 and 1101. *In* P. F. Barker et al. (Eds), *Proceedings of the Ocean Drilling Program, Scientific Results,* College Station, TX (Ocean Drilling Program), 178: 1-33.

Hilmers, C. 1906. *Zur Kenntniss der Collosphaeriden*. Kiel, C. Schaid, 93pp.

Hodell, D. A. & K. A. Venz-Curtis. 2006. Late Neogene history of deepwater ventilation in the Southern Ocean, *Geochemistry, Geophysics, Geosystems*, 7: Q09001.

Hollande, A. & D. Carré. 1974. Les xanthelles des radiolaires sphaerocollides, des acanthaires et de *Velella velella*: infrastructure, cytochimie, taxonomie. *Protistlogica* 10(4): 573-601.

Hollande, A. & M. Enjumet. 1953. Contribution à l'étude biologique des Sphaerocollides (Radiolaires Collodaires et Radiolaires Polycyttaires) et de leur parasites. *Annales des Sciences Naturelles, Zoologie, 11e série,* 15: 99-183.

——. 1954. Sur l'existence d'axopodes et d'un complexe centroplastique chez les Radiolaires. *Comptes Rendus de des scéances de l'Académie des Sciences*, 238: 1841-1843.

——. 1960. Cytologie, évolution et systématique des Sphaeroïdés (Radiolaires). *Archives du Muséum National d'Histoire Naturelle*, 7: 1-134.

Hollis, C. J. 2002. Biostratigraphy and paleoceanographic significance of Paleocene radiolarians from offshore Eastern New Zealand. *Marine Micropaleontology*, 46: 265-316.

Honigsberg, B. M. Subphylum Sarcomastigophora nom. nov. to embrace the flagellate and amoeboid assemblages of protozoans. *Journal of Protozoology,* 10 (sup3): 27.

Horn, H. 1966. Measurement of 'overlap' in comparative ecological studies. *American Naturalist*, 100: 419-424.

Hsü, K. J., W. B. F. Ryan & M. B. Cita. 1973. Late Miocene Desiccation of the Mediterranean. *Nature,* 242: 240-244.

Hull, D. M. 1996. Paleoceanography and biostratigraphy of Paleogene radiolarians from the Norwegian-Greenland Sea. *In* J. Thiede et al. (Eds). *Proceedings of the Ocean Drilling Program, Scientific Results,* College Station, TX (Ocean Drilling Program), 151: 125-152.

Hülsemann, K. 1963. Radiolaria in plankton from the Arctic drifting station T-3, including description of three new species. *Arctic Institute of North America, Technical Paper*, 13: 1-52.

Itaki, T. 2009. Late glacial to Holocene Polycystine radiolarians from the Japan Sea. *News of Osaka Micropaleontologists, Special Volume*, 14: 43-89.

Itaki, T. & K. R. Bjørklund. 2006. Bailey's (1856) radiolarian types from the Bering Sea re-examined. *Micropaleontology,* 52(5): 449-463.

Itaki, T., B.-K. Khim & K. Ikehara. 2008. Last glacial-Holocene water structure in the southwestern Okhotsk Sea inferred from radiolarian assemblages. *Marine Micropaleontology*, 67: 191-215.

Johnson, D. A. & C. Nigrini, 1980. Radiolarian biogeography in surface sediments of the western Indian Ocean. *Marine Micropaleontology,* 5(2): 111-152.

Jørgensen, E. 1900. Protophyten und Protozöen in Plankton aus der norwegischen Westküste. *Bergens Museums Aarbog*, 6: 51-112.

——. 1905. The Protist plankton and the diatoms in bottom samples. VII. Radiolaria. *In* O. Nordgaard (Ed.), Hydrographical and Biological investigations in Norwegian Fiords, *Bergen Museum Skrifter*, 114-141.

Kamikuri, S. 2010. New late Neogene radiolarian species from the middle to high latitudes of the North Pacific. *Revue de Micropaléontologie*, 53(2): 85-106.

Kamikuri, S., I. Motoyama & A. Nishimura. 2008. Radiolarian assemblages in surface sediments along longitude 175°E in the Pacific Ocean. *Marine micropaleontology,* 69: 151-172.

Kaminski, M. A., E. Setoyama & C. G. Cetean. 2010. The phanerozoic diversity of agglutinated foraminifera: origination and extinction rates. *Acta Palaeontologica Polonica*, 55(3): 529-539.

Keany, J. 1979. Early Pliocene radiolarian taxonomy and biostratigraphy in the Antarctic region. *Micropaleontology*, 25(1): 50-74.

Keeling, P., G. Burger, D. G. Durnford, B. F. Lang, R. W. Lee, R. E. Pearlman, A. J. Roger & M. W. Gray. 2005. The Tree of Eukaryotes. *Trends in Ecology and Evolution,* 20(12): 670-676.

Keith, T. H., R. Bivand, E. Pebesma & B. Rowlingson. 2012. rgdal: Bindings for the Geospatial Data Abstraction Library. R. package version 0.7-8.

Kellogg, D. E. 1975. The role of phyletic change in the evolution of *Pseudocubus vema* (Radiolaria). *Paleobiology*, 1(4): 359-370.

Kemple, W. G., P. M. Sadler & D. J. Strauss. 1995. Extending graphic correlation to many dimensions: stratigraphic correlation as constrained optimization. *In* K. O. Mann & H. R. Lane (Eds), Graphic correlation, *Special Publications of the Society of Economic Paleontologists and Mineralogists,* 53: 65-82.

Kennett, J. P. 1995. A review of polar climatic evolution during the Neogene, based on the marine sediment record. *In* E. Vrba et al. (Eds), *Paleoclimate and Evolution with Emphasis on Human Origins*, New Haven (Yale University Press): 49-64.

Kennett, J. P. & P. F. Barker. 1990. Latest Cretaceous to Cenozoic climate and oceanographic developments in the Wedell Sea, Antarctica: an Ocean-Drilling perspective. In P. F. Barker et al. (Eds), *Proceedings of the Ocean Drilling Program, Scientific Results*, College Station, TX (Ocean Drilling Program), 113: 937-960.

Kennett, J. P. & L. D. Stott. 1990. Proteus and Proto-oceanus: ancestral Paleogene oceans as revealed from Antarctic stable isotopic results; ODP Leg 113. In P. F. Barker et al. (Eds), *Proceedings of the Ocean Drilling Program, Scientific Results*, College Station, TX (Ocean Drilling Program), 113: 865-880.

Kennett, J. P. & C. C. von der Borch. 1986. Southwest Pacific Cenozoic Paleoceanography. *In* J. P. Kennett et al. (Eds), *Initial Reports of the Deep Sea Drilling Project*, Washington (U.S. Govt. Printing Office), 90: 1493-1517.

Kiessling, W. & T. Danelian. 2011. Trajectories of late Permian- Jurassic radiolarian extinction rates: no evidence for an end-Triassic mass extinction. *Fossil Record*, 14(1): 95-101.

Kirkpatrick, S., C. D. Gelatt & M. P. Vecchi. 1983. Optimization by Simulated Annealing. *Science*, 220(4598): 671-680.

Kling, S. A. 1973. Radiolaria from the eastern North Pacific, Deep Sea Drilling Project, Leg 18. *In* L. D. Kulm et al. (Eds), *Initial Reports of the Deep Sea Drilling Project*, Washington (U.S. Govt. Printing Office), 18: 617-671.

Koch, C. F. 1978. Bias in the published fossil record. *Paleobiology*, 4(3): 367-372.

Kozur, H. & H. Mostler. 1982. Entactinaria subordo nov., a new radiolarian suborder. *Geologisch-Paläontlogische Mitteilungen Innsbruck*, 11 (1) 399-414.

Krabberød, A., J. Bråte, J. K. Dolven, R. F. Ose, D. Klaveness, T. Kristensen, K. R. Bjørklund & K. Shalchian-Tabrizi. 2011. Radiolaria divided into Polycystina and Spasmaria in combined 18S and 28S rDNA phylogeny. *PLoS ONE,* 6(8): e23526.

Krijgsman, W., F. J. Hilgen, I. Raffi, F. J. Sierro & D. S. Wilson. 1999. Chronology, causes and progression of the Messinian salinity crisis. *Nature,* 400: 652-655.

Kruglikova, S. B. 1978. Novye vidy radiolyarii miotsena-golotsena ekvatorialnoi zony Tikhogo okeana. *In* A. P. Zhuze (Ed), *Morskaya Mikropaleontologiya (diatomei, radiolyarii, silikoflyagellyaty, foraminifery i izvestkovyi nannoplankton),* 87-90. Nauka, Moskow.

Lawver, L. A. & L. M. Gahagan. 2003. Evolution of Cenozoic seaways in the circum-Antarctic region. *Palaeogeography, Palaeoclimatology, Palaeoecology,* 198: 11-37.

Lazarus, D.B. 1990. Middle Miocene to Recent radiolarians from the Weddell sea, Antarctica, ODP Leg 113. *In* J. P. Kennett et al. (Eds), *Proceedings of the Ocean Drilling Program, Scientific Results*, College Station, TX (Ocean Drilling Program), 113: 709–727.

——. 1992. Antarctic Neogene radiolarians from the Kerguelen Plateau, Legs 119 and 120. *In* S. W. Wise Jr et al. (Eds), *Proceedings of the Ocean Drilling Program, Scientific Results*, College Station, TX (Ocean Drilling Program), 120: 785-809.

——. 1994. Neptune: a marine micropaleontology database. *Mathematical Geology*, 26(7), 817-832.

——. 2001. Late Miocene to Early Pliocene radiolarians from glaciomarine drift deposits, ODP Leg 178, Hole 1095B (Bellinghausen Basin, Antarctic Ocean). *In* P. F. Barker et al. (Eds), *Proceedings of the Ocean Drilling Program, Scientific Results,* 178: 22pp.

——. 2002. Environmental control of diversity, evolutionary rates and taxa longevities in Antarctic Neogene Radiolaria. *Palaeontologia Electronica*, 5(1): 32pp.

——. 2006. The Micropaleontological Reference Center Network. *Scientific Drilling*, 3: 46-49.

——. 2011. The deep-sea microfossil record of macroevolutionary change in plankton and its study. *In* A. J. McGowan and A. B. Smith (Eds), Comparing the geological and fossil records: implications for biodiversity studies. *Geological Society of London, Special Publications*, 358: 141-166.

——. submitted. The legacy of early radiolarian taxonomists, with a focus on the species published by German workers. *Journal of Micropalaeontology.*

Lazarus, D. B. and J.-P. Caulet. 1994. Cenozoic Southern Ocean reconstructions from sedimentologic, radiolarian and other microfossil data. *In* J. P. Kennett and D. A. Warnke (Eds), The Antarctic Paleoenvironment: a perspective on global change. *Antarctic Research Series*, 60: 145-174.

Lazarus, D. B. & A. Pallant. 1989. Oligocene and Neogene radiolarians from the Labrador Sea, ODP Leg 105. *In* S. P. Srivastava et al. (Eds), *Proceedings of the Ocean Drilling Program, Scientific Results*, College Station, TX (Ocean Drilling Program), 105: 349-380.

Lazarus, D. B., R. P. Scherer & D. R. Prothero. 1985. Evolution of the radiolarian species-complex *Pterocanium*: a preliminary survey. *Journal of Paleontology*, 59(1): 183-220.

Lazarus, D. B., C. Spencer-Cervato, M. Pika-Biolzi, J. P. Beckmann, K. von Salis, H. Hilbrecht and H. R. Thierstein. 1995. Revised chronology of Neogene DSDP Holes from the World Ocean. *Ocean Drilling Program Technical Notes*, 24: 312pp.

Lazarus, D. B., K. Faust & I. Popova-Goll. 2005. New species of prunoid radiolarians from the Antarctic Neogene. *Journal of Micropaleontology*, 24(2): 97-121.

Lazarus, D. B., M. Weinkauf and P. Diver. 2012. Pacman profiling: a simple procedure to identify stratigraphic outliers in high-density deep-sea microfossil data. *Paleobiology*, 38(1): 858-875.

Lees, J. M. 2010. GEOmap: Topographic and Geologic Mapping. R package version 1.5-4.

Levine, N. D., J. O. Corliss, F. E. G. Cox, G. Deroux, J. Grain, B. M. Honigsberg, G. F. Leedale, A. R. Loeblich III, J. Lom, D. Lynn, E. G. Merinfeld, F. C. Page, G. Poljansky, V. Sprague, J. Vavra & F. G: Wallace. 1980. A Newly Revised Classification of Protozoa. *Journal of Protozoology,* 27(1): 37-58.

Lewin-Koh, N. J. & R. Bivand. 2012. maptools: Tools for reading and handling spatial objects. R package version 0.8-14.

Ling, H.-Y. 1973. Radiolaria: Leg 19 of the Deep Sea Drilling Project. *In* J. S. Creager et al. (Eds), *Initial Reports of the Deep Sea Drilling Project*, Washington (U.S. Govt. Printing Office), 19: 777-797.

Ling, H.-Y., C. J. Stadum & M. L. Welch. 1971. Polycystine Radiolaria from Bering Sea surface sediments. *Proceedings of the 2nd Planktonic Conference*, *Rome 1970*, 2: 705-729.

Liow, L. H., H. J. Skaug, T. Ergon & T. Schweder. 2010. Global occurences trajectories of microfossils: environmental volatility and the rise and fall of individual species. *Paleobiology*, 36(2): 224-252.

Lipps, J. H. 1981. What, if anything, is micropaleontology? *Paleobiology*, 7(2): 167-199.

Lipps, J. H. & J. W. Valentine. 1970. The role of foraminifera in the trophic structure of marine communities. *Lethaia*, 3(3): 279-286.

Lloyd, G. T., A. B. Smith & J. R. Young. 2011. Quantifying the deep-sea rock and fossil record bias using coccolithophores. *In* A. J. McGowan and A. B. Smith (Eds), Comparing the geological and fossil records: implications for biodiversity studies. *Geological Society of London, Special Publications*, 358: 141-166.

Loeblich, A. R. Jr & H. N. Tappan. 1961. Remarks on the systematics of the Sarcodina (Protozoa), renamed homonyms and new and validated genera. *Proceedings of the Biological Society of Washington*, 74: 213-234.

Lombari, G. & D. B. Lazarus. 1988. Neogene cycladophorid radiolarians from North Atlantic, Antarctic, and North Pacific deep-sea sediments. *Micropaleontology*, 34(2): 97-135.

Longhurst, A. 1995. Ecological biogeography of the pelagial. *In* A. C. Pierrot-Bults & S. van der Spoel (Eds.), *Pelagic Biogeography ICoPB II: Proceedings of the 2nd International Conference. Final reports of SCOR/IOC Working Group 93. IOC Workshop Report*, 142: 239-249.

Longhurst, A. 1998. *Ecological Geography of the Sea*. Academic Press, San Diego.

Lunt, D. J., P. J. Valdes, A. Haywood & I. C. Rutt. 2008. Closure of the Panama Seaway during the Pliocene: implications for climate and Northern Hemisphere glaciation. *Climate Dynamics,* 30: 1-18.

Mackensen, A., E. Barrera and H.-W. Hubberten. 1992. Neogene circulation in the Southern Indian Ocean: evidence from benthic foraminifers, carbonate data and stable isotope analyses (Site 751). *In* S. W. Wise Jr et al. (Eds), *Proceedings of the Ocean Drilling Program, Scientific Results*, College Station, TX (Ocean Drilling Program), 120: 867-878.

Maharapatra, A. K. & V. Sharma. 1994. Trissocyclid Radiolaria from the late Early Miocene sequences of Colebrook, North Passage and Great Nicobar Islands, northeast Indian Ocean. *Micropaleontology,* 40(2): 157-168.

Maletz, J. 2011. Radiolarian skeletal structures and biostratigraphy in the early Palaeozoic (Cambrian-Ordovician). *Palaeoworld,* 20: 116-133.

Martin, G. C. 1904. Radiolaria. *In* W. B. Clark et al. (Eds), Systematic Paleontology of the Miocene Deposits of Maryland: Baltimore. *Maryland Geological Survey*, 447-459. Johns Hopkins Press.

Mast, H. 1910. Die Astrosphaeriden. *Wissenschaftliche Ergebnisse der deutschen Tiefsee-Expedition auf dem Dampfer "Valdivia" 1898-1899*, 19(4): 123-190.

Matsuoka, A. 2007. Living radiolarian feeding mechanisms: new light on past marine ecosystems. *Swiss Journal of Geosciences,* 100: 273-279.

Meyers, S. R. & L. A. Hinnov. 2010. Northern Hemisphere glaciation and the evolution of Plio-Pleistocene. *Paleoceanography,* 25: PA3207.

Moore, T. C. 1972. Mid-Tertiary evolution of the radiolarian genus *Calocycletta*. *Micropaleontology*, 18(2): 144-152.

——. 1973. Method of randomly distributing grains for microscope examination. *Journal of Sedimentary Petrology*, 43(3): 904-906.

Moreira, D. S. von der Heyden, D. Bass, P. López-García, E. Chao & T. Cavalier-Smith. 2007. Global Eukaryote Phylogeny: Combined small- and large-subunit ribosomal DNA trees

support monophyly of Rhizaria, Retaria and Excavata. *Molecular Phylogenetics and Evolution*, 44: 255-266.

Morisita, M. 1959. Measuring of interspecific association and similarity between communities. *Memoirs of the Faculty of Science, Kyushu University, Serie E (Biology)*, 3: 65-80.

Morley, J. J. & C. Nigrini. 1995. Miocene to Pleistocene radiolarian biostratigraphy of North Pacific sites 881, 884, 885, 886 and 887. *In* D. K. Rea et al. (Eds), *Proceedings of the Ocean Drilling Program, Scientific Results*, College Station, TX (Ocean Drilling Program), 145: 55-91.

Motoyama, I. 1996. Late Neogene radiolarian biostratigraphy in the subarctic Northwest Pacific. *Micropaleontology,* 42(3): 221-262.

——. 1997. Origin and evolution of Cycladophora davisiana Ehrenberg (Radiolarian) in DSDP Site 192, Northwest Pacific. *Marine micropaleontology,* 30(1-3): 45-63.

Mudelsee, M. & M. E. Raymo. 2005. Slow dynamics of the Northern Hemisphere glaciation. *Paleoceanography,* 20: PA4022.

Müller, D. W., D. A: Hodell & P. F. Cieselski. 1991. Late Miocene to earliest Pliocene (9.8-4.5 Ma) paleoceanography of the subantarctic southeast Atlantic: stable isotopic, sedimentologic, and microfossil evidence. *In* P. F. Cieselski et al. (Eds), *Proceedings of the OCean Drilling Program, Scientific Results,* College Station, TX (Ocean Drilling Program), 114: 459-474.

Müller, J. 1855. Über *Sphaerozoum* und *Thalassicolla*. *Königlichen Preußischen Akademie der Wissenschaften zu Berlin, Bericht, Jahre 1855*, 229-253.

——. 1857. Über die Thalassicollen, Polycystinen und Acanthometren des Mittelmeeres. *Königlichen Preußischen Akademie der Wissenschaften zu Berlin, Monatsbericht, Jahre 1856*, 474-503.

——. 1858. Über die Thalassicollen, Polycystinen und Acanthometren des Mittelmeeres. *Königlichen Preußischen Akademie der Wissenschaften zu Berlin, Abhandlungen, Jahre 1858*, 1-62.

Mullineaux, L. S. & M. J. Westberg-Smith. 1986. Radiolarians as paleoceanographic indicators in the Miocene Monterey Formation, Upper Newport Bay, California. *Micropaleontology,* 32(1): 48-71.

Murray, J. 1876. Preliminary Reports on Specimens of the Sea-bottoms obtained in the soundings, dredgins and trawlings of H.M.S. Challenger, in the years 1873-75, between England and Valparaiso. *Proceedings of the Royal Society of London,* 24: 471-544.

——. 1885. The Radiolaria. *Report on the Scientific Results of the voyage of H.M.S. Challenger during the years 1873-1876, Narrative*, 1: 219-227.

Nakaseko K. 1955. Miocene radiolarian fossil assemblage from the southern Tojama Prefecture in Japan. *Science Reports, College of General Education, Osaka University*, 4: 65-127.

——. 1959. On superfamily Liosphaericae (Radiolaria) from sediments in the sea near Antarctica. *Special Publications from the Seto Marine Biology Laboratory, Osaka, Japan*, 1-21.

——. 1963. Neogene Cyrtoidea (Radiolaria) from the Isozaki Formation in Ibaraki Prefecture, Japan. *Science Reports, College of General Education, Osaka University,* 12(2): 165-198.

——. 1972. On some species of the genus *Thecosphaera* from the Neogene Formations, Japan. *Science Reports, College of General Education, Osaka University*, 20(2): 59-66.

Nakaseko, K. & A. Nishimura. 1974. Miocene radiolarian fossils of the Oki Islands in Shimane Prefecture, Japan. *Science Reports, College of General Education, Osaka University*, 23(1): 45-73.

Nakaseko, K. & K. Sugano. 1973. Neogene radiolarian zonation in Japan. *The memoirs of the Geological Society of Japan,* 8: 23-34.

Nakaseko, K., K. Nagata & A. Nishimura. 1982. Discovery of Miocene Radiolaria belonging to Pentactinocarpinae in Japan (Preliminary Report). N*ews of Osaka Micropaleontologists, Special Volume*, 5: 423-425.

——. 1983. *Pentactinosphaera hokurikuensis* (Nakaseko): a revised Early Miocene Radiolaria. *Science Reports, College of General Education, Osaka University*, 32(1): 31-37.

Naish, T. R. Powell, R. Levy, G. Wilson, R. Scherer, F. Talarico, L. Krissek, F. Niessen, M. Pompilio, T. Wilson, L. Carter, R. De Conto, P. Huybers, R. McKay, D. Pollard, J. Ross, D. Winter, P. Barrett, G. Browne, R. Cody, E. Cowan, J. Crampton, G. Dunbar, N. Dunbar, F. Florindo, C. Gebhardt, I. Graham, M. Hannah, D. Hansaraj, D. Harwood, D. Helling, S. Henrys, L. Hinnov, G. Kuhn, P. Kyle, A. Läufer, P. Maffioli, D. Magens, K. Mandernack, W. McIntosh, C. Millan, R. Morin, C. Ohneiser, T. Paulsen, D. Persico, I. Raine, J. Reed, C. Riesselman, L. Sagnotti, D. Schmitt, C. Sjunneskog, P. Strong, M. Taviani, S. Vogel, T. Wilch & T. Williams. 2009. Obliquity-paced Pliocene West Antarctic Icee Sheet oscillations. *Nature*, 458: 322-328.

Nelson, C. S. & P. J. Cooke. 2001. History of oceanic front development in the New Zealand sector of the Southern Ocean during the Cenozoic - a Synthesis. *New Zealand Journal of Geology and Geophysics,* 44(4): 535-553.

Nigrini, C. 1967. Radiolaria in pelagic sediments from the Indian and Atlantic Oceans. *Bulletin of the Scripps Institution of Oceanography, University of California, San Diego, La Jolla, California*, 11: 1-125.

——. 1968. Radiolaria from eastern tropical Pacific Sediments. *Micropaleontology*, 14(1): 51-63.

——. 1977. Tropical Cenozoic Artostrobiidae (Radiolaria). *Micropaleontology*, 23(3): 241-269.

Nigrini, C. & J.-P. Caulet. 1992. Late Neogene radiolarian assemblages characteristics of Indo-Pacific areas of upwelling. *Micropaleontology,* 38(2): 139-164.

Nigrini, C. & T. C. Moore. 1979. A guide to modern Radiolaria. *Cushman Foundation for Foraminiferal Research, Special Publication*, 16: 1-248.

Nikolaev, S. I., C. Berney, J. F. Fahrni, I. BOlivar, S. Polet, A. P. Mylkinov, V. V. Aleshin, N. B. Petrov & J. Pawlowski. 2004. The twilight of Heliozoa and rise of Rhizaria, an emerging supergroup of amoeboid eukaryotes. *Proceedings of the National Academy of Science,* 101(21): 8066-8071.

Nishimura, A. 2003. The skeletal structure of *Prunopyle antarctica* Dreyer (Radiolaria) in sediment samples from the Antarctic Ocean. *Micropaleontology,* 49(2): 197-200.

Nishimura, A. & M. Yamauchi. 1984. Radiolarians from the Nankai Trough in the Northwest Pacific. *News of Osaka Micropaleontologist, Special Volume*, 6: 1-148.

Nishimura, H. 1990. Taxonomic study on Cenozoic Nassellaria (Radiolaria). *Science Report of the Institute of Geosciences, University of Tsukuba, section B*, 11: 69-172.

Not, F., R. Gausling, F. Azam, J. F. Heidelberg & A. Z. Worden. 2007. Vertical distribution of picoeukaryotic diversity in the Sargasso Sea. *Environmental microbiology*, 9(5): 1233-1252.

Not, F., J. del Campo, V. Balagué, C. de Vargas & R. Massana. 2009. New insights into the diversity of marine picoeukaryotes. *PLoS ONE*, 4(9): e7143.

O'Connor, B. 1994. Seven new radiolarian species from the Oligocene of New Zealand. *Micropaleontology*, 40(4): 337-350.

——. 1997a. Lower Miocene Radiolaria from Te Kopua Point, Kaipara Harbour, New Zealand. *Micropaleontology,* 43(2): 101-128.

——. 1999a. Distribution and biostratigraphy of latest Eocene to latest Oligocene Radiolaria from the Mahurangi Limestone, Northland, New Zealand. *New Zealand Journal of Geology and Geophysics*, 42: 489-511.

——. 1999b. Radiolaria from the late Eocene Oamaru diatomite, South Island, New Zealand. *Micropaleontology*, 45(1): 1-55.

Ogane, K., N. Suzuki, Y. Aita, T. Sakai & D. B. Lazarus. 2009a. Ehrenberg's Radiolarian Collection from Barbados. *In* Y. Tanimura & Y. Aita (Eds), Joint Haeckel and Ehrenberg Project: Reexamination of the Haeckel and Ehrenberg Microfossil Collection as a Historical and Scientific Legacy, *National Museum of Nature and Science Monographs*, Tokyo, 40: 97-106.

Ogane, K., A. Tuji, N. Suzuki, T. Kurihara & A. Matsuoka. 2009b. First application of PDMPO to examine silicification in polycystine Radiolaria. *Plankton & Benthos Research,* 4(3): 89-94.

Ogane, K., A. Tuji, N. Suzuki, A. Matsuoka, T. Kurihara & R. Hori. 2010. Direct observation of the skeletal growth patterns of polycystine radiolarians using fluorescent marker. *Marine Micropaleontology,* 77: 137-144.

Okamoto, N., C. Chantangsi, A. Horák, B. S. Leander & P. J. Keeling. 2009. Molecular phylogeny and description of the novel Katablepharid *Roombia truncata* gen. et sp. nov., and establishment of the Hacrobia taxon nov. *PLoS ONE,* 4(9): e7080.

Orsi, A. H., T. Whitsworth III & W. D. Nowlin Jr. 1995. On the meridional extent and fronts of the Antarctic Circumpolar Current. *Deep-Sea Research I,* 42(5): 641-673.

Orsi, A. H. G. C. Johnson & J. L. Bullister. 1999. Circulation, mixing and production of Antarctic Bottom Water. *Progress in Oceanography,* 43: 55-109.

Pawlowski. J. 2008. The twilight of Sarcodina: a molecular perspective on the polyphyletic origin of amoeboid protists. *Protistology,* 5(4): 281-302.

Petrushevskaya, M. G. 1965. Osobennosti i konstruktsii skeleta radiolyarii Botryoidae (otr. Nassellaria). *Trudy Zoologicheskogo Instituta*, 35: 79-118.

——. 1967. Radiolaryii otryadov Spumellaria i Nasselaria antarkticheskoi oblasti. *Issledovaniya Fauny Morei*, 4(12): 2-186.

——. 1968. Gomologii v skeletakh radiolyarii Nasselaria. 1. Osnovnye dugi v semeistve Cyrtoidea. *Zoologicheskii Zhurnal*, 47(9): 1296-1310.

——. 1971. Radiolyarii nassellaria v planktone mirovogo okeana. *Issledovaniya Fauny Morei*, 9(17): 1-294.

——. 1975. Cenozoic radiolarians of the Antarctic, Leg 29, Deep Sea Drilling Project. *In* J. P. Kennett et al. (Eds), *Initial Reports of the Deep Sea Drilling Project*, Washington (U.S. Govt. Printing Office), 29: 541-676.

——. 1986. Evolution of the *Antarctissa* Group. *Marine Micropaleontology*, 11(1-3): 185-195.

Petrushevskaya, M. G. & G. E. Kozlova. 1972. Radiolaria: Leg 14, Deep Sea Drilling Project. *In* D. E. Hayes et al. (Eds), *Initial Reports of the Deep Sea Drilling Project*, Washington (U.S. Govt. Printing Office), 14: 495-648.

——. 1979. Opisanie rodov i vidov Radiolyarii. *Issledovaniya Fauny Morei*, 23: 86-157.

Polet, S., C. Berney, J. Fahrni & J. Pawlowski. 2004. Small-subunit ribosomal RNA gene sequences of Phaeodarea challenge the monophyly of Haeckel's Radiolaria. *Protist,* 155: 53-63.

Popofsky, A. 1908. Die Radiolarien der Antarktis. *Deutsche Südpolar-Expedition 1901-1903*, 10 (Zool., 2): 183-305.

——. 1912. Die Sphaerellarien des Warmwassergebietes. *Deutsche Südpolar-Expedition 1901-1903*, 13(Zool., 5): 73-159.

——. 1913. Die Nassellarien des Warmwassergebietes. *Deutsche Südpolar-Expedition 1901-1903*, 14 (Zool., 6): 217-416.

——. 1917. Die Collosphaeriden der Deutschen Sudpolar-Expedition 1901-1903. Mit Nachtrag zu den Spumellarien und Nassellarien. *Deutsche Südpolar-Expedition 1901-1903*, 16(Zool. 8): 235-278.

Pouille, L., O. Obut, T. Danelian & N. Sennikov. 2011. Lower Cambrian (Botomian) polycystine Radiolaria from the Altai Mountains (southern Siberia, Russia). *Comptes Rendus Palevol,* 10(8): 627-633.

R development core team 2011. *R: a language and environment for statistical computing*. R Foundation for Statistical Computing, Vienna, Austria.

Rabosky, D. L. & U. Sorhannus 2009. Diversity dynamics of marine planktonic diatoms across the Cenozoic. *Nature*, 457: 183-186.

Reid, J. L. 1979. On the contribution of the Mediterranean Sea outflow to the Norwegian-Greenland Sea. *Deep-Sea Research,* 26A: 1199-1223.

Renaudie, J. & D. B. Lazarus. 2012. New species of neogene radiolarians from the Southern Ocean. *Journal of Micropalaeontology*, 31(1): 1-24.

——. in press. New species of neogene radiolarians from the Southern Ocean - Part II. *Journal of Micropalaeontology*.

——. submitted. On the accuracy of paleodiversity reconstructions: a case study in Antarctic Neogene radiolarians. *Paleobiology*.

Renz, G. W. 1974. Radiolaria from Leg 27 of the Deep Sea Drilling Poject. *In* J. J. Veevers et al. (Eds), *Initial Reports of the Deep Sea Drilling Project,* Washington (U. S. Govt Printing Office), 27: 769-841.

——. 1976. The distribution and ecology of Radiolaria in the Central Pacific: plankton and surface sediments. *Bulletin of the Scripps Institution of Oceanography,* 22: 1-267.

Reynolds, R. A. 1980. Radiolarians from the western north Pacific, Leg 57, Deep Sea Drilling Project. *In* M. Langseth et al (Eds), *Initial Reports of the Deep Sea Drlling Project*, Washington (U. S. Govt Printing Office), 56: 735-769.

Riedel, W. R. 1958. Radiolaria in Antarctic sediments. *Reports of the B.A.N.Z. Antarctic Research Expedition, Series B*, 6(10): 218-254.

——. 1959. Oligocene and lower Miocene Radiolaria in tropical Pacific sediments. *Micropaleontology,* 5(3): 285-302.

——. 1967. Some new families of Radiolaria. *Proceedings of the Geological Society of London*, 1640: 148-149.

Riedel, W. R. & A. S. Campbell. 1952. A new Eocene radiolarian genus, *Journal of Paleontology,* 26(4): 667-669.

Riedel, W. R. & A. Sanfilippo. 1970. Radiolaria, Leg 4, Deep Sea Drilling Project. *In* R. G. Bader et al. (Eds), *Initial Reports of the Deep Sea Drlling Project*, Washington (U. S. Govt Printing Office), 4: 503-575.

——. 1971. Cenozoic Radiolaria from the western tropical Pacific, Leg 7. *In* E. L. Winterer et al. (Eds), *Initial Reports of the Deep Sea Drlling Project*, Washington (U. S. Govt Printing Office), 7: 1529-1672.

——. 1973. Cenozoic Radiolaria from the Caribbean, Deep Sea Drilling Project, Leg 15. *In* N. T: Edgar et al. (Eds), *Initial Reports of the Deep Sea Drlling Project*, Washington (U. S. Govt Printing Office), 15: 705-751.

Riisberg, I., R. J. S. Orr, R. Kluge, K. Shalchian-Tabrizi, H. A. Bowers, V. Patil, B. Edvardsen & K. S. Jakobsen. 2009. Seven gene phylogeny of Heterokonts. *Protist,* 160: 191-204.

Rüst, D. 1885. Beitrage zur Kenntniss der fossilen Radiolarien aus Gesteinen der Kreide. *Palaeontographica*, 34: 181-213.

——. 1892. Beitrage zur Kenntnis der fossilen Radiolarien aus Gesteinen derTrias und der palaeozoischen Schichten. *Paleontographica,* 38: 107-179.

Sadler, P. M. 2007. Constrained Optimization Approaches to the Paleobiologic Correlation and Seriation Problems: Part 1 (A Users Guide to the CONOP Program Family) and Part 2 (A Reference Manual to the CONOP Program Family). UC Riverside, Riverside, CA.

Sakai, T. 1980. Radiolarians from Sites 434, 435, and 436, Northwest Pacific, Leg 56, Deep Sea Drilling Project. *In* M. Langseth et al (Eds), *Initial Reports of the Deep Sea Drlling Project*, Washington (U. S. Govt Printing Office), 56: 695-733.

Sanders, H. L. 1968. Marine benthic diversity: a comparative study. *The American Naturalist*, 102(935): 243-282.

Sanfilippo, A. & J.-P. Caulet. 1998. Taxonomy and evolution of Paleogene Antarctic and tropical Lophocyrtid radiolarians. *Micropaleontology*, 44(1): 1-43.

Sanfilippo, A. & W. R. Riedel. 1970. Post-Eocene "closed" theoperid radiolarians. *Micropaleontology,* 16(4): 446-462.

——. 1973. Cenozoic Radiolaria (exclusive of Theoperids, Artostrobiids and Amphipyndacids) from the Gulf of Mexico, DSDP Leg 10. *In* J. L. Worzel et al. (Eds), *Initial Reports of the Deep Sea Drlling Project*, Washington (U. S. Govt Printing Office), 10: 475-611.

——. 1980. A revised generic and suprageneric classification of the Artiscins (Radiolaria). *Journal of Paleontology*, 54(5): 1008-1011.

Scher, H. D. & E. E. Martin. 2006. Timing and climatic consequences of the opening of the Drake Passage. *Science,* 312: 428-430.

Scherer, R. P., A. Aldahan, S. Tulaczyk, G. Possnert, H. Engelhardt & B. Kamb. 1998. Pleistocene Collapse of the West Antarctic Ice Sheet. *Science*, 281: 82-85.

Schlüter, P. & G. Ünzelmann-Neben. 2008. Indications for bottom current activity since Eocene times: the climate and ocean gateway archive of the Transkei Basin, South Africa. *Global and Planetary Change,* 60: 416-428.

Schmarda, L. K. 1871. *Zoologie.* Braumüller, Oxford, 584pp.

Schmidt, D. N. 2007. The closure history of the Central American Seaway: evidence from isotopes and fossils to models and molecules. *In* W. M. Haywood et al. (Eds), Deep-Time perspectives on climate change: marrying the signall from computer models and biological proxies, *The Micropalaeontological Society, Special Publications,* London (The Geological Society), 427-442.

Shannon, C. E. 1948. A mathematical theory of communication. *Bell System Technical Journal*, 27: 379-423.

Shaw, A. B. 1964. *Time in Stratigraphy*. McGraw Hill, New York, 365pp.

Shinozaki, K. 1963. Note on the species-area curve. *Proceedings of the 10th annual meeting of the Ecological Society of Japan*: 5.

Shipboard Scientific Party. 1988a. Site 689. *In* P. E. Barker et al. (Eds), *Proceedings of the Ocean Drilling Program, Initial Reports*, College Station, TX (Ocean Drilling Program), 113: 89-181.

——. 1988b. Site 690. *In* P. E. Barker et al. (Eds), *Proceedings of the Ocean Drilling Program, Initial Reports*, College Station, TX (Ocean Drilling Program), 113: 183-292.

——. 1988c. Site 693. *In* P. E. Barker et al. (Eds), *Proceedings of the Ocean Drilling Program, Initial Reports*, College Station, TX (Ocean Drilling Program), 113: 329-447.

——. 1989a. Site 737. *In* J. Barron et al. (Eds), *Proceedings of the Ocean Drilling Program, Initial Reports*, College Station, TX (Ocean Drilling Program), 119: 159-227.

——. 1989b. Site 738. *In* J. Barron et al. (Eds), *Proceedings of the Ocean Drilling Program, Initial Reports*, College Station, TX (Ocean Drilling Program), 119: 229-288.

——. 1989c. Site 744. *In* J. Barron et al. (Eds), *Proceedings of the Ocean Drilling Program, Initial Reports*, College Station, TX (Ocean Drilling Program), 119: 477-504.

——. 1989d. Site 745. *In* J. Barron et al. (Eds), *Proceedings of the Ocean Drilling Program, Initial Reports*, College Station, TX (Ocean Drilling Program), 119: 505-535.

——. 1989e. Site 746. *In* J. Barron et al. (Eds), *Proceedings of the Ocean Drilling Program, Initial Reports*, College Station, TX (Ocean Drilling Program), 119: 537-553.

——. 1989f. Site 747. *In* R. Schlich et al. (Eds), *Proceedings of the Ocean Drilling Program, Initial Reports*, College Station, TX (Ocean Drilling Program), 119: 89-156.

——. 1989g. Site 748. *In* R. Schlich et al. (Eds), *Proceedings of the Ocean Drilling Program, Initial Reports*, College Station, TX (Ocean Drilling Program), 119: 157-235.

——. 1989h. Site 751. *In* R. Schlich et al. (Eds), *Proceedings of the Ocean Drilling Program, Initial Reports*, College Station, TX (Ocean Drilling Program), 119: 339-373.

——. 2000. Site 1138. *In* M. F. Coffey et al. (Eds), *Proceedings of the Ocean Drilling Program, Initial Reports,* College Station, TX (Ocean Drilling Program), 183: 205pp.

Smith, A. B. & A. J. McGowan. 2011. The ties linking rock and fossil records and why they are important for palaeodiversity studies. *In* A. J. McGowan and A. B. Smith (Eds), Comparing the geological and fossil records: implications for biodiversity studies. *Geological Society of London, Special Publications*, 358: 1-8.

Sorlien, C. S., B. P. Luyendyk, D.S. Wilson, R. C. Decesari, L. R. Bartek & J. B. Diebold. 2007. Oligocene development of the West Antarctic Ice Sheet recorded in eastern Ross Sea strata. *Geology,* 35(5): 467-470.

Sournia, A. 1994. Pelagic biogeography and fronts. *Progress in Oceanography*, 34: 109-120.

Spencer-Cervato, C. 1999. The Cenozoic deep-sea microfossil record: explorations of the DSDP/ODP sample set using the Neptune database. *Palaeontologia electronica*, 2(2): 270pp.

Stadum, C. J & H.-Y. Ling. 1969. Tripylean Radiolaria in deep-sea sediments of the Norwegian Sea. *Micropaleontology,* 15(4): 481-489.

Stepanjants, S. D., G. Cortese, S. B. Kruglikova & K. R. Bjørklund. 2006. A review of bipolarity concepts: history and examples from Radiolaria and Medusozoa (Cnidaria). *Marine Biology Research*, 2: 200-241.

Stickley, C. E., H. Brinkhuis, S. A. Schellenberg, A. Sluijs, U. Röhl, M. Fuller, M. Grauert, M. Huber, J. Warnaar & G. L. Williams. 2004. Timing and nature of the deepening of the Tasmanian Gateway. *Paleoceanography,* 19: PA4027.

Stöhr, E. 1880. Die Radiolarienfauna der Tripoli von Grotte, Provinz Girgenti in Sicilien. *Palaeontographica*, 26 (2): 71-124.

Strelkov, A. A. & V. V. Reshetnjak. 1971. Koloniyalnie radiolyarii Spumellaria mirovogo okeana. *Issledovaniya Fauny Morei*, 9(17): 295-373.

Su, X. 1982. Description of 11 new species of Radiolaria from the Xisha Islands, Guangdong Province, China. *Oceanologia et Limnologia Sinica*, 13(3): 275-284.

Sugiyama, K. 1992a. *Syscioscenium velamen* gen. et sp. nov., a new sethoformid Radiolaria from the lower to middle Miocene of central Japan. *Bulletin of the Mizunami Fossil Museum*, 19: 215-218.

——. 1992b. New spumellarians (Radiolaria) from the lower Miocene Toyohama Formation, Morozaki Group, central Japan. *Bulletin of the Mizunami Fossil Museum,* 19: 193-197.

——. 1993. Skeletal structures of lower and middle Miocene lophophaenids (Radiolaria) from central Japan. *Transactions and Proceedings of the Palaeontological society of Japan, New Series*, 169: 44-72.

——. 1994. Lower Miocene New Nassellarians (Radiolaria) from the Toyohama Formation, Morozaki Group, Central Japan. *Bulletin of the Mizunami Fossil Museum*, 21: 1-11.

——. 1998. Nassellarian fauna from the Middle Miocene Oidawara Formation, Mizunami Group, central Japan. *News of Osaka Micropaleontologists, Special Volume*, 11: 227-250.

Sugiyama, K. & O. R. Anderson. 1998. The fine structure of some living Spyrida (Nassellaria, Radiolaria) and their implications for nassellarian classification. *Paleontological Research,* 2(2): 75-88.

Sugiyama, K. & H. Furutani. 1992. Middle Miocene radiolarians from the Oidawara Formation, Mizunami Group, Gifu Prefecture, central Japan. *Bulletin of the Mizunami Fossil Museum*, Dr. Junji Itoigawa memorial volume, 19: 199-213.

Sugiyama, K., R. S. Hori, Y. Kusunoki & A. Matsuoka. 2008. Pseudopodial features and feeding behavior of living nassellarians *Eucyrtidium hexagonatum* Haeckel, *Pterocorys zancleus* (Müller) and *Dictyocodom prometheus* (Haeckel). *Paleontological Research,* 12(3): 209-222.

Sugiyama, K., T. Nobuhara & K. Inoue. 1992. Preliminary report on Pliocene radiolarians from the Nobori Formation, Tonohama Group, Shikoku, Southwest Japan. *Journal of Earth and Planetary Science, Nagoya University*, 39: 1-30.

Suzuki, N. 2006. Ontogenetic growth and variation in the skeletal structure of two late Neogene *Sphaeropyle* species (Polycystine radiolarians). *Journal of Paleontology*, 80(5): 849-866.

Suzuki, N. & Y. Aita. 2011. Radiolaria: achievements and unresolved issues: taxonomy and cytology. *Plankton & Benthos Research,* 6(2): 69-91.

Suzuki, N. D. Lazarus, K. Ogane, Y. Aita & T. Sakai. 2009a. General results of reexamination of Ehrenberg's radiolarian collections: with instructions on efficient methods to find microfossils from the collection. *In* Y. Tanimura & Y. Aita (Eds), Joint Haeckel and Ehrenberg Project: Reexamination of the Haeckel and Ehrenberg Microfossil Collection as a Historical and Scientific Legacy, *National Museum of Nature and Science Monographs*, Tokyo, 40: 71-86.

Suzuki, N., K. Ogane, Y. Aita, M. Kato, S. Sakai, T. Kurihara, A. Matsuoka, S. Ohtsuka, A. Go, K, Nakaguchi, S. Yamaguchi, T. Takahashi & A. Tuji. 2009b. Distribution patterns of the radiolarian nuclei and symbionts using DAPI-fluorescence. *Bulletin of the National Museum of Science, Series B,* 35(4): 169-182.

Suzuki, N., T. Kurihara & A. Matsuoka. 2009c. Sporogenesis of an extracellular cell chain from the spheroidal radiolarian host *Haliomma capillaceum* (Haeckel), Polycystina, Protista. *Marine micropaleontology*, 72: 157-164.

Swanberg, N. R. 1979. *The ecology of colonial radiolarians: their colony morphology, trophic interactions and associations, behavior, distribution, and the photosynthesis of their symbiont*s. PhD thesis, Massachusetts Institute of Technology and Woods Hole Oceanographic Institution, 198pp.

Swanberg, N. R. & O. R. Anderson. 1981. *Collozoum caudatum* sp. nov.: a giant colonial radiolarian from equatorial and Gulf Stream waters. *Deep-Sea Resaerch*, 28A(9): 1033-1047.

——. 1985. The nutrition of radiolarians: trophic activity of some solitary Spumellaria. *Limnology and Oceanography*, 30(3): 646-652.

Swanberg, N. R. & D. A. Caron. 1991. Patterns of sarcodine feeding in epipelagic oceanic plankton. *Journal of Plankton Research,* 13(2): 287-312.

Swanberg, N. R. & G. R. Harbison. 1980. The ecology of *Collozoum longiforme*, sp. nov., a new colonial radiolarian from the equatorial Atlantic Ocean. *Deep-Sea Research*, 27A: 715-732.

Swanberg, N. R., O. R. Anderson & P. Bennett. 1985. Spongiose spumellarian Radiolaria: the functional morphology of the radiolarian skeleton with a description of *Spongostaurus*, a new genus. *Marine Micropaleontology,* 9: 455-464.

Takahashi, K. 1987. Radiolarian flux and seasonality: climatic and El Niño response in the Subarctic Pacific, 1982-1984. *Global Biogeochemical Cycles*, 1(3): 213-231.

——. 1991. Radiolaria: flux, ecology and taxonomy in the Pacific and Atlantic. *In* S. Honjo. *Ocean Biocoenosis Series*, Woods Hole, MA, (Woods Hole Oceanographic Institution), 3: 1-303.

Takahashi, K. & S. Honjo. 1981. Vertical flux of Radiolaria: a taxon-quantitative sediment trap study from the western tropical Atlantic. *Micropaleontology,* 27(2): 140-190.

Takahashi, O., T. Yuasa, D. Honda & S. Mayama. 2004. Molecular phylogeny of solitary shell-bearing Polycystinea (Radiolaria). *Revue de Micropaléontologie,* 47: 111-118.

Takemura, A. 1992. Radiolarian Paleogene biostratigraphy in the southern Indian Ocean, Leg 120. *In* S. W. Wise Jr. et al (Eds), *Proceedings of the Ocean Drilling Program, Scientific Results,* College Station, TX (Ocean Drilling Program), 120: 735-756.

Tanaka, S. & K. Takahashi. 2008. Detailed vertical distribution of radiolarian assemblage (0-3000m, fifteen layers) in the central subarctic Pacific, June 2006. *Memoirs of the Faculty of Science, Kyushu University, Series D Earth and Planetary Sciences*, 32(1): 49-72.

Tanimura, Y., A. Tuji, Y. Aita, N. Suzuki, K. Ogane & T. Sakai. 2009. Joint Haeckel and Ehrenberg project "Reexamination of the Haeckel and Ehrenberg microfossil collections as a historical and scientific legacy": a summary. *In* Y. Tanimura & Y. Aita (Eds), Joint Haeckel and Ehrenberg Project: Reexamination of the Haeckel and Ehrenberg Microfossil Collection as a Historical and Scientific Legacy, *National Museum of Nature and Science Monographs*, Tokyo, 40: 1-6.

Tchernia, P. 1980. Descriptive Regional Oceanography. *Pergamon Marine Series,* Exeter (Pergamon Press), 3: 253pp.

Tedford, R. A. & D. C. Kelly. 2004. A deep-sea record of the late Miocene carbon shift from the Southern Tasman Sea. *In* N. Exon et al. (Eds), The Cenozoic Southern Ocean: tectonics, sedimentation and climate change between Australia and Antarctica. *Geophysical Monograph*, 151: 273-290.

Van de Paverd, P. J. 1995. *Recent polycystine Radiolaria from the Snellius-II Expedition*. PhD thesis, Vrije Universiteit, Amsterdam, 351pp.

van Leeuwenhoek, A. 1674. More observations from Mr Leewenhook in a letter of Sept. 7, 1674 sent to the publisher. *Philosophical transactions of the Royal Society of London,* 9: 178-182.

Vigour, R. & D. B. Lazarus. 2002. Biostratigraphy of late Miocene–early Pliocene radiolarians from ODP Leg 183 Site 1138. *In* F. A. Frey et al. (Eds), *Proceedings of the Ocean Drilling Program, Scientific Results*, College Station, TX (Ocean Drilling Program), 183: 1–17.

Vincent, E., J. S. Killingley & W. H. Berger. 1980. The magnetic epoch-6 carbon shift: a change in the ocean's $^{13}C/^{12}C$ ratio 6.2 million years ago. *Marine Micropaleontology*, 5: 185-203.

Vinassa de Regny, P. E., 1900. Radiolari Miocenici Italiani. *Memorie della Reale Accademia delle scienze dell'Istituto di Bologna,* 5(8): 227-257.

VLIZ. 2009. Longhurst Biogeographical Provinces. Available online at http://www.vliz.be/vmdcdata/vlimar/downloads.php. Consulted on 2012-06-13.

Waddell, L. M., I. L. Hendy, T. C. Moore & M. W. Lyle. 2009. Ventilation of the Southern Ocean during the late Neogene: a new perspective from the subantarctic Pacific. *Paleoceanography*, 24: PA3206.

Wallich, G. C. 1869. On some undescribed Testaceous Rhizopods from the North Atlantic deposits. *The Monthly Microscopical Journal,* 1: 104-110.

Wang, Y. & Q. Yang. 1992. Neogene and Quaternary radiolarians from leg 125. *In* P. Fryer et al. (Eds), *Proceedings of the Ocean Drilling Program, Scientific Results*, College Station, TX (Ocean Drilling Program), 125: 95-112.

Weaver, F. M. 1976. Antarctic Radiolaria from the southeast Pacific Basin, Deep Sea Drilling Project, Leg 35. *In* C. D. Hollister et al. (Eds), *Initial Reports of the Deep Sea Drilling Project*, Washingtion (U. S. Govt. Printing Office), 35: 569-603.

——. 1983. Cenozoic radiolarians from the Southwest Atlantic, Falkland Plateau region, Deep Sea Drilling Project, Leg 71. *In* W. J. Ludwig et al. (Eds), *Initial Reports of the Deep Sea Drilling Project*, Washingtion (U. S. Govt. Printing Office), 71: 667-686.

Wei, W. & A. Peleo-Alampay. 1997. Onset of the North Atlantic Deep Water 11.5 million years ago triggered by climate cooling. *In* P. Wang & W. A. Berggren (Eds), *Marine Geology and Palaeocenography, Proceedings of the 30th International Geological Congress*: 57-64.

Westberg-Smith M. J. & W. R. Riedel. 1985. Radiolarians from the western margin of the Rockall Plateau, Deep Sea Drilling Project Leg 81. *In* D. G. Roberts et al. (Eds), *Initial Reports of the Deep Sea Drilling Project*, Washington (U. S. Govt. Printing Office), 81: 479-501.

Won, M.-Z. & R. Below. 1999. Cambrian Radiolaria from the Georgina Basin, Queensland, australia. *Micropaleontology,* 45(4): 325-363.

Wright, J. D. & K. G. Miller. 1992. Miocene stable isotope stratigraphy, site 747, Kerguelen Plateau. *In* S. W. Wise Jr et al. (Eds), *Proceedings of the Ocean Drilling Program, Scientific Results*, College Station, TX (Ocean Drilling Program), 120: 855-866.

Wright, J. D., Miller, K. G. & R. G. Fairbanks. 1992. Early and middle Miocene stable isotopes: implications for deepwater circulation and climate. *Paleoceanography,* 7(3): 357-389.

Yuasa, T., O. Takahashi, D. Honda & S. Mayama. 2005. Phylogenetic analyses of the polycystine Radiolaria based on the 18S rDNA sequences of the Spumellarida and the Nassellarida. *European Journal of Protistology,* 41: 287-298.

Zachos, J., M. Pagani, L. Sloan, E. Thomas & K. Billups. 2001. Trends, rhythms, and aberrations in global climate 65Ma to Present. *Science,* 292: 686-693.

Zittel, K. A. 1876. Über einige fossile Radiolarien aus der norddeutschen Kreiden. *Zeitschrift der deutschen geologischen Gesellschaft*, 28: 75-87.

NeptuneCompanion-package

R Documentation

Palaeodiversity analysis using DSDP-ODP data from the Neptune database

Description

Palaeodiversity analysis using DSDP-ODP data from the Neptune database

Details

Package: NeptuneCompanion
Type: Package
Version: 1.0
Date: 2012-04-27
Depends: RCurl, XML
License: None

Author(s)

Johan Renaudie.

Maintainer: Johan Renaudie <Johan.Renaudie@mfn-berlin.de>

ace

R Documentation

Abundance-based Coverage Estimator

Description

Function to compute Chao & Lee's ACE for a given dataset.

Usage

```
ace(mat)
```

Arguments

`mat`
Input data: abundance of each species in a given sample (vector)

Value

Return the ACE value (i. e. an estimate of the real diversity through extrapolation) for the sample (numeric).

Author(s)

Chao & Lee (1992) for the equation, Johan Renaudie for the code.

References

Chao, A. & S.-M. Lee. 1992. Estimating the number of classes via sample coverage. Journal of the american Statistical Association, 87(417): 210-217.

See Also

`caprariis`

Examples

```
## The function is currently defined as
function (mat)
{
  S <- sum(mat > 0)
  Srar <- sum(mat > 0 & mat <= 10)
  snfn <- 0
  for (i in 1:10) {snfn <- snfn + i * sum(mat == i)}
  snn1fn <- 0
  for (i in 1:10) {snn1fn <- snn1fn + i * (i - 1) * sum(mat == i)}
  f1 <- sum(mat == 1)
  Cace <- 1 - f1/snfn
  gamma <- max(c(((snn1fn * Srar)/(Cace * snfn * (snfn - 1)) - 1), 0))
  ACE <- (S - Srar) + (Srar/Cace) + (f1/Cace) * gamma
  return(ACE)
 }
```

bin.summary

R Documentation

Summarize a binned Neptune dataset.

Description

Given specific time bins, this function summarize the needed informations from a given dataset extracted from Neptune to help deining the quotas for the subsamplings procedures.

Usage

```
bin.summary(neptune, age_min, age_max, bin_length)
```

Arguments

`neptune`
The dataset to summarize (the compulsory fields are: age_ma, taxon_id, site and depth_mbsf).

`age_min`
Youngest age for the time bins (in Ma)

`age_max`
Oldest age for the time bins (in Ma)

`bin_length`
Length of the time bins (in My)

Value

`"# Occurrences"`
Number of Occurrences per time bin (for Occurence-Weighted by-list subsamplings)

`"# Collections"`
Number of Collections per time bin (for Unweighted By-list subsampling)

`"# Species"`
Number of Species per time bin

`"Good's u"`
Good (1953) coverage estimator per time bin (for SQS subsampling)

`# Occurence-Squared`
Number of squared occurrences per time bin (for O2W subsampling)

Reference

Good, I. J. 1953. The population frequencies of species and the estimation of population parameters. Biometrika, 40(3-4): 237-264.

Author(s)

Johan Renaudie.

See Also

UW, OW, O2W, CR, sqs.

Examples

```
## The function is currently defined as
function (neptune, age_min, age_max, bin_length)
{
  bin <- seq(age_min, age_max, by = bin_length)
  vl <- length(bin) - 1
  binmid <- numeric(vl)
  for (i in 1:vl) {
    binmid[i] <- (bin[i] + bin[i + 1])/2
  }
  occ <- numeric(vl)
  rawsp <- numeric(vl)
  occbinned <- list()
  ncoll <- numeric(vl)
  collbinned <- list()
  mostfrequent <- numeric(vl)
  ab <- list()
  freq <- list()
  u <- numeric(vl)
  single <- numeric(vl)
  occ2 <- numeric(vl)
  for (i in 1:vl) {
    occbinned[[i]] <- subset(neptune, bin[i] < age_ma & bin[i +
      1] > age_ma)
    occ[i] <- nrow(occbinned[[i]])
    rawsp[i] <- length(unique(occbinned[[i]]$taxon_id))
    collbinned[[i]] <- unique(neptune[neptune$age_ma < bin[i +
      1] & neptune$age_ma > bin[i], ][, c(5, 2)])
    collbinned[[i]] <- collbinned[[i]][order(collbinned[[i]][,
      1]), ]
    ncoll[i] <- nrow(collbinned[[i]])
    ab[[i]] <- summary(occbinned[[i]]$taxon_id, maxsum = 1000)
    ab[[i]] <- ab[[i]][ab[[i]] != 0]
    single[i] <- sum(ab[[i]] == 1)
    u[i] <- 1 - single[i]/occ[i]
    for (k in 1:nrow(collbinned[[i]])) {
      occ2[i] <- occ2[i] + nrow(subset(neptune, site ==
        collbinned[[i]][k, 1] & depth_mbsf == collbinned[[i]][k,
        2]))^2
    }
  }
  summary_mat <- cbind(occ, ncoll, rawsp, u, occ2)
  colnames(summary_mat) <- c("# Occurences", "# Collections",
    "# Species", "Good's u", "# Occurence-Squared")
  return(summary_mat)
 }
```

boundcross

R Documentation

Range-through diversities for abundance matrices.

Description

Computes a serie of range-through diversities for a given abundance matrix.

Usage

```
boundcross(site, age, age_min, age_max, bin_length)
```

Arguments

`site`
Abundance matrix with taxa as rows and samples (ordered from the youngest to the oldest) as columns.

`age`
Vector of age for the samples (in Ma).

`age_min`
Youngest age for the time bins (in Ma).

`age_max`
Oldest age for the time bins (in Ma).

`bin_length`
Time length for the time bins (in My).

Value

The returned value is a list containing the following elements:

`'Bins midpoints'`
Midpoint of the time bins (for plotting purposes).

`'Total diversity'`
Classic range-through diversity.

`'Total diversity minus singletons'`
Classic range-through diversity (minus singletons).

`'Bottom Boundary crossers'`
Foote (2000)'s bottom boundary crossers.

`"Standing mean diversity"`
Foote (2000)'s standing mean diversity (i. e. mean between bottom and top boundary crossers).

`'Extinction Rate'`
Foote (2000)'s extinction rate.

`'Origination Rate'`

Foote (2000)'s origination rate.

Author(s)

Johan Renaudie.

References

Foote, M. 2000. Origination and extinction components of taxonomic diversity: general problems. Paleobiology, 26(sp4): 74-102.

See Also

`lofo`, `RT`

Examples

```
## The function is currently defined as
function(site, age, age_min, age_max, bin_length){
bin<-seq(age_min, age_max, by=bin_length)
binsp<-array(0,dim=c(nrow(site),length(bin)-1))
for(j in 1:(length(bin)-1)){
      for(i in 1:ncol(site)){
            if(age[i]>=bin[j]&age[i]<bin[j+1]){
                  for (k in 1:nrow(site)){
                        if(site[k,i]>0){
                              if(binsp[k,j]==0){binsp[k,j]<-binsp[k,j]+1}
                        }
                  }
            }
      }
}
colSums(binsp)->nspbin
nspbin[nspbin==0]<-NA

FL<-bL<-Ft<-bt<-numeric(length(bin)-1)

for (k in 1:nrow(binsp)){
      if(binsp[k,1]==1 & sum(binsp[k,2:ncol(binsp)])==0){FL[1]<-FL[1]+1}
      if(binsp[k,1]==1 & sum(binsp[k,2:ncol(binsp)])>0){bL[1]<-bL[1]+1}
      if(binsp[k,ncol(binsp)]==1 & sum(binsp[k,1:(ncol(binsp)-1)])==0)
{FL[length(bin)-1]<-FL[length(bin)-1]+1}
      if(binsp[k,ncol(binsp)]==1 & sum(binsp[k,1:(ncol(binsp)-1)])>0)
{Ft[length(bin)-1]<-Ft[length(bin)-1]+1}
      for(j in 2:(ncol(binsp)-1)){
            if(sum(binsp[k,1:(j-1)])>0 & sum(binsp[k,(j+1):ncol(binsp)])>0)
{bt[j]<-bt[j]+1}
            if(binsp[k,j]==1){
                  if(sum(binsp[k,1:(j-1)])==0 & sum(binsp[k,(j
+1):ncol(binsp)])>0){bL[j]<-bL[j]+1}
                  if(sum(binsp[k,1:(j-1)])>0 & sum(binsp[k,(j
+1):ncol(binsp)])==0){Ft[j]<-Ft[j]+1}
                  if(sum(binsp[k,1:(j-1)])==0 & sum(binsp[k,(j
+1):ncol(binsp)])==0){FL[j]<-FL[j]+1}
                  }
            }
```

```
      }

bc<-bL+bt
div<-bc+Ft
bindiv<-div+FL
smd<-((bL+bt)+(Ft+bt))/2

bc[bc==0]<-NA
div[div==0]<-NA
bindiv[bindiv==0]<-NA
smd[smd==0]<-NA

-log(bt/bc)->ext
-log(bt/(bt+Ft))->ori

ext[is.na(nspbin)]<-NA
ori[is.na(nspbin)]<-NA

binmid<-numeric(length(bin)-1)
for(i in 1:length(bin)-1){binmid[i]<-(bin[i]+bin[i+1])/2}

Foote<-list('Bins midpoints'=binmid,'Total diversity'=bindiv,'Total diversity
minus singletons'=div,'Bottom Boundary crossers'=bc, "Standing mean
diversity"=smd, 'Extinction Rate'=ext, 'Origination Rate'=ori)

return(Foote)
}
```

caprariis

R Documentation

De Caprariis curve fitting

Description

Estimates the total diversity from the shape of a collector's curve.

Usage

```
caprariis(AccuTot)
```

Arguments

`AccuTot`
A matrix of two columns, defining the species accumulation curve (first column is the number of specimens, 2nd column the number of species).

Value

Returned value is a list containing:

`Informations`
Gives the equation used, the optimization method and the distance measure used: to date, only de Caprariis et al. 1981 equation, BFGS optimization and absolution value as misfit distance measure are implemented.

`Curve.fitting`
A 3 column matrix: first column is the number of specimen, 2nd column the number of species observed, 3rd column the number of species of the fitted curve.

`Summary`
Gives 5 values: Smax (the asymptote of the fitted curve, i. e. the extrapolated diversity), b, Misfit (the total measured misfit between the real species-accumulation curve and the fitted curve), Pearson and Pearson-squared (the correlation coefficient between the species-accumulation curve and the fitted curve).

Author(s)

De Caprariis et al. (1976; 1981) for the equation, Johan Renaudie for the code.

References

De Caprariis, P., R. H. Lindemann & C. M. Collins. 1976. A method for determining optimum sample size in species diversity studies. Mathematical Geology, 8(5): 575-581. De Caprariis, P., R. H. Lindemann & R. Haimes. 1981. A relationship between sample size and accuracy of species richness predictions. Mathematical Geology, 13(4): 351-355.

See Also

`ace`

Examples

```
## The function is currently defined as
function (AccuTot)
{
  caprariis.misfit <- function(parametres, x) {
    A <- parametres[1]
    B <- parametres[2]
    FIT <- c()
    misfit <- 0
    for (i in 1:nrow(x)) {
      FIT[i] <- (A * i)/(B + i)
      misfit <- sum(abs(FIT[i] - x[i, 2])) + misfit
    }
    return(misfit)
  }
  OPT <- optim(c(50, 10), caprariis.misfit, method = "BFGS",
    x = AccuTot, control = list(trace = 1))
  Smax <- OPT$par[1]
  b <- OPT$par[2]
  FIT <- c()
  caprar <- list()
  misfit <- 0
  for (i in 1:nrow(AccuTot)) {
    FIT[i] <- (Smax * i)/(b + i)
    misfit <- sum(abs(FIT[i] - AccuTot[i, 2])) + misfit
  }
  caprar$Informations <- matrix(c("(Smax*N)/(N+b)", "BFGS",
    "Absolute"), nrow = 3, ncol = 1)
  rownames(caprar$Informations) <- c("Formula", "Optimization method",
    "Misfit measurement")
  caprar$Curve.fitting <- cbind(AccuTot, FIT)
  colnames(caprar$Curve.fitting) <- c("N", "SAC", "Fitting")
  pearson <- cor(FIT, AccuTot[, 2])
  pearson.squared <- pearson^2
  all <- array(c(Smax, b, misfit, pearson, pearson.squared),
    dim = c(5, 1))
  rownames(all) <- c("Smax", "b", "Misfit", "Pearson", "Pearson squared")
  caprar$Summary <- all
  return(caprar)
 }
```

hat.fitting

R Documentation

'Hat' fitting

Description

Fits Liow et al. 2010 'hat' model to the abundance curve of a species.

Usage

```
hat.fitting(X, Tinc, Tdec)
```

Arguments

`X`
Abundance values for a given species along a stratigraphic sequence. Should be a two column matrix: first column is the age of the sample, second column is the number of specimens in the sample.

`Tinc`
Approximative time of increased abundance

`Tdec`
Approximative time of decreased abundance

Value

The returned value is a list:

`Curve-fitting`
4-column matrix: age of the sample, frequency of the species in said sample, fitted value, residual

`Summary`
Gives 8 values: Estimated theoretical maximum of occurence, Max rate of increase, Max rate of decrease, ime of inflection of increase, Time of inflection of decrease, Misfit, Pearson and Pearson squared

Author(s)

Liow et al. 2010 for the concept and the equations; Johan Renaudie for the code,

References

Liow et al. 2010. Global occurrence of trajectories of microfossils: environmental volatility and the rise and fall of individual species. Paleobiology, 36(2): 224-252.

Examples

```
## The function is currently defined as
function (X, Tinc, Tdec)
{
```

```
  if (Tinc > max(X[, 1], na.rm = TRUE)) {
    Tinc <- floor(max(X[, 1], na.rm = TRUE))
  }
  if (Tdec < min(X[, 1], na.rm = TRUE)) {
    Tdec <- ceiling(min(X[, 1], na.rm = TRUE))
  }
  init.param <- c(0.1, 1, -1, Tinc, Tdec)
  X[, 2] <- X[, 2]/sum(X[, 2])
  l <- function(x) {
    y <- 1/(1 + exp(-x))
    return(y)
  }
  hat.misfit <- function(parameters, sp) {
    L <- parameters[1]
    lambdaS <- parameters[2]
    lambdaR <- parameters[3]
    S <- parameters[4]
    R <- parameters[5]
    t <- sp[, 1]
    n <- sp[, 2]
    h <- vector(length = length(t))
    misfit <- 0
    for (i in 1:length(t)) {
      h[i] <- L * (l(lambdaS * (t[i] - S))) * (l(lambdaR *
        (t[i] - R)))
      misfit <- misfit + abs(h[i] - n[i])
    }
    return(misfit)
  }
  OPT <- optim(init.param, hat.misfit, method = "L-BFGS-B",
    sp = X, control = list(trace = 1), lower = c(0, 0, -Inf,
      0, 0), upper = c(1, Inf, 0, Inf, Inf))
  L <- OPT$par[1]
  lambdaS <- OPT$par[2]
  lambdaR <- OPT$par[3]
  S <- OPT$par[4]
  R <- OPT$par[5]
  h <- residual <- vector(length = length(X[, 1]))
  misfit <- 0
  for (i in 1:nrow(X)) {
    h[i] <- L * (l(lambdaS * (X[i, 1] - S))) * (l(lambdaR *
      (X[i, 1] - R)))
    residual[i] <- X[i, 2] - h[i]
    misfit <- misfit + abs(residual[i])
  }
  hat <- list()
  hat$Curve.fitting <- cbind(X, h, residual)
  colnames(hat$Curve.fitting) <- c("t", "n", "h", "r")
  rho <- cor(h, X[, 2])
  rho.squared <- rho^2
  all <- array(c(L, lambdaS, lambdaR, S, R, misfit, rho, rho.squared),
    dim = c(8, 1))
  rownames(all) <- c("Estimated theoretical maximum of occurence",
    "Max rate of increase", "Max rate of decrease", "Time of inflection of
increase",
    "Time of inflection of decrease", "Misfit", "Pearson",
    "Pearson squared")
  hat$Summary <- all
  return(hat)
 }
```

lofo

R Documentation

LO and FO.

Description

From an abundance matrix, extract the first and last observed occurrences of all species.

Usage

```
lofo(site)
```

Arguments

`site`
Abundance matrix with taxa as rows and samples as columns. Samples have to be in chronological order (youngest to oldest) and the first row has to be either the age or the depth for each sample.

Value

The returned value is a matrix in with each row is a species. First column is LO and second column FO.

Author(s)

Johan Renaudie.

See Also

`boundcross`, `RT`

Examples

```
## The function is currently defined as
function (site)
{
  pba <- 0
  pb <- txtProgressBar(0, (nrow(site) - 1) * (ncol(site) -
    2), style = 3)
  site <- site[rowSums(site) > 0, ]
  lofo <- array(dim = c(nrow(site), 2))
  rownames(lofo) <- rownames(site)
  colnames(lofo) <- c("LO", "FO")
  for (i in 2:ncol(site) - 1) {
    for (j in 2:nrow(site)) {
      if (sum(site[j, 1:i]) == 0 & site[j, i + 1] > 0) {
        lofo[j, 1] <- site[1, i + 1]
      }
      if (sum(site[j, (i + 1):ncol(site)]) == 0 & site[j,
        i] > 0) {
```

```
        lofo[j, 2] <- site[1, i]
      }
      pba <- pba + 1
      Sys.sleep(0.01)
      setTxtProgressBar(pb, pba)
    }
  }
  lofo <- lofo[-1, ]
  lofo[is.na(lofo[, 1]), 1] <- site[1, 1]
  lofo[is.na(lofo[, 2]), 2] <- site[1, ncol(site)]
  return(lofo)
}
```

pacman

R Documentation

Pacman profiling and trimming

Description

Flag and trim anomalous occurrences given a certain percentage on a Neptune occurrence dataframe

Usage

```
pacman(neptune, perc_top = 5, perc_bottom = 3)
```

Arguments

`neptune`
A dataframe extracted from Neptune (need at a field `taxon_id`,`age_ma`, `depth_mbsf` and `site`)

`perc_top`
Percentage to trim at the top of the ranges, default to 5%

`perc_bottom`
Percentage to trim at the bottom of the ranges, default to 3%

Value

The returned value is a list:

`Trimming`
Trimmed dataframe

`Profiling`
3-column matrix: site, depth, number of outliers

Author(s)

Lazarus et al. 2012 for the algorithm, Johan Renaudie for the code.

References

Lazarus et al. 2012. Pacman profiling: a simple procedure to identify stratigraphic outliers in high-density deep-sea microfossil data. Paleobiology, 38(1): 858-875.

Examples

```
## The function is currently defined as
function (neptune, perc_top = 5, perc_bottom = 3)
{
  species <- unique(neptune$taxon_id)
  sp <- list()
  noc <- c()
```

```
  for (i in 1:length(species)) {
    sp[[i]] <- neptune[neptune$taxon_id == species[i], ]
    sp[[i]] <- sp[[i]][order(sp[[i]]$age_ma), ]
    noc[i] <- nrow(sp[[i]])
  }
  n1 <- cbind(neptune$site, neptune$depth_mbsf)
  samples <- unique(n1[, 1:2])
  outlier <- rep(0, nrow(samples))
  res <- c()
  for (i in 1:length(species)) {
    spe <- sp[[i]]
    nb_top <- floor(noc[i] * perc_top/100)
    nb_bottom <- floor(noc[i] * perc_bottom/100)
    if (nb_top >= 1) {
      for (k in 1:nb_top) {
        out <- samples[, 1] == spe$site[k] & samples[,
         2] == spe$depth_mbsf[k]
        outlier[out] <- outlier[out] + 1
      }
      spe <- spe[-(1:nb_top), ]
    }
    if (nb_bottom >= 1) {
      for (k in ((nrow(spe) - nb_bottom + 1):nrow(spe))) {
        out <- samples[, 1] == spe$site[k] & samples[,
         2] == spe$depth_mbsf[k]
        outlier[out] <- outlier[out] + 1
      }
      spe <- spe[-((nrow(spe) - nb_bottom + 1):nrow(spe)),
        ]
    }
    res <- rbind(res, spe)
  }
  outlier <- cbind(samples, outlier)
  colnames(res) <- names(neptune)
  res <- as.data.frame(res)
  colnames(outlier) <- c("site", "depth_mbsf", "nb_outliers")
  reslist <- list(Trimming = res, Profiling = outlier)
  return(reslist)
}
```

Pangea

R Documentation

Functions to deal with data from Pangea

Description

A serie of functions to retrieve and work with datasets from Pangea, the online depository for paleoceanographical datasets.

Usage

```
searchPangea(string, output = FALSE)
getPangeaData(DOI)
getPangeaList(DOI)
readPangea(file1, label.col = 1)
```

Arguments

`string`
A string of keywords for the search

`DOI`
DOI (as retrieved by searchPangea) of a dataset or a reference.

`output`
if TRUE, the resulting dataframe is sinked into a tabulated txt file.

`file1`
File downloaded from Pangea to read.

`label.col`
Index of the column (or columns) that contains the unique identifiers of each entry.

Details

`searchPangea` searches datasets corresponding to the keywords given in `string`. `getPangeaData` extracts a dataset from Pangea, given the DOI of the dataset.`getPangeaList` extracts a list of datasets corresponding to one reference from Pangea, given the DOI of the reference. `readPangea` reads a file downloaded (as tabulated text) from Pangea.

Value

The returned value of `searchPangea` and `getPangeaList` is a dataframe in which the first element is the name (when available) of the dataset or of the reference from which the dataset comes from, the second element the number of dataset said reference contains or the number of datapoints said dataset contains, the third element is the DOI of the dataset/reference and the fourth element the relevance score given by Pangea to the dataset/reference with regards to the keywords entered in `string`. The returned value of `getPangeaData` is a list containing:

`Citation`
Metadata allowing the user to be able to cite his/her source.

`Parameters`
Informations on each column of the dataset

`Dataset`
The dataset as a matrix.

Author(s)

Johan Renaudie.

Examples

```
library(RCurl)
library(XML)

#Search online for datasets on Miocene carbon isotopes
searchPangea("d13C miocene")->d13C
d13C

#Select, get and plot one of the datasets from Swart & Eberli 2005
d13C[grep("Swart",d13C[,1]),3]->doi1
getPangeaList(doi1)->Swart_Eberli
Swart_Eberli[1,3]->doi2
getPangeaData(doi2)->swart_eberli1
plot(swart_eberli1$Dataset[,4], swart_eberli1$Dataset[,3]/1000, pch=20,
ylim=c(23,5.3), xlab=expression(paste(delta^13,C, sep="")), ylab="Age(Ma)",
main="Bahama Bank")

#Select datasets on New Zealand
d13C[grep("New Zealand",d13C[,1]),]->NZd13C

#Pick, get and plot one with a high relevance score
NZd13C[ NZd13C$Score %in% head(d13C$Score,5) ,3 ]->doi3
getPangeaData(doi3)->ando2011
grep("d13C",ando2011$Parameters$Name)->c13
grep("DEPTH",ando2011$Parameters$Name)->d
plot(ando2011$Dataset[,c13], ando2011$Dataset[,d], pch=20, ylim=c(250,0),
yaxs="i", xlab=expression(paste(delta^13,C, sep="")), ylab="Depth(mbsf)")

## The functions are currently defined as
searchPangea<-function (string, output = FALSE)
{
  require(XML)
  outname <- string
  string <- strsplit(string, split = " ")[[1]]
  query <- string[1]
  if (length(string) > 1) {
    for (i in 2:length(string)) {
      query <- paste(query, string[i], sep = "+")
    }
  }
  results <- readHTMLTable(URLencode(paste("http://www.pangea.de/search?q=",
    query, "&count=", 1000, sep = "")), which = -(1:3))
  n <- length(results)
  if (n == 0) {
    stop("No result for that query")
  }
  art <- siz <- doi <- sco <- vector(length = n)
```

```
  for (i in 1:n) {
    if (nrow(results[[i]]) == 4) {
      art[i] <- as.character(results[[i]][2, 2])
      siz[i] <- as.character(results[[i]][3, 2])
      a1 <- results[[i]][4, 1]
    }
    if (nrow(results[[i]]) == 3) {
      art[i] <- as.character(results[[i]][1, 2])
      siz[i] <- as.character(results[[i]][2, 2])
      a1 <- results[[i]][3, 1]
    }
    if (nrow(results[[i]]) == 2) {
      art[i] <- NA
      siz[i] <- as.character(results[[i]][1, 2])
      a1 <- results[[i]][2, 1]
    }
    a2 <- strsplit(as.character(a1), split = " - ")[[1]]
    doi[i] <- gsub("doi:", "", a2[1])
    sco[i] <- strsplit(a2[2], split = ": ")[[1]][2]
    rm(a1, a2)
  }
  result <- data.frame(Article = art, Size = siz, DOI = doi,
    Score = sco)
  if (output == TRUE) {
    write.table(result, file = paste(outname, " on pangea.txt",
      sep = ""), sep = "\t", col.names = TRUE, row.names = FALSE,
      quote = FALSE)
  }
  if (output == FALSE) {
    return(result)
  }
 }

getPangeaData<-function(DOI)
{
      require(XML)
      as.character(DOI)->DOI
      URLencode(paste("http://doi.pangaea.de/",DOI,sep=""))->doi.url
      URLencode(paste("http://doi.pangaea.de/",DOI,"?
format=textfile",sep=""))->dl
      readLines(doi.url)->p
      options(warn=-1)
      p[grep("description",p)][1]->p1
      gsub("<meta name=\"description\" content=\"","",p1)->p1
      strsplit(p1,", Supplement to: ")[[1]]->p1
      strsplit(p1[1]," doi:")[[1]][1]->p1[1]
      strsplit(p1[2],", doi:")[[1]][1]->p1[2]
      c(p1,DOI)->p1
      names(p1)<-c("Dataset name:", "Supplement to:", "DOI:")
      readHTMLTable(p[grep("Parameter",p):tail(grep("/table",p),1)])[[1]]-
>params
      url(dl)->f
      readLines(f)->g
      (1:length(g))[g=="*/"]->metaskip
      strsplit(g[metaskip+1],split="\t",perl=TRUE)[[1]]->cn
      read.table(f,header=FALSE,sep="\t",skip=metaskip+1)->result
      colnames(result)<-cn
      res<-list(Citation=p1,Parameters=params,Dataset=result)
      options(warn=0)
      return(res)
```

```
 }

getPangeaList<-function (DOI)
{
  require(XML)
  DOI <- as.character(DOI)
  doi.url <- URLencode(paste("http://doi.pangaea.de/", DOI,
    sep = ""))
  p <- readLines(doi.url)
  p2 <- p[grep("<li>", p)]
  p3 <- strsplit(p2, split = "strong")
  aut <- tit <- doi <- vector(length = length(p3))
  for (i in 1:length(p3)) {
    aut[i] <- gsub(">", "", gsub(": </", "", p3[[i]][2]))
    tit[i] <- gsub(">", "", strsplit(p3[[i]][3], split = ". doi")[[1]][1])
    doi[i] <- gsub("\"><", "", strsplit(p3[[i]][1], split =
"doi.pangaea.de/")[[1]][2])
  }
  result <- data.frame(Source = aut, Name = tit, DOI = doi)
  return(result)
 }

readPangea<-function (file1, label.col = 1)
{
  k <- file(file1)
  k1 <- readLines(k)
  close(k)
  metastop <- grep("*/", k1, fixed = TRUE)
  k2 <- k1[(metastop + 1):length(k1)]
  headernames <- strsplit(k2, split = "\t")[[1]]
  m <- length(headernames)
  classcol <- rep("numeric", m)
  if (!is.na(label.col[1])) {
    classcol[label.col] <- "character"
  }
  res1 <- read.table(file1, sep = "\t", header = T, colClasses = classcol,
    skip = metastop, row.names = NULL)
  return(res1)
 }
```

RT

R Documentation

Range-through diversity for occurrence dataframe.

Description

Computes Foote (2000)'s range-through diversity for a given occurrence dataframe.

Usage

```
RT(data, age_min, age_max, bin_length)
```

Arguments

`data`
Occurrence dataframe. Compulsory fields: `taxon_id`, `age_ma`, `depth_mbsf` and `site`.

`age_min`
Youngest age for the time bins (in Ma).

`age_max`
Oldest age for the time bins (in Ma).

`bin_length`
Time length for the time bins (in My).

Value

The returned value is a 4-columns matrix: Bin midpoint (for plotting purposes), Foote (2000)'s boundary crossers (standing mean diversity), Foote (2000)'s extinction and origination rates.

Author(s)

Johan Renaudie.

References

Foote, M. 2000. Origination and extinction components of taxonomic diversity: general problems. Paleobiology, 26(sp4): 74-102.

See Also

`boundcross`, `lofo`

Examples

```
## The function is currently defined as
function (data, age_min, age_max, bin_length)
{
  bin <- seq(age_min, age_max, by = bin_length)
  vl <- length(bin) - 1
  binmid <- numeric(vl)
```

```
  for (i in 1:vl) {
    binmid[i] <- (bin[i] + bin[i + 1])/2
  }
  sib <- array(0, dim = c(length(levels(data$taxon_id)),
    vl))
  for (j in 1:vl) {
    in_bin <- subset(data, age_ma > bin[j] & age_ma <
      bin[j + 1])
    sib[in_bin, j] <- 1
  }
  sib <- sib[rowSums(sib) != 0, ]
  bL <- bt <- bcRaw <- numeric(vl)
  for (k in 1:nrow(sib)) {
    if (sib[k, 1] == 1 & sum(sib[k, 2:ncol(sib)]) > 0) {
      bL[1] <- bL[1] + 1
    }
    if (sib[k, vl] == 1 & sum(sib[k, 1:(vl - 1)]) > 0) {
      Ft[vl] <- Ft[vl] + 1
    }
    for (j in 2:(vl - 1)) {
      if (sum(sib[k, 1:(j - 1)]) > 0 & sum(sib[k, (j +
        1):vl]) > 0) {
        bt[j] <- bt[j] + 1
      }
      if (sum(sib[k, 1:(j - 1)]) == 0 & sib[k, j] == 1 &
        sum(sib[k, (j + 1):vl]) > 0) {
        bL[j] <- bL[j] + 1
      }
      if (sum(sib[k, 1:(j - 1)]) > 0 & sib[k, j] == 1 &
        sum(sib[k, (j + 1):vl]) == 0) {
        bL[j] <- bL[j] + 1
      }
    }
  }
  bcRaw <- ((bL + bt) + (Ft + bt))/2
  rateRaw <- -log(bt/(bL + bt))
  origRaw <- -log(bt/(Ft + bt))
  result <- cbind(`Mid-bin age` = binmid, `Boundary Crossers` = bcRaw,
    `Extinction Rate` = rateRaw, `Origination Rate` = origRaw)
  return(result)
}
```

sample.depth

R Documentation

From sample name to sample depth.

Description

From a vector of sample names (DSDP/ODP), get the corresponding depth (in mbsf) using Janus online database.

Usage

```
sample.depth(samples, toponly = FALSE, intervalsep = "/")
```

Arguments

`samples`
Vector of sample names (as characters). Should include the Leg information.

`toponly`
TRUE if only the top of the interval is given (e.g. "120-747A-4H-3, 20"); FALSE otherwise (e.g. "120-747A-4H-3, 20/22cm")

`intervalsep`
What character string separated the top to the bottom of the interval if toponly=FALSE.

Value

The returned value is a matrix with 1 column (the depth of the sample in meters below sea-floor).

Author(s)

Johan Renaudie

Examples

```
library(RCurl)
library(XML)
searchPangea("marine isotope stages")->mis
mis[grep("Thunell",mis[,1]),3][1]->doi1
getPangeaData(doi1)->thunell
thunell # This dataset lacks the depth parameter.

as.character(thunell$Dataset[,4])->samples
sample.depth(samples, toponly=FALSE, intervalsep="-")->depth
depth # ...and here it is.

## The function is currently defined as
function (samples, toponly = FALSE, intervalsep = "/")
{
  pba <- 0
  pb <- txtProgressBar(0, length(samples), style = 3)
```

```
  if (!is.logical(toponly)) {
    stop("toponly must be logical:\n\tTRUE if only the top of the interval is
given (e.g. \"120-747A-4H-3, 20\"),\n\tFALSE otherwise (e.g. \"120-747A-4H-3,
20/22cm\")")
  }
  for (i in 1:length(samples)) {
    if (length(grep(",", samples[i])) != 0) {
      if (length(grep(", ", samples[i])) == 0) {
        b <- strsplit(samples[i], split = ",")[[1]]
        samples[i] <- paste(b[1], b[2], sep = ", ")
      }
    }
  }
  samp_temp <- strsplit(samples, split = ", ")
  mbsf <- rep(NA, length(samples))
  Janus.CorScRequest <- function(leg, site, ...) {
    require(RCurl)
    require(XML)
    a <- getForm("http://iodp.tamu.edu/janusweb/coring_summaries/
coresumm.cgi", leg = leg, site = site, ...)
    a1 <- htmlTreeParse(a, useInternalNodes = TRUE)
    a2 <- xpathApply(a1, path = "//pre", xmlValue)[[1]]
    a3 <- strsplit(a2, split = "\n")[[1]]
    a3 <- a3[a3 != ""]
    a4 <- strsplit(a3, split = "\t")
    a5 <- array(dim = c(length(a4), 10))
    for (i in 1:length(a4)) {
      a5[i, ] <- a4[[i]][1:10]
    }
    a5[, 1:9] <- gsub(" ", "", a5[, 1:9])
    a5 <- a5[-1, ]
    leg1 <- as.integer(a5[, 1])
    site1 <- as.integer(a5[, 2])
    core1 <- as.integer(a5[, 4])
    hole1 <- as.character(a5[, 3])
    type1 <- as.character(a5[, 5])
    sc1 <- as.character(a5[, 6])
    comment <- as.character(a5[, 10])
    ll <- as.numeric(a5[, 7])
    cl <- as.numeric(a5[, 8])
    top <- as.numeric(a5[, 9])
    res <- data.frame(Leg = leg1, Site = site1, H = hole1,
      Cor = core1, T = type1, Sc = sc1, LL = ll, CL = cl,
      Top = top, Comment = comment)
    return(res)
  }
  for (i in 1:length(samples)) {
    sct_temp <- strsplit(samp_temp[[i]][1], split = "-")[[1]]
    leg <- sct_temp[1]
    n <- length(strsplit(sct_temp[2], split = "")[[1]])
    site <- substr(sct_temp[2], 1, (n - 1))
    hole <- substr(sct_temp[2], n, n)
    core_summary <- Janus.CorScRequest(leg = leg, site = site,
      hole = hole)
    if (!hole %in% core_summary[, 3]) {
      if (leg == TRUE & toponly == FALSE) {
        stop(paste("In row ", i, paste(", the syntax should be
\"120-747A-1H-1, 45",
          "47cm\"\nIf no Hole, try *\n", sep = intervalsep)))
      }
```

```
      if (leg == FALSE & toponly == FALSE) {
        stop(paste("In row", i, paste(", the syntax should be \"747A-1H-1,
45",
         "47cm\"\nIf no Hole, try *\n", sep = intervalsep)))
      }
      if (leg == TRUE & toponly == TRUE) {
        stop(paste("In row", i, ", the syntax should be \"120-747A-1H-1,
45\"\nIf no Hole, try *\n"))
      }
      if (leg == FALSE & toponly == TRUE) {
        stop(paste("In row", i, ", the syntax should be \"747A-1H-1, 45\"\nIf
no Hole, try *\n"))
      }
    }
    m <- length(strsplit(sct_temp[3], split = "")[[1]])
    core <- substr(sct_temp[3], 1, (m - 1))
    type <- substr(sct_temp[3], m, m)
    section <- sct_temp[4]
    if (length(samp_temp[[i]]) == 1) {
      top <- 0
    }
    if (length(samp_temp[[i]]) != 1) {
      if (toponly == FALSE) {
        top <- strsplit(samp_temp[[i]][2], split = intervalsep)[[1]][1]
      }
      else {
        top <- samp_temp[[i]][2]
      }
    }
    if (section != "CC") {
      section_top <- core_summary[((core_summary[, 2] ==
        as.numeric(site)) & (core_summary[, 3] == hole) &
        (core_summary[, 4] == as.numeric(core)) &
(as.character(core_summary[, 6]) == section)), 9]
    }
    if (section == "CC") {
      top_temp <- core_summary[((core_summary[, 2] == as.numeric(site)) &
        (core_summary[, 3] == hole) & (core_summary[, 4] ==
as.numeric(core))), ]
      section_top <- top_temp[grep("CC", top_temp[, 6]), 9]
    }
    if (length(section_top) == 0) {
      mbsf[i] <- NA
    }
    if (length(section_top) != 0) {
      depth <- as.numeric(section_top) + (as.numeric(top)/100)
      mbsf[i] <- depth
    }
    pba <- pba + 1
    Sys.sleep(0.01)
    setTxtProgressBar(pb, pba)
  }
  result <- matrix(mbsf, ncol = 1)
  colnames(result) <- "Depth (mbsf)"
  rownames(result) <- samples
  return(result)
 }
```

subsamplings

R Documentation

Subsampling procedures.

Description

Classical rarefaction, unweighted by-list, occurrence-weighted by-list, occurrence-squared weighted by-list and Shareholders Quorum Subsamplings methods.

Usage

```
CR(data, quota, trials = 100, age_min, age_max, bin_length)
UW(data, quota, trials = 100, age_min, age_max, bin_length)
OW(data, quota, trials = 100, age_min, age_max, bin_length)
O2W(data, quota, trials = 100, age_min, age_max, bin_length)
sqs(data, quota, trials = 100, dominant = "include", age_min,
age_max, bin_length)
```

Arguments

`data`
Neptune dataframe (compulsory fields are `taxon_id`, `site`, `depth_mbsf` and `age_ma`).

`quota`
Quota for the subsampling (`numeric`).

`trials`
Number of trials (default to 100).

`dominant`
For `sqs` function: if '`exclude`' the dominant taxa is excluded (i. e. it won't be picked by the subsampling algorithm) and if '`include`' it will be.

`age_min`
Youngest age for the time binning (in Ma).

`age_max`
Older age for the time binning (in Ma).

`bin_length`
Length of the time bins (in My).

Details

1. CR: Classical rarefaction (Sanders 1968). The `quota` is a number of occurrences. Occurrences are picked until the quota is reached.

2. UW: Unweighted by-list subsampling (Shinozaki 1963). The `quota` is a number of collections. Collections are picked until the quota is reached.

3. OW: Occurrence-weighted by-list subsampling (Alroy 1996). The `quota` is a number of occurrences. Collections are picked until the quota of total occurrences is reached.

4. O2W: Occurrence-squared-weighted by-list subsampling (Alroy 2000). The `quota` is a number of squared occurrences. Collections are picked until the sum of the squared number of occurrences for each collection reaches the quota.

5. sqs: 'Shareholder Quorum' subsampling (Alroy 2010). The `quota` is a coverage estimator (Good (1953)'s u) between 0 and 1. Species are picked until the sum of each species frequency in the bin reaches the quota.

Value

The result is a list containing the following elements:

`'SQS subsampling value for 100 trials'`
Matrix containing the raw results for each single trials (rows are trials and columns are time bins).

`'SQS Boundary crossers for 100 trials'`
Matrix containing the range-through diversity (Boundary Crossers methods) for each single trials (rows are trials and columns are time bins).

`'SQS Subsampling summary'`
Matrix with time bins as columns and containing several elements as rows: `` `Bin Mid-point` `` the time bin midpoints (for plotting purposes),`` `subsampled diversity` `` the mean raw diversity, `` `Boundary Crossers` `` the mean range-through diversity (Boundary Crossers methods; Foote 2000), `` `Extinction rate` `` and `` `Origination rate` `` mean extinction and origination rates (Foote 2000 method).

Author(s)

Johan Renaudie. The `sqs` function is adapted from John Alroy own `sqs` function (available on his personal website) and the other functions are loosely based on functions teached by John Alroy during the 2010 PaleoBiology DataBase Intensive Workshop on Analytical Paleobiology.

References

Alroy, J. 1996. Constant extinction, constrained diversification, and uncoordinated stasis in North American mammals. Palaeogeography, Palaeoclimatology, Palaeoecology, 127:285-311.

Alroy, J. 2000. New methods for quantifying macroevolutionary patterns and processes. Paleobiology, 26(4): 707-733.

Alroy, J. 2010b. Fair sampling of taxonomic richness and unbiased estimation of origination and extinction rates. In J. Alroy and G. Hunt, eds. Quantitative methods in paleobiology. The Paleontological Society Papers, 16: 55-80.

Foote, M. 2000. Origination and extinction components of taxonomic diversity: general problems. Paleobiology, 26(sp4): 74-102. Good, I. J. 1953. The population frequencies of species and the estimation of population parameters. Biometrika, 40(3-4): 237-264.

Sanders, H. L. 1968. Marine benthic diversity: a comparative study. The American Naturalist, 102(935): 243-282.

Shinozaki, K. 1963. Note on the species-area curve. Proceedings of the 10th annual meeting of the Ecological Society of Japan: 5.

Examples

```
## The function is currently defined as
UW<-function (data, quota, trials = 100, age_min, age_max, bin_length)
{
  bin <- seq(age_min, age_max, by = bin_length)
  vl <- length(bin) - 1
  binmid <- numeric(vl)
  for (i in 1:vl) {
    binmid[i] <- (bin[i] + bin[i + 1])/2
  }
  occ <- numeric(vl)
  occbinned <- list()
  ncoll <- numeric(vl)
  collbinned <- list()
  for (i in 1:vl) {
    occbinned[[i]] <- subset(data, bin[i] < age_ma & bin[i +
      1] > age_ma)
    occ[i] <- nrow(occbinned[[i]])
    o1 <- cbind(occbinned[[i]]$site, occbinned[[i]]$depth_mbsf)
    collbinned[[i]] <- unique(o1[, 1:2])
    collbinned[[i]] <- collbinned[[i]][order(collbinned[[i]][,
      1]), ]
    ncoll[i] <- nrow(collbinned[[i]])
  }
  Sys.sleep(0.01)
  cat("\nUW\n")
  bcUW <- uwSpecies <- rateUW <- origUW <- array(0, dim = c(trials,
    vl))
  pba <- 0
  pb <- txtProgressBar(0, vl * trials, style = 3)
  for (t in 1:trials) {
    seen <- array(0, dim = c(length(levels(data$taxon_id)),
      vl))
    for (i in 1:vl) {
      temp <- collbinned[[i]]
      collsamp <- 0
      uwsampled <- c()
      ncollLeft <- ncoll[i]
      if (ncoll[i] < quota) {
        uwSpecies[t, i] <- NA
      }
      else {
        while (collsamp < quota) {
         cellNo <- floor(runif(1, min = 1, max = ncollLeft +
          1))
         picked <- data[(data$site == temp[cellNo, 1] &
          data$depth_mbsf == temp[cellNo, 2]), ]
         uwsampled <- rbind(uwsampled, picked)
         seen[picked$taxon_id, i] <- 1
         temp[cellNo, ] <- temp[ncollLeft, ]
         collsamp <- collsamp + 1
         ncollLeft <- ncollLeft - 1
        }
        uwSpecies[t, i] <- length(unique(uwsampled$taxon_id))
      }
```

```
      pba <- pba + 1
      Sys.sleep(0.01)
      setTxtProgressBar(pb, pba)
    }
    bL <- Ft <- bt <- numeric(vl)
    for (k in 1:nrow(seen)) {
      if (seen[k, 1] == 1 & sum(seen[k, 2:vl]) > 0) {
        bL[1] <- bL[1] + 1
      }
      if (seen[k, vl] == 1 & sum(seen[k, 1:(vl - 1)]) >
        0) {
        Ft[vl] <- Ft[vl] + 1
      }
      for (j in 2:(vl - 1)) {
        if (sum(seen[k, 1:(j - 1)]) > 0 & sum(seen[k,
         (j + 1):vl]) > 0) {
         bt[j] <- bt[j] + 1
        }
        if (seen[k, j] == 1) {
         if (sum(seen[k, 1:(j - 1)]) == 0 & sum(seen[k,
          (j + 1):vl]) > 0) {
          bL[j] <- bL[j] + 1
         }
         if (sum(seen[k, 1:(j - 1)]) > 0 & sum(seen[k,
          (j + 1):vl]) == 0) {
          Ft[j] <- Ft[j] + 1
         }
        }
      }
    }
    bcUW[t, ] <- ((bL + bt) + (bt + Ft))/2
    rateUW[t, ] <- -log(bt/(bL + bt))
    origUW[t, ] <- -log(bt/(Ft + bt))
  }
  uwSpeciesM <- bcUWM <- rateUWM <- origUWM <- numeric(vl)
  for (i in 1:vl) {
    uwSpeciesM[i] <- mean(uwSpecies[, i], na.rm = T)
    bcUWM[i] <- mean(bcUW[, i], na.rm = T)
    rateUWM[i] <- mean(rateUW[, i], na.rm = T)
    origUWM[i] <- mean(origUW[, i], na.rm = T)
  }
  uwmat <- rbind(`Bin Mid-point` = binmid, `UW subsampled diversity` =
uwSpeciesM,
    `Boundary Crossers on UW` = bcUWM, `Extinction rate` = rateUWM,
    `Origination rate` = origUWM)
  for (i in 1:vl) {
    if (uwmat[3, i] == 0) {
      uwmat[3, i] <- NA
    }
  }
  result <- list(`UW subsampling value for 100 trials` = uwSpecies,
    `UW Boundary crossers in 100 trials` = bcUW, `UW Subsampling summary` =
uwmat)
  return(result)
 }

OW<-function (data, quota, trials = 100, age_min, age_max, bin_length)
{
  bin <- seq(age_min, age_max, by = bin_length)
  vl <- length(bin) - 1
```

```
binmid <- numeric(vl)
for (i in 1:vl) {
  binmid[i] <- (bin[i] + bin[i + 1])/2
}
occ <- numeric(vl)
occbinned <- list()
ncoll <- numeric(vl)
collbinned <- list()
for (i in 1:vl) {
  occbinned[[i]] <- subset(data, bin[i] < age_ma & bin[i +
    1] > age_ma)
  occ[i] <- nrow(occbinned[[i]])
  o1 <- cbind(occbinned[[i]]$site, occbinned[[i]]$depth_mbsf)
  collbinned[[i]] <- unique(o1[, 1:2])
  collbinned[[i]] <- collbinned[[i]][order(collbinned[[i]][,
    1]), ]
  ncoll[i] <- nrow(collbinned[[i]])
}
cat("\nOW\n")
bcOW <- owSpecies <- rateOW <- origOW <- array(0, dim = c(trials,
  vl))
pba <- 0
pb <- txtProgressBar(0, vl * trials, style = 3)
for (t in 1:trials) {
  seen <- array(0, dim = c(length(levels(data$taxon_id)),
    vl))
  for (i in 1:vl) {
    temp <- collbinned[[i]]
    occsamp <- 0
    owsampled <- c()
    ncollLeft <- ncoll[i]
    if (occ[i] < quota) {
      owSpecies[t, i] <- NA
    }
    else {
      while (occsamp < quota) {
       cellNo <- floor(runif(1, min = 1, max = ncollLeft +
        1))
       picked <- data[(data$site == temp[cellNo, 1] &
        data$depth_mbsf == temp[cellNo, 2]), ]
       owsampled <- rbind(owsampled, picked)
       seen[picked$taxon_id, i] <- 1
       temp[cellNo, ] <- temp[ncollLeft, ]
       occsamp <- occsamp + nrow(picked)
       ncollLeft <- ncollLeft - 1
      }
      owSpecies[t, i] <- length(unique(owsampled$taxon_id))
    }
    pba <- pba + 1
    Sys.sleep(0.01)
    setTxtProgressBar(pb, pba)
  }
  bL <- bt <- Ft <- numeric(vl)
  for (k in 1:nrow(seen)) {
    if (seen[k, 1] == 1 & sum(seen[k, 2:vl]) > 0) {
      bL[1] <- bL[1] + 1
    }
    if (seen[k, vl] == 1 & sum(seen[k, 1:(vl - 1)]) >
      0) {
      Ft[vl] <- Ft[vl] + 1
```

```
      }
      for (j in 2:(vl - 1)) {
        if (sum(seen[k, 1:(j - 1)]) > 0 & sum(seen[k,
         (j + 1):vl]) > 0) {
         bt[j] <- bt[j] + 1
        }
        if (seen[k, j] == 1) {
         if (sum(seen[k, 1:(j - 1)]) == 0 & sum(seen[k,
          (j + 1):vl]) > 0) {
          bL[j] <- bL[j] + 1
         }
         if (sum(seen[k, 1:(j - 1)]) > 0 & sum(seen[k,
          (j + 1):vl]) == 0) {
          Ft[j] <- Ft[j] + 1
         }
        }
      }
    }
    bcOW[t, ] <- ((bL + bt) + (bt + Ft))/2
    rateOW[t, ] <- -log(bt/(bL + bt))
    origOW[t, ] <- -log(bt/(Ft + bt))
  }
  owSpeciesM <- bcOWM <- rateOWM <- origOWM <- numeric(vl)
  for (i in 1:vl) {
    owSpeciesM[i] <- mean(owSpecies[, i], na.rm = T)
    bcOWM[i] <- mean(bcOW[, i], na.rm = T)
    rateOWM[i] <- mean(rateOW[, i], na.rm = T)
    origOWM[i] <- mean(origOW[, i], na.rm = T)
  }
  owmat <- rbind(`Bin Mid-point` = binmid, `OW subsampled diversity` =
owSpeciesM,
    `Boundary Crossers on OW` = bcOWM, `Extinction rate` = rateOWM,
    `Origination rate` = origOWM)
  for (i in 1:vl) {
    if (owmat[3, i] == 0) {
      owmat[3, i] <- NA
    }
  }
  result <- list(`OW subsampling value for 100 trials` = owSpecies,
    `OW Boundary crossers in 100 trials` = bcOW, `OW Subsampling summary` =
owmat)
  return(result)
 }

O2W<-function (data, quota, trials = 100, age_min, age_max, bin_length)
{
  bin <- seq(age_min, age_max, by = bin_length)
  vl <- length(bin) - 1
  binmid <- numeric(vl)
  for (i in 1:vl) {
    binmid[i] <- (bin[i] + bin[i + 1])/2
  }
  occ <- numeric(vl)
  occbinned <- list()
  ncoll <- numeric(vl)
  collbinned <- list()
  for (i in 1:vl) {
    occbinned[[i]] <- subset(data, bin[i] < age_ma & bin[i +
      1] > age_ma)
    occ[i] <- nrow(occbinned[[i]])
```

```
    o1 <- cbind(occbinned[[i]]$site, occbinned[[i]]$depth_mbsf)
    collbinned[[i]] <- unique(o1[, 1:2])
    collbinned[[i]] <- collbinned[[i]][order(collbinned[[i]][,
      1]), ]
    ncoll[i] <- nrow(collbinned[[i]])
    for (k in 1:nrow(collbinned[[i]])) {
      occ2[i] <- occ2[i] + nrow(subset(data, site ==
        collbinned[[i]][k, 1] & depth_mbsf == collbinned[[i]][k,
        2]))^2
    }
  }
  Sys.sleep(0.01)
  cat("\nO2W\n")
  bc3 <- ow2Species <- rateO2W <- origO2W <- array(0, dim = c(trials,
    vl))
  pba <- 0
  pb <- txtProgressBar(0, vl * trials, style = 3)
  occ2 <- numeric(vl)
  for (t in 1:trials) {
    seen <- array(0, dim = c(length(levels(data$taxon_id)),
      vl))
    for (i in 1:vl) {
      temp <- collbinned[[i]]
      spsamp <- 0
      ow2sampled <- c()
      ncollLeft <- ncoll[i]
      if (occ2[i] < quota) {
        ow2Species[t, i] <- NA
      }
      else {
        while (spsamp < quota) {
         cellNo <- floor(runif(1, min = 1, max = ncollLeft +
          1))
         selected <- subset(data, site == temp[cellNo,
          1] & depth_mbsf == temp[cellNo, 2])
         ow2sampled <- rbind(ow2sampled, selected)
         seen[selected$taxon_id, i] <- 1
         temp[cellNo, ] <- temp[ncollLeft, ]
         spsamp <- spsamp + nrow(selected)^2
         ncollLeft <- ncollLeft - 1
        }
        ow2Species[t, i] <- length(unique(ow2sampled$taxon_id))
      }
      pba <- pba + 1
      Sys.sleep(0.01)
      setTxtProgressBar(pb, pba)
    }
    bL <- bt <- Ft <- numeric(vl)
    for (k in 1:nrow(seen)) {
      if (seen[k, 1] == 1 & sum(seen[k, 2:vl]) > 0) {
        bL[1] <- bL[1] + 1
      }
      if (seen[k, vl] == 1 & sum(seen[k, 1:(vl - 1)]) >
        0) {
        Ft[vl] <- Ft[vl] + 1
      }
      for (j in 2:(vl - 1)) {
        if (sum(seen[k, 1:(j - 1)]) > 0 & sum(seen[k,
         (j + 1):vl]) > 0) {
         bt[j] <- bt[j] + 1
```

```
        }
        if (seen[k, j] == 1) {
         if (sum(seen[k, 1:(j - 1)]) == 0 & sum(seen[k,
          (j + 1):vl]) > 0) {
          bL[j] <- bL[j] + 1
         }
         if (sum(seen[k, 1:(j - 1)]) > 0 & sum(seen[k,
          (j + 1):vl]) == 0) {
          Ft[j] <- Ft[j] + 1
         }
        }
      }
    }
    bc3[t, ] <- ((bL + bt) + (bt + Ft))/2
    rateO2W[t, ] <- -log(bt/(bL + bt))
    origO2W[t, ] <- -log(bt/(Ft + bt))
  }
  ow2SpeciesM <- bc3M <- rateO2WM <- origO2WM <- numeric(vl)
  for (i in 1:vl) {
    ow2SpeciesM[i] <- mean(ow2Species[, i], na.rm = T)
    bc3M[i] <- mean(bc3[, i], na.rm = T)
    rateO2WM[i] <- mean(rateO2W[, i], na.rm = T)
    origO2WM[i] <- mean(origO2W[, i], na.rm = T)
  }
  ow2mat <- rbind(`Bin Mid-point` = binmid, `O2W subsampled diversity` =
ow2SpeciesM,
    `Boundary Crossers on O2W` = bc3M, `Extinction rate` = rateO2WM,
    `Origination rate` = origO2WM)
  for (i in 1:vl) {
    if (ow2mat[3, i] == 0) {
      ow2mat[3, i] <- NA
    }
  }
  result <- list(`OW2 subsampling value for 100 trials` = ow2Species,
    `OW2 Boundary crossers in 100 trials` = bc3, `OW2 Subsampling summary` =
ow2mat)
  return(result)
 }

CR<-function(data,quota,trials=100,age_min,age_max,bin_length)
{
      bin<-seq(age_min,age_max,by=bin_length)
      length(bin)-1->vl
      binmid<-numeric(vl)
      for(i in 1:vl){binmid[i]<-(bin[i]+bin[i+1])/2}
      occ<-numeric(vl)
      occbinned<-list()
      for (i in 1:vl){
            occbinned[[i]]<-subset(data,bin[i]<age_ma & bin[i+1]>age_ma)
            occ[i]<-nrow(occbinned[[i]])
            }
      Sys.sleep(0.01)
      cat("\nCR\n")
            rarefied<-bc4<-rateRar<-origRar<-array(dim=c(trials,vl))
            pba<-0
            pb<-txtProgressBar(0,trials,style=3)
            for(t in 1:trials){
                  seen<-array(0,dim=c(length(levels(data$taxon_id)),vl))
                  for(i in 1:vl){
                        if(occ[i]<quota){rarefied[t,i]<-NA}
```

```
                        else{
                              occbinned[[i]]
[sample(nrow(occbinned[[i]]),quota),]->selected
                              length(unique(selected$taxon_id))->rarefied[t,i]
                              seen[unique(selected$taxon_id),i]<-1
                              }
                        }
                  bL<-bt<-Ft<-numeric(vl)
                  for (k in 1:nrow(seen)){
                        if(seen[k,1]==1 & sum(seen[k,2:vl])>0){bL[1]<-
bL[1]+1}
                        if(seen[k,vl]==1 & sum(seen[k,1:(vl-1)])>0){Ft[vl]<-
Ft[vl]+1}
                        for(j in 2:(vl-1)){
                              if(sum(seen[k,1:(j-1)])>0 & sum(seen[k,(j
+1):vl])>0){bt[j]<-bt[j]+1}
                              if(seen[k,j]==1){
                                    if(sum(seen[k,1:(j-1)])==0 & sum(seen[k,(j
+1):vl])>0){bL[j]<-bL[j]+1}
                                    if(sum(seen[k,1:(j-1)])>0 & sum(seen[k,(j
+1):vl])==0){Ft[j]<-Ft[j]+1}
                                    }
                              }
                        }
                  bc4[t,]<-((bL+bt)+(bt+Ft))/2
                  rateRar[t,]<- -log(bt/(bL+bt))
                  origRar[t,]<- -log(bt/(Ft+bt))
                  pba<-pba+1
                  Sys.sleep(0.01)
                  setTxtProgressBar(pb,pba)
            }
            rarefiedM<-bc4M<-rateRarM<-origRarM<-numeric(vl)
            for(i in 1:vl){
                  mean(rarefied[,i],na.rm=T)->rarefiedM[i]
                  mean(bc4[,i],na.rm=T)->bc4M[i]
                  mean(rateRar[,i],na.rm=T)->rateRarM[i]
                  mean(origRar[,i],na.rm=T)->origRarM[i]
                  }
            rbind("Bin Mid-point"=binmid,"Rarefied
diversity"=rarefiedM,"Boundary Crossers"=bc4M,"Extinction rate"=rateRarM,
"Origination rate"=origRarM)->Rarmat
            for(i in 1:vl){if(Rarmat[3,i]==0){Rarmat[3,i]<-NA}}
            result<-list("Classic Rarefaction value for 100 trials"=rarefied,
"Boundary crossers in 100 trials"=bc4, "Rarefaction summary"=Rarmat)
            return(result)
            }

sqs<-function (data, quota, trials = 100, dominant = "include", age_min,
  age_max, bin_length)
{
  bin <- seq(age_min, age_max, by = bin_length)
  vl <- length(bin) - 1
  binmid <- numeric(vl)
  for (i in 1:vl) {
    binmid[i] <- (bin[i] + bin[i + 1])/2
  }
  occ <- numeric(vl)
  occbinned <- list()
  mostfrequent <- numeric(vl)
  ab <- list()
```

```
  freq <- list()
  u <- numeric(vl)
  single <- numeric(vl)
  for (i in 1:vl) {
    occbinned[[i]] <- subset(data, bin[i] < age_ma & bin[i +
      1] > age_ma)
    occ[i] <- nrow(occbinned[[i]])
    ab[[i]] <- summary(occbinned[[i]]$taxon_id, maxsum = 1000)
    ab[[i]] <- ab[[i]][ab[[i]] != 0]
    single[i] <- sum(ab[[i]] == 1)
    u[i] <- 1 - single[i]/occ[i]
    if (length(ab[[i]]) != 0) {
      mostfrequent[i] <- names(ab[[i]])[ab[[i]] == max(ab[[i]],
        na.rm = T)]
    }
    freq[[i]] <- ab[[i]]/occ[i]
  }
  q <- quota
  Sys - sleep(0.01)
  cat("\nSQS\n")
  SQSspecies <- array(0, dim = c(trials, vl))
  bcSQS <- array(0, dim = c(trials, vl))
  rateSQS <- array(0, dim = c(trials, vl))
  origSQS <- array(0, dim = c(trials, vl))
  pba <- 0
  pb <- txtProgressBar(0, vl * trials, style = 3)
  for (t in 1:trials) {
    seen <- array(0, dim = c(length(levels(data$taxon_id)),
      vl))
    for (i in 1:vl) {
      if (nrow(occbinned[[i]]) != 0) {
        pool <- occbinned[[i]]
        left <- nrow(pool)
        sumfreq <- 0

                if (q <= u[i]) {
                  while (sumfreq < q) {
                    x <- floor(runif(1, min = 1, max = left +
                      1))
                    if (seen[as.integer(pool$taxon_id[x]), i] ==
                      0) {
                      if (pool$taxon_id[x] != mostfrequent[i] |
                        dominant == "include") {
                        sumfreq <- sumfreq + as.numeric(freq[[i]]
[names(freq[[i]]) ==
                          pool$taxon_id[x]])
                      }
                      seen[as.integer(pool$taxon_id[x]), i] <- 1
                      SQSspecies[t, i] <- SQSspecies[t, i] +
                        1
                    }
                    pool[x, ] <- pool[left, ]
                    left <- left - 1
                  }
                }
            }
            pba <- pba + 1
            Sys.sleep(0.01)
            setTxtProgressBar(pb, pba)
        }
```

```
        bL <- bt <- Ft <- numeric(vl)
        for (k in 1:nrow(seen)) {
            if (seen[k, 1] == 1 & sum(seen[k, 2:vl]) > 0) {
                bL[1] <- bL[1] + 1
            }
            if (seen[k, vl] == 1 & sum(seen[k, 1:(vl - 1)]) >
                0) {
                Ft[vl] <- Ft[vl] + 1
            }
            for (j in 2:(vl - 1)) {
                if (sum(seen[k, 1:(j - 1)]) > 0 & sum(seen[k,
                  (j + 1):vl]) > 0) {
                  bt[j] <- bt[j] + 1
                }
                if (seen[k, j] == 1) {
                  if (sum(seen[k, 1:(j - 1)]) == 0 & sum(seen[k,
                    (j + 1):vl]) > 0) {
                    bL[j] <- bL[j] + 1
                  }
                  if (sum(seen[k, 1:(j - 1)]) > 0 & sum(seen[k,
                    (j + 1):vl]) == 0) {
                    Ft[j] <- Ft[j] + 1
                  }
                }
            }
        }
        bcSQS[t, ] <- ((bL + bt) + (bt + Ft))/2
        rateSQS[t, ] <- -log(bt/(bL + bt))
        origSQS[t, ] <- -log(bt/(Ft + bt))
    }
    bcSQSM <- SQSspeciesM <- rateSQSM <- origSQSM <- numeric(vl)
    for (i in 1:vl) {
        bcSQSM[i] <- mean(bcSQS[, i], na.rm = T)
        rateSQSM[i] <- mean(rateSQS[, i], na.rm = T)
        origSQSM[i] <- mean(origSQS[, i], na.rm = T)
        SQSspeciesM[i] <- mean(SQSspecies[, i], na.rm = T)
    }
    sqsmat <- rbind(`Bin Mid-point` = binmid, `SQS subsampled diversity` =
SQSspeciesM,
        `Boundary Crossers on SQS` = bcSQSM, `Extinction rate` = rateSQSM,
        `Origination rate` = origSQSM)
    for (i in 1:vl) {
        if (sqsmat[3, i] == 0) {
            sqsmat[3, i] <- NA
        }
    }
    result <- list(`SQS subsampling value for 100 trials` = SQSspecies,
        `SQS Boundary crossers in 100 trials` = bcSQS, `SQS Subsampling
summary` = sqsmat)
    return(result)
  }
```

CONOPcompanion-package

R Documentation

An R companion to quantitative biostratigraphy using CONOP9 (Sadler 2007)

Description

Provides functions to prepare the main input files for CONOP9, read the main output files and start the analysis.

Details

Package:	CONOPcompanion
Type:	Package
Version:	1.0
Date:	2012-04-12
Depends:	grDevices
License:	None.

Author(s)

Johan Renaudie

Maintainer: Johan Renaudie <Johan.Renaudie@mfn-berlin.de>

References

Sadler, P. M. 2007. CONOP9 version 7.43

compact.ordinal

R Documentation

Compact the ordinal composite sequence.

Description

Take the ordinal composite sequence of events and compact it so that events that are not differentiable temporally are projected to the same level.

Usage

```
compact.ordinal(plcdfile, composfile)
```

Arguments

`plcdfile`
Array containing the CONOP9 output file corresponding to the field PLCDFILE in the conop9.cfg file

`composfile`
Array containing the CONOP9 output file corresponding to the field COMPOSFILE in the conop9.cfg file

Value

The output is in any way similar to the ordinal composite sequence of event.

Author(s)

Johan Renaudie.

Examples

```
## The function is currently defined as
function (plcdfile, composfile)
{
  lev <- unique(plcdfile[, 3:ncol(plcdfile)])
  id <- function(X) {
    a <- vector(length = nrow(plcdfile))
    for (i in 1:nrow(plcdfile)) {
      a[i] <- identical(plcdfile[i, 3:ncol(plcdfile)],
        lev[X, ])
    }
    b <- plcdfile[a, 1:2]
    return(b)
  }
  ord <- lapply(1:nrow(lev), FUN = id)
  ord <- rev(ord)
  ord_depth <- seq(1000, 2000, by = 1000/(length(ord) - 1))
  composfile_ord <- composfile
  n <- c()
  m <- 1
  for (i in 1:length(ord)) {
    n[i] <- length(ord[[i]])/2
```

```
   composfile_ord[m:(m + n[i] - 1), 4] <- ord_depth[i]
   composfile_ord[m:(m + n[i] - 1), 5] <- i
   m <- m + n[i]
 }
 return(composfile_ord)
}
```

LOC

R Documentation

Line of correlation.

Description

Four functions to derive an age model from the composite sequence.

Usage

```
LOC.tiepoints(composfile, obsdfile, sectfile, saveLOC = FALSE)
printLOC(sectfile, obsdfile, composfile)
composite.age(agemodels,tie.points,composfile,age.span,pch,bg)
printLOC.age(sectfile, obsdfile, composfile, age.old = 14,
age.young = 0)
```

Arguments

`composfile`
Conop output referred to as `composfile` on the CONFIG file.

`obsdfile`
Conop output referred to as `obsdfile` on the CONFIG file (i.e. depth of observed events on each site).

`sectfile`
Conop input file referred to as `sectfile` on the conop9.cfg file.

`agemodels`
A list of known age models with one element for each site (in the order defined in `sectfile`). Each element is a Two-column matrix: first column is the age value (in Ma) and the second column is the depth (in mbsf). The user can provide existing age models for any number of sites that he want (max is the number of site included in `sectfile`). Sites that are included in `sectfile` but for which no age models is given needs to be `NA`. E. G. two sites are present in `sectfile`, the first site is not provided with an age models but the second site have two tie points (10mbsf -> 1Ma and 50mbsf ->3Ma), `agemodels` should therefore be as follow: [[1]]NA [[2]][,1]10 50 [,2]1 3

`tie.points`
Output from function `LOC.tiepoints`

`age.span`
Vector of two age values (oldest, youngest).

`pch`
See `par`.

`bg`
See `par`.

`saveLOC`
If `TRUE`, plots and LOC are saved in the working directory.

`age.old`
Numeric. Oldest age to be displayed on the plot.

`age.young`
Numeric. Youngest age to be displayed on the plot.

Details

- `LOC.tiepoints`: Prompt the user to interactively draw a line of correlation on depth vs composite depth diagram and return the set of tie points thus selected.
- `printLOC`: Plot and print depth vs composite depth diagram.
- `composite.age`: From a given set of tie points, translate COMPOSFILE from composite depth to numerical age values.
- `printLOC.age`: Plot and print age vs depth diagram.

Value

The output of `LOC.tiepoints` is a list which elements corresponds to a site (the index is the same as in `sectfile`). In each element, an age-depth matrix is stored. The output of codecomposite.age is a matrix similar to COMPOSFILE with numerical age value instead of composite depth.

Author(s)

Johan Renaudie.

Examples

```
## The function is currently defined as
LOC.tiepoints <- function (composfile, obsdfile, sectfile, saveLOC = FALSE)
{
  obsdfile[obsdfile == 0] <- NA
  Nsect <- nrow(sectfile)
  tie.points <- list()
  for (SITE in 1:Nsect) {
    layout(matrix(c(0, 1, 2, 3), nrow = 2, byrow = T), width = c(3,
      20), height = c(3, 20))
    par(mar = c(0, 0, 5, 5))
    plot(0, 0, type = "n", xlim = c(min(composfile[, 4]),
      max(composfile[, 4])), ylim = c(0, 10), xaxt = "n",
      yaxt = "n", yaxs = "i", xaxs = "i", xlab = "", ylab = "",
      bty = "n")
    for (i in 1:length(unique(composfile[, 4]))) {
      lines(c(unique(composfile[, 4])[i], unique(composfile[,
        4])[i]), c(0, 10), lty = 1, col = "black")
    }
    axis(3, at = seq(min(composfile[, 4]), max(composfile[,
      4]), by = 100))
    box()
    par(mar = c(5, 5, 0, 0))
    plot(0, 0, type = "n", ylim = c(min(obsdfile[, SITE +
      2], na.rm = T), max(obsdfile[, SITE + 2], na.rm = T)),
```

```
    xlim = c(0, 10), xaxt = "n", yaxt = "n", yaxs = "i",
    xaxs = "i", xlab = "", ylab = "", bty = "n")
  for (i in 1:length(unique(obsdfile[, SITE + 2]))) {
    lines(c(0, 10), c(unique(obsdfile[, SITE + 2])[i],
      unique(obsdfile[, SITE + 2])[i]), lty = 1, col = "black")
  }
  axis(2, at = seq(min(obsdfile[, SITE + 2], na.rm = T),
    max(obsdfile[, SITE + 2], na.rm = T), by = 10), las = 2)
  box()
  b <- cbind(rev(composfile[, 4]), obsdfile[, SITE + 2],
    obsdfile[, 2])
  b[b[, 2] == 0] <- NA
  b <- b[!is.na(b[, 2]), ]
  d <- unique(b[, 1:2])
  f <- vector(length = nrow(d))
  for (i in 1:nrow(d)) {
    for (j in 1:nrow(b)) {
      if (b[j, 1] == d[i, 1] & b[j, 2] == d[i, 2]) {
       f[i] <- f[i] + 1
      }
    }
  }
  f[f > 10] <- 10
  g <- vector(length = nrow(b))
  for (i in 1:nrow(d)) {
    for (j in 1:nrow(b)) {
      if (b[j, 1] == d[i, 1] & b[j, 2] == d[i, 2]) {
       g[j] <- f[i]
      }
    }
  }
  lofo.pch <- c()
  for (i in 1:nrow(b)) {
    if (b[i, 3] == 1) {
      lofo.pch[i] <- 24
    }
    if (b[i, 3] == 2) {
      lofo.pch[i] <- 25
    }
  }
  par(mar = c(5, 0, 0, 5))
  palette(rev(heat.colors(10)))
  plot(b[, 1], b[, 2], pch = lofo.pch, xaxs = "i", yaxs = "i",
    yaxt = "n", xlab = "", ylab = "", xaxt = "n", bty = "o",
    ylim = c(min(obsdfile[, SITE + 2], na.rm = T), max(obsdfile[,
      SITE + 2], na.rm = T)), xlim = c(min(composfile[,
      4]), max(composfile[, 4])), bg = g, cex = 3)
  title(sub = paste(sectfile[SITE, 4], " vs Composite Section",
    sep = ""), line = 2, cex.sub = 2)
  box()
  tie.points[[SITE]] <- locator(type = "o", pch = 3, lty = 2)
  if (saveLOC == TRUE) {
    dev.copy2pdf(width = 10, height = 10, file = paste(sectfile[SITE,
      2], "_LOC.pdf", sep = ""))
  }
  dev.off()
 }
 return(tie.points)
}
```

```
printLOC <- function (sectfile, obsdfile, composfile)
{
  require(grDevices)
  redscale <- rev(heat.colors(10))
  bluescale <- c("aliceblue", "cadetblue1", "lightskyblue",
    "skyblue1", "steelblue2", "deepskyblue", "cornflowerblue",
    "blue", "darkblue", "black")
  for (SITE in 1:nrow(sectfile)) {
    b1 <- cbind(rev(composfile[, 4]), obsdfile[, SITE + 2],
      obsdfile[, 2])
    b <- array(dim = dim(b1))
    for (i in 1:nrow(b1)) {
      for (j in 1:ncol(b1)) {
        b[i, j] <- as.numeric(b1[i, j])
      }
    }
    b[b[, 2] == 0] <- NA
    b <- b[!is.na(b[, 2]), ]
    d <- unique(b[, 1:2])
    f <- vector(length = nrow(d))
    for (i in 1:nrow(d)) {
      for (j in 1:nrow(b)) {
        if (b[j, 1] == d[i, 1] & b[j, 2] == d[i, 2]) {
         f[i] <- f[i] + 1
        }
      }
    }
    f[f > 10] <- 10
    g <- vector(length = nrow(b))
    for (i in 1:nrow(d)) {
      for (j in 1:nrow(b)) {
        if (b[j, 1] == d[i, 1] & b[j, 2] == d[i, 2]) {
         g[j] <- f[i]
        }
      }
    }
    pdf(file = paste(sectfile[SITE, 4], "_LOC.pdf", sep = ""),
      width = 10, height = 10)
    layout(matrix(c(0, 1, 0, 2, 3, 4), nrow = 2, byrow = T),
      width = c(3, 20, 4), height = c(3, 20))
    par(mar = c(0, 0, 5, 0))
    plot(0, 0, type = "n", xlim = c(1000, max(b[, 1])), ylim = c(0,
      10), xaxt = "n", yaxt = "n", yaxs = "i", xaxs = "i",
      xlab = "", ylab = "", bty = "n")
    for (i in 1:length(unique(composfile[, 4]))) {
      lines(c(unique(composfile[, 4])[i], unique(composfile[,
        4])[i]), c(0, 10), lty = 1, col = "black")
    }
    axis(3, at = seq(1000, max(b[, 1]), by = 100), cex.axis = 2)
    box()
    par(mar = c(5, 5, 0, 0))
    plot(0, 0, type = "n", ylim = c(min(b[, 2]), max(b[,
      2])), xlim = c(0, 10), xaxt = "n", yaxt = "n", yaxs = "i",
      xaxs = "i", xlab = "", ylab = "", bty = "n")
    for (i in 1:length(unique(obsdfile[, SITE + 2]))) {
      lines(c(0, 10), c(unique(obsdfile[, SITE + 2])[i],
        unique(obsdfile[, SITE + 2])[i]), lty = 1, col = "black")
    }
    axis(2, at = seq(max(obsdfile[, SITE + 2]), min(obsdfile[,
      SITE + 2]), by = -10), las = 2, cex.axis = 2)
```

```
    box()
    par(mar = c(5, 0, 0, 0))
    plot(b[, 1], b[, 2], xaxs = "i", yaxs = "i", yaxt = "n",
      xlab = "", ylab = "", xaxt = "n", bty = "o", ylim = c(min(b[,
        2]), max(b[, 2])), xlim = c(1000, max(b[, 1])),
      type = "n")
    for (i in 1:nrow(b)) {
      if (b[i, 3] %in% c(1, -1)) {
        points(b[i, 1], b[i, 2], pch = 24, bg = redscale[g[i]],
         cex = 3)
      }
      if (b[i, 3] %in% c(2, -2)) {
        points(b[i, 1], b[i, 2], pch = 25, bg = bluescale[g[i]],
         cex = 3)
      }
    }
    title(sub = paste(sectfile[SITE, 4], " vs Composite Section",
      sep = ""), line = 2, cex.sub = 2)
    box()
    par(mar = c(5, 1, 0, 5))
    plot(0, 0, type = "n", xlim = c(0, 2), ylim = c(0, 10),
      xaxs = "i", yaxs = "i", ylab = "", xlab = "", xaxt = "n",
      yaxt = "n")
    for (i in 1:10) {
      rect(0, (i - 1), 1, i, border = "black", col = redscale[i])
    }
    for (i in 1:10) {
      rect(1, (i - 1), 2, i, border = "black", col = bluescale[i])
    }
    mtext("FO", side = 3, at = c(0.5, 11))
    mtext("LO", side = 3, at = c(1.5, 11))
    axis(4, las = 2, at = seq(0.5, 9.5, by = 1), labels = c(1,
      2, 3, 4, 5, 6, 7, 8, 9, "10+"), tick = FALSE, cex.axis = 2)
    dev.off()
  }
 }

printLOC.age <-function (sectfile, obsdfile, composfile, age.old = 14,
age.young = 0)
{
  require(grDevices)
  redscale <- rev(heat.colors(10))
  bluescale <- c("aliceblue", "cadetblue1", "lightskyblue",
    "skyblue1", "steelblue2", "deepskyblue", "cornflowerblue",
    "blue", "darkblue", "black")
  for (SITE in 1:nrow(sectfile)) {
    b1 <- cbind(rev(composfile[, 4]), obsdfile[, SITE + 2],
      obsdfile[, 2])
    b <- array(dim = dim(b1))
    for (i in 1:nrow(b1)) {
      for (j in 1:ncol(b1)) {
        b[i, j] <- as.numeric(b1[i, j])
      }
    }
    b[b[, 2] == 0] <- NA
    b <- b[!is.na(b[, 2]), ]
    d <- unique(b[, 1:2])
    f <- vector(length = nrow(d))
    for (i in 1:nrow(d)) {
      for (j in 1:nrow(b)) {
```

```
      if (b[j, 1] == d[i, 1] & b[j, 2] == d[i, 2]) {
       f[i] <- f[i] + 1
      }
    }
  }
  f[f > 10] <- 10
  g <- vector(length = nrow(b))
  for (i in 1:nrow(d)) {
    for (j in 1:nrow(b)) {
      if (b[j, 1] == d[i, 1] & b[j, 2] == d[i, 2]) {
       g[j] <- f[i]
      }
    }
  }
  pdf(file = paste(sectfile[SITE, 4], "_LOC.pdf", sep = ""),
    width = 10, height = 10)
  layout(matrix(c(0, 1, 0, 2, 3, 4), nrow = 2, byrow = T),
    width = c(3, 20, 4), height = c(3, 20))
  par(mar = c(0, 0, 5, 0))
  plot(0, 0, type = "n", xlim = c(age.old, age.young),
    ylim = c(0, 10), xaxt = "n", yaxt = "n", yaxs = "i",
    xaxs = "i", xlab = "", ylab = "", bty = "n")
  for (i in 1:length(unique(composfile[, 4]))) {
    lines(c(unique(composfile[, 4])[i], unique(composfile[,
      4])[i]), c(0, 10), lty = 1, col = "black")
  }
  axis(3, at = seq(age.old, age.young, by = -2), cex.axis = 2)
  box()
  par(mar = c(5, 5, 0, 0))
  plot(0, 0, type = "n", ylim = c(min(b[, 2]), max(b[,
    2])), xlim = c(0, 10), xaxt = "n", yaxt = "n", yaxs = "i",
    xaxs = "i", xlab = "", ylab = "", bty = "n")
  for (i in 1:length(unique(obsdfile[, SITE + 2]))) {
    lines(c(0, 10), c(unique(obsdfile[, SITE + 2])[i],
      unique(obsdfile[, SITE + 2])[i]), lty = 1, col = "black")
  }
  axis(2, at = seq(max(obsdfile[, SITE + 2]), min(obsdfile[,
    SITE + 2]), by = -10), las = 2, cex.axis = 2)
  box()
  par(mar = c(5, 0, 0, 0))
  plot(b[, 1], b[, 2], xaxs = "i", yaxs = "i", yaxt = "n",
    xlab = "", ylab = "", xaxt = "n", bty = "o", ylim = c(min(b[,
      2]), max(b[, 2])), xlim = c(age.old, age.young),
    type = "n")
  for (i in 1:nrow(b)) {
    if (b[i, 3] %in% c(1, -1)) {
      points(b[i, 1], b[i, 2], pch = 24, bg = redscale[g[i]],
       cex = 3)
    }
    if (b[i, 3] %in% c(2, -2)) {
      points(b[i, 1], b[i, 2], pch = 25, bg = bluescale[g[i]],
       cex = 3)
    }
  }
  title(sub = paste(sectfile[SITE, 4], " vs Composite Section",
    sep = ""), line = 2, cex.sub = 2)
  box()
  par(mar = c(5, 1, 0, 5))
  plot(0, 0, type = "n", xlim = c(0, 2), ylim = c(0, 10),
    xaxs = "i", yaxs = "i", ylab = "", xlab = "", xaxt = "n",
```

```
      yaxt = "n")
    for (i in 1:10) {
      rect(0, (i - 1), 1, i, border = "black", col = redscale[i])
    }
    for (i in 1:10) {
      rect(1, (i - 1), 2, i, border = "black", col = bluescale[i])
    }
    mtext("FO", side = 3, at = c(0.5, 11))
    mtext("LO", side = 3, at = c(1.5, 11))
    axis(4, las = 2, at = seq(0.5, 9.5, by = 1), labels = c(1,
      2, 3, 4, 5, 6, 7, 8, 9, "10+"), tick = FALSE, cex.axis = 2)
    dev.off()
  }
 }

composite.age<-function(agemodels,tie.points,composfile,age.span,pch,bg){
            if(!exists("age.span",inherits=FALSE)){
                  age.span<-c()
                  for(i in 1:length(agemodels)){if(length(agemodels[[i]])!=0)
{range(c(age.span,agemodels[[i]][,2]),na.rm=T)->age.span}}
                  }
            max(age.span)->age.old
            min(age.span)->age.young
            if(!exists("pch",inherits=FALSE)){pch<-rep(21,length(agemodels))}
            if(!exists("bg",inherits=FALSE)){bg<-rainbow(length(agemodels))}

            layout(matrix(c(1,2),nrow=2,byrow=T),width=20,height=c(3,20))
            par(mar=c(0,3,3,3))
            plot(0,0,type="n",xlim=c(min(composfile[,4]),max(composfile[,
4])),ylim=c(0,10),xaxt="n",yaxt="n",yaxs="i",xaxs="i",xlab="",ylab="",bty="n"
)
            for(i in 1:length(unique(composfile[,4])))
{lines(c(unique(composfile[,4])[i],unique(composfile[,4])
[i]),c(0,10),lty=1,col="black")}
            axis(3,at=seq(min(composfile[,4]),max(composfile[,4]),by=100))
            box()
            par(mar=c(3,3,0,3))


plot(0,0,xaxs="i",yaxs="i",yaxt="n",xlab="",ylab="",xaxt="n",bty="o",ylim=c(a
ge.old,age.young),xlim=c(min(composfile[,4]),max(composfile[,4])),type="n")

            for(SITE in 1:length(agemodels)){
                  if(length(agemodels[[SITE]])!=0){
                        if(agemodels[[SITE]][1,2]>=0){-1 * agemodels[[SITE]]
[,2]->agemodels[[SITE]][,2]}
                        cbind(approx(tie.points[[SITE]]$y,tie.points[[SITE]]
$x,xout=agemodels[[SITE]][,2],rule=1)$y,agemodels[[SITE]][,1])->am
                        points(am,pch=pch[SITE],bg=bg[SITE],cex=3)
                        }
                  }

            title(sub="Age models vs Composite Section",line=2,cex.sub=2)
            axis(2,at=seq(age.old,age.young,by=-1),las=2)
            box()

            locator(type="o",pch=3,lty=2)->age.model
            dev.copy2pdf(file="Age model.pdf",width=10,height=10)
            dev.off()
```

```
            unique(composfile[,4])->depth
            approx(age.model$x,age.model$y,depth,rule=2)->c.age
            cbind(c.age$x,c.age$y)->c.age
            compage<-composfile
            for(i in 1:nrow(compage)){compage[i,4]<-c.age[c.age[,
1]==composfile[i,4],2]}

            return(compage)
            }
```

lofo

R Documentation

Bioevents

Description

Find the FO, FCO, Acme, LCO and LO for each species of the dataset on the studied site.

Usage

```
lofo(site, remove.na = TRUE)
acme(site, quota = 5)
```

Arguments

`site`
Abundance matrix for a given site (species as rows, samples ordered from the youngest to the oldest as columns and first row is the sample depth)

`remove.na`
If the species is contained in the last sample or in the first sample, `remove.na=TRUE` will output the depth of the last or the first sample as its LO or FO.

`quota`
LCO, FCO and acme will be computed only for species that reach the quota (in percentage, default is 5%) at least once during their range.

Value

The output is a matrix whre each row is a species For function `acme`, the columns are LCO, Acme and FCO; for function `lofo`, the columns are LO and FO. Values given are the depth (first row of the input matrix) for each event.

Author(s)

Johan Renaudie.

Examples

```
## The function is currently defined as
lofo <- function (site, remove.na = TRUE)
{
  site <- site[rowSums(site) > 0, ]
  lofo <- array(dim = c(nrow(site), 2))
  rownames(lofo) <- rownames(site)
  colnames(lofo) <- c("LO", "FO")
  for (i in 2:ncol(site) - 1) {
    for (j in 2:nrow(site)) {
      if (sum(site[j, 1:i]) == 0 & site[j, i + 1] > 0) {
        lofo[j, 1] <- site[1, i + 1]
      }
      if (sum(site[j, (i + 1):ncol(site)]) == 0 & site[j,
        i] > 0) {
```

```
        lofo[j, 2] <- site[1, i]
      }
    }
  }
  lofo <- lofo[-1, ]
  if (remove.na == TRUE) {
    lofo[is.na(lofo[, 1]), 1] <- site[1, 1]
    lofo[is.na(lofo[, 2]), 2] <- site[1, ncol(site)]
  }
  a <- c()
  for (i in 1:nrow(lofo)) {
    if (is.na(lofo[i, 1]) & is.na(lofo[i, 2])) {
      a <- c(a, i)
    }
  }
  if (length(a) != 0) {
    lofo <- lofo[!a, ]
  }
  return(lofo)
 }

acme <- function (site, quota = 5)
{
  site <- site[rowSums(site) > 0, ]
  for (i in 1:ncol(site)) {
    site[2:nrow(site), i] <- site[2:nrow(site), i] * 100/
colSums(site[2:nrow(site),
      ])[i]
  }
  acme <- matrix(nrow = nrow(site), ncol = 3)
  rownames(acme) <- rownames(site)
  colnames(acme) <- c("LCO", "Acme", "FCO")
  for (i in 2:nrow(site)) {
    if (max(site[i, ]) >= quota) {
      temp <- site[1, site[i, ] >= quota]
      acme[i, 3] <- temp[[length(temp)]]
      acme[i, 1] <- temp[[1]]
      acme[i, 2] <- site[1, site[i, ] == max(site[i, ])]
    }
  }
  acme <- acme[-1, ]
  acme <- acme[!is.na(acme[, 1]), ]
  return(acme)
 }
```

pacman

R Documentation

Pacman profiling and trimming

Description

Flag and trim anomalous occurrences given a certain percentage on an abundance matrix

Usage

```
pacman(neptune, perc_top = 5, perc_bottom = 3)
```

Arguments

`ab_mat`
An abundance matrix with samples as rows and taxa as columns.

`perc_top`
Percentage to trim at the top of the ranges, default to 5%

`perc_bottom`
Percentage to trim at the bottom of the ranges, default to 3%

Value

The returned value is a list:

`Trimming`
Trimmed Matrix

`Profiling`
Vector: number of outliers in each sample.

Author(s)

Lazarus et al. 2012 for the algorithm, Johan Renaudie for the code.

References

Lazarus et al. 2012. Pacman profiling: a simple procedure to identify stratigraphic outliers in high-density deep-sea microfossil data. Paleobiology, 38(1): 858-875.

Examples

```
## The function is currently defined as
function(ab_mat,perc_top=5,perc_bottom=3){
      outlier<-rep(0,nrow(ab_mat))
      lim_top<-rep(0,ncol(ab_mat))
      lim_bottom<-rep(nrow(ab_mat),ncol(ab_mat))
      for(j in 1:ncol(ab_mat)){
            ab_mat[,j]->sp_ab
            as.vector(sp_ab)->sp_ab
```

```
            nb_top<-sum(sp_ab)*perc_top/100
            nb_bottom<-sum(sp_ab)*perc_bottom/100
            for(i in 1:length(sp_ab)){
                  if(sum(sp_ab[1:i])<=nb_top){i->lim_top[j]}
                  if(sum(sp_ab[i:length(sp_ab)])>=nb_bottom){i-
>lim_bottom[j]}
                  }
            if(lim_top[j]%in%(1:2)){lim_top[j]<-0}
            if(lim_bottom[j]%in%((length(sp_ab)-1):length(sp_ab)))
{lim_bottom[j]<-length(sp_ab)}
            if(lim_top[j]>0){
                  if(lim_bottom[j]<length(sp_ab)){c(1:lim_top[j],
(lim_bottom[j]+1):length(sp_ab))->out}
                  if(lim_bottom[j]==length(sp_ab)){c(1:lim_top[j])->out}}
            if(lim_top[j]==0){
                  if(lim_bottom[j]<length(sp_ab)){c((lim_bottom[j]
+1):length(sp_ab))->out}
                  if(lim_bottom[j]==length(sp_ab)){c()->out}}
            outlier[out]<-outlier[out]+sp_ab[out]
            sp_ab[out]<-0
            ab_mat[,j]<-sp_ab
            }
      names(outlier)<-row.names(ab_mat)
      list(Trimming=ab_mat,Profiling=outlier)->paclist
      return(paclist)
      }
```

prep.conop

R Documentation

Prepares CONOP9 input files.

Description

Functions to prepare CONOP input files referred to as `eventfile` and `loadfile`. Functions `prep.magn`, `prep.weight`, `prep.acme` allow the user to modify `eventfile` and `loadfile` to include respectively magnetostratigraphic data, weights (to deal with outliers) and abundance-based bioevents.

Usage

```
write.eventfile(taxa_list)
prep.level(sectfile, magn, samples)
prep.conop(lofo, levelfile, eventfile, relaxed = FALSE, paired =
TRUE)
prep.magn(magn, eventfile, sectfile, scale, levelfile)
prep.weight(loadfile, eventfile, sectfile, method =
"badspecies", bad, weight.bad = "0.50", inconsistent,
weight.inconsistent = "0.50", paclist, abmat, mbsf,
pacman.sample.ratio = 0.1, weight.pacman = "0.50")
prep.acme(acme, Nsect, levelfile, eventfile)
```

Arguments

`taxa_list`
Vector of taxa names to be used in the analysis (for non-bioevents, it will need to be modified later manually or with other functions such as `prep.magn`)

`lofo`
List where each element correspond to the output of function `lofo` for one of the sites (in the order given by sectfile.

`acme`
Output of function `acme`.

`levelfile`
Output of function `prep.level`.

`eventfile`
Conop input referred to as `eventfile` on the conop9.cfg file (or output of function `write.eventfile`).

`loadfile`
Output of function `prep.conop`.

`sectfile`
Conop input file referred to as `sectfile` on the conop9.cfg file.

`relaxed`

If FALSE, FO will be able to more down a section but not up and LO inversely. If TRUE, they will both be able to more up or down a section.

paired
If TRUE, FO and LO are paired events.

magn
Matrix of magnetostratigraphic data (can be NULL for prep.level). One row for each magnetostratigraphic events. First column should be the chron name as per convention (e.g. "C1n.1n"), second column is the usual chron name (e.g. "Brunhes"), third is T for Top and B for bottom, the following columns correspond to each site (in the order of sectfile).

scale
Correspondance table (e. g. Cande & Kent 1992; Berggren et al. 1995, 2004) for the age of the magnetostratigraphic datum. (NB: should be provided with the package as .Rdata files).

samples
Vector of samples depth (in mbsf): the name of each element needs to be of the form "Site.Sample" with the "Site" part included present in the complete name of the site as stated in the fourth column of sectfile.

method
prep.weight should be used one method at a time. The methods are as follow: badspecies, badevent, inconsistent and pacman. For inconsistent and badspecies, the function weights down species that are thought to be diachronic (bad and weight.bad needed) or with inconsistent ranges(inconsistent and weight.inconsistant needed). For badevent, the function weights down an a priori diachronic event (bad and weight.bad needed). For pacman (paclist,), the function weights down a sample according to a pacman profiling (Lazarus et al. 2012).

bad
For badspecies method, a vector of species name to weight down. For badevent method, a two-column matrix: first column is the name of the species for which the FO will be weight down, second column is the name of the species for which the LO is desired to be weighted down.

weight.bad
Weight (from 0 to 1) for badspecies and badevent method.

inconsistent
For inconstistent, a vector of species names to be weighted down.

weight.inconsistent
Weight (from 0 to 1) for inconsitent method.

paclist
Output of function pacman.

abmat
For pacman method, same matrix as used to create paclist

mbsf
Vector of sample depth (same order as the samples in abmat).

`pacman.sample.ratio`
Ratio of anomalous occurrences per sample above which the function is desired to weight down the sample (numeric value from 0 to 1).

`weight.pacman`
Weight (from 0 to 1) for `pacman` method.

`Nsect`
Index of the site used.

Value

The output of `write.eventfile` and `prep.conop` are respectively the CONOP input file `eventfile` and `loadfile`.

`prep.magn` modifies both those above-mentionned outputs.

`prep.acme` creates a piece of matrix that need to be appended to `loadfile` (which consequently needs to be reordered).

`prep.weight` modifies `loadfile`.

`prep.level` creates a conversion table which gives the rank of one sample in one site (needed to create `loadfile`).

Author(s)

Johan Renaudie.

References

Lazarus et al. 2012. Pacman profiling: a simple procedure to identify stratigraphic outliers in high-density deep-sea microfossil data. Paleobiology, 38(1): 858-875.

Sadler, 2007. CONOP version 7.43

Examples

```
## The function is currently defined as
prep.conop<-function (lofo, levelfile, eventfile, relaxed = FALSE, paired =
TRUE)
{
  loadfile <- c()
  for (k in 1:length(lofo)) {
    j <- 1
    siteevent <- array(dim = c(length(lofo[[k]][!is.na(lofo[[k]])]),
      8))
    siteevent[, 3] <- k
    for (i in 1:nrow(lofo[[k]])) {
      if (paired == TRUE) {
        siteevent[j + 1, 1] <- siteevent[j, 1] <- eventfile[eventfile[,
         3] == rownames(lofo[[k]])[i], 1]
        siteevent[j, 2] <- 1
        siteevent[j + 1, 2] <- 2
```

```
        siteevent[j, 4] <- lofo[[k]][i, 2]
        siteevent[j + 1, 4] <- lofo[[k]][i, 1]
        if (relaxed == FALSE) {
         siteevent[j, 6] <- 1
         siteevent[j + 1, 6] <- 2
        }
        if (relaxed == TRUE) {
         siteevent[j, 6] <- 3
         siteevent[j + 1, 6] <- 3
        }
        siteevent[j:j + 1, 7:8] <- "1.00"
        j <- j + 2
      }
      if (paired == FALSE) {
        siteevent[j, 1] <- eventfile[eventfile[, 3] ==
         rownames(lofo[[k]])[i], 1]
        if (is.na(lofo[[k]][i, 1])) {
         siteevent[j, 2] <- -1
         siteevent[j, 4] <- lofo[[k]][i, 2]
         if (relaxed == FALSE) {
          siteevent[j, 6] <- 1
         }
         if (relaxed == TRUE) {
          siteevent[j, 6] <- 3
         }
         siteevent[j, 7:8] <- "1.00"
         j <- j + 1
        }
        if (is.na(lofo[[k]][i, 2])) {
         siteevent[j, 2] <- -2
         siteevent[j, 4] <- lofo[[k]][i, 1]
         if (relaxed == FALSE) {
          siteevent[j, 6] <- 2
         }
         if (relaxed == TRUE) {
          siteevent[j, 6] <- 3
         }
         siteevent[j, 7:8] <- "1.00"
         j <- j + 1
        }
      }
    }
    for (l in 1:nrow(siteevent)) {
      siteevent[l, 5] <- levelfile[levelfile[, 1] == k &
        levelfile[, 2] == siteevent[l, 4], 3]
      siteevent[l, 4] <- paste("-", siteevent[l, 4], sep = "")
    }
    loadfile <- rbind(loadfile, siteevent)
  }
  loadfile <- loadfile[order(as.numeric(loadfile[, 1]), as.numeric(loadfile[,
    2]), as.numeric(loadfile[, 3])), ]
  write.table(loadfile, "load.dat", sep = " ", row.names = FALSE,
    col.names = FALSE, quote = FALSE)
  return(loadfile)
 }

prep.weigth <- function (loadfile, eventfile, sectfile, method =
"badspecies",
  bad, weight.bad = "0.50", inconsistent, weight.inconsistent = "0.50",
  paclist, abmat, mbsf, pacman.sample.ratio = 0.1, weight.pacman = "0.50")
```

```
{
  if (method == "badspecies") {
    for (i in 1:length(bad)) {
      bad[i] <- gsub("^\ +|| +$", "", bad[i])
      code <- eventfile[eventfile[, 3] == bad[i], 1]
      loadfile[loadfile[, 1] == code, 8] <- format(as.numeric(weight.bad) *
as.numeric(loadfile[loadfile[, 1] == code, 8]), digits = 2, nsmall = 2)
      loadfile[loadfile[, 1] == code, 7] <- format(as.numeric(weight.bad) *
as.numeric(loadfile[loadfile[, 1] == code, 7]), digits = 2, nsmall = 2)
    }
  }
  if (method == "badevent") {
    for (i in 1:nrow(bad)) {
      bad[i, 1] <- gsub("^\ +|| +$", "", bad[i, 1])
      bad[i, 2] <- gsub("^\ +|| +$", "", bad[i, 2])
      codeFO <- eventfile[eventfile[, 3] == bad[i, 1],
        1]
      codeLO <- eventfile[eventfile[, 3] == bad[i, 2],
        1]
      loadfile[loadfile[, 1] == codeFO & loadfile[, 2] %in%
        c(-1, 1), 8] <- format(as.numeric(weight.bad) *
as.numeric(loadfile[loadfile[, 1] == codeFO & loadfile[, 2] %in% c(-1, 1),
8]), digits = 2, nsmall = 2)
      loadfile[loadfile[, 1] == codeFO & loadfile[, 2] %in% c(-1, 1), 7] <-
format(as.numeric(weight.bad) * as.numeric(loadfile[loadfile[, 1] == codeFO &
loadfile[, 2] %in% c(-1, 1), 7]), digits = 2, nsmall = 2)
    }
  }
  if (method == "pacman" | method == "pac") {
    outsamples <- names(paclist$Profiling[(paclist$Profiling/rowSums(abmat))
>= pacman.sample.ratio])
    if (length(outsamples) != 0) {
      Code_Sect <- function(X) {
        code <- 0
        if (length(grep(X, sectfile[, 4])) != 0) {
         code <- sectfile[grep(X, sectfile[, 4]), 1]
        }
        return(code)
      }
      decomp <- strsplit(outsamples, split = ".", fixed = TRUE)
      sites <- c()
      for (i in 1:length(decomp)) {
        sites[i] <- strsplit(decomp[[i]][1], split = "X")[[1]][2]
        if (is.na(sites[i])) {
         sites[i] <- decomp[[i]][1]
        }
      }
      outcodes <- as.vector(sapply(sites, FUN = Code_Sect))
      outmbsf <- mbsf[(paclist$Profiling/rowSums(abmat)) >=
        pacman.sample.ratio]
      for (i in 1:length(outcodes)) {
        loadfile[loadfile[, 3] == outcodes[i] & loadfile[,
         4] == (-1) * as.vector(t(outmbsf))[i], 8] <-
format(as.numeric(weight.pacman) *
          as.numeric(loadfile[loadfile[, 3] == outcodes[i] &
           loadfile[, 4] == (-1) * as.vector(t(outmbsf))[i],
           8]), digits = 2, nsmall = 2)
        loadfile[loadfile[, 3] == outcodes[i] & loadfile[,
         4] == (-1) * as.vector(t(outmbsf))[i], 7] <-
format(as.numeric(weight.pacman) *
```

```
          as.numeric(loadfile[loadfile[, 3] == outcodes[i] &
           loadfile[, 4] == (-1) * as.vector(t(outmbsf))[i],
           7]), digits = 2, nsmall = 2)
      }
    }
  }
  if (method == "inconsistent" | method == "gap") {
    for (i in 1:length(inconsistent)) {
      inconsistent[i] <- gsub("^\ +|| +$", "", inconsistent[i])
      code <- eventfile[eventfile[, 3] == inconsistent[i],
        1]
      loadfile[loadfile[, 1] == code, 7] <-
format(as.numeric(weight.inconsistent) *
        as.numeric(loadfile[loadfile[, 1] == code, 7]),
        digits = 2, nsmall = 2)
      loadfile[loadfile[, 1] == code, 8] <-
format(as.numeric(weight.inconsistent) *
        as.numeric(loadfile[loadfile[, 1] == code, 8]),
        digits = 2, nsmall = 2)
    }
  }
  return(loadfile)
 }

write.eventfile <- function (taxa_list)
{
  trim.white <- function(x) gsub("^\ +|| +$", "", x)
  taxa_list <- trim.white(taxa_list)
  taxa <- unique(taxa_list)
  a <- strsplit(taxa, split = " ")
  taxa <- paste("'", taxa, "'", sep = "")
  abb <- c()
  for (i in 1:length(taxa)) {
    g <- a[[i]][1]
    s <- a[[i]][2]
    g1 <- substr(g, 1, 3)
    s1 <- substr(s, 1, 3)
    abb[i] <- paste("'", g1, " ", s1, "'", sep = "")
  }
  eventfile <- cbind(1:length(taxa), abb, taxa)
  eventfile <- eventfile[order(eventfile[, 3]), ]
  write.table(eventfile, file = "EVENTFILE.evt", quote = FALSE,
    sep = " ", row.names = FALSE, col.names = FALSE)
  taxa <- gsub("'", "", taxa)
  eventfile <- cbind(1:length(taxa), abb, taxa)
  return(eventfile)
 }

prep.level <- function (sectfile, magn, samples)
{
  Code_Sect <- function(X) {
    code <- sectfile[grep(X, sectfile[, 4]), 1]
    return(code)
  }
  sites1 <- sites2 <- Nlev <- c()
  if (!is.null(magn)) {
    decomp1 <- strsplit(colnames(magn[, 4:ncol(magn)]), split = "X")
    for (i in 1:length(decomp1)) {
      sites1[i] <- decomp1[[i]][2]
    }
```

```
    magn_codes <- as.vector(sapply(sites1, FUN = Code_Sect))
    magn2 <- magn[, 4:ncol(magn)]
    N <- length(magn2[!is.na(magn2)])
    MagLev <- array(dim = c(N, 2))
    n <- 1
    for (j in 1:ncol(magn2)) {
      for (i in 1:nrow(magn2)) {
        if (!is.na(magn2[i, j])) {
         MagLev[n, 1] <- magn_codes[j]
         MagLev[n, 2] <- magn2[i, j]
         n <- n + 1
        }
      }
    }
  }
  decomp2 <- strsplit(colnames(samples), split = ".", fixed = TRUE)
  for (i in 1:length(decomp2)) {
    sites2[i] <- strsplit(decomp2[[i]][1], split = "X")[[1]][2]
    if (is.na(sites2[i])) {
      sites2[i] <- decomp2[[i]][1]
    }
  }
  samp_codes <- as.vector(sapply(sites2, FUN = Code_Sect))
  SampLev <- cbind(samp_codes, t(samples))
  if (!is.null(magn)) {
    Lev <- rbind(MagLev, SampLev)
  }
  else {
    Lev <- SampLev
  }
  Lev <- unique(Lev[, 1:2])
  Lev <- Lev[order(Lev[, 1], Lev[, 2]), ]
  for (i in 1:length(sectfile[, 1])) {
    a <- sum(Lev[, 1] == sectfile[i, 1])
    Nlev <- c(Nlev, a:1)
  }
  levelfile <- cbind(Lev, Nlev)
  write.table(levelfile, file = "levelfile.txt", sep = " ",
    row.names = F, col.names = F)
  return(levelfile)
 }

prep.magn <- function (magn, eventfile, sectfile, scale, levelfile)
{
  eventfileSUITE <- array(dim = c(nrow(magn), 3))
  start <- tail(eventfile, 1)[, 1]
  eventfileSUITE[, 1] <- (start + 1):(start + nrow(magn))
  for (i in 1:nrow(magn)) {
    eventfileSUITE[i, 2] <- paste(magn[i, 3], magn[i, 2],
      sep = " ")
    if (magn[i, 3] == "B") {
      eventfileSUITE[i, 3] <- paste(magn[i, 3], magn[i,
        1], sep = "ottom of Chron ")
    }
    if (magn[i, 3] == "T") {
      eventfileSUITE[i, 3] <- paste(magn[i, 3], magn[i,
        1], sep = "op of Chron ")
    }
  }
  eventfile <- rbind(eventfile, eventfileSUITE)
```

```
  eventfile[, 1] <- as.integer(eventfile[, 1])
  write.table(eventfile, file = "EVENTFILE.evt", sep = " ",
    quote = TRUE, row.names = FALSE, col.names = FALSE)
  magnevent <- array(dim = c(sum(!is.na(magn[, 4:ncol(magn)])),
    8))
  n <- 1
  decomp1 <- strsplit(colnames(magn[, 4:ncol(magn)]), split = "X")
  sites1 <- c()
  for (i in 1:length(decomp1)) {
    sites1[i] <- decomp1[[i]][2]
  }
  for (j in 4:ncol(magn)) {
    for (i in 1:nrow(magn)) {
      if (!is.na(magn[i, j])) {
        magnevent[n, 3] <- sectfile[grep(sites1[j - 3],
         sectfile[, 4]), 1]
        magnevent[n, 4] <- magn[i, j]
        magnevent[n, 1] <- start + i
        magnevent[n, 2] <- 5
        magnevent[n, 6] <- 0
        if (magn[i, 3] == "B") {
         magnevent[n, 8] <- magnevent[n, 7] <- scale[which(scale[,
          3] == magn[i, 1]), 2]
        }
        if (magn[i, 3] == "T") {
         magnevent[n, 8] <- magnevent[n, 7] <- scale[which(scale[,
          3] == magn[i, 1]), 1]
        }
        n <- n + 1
      }
    }
  }
  for (k in 1:nrow(magnevent)) {
    magnevent[k, 5] <- levelfile[levelfile[, 1] == as.numeric(magnevent[k,
      3]) & levelfile[, 2] == as.numeric(magnevent[k, 4]),
      3]
    magnevent[k, 4] <- paste("-", magnevent[k, 4], sep = "")
  }
  return(magnevent)
 }

prep.acme <- function (acme, Nsect, levelfile, eventfile)
{
  acmeevent <- array(dim = c(nrow(acme), 8))
  acmeevent[, 7:8] <- "1.00"
  acmeevent[, 3] <- Nsect
  j <- 1
  for (i in 1:nrow(acme)) {
    acmeevent[j, 1] <- eventfile[which(eventfile[, 3] ==
      rownames(acme)[i]), 1]
    acmeevent[j, 2] <- 3
    acmeevent[j, 4] <- acme[i, 2]
    acmeevent[j, 6] <- 3
    j <- j + 1
  }
  for (k in 1:nrow(acmeevent)) {
    acmeevent[k, 5] <- levelfile[levelfile[, 1] == Nsect &
      levelfile[, 2] == acmeevent[k, 4], 3]
    acmeevent[k, 4] <- paste("-", acmeevent[k, 4], sep = "")
  }
```

```
 return(acmeevent)
}
```

readCONOP

R Documentation

Functions to read the outputs of CONOP9.

Description

`read.unloadmain` reads the Conop output file referred to as `unloadmain` in the conop9.cfg file. `read.unloadevnt` reads the Conop output file referred to as`unloadevnt` in the conop9.cfg file. `read.unloadsect` reads the Conop output file referred to as `unloadsect` in the conop9.cfg file. `read.config` reads the conop9.cfg file. `read.cpchrt` reads the additional Conop output file `cpchrt`. `read.extension` reads the additional Conop output file `extension`.

Usage

```
read.unloadmain(file)
read.unloadevnt(file, nevent)
read.unloadsect(file, sectfile, nevent)
read.config(file)
read.cpchrt(file)
read.extension(file)
```

Arguments

`file`
File to read (can be `file.choose()` for interactive selection).

`nevent`
Number of events in the CONOP analysis.

`sectfile`
Conop input file referred to as `sectfile` in the conop9.cfg file.

Value

The returned value for `read.unloadmain` is a list of 4 elements (corresponding to the four main parts of the UNLOADMAIN file):

`'OBSERVED HORIZONS'`
Corresponds more or less to the `OBSDFILE`.

`'THE LINE OF CORRELATION'`
Corresponds more or less to the `PLCDFILE`.

`'INCREMENTAL RANGE EXTENSION MEASURED BY LEVELS'`
Corresponds more or less to the `extension` file.

`COMPOSITE`
Corresponds more or less to the `COMPOSFILE`.

The returned value for `read.config` is a list of 4 elements (corresponding to the four parts of the `conop9.cfg` file). The returned value for `read.unloadsect` is a list containing one

element for each site (in the order implied by SECTFILE). The returned value for `read.unloadevnt`, `read.cpchrt` and `read.extension` are matrices, equivalent to the corresponding files in all aspects (except metadata).

Author(s)

Johan Renaudie.

Examples

```
# All other output file of CONOP9 for which no function have been writen
(".dat" files, including COMPOSFILE, OBSDFILE & PLCDFILE) can be directly
"batch-read" the following way:

dir1<-dirname(file.choose()) # Select here the CONOP9 working directory where
all output files were sinked.
DatFiles<-dir(dir1,pattern="dat")
DatOutput<-sub(".dat","",DatFiles)
for(j in 1:length(DatFiles)){
      readLines(paste(dir1,DatFiles[j],sep="/"))->yyy
      strsplit(yyy,split=" ")->yy
      for(i in 1:length(yy)){yy[[i]][yy[[i]]!=""]->yy[[i]]}
      length(yy[[1]])->ycol
      length(yy)->yrow
      y<-array(dim=c(yrow,ycol))
      for(i in 1:length(yy)){as.numeric(yy[[i]])->y[i,]}
      assign(DatOutput[j],y)
      }

## The functions are currently defined as
read.unloadmain <- function (file)
{
  temp <- readLines(file)
  Nsect <- as.integer(gsub(" ", "", gsub("Number of sections:",
    "", temp[grep("Number of sections:", temp)])))
  Nevents <- as.integer(gsub(" ", "", gsub("Total number of events:",
    "", temp[grep("Total number of events:", temp)])))
  index <- grep("INCREMENTAL RANGE EXTENSION MEASURED BY LEVELS",
    temp)
  x <- temp[(index + 13):(index + 12 + Nevents)]
  y <- strsplit(x, split = "[", fixed = TRUE)
  for (i in 1:length(y)) {
    y[[i]][2] <- strsplit(y[[i]][2], split = "]", fixed = TRUE)[[1]][2]
    x[i] <- paste(y[[i]][1], y[[i]][2], sep = " ")
  }
  y <- strsplit(x, split = " ", fixed = TRUE)
  level_extension <- matrix(nrow = length(y), ncol = 2 + Nsect)
  for (i in 1:length(y)) {
    z <- y[[i]]
    z <- z[z != ""]
    options(warn = -1)
    level_extension[i, ] <- as.numeric(z)
    options(warn = 0)
  }
  options(warn = -1)
  sectcode <- strsplit(gsub(")", "", gsub("(sections:", "",
    temp[grep("sections: ", temp)][3], extended = FALSE)),
    split = " ")[[1]]
```

```
  options(warn = 0)
  sectcode <- sectcode[sectcode != ""]
  colnames(level_extension) <- c("Event", "type", sectcode)
  x <- temp[(grep("COMPOSITE", temp) + 2):(grep("COMPOSITE",
    temp) + 1 + Nevents)]
  y <- strsplit(x, split = "{", fixed = TRUE)
  for (i in 1:length(y)) {
    x[i] <- y[[i]][1]
  }
  y <- strsplit(x, split = " ")
  composite <- matrix(nrow = length(y), ncol = 5)
  colnames(composite) <- c("Event", "Type", "Space-below",
    "Level-placed", "Sections")
  for (i in 1:length(y)) {
    z <- y[[i]]
    z <- z[z != ""]
    options(warn = -1)
    composite[i, ] <- as.numeric(z)
    options(warn = 0)
  }
  x <- temp[(grep("OBSERVED HORIZONS", temp) + 6):(grep("OBSERVED HORIZONS",
    temp) + 5 + Nevents)]
  y <- strsplit(x, split = "[", fixed = TRUE)
  for (i in 1:length(y)) {
    y[[i]][2] <- strsplit(y[[i]][2], split = "]", fixed = TRUE)[[1]][2]
    x[i] <- paste(y[[i]][1], y[[i]][2], sep = " ")
  }
  y <- strsplit(x, split = " ", fixed = TRUE)
  horizon1 <- matrix(nrow = length(y), ncol = 2 + Nsect)
  for (i in 1:length(y)) {
    z <- y[[i]]
    z <- z[z != ""]
    z <- gsub("none", "NA", z)
    options(warn = -1)
    horizon1[i, ] <- as.numeric(z)
    options(warn = 0)
  }
  colnames(horizon1) <- c("Event", "type", sectcode)
  x <- temp[(grep("THE LINE OF CORRELATION", temp) + 9):(grep("THE LINE OF
CORRELATION",
    temp) + 8 + Nevents)]
  y <- strsplit(x, split = "[", fixed = TRUE)
  for (i in 1:length(y)) {
    y[[i]][2] <- strsplit(y[[i]][2], split = "]", fixed = TRUE)[[1]][2]
    x[i] <- paste(y[[i]][1], y[[i]][2], sep = " ")
  }
  y <- strsplit(x, split = " ", fixed = TRUE)
  horizon2 <- matrix(nrow = length(y), ncol = 2 + Nsect)
  for (i in 1:length(y)) {
    z <- y[[i]]
    z <- z[z != ""]
    options(warn = -1)
    horizon2[i, ] <- as.numeric(z)
    options(warn = 0)
  }
  colnames(horizon2) <- c("Event", "type", sectcode)
  unloadmain <- list(`OBSERVED HORIZONS` = horizon1, `THE LINE OF
CORRELATION` = horizon2,
    `INCREMENTAL RANGE EXTENSION MEASURED BY LEVELS` = level_extension,
    COMPOSITE = composite)
```

```
  return(unloadmain)
 }

read.unloadevnt <- function (file, nevent)
{
  y <- readLines(file)[9:(nevent + 8)]
  close(file)
  yyy <- matrix(nrow = nevent, ncol = 5)
  colnames(yyy) <- c("Event", "Type", "Extension", "Penalty",
    "Sections")
  rownames(yyy) <- 1:nevent
  for (i in 1:length(y)) {
    yy <- strsplit(y[[i]], split = "{", fixed = TRUE)[[1]][1]
    z <- strsplit(yy, split = " ")[[1]]
    z <- z[z != ""]
    yyy[i, ] <- as.numeric(z[c(1, 3:6)])
  }
  return(yyy)
 }

read.unloadsect <- function (file, sectfile, nevent)
{
  Output_Section <- list()
  temp <- readLines(file)
  for (j in 1:nrow(sectfile)) {
    y <- temp[(grep(substr(sectfile[j, 4], 1, 20), temp) +
      3):(grep(substr(sectfile[j, 4], 1, 20), temp) + 2 +
      nevent)]
    y <- sub("not seen", "NA", y)
    y <- sub("unseen", "NA", y)
    yy <- strsplit(y, split = "{", fixed = TRUE)
    yyy <- matrix(nrow = length(yy), ncol = 7)
    colnames(yyy) <- c("Event n\302\260", "Event type", "Observed",
      "Placed", "Unweighted misfit", "Weighted misfit",
      "Level misfit")
    rownames(yyy) <- 1:length(yy)
    for (i in 1:length(yy)) {
      z <- strsplit(yy[[i]][1], split = " ")[[1]]
      z <- z[z != ""]
      options(warn = -1)
      if (z[2] == "-") {
        yyy[i, 1:7] <- as.numeric(z[c(1, 3:8)])
      }
      if (z[2] != "-") {
        yyy[i, ] <- as.numeric(gsub("--", "-", z))
      }
      options(warn = 0)
    }
    rm(y, yy, z)
    Output_Section[[j]] <- yyy
    names(Output_Section)[j] <- as.character(sectfile[j,
      4])
    rm(yyy)
  }
  return(Output_Section)
 }
read.config <- function (file)
{
  x <- readLines(file)
  x <- x[!x %in% c("", " ", "  ", "   ", "   ")]
```

```
  y <- grep("/", x)
  x <- gsub(" *$", "", x)
  getinn <- x[2:(y[1] - 1)]
  getans <- x[(y[1] + 2):(y[2] - 1)]
  getrun <- x[(y[2] + 2):(y[3] - 1)]
  getout <- x[(y[3] + 2):(y[4] - 1)]
  getinn_list <- strsplit(getinn, split = "=")
  getinn_row <- c()
  getinn_value <- c()
  for (i in 1:length(getinn_list)) {
    getinn_row[i] <- getinn_list[[i]][1]
    getinn_value[i] <- getinn_list[[i]][2]
    getinn_value[i] <- gsub("'", "", getinn_value[i], fixed = T)
  }
  getinn <- data.frame(getinn_value, row.names = getinn_row)
  getout_list <- strsplit(getout, split = "=")
  getout_row <- c()
  getout_value <- c()
  for (i in 1:length(getout_list)) {
    getout_row[i] <- getout_list[[i]][1]
    getout_value[i] <- getout_list[[i]][2]
    getout_value[i] <- gsub("'", "", getout_value[i], fixed = T)
  }
  getout <- data.frame(getout_value, row.names = getout_row)
  getans_list <- strsplit(getans, split = "=")
  getans_row <- c()
  getans_value <- c()
  for (i in 1:length(getans_list)) {
    getans_row[i] <- getans_list[[i]][1]
    getans_value[i] <- getans_list[[i]][2]
    getans_value[i] <- gsub("'", "", getans_value[i], fixed = T)
  }
  getans <- data.frame(getans_value, row.names = getans_row)
  getrun_list <- strsplit(getrun, split = "=")
  getrun_row <- c()
  getrun_value <- c()
  for (i in 1:length(getrun_list)) {
    getrun_row[i] <- getrun_list[[i]][1]
    getrun_value[i] <- getrun_list[[i]][2]
    getrun_value[i] <- gsub("'", "", getrun_value[i], fixed = T)
  }
  getrun <- data.frame(getrun_value, row.names = getrun_row)
  config <- list(`PARAMETERS THAT IDENTIFY THE INPUT DATA` = getinn,
    `PARAMETERS THAT ALTER THE BEST SOLUTION` = getans, `PARAMETERS THAT
INFLUENCE EFFICIENCY OF SEARCH FOR BEST SOLUTION` = getrun,
    `PARAMETERS THAT DETERMINE THE NATURE AND LOCATION OF OUTPUT` = getout)
  return(config)
 }

read.cpchrt <- function (file = file.choose())
{
  a <- readLines(file)
  a <- a[12:length(a)]
  b <- strsplit(a, split = "[", fixed = TRUE)
  chart <- matrix(nrow = length(a), ncol = 4)
  sp <- c()
  for (i in 1:length(b)) {
    bi <- strsplit(b[[i]][1], split = " ")[[1]]
    bi <- bi[bi != ""]
    chart[i, ] <- as.numeric(bi[1:4])
```

```
    if (length(bi) == 6) {
      sp[i] <- paste(bi[5], bi[6], sep = " ")
    }
    if (length(bi) == 7) {
      sp[i] <- paste(bi[5], bi[6], bi[7], sep = " ")
    }
    if (length(bi) > 7) {
      sp[i] <- paste(bi[5], bi[6], sep = " ")
    }
  }
  if (is.na(chart[nrow(chart), 1])) {
    chart <- chart[-nrow(chart), ]
  }
  rownames(chart) <- sp
  return(chart)
 }

read.extension <- function (file)
{
  temp <- readLines(file)
  N <- grep("Number of sections:", temp)
  Nsect <- as.integer(gsub(" ", "", gsub("Number of sections:",
    "", temp[N])))
  N <- grep("Total number of events:", temp)
  Nevents <- as.integer(gsub(" ", "", gsub("Total number of events:",
    "", temp[N])))
  index <- grep("INCREMENTAL RANGE EXTENSION MEASURED BY LEVELS",
    temp)
  x <- temp[(index + 13):(index + 12 + Nevents)]
  y <- strsplit(x, split = "[", fixed = TRUE)
  for (i in 1:length(y)) {
    y[[i]][2] <- strsplit(y[[i]][2], split = "]", fixed = TRUE)[[1]][2]
    x[i] <- paste(y[[i]][1], y[[i]][2], sep = " ")
  }
  y <- strsplit(x, split = " ", fixed = TRUE)
  yy <- matrix(nrow = length(y), ncol = 2 + Nsect)
  for (i in 1:length(y)) {
    z <- y[[i]]
    z <- z[z != ""]
    options(warn = -1)
    yy[i, ] <- as.numeric(z)
    options(warn = 0)
  }
  options(warn = -1)
  sectcode <- strsplit(gsub(")", "", gsub("(sections:", "",
    temp[grep("sections: ", temp)][3], extended = FALSE)),
    split = " ")[[1]]
  options(warn = 0)
  sectcode <- sectcode[sectcode != ""]
  colnames(yy) <- c("Event", "type", sectcode)
  return(yy)
 }
```

site2composite

R Documentation

From site depth to composite depth.

Description

Translate the depth of a sample in its 'depth' on the composite sequence.

Usage

```
site2composite(mbsf, Nsect, plcdfile, composfile)
```

Arguments

`mbsf`
Vector of depths to translate.

`Nsect`
Index of the site (see sectfile).

`plcdfile`
CONOP9 output corresponding to `plcdfile` in the configuration file.

`composfile`
CONOP9 output corresponding to `composfile` in the configuration file.

Value

Vector of composite depths.

Author(s)

Johan Renaudie.

Examples

```
## The function is currently defined as
function (mbsf, Nsect, plcdfile, composfile)
{
  equiv <- matrix(nrow = nrow(composfile), ncol = ncol(plcdfile) -
    1)
  for (i in 1:nrow(composfile)) {
    equiv[i, ] <- c(composfile[i, 4], plcdfile[plcdfile[,
      1] == composfile[i, 1] & plcdfile[, 2] == composfile[i,
      2], 3:ncol(plcdfile)])
  }
  result <- approx(equiv[, Nsect + 1], equiv[, 1], (-1) * mbsf,
    rule = 2, ties = "ordered")$y
  return(result)
 }
```

drawCONOP

R Documentation

Classical, useful plots from CONOP output.

Description

`draw.ranges` plots a range-chart. `culling` shows the full range of positions where an event may be placed in the optimal sequence. `fence.depth` plots a fence diagram.

Usage

```
draw.ranges(composfile, eventfile, order = "FAD", method =
"depth", ...)
fence.depth(plcdfile, sectfile, tag = 1)
culling(composfile, cpcht, age.span = c(25, 0), FO.col = "blue",
LO.col = "red")
```

Arguments

`composfile`
Conop output referred to as `composfile` on the conop9.cfg file.

`eventfile`
Conop input referred to as `eventfile` on the conop9.cfg file (see `write.eventfile`).

`plcdfile`
Conop output referred to as `plcdfile` on the conop9.cfg file (i. e. depth of placed event on each site). Can be replaced by the output `obsdfile` if needed.

`sectfile`
Conop input file referred to as `sectfile` on the conop9.cfg file.

`tag`
Two possible values: if `1` then each sites will be named after its abridged name, if `2` after its complete name (respectively columns 2 and 4 of the input file SECTFILE).

`order`
The rangechart can be ordered by `"FAD"` or by `"LAD"`.

`method`
If `"depth"`, then the rangechart is plotted according to the composite sequence 'depth'. If `"age"` it is plotted according to the age of the events: in that case `composfile` needs to be supplied by the output of function `composite.age`.

`cpcht`
Additional Conop output `cpchrt`.

`age.span`
Age range (vector of two ages).

`FO.col`
Color for FO.

`LO.col`
Color for LO.

`...`
Any argument that could be passed to `segments`.

Author(s)

Johan Renaudie.

Examples

```
## The function is currently defined as
draw.ranges <- function (composfile, eventfile, order = "FAD", method =
"depth",
  ...)
{
  if (order == "FAD") {
    a <- 1
  }
  if (order == "LAD") {
    a <- 2
  }
  if (method == "depth") {
    b <- 4
    d <- 50
    MetLab <- "Composite section depth"
  }
  if (method == "rank") {
    b <- 5
    d <- 2
    MetLab <- "Rank n\302\260"
  }
  if (method == "age") {
    b <- 4
    d <- -1
    MetLab <- "Age\n(Ma)"
  }
  par(mar = c(1, 5, 5, 1))
  if (method != "age") {
    y1 <- min(composfile[, b])
    y2 <- max(composfile[, b])
  }
  if (method == "age") {
    y1 <- max(composfile[, b])
    y2 <- min(composfile[, b])
  }
  plot(0, 0, ylim = c(y1, y2), xlim = c(0,
length(unique(composfile[composfile[,
    2] != 5, 1])) + 1), type = "n", xaxt = "n", xlab = "",
    ylab = "", yaxt = "n", xaxs = "i", yaxs = "i")
  axis(2, at = seq(floor(y1), floor(y2), by = d), las = 2,
    cex.lab = 10)
  mtext(MetLab, side = 2, line = 3)
  evtorder <- composfile[composfile[, 2] == a, 1]
  evtorder <- cbind(evtorder, 1:length(evtorder))
  for (X in unique(composfile[composfile[, 2] != 5, 1])) {
    Xrange <- composfile[composfile[, 1] == X, ]
```

```
    segments(evtorder[evtorder[, 1] == X, 2], Xrange[Xrange[,
      2] %in% c(-1, 1), b], evtorder[evtorder[, 1] == X,
      2], Xrange[Xrange[, 2] == 2, b], ...)
    mtext(eventfile[eventfile[, 1] == X, 3], font = 3, las = 2,
      at = evtorder[evtorder[, 1] == X, 2], line = 0.5,
      cex = 0.3)
  }
 }

 fence.depth <- function (plcdfile, sectfile, tag = 1)
{
  plot(c(0, 10 * nrow(sectfile) - 5), c(max(plcdfile[, 3:7],
    na.rm = T), min(plcdfile[, 3:7], na.rm = T)), ylim = c(min(plcdfile[,
    3:7], na.rm = T), max(plcdfile[, 3:7], na.rm = T)), yaxt = "n",
    bty = "n", xaxt = "n", ylab = "Depth", xlab = "", type = "n")
  for (i in 1:nrow(sectfile)) {
    rect((sectfile[i, 3] - 1) * 10, max(plcdfile[, 2 + i],
      na.rm = T), 5 + (sectfile[i, 3] - 1) * 10, min(plcdfile[,
      2 + i], na.rm = T), col = "white")
    for (j in 1:length(unique(plcdfile[, 2 + i]))) {
      lines(c((sectfile[i, 3] - 1) * 10, 5 + (sectfile[i,
        3] - 1) * 10), c(unique(plcdfile[, 2 + i])[j],
        unique(plcdfile[, 2 + i])[j]))
    }
    text(2.5 + (sectfile[i, 3] - 1) * 10, max(plcdfile[,
      2 + i], na.rm = T) + 5, sectfile[i, 2 * tag])
  }
  axis(2, at = seq(floor(min(plcdfile[, 3:7], na.rm = T)),
    ceiling(max(plcdfile[, 3:7], na.rm = T)), by = 50), las = 2,
    cex = 0.8)
  for (i in 1:(nrow(sectfile) - 1)) {
    for (j in 1:nrow(plcdfile)) {
      if (plcdfile[j, 2] != 5) {
        lines(c(5 + (i - 1) * 10, 10 + (i - 1) * 10),
         c(plcdfile[j, as.vector(sectfile[sectfile[,
          3] == i, 1]) + 2], plcdfile[j, as.vector(sectfile[sectfile[,
          3] == i + 1, 1]) + 2]), col = "blue", lwd = 1)
      }
      if (plcdfile[j, 2] == 5) {
        lines(c(5 + (i - 1) * 10, 10 + (i - 1) * 10),
         c(plcdfile[j, as.vector(sectfile[sectfile[,
          3] == i, 1]) + 2], plcdfile[j, as.vector(sectfile[sectfile[,
          3] == i + 1, 1]) + 2]), col = "orange", lwd = 1)
      }
    }
  }
 }

culling <- function (composfile, cpcht, age.span = c(25, 0), FO.col = "blue",
  LO.col = "red")
{
  agem <- composfile[composfile[, 7] > 1, c(4, 7)]
  b <- array(dim = c(nrow(cpcht), 4))
  for (i in 1:4) {
    b[, i] <- approx(agem[, 1], agem[, 2], cpcht[, i], rule = 2,
      ties = "ordered")$y
  }
  maxb <- max(b, na.rm = T)
  minb <- min(b, na.rm = T)
  par(mar = c(4, 3, 2, 2))
```

```
 plot(c(-0.5, 0.5), c(minb, maxb), type = "n", xaxt = "n",
   xlab = "", ylab = "", yaxt = "n", ylim = age.span, asp = 1,
   yaxs = "i", xaxs = "i")
 mtext("Composite section", side = 1, line = 1.5)
 axis(2, at = seq(age.span[2], age.span[1], by = 2), las = 2)
 rect(-0.05, minb, 0.05, maxb)
 for (i in 1:nrow(cpcht)) {
   circle.diam(0, b[i, 1], 0, b[i, 2], col = FO.col)
   if (!is.na(b[i, 3])) {
     circle.diam(0, b[i, 3], 0, b[i, 4], col = LO.col)
   }
 }
}
```

circle

R Documentation

Draw a circle.

Description

`circle` draws a circle given its center and its radius; `circle.diam` given its diameter. Functions needed for some CONOP9 graphical output such as `culling`.

Usage

```
circle(r, x0, y0, new = FALSE, ...)
circle.diam(x1, y1, x2, y2, new = FALSE, ...)
```

Arguments

`r`
Circle radius

`x0`
Center abscissa

`y0`
Center ordinate

`x1`
Abscissa of one end of the diameter

`y1`
Ordinate of one end of the diameter

`x2`
Abscissa of the other end of the diameter

`y2`
Ordinate of the other end of the diameter

`new`
Wether or not the circle should be drawn on a new plot (`TRUE`) or an existing one (`FALSE`)

`...`
Any other arguments that can be passed to `lines` or `plot`

Examples

```
##The functions are currently defined as
circle<-
function (r, x0, y0, new = FALSE, ...)
{
  t <- seq(0, 2 * pi, by = 0.01)
  x <- r * cos(t) + x0
  y <- r * sin(t) + y0
  if (new == FALSE) {
```

```
    lines(x, y, ...)
  }
  if (new == TRUE) {
    plot(x, y, type = "l", ...)
  }
 }
circle.diam<-
function (x1, y1, x2, y2, new = FALSE, ...)
{
  t <- seq(0, 2 * pi, by = 0.01)
  x0 <- (x1 + x2)/2
  y0 <- (y1 + y2)/2
  r <- sqrt((x0 - x1)^2 + (y0 - y1)^2)
  x <- r * cos(t) + x0
  y <- r * sin(t) + y0
  if (new == FALSE) {
    lines(x, y, ...)
  }
  if (new == TRUE) {
    plot(x, y, type = "l", ...)
  }
 }
```

trim.white

R Documentation

White trimming

Description

Trim heading and trailing whites in a character string (function needed to assure consistency of character strings in the function to write the input or read the output of CONOP9)

Usage

```
trim.white(x)
```

Arguments

`x`
Character string to be trimmed

Examples

```
## The function is currently defined as
function(x) gsub("^\ +|| +$","",x)
```

Erklärung

Hiermit erkläre ich, die Dissertation selbständig und nur unter Verwendung der angegebenen Hilfen und Hilfsmittel angefertigt habe.

Ich habe mich anderwärts nicht um einen Doktorgrad beworben und besitze einen entsprechenden Doktorgrad nicht.

Ich erkläre die Kenntnisnahme der dem Verfahren zugrunde liegenden Promotionsordnung der Mathematisch-Naturwissenschaftlichen Fakultät I der Humboldt-Universität zu Berlin.

Berlin, 12. Juli 2012,

Johan Renaudie.